

# Leveraging Chemical Biology to Modulate Antigen Presentation

Joseph John Kelly

B.S. Bioengineering, Lehigh University, 2020

A Dissertation

Presented to the Graduate Faculty of the University of Virginia in Candidacy for the  
Degree of Doctor of Philosophy

Department of Chemistry

University of Virginia

May 2025

© 2025 Copyright

Joseph J. Kelly

## Abstract

The immune system possesses a remarkable ability to distinguish between “self” and “non-self” antigens to help maintain homeostasis. A key mechanism underlying this capability is the presentation of peptides on the major histocompatibility complex (MHC). This process is essential for mounting immune responses against infectious disease and cancer. Notably, many FDA-approved cancer immunotherapies, including checkpoint inhibitors and cancer vaccines rely on the recognition of MHC-displayed antigens by effector immune cells. However, the continued success of these therapies depends on the identification of conserved cancer antigens and a deeper understanding of the biological mechanisms governing antigen presentation.

Cancers can escape immune detection by eliminating cancer-specific antigens. One class of these antigens includes neoantigens, which are modified peptides presented on MHC that arise from tumor-specific alterations. Cancer cells can avoid immune recognition of their neoantigens by either (1) losing neoantigen expression or (2) downregulating MHC molecules, thereby reducing antigen presentation. Given the central role of antigen presentation in immune surveillance, understanding the mechanisms that drive neoantigen loss and MHC downregulation is critical for developing more effective immunotherapies. Additionally, understanding the biological pathways behind the generation of neoantigens also aids in identifying promising neoantigens to target. By elucidating these pathways, we can refine existing immunotherapies and identify new approaches to improve immune targeting of cancer cells.

Chapter 3 details the selective delivery of a neoantigen to cancer cells using a pH(low) insertion peptide (pHLIP). pHLIP selectively integrates into the membranes of cells in acidic environments and facilitates the transport of large molecules, including peptides, across the cell membrane. The acidic tumor microenvironment is a well-conserved feature across cancer, driven by the increased energy demand and the resulting production of lactic acid through glycolysis. Here, we demonstrate that pHLIP can efficiently deliver a model neoantigen across the cell membrane and into the antigen presentation pathway in a pH-dependent manner. Furthermore, brief treatment with the

conjugate enables neoantigen-specific T cells to recognize the peptide-MHC complex, highlighting the potential of this strategy for enhancing immune targeting of tumors.

Next, we addressed the challenge of MHC-I downregulation, a common immune evasion strategy, by developing a screening platform to identify small molecules that enhance MHC-I surface expression. Loss of MHC-I is observed in various tumor types, including colorectal cancer, and is associated with resistance to checkpoint inhibition therapy. In Chapter 4, we identify promising chemical scaffolds that increase MHC-I display on colorectal cancer cells. Through screening diverse classes of compounds reported to upregulate MHC-I, we found that a purine-based scaffold derived from heat shock protein 90 inhibitors exhibited the most robust activity. To further optimize this scaffold, we employed a click-chemistry-based approach to rapidly generate and evaluate hundreds of derivatives, selecting those that enhance MHC-I expression while minimizing toxicity relative to the parent compound.

In Chapter 5, we investigated how enzymatic post-translational modifications (PTMs) influence the antigen presentation pathway. Peptides modified with PTMs represent a significant class of cancer-specific neoantigens. However, the molecular basis of their immunomodulatory effects remains poorly understood for most PTMs. We hypothesized that PTMs play a critical role in modulating peptide affinity for MHC-I as well as recognition by T cells through their T cell receptors (TCRs). To test this, we integrated experimental data with computational modeling to assess the impact of various PTMs on peptide-MHC-I binding affinity. Additionally, we observed substantial changes in TCR recognition of modified peptides, suggesting that TCR specificity is a key determinant in the immune response to modified self-antigens.

While most modified self-antigens presented on MHC-I arise from nonenzymatic modifications, their impact on the immune response remains less understood. In Chapter 6, we investigated how nonenzymatic modifications influence the antigen presentation pathway. Specifically, we assessed their effects on MHC-I binding affinity and TCR recognition. Additionally, we also identify key changes in peptide presentation between unmodified and modified cancer-associated MHC peptides. Finally, we are developing an enrichment strategy to map sites of nonenzymatic modifications displayed on MHC to

provide insights onto the role of the modification on immune responses. This is particularly significant given that many inflammatory conditions involve the release of electrophilic molecules capable of nonenzymatically modifying proteins, potentially shaping immune recognition and response.

Finally, in Chapter 7, we examine how intracellular pathogens evade both immune defenses and antibiotic treatment. Bacteria have evolved strategies that allow them to survive within host cells, where they are shielded from immune effectors and antimicrobial agents. A key challenge in treating intracellular infections is determining whether reduced antibiotic efficacy stems from bacterial phenotypic changes or limited antibiotic accumulation within intracellular compartments. To address this, we developed a method to incorporate a bioorthogonal alkyne handle into the peptidoglycan of *Staphylococcus aureus*, enabling the quantification of azide-modified antibiotic accumulation. By comparing the kinetics of azide-modified antibiotic accumulation with alkyne-labeled peptidoglycan in *S. aureus* residing within macrophages, we aimed to elucidate the extent to which antibiotics reach intracellular pathogens.

## **Acknowledgments**

I would like to thank my parents, Kristin and Sean, for their continued love and support. I would also like to thank my mentor Marcos Pires for his guidance throughout my doctoral studies. Finally, I am incredibly thankful to Brianna Dalesandro for her constant love and support given to me throughout my journey in becoming a Doctor of Philosophy.

## Table of Contents

<b>Abstract</b> .....	<b>iii</b>
<b>Chapter 1 Introduction</b> .....	<b>11</b>
1.1 Major Histocompatibility Complex .....	11
1.2 Major Histocompatibility Complex Class II .....	13
1.3 T Cell Response to MHC .....	14
1.4 Neoantigen Presentation in Cancer .....	15
1.5 Cancer Immune Evasion Mechanisms .....	17
1.6 Summary and Future Outlook .....	18
1.7 References .....	19
<b>Chapter 2 Post-Translationally Modified Peptide Display on MHC</b> .....	<b>26</b>
2.1 Identification of MHC-Associated Peptides .....	26
2.2 Post-Translationally Modified Peptides .....	28
2.3 Enzymatic PTMs .....	30
2.3.1 Phosphorylation .....	30
2.3.2 Glycosylation .....	31
2.3.3 Citrullination .....	33
2.3.4 Other Enzymatic Modifications .....	34
2.4 Nonenzymatic PTMs .....	35
2.4.1 Cysteinylation .....	35
2.4.2 Oxidation .....	36
2.5 Hapten Display on MHC .....	37
2.6 Summary and Future Outlook .....	39
2.7 References .....	40
<b>Chapter 3 Targeted Acidosis Delivery of Antigenic MHC-Binding Peptides</b> .....	<b>51</b>
3.1 Abstract .....	51
3.2 Introduction .....	51
3.3 Results and Discussion .....	54
3.3.1 Strategic placement of cysteine handle .....	55

3.3.2 Assessing the ability of pHILIP-CysOVA to insert into membranes in acidic environments .....	57
3.3.3 Analyzing pHILIP-CysOVA delivery into antigen presentation pathway .....	58
3.4 Conclusion .....	60
3.5 Summary and Future Outlook .....	61
3.6 Materials and Methods .....	62
3.7 Supplementary Figures .....	66
3.8 References .....	68
<b>Chapter 4 Evaluation and Diversification of Small Molecule Inducers of MHC-I Surface Expression .....</b>	<b>75</b>
4.1 Abstract .....	75
4.2 Introduction .....	75
4.3 Results and Discussion .....	78
4.3.1 Screening small molecules for their MHC-I upregulation activity .....	78
4.3.2 Screening Hsp90 inhibitors for MHC-I surface upregulation activity .....	79
4.3.3 High-throughput click chemistry diversification strategy of Hsp90 inhibitor ...	82
4.3.4 ClIMB-325 enhances MHC-I surface expression and T cell activation .....	86
4.4 Conclusion .....	87
4.5 Summary and Future Outlook .....	88
4.6 Materials and Methods .....	88
4.7 Supplementary Figures .....	91
4.8 References .....	98
<b>Chapter 5 A Chemical Approach to Assess Impact of Post-Translational Modifications on MHC Peptide Binding and Effector Cell Engagement .....</b>	<b>105</b>
5.1 Abstract .....	105
5.2 Introduction .....	105
5.3 Results and Discussion .....	108
5.3.1 PTMs alter peptide binding affinity to MHC .....	108
5.3.2 TCR recognition of pMHC is distinctly altered by PTMs compared to MHC	

affinity .....	110
<b>5.3.3</b> Assessing influence of PTMs on display of disease relevant peptides .....	113
<b>5.3.4</b> Modeling PTM influence on peptide-MHC binding affinity .....	115
<b>5.4</b> Conclusion .....	119
<b>5.5</b> Summary and Future Outlook .....	119
<b>5.6</b> Materials and Methods .....	120
<b>5.7</b> Supplementary Figures .....	123
<b>5.8</b> References .....	133
<b>Chapter 6 Impact of Non-Enzymatic Modifications to Peptides on MHC Peptide Binding and TCR Engagement .....</b>	<b>144</b>
<b>6.1</b> Abstract .....	144
<b>6.2</b> Introduction .....	144
<b>6.3</b> Results and Discussion .....	147
<b>6.3.1</b> Impact of modifications on MHC-I affinity .....	149
<b>6.3.2</b> Impact of modifications on TCR recognition .....	150
<b>6.3.3</b> Identification of acylation sites displayed on MHC-I .....	151
<b>6.4</b> Conclusion .....	153
<b>6.5</b> Summary and Future Outlook .....	154
<b>6.6</b> Materials and Methods .....	155
<b>6.7</b> References .....	157
<b>Chapter 7 Measurement of Accumulation of Antibiotics to <i>Staphylococcus aureus</i> in Phagosomes of Live Macrophages.....</b>	<b>166</b>
<b>7.1</b> Abstract .....	166
<b>7.2</b> Introduction .....	166
<b>7.3</b> Results and Discussion .....	168
<b>7.3.1</b> Optimizing D-DapD labeling conditions for <i>S. aureus</i> .....	171
<b>7.3.2</b> Assessing accessibility of antibiotics to cell surface of <i>S. aureus</i> .....	175
<b>7.3.3</b> Investigating accumulation of antibiotics to MRSA .....	177
<b>7.3.4</b> Measuring antibiotic permeability to intracellular pathogens .....	180

7.4 Conclusion .....	182
7.5 Summary and Future Outlook .....	182
7.6 Materials and methods .....	183
7.7 Supplementary Figures .....	187
7.7 References .....	195
<b>Chapter 8 Summary and Future Outlook .....</b>	<b>203</b>
<b>Appendix .....</b>	<b>208</b>
<b>A.3 Synthesis and Characterization of Compounds in Chapter 3 .....</b>	<b>208</b>
<b>A.4 Synthesis and Characterization of Compounds in Chapter 4 .....</b>	<b>222</b>
<b>A.5 Synthesis and Characterization of Compounds in Chapter 5 .....</b>	<b>229</b>
<b>A.6 Synthesis and Characterization of Compounds in Chapter 6 .....</b>	<b>300</b>
<b>A.7 Synthesis and Characterization of Compounds in Chapter 7 .....</b>	<b>349</b>

## **Chapter 1 Introduction**

### **1.1 Major Histocompatibility Complex**

The Major Histocompatibility Complex (MHC) plays a crucial role for the immune system by enabling the identification and elimination of foreign entities. It was first identified in 1936 when researchers sought to understand the molecular mechanisms underlying organ transplant rejection.<sup>1</sup> Since then, extensive investigations have focused on its role in antigen presentation and immune detection. MHC proteins, also known as MHC molecules, function primarily by displaying antigens on cell surfaces, where they are recognized by specific immune cells.<sup>2</sup> There are two main classes of MHC molecules: MHC class I (MHC-I) and MHC class II (MHC-II). These classes differ in the types of antigens they present, the cells that express these proteins, and the immune cells they interact with.<sup>3</sup> Both MHC-I and MHC-II are essential for mounting immune response against pathogens and cancer.<sup>4</sup>

MHC-I is responsible for presenting peptides derived from the cytosol to CD8+ T cells. It is expressed on the surface of all nucleated cells, allowing for continuous immune surveillance.<sup>5</sup> If a peptide being presented is a foreign antigen, the interaction between the peptide MHC-I complex (pMHC) and the T cell receptor (TCR) on CD8+ T cells triggers their differentiation into cytotoxic T lymphocytes (CTLs).<sup>6</sup> These CTLs then target and destroy the cells displaying the peptide antigen. While most pMHC complexes present endogenous peptides, virally infected cells will have viral proteins present in the cytosol. These proteins are degraded into peptide fragments and presented on MHC-I, forming virus-specific pMHC complexes. This enables CTLs to recognize and eliminate infected cells by detecting viral peptides through their TCRs.<sup>7</sup> Besides viral infections, MHC-I can also display peptides from other intracellular pathogens like bacteria<sup>8</sup> and fungi<sup>8</sup> as well as disease-associated peptides in conditions such as cancer<sup>9</sup> and autoimmunity.<sup>10</sup>

MHC-I has evolved several mechanisms to present various peptides derived from diverse sources. A key mechanism is its promiscuous peptide-binding groove, which allows a single MHC-I molecule to display thousands of unique peptide sequences.<sup>11</sup> Additionally,

each individual expresses six MHC-I alleles, selected from over 35,000 known alleles in the human population.<sup>12</sup> The high degree of polymorphism in MHC-I genes enhances the ability of the immune system to recognize a broad range of pathogens. The vast diversity of MHC-I molecules and the peptides they can present ensure effective antigenic peptides to CTLs and improve the population's ability to respond to various infectious agents.

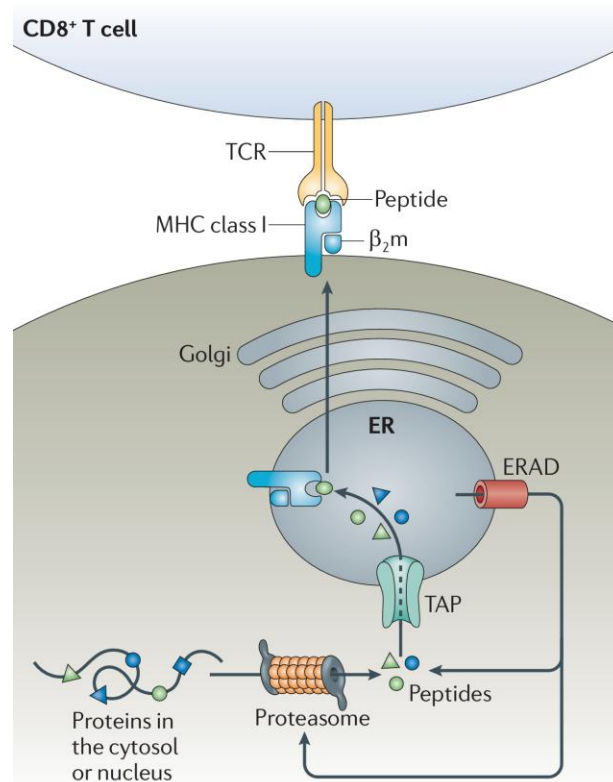


**Figure 1.1** MHC-I antigen presentation pathway

Reproduced from<sup>2</sup>.

Peptides presented on MHC-I are primarily derived from the cytosol, typically as products of protein degradation by the proteasome<sup>13</sup> or from errors in protein translation, such as defective ribosomal products.<sup>14</sup> While most cytosolic peptides are fully degraded by cytosolic proteases, some are transported from the cytosol to the endoplasmic reticulum (ER) via the transporter associated with antigen processing (TAP).<sup>15</sup> In the ER, these peptides can interact with MHC-I molecules. If necessary, the proteases ERAP1 and ERAP2 can further trim the peptides to the correct length (typically 8-12 amino acids) to

ensure proper binding into the MHC-I peptide binding groove.<sup>16</sup> Additionally, numerous chaperone proteins, including TAP, tapasin, Erp57, and calreticulin, form the peptide loading complex (PLC) to help stabilize MHC-I and facilitate peptide loading.<sup>17</sup> If a peptide fails to bind to MHC-I, then it is translocated back into the cytosol and degraded.<sup>18</sup> Once a peptide is successfully loaded onto MHC-I, the pMHC is transported to the cell membrane to display the peptide antigen to CTLs for immune surveillance (Figure 1.1).<sup>19</sup>

## 1.2 Major Histocompatibility Complex Class II

MHC-II, however, differs from MHC-I in that MHC-II expression is primarily restricted to a subset of immune cells known as professional antigen presenting cells (APCs) such as dendritic cells, macrophages, and B cells.<sup>4</sup> Additionally, MHC-II presents peptides to a distinct type of T cells known as CD4+ T cells.<sup>20</sup> CD4+ T cells recognize antigens presented on MHC-II through their TCRs, but unlike CD8+ T cells, their activation typically does not result in a cytotoxic response. Instead, antigen recognition by CD4+ T cells promotes their differentiation into T helper (Th) cells.<sup>21</sup> These T helper cell cells are critical in supporting the immune response by secreting cytokines that enhance CTL activity.<sup>22</sup>

MHC-II also differs from MHC-I in the source of peptides it presents, and the mechanism by which the peptides are loaded. Instead of primarily presenting intracellularly derived peptides, APCs mainly acquire extracellular material through various processes such as micropinocytosis, phagocytosis, and endocytosis, as well as some cytosolic material through autophagy.<sup>4</sup> Once trapped in an early endosome, captured proteins can be processed either in lysosomes or in late endosomes/MHC class II-enriched compartment (MIIC). From here, endosomal proteases, such as the various types of cathepsins, degrade endosomal trapped proteins. Importantly, if the protein being processed contains disulfide bonds, they can be reduced in the lysosome by gamma-interferon-inducible lysosomal thiol reductase (GILT).<sup>23</sup> Additionally, before MHC-II is loaded with new peptide it is first bound to the class II-associated invariant chain peptide (CLIP).<sup>24</sup> CLIP can be released by the glycoprotein DM to allow for endosomal trapped peptide to bind to MHC-II.<sup>25, 26</sup> Once loaded, the pMHC-II complex is transported from the endosome to the cell surface. The exact mechanisms of this transport are not well understood and may vary

among different types of APC.<sup>27, 28</sup> However, once on the cell surface, the pMHC-II complex is displayed for recognition by CD4+ T cells (Figure 1.2).

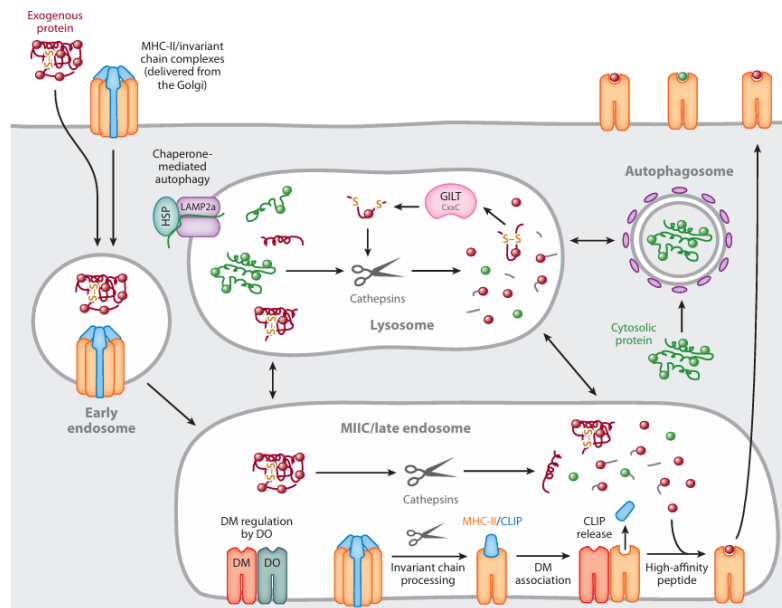


**Figure 1.2** MHC-II antigen presentation pathway

*Adapted from<sup>4</sup>.*

### 1.3 T Cell Response to MHC

As mentioned previously, the different classes of MHC present peptides to distinct T cell populations that have distinctive functions. In the case of MHC-I, the pMHC complex is presented to TCRs on CD8+ T cells that initiate a cytotoxic immune response. The TCR is composed of an  $\alpha$  and  $\beta$  chain, each containing both a variable and a constant domain.<sup>29</sup> The variable domains are responsible for recognizing the specific pMHC-I it has been trained to detect. The constant domain consists of a transmembrane domain that anchors the receptor to the cell membrane and interacts with CD3 which is a critical signaling component.<sup>30</sup> A recognition event between the variable domain of the TCR and the pMHC-I recruits the kinase Lck to phosphorylate CD3 and induce a downstream signaling cascade.<sup>31</sup> Critically, the TCR signaling must be accompanied by a co-stimulatory signal to fully activate the CD8+ T cell and enable a cytotoxic response.<sup>32</sup> This typically involves CD28 receptors on CD8+ T cells binding to the co-stimulatory ligand B7.1 or B7.2 on the antigen-presenting cell. Once fully active, CD8+ T cells secrete the

pore forming protein, perforin, along with various granzyme proteases that trigger apoptosis in the target cell.<sup>33</sup>

In addition to positive modulators of TCR activation, CD8+ T cells also express negative modulators of activation known as immune checkpoints. The most studied immune checkpoints are programmed cell death receptor 1 (PD-1) along with cytotoxic T-lymphocyte associated protein 4 (CTLA-4).<sup>34-36</sup> This family of proteins is responsible for binding to their respective ligands on other endogenous cells to ensure that T cell activation does not become uncontrolled.<sup>37</sup> Immune checkpoints also are known markers of T cell exhaustion in which the CD8+ T cells have reduced cytotoxic capabilities.<sup>38</sup>

In the case of MHC-II, peptides presented on MHC-II are recognized by CD4+ T cells which then differentiate into various subsets types of Th cells.<sup>39</sup> Upon antigen recognition, CD4+ T cells differentiate into T helper 1 (Th1), T helper 2 (Th2), T helper 17 (Th17), follicular helper T cells (Tfh), or regulatory T cells (Tregs).<sup>40</sup> Each of these subsets have specialized roles in immunity, including responses to intracellular pathogens, extracellular bacteria, allergies, and immune regulation.<sup>41</sup> The differentiation of CD4+ T cells into these subsets depends on the type of APC presenting the antigen, as well as the cytokine environment during activation.<sup>42</sup>

Th1 cells and Tregs play the most significant roles in terms of modulating CD8+ T cell activity. Th1 cells primarily secrete the pro-inflammatory cytokines interferon-gamma (IFN $\gamma$ ) and interleukin-2 (IL-2) which enhance CD8+ T cell response. IFN $\gamma$  promotes the activation and expansion of CD8+ T cells while IL-2 helps promote the differentiation of CD8+ T cells into memory T cells ensuring a durable immune response.<sup>42</sup> However, Tregs play an important role in preventing overactive immune responses. Tregs achieve this through the secretion of anti-inflammatory cytokines such as IL-10, IL-35, and transforming growth factor-beta (TGF- $\beta$ ). These cytokines suppress CD8+ T cell response to prevent autoimmunity or excessive inflammation.<sup>43</sup>

#### 1.4 Neoantigen Presentation in Cancer

The biological function of antigen presentation through MHC has traditionally been recognized for its role in combating infectious diseases. However, there is growing

interest in leveraging antigen presentation via MHC for cancer treatment. Typically, T cells undergo negative selection in the thymus which removes CTLs that recognize endogenous peptides to prevent autoimmunity.<sup>44</sup> However, in cancer, alterations in the proteome of tumor cells can generate novel peptide sequences not found in healthy cells. Therefore, these new peptides, or neoantigens, are not subject to negative selection and can be recognized by the immune system enabling a cancer-specific response. Many neoantigens result from DNA mutations which are a hallmark of cancer development.<sup>45</sup> Additionally, neoantigens can also arise from aberrant post-translational modifications (PTMs), dysregulated RNA splicing, integrated viral DNA, and a variety of other mechanism.<sup>9</sup>

Neoantigens are unique in that their expression is restricted to cancer cells.<sup>46</sup> In contrast, most targeted therapeutics for cancer therapy obtain their specificity to cancer by targeting biomarkers that are highly abundant on cancer, but are also present in low levels on other tissue types. This can lead to significant on-target off-tumor toxicity issues. Therefore, extensive work has been done to create therapeutics to target neoantigens presented on MHC-I through interventions such as vaccination,<sup>47, 48</sup> adoptive T cell therapy,<sup>49, 50</sup> and TCR-mimic antibodies.<sup>51</sup> These treatments work by either directly engaging and eliminating cells presenting neoantigens in the context of MHC-I, or by training the immune system to recognize and eliminate cells presenting specific neoantigens.

However, targeting cancer cells through neoantigen presentation presents several challenges. While tumors with a high mutational burden are more likely to display neoantigens, their heterogenous neoantigen expression within the tumor can impede complete eradication resulting in the development of resistance.<sup>52</sup> Additionally, variability in neoantigen expression between patients complicates the development of universal “off-the-shelf” therapies.<sup>53</sup> Personalized vaccines containing patient-specific neoantigens may improve treatment outcomes in such cases.<sup>54</sup> Conversely, tumors with a low mutational burden present fewer neoantigens, further restricting therapeutic options and necessitating alternative approaches.<sup>55</sup> When targeting conserved neoantigens is unfeasible, alternative strategies to enhance neoantigen presentation may be beneficial.

Recent advances in this area include utilizing delivery platforms such as engineered bacteria<sup>56</sup> and peptides<sup>57</sup>, which facilitated neoantigen transport to cancer cells and improve their display on MHC molecules for immune-mediated clearance.

### 1.5 Cancer Immune Evasion Mechanisms

Due to the selective pressure exerted by the immune system onto cancer cells, cancer often evolves sophisticated mechanisms to avoid immune-mediated clearance. Many of these strategies involve avoiding recognition, interfering with immune signaling pathways, or blocking cytotoxic activity of immune cells.<sup>58</sup> One prominent mechanism to inhibit activity of cytotoxic T cells is through upregulation of immune checkpoints such as protein death ligand-1 (PD-L1). PD-L1 is the protein ligand of PD-1 on CTLs which plays an important negative feedback role to prevent autoimmunity.<sup>59</sup> However, increased expression of PD-L1 in cancer can prevent T cells from eliminating the tumor and can even contribute to T cell exhaustion.<sup>60</sup> To circumvent this immune evasion mechanism, antibodies blocking the PD-L1/PD-1 interactions have shown impressive clinical efficacy (Figure 1.3).<sup>61</sup>

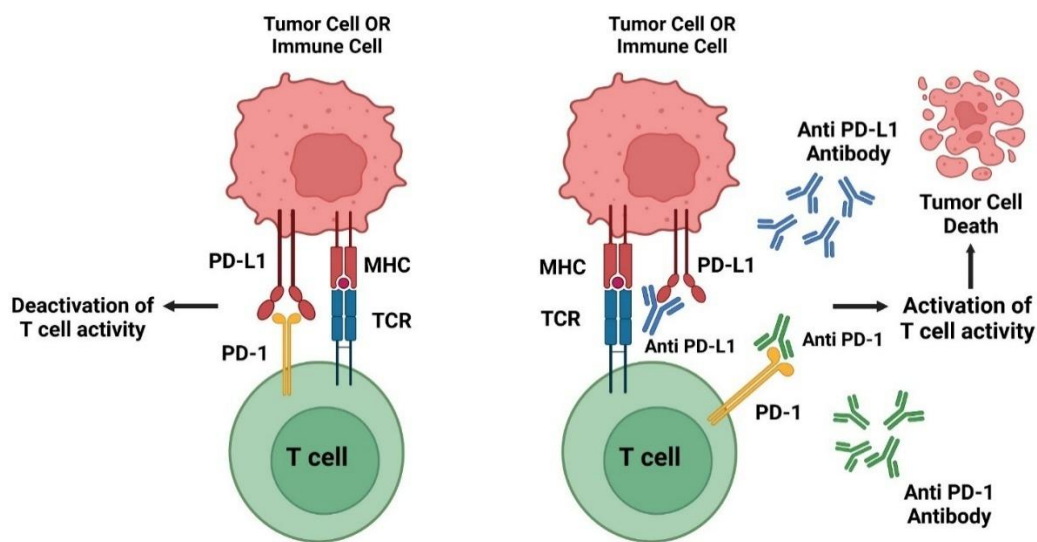


**Figure 1.3** Immune checkpoint inhibition

*Adapted from*<sup>62</sup>.

Another mechanism by which the immune system avoids detection is through the downregulation of MHC-I. Downregulation of MHC-I has been seen in multiple tumor types including colorectal, melanoma, and cervical cancers and can be caused through

a variety of mechanisms such as genetic mutations, transcriptional downregulation, and altering signaling pathways.<sup>63</sup> Importantly, disruptions in MHC-I surface expression is reported to be a prominent resistance mechanisms in response to PD-1 blockade therapy.<sup>46</sup> In response to this, screening efforts to enhance the expression of MHC-I in cancer cells are being used to identify potential clinical candidates to improve immunotherapy treatments.<sup>64-66</sup>

## 1.6 Summary and Future Outlook

Chapter 1 explores the biological role of antigen presentation through MHC-I and MHC-II in response to infectious disease and cancer. MHC-I presentation enables the immune system to detect intracellular antigens, including viral peptides and tumor-associated neoantigens, allowing for the elimination of unhealthy or infected cells. In contrast, MHC-II antigen presentation plays a crucial role in initiating and regulating adaptive immune responses by displaying extracellular antigens to CD4+ T cells. Enhancing these processes has shown great promise in advancing cancer treatment options. The presence of cancer-specific neoantigens on MHC molecules provides a unique therapeutic opportunity, as these antigens are absent on healthy cells and selectively recognized by immune cells. This combination allows for the targeted elimination of cancer cells while minimizing off-target toxicity.

A comprehensive understanding of the biological pathways governing antigen processing and presentation, as well as T cell response to pMHC complexes, is essential for improving immunotherapy strategies. These efforts have driven major advances in checkpoint blockade, adoptive T cell therapy, and cancer vaccine development. However, key challenges remain, including the identification of patient-specific neoantigens. Additionally, understanding the molecular mechanisms driving the presentation of different neoantigens would provide an avenue into developing more effective therapeutics. Addressing these obstacles requires a deeper understanding of the factors that drive neoantigen presentation on MHC and improved methods for neoantigen detection.

## 1.7 References

1. Gorer, P. A. (1936) The detection of antigenic differences in mouse erythrocytes by the employment of immune sera., *Brit J Exp Pathol* 17, 42-50.
2. Neefjes, J., Jongstra, M. L., Paul, P., and Bakke, O. (2011) Towards a systems understanding of MHC class I and MHC class II antigen presentation, *Nat Rev Immunol* 11, 823-836.
3. Rock, K. L., Reits, E., and Neefjes, J. (2016) Present Yourself! By MHC Class I and MHC Class II Molecules, *Trends Immunol* 37, 724-737.
4. Blum, J. S., Wearsch, P. A., and Cresswell, P. (2013) Pathways of antigen processing, *Annu Rev Immunol* 31, 443-473.
5. Hulpke, S., and Tampe, R. (2013) The MHC I loading complex: a multitasking machinery in adaptive immunity, *Trends Biochem Sci* 38, 412-420.
6. Koh, C. H., Lee, S., Kwak, M., Kim, B. S., and Chung, Y. (2023) CD8 T-cell subsets: heterogeneity, functions, and therapeutic potential, *Exp Mol Med* 55, 2287-2299.
7. Pishesha, N., Harmand, T. J., and Ploegh, H. L. (2022) A guide to antigen processing and presentation, *Nat Rev Immunol* 22, 751-764.
8. Pfeifer, J. D., Wick, M. J., Roberts, R. L., Findlay, K., Normark, S. J., and Harding, C. V. (1993) Phagocytic processing of bacterial antigens for class I MHC presentation to T cells, *Nature* 361, 359-362.
9. Xie, N., Shen, G., Gao, W., Huang, Z., Huang, C., and Fu, L. (2023) Neoantigens: promising targets for cancer therapy, *Signal Transduct Target Ther* 8, 9.
10. Fernando, M. M., Stevens, C. R., Walsh, E. C., De Jager, P. L., Goyette, P., Plenge, R. M., Vyse, T. J., and Rioux, J. D. (2008) Defining the role of the MHC in autoimmunity: a review and pooled analysis, *PLoS Genet* 4, e1000024.
11. Stopfer, L. E., D'Souza, A. D., and White, F. M. (2021) 1,2,3, MHC: a review of mass-spectrometry-based immunopeptidomics methods for relative and absolute quantification of pMHCs, *Immuno-oncol Technol* 11, 100042.
12. Arrieta-Bolanos, E., Hernandez-Zaragoza, D. I., and Barquera, R. (2023) An HLA map of the world: A comparison of HLA frequencies in 200 worldwide populations reveals diverse patterns for class I and class II, *Front Genet* 14, 866407.

13. Liepe, J., Marino, F., Sidney, J., Jeko, A., Bunting, D. E., Sette, A., Kloetzel, P. M., Stumpf, M. P., Heck, A. J., and Mishto, M. (2016) A large fraction of HLA class I ligands are proteasome-generated spliced peptides, *Science* 354, 354-358.
14. Yewdell, J. W., Anton, L. C., and Bennink, J. R. (1996) Defective ribosomal products (DRiPs): a major source of antigenic peptides for MHC class I molecules?, *J Immunol* 157, 1823-1826.
15. Spies, T., and DeMars, R. (1991) Restored expression of major histocompatibility class I molecules by gene transfer of a putative peptide transporter, *Nature* 351, 323-324.
16. Saveanu, L., Carroll, O., Lindo, V., Del Val, M., Lopez, D., Lepelletier, Y., Greer, F., Schomburg, L., Fruci, D., Niedermann, G., and van Endert, P. M. (2005) Concerted peptide trimming by human ERAP1 and ERAP2 aminopeptidase complexes in the endoplasmic reticulum, *Nat Immunol* 6, 689-697.
17. Sadasivan, B., Lehner, P. J., Ortmann, B., Spies, T., and Cresswell, P. (1996) Roles for calreticulin and a novel glycoprotein, tapasin, in the interaction of MHC class I molecules with TAP, *Immunity* 5, 103-114.
18. Koopmann, J. O., Albring, J., Huter, E., Bulbuc, N., Spee, P., Neefjes, J., Hammerling, G. J., and Momburg, F. (2000) Export of antigenic peptides from the endoplasmic reticulum intersects with retrograde protein translocation through the Sec61p channel, *Immunity* 13, 117-127.
19. Vyas, J. M., Van der Veen, A. G., and Ploegh, H. L. (2008) The known unknowns of antigen processing and presentation, *Nat Rev Immunol* 8, 607-618.
20. Bawden, E., and Gebhardt, T. (2023) The multifaceted roles of CD4(+) T cells and MHC class II in cancer surveillance, *Curr Opin Immunol* 83, 102345.
21. Bevan, M. J. (2004) Helping the CD8(+) T-cell response, *Nat Rev Immunol* 4, 595-602.
22. Topchyan, P., Lin, S., and Cui, W. (2023) The Role of CD4 T Cell Help in CD8 T Cell Differentiation and Function During Chronic Infection and Cancer, *Immune Netw* 23, e41.

23. Arunachalam, B., Phan, U. T., Geuze, H. J., and Cresswell, P. (2000) Enzymatic reduction of disulfide bonds in lysosomes: characterization of a gamma-interferon-inducible lysosomal thiol reductase (GILT), *Proc Natl Acad Sci U S A* 97, 745-750.
24. Riberdy, J. M., Newcomb, J. R., Surman, M. J., Barbosa, J. A., and Cresswell, P. (1992) HLA-DR molecules from an antigen-processing mutant cell line are associated with invariant chain peptides, *Nature* 360, 474-477.
25. Sherman, M. A., Weber, D. A., and Jensen, P. E. (1995) DM enhances peptide binding to class II MHC by release of invariant chain-derived peptide, *Immunity* 3, 197-205.
26. Fung-Leung, W. P., Surh, C. D., Liljedahl, M., Pang, J., Leturcq, D., Peterson, P. A., Webb, S. R., and Karlsson, L. (1996) Antigen presentation and T cell development in H2-M-deficient mice, *Science* 271, 1278-1281.
27. Vascotto, F., Lankar, D., Faure-Andre, G., Vargas, P., Diaz, J., Le Roux, D., Yuseff, M. I., Sibarita, J. B., Boes, M., Raposo, G., Mougneau, E., Glaichenhaus, N., Bonnerot, C., Manoury, B., and Lennon-Dumenil, A. M. (2007) The actin-based motor protein myosin II regulates MHC class II trafficking and BCR-driven antigen presentation, *J Cell Biol* 176, 1007-1019.
28. van Niel, G., Wubbolts, R., Ten Broeke, T., Buschow, S. I., Ossendorp, F. A., Melief, C. J., Raposo, G., van Balkom, B. W., and Stoorvogel, W. (2006) Dendritic cells regulate exposure of MHC class II at their plasma membrane by oligoubiquitination, *Immunity* 25, 885-894.
29. Raskov, H., Orhan, A., Christensen, J. P., and Gogenur, I. (2021) Cytotoxic CD8(+) T cells in cancer and cancer immunotherapy, *Br J Cancer* 124, 359-367.
30. Bettini, M. L., Guy, C., Dash, P., Vignali, K. M., Hamm, D. E., Dobbins, J., Gagnon, E., Thomas, P. G., Wucherpfennig, K. W., and Vignali, D. A. (2014) Membrane association of the CD3epsilon signaling domain is required for optimal T cell development and function, *J Immunol* 193, 258-267.
31. Weiss, A., and Littman, D. R. (1994) Signal transduction by lymphocyte antigen receptors, *Cell* 76, 263-274.
32. Zumerle, S., Molon, B., and Viola, A. (2017) Membrane Rafts in T Cell Activation: A Spotlight on CD28 Costimulation, *Front Immunol* 8, 1467.

33. Gordy, C., and He, Y. W. (2012) Endocytosis by target cells: an essential means for perforin- and granzyme-mediated killing, *Cell Mol Immunol* 9, 5-6.
34. Nishimura, H., Minato, N., Nakano, T., and Honjo, T. (1998) Immunological studies on PD-1 deficient mice: implication of PD-1 as a negative regulator for B cell responses, *Int Immunol* 10, 1563-1572.
35. Nishimura, H., Nose, M., Hiai, H., Minato, N., and Honjo, T. (1999) Development of lupus-like autoimmune diseases by disruption of the PD-1 gene encoding an ITIM motif-carrying immunoreceptor, *Immunity* 11, 141-151.
36. Krummel, M. F., and Allison, J. P. (1995) CD28 and CTLA-4 have opposing effects on the response of T cells to stimulation, *J Exp Med* 182, 459-465.
37. Wang, J., Yuan, R., Song, W., Sun, J., Liu, D., and Li, Z. (2017) PD-1, PD-L1 (B7-H1) and Tumor-Site Immune Modulation Therapy: The Historical Perspective, *J Hematol Oncol* 10, 34.
38. Thommen, D. S., and Schumacher, T. N. (2018) T Cell Dysfunction in Cancer, *Cancer Cell* 33, 547-562.
39. Luckheeram, R. V., Zhou, R., Verma, A. D., and Xia, B. (2012) CD4(+)T cells: differentiation and functions, *Clin Dev Immunol* 2012, 925135.
40. Kan, A. K. C., Tang, W. T., and Li, P. H. (2024) Helper T cell subsets: Development, function and clinical role in hypersensitivity reactions in the modern perspective, *Heliyon* 10, e30553.
41. Zhu, J. (2018) T Helper Cell Differentiation, Heterogeneity, and Plasticity, *Cold Spring Harb Perspect Biol* 10.
42. Schmitt, N., and Ueno, H. (2015) Regulation of human helper T cell subset differentiation by cytokines, *Curr Opin Immunol* 34, 130-136.
43. Sumida, T. S., Cheru, N. T., and Hafler, D. A. (2024) The regulation and differentiation of regulatory T cells and their dysfunction in autoimmune diseases, *Nat Rev Immunol* 24, 503-517.
44. Palmer, E. (2003) Negative selection--clearing out the bad apples from the T-cell repertoire, *Nat Rev Immunol* 3, 383-391.

45. Borden, E. S., Buetow, K. H., Wilson, M. A., and Hastings, K. T. (2022) Cancer Neoantigens: Challenges and Future Directions for Prediction, Prioritization, and Validation, *Front Oncol* 12, 836821.
46. Zaretsky, J. M., Garcia-Diaz, A., Shin, D. S., Escuin-Ordinas, H., Hugo, W., Hu-Lieskovan, S., Torrejon, D. Y., Abril-Rodriguez, G., Sandoval, S., Barthly, L., Saco, J., Homet Moreno, B., Mezzadra, R., Chmielowski, B., Ruchalski, K., Shintaku, I. P., Sanchez, P. J., Puig-Saus, C., Cherry, G., Seja, E., Kong, X., Pang, J., Berent-Maoz, B., Comin-Anduix, B., Graeber, T. G., Tumei, P. C., Schumacher, T. N., Lo, R. S., and Ribas, A. (2016) Mutations Associated with Acquired Resistance to PD-1 Blockade in Melanoma, *N Engl J Med* 375, 819-829.
47. Ye, L., Creaney, J., Redwood, A., and Robinson, B. (2021) The Current Lung Cancer Neoantigen Landscape and Implications for Therapy, *J Thorac Oncol* 16, 922-932.
48. Sahin, U., Derhovanessian, E., Miller, M., Kloke, B. P., Simon, P., Lower, M., Bukur, V., Tadmor, A. D., Luxemburger, U., Schrors, B., Omokoko, T., Vormehr, M., Albrecht, C., Paruzynski, A., Kuhn, A. N., Buck, J., Heesch, S., Schreeb, K. H., Muller, F., Ortseifer, I., Vogler, I., Godehardt, E., Attig, S., Rae, R., Breitkreuz, A., Tolliver, C., Suchan, M., Martic, G., Hohberger, A., Sorn, P., Diekmann, J., Ciesla, J., Waksman, O., Bruck, A. K., Witt, M., Zillgen, M., Rothermel, A., Kasemann, B., Langer, D., Bolte, S., Diken, M., Kreiter, S., Nemecek, R., Gebhardt, C., Grabbe, S., Holler, C., Utikal, J., Huber, C., Loquai, C., and Tureci, O. (2017) Personalized RNA mutanome vaccines mobilize poly-specific therapeutic immunity against cancer, *Nature* 547, 222-226.
49. Xie, G., Ivica, N. A., Jia, B., Li, Y., Dong, H., Liang, Y., Brown, D., Romee, R., and Chen, J. (2021) CAR-T cells targeting a nucleophosmin neopeptide exhibit potent specific activity in mouse models of acute myeloid leukaemia, *Nat Biomed Eng* 5, 399-413.
50. Anderson, K. G., Voillet, V., Bates, B. M., Chiu, E. Y., Burnett, M. G., Garcia, N. M., Oda, S. K., Morse, C. B., Stromnes, I. M., Drescher, C. W., Gottardo, R., and Greenberg, P. D. (2019) Engineered Adoptive T-cell Therapy Prolongs Survival in a Preclinical Model of Advanced-Stage Ovarian Cancer, *Cancer Immunol Res* 7, 1412-1425.

51. Hsiue, E. H., Wright, K. M., Douglass, J., Hwang, M. S., Mog, B. J., Pearlman, A. H., Paul, S., DiNapoli, S. R., Konig, M. F., Wang, Q., Schaefer, A., Miller, M. S., Skora, A. D., Azurmendi, P. A., Murphy, M. B., Liu, Q., Watson, E., Li, Y., Pardoll, D. M., Bettgowda, C., Papadopoulos, N., Kinzler, K. W., Vogelstein, B., Gabelli, S. B., and Zhou, S. (2021) Targeting a neoantigen derived from a common TP53 mutation, *Science* 371.
52. Roerden, M., Castro, A. B., Cui, Y., Harake, N., Kim, B., Dye, J., Maiorino, L., White, F. M., Irvine, D. J., Litchfield, K., and Spranger, S. (2024) Neoantigen architectures define immunogenicity and drive immune evasion of tumors with heterogenous neoantigen expression, *J Immunother Cancer* 12.
53. Chen, I., Chen, M. Y., Goedegebuure, S. P., and Gillanders, W. E. (2021) Challenges targeting cancer neoantigens in 2021: a systematic literature review, *Expert Rev Vaccines* 20, 827-837.
54. Blass, E., and Ott, P. A. (2021) Advances in the development of personalized neoantigen-based therapeutic cancer vaccines, *Nat Rev Clin Oncol* 18, 215-229.
55. Budczies, J., Kazdal, D., Menzel, M., Beck, S., Kluck, K., Altburger, C., Schwab, C., Allgauer, M., Ahadova, A., Kloor, M., Schirmacher, P., Peters, S., Kramer, A., Christopoulos, P., and Stenzinger, A. (2024) Tumour mutational burden: clinical utility, challenges and emerging improvements, *Nat Rev Clin Oncol* 21, 725-742.
56. Redenti, A., Im, J., Redenti, B., Li, F., Rouanne, M., Sheng, Z., Sun, W., Gurbatri, C. R., Huang, S., Komaranchath, M., Jang, Y., Hahn, J., Ballister, E. R., Vincent, R. L., Vardoshivilli, A., Danino, T., and Arpaia, N. (2024) Probiotic neoantigen delivery vectors for precision cancer immunotherapy, *Nature* 635, 453-461.
57. Yurkevicz, A. M., Liu, Y., Katz, S. G., and Glazer, P. M. (2025) Tumor-Specific Antigen Delivery for T-cell Therapy via a pH-Sensitive Peptide Conjugate, *Mol Cancer Ther* 24, 105-117.
58. Galassi, C., Chan, T. A., Vitale, I., and Galluzzi, L. (2024) The hallmarks of cancer immune evasion, *Cancer Cell* 42, 1825-1863.
59. Tang, Q., Chen, Y., Li, X., Long, S., Shi, Y., Yu, Y., Wu, W., Han, L., and Wang, S. (2022) The role of PD-1/PD-L1 and application of immune-checkpoint inhibitors in human cancers, *Front Immunol* 13, 964442.

60. Baessler, A., and Vignali, D. A. A. (2024) T Cell Exhaustion, *Annu Rev Immunol* 42, 179-206.
61. Liu, J., Chen, Z., Li, Y., Zhao, W., Wu, J., and Zhang, Z. (2021) PD-1/PD-L1 Checkpoint Inhibitors in Tumor Immunotherapy, *Front Pharmacol* 12, 731798.
62. Parvez, A., Choudhary, F., Mudgal, P., Khan, R., Qureshi, K. A., Farooqi, H., and Aspatwar, A. (2023) PD-1 and PD-L1: architects of immune symphony and immunotherapy breakthroughs in cancer treatment, *Front Immunol* 14, 1296341.
63. Taylor, B. C., and Balko, J. M. (2022) Mechanisms of MHC-I Downregulation and Role in Immunotherapy Response, *Front Immunol* 13, 844866.
64. Dong, H., Wen, C., He, L., Zhang, J., Xiang, N., Liang, L., Hu, L., Li, W., Liu, J., Shi, M., Hu, Y., Chen, S., Liu, H., and Yang, X. (2024) Nilotinib boosts the efficacy of anti-PDL1 therapy in colorectal cancer by restoring the expression of MHC-I, *J Transl Med* 22, 769.
65. Yu, Q., Dong, Y., Wang, X., Su, C., Zhang, R., Xu, W., Jiang, S., Dang, Y., and Jiang, W. (2024) Pharmacological induction of MHC-I expression in tumor cells revitalizes T cell antitumor immunity, *JCI Insight* 9.
66. Tripathi, C., Tovar Perez, J. E., Kapoor, S., Muhsin, A., Dashwood, W. M., Demirhan, Y., Demirhan, M., Shapiro, A., Mohammed, A., Sei, S., Thompson, J., Zaheer, M., Sinha, K. M., Brown, P. H., Savage, M. I., Vilar, E., Rajendran, P., and Dashwood, R. H. (2025) Antitumor efficacy of intermittent low-dose erlotinib plus sulindac via MHC upregulation and remodeling of the immune cell niche, *Int J Cancer*.

## **Chapter 2 Post-Translationally Modified Peptide Display on MHC**

### *2.1 Identification of MHC-Associated Peptides*

A significant challenge in creating MHC-I targeting therapeutics is identifying which peptides are presented by cancer cells. Most efforts to characterize the cancer immunopeptidome utilized mass spectrometry (MS)-based techniques.<sup>1</sup> This approach involves isolating peptides bound to MHC-I molecules, followed by the identification of their sequence using liquid chromatograph coupled with tandem mass-spectrometry (LC-MS/MS). Advances in MS-based techniques have further enhanced the sensitivity and specificity of immunopeptidome mapping. LC-MS/MS remains a powerful tool and have been used to identify tumor-associated peptides in cancers such as melanoma<sup>2</sup>, colorectal cancer<sup>3</sup>, breast<sup>4</sup>, lung<sup>5</sup>, and others<sup>6-9</sup>. Furthermore, MS-based approaches have provided insights into peptide properties that enhance binding to specific MHC-I allotypes, informing the development of more effective immunotherapies.

Two main approaches are used to isolate the immunopeptidome for analysis via LC-MS/MS. The first approach, known as mild acid elution (MAE), involves briefly incubating cells with a citric acid buffer at pH 3. This treatment causes the dissociation of the  $\beta$ 2-microglobulin subunit from MHC-I molecules, leading to the release of bound peptides while minimizing effects on cell viability.<sup>10, 11</sup> Using this method, Rammensee et al. were the first to identify virus-derived peptide sequences that were displayed on MHC-I validating this approach.<sup>12</sup> MAE still remains as a commonly used method to map out the immunopeptidome of various cell types.

The other approach involves isolating and purifying pMHC complexes through immunoprecipitation and was first developed by Hunt et al.<sup>13</sup> In this method, cells are lysed, and pMHC complexes are captured using antibodies (typically using the W6/32 clone) that recognizes MHC-I heavy chains.<sup>14</sup> Both immunoprecipitation and MAE approaches yield reproducible and comparable results (Figure 2.1). However, immunoprecipitation is generally preferred as it has been shown to recover higher yields of peptide.<sup>15</sup> Additionally, immunoprecipitation is compatible with frozen tissues whereas MAE is not.<sup>11</sup> This is especially advantageous in a clinical setting in which patient-derived

tumor samples are often stored as frozen tissue. One drawback of this approach is that immunoprecipitation is primarily limited to human cells as effective antibodies for enriching MHC molecules from other species are limited.<sup>16</sup>

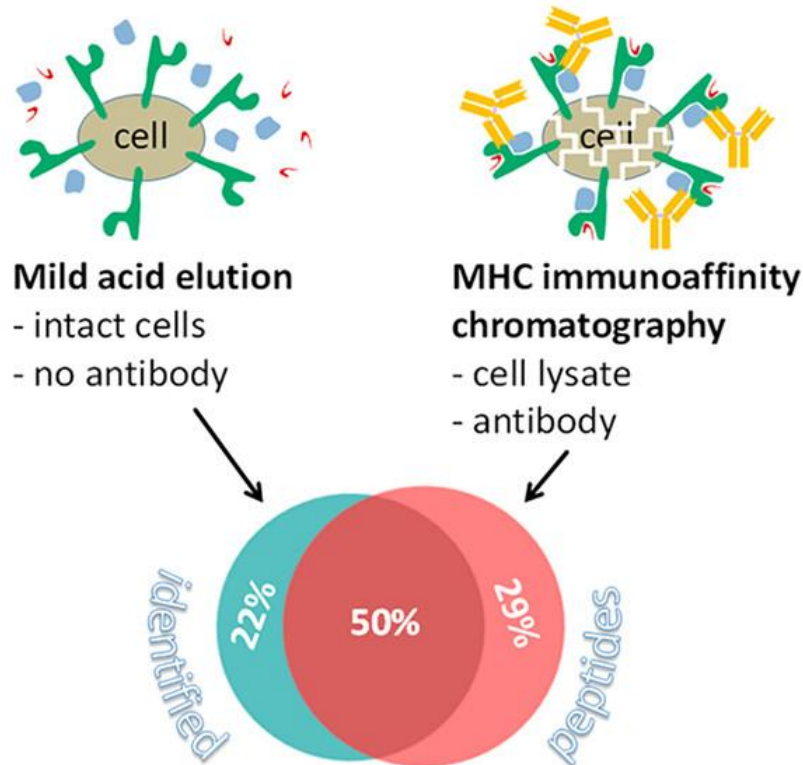


**Figure 2.1** Schematic of mild acid elution and immunoaffinity chromatography for isolation of MHC-associated peptides. Reproduced from<sup>17</sup>.

In addition to LC-MS/MS, DNA and RNA sequencing are also valuable tools for identifying potential neoantigens. Tumors exhibit varying degrees of mutational burden, which can give rise to neoantigens. The advantage of identifying neoantigens through genetic sequencing is that the peptides identified will be tumor specific antigens (TSA) rather than tumor associated antigens (TAA).<sup>18</sup> Unlike TAAs which may also be expressed in healthy tissue, TSAs arise exclusively from tumor-specific mutations, reducing the risk of off-target immune responses. Ideally, neoantigens selected through genetic sequencing will correspond to driver mutations in a specific cancer type, as targeting these mutations reduces the likelihood of immune evasion through loss of neoantigen expression.<sup>19</sup> However, a key limitation of genomic information by itself is that it does not provide

information on whether a mutation is likely to be represented via display on MHC-I. To address this, genomic sequencing information is often combined with computational prediction algorithms to identify neoantigens most likely to have high affinity to specific MHC isoforms.<sup>20</sup> NetMHCpan is one of the most widely used prediction software that uses machine learning to predict peptide affinity to MHC molecules.<sup>21</sup>

## *2.2 Post-Translationally Modified Peptides*

While neoantigens arise from genetic mutations, another important class of TSAs and TAAs includes peptides modified with post-translational modifications (PTMs). These modifications can alter peptide binding to MHC-I, affect immune recognition by CTLs, and influence peptide processing by antigen presentation machinery.<sup>22</sup> Importantly, these modifications expand on the diversity of the immunopeptidome beyond what is predicted by genomic sequencing alone. Additionally, the dysregulation of PTMs is a known hallmark of diseases such as cancer and autoimmunity which results in enhanced presentation of peptides bearing PTMs in these conditions.<sup>23</sup> PTM modified peptides play a crucial role in antigen presentation, as they have been shown to be more efficient in triggering an immune response.<sup>1</sup> This enhanced immunogenicity is likely due to PTM-modified antigens being absent during thymic negative selection thereby allowing PTM-specific T cells to persist in circulation.<sup>24</sup> In support of this, aberrant changes in protein “writers” (enzymes that add modifications) and “erasers” (enzymes that remove modifications) within cancer cells have been shown to generate cancer-specific PTM antigens presented on MHC-I. Identifying these PTM antigens remains a growing area of research to expand the potential pool of TAAs for immunotherapy applications.

One of the key challenges in identifying MHC-associated peptides using MS-based and genomics-based methods is their limited ability to detect PTM modified peptides. A major difficulty arises from the promiscuous binding nature of MHC molecules, where a single isoform can present more than 10,000 distinct peptide sequences.<sup>25</sup> Therefore, identification of MHC-associated peptides require enough sensitivity to distinguish between the different peptide sequences presented. Identification of PTMs can also be challenging if the modified antigen is not abundant. However, even a small number of pMHC complexes can be biologically important as T cells are known to be able to activate

against cells presenting only one pMHC on its surface. Additionally, sample preparation and MS analysis can introduce artificial modifications that do not accurately reflect the native immunopeptidome, further complicating the identification of true PTM-modified peptides.<sup>26</sup> Therefore, it is crucial to distinguish genuine PTMs on MHC-associated peptides from artifacts introduced during sample processing (Figure 2.2). To mitigate these issues and improve detection, enrichment methods can be used to help identify modified peptides.<sup>27</sup>

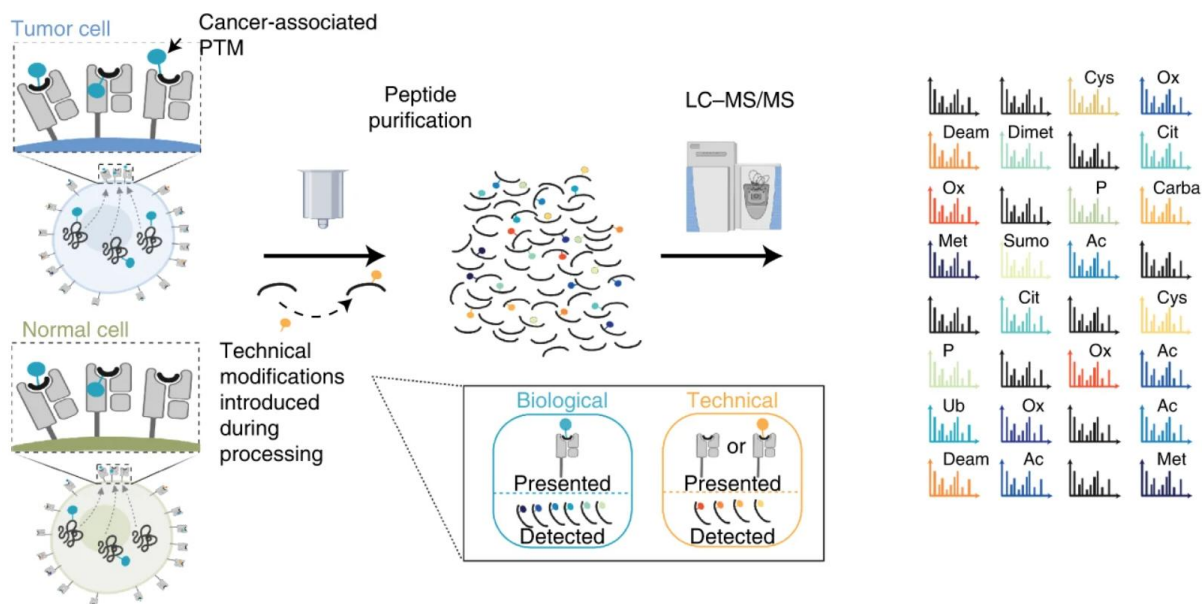


**Figure 2.2** MS-based identification of modified peptides.

*Reproduced from<sup>28</sup>.*

Tandem mass-spectrometry analysis relies on peak annotations matched to known peptide sequences, often obtained from databases. However, incorporating various PTMs significantly expands the search space, making peptide identification more computationally intensive. With approximately 400 known PTMs, including all of them in MS-based searches is currently impractical due to hardware and software limitations, which can contribute to high false discovery rates.<sup>22, 29</sup> To address these technical challenges, researchers have focused on identifying and characterizing some of the most common PTMs to evaluate their impact on the immunopeptidome. These efforts have

started to shed light on the ways that certain PTMs can enhance or alter MHC display and immune recognition of the modified peptides.

## ***2.3 Enzymatic PTMs***

### ***2.3.1 Phosphorylation***

Phosphorylation was one of the first PTMs identified in MHC-associated peptides.<sup>30</sup> A pivot finding regarding phosphorylated MHC-associated peptides was their preferential presentation in melanoma cells and recognition by phosphopeptide-specific CD8+ CTLs.<sup>31</sup> It was demonstrated that phosphopeptide-specific CTLs could distinguish phosphorylated peptides from their non-phosphorylated counterparts and lead to a cancer specific response.<sup>32</sup> The underlying mechanism for this selectivity is that dysregulated kinase signaling cascades in cancer cells led to the generation of phosphorylated peptides that are not present in healthy tissue. This phenomenon was later observed in other cancer types including lung, colorectal, and certain carcinomas.<sup>33</sup> Early clinical trial data further suggested that vaccination with a phosphopeptide epitope provided modest tumor growth control in mice. Additionally, vaccination with phosphorylated neoantigens pIRS2<sub>1097-1105</sub> and pBCAR3<sub>126-134</sub> elicited a T-cell response in 40% of melanoma patients in the study.<sup>34</sup>

Mechanistically, the effects of phosphorylation have been studied on a subset of immunogenic peptides presented for HLA A\*02:01. In one study, the crystal structure of three immunogenic phosphorylated peptides and their unmodified counterparts were solved to assess the impact of phosphorylation on MHC binding. In all cases, the phosphate group was primarily solvent exposed and likely served as a TCR contact site (Figure 2.3). Additionally, two of the three peptides exhibited negligible changes in MHC-I binding affinity, while one of the phosphorylated peptides greatly showed significantly enhanced binding affinity. This indicates that phosphorylation may act as an MHC-I stabilizing modification for certain pMHC complexes potentially increasing their display on cells.<sup>35</sup> Supporting this, another study found that among previously identified phosphopeptide, the majority with phosphorylation at position 4 of the peptide chain exhibited improved binding to HLA-A\*02:01 compared to their unmodified counterparts.<sup>36</sup>

Overall, these studies suggest that phosphorylation plays a role in modulating peptide presentation on MHC and influences CTL recognition.

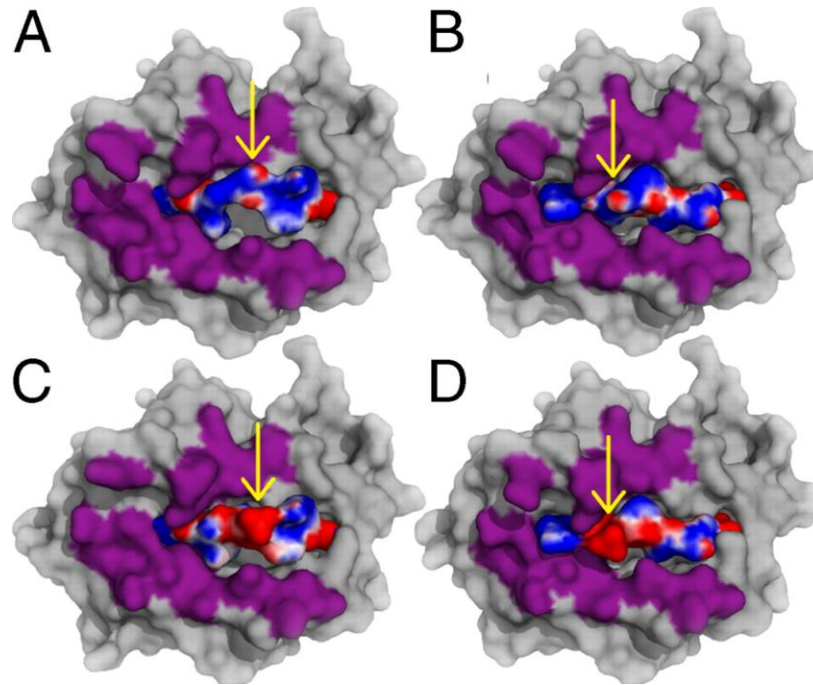


**Figure 2.3** Crystal structure of IRS2 (A) CDC25 (B) IRS2-phospho (C) and CDC25-phospho (D). Arrows indicate peptide phosphorylation site. Electrostatic potential shown in blue (positive) and red (negative). Putative TCR contact sites shown in purple.

Reproduced from<sup>35</sup>.

### 2.3.2 Glycosylation

Glycosylation is one of the most common class of PTMs.<sup>37</sup> Early studies on glycosylation in MHC-associated peptides involved synthesizing glycosylated peptides to assess their effects on MHC binding and the activation of glycosylation-specific CTLs. These studies demonstrated that both N-linked and O-linked glycopeptides could be processed by TAP and that glycosylated MHC-associated peptides could be selectively enriched using lectin affinity columns. Notably, glycosylated peptides were estimated to constitute approximately 1% of the total MHC peptidome.<sup>38</sup> Additionally, peptide bearing extended glycan chains have been shown to be presented in the context of MHC.<sup>39</sup>

It was also demonstrated that O-linked and N-linked glycosylation of a Sendai virus peptide could lead to glycosylation-specific CTL responses.<sup>40</sup> Additionally, an

immunodominant epitope of the lymphocytic choriomeningitis virus (LCMV) was found to contain a glycosylation motif. The glycosylated form of this epitope, along with its unmodified counterpart, exhibited comparable binding affinities to the mouse MHC molecule H-2D<sup>b</sup> but activated distinct CTL populations.<sup>41</sup> This suggests that glycosylation may diversify immune responses to infectious diseases by generating neoepitopes that engage different T cell repertoires. Similar results were also seen for a glycosylated version of an immunodominant peptide in vesicular stomatitis virus,<sup>42</sup> tuberculosis,<sup>43</sup> HIV,<sup>44</sup> and SARS-CoV-2.<sup>45</sup>

In addition to their role in infectious diseases, glycosylated peptides are also presented on HLA molecules. While most N-linked glycosylated peptides are cleaved by peptide: N-glycosidase (PNGase) during antigen processing, O-linked glycosylated peptides have been identified in the context of MHC presentation.<sup>46</sup> One study identified 36 O-GlcNAcetylated peptides, the majority of which were absent in healthy tissue.<sup>47</sup> This suggests that O-linked glycosylation may generate tumor-specific neoantigens with potential implications for cancer immunotherapy. Additionally, a glycosylated neoantigen derived from p53, a tumor suppressor protein commonly mutated in cancer, has been identified in HLA-A\*24:02.<sup>48</sup> The majority of the glycosylated neoantigens identified have their sugar moieties surface-exposed which may influence TCR engagement and immune recognition.<sup>49, 50</sup> Recently, advances in methodologies to analyze previously published MS databanks have further identified an order of magnitude higher number of glycopeptides presented on HLA class II further underscoring their importance in the immunopeptidome.<sup>50</sup>

In many cases, glycosylated MHC-associated peptides also contribute to the progression of autoimmune disease, such as rheumatoid arthritis (RA), through their presentation on MHC-II. While N-linked glycosylation is not typically observed in MHC-I, N-linked glycosylated antigens have been identified in the context of MHC-II. Early studies demonstrated that MHC-II can present peptides with either a single monosaccharide or an extended polysaccharide chain.<sup>51, 52</sup> Subsequent research revealed that that distinct T cell clones reacted differently to the glycosylated and unmodified epitope of type II collagen<sub>260-270</sub>, suggesting that the glycosylated form is more arthritogenic than its

unmodified counterpart.<sup>53, 54</sup> Later, it was discovered that peripheral blood mononuclear cells (PBMCs) from RA patients contained T cells that specifically recognized different glycosylated variants of the type II collagen peptide further supporting a role for glycosylation in driving autoimmune inflammation.<sup>55</sup>

### **2.3.3 Citrullination**

Another PTM commonly implicated in autoimmunity is the conversion of arginine to citrulline by peptidyl arginine deiminase (PAD) enzymes. Citrullination of myelin basic protein (MBP) is a well-established driver of multiple sclerosis (MS), with the extent of citrullination correlating strongly with disease progression.<sup>56</sup> While citrullination does not introduce significant steric changes in a peptide sequence, it alters the charge of the arginine side chain from positively charged to neutral, which can influence antigen processing, MHC binding affinity, and TCR recognition. Studies in an animal model of MS demonstrated that citrullination of the immunodominant T cell epitope from MBP enhanced its immunogenicity.<sup>57</sup> Further research revealed that PBMCs from MS patients differentiated into Th1 CD4+ T cells when stimulated with various citrullinated peptides, suggesting citrullinated MHC-associated peptides play a role in disease progression.<sup>58</sup> Surprisingly, this effect was also identified in healthy individuals indicating that the enhanced presentation of citrullinated epitopes on MHC-II in MS patients may be a key factor in breaking immune tolerance and triggering autoimmunity.<sup>59</sup>

Citrullination also plays a role in RA. Early studies demonstrated that citrullination of vimentin, a prominent joint-derived protein that is often a target of autoreactive antibodies, enhances its binding affinity to HLA-DRB1\*0401 and elicited a citrullination specific CD4+ T cell response.<sup>60</sup> The molecular mechanism underlying this response was later elucidated through the crystal structure of citrullinated vimentin peptide complexed with HLA-DRB1\*0401, revealing that the citrullination improved binding interactions with the MHC-II molecule.<sup>61</sup> Ting et al. further expanded these findings to closely related MHC-II alleles, demonstrating that citrullination at the P4 position generally increases peptide affinity for MHC-II, potentially broadening the pool of self-antigens available for presentation.<sup>62</sup> More recently, a study described how citrullination influences the antigen

presentation pathway in MS by altering the stability of proteins and their degradation patterns leading to the generation of cryptic citrullinated antigens.<sup>63</sup>

### *2.3.4 Other Enzymatic Modifications*

While phosphorylation, glycosylation, and citrullination are among the most thoroughly studied enzymatically induced PTMs, recent advances in computational processing have expanded the scope of identified PTM-modified MHC-associated peptides.<sup>28, 64</sup> Among these newly identified PTMs, methylation and acetylation have emerged as the next most abundant modifications of MHC-associated peptides. Methylation plays a key role in modulating the activity of DNA and RNA binding proteins. One study identified a demethylated arginine peptide derived from heterogenous nuclear ribonucleoprotein (hnRNP) displayed on HLA-B\*3910, though the immunological consequences of this modification were never determined.<sup>65</sup> Methylated arginine peptides were also identified in healthy donors in which T cells reacted specifically to the modified version rather than the unmodified peptide suggesting that the modification may be important for immune recognition.<sup>47</sup> A later report described 149 arginine (di)methylated MHC-associated peptides indicating that methylation may be a more frequent feature of antigen processing than previously appreciated.<sup>66</sup>

N-terminal acetylation is another major class of PTM-modified peptides and has been identified as the most frequently occurring PTMs in cancer cells.<sup>67</sup> This modification is typically catalyzed by a family of N-terminal acetyltransferases, which regulate protein stability and function.<sup>68</sup> The role of N-terminal acetylation in antigen presentation was first recognized in the 1980s, when it was discovered that N-terminal acetylation was required for the activation of T cells against a peptide derived from MBP and potentially contributed to encephalomyelitis.<sup>69</sup> A subsequent crystal structure of the pMHC complex revealed that the N-terminal acetylation enhanced interactions with MHC-I.<sup>70</sup> Further studies confirmed that N-acetylated peptides are naturally presented on MHC-I molecules, with the majority of acetylated peptides displaying improved binding affinity compared to their non-acetylated counterparts.<sup>71</sup>

Additionally, lysine acetylation has been shown to influence the antigen presentation pathway. One study showed that acetylation of a lysine residue at position 120 of p53 led

to the display of an acetylated p53 epitope that could be recognized by specific CD4+ T cell clones. Interestingly, this study also revealed that treatment with a histone deacetylase inhibitor increased the expression of the acetylated protein and lead to enhanced T cell activation.<sup>72</sup> These findings suggest that inhibitors targeting PTM writers or erasers may have potential applications in immunotherapy by modulating antigen presentation and T cell recognition.

## 2.4 Non-enzymatic PTMs

Another major class of modifications found in MHC-associated peptides are non-enzymatic modifications, which can arise under conditions of oxidative stress. These modifications typically occur on cysteine, methionine, tyrosine, tryptophan, and proline residues and can be presented by both MHC class I and MHC class II molecules (Figure 2.4).<sup>28</sup> Unlike enzymatic PTMs, non-enzymatic modifications occur spontaneously, often as a result of inflammation, which generates high concentration of reactive oxygen species (ROS).

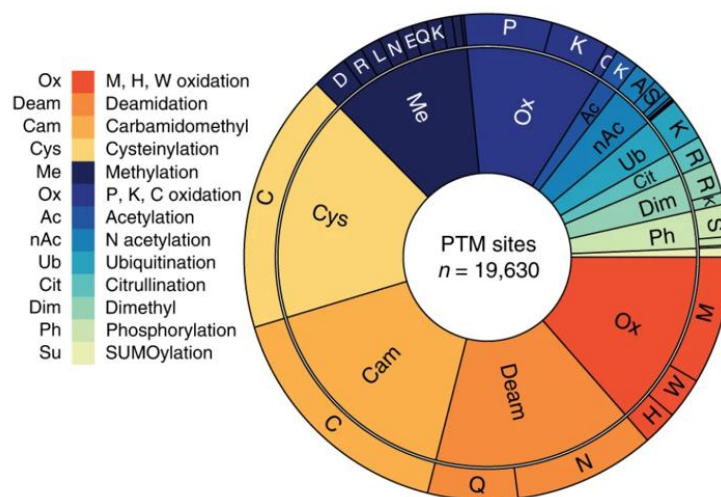


**Figure 2.4** Identified PTMs identified on MHC-associated peptides.

Reproduced from<sup>28</sup>.

### 2.4.1 Cysteinylation

Cysteinylation, the formation of a disulfide bond between a free cysteine residue and another cysteine containing molecule, is one of the most common non-enzymatic PTMs

and has been shown to influence immune recognition when presented on MHC. Although cysteinylolation typically does not occur under the reducing conditions of the cytosol, oxidative stress can alter these conditions, allowing cysteinylolation to take place. Additionally, this modification can occur in more oxidative environments such as the ER or intracellular vesicle before peptide loading onto MHC.

One of the first immunological roles of cysteinylolation of MHC-associated peptides was identified in the context of graft-versus-host disease. The male-specific H-Y antigen was known to contribute to the rejection of male-to-female skin grafts in mice. Researchers discovered that a cysteinylolated version of an H-Y antigen-derived peptide activated a distinct T-cell population, suggesting a role for this PTM in immune recognition.<sup>73, 74</sup> Similarly, another study found that cysteinylolated peptides formed during influenza infection. While cysteinylolation did not affect binding to H-2K<sup>b</sup>, it did result in the induction of cysteinylolation-specific T cells in mice.<sup>75</sup> Cysteinylolation may also be involved in autoimmune disease as it was found that CD4<sup>+</sup> T cells from donors with type 1 diabetes recognized a cysteinylolated insulin peptide, whereas healthy donors did not respond to the modified peptide.<sup>76</sup> This finding suggests that cysteinylolation may contribute to the breakdown of immune tolerance in certain autoimmune conditions.

#### ***2.4.2 Oxidation***

Inflammation and cancer can generate reactive oxygen species (ROS), which may contribute to the presentation of oxidized peptides on MHC. However, a major challenge in studying oxidation's role in antigen presentation is distinguishing between peptides that are naturally oxidized *in vivo* and those that undergo oxidation during sample preparation. Despite this technical limitation, oxidation remains one of the most frequently identified classes of PTMs on MHC-associated peptides.<sup>28, 77</sup> The functional impact of oxidation on antigen presentation, however, remains unclear. As a proof of concept, one study demonstrated that exposing hen egg-white lysozyme (HEL) to nitric oxide enhanced its uptake and processing by antigen presenting cells (APCs) through the oxidation of tyrosine residues.<sup>78</sup> This result suggests that oxidation could play a role in modulating the antigen presentation pathway in ways that are separate from influencing MHC binding or T cell recognition. Similarly, another group found that

nitration of a pollen allergen enhanced the presentation of allergen-associated MHC peptides.<sup>79</sup> However the impact of oxidation on MHC binding and T cell interaction remains largely unexplored.

### *2.5 Hapten Display on MHC*

An emerging class of PTMs on MHC-associated peptides arise from reactions with electrophilic molecules, leading to permanent, covalent modifications of proteins. These modifications have been implicated in both allergic responses and cancer. Their significance was first recognized in the context of drug hypersensitivity, where chemically reactive drugs or their metabolites modify self-proteins and trigger an immune response.<sup>80</sup> One of the primary models proposed to explain how these modifications influence antigen presentation and immune activation is the hapten model. This model suggests that small reactive molecules covalently modify proteins, leading to the generation of altered peptides that can be processed and presented on MHC molecules. Once displayed, these modified peptides can activate T cells, potentially driving immune response against the covalent moiety.<sup>81</sup>

$\beta$ -lactams were among the first identified agents supporting the hapten model, particularly in cases involving piperacillin and benzylpenicillin. The four-member  $\beta$ -lactam ring of penicillin is highly reactive and readily forms covalent bonds with nucleophilic residues in proteins. Notably, treatment with piperacillin or benzylpenicillin modifies human serum albumin (HAS), allowing the altered protein to be processed and presented by APCs, ultimately activating HAS-specific T cell clones.<sup>76, 82</sup> These findings have since been extended to identifying benzylpenicillin and amoxicillin-specific CD4+ T cells in patients with penicillin allergies.<sup>83, 84</sup>

Beyond  $\beta$ -lactams, another drug metabolite known to form haptens that trigger a T cell-specific response is sulfamethoxazole (SMX). Oxidized metabolites of SMX, such as nitroso-sulfamethoxazole (SMX-NO) and sulfamethoxazole hydroxylamine (SMX-NHOH), react with thiol groups in biological systems.<sup>85</sup> Notably, exposure to SMX-NO has been shown to induce SMX-NO-specific T cell activation in lymphocytes from 90% of donors, providing strong evidence of its role in immune response.<sup>86</sup>

More recently, haptens have been explored as a strategy to target cancer-specific covalent modification. The Craik lab ingeniously leveraged sotorasib, a covalent inhibitor of the KRAS G12C mutation, to generate recombinant antibodies and bispecific T cell engagers that selectively recognize and attack cancer cells (Figure 2.5).<sup>87</sup> Building on this approach, they further adapted the technology for use in combination with radiotherapy, enabling the targeted delivery of radioligands to the surface of cancer cells.<sup>88</sup> This work highlights the potential of cancer-specific hapten as a foundation for developing novel immunotherapy strategies.

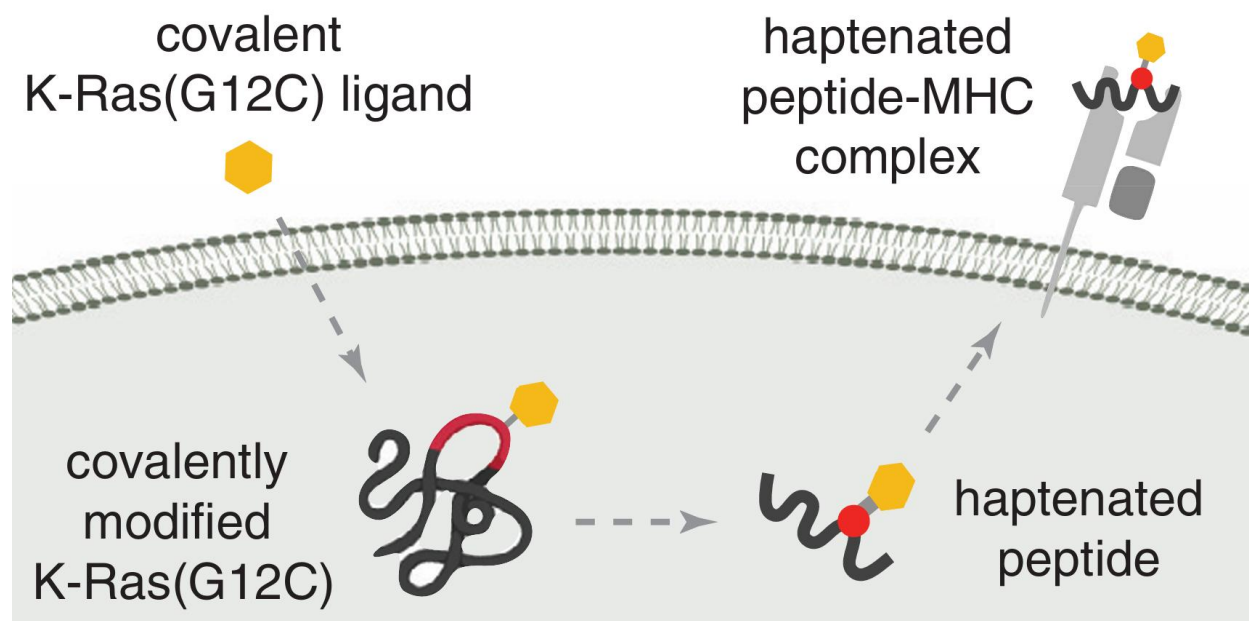


**Figure 2.5** Cancer specific display of hapten ligand derived for sotorasib modified K-Ras(G12C). Reproduced from<sup>87</sup>.

An emerging area of research focuses on identifying metabolites that generate modified peptides displayed on MHC. A recent study investigating PTMs associated with ankylosing spondylitis (AS) uncovered a connection between 3-hydroxypropionate (3-HPA) and neoantigen presentation to CD4<sup>+</sup> T cells. This research demonstrated that 3-HPA, a metabolite produced by commensal gut microbes, induces carboxyethylation of a cysteine residue. This modification resulted in peptide presentation on HLA-DRA\*01, where it was specifically recognized by CD4<sup>+</sup> T cells in patients with AS.<sup>89</sup>

## ***2.6 Summary and Future Outlook***

There are fundamental molecular aspects of cancer and autoimmune disease that remain largely unknown. A prevailing theory centers on the loss of self-tolerance, where the immune system fails to recognize and tolerate self-antigens. This breakdown in self-tolerance can result in the immune system attacking healthy cells. While detrimental in terms of autoimmunity, this response can be beneficial for eliminating cancer.

Identifying MHC-associated peptides with biological responses has been a major step toward understanding these mechanisms. MHC-associated peptides bearing PTMs represent a promising class of biologically active peptides to study due to their immune privilege, as they are often not subject to negative selection during thymic development. Recent advances in mass spectrometry have expanded the known repertoire of PTM-modified MHC-associated peptides. However, most studies investigating their biological impact on antigen presentation have focused on a limited subset of PTMs, such as phosphorylation, glycosylation, and citrullination. The broader influence of PTMs on antigen display and immune recognition remains largely unexplored.

Furthermore, the emerging understanding of how reactive chemical species modulate immune signaling provides insights into the mechanisms underlying autoimmunity and allergic responses. At the same time, this knowledge can also be leveraged to develop novel cancer-specific immunotherapies. To fully realize the therapeutic potential of modified antigens, future research must integrate structural, functional, and immunological studies to systematically define the impact of diverse PTMs on antigen presentation and immune recognition.

## 2.7 References

1. Kote, S., Pirog, A., Bedran, G., Alfaro, J., and Dapic, I. (2020) Mass Spectrometry-Based Identification of MHC-Associated Peptides, *Cancers (Basel)* 12.
2. Bassani-Sternberg, M., Pletscher-Frankild, S., Jensen, L. J., and Mann, M. (2015) Mass spectrometry of human leukocyte antigen class I peptidomes reveals strong effects of protein abundance and turnover on antigen presentation, *Mol Cell Proteomics* 14, 658-673.
3. Kloor, M., Reuschenbach, M., Karbach, J., Rafiyan, M., Al-Batran, S. E., Pauligk, C., Jaeger, E., and Doeberitz, M. V. (2015) Vaccination of MSI-H colorectal cancer patients with frameshift peptide antigens: A phase I/IIa clinical trial., *J Clin Oncol* 33.
4. Sueangoen, N., Thuwajit, P., Yenchitsomanus, P. T., and Thuwajit, C. (2024) Public neoantigens in breast cancer immunotherapy (Review), *Int J Mol Med* 54.
5. Ye, L., Creaney, J., Redwood, A., and Robinson, B. (2021) The Current Lung Cancer Neoantigen Landscape and Implications for Therapy, *J Thorac Oncol* 16, 922-932.
6. Rivero-Hinojosa, S., Grant, M., Panigrahi, A., Zhang, H., Caisova, V., Bollard, C. M., and Rood, B. R. (2021) Proteogenomic discovery of neoantigens facilitates personalized multi-antigen targeted T cell immunotherapy for brain tumors, *Nat Commun* 12, 6689.
7. Toubaji, A., Achar, M., Provenzano, M., Herrin, V. E., Behrens, R., Hamilton, M., Bernstein, S., Venzon, D., Gause, B., Marincola, F., and Khleif, S. N. (2008) Pilot study of mutant ras peptide-based vaccine as an adjuvant treatment in pancreatic and colorectal cancers, *Cancer Immunol Immunother* 57, 1413-1420.
8. Wu, M., and Zhou, S. (2023) Harnessing tumor immunogenomics: Tumor neoantigens in ovarian cancer and beyond, *Biochim Biophys Acta Rev Cancer* 1878, 189017.
9. Subudhi, S. K., Vence, L., Zhao, H., Blando, J., Yadav, S. S., Xiong, Q., Reuben, A., Aparicio, A., Corn, P. G., Chapin, B. F., Pisters, L. L., Troncso, P., Tidwell, R. S., Thall, P., Wu, C. J., Zhang, J., Logothetis, C. L., Futreal, A., Allison, J. P., and Sharma, P. (2020) Neoantigen responses, immune correlates, and favorable outcomes after ipilimumab treatment of patients with prostate cancer, *Sci Transl Med* 12.

10. Sugawara, S., Abo, T., and Kumagai, K. (1987) A simple method to eliminate the antigenicity of surface class I MHC molecules from the membrane of viable cells by acid treatment at pH 3, *J Immunol Methods* 100, 83-90.
11. Bassani-Sternberg, M., Braunlein, E., Klar, R., Engleitner, T., Sinitcyn, P., Audehm, S., Straub, M., Weber, J., Slotta-Huspenina, J., Specht, K., Martignoni, M. E., Werner, A., Hein, R., D, H. B., Peschel, C., Rad, R., Cox, J., Mann, M., and Krackhardt, A. M. (2016) Direct identification of clinically relevant neoepitopes presented on native human melanoma tissue by mass spectrometry, *Nat Commun* 7, 13404.
12. Rotzschke, O., Falk, K., Deres, K., Schild, H., Norda, M., Metzger, J., Jung, G., and Rammensee, H. G. (1990) Isolation and analysis of naturally processed viral peptides as recognized by cytotoxic T cells, *Nature* 348, 252-254.
13. Hunt, D. F., Henderson, R. A., Shabanowitz, J., Sakaguchi, K., Michel, H., Sevilir, N., Cox, A. L., Appella, E., and Engelhard, V. H. (1992) Characterization of peptides bound to the class I MHC molecule HLA-A2.1 by mass spectrometry, *Science* 255, 1261-1263.
14. Kuznetsov, A., Voronina, A., Govorun, V., and Arapidi, G. (2020) Critical Review of Existing MHC I Immunopeptidome Isolation Methods, *Molecules* 25.
15. Lanoix, J., Durette, C., Courcelles, M., Cossette, E., Comtois-Marotte, S., Hardy, M. P., Cote, C., Perreault, C., and Thibault, P. (2018) Comparison of the MHC I Immunopeptidome Repertoire of B-Cell Lymphoblasts Using Two Isolation Methods, *Proteomics* 18, e1700251.
16. Sirois, I., Isabelle, M., Duquette, J. D., Saab, F., and Caron, E. (2021) Immunopeptidomics: Isolation of Mouse and Human MHC Class I- and II-Associated Peptides for Mass Spectrometry Analysis, *J Vis Exp*.
17. Sturm, T., Sautter, B., Worner, T. P., Stevanovic, S., Rammensee, H. G., Planz, O., Heck, A. J. R., and Aebersold, R. (2021) Mild Acid Elution and MHC Immunoaffinity Chromatography Reveal Similar Albeit Not Identical Profiles of the HLA Class I Immunopeptidome, *J Proteome Res* 20, 289-304.
18. Lang, F., Schrors, B., Lower, M., Tureci, O., and Sahin, U. (2022) Identification of neoantigens for individualized therapeutic cancer vaccines, *Nat Rev Drug Discov* 21, 261-282.

19. Zapata, L., Pich, O., Serrano, L., Kondrashov, F. A., Ossowski, S., and Schaefer, M. H. (2018) Negative selection in tumor genome evolution acts on essential cellular functions and the immunopeptidome, *Genome Biol* 19, 67.
20. Reynisson, B., Alvarez, B., Paul, S., Peters, B., and Nielsen, M. (2020) NetMHCpan-4.1 and NetMHCIIpan-4.0: improved predictions of MHC antigen presentation by concurrent motif deconvolution and integration of MS MHC eluted ligand data, *Nucleic Acids Res* 48, W449-W454.
21. Mei, S., Li, F., Leier, A., Marquez-Lago, T. T., Giam, K., Croft, N. P., Akutsu, T., Smith, A. I., Li, J., Rossjohn, J., Purcell, A. W., and Song, J. (2020) A comprehensive review and performance evaluation of bioinformatics tools for HLA class I peptide-binding prediction, *Brief Bioinform* 21, 1119-1135.
22. de Wit, A. S., Bianchi, F., and van den Bogaart, G. (2025) Antigen presentation of post-translationally modified peptides in major histocompatibility complexes, *Immunol Cell Biol* 103, 161-177.
23. Engelhard, V. H., Altrich-Vanlith, M., Ostankovitch, M., and Zarlring, A. L. (2006) Post-translational modifications of naturally processed MHC-binding epitopes, *Curr Opin Immunol* 18, 92-97.
24. Raposo, B., Merky, P., Lundqvist, C., Yamada, H., Urbonaviciute, V., Niaudet, C., Viljanen, J., Kihlberg, J., Kyewski, B., Ekwall, O., Holmdahl, R., and Backlund, J. (2018) T cells specific for post-translational modifications escape intrathymic tolerance induction, *Nat Commun* 9, 353.
25. Engelhard, V. H. (1994) Structure of peptides associated with MHC class I molecules, *Curr Opin Immunol* 6, 13-23.
26. Engelhard, V. H., Appella, E., Benjamin, D. C., Bodnar, W. M., Cox, A. L., Chen, Y., Henderson, R. A., Huczko, E. L., Michel, H., Sakaguichi, K., and et al. (1993) Mass spectrometric analysis of peptides associated with the human class I MHC molecules HLA-A2.1 and HLA-B7 and identification of structural features that determine binding, *Chem Immunol* 57, 39-62.
27. Brandi, J., Noberini, R., Bonaldi, T., and Cecconi, D. (2022) Advances in enrichment methods for mass spectrometry-based proteomics analysis of post-translational modifications, *J Chromatogr A* 1678, 463352.
28. Kacen, A., Javitt, A., Kramer, M. P., Morgenstern, D., Tsaban, T., Shmueli, M. D., Teo, G. C., da Veiga Leprevost, F., Barnea, E., Yu, F., Admon, A., Eisenbach, L.,

- Samuels, Y., Schueler-Furman, O., Levin, Y., Nesvizhskii, A. I., and Merbl, Y. (2023) Post-translational modifications reshape the antigenic landscape of the MHC I immunopeptidome in tumors, *Nat Biotechnol* *41*, 239-251.
29. Aebersold, R., Agar, J. N., Amster, I. J., Baker, M. S., Bertozzi, C. R., Boja, E. S., Costello, C. E., Cravatt, B. F., Fenselau, C., Garcia, B. A., Ge, Y., Gunawardena, J., Hendrickson, R. C., Hergenrother, P. J., Huber, C. G., Ivanov, A. R., Jensen, O. N., Jewett, M. C., Kelleher, N. L., Kiessling, L. L., Krogan, N. J., Larsen, M. R., Loo, J. A., Ogorzalek Loo, R. R., Lundberg, E., MacCoss, M. J., Mallick, P., Mootha, V. K., Mrksich, M., Muir, T. W., Patrie, S. M., Pesavento, J. J., Pitteri, S. J., Rodriguez, H., Saghatelian, A., Sandoval, W., Schluter, H., Sechi, S., Slavoff, S. A., Smith, L. M., Snyder, M. P., Thomas, P. M., Uhlen, M., Van Eyk, J. E., Vidal, M., Walt, D. R., White, F. M., Williams, E. R., Wohlschlagler, T., Wysocki, V. H., Yates, N. A., Young, N. L., and Zhang, B. (2018) How many human proteoforms are there?, *Nat Chem Biol* *14*, 206-214.
  30. Zarling, A. L., Ficarro, S. B., White, F. M., Shabanowitz, J., Hunt, D. F., and Engelhard, V. H. (2000) Phosphorylated peptides are naturally processed and presented by major histocompatibility complex class I molecules in vivo, *J Exp Med* *192*, 1755-1762.
  31. Zarling, A. L., Polefrone, J. M., Evans, A. M., Mikesch, L. M., Shabanowitz, J., Lewis, S. T., Engelhard, V. H., and Hunt, D. F. (2006) Identification of class I MHC-associated phosphopeptides as targets for cancer immunotherapy, *Proc Natl Acad Sci U S A* *103*, 14889-14894.
  32. Andersen, M. H., Bonfill, J. E., Neisig, A., Arsequell, G., Sondergaard, I., Neefjes, J., Zeuthen, J., Elliott, T., and Haurum, J. S. (1999) Phosphorylated peptides can be transported by TAP molecules, presented by class I MHC molecules, and recognized by phosphopeptide-specific CTL, *J Immunol* *163*, 3812-3818.
  33. Apoorvi, T., Yury, P., Iryna, V., and Michelle, K. (2024) Phosphopeptide Neoantigens as Emerging Targets in Cancer Immunotherapy, *J Cancer Immunol (Wilmington)* *6*, 135-147.
  34. Engelhard, V. H., Obeng, R. C., Cummings, K. L., Petroni, G. R., Ambakhutwala, A. L., Chianese-Bullock, K. A., Smith, K. T., Lulu, A., Varhegyi, N., Smolkin, M. E., Myers, P., Mahoney, K. E., Shabanowitz, J., Buettner, N., Hall, E. H., Haden, K., Cobbold, M., Hunt, D. F., Weiss, G., Gaughan, E., and Slingluff, C. L., Jr. (2020)

- MHC-restricted phosphopeptide antigens: preclinical validation and first-in-humans clinical trial in participants with high-risk melanoma, *J Immunother Cancer* 8.
35. Petersen, J., Wurzbacher, S. J., Williamson, N. A., Ramarathinam, S. H., Reid, H. H., Nair, A. K., Zhao, A. Y., Nastovska, R., Rudge, G., Rossjohn, J., and Purcell, A. W. (2009) Phosphorylated self-peptides alter human leukocyte antigen class I-restricted antigen presentation and generate tumor-specific epitopes, *Proc Natl Acad Sci U S A* 106, 2776-2781.
  36. Mohammed, F., Cobbold, M., Zarling, A. L., Salim, M., Barrett-Wilt, G. A., Shabanowitz, J., Hunt, D. F., Engelhard, V. H., and Willcox, B. E. (2008) Phosphorylation-dependent interaction between antigenic peptides and MHC class I: a molecular basis for the presentation of transformed self, *Nat Immunol* 9, 1236-1243.
  37. Wolfert, M. A., and Boons, G. J. (2013) Adaptive immune activation: glycosylation does matter, *Nat Chem Biol* 9, 776-784.
  38. Haurum, J. S., Hoier, I. B., Arsequell, G., Neisig, A., Valencia, G., Zeuthen, J., Neefjes, J., and Elliott, T. (1999) Presentation of cytosolic glycosylated peptides by human class I major histocompatibility complex molecules in vivo, *J Exp Med* 190, 145-150.
  39. Marino, F., Bern, M., Mommen, G. P. M., Leney, A. C., van Gaans-van den Brink, J. A. M., Bonvin, A., Becker, C., van Els, C., and Heck, A. J. R. (2015) Extended O-GlcNAc on HLA Class-I-Bound Peptides, *J Am Chem Soc* 137, 10922-10925.
  40. Haurum, J. S., Arsequell, G., Lellouch, A. C., Wong, S. Y., Dwek, R. A., McMichael, A. J., and Elliott, T. (1994) Recognition of carbohydrate by major histocompatibility complex class I-restricted, glycopeptide-specific cytotoxic T lymphocytes, *J Exp Med* 180, 739-744.
  41. Hudrisier, D., Riond, J., Mazarguil, H., Oldstone, M. B., and Gairin, J. E. (1999) Genetically encoded and post-translationally modified forms of a major histocompatibility complex class I-restricted antigen bearing a glycosylation motif are independently processed and co-presented to cytotoxic T lymphocytes, *J Biol Chem* 274, 36274-36280.

42. Speir, J. A., Abdel-Motal, U. M., Jondal, M., and Wilson, I. A. (1999) Crystal structure of an MHC class I presented glycopeptide that generates carbohydrate-specific CTL, *Immunity* 10, 51-61.
43. Harriff, M. J., Wolfe, L. M., Swarbrick, G., Null, M., Cansler, M. E., Canfield, E. T., Vogt, T., Toren, K. G., Li, W., Jackson, M., Lewinsohn, D. A., Dobos, K. M., and Lewinsohn, D. M. (2017) HLA-E Presents Glycopeptides from the Mycobacterium tuberculosis Protein MPT32 to Human CD8(+) T cells, *Sci Rep* 7, 4622.
44. Olvera, A., Cedeño, S., Llano, A., Mothe, B., Sanchez, J., Arsequell, G., and Brander, C. (2021) Does Antigen Glycosylation Impact the HIV-Specific T Cell Immunity?, *Front Immunol* 11.
45. Parker, R., Partridge, T., Wormald, C., Kawahara, R., Stalls, V., Aggelakopoulou, M., Parker, J., Powell Doherty, R., Ariosa Morejon, Y., Lee, E., Saunders, K., Haynes, B. F., Acharya, P., Thaysen-Andersen, M., Borrow, P., and Ternette, N. (2021) Mapping the SARS-CoV-2 spike glycoprotein-derived peptidome presented by HLA class II on dendritic cells, *Cell Rep* 35, 109179.
46. Suzuki, T., Huang, C., and Fujihira, H. (2016) The cytoplasmic peptide:N-glycanase (NGLY1) - Structure, expression and cellular functions, *Gene* 577, 1-7.
47. Malaker, S. A., Penny, S. A., Steadman, L. G., Myers, P. T., Loke, J. C., Raghavan, M., Bai, D. L., Shabanowitz, J., Hunt, D. F., and Cobbold, M. (2017) Identification of Glycopeptides as Posttranslationally Modified Neoantigens in Leukemia, *Cancer Immunol Res* 5, 376-384.
48. Nguyen, T. B., Lane, D. P., and Verma, C. S. (2021) Can Glycosylation Mask the Detection of MHC Expressing p53 Peptides by T Cell Receptors?, *Biomolecules* 11.
49. Malaker, S. A., Ferracane, M. J., Depontieu, F. R., Zarling, A. L., Shabanowitz, J., Bai, D. L., Topalian, S. L., Engelhard, V. H., and Hunt, D. F. (2017) Identification and Characterization of Complex Glycosylated Peptides Presented by the MHC Class II Processing Pathway in Melanoma, *J Proteome Res* 16, 228-237.
50. Bedran, G., Polasky, D. A., Hsiao, Y., Yu, F., da Veiga Leprevost, F., Alfaro, J. A., Cieslik, M., and Nesvizhskii, A. I. (2023) Unraveling the glycosylated immunopeptidome with HLA-Glyco, *Nat Commun* 14, 3461.
51. Michaelsson, E., Broddefalk, J., Engstrom, A., Kihlberg, J., and Holmdahl, R. (1996) Antigen processing and presentation of a naturally glycosylated protein elicits

- major histocompatibility complex class II-restricted, carbohydrate-specific T cells, *Eur J Immunol* 26, 1906-1910.
52. Dengjel, J., Rammensee, H. G., and Stevanovic, S. (2005) Glycan side chains on naturally presented MHC class II ligands, *J Mass Spectrom* 40, 100-104.
  53. Corthay, A., Backlund, J., Broddefalk, J., Michaelsson, E., Goldschmidt, T. J., Kihlberg, J., and Holmdahl, R. (1998) Epitope glycosylation plays a critical role for T cell recognition of type II collagen in collagen-induced arthritis, *Eur J Immunol* 28, 2580-2590.
  54. Backlund, J., Treschow, A., Bockermann, R., Holm, B., Holm, L., Issazadeh-Navikas, S., Kihlberg, J., and Holmdahl, R. (2002) Glycosylation of type II collagen is of major importance for T cell tolerance and pathology in collagen-induced arthritis, *Eur J Immunol* 32, 3776-3784.
  55. Snir, O., Backlund, J., Bostrom, J., Andersson, I., Kihlberg, J., Buckner, J. H., Klareskog, L., Holmdahl, R., and Malmstrom, V. (2012) Multifunctional T cell reactivity with native and glycosylated type II collagen in rheumatoid arthritis, *Arthritis Rheum* 64, 2482-2488.
  56. Yang, L., Tan, D., and Piao, H. (2016) Myelin Basic Protein Citrullination in Multiple Sclerosis: A Potential Therapeutic Target for the Pathology, *Neurochem Res* 41, 1845-1856.
  57. de Haan, E. C., Wagenaar-Hilbers, J. P., Liskamp, R. M., Moret, E. E., and Wauben, M. H. (2005) Limited plasticity in T cell recognition of modified T cell receptor contact residues in MHC class II bound peptides, *Mol Immunol* 42, 355-364.
  58. Deraos, G., Chatzantoni, K., Matsoukas, M. T., Tselios, T., Deraos, S., Katsara, M., Papathanasopoulos, P., Vynios, D., Apostolopoulos, V., Mouzaki, A., and Matsoukas, J. (2008) Citrullination of linear and cyclic altered peptide ligands from myelin basic protein (MBP(87-99)) epitope elicits a Th1 polarized response by T cells isolated from multiple sclerosis patients: implications in triggering disease, *J Med Chem* 51, 7834-7842.
  59. Martin Monreal, M. T., Hansen, B. E., Iversen, P. F., Enevold, C., Odum, N., Sellebjerg, F., Hojrup, P., Rode von Essen, M., and Nielsen, C. H. (2023) Citrullination of myelin basic protein induces a Th17-cell response in healthy individuals and enhances the presentation of MBP85-99 in patients with multiple sclerosis, *J Autoimmun* 139, 103092.

60. Hill, J. A., Southwood, S., Sette, A., Jevnikar, A. M., Bell, D. A., and Cairns, E. (2003) Cutting edge: the conversion of arginine to citrulline allows for a high-affinity peptide interaction with the rheumatoid arthritis-associated HLA-DRB1\*0401 MHC class II molecule, *J Immunol* 171, 538-541.
61. Scally, S. W., Petersen, J., Law, S. C., Dudek, N. L., Nel, H. J., Loh, K. L., Wijeyewickrema, L. C., Eckle, S. B., van Heemst, J., Pike, R. N., McCluskey, J., Toes, R. E., La Gruta, N. L., Purcell, A. W., Reid, H. H., Thomas, R., and Rossjohn, J. (2013) A molecular basis for the association of the HLA-DRB1 locus, citrullination, and rheumatoid arthritis, *J Exp Med* 210, 2569-2582.
62. Ting, Y. T., Petersen, J., Ramarathinam, S. H., Scally, S. W., Loh, K. L., Thomas, R., Suri, A., Baker, D. G., Purcell, A. W., Reid, H. H., and Rossjohn, J. (2018) The interplay between citrullination and HLA-DRB1 polymorphism in shaping peptide binding hierarchies in rheumatoid arthritis, *Journal of Biological Chemistry* 293, 3236-3251.
63. Curran, A. M., Girgis, A. A., Jang, Y., Crawford, J. D., Thomas, M. A., Kawalerski, R., Coller, J., Bingham, C. O., 3rd, Na, C. H., and Darrah, E. (2023) Citrullination modulates antigen processing and presentation by revealing cryptic epitopes in rheumatoid arthritis, *Nat Commun* 14, 1061.
64. Mangalaparthy, K. K., Madugundu, A. K., Ryan, Z. C., Garapati, K., Peterson, J. A., Dey, G., Prakash, A., and Pandey, A. (2021) Digging deeper into the immunopeptidome: characterization of post-translationally modified peptides presented by MHC I, *J Proteins Proteom* 12, 151-160.
65. Yagüe, J., Vázquez, J., and De Castro, J. A. L. (2000) A post-translational modification of nuclear proteins, -dimethyl-Arg, found in a natural HLA class I peptide ligand, *Protein Sci* 9, 2210-2217.
66. Marino, F., Mommen, G. P., Jeko, A., Meiring, H. D., van Gaans-van den Brink, J. A., Scheltema, R. A., van Els, C. A., and Heck, A. J. (2017) Arginine (Di)methylated Human Leukocyte Antigen Class I Peptides Are Favorably Presented by HLA-B\*07, *J Proteome Res* 16, 34-44.
67. Yi, X., Liao, Y., Wen, B., Li, K., Dou, Y., Savage, S. R., and Zhang, B. (2021) caAtlas: An immunopeptidome atlas of human cancer, *iScience* 24, 103107.
68. Ree, R., Varland, S., and Arnesen, T. (2018) Spotlight on protein N-terminal acetylation, *Exp Mol Med* 50, 1-13.

69. Zamvil, S. S., Mitchell, D. J., Moore, A. C., Kitamura, K., Steinman, L., and Rothbard, J. B. (1986) T-cell epitope of the autoantigen myelin basic protein that induces encephalomyelitis, *Nature* 324, 258-260.
70. He, X. L., Radu, C., Sidney, J., Sette, A., Ward, E. S., and Garcia, K. C. (2002) Structural snapshot of aberrant antigen presentation linked to autoimmunity: the immunodominant epitope of MBP complexed with I-Au, *Immunity* 17, 83-94.
71. Sun, M., Liu, J., Qi, J., Tefsen, B., Shi, Y., Yan, J., and Gao, G. F. (2014) Nalpha-terminal acetylation for T cell recognition: molecular basis of MHC class I-restricted nalpha-acetylpeptide presentation, *J Immunol* 192, 5509-5519.
72. Kumai, T., Ishibashi, K., Oikawa, K., Matsuda, Y., Aoki, N., Kimura, S., Hayashi, S., Kitada, M., Harabuchi, Y., Celis, E., and Kobayashi, H. (2014) Induction of tumor-reactive T helper responses by a posttranslational modified epitope from tumor protein p53, *Cancer Immunol Immunother* 63, 469-478.
73. Meadows, L., Wang, W., den Haan, J. M., Blokland, E., Reinhardus, C., Drijfhout, J. W., Shabanowitz, J., Pierce, R., Agulnik, A. I., Bishop, C. E., Hunt, D. F., Goulmy, E., and Engelhard, V. H. (1997) The HLA-A\*0201-restricted H-Y antigen contains a posttranslationally modified cysteine that significantly affects T cell recognition, *Immunity* 6, 273-281.
74. Pierce, R. A., Field, E. D., den Haan, J. M., Caldwell, J. A., White, F. M., Marto, J. A., Wang, W., Frost, L. M., Blokland, E., Reinhardus, C., Shabanowitz, J., Hunt, D. F., Goulmy, E., and Engelhard, V. H. (1999) Cutting edge: the HLA-A\*0101-restricted HY minor histocompatibility antigen originates from DFFRY and contains a cysteinylated cysteine residue as identified by a novel mass spectrometric technique, *J Immunol* 163, 6360-6364.
75. Chen, W., Yewdell, J. W., Levine, R. L., and Bennink, J. R. (1999) Modification of cysteine residues in vitro and in vivo affects the immunogenicity and antigenicity of major histocompatibility complex class I-restricted viral determinants, *J Exp Med* 189, 1757-1764.
76. Mannering, S. I., Harrison, L. C., Williamson, N. A., Morris, J. S., Thearle, D. J., Jensen, K. P., Kay, T. W., Rossjohn, J., Falk, B. A., Nepom, G. T., and Purcell, A. W. (2005) The insulin A-chain epitope recognized by human T cells is posttranslationally modified, *J Exp Med* 202, 1191-1197.

77. Mei, S., Ayala, R., Ramarathinam, S. H., Illing, P. T., Faridi, P., Song, J., Purcell, A. W., and Croft, N. P. (2020) Immunopeptidomic Analysis Reveals That Deamidated HLA-bound Peptides Arise Predominantly from Deglycosylated Precursors, *Mol Cell Proteomics* 19, 1236-1247.
78. Herzog, J., Maekawa, Y., Cirrito, T. P., Illian, B. S., and Unanue, E. R. (2005) Activated antigen-presenting cells select and present chemically modified peptides recognized by unique CD4 T cells, *Proc Natl Acad Sci U S A* 102, 7928-7933.
79. Karle, A. C., Oostingh, G. J., Mutschlechner, S., Ferreira, F., Lackner, P., Bohle, B., Fischer, G. F., Vogt, A. B., and Duschl, A. (2012) Nitration of the pollen allergen bet v 1.0101 enhances the presentation of bet v 1-derived peptides by HLA-DR on human dendritic cells, *PLoS One* 7, e31483.
80. Sakamoto, E., Katahira, Y., Mizoguchi, I., Watanabe, A., Furusaka, Y., Sekine, A., Yamagishi, M., Sonoda, J., Miyakawa, S., Inoue, S., Hasegawa, H., Yo, K., Yamaji, F., Toyoda, A., and Yoshimoto, T. (2023) Chemical- and Drug-Induced Allergic, Inflammatory, and Autoimmune Diseases Via Haptenation, *Biology (Basel)* 12.
81. Adair, K., Meng, X., and Naisbitt, D. J. (2021) Drug hapten-specific T-cell activation: Current status and unanswered questions, *Proteomics* 21, e2000267.
82. Yildiz, O., Hunt, G. P., Schroth, J., Dhillon, G., Spargo, T. P., Al-Chalabi, A., Koks, S., Turner, M. R., Shaw, P. J., Henson, S. M., Iacoangeli, A., and Malaspina, A. (2025) Lipid-mediated resolution of inflammation and survival in amyotrophic lateral sclerosis, *Brain Commun* 7, fcae402.
83. Azoury, M. E., Fili, L., Bechara, R., Scornet, N., de Chaisemartin, L., Weaver, R. J., Claude, N., Maillere, B., Parronchi, P., Joseph, D., and Pallardy, M. (2018) Identification of T-cell epitopes from benzylpenicillin conjugated to human serum albumin and implication in penicillin allergy, *Allergy* 73, 1662-1672.
84. Tailor, A., Meng, X. L., Adair, K., Farrell, J., Waddington, J. C., Daly, A., Pirmohamed, M., Dear, G., Park, B. K., and Naisbitt, D. J. (2020) HLA DaB1\*15:01-DQB1\*06:02-Restricted Human CD4+T Cells Are Selectively Activated With Amoxicillin-Peptide Adducts, *Toxicol Sci* 178, 115-126.
85. Naisbitt, D. J., Hough, S. J., Gill, H. J., Pirmohamed, M., Kitteringham, N. R., and Park, B. K. (1999) Cellular disposition of sulphamethoxazole and its metabolites: implications for hypersensitivity, *Brit J Pharmacol* 126, 1393-1407.

86. Castrejon, J. L., Berry, N., El-Ghaiesh, S., Gerber, B., Pichler, W. J., Park, B. K., and Naisbitt, D. J. (2010) Stimulation of human T cells with sulfonamides and sulfonamide metabolites, *J Allergy Clin Immun* 125, 411-418.
87. Zhang, Z. Y., Rohweder, P. J., Ongpipattanakul, C., Basu, K., Bohn, M. F., Dugan, E. J., Steri, V., Hann, B., Shokat, K. M., and Craik, C. S. (2022) A covalent inhibitor of K-Ras(G12C) induces MHC class I presentation of haptened peptide neoepitopes targetable by immunotherapy, *Cancer Cell* 40, 1060-+.
88. Pandey, A., Rohweder, P. J., Chan, L. M., Ongpipattanakul, C., Chung, D. H., Paoella, B., Quimby, F. M., Nguyen, N., Verba, K. A., Evans, M. J., and Craik, C. S. (2025) Therapeutic Targeting and Structural Characterization of a Sotorasib-Modified KRAS G12C-MHC I Complex Demonstrate the Antitumor Efficacy of Hapten-Based Strategies, *Cancer Res* 85, 329-341.
89. Zhai, Y., Chen, L., Zhao, Q., Zheng, Z. H., Chen, Z. N., Bian, H., Yang, X., Lu, H. Y., Lin, P., Chen, X., Chen, R., Sun, H. Y., Fan, L. N., Zhang, K., Wang, B., Sun, X. X., Feng, Z., Zhu, Y. M., Zhou, J. S., Chen, S. R., Zhang, T., Chen, S. Y., Chen, J. J., Zhang, K., Wang, Y., Chang, Y., Zhang, R., Zhang, B., Wang, L. J., Li, X. M., He, Q., Yang, X. M., Nan, G., Xie, R. H., Yang, L., Yang, J. H., and Zhu, P. (2023) Cysteine carboxyethylation generates neoantigens to induce HLA-restricted autoimmunity, *Science* 379, eabg2482.

### **Chapter 3 Targeted Acidosis Mediated Delivery of Antigenic MHC-Binding Peptides**

Adapted from: Kelly, J. J.; Ankrom, E. N.; Newkirk, S. E.; Thévenin, D.; Pires, M. M., Targeted acidosis mediated delivery of antigenic MHC-binding peptides *Front. Immunol.* **2024**, 15:1337973.

#### **3.1 Abstract**

Cytotoxic T lymphocytes are the primary effector immune cells responsible for protection against cancer, as they target peptide neoantigens presented through the major histocompatibility complex (MHC) on cancer cells, leading to cell death. Targeting peptide-MHC (pMHC) complex offers a promising strategy for immunotherapy due to their specificity and effectiveness against cancer. In this work, we exploit the acidic tumor micro-environment to selectively deliver antigenic peptides to cancer using pH(low) insertion peptides (pHLIP). We demonstrated the delivery of MHC binding peptides directly to the cytoplasm of melanoma cells resulted in the presentation of antigenic peptides on MHC, and activation of T cells. This work highlights the potential of pHLIP as a vehicle for the targeted delivery of antigenic peptides and its presentation via MHC bound complexes on cancer cell surface for activation of T cells with implications for enhancing anti-cancer immunotherapy.

#### **3.2 Introduction**

The unmet need for effective and innovative treatments against cancer has underscored the importance of targeted delivery of therapeutic agents for cancer therapy.<sup>1</sup> Cytotoxic effects associated with conventional cancer treatments have significantly limited their overall effectiveness.<sup>2</sup> In addition, off-target effects also pose challenges in terms of dosing and administration by causing unwanted side effects to normal cells.<sup>3</sup> Balancing the therapeutic benefits with the risk of toxicity is critical in minimizing damage to healthy tissue and to improve existing treatments. To overcome these limitations, there is an increasing demand for innovative cancer treatment strategies that can overcome the cytotoxicity-associated drawbacks and improve pharmacological properties.

An effective method to mitigate off-target impact involves linking therapeutic agents to well-defined carriers to precisely target cancer cells. Current advances in targeted cancer treatment primarily leverage the overexpression of specific biomarkers on cancer cell surfaces to administer high doses of therapeutic compounds more precisely. An important consideration in designing these types of therapeutics is the specific covalent attachment used to link the therapeutic payload.<sup>4</sup> Numerous covalent linkers, including peptides, disulfides, and thioethers, have been employed to conjugate the therapeutic payload to the antibody.<sup>5-9</sup> Additionally, other delivery systems such as nanoparticles, liposomes, and dendrimers have been engineered to target overexpressed biomarkers such as epidermal growth factor receptors, folate receptors, surface glycoproteins, and transferrin receptors to effectively target cancer.<sup>10-15</sup> While targeting overexpressed biomarkers has been successful in increasing the effective concentration of therapeutic compounds in cells, the same biomarkers expressed at low levels on healthy cells have contributed to significant levels of on-target off-tumor toxicity, highlighting the need to develop alternative strategies.<sup>16</sup>

Alternatively, a strategy to enhance targeted delivery toward tumors involves exploiting the acidic microenvironment that is characteristic of solid tumors. Most tumors display rapid growth levels, which demands increased energy production via glycolysis. This metabolic shift results in the production of lactic acid as a byproduct and the expulsion of protons from the cancer cells into the extracellular space, a phenomenon known as the Warburg effect.<sup>17</sup> As a result, the extracellular space surrounding cancer cells typically has an acidic pH ranging from 6.7 to 7.1 as opposed to a healthy pH range of 7.35 to 7.45. Interestingly, the environment closest to the cell surface is even more acidic; the pH can reach 6.1, making them an ideal target for pH(low) insertion peptides (pHLIPs).<sup>18</sup> The distinctive feature of pHLIP centers on its ability to specifically target the acidic microenvironment by undergoing a pH-dependent rearrangement. This pH-dependent change leads to the insertion of its C-terminus across the cell membrane, forming a transmembrane  $\alpha$ -helix.<sup>19, 20</sup> Importantly, pHLIP can effectively target tumors, transport cargo, and facilitate the translocation of various payloads into the cytosol without needing cell receptor interactions or membrane pore formation.<sup>21-26</sup> Previous studies have

successfully harnessed pHLP to deliver various drug molecules (including peptides) into solid tumors and metastatic sites in animal models.<sup>27-32</sup>

A promising payload for targeted tumor therapies involves antigenic peptides for presentation on the major histocompatibility complex (MHC). MHC molecules can present antigenic peptides to cytotoxic T lymphocytes, initiating an immune response.<sup>33</sup> Specifically, antigenic peptides presented on MHC class I molecules can be recognized by cytotoxic CD8+ T cell receptors (TCRs), triggering the release of perforin and granzyme B, ultimately leading to target cell death.<sup>34, 35</sup> In the context of cancer, cancer cells often display unique peptide-MHC complexes due to various alterations in their proteome, such as protein mutations, aberrant post-translational modifications, and other cellular processes.<sup>36-38</sup> These unique peptides, called neoantigens, are absent in healthy cells and enable the immune system to selectively target and eliminate cancer cells with high efficiency, particularly in cancers with a high mutational burden.<sup>39</sup> However, targeting neoantigens in cancers with a low mutational burden or heterogeneous neoantigen expression has shown limited success.<sup>40</sup> Additionally, the negative selection of self-reactive T cells can prevent neoantigens from having strong anti-cancer activity.<sup>41</sup> Therefore, delivering highly antigenic peptides that are orthogonal to endogenous neoantigens and prompting their presentation on MHC molecules represents a potential strategy for enhancing treatment outcomes.

Prior work by Irvine and colleagues highlighted the benefit of delivering antigenic peptides in a non-specific manner by using cell-penetrating peptides. This approach led to the improved display of antigenic peptides on MHC and the development of T cells specifically targeting the desired epitope.<sup>42</sup> An advantage of cytosolic delivery of antigenic peptides is that it bypasses endosomal processing of peptides, which can lead to significant degradation of MHC-binding peptide epitopes before they can be presented on MHC.<sup>43</sup> Additionally, recent clinical trials have demonstrated the effectiveness of delivering cancer-specific neoantigens for display on MHC in use for cancer therapy.<sup>44</sup>

Building upon these findings, we posed that pHLP could deliver antigenic peptides to cancer cells and this would offer a novel approach to selectively activate the immune system against cancer cells. Here, we showed that pHLP conjugated to the model

antigen SIINFEKL selectively translocated through the membrane of cells in low pH environments and becomes displayed on MHC (**Figure 3.1**). The peptide epitope SIINFEKL (OVA) comes from ovalbumin and there are no known human equivalents, thus making it an orthogonal antigenic peptide with high affinity towards MHC molecules. Notably, melanoma cells in acidic environments showed enhanced MHC display of the target epitope and increased recognition and activation by CD8<sup>+</sup> T cells. These findings highlight the potential of pHLP-mediated delivery of immunomodulatory agents.

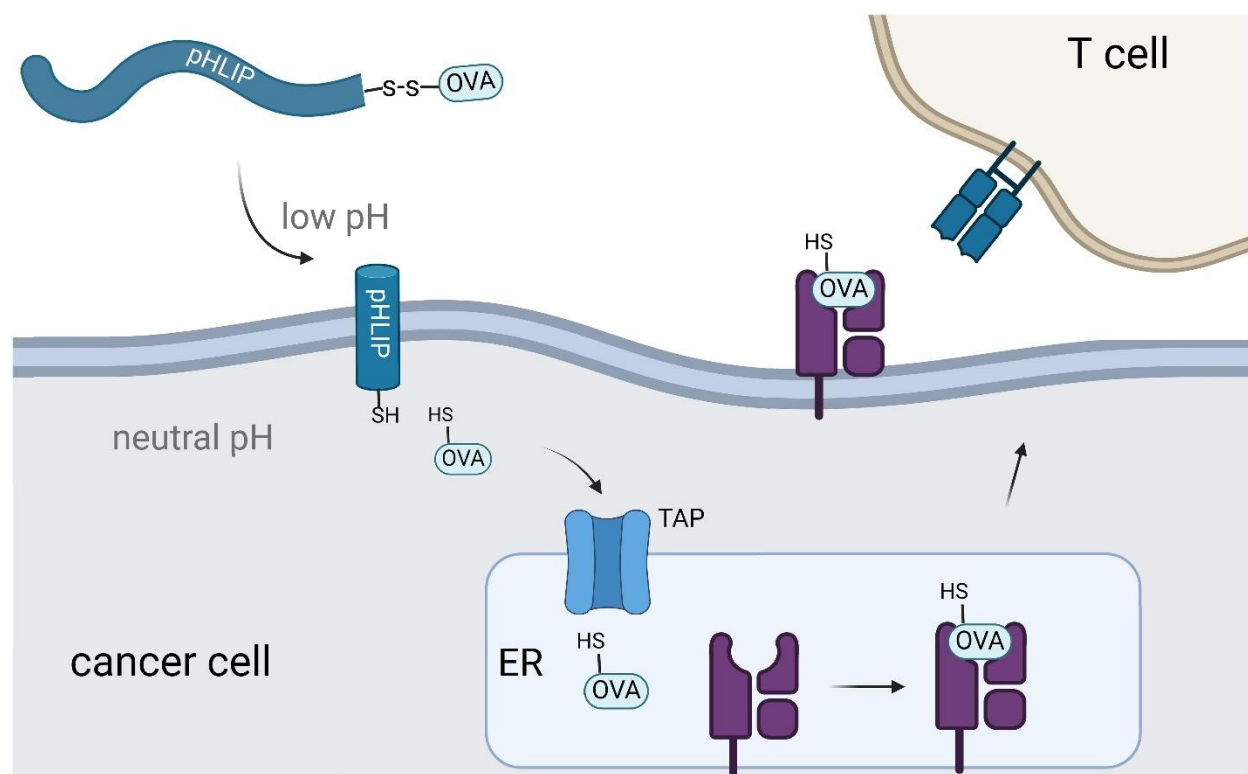


**Figure 3.1** Schematic representation of pHLP-mediated translocation of antigenic peptides for display on MHC. Intracellular delivery of the OVA peptide results in transportation to the endoplasmic reticulum for eventual display on MHC.

### 3.3 Results and Discussion

We sought to link the OVA peptide to pHLP via a chemical handle that would selectively uncouple upon arrival in the cytosolic space. While there are a number of strategies that would be compatible with our system, we selected to connect OVA to pHLP via a disulfide bond. The selection of OVA was based on its considerable precedence as a model MHC

binding antigen, and the rationale behind employing disulfide conjugation was to facilitate the release of the peptide in the reducing cytosolic environment to enable its entry into the antigen presentation pathway. To accomplish this strategy, it would be necessary to introduce a thiol group into the sequence of OVA. Our initial goal was to identify a site on OVA where adding a cysteine would have minimal impact on MHC binding and maintain recognition by OVA-specific TCRs, considering that structural alterations on peptide sequences can significantly influence both parameters.<sup>45, 46</sup>

### 3.3.1 Strategic placement of cysteine handle

To assess changes in peptide affinity to MHC complexes (including thiol-modified OVA peptides), we used the RMA-S stabilization assay. The RMA-S cell line, which lacks the transporter associated with antigen processing (TAP), can be used to isolate the effect of peptide affinity because it lacks the ability to intracellularly process peptides for presentation.<sup>47, 48</sup> Under low-temperature conditions (22-26°C), RMA-S cells present low-affinity pMHC complex on their cell surface. Increasing the temperature to 37°C causes the low-affinity pMHC complex to dissociate and become internalized and degraded. By introducing peptides with high affinity to bind to the MHC molecules, the pMHC complex remains stable on the cell surface at 37°C. The quantification of the peptide-MHC binding affinity, specifically to the H-2K<sup>b</sup> haplotype on RMA-S cells, is determined using flow cytometry with a fluorescent anti-H-2K<sup>b</sup> antibody.

Cysteine-containing OVA peptides were synthesized using a standard solid-phase peptide synthesis (SPPS) approach. Cysteine residues were introduced in sites within the OVA peptide that we projected would minimally impact binding to MHC molecules. These included the addition of cysteine to the termini of the sequence and replacement of residues for cysteine. Subsequently, RMA-S cells were incubated with the synthesized peptides at 26°C, allowing for the exchange of existing low-affinity pMHC complexes. Afterwards, the cells were then warmed to 37°C and treated with an APC-conjugated anti-mouse H-2K<sup>b</sup> antibody. As expected, RMA-S cells treated with unmodified OVA peptide displayed high levels of MHC presentation on the cell surface (**Figure 3.2A**). The peptide SNFVSAGI (**cntPEP**) was used as a negative control as it has been reported to not appreciably bind to MHC.<sup>45, 49</sup> Satisfyingly, the introduction of cysteine was well tolerated

in most of the cysteine-modified OVA peptides; in particular, the cysteine introduction was better tolerated when the cysteine residues were located near the N-terminus. Nonetheless, all the cysteine-modified OVA peptides demonstrated substantial stabilization of the pMHC complex.

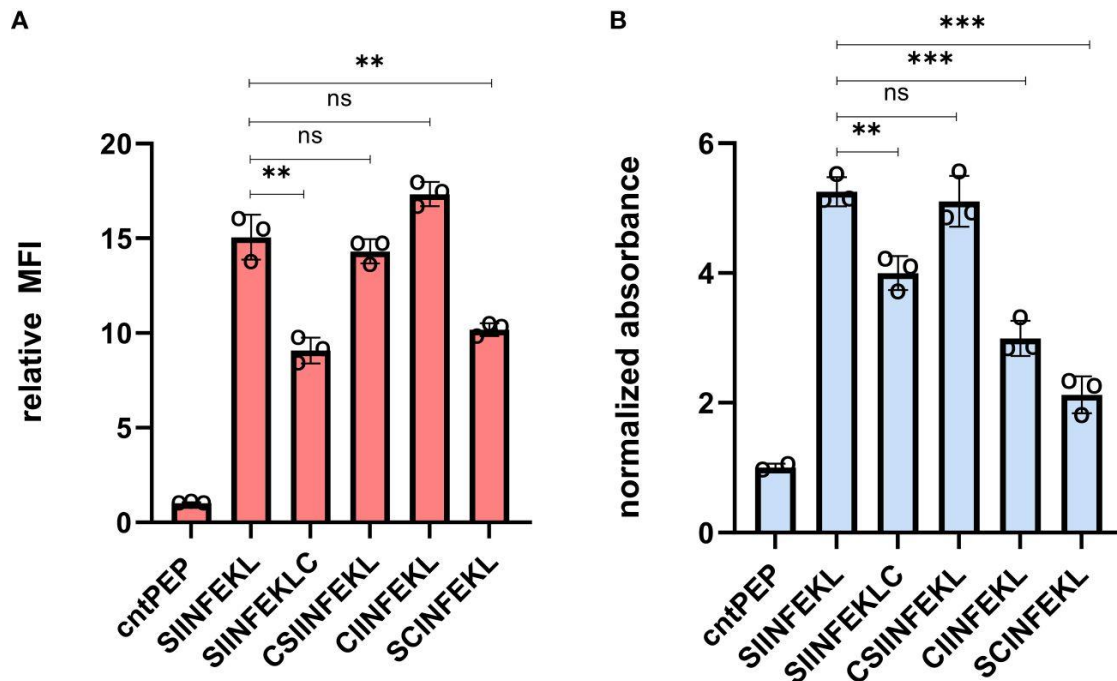


**Figure 3.2** (A) Flow cytometry analysis of RMA-S cells. RMA-S cells were incubated with 20  $\mu\text{M}$  peptide for 6 hours and pMHC complex display was quantified via APC conjugated anti-mouse H-2K<sup>b</sup> antibodies. MFI is mean fluorescence intensity of the level of fluorescence relative to the control peptide. (B) RMA-S cells were incubated with 20  $\mu\text{M}$  peptide and co-cultured with B3Z T cells for 8 hours at an effector-to-target ratio of 1:1.  $\beta$ -galactosidase expression was analyzed by measuring the hydrolysis of the colorimetric reagent CPRG on a plate reader at 570 nm and the data presented has been normalized to the absorbance from **cntPEP**. Data are represented as mean  $\pm$  SD of biological replicates ( $n=3$ ). P-values were determined by a two-tailed t-test (\*\* $p < 0.01$ , \*\*\* $p < 0.001$ , ns, not significant).

Presentation of a cysteine-modified OVA peptide on MHC is critical for the success of our strategy; However, we appreciated that the cysteine modification could also alter the recognition of T cells by the OVA-specific TCR. TCRs can display altered binding affinity

towards modified peptide sequences, prompting us to empirically assess how the position of cysteine might impact T cell activation. Previous findings, conducted by us and others, have indicated that changes to the OVA structure can potentially abolish TCR binding and subsequent T cell activation.<sup>45, 50</sup> Additionally, we introduced cysteines in places reported to have the least disruptive effects to minimize any unfavorable interactions with SIINFEKL-specific TCRs.<sup>51</sup>

We used the effector cells, B3Z T cells, to evaluate T cell activation of target cells displaying cysteine modified OVA peptides. These cells have OVA-specific TCRs and express the enzyme  $\beta$ -galactosidase under the control of an IL-2 inducible promoter upon activation of target cells. The hydrolysis of chlorophenol red- $\beta$ -D-galactopyranoside (CPRG) by  $\beta$ -galactosidase leads to a measurable color change, reflecting the levels of T cell activation. RMA-S cells were incubated with the peptides at 26°C before being co-cultured with B3Z T cells at 37°C. In this assay,  $\beta$ -galactosidase expression was quantified by measuring the hydrolysis of CPRG at 570 nm. All cysteine-containing OVA peptides demonstrated the capability to activate T cells to varying levels (**Figure 3.2B**). However, amongst the peptides tested, CSIINFEKL (**CysOVA**) exhibited both high MHC binding and TCR activation levels, comparable to those of the wild-type OVA peptide. Therefore, we proceeded with **CysOVA** for conjugation to pHLIP.

### **3.3.2** *Assessing the ability of pHLIP-CysOVA to insert into membranes in acid environments*

Next, pHLIP was synthesized using SPPS and it included a corresponding cysteine added on its C-terminus. The disulfide conjugation between **CysOVA** and pHLIP was performed in solution, and the resulting conjugate (**pHLIP-CysOVA**) was purified via reverse phase high performance liquid chromatography (RP-HPLC). To determine the secondary structures of **pHLIP-CysOVA** in the presence of a lipid bilayer at neutral and acidic pH, we utilized far-ultraviolet circular dichroism (CD) spectroscopy. pHLIP-OVA was incubated in the presence of 200 nM 1-palmitoyl-2-oleoyl-sn-glycero-3-phosphocholine (POPC) liposomes at pH 7.4 or pH 5.0. As shown in **Figure 3.3A**, a pH-dependent conformational shift from an unstructured random coil (pH 7.4) to an  $\alpha$ -helix (pH 5.0) characteristic of pHLIP's behavior was observed. Tryptophan (Trp) fluorescence

spectroscopy was also employed to validate the pH-dependent membrane insertion propensity of **pHLIP-CysOVA**. Fluorescence emission from the two Trp residues in the sequence of pHLIP is sensitive to environment polarity and thus reports on lipid membrane insertion. When the pH was lowered from pH 7.4 to pH 5.0, we observed a  $\lambda_{\max}$  blue shift indicating the Trp residues have transitioned to the hydrophobic environment of the lipid bilayer (**Figure 3.3B**). Together with the CD spectra, these results indicate that conjugation to **CysOVA** does not significantly impact the ability of pHLIP to insert across lipid membranes. This result agrees with the many previous studies showing that pHLIP can translocate a wide variety of C-terminally linked peptide cargoes across lipid bilayers.<sup>23, 24, 26, 28, 52</sup>

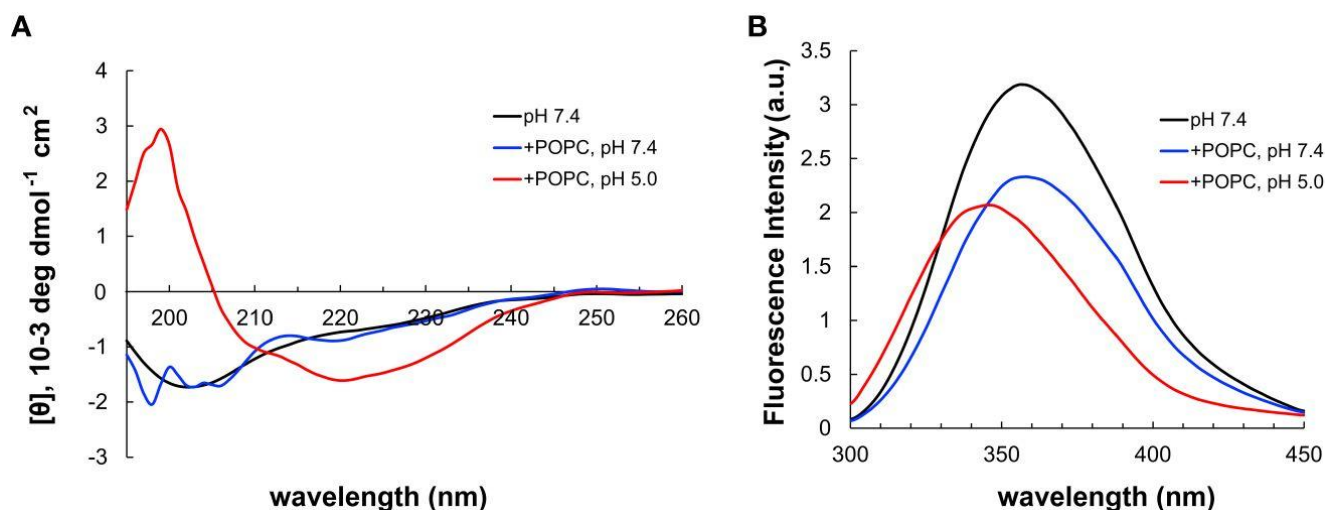


**Figure 3.3** (A) CD spectrum of **pHLIP-CysOVA** in the presence of POPC vesicles at pH 7.4 or 5.0. (B) Tryptophan fluorescence spectra of **pHLIP-CysOVA** (20  $\mu\text{M}$ ) in the presence of POPC vesicles at pH 7.4 or 5.0

### 3.3.3 Analyzing **pHLIP-CysOVA** delivery into antigen presentation pathway

Given that the length of peptides that bind to MHC class I molecules are in the range of 8-12 amino acids, we anticipated that the disulfide bond would have to be reduced to generate **CysOVA** before proper MHC binding. Therefore, we set out to investigate whether **pHLIP-CysOVA** needs to be reduced for enhanced antigen presentation on MHC. For this, we used the RMA-S stabilization assay to assess the relative affinity of the peptide to MHC before and after disulfide reduction at physiological pH. In this assay,

RMA-S cells were incubated in the presence or absence of  $\beta$ -mercaptoethanol (BME) to cleave the disulfide linkage to assess changes in MHC binding affinity. Our results showed that cleaving the disulfide bond to generate **CysOVA** stabilized the peptide-MHC complex on RMA-S cells and significantly improved antigen presentation on the cell surface (**Figure 3.4A**). We observed cytotoxic effects of the RMA-S cells with higher concentrations of BME. Therefore, we believe that there may be an incomplete reduction of the **pHLIP-CysOVA** in the presence of BME. There is also the possibility that **CysOVA** produces an *in situ* adduct with BME, which would change the stabilization levels. Overall, these results indicate that **pHLIP-CysOVA** must be reduced into **CysOVA** for optimal display on MHC.

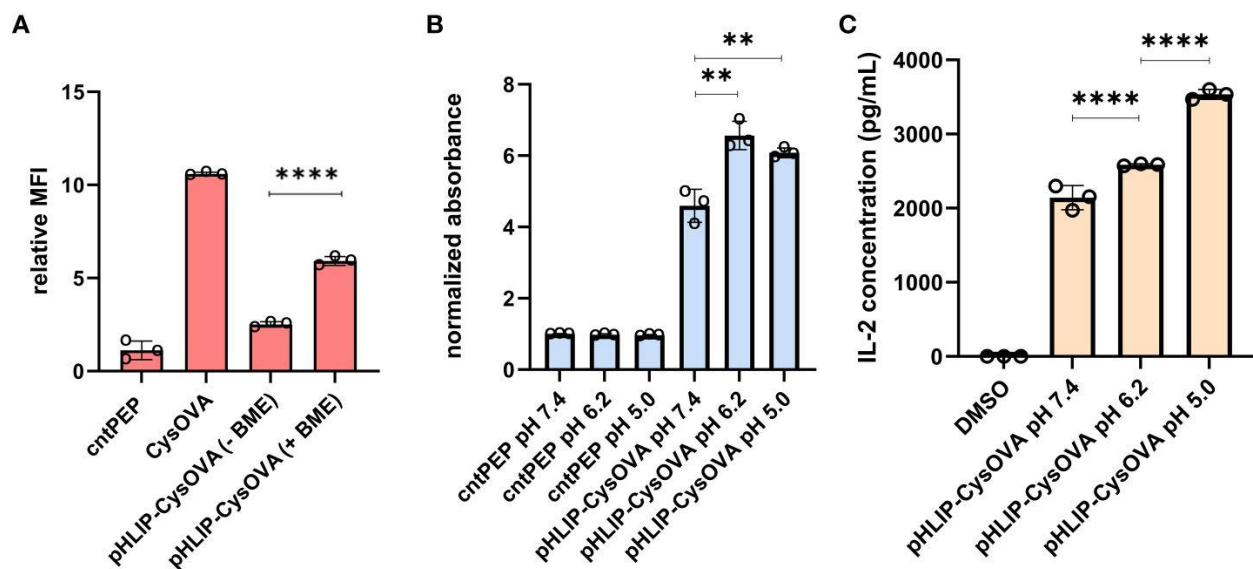


**Figure 3.4** (A) RMA-S cells at physiological pH were incubated with  $2.5 \mu\text{M}$  **pHLIP-CysOVA** for 6 hours in the presence or absence of BME. Cells were then labeled with anti-mouse H-2K<sup>b</sup> antibody and analyzed via flow cytometry. MFI is mean fluorescence intensity of the level of fluorescence relative to the control peptide (B)  $2.5 \mu\text{M}$  **pHLIP-CysOVA** was incubated with B16 cells for 5 mins before adjusting to the indicated pH for 10 mins. Cells were washed and co-cultured with B3Z T cells for 8 hours before lysing and measuring  $\beta$ -galactosidase activity via the colorimetric reagent CPRG on a plate reader at 570 nm and the data presented has been normalized to the absorbance from **cntPEP**. (C) B16 cells were treated with **pHLIP-CysOVA** for 5 mins before adjusting to pH 5 for 10 mins. Subsequently, these cells were washed and co-cultured

*with B3Z T cells overnight, with secreted IL-2 levels measured through ELISA. Data are represented as mean  $\pm$  SD of biological replicates (n= 3). P-values were determined by a two-tailed t-test (\*\*p<0.01, \*\*\*\*p < 0.0001).*

To evaluate the efficacy of **pHLIP-CysOVA** in enabling antigen presentation on MHC in cells within acidic microenvironments, DC2.4 dendritic cells were subjected to incubation with **pHLIP-CysOVA** under neutral and acidic conditions. Cells were treated with **pHLIP-CysOVA** at either pH 7.4 or 5.0 for 10 mins at 37°C. Subsequently, cells were washed and were incubated with APC-conjugated 25-D1.16 antibodies (specific to SIINFEKL bound to H-2K<sup>b</sup>) to quantify antigen presentation on MHC. Our data demonstrated a significant increase in antigen presentation on MHC in cells treated at low pH, indicating successful translocation of **pHLIP-CysOVA** across the membrane and entry into the antigen presentation pathway (**Figure S3.1**).

Finally, to demonstrate that treatment at low pH enables selective immune activation of **pHLIP-CysOVA** in a clinically relevant model, B16 melanoma cells were employed. B16 cells were incubated with **pHLIP-CysOVA** at either physiological or low pH for 10 min. Following this incubation, the cells were washed and co-cultured with effector cells (B3Z T cells). Once again, treatment at lower pH conditions significantly enhanced T cell activations against the target B16 cells (**Figure 3.4B**). Satisfyingly, **pHLIP-CysOVA** also shows improved T cell activation against the melanoma model at a more physiologically relevant pH of 6.2 (**Figure 3.4B**). Noteworthy, cells treated with **CysOVA** peptide alone did not show any pH dependent T cell activation (**Figure S3.2**). Additionally, ELISA results confirmed that **pHLIP-CysOVA** treatment at low pH induced significant T cell activation through elevated IL-2 cytokine secretion from B3Z T cells (**Figure 3.4C**). Taken together, these findings demonstrate selective activation of T cells in response to **pHLIP-CysOVA** treatment within acidic environments.

### 3.4 Conclusion

In this study, we have described a targeted approach to deliver antigenic peptides specifically to cancer cells, thereby aiding their presentation on MHC molecules to enhance immune activation. Our method used pHLIP to deliver **CysOVA** directly to the cytosol, allowing for the cytoplasmic delivery of exogenously derived peptides.

Traditionally, antigen-presenting cells would be required to translocate exogenous peptides into the cytosol for display on MHC class I through a process called cross-presentation.<sup>53</sup> By avoiding this step, we can deliver peptides to non-antigen presenting cells.

A key advantage of our approach is the versatility of pHLIP, which has previously demonstrated the ability to translocate a wide range of molecules, including hydrophilic peptides, across cell membranes.<sup>28</sup> We envision that our strategy can be adapted to deliver various potential neoantigens, thereby broadening its applicability and therapeutic potential. Additionally, it was recently reported that MHC peptides tagged with distinct covalent small-molecule inhibitors can be targeted by immune cells for immunotherapy applications.<sup>54</sup> Consequently, we anticipate that pHLIP can serve as a delivery vehicle for chemically modified peptides, potentially used alongside antibodies or CAR-T cells to enable precision immunotherapy against cancer.<sup>55</sup>

However, developing a robust T cell response towards pMHC complexes is hindered by the variety of ways in which cancer evades immune recognition. One widely reported mechanism for immune escape is the downregulation of MHC which impairs their ability to display antigenic peptides.<sup>56, 57</sup> Indeed, non-responders to immune checkpoint inhibition often possess cancer mutations that decrease the presentation of peptides on the cell surface via MHC.<sup>58</sup> Furthermore, the acidic cancer microenvironment is known to diminish T cells activity against tumors.<sup>59-61</sup> Another means by which CD8+ T cells become less effective against tumors is through the immunosuppressive activity of regulatory CD4+ T cells.<sup>62</sup> Therefore, effective immunotherapy strategies will likely require a multifactorial approach in order to overcome these limitations related to immune evasion.

### 3.5 Summary and Future Outlook

In Chapter 3, we leveraged pHLIP to selectively deliver immunogenic peptides to cancer cells, enhancing T cell recognition. Tumors often exhibit heterogeneous neoantigen expression which can hinder complete eradication by the immune system. Moreover, few neoantigens are shared across individuals, limiting broad therapeutic application. An alternative strategy to engage T cells more effectively involves the direct delivery of

immunogenic peptides to malignant cells. Here, we exploited the acidic tumor microenvironment, a conserved hallmark of many cancers, as a targeting mechanism for peptide delivery. By capitalizing on this feature, we facilitated antigenic peptide presentation on MHC-I molecules and promoted T cell recognition.

A key advantage of employing pHLIP as a delivery vehicle lies in its ability to transport peptides significantly larger and more polar than typical MHC-I ligands. This inherent versatility suggests that pHLIP-mediated delivery can be readily adapted to various neoantigens of interest. However, for MHC haplotypes beyond H-2Kb, it will be necessary to empirically determine whether the N- or C-terminus is more amenable to cysteine modifications for disulfide linkage to ensure optimal display on MHC-I molecules and recognition by cognate TCRs. Establishing a broadly applicable platform for neoantigen delivery could ultimately enhance personalized cancer immunotherapy against diverse tumor types.

### **3.6 Materials and Methods**

**Materials.** All peptide related reagents and protected amino acids were purchased from Chem-Impex. APC-labeled anti-mouse H-2Kd/H-2Dd antibody was purchased from Biolegend. Pooled Human Serum was purchased from Sigma Aldrich. Dulbecco's Modified Eagle's Medium (DMEM) and Roswell Park Memorial Institute (RPMI) 1640 medium were purchased from VWR. Fetal Bovine Serum (FBS) was purchased from R&D Systems. Penicillin-streptomycin and mouse IL-2 ELISA kits was purchased from Sigma-Aldrich. All other organic chemical reagents were purchased from Fisher Scientific or Sigma Aldrich and used without further purification. All compounds are >95% pure by HPLC analysis.

**Mammalian Cell Culture.** RMA-S cells were a kind gift from Dr. John Sampson. RMA-S cells were maintained in RPMI 1640 media supplemented with 10% fetal bovine serum, 50 IU/mL penicillin, 50  $\mu$ g/mL streptomycin, 1X a MEM non-essential amino acid solution (ThermoFisher) and cultured in a humidified atmosphere of 5% CO<sub>2</sub> at 37°C. B3Z cells were kindly provided by Dr. Aaron Esser-Kahn and maintained in RPMI 1640 media supplemented with 10% fetal bovine serum, 50 IU/mL penicillin, 50  $\mu$ g/mL streptomycin

and cultured in a humidified atmosphere of 5% CO<sub>2</sub> at 37°C. B16 cells were kindly provided by Dr. Victor Engelhard and also maintained in RPMI 1640 media supplemented with 10% fetal bovine serum, 50 IU/mL penicillin, 50 µg/mL streptomycin and cultured in a humidified atmosphere of 5% CO<sub>2</sub> at 37°C.

**RMA-S Stabilization Assay.** 10<sup>5</sup> RMA-S cells were seeded in a treated 96 well plate at 37°C overnight. The next day, RMA-S cells were moved to a 26°C incubator for 24-48 hours. Following the incubation period, cells were incubated with 20 µM peptides in culture media at indicated concentrations for 1 hour at 26°C before being moved to the 37°C incubator for 6 hours. For assays involving β-mercaptoethanol, 100 µM of BME was added along with peptide during these incubation periods. The media was then replaced with a 1:100 dilution of APC labeled anti-mouse H-2Kd/H-2Dd antibody in culture media for 1 hour at 4°C. Cells were removed from the well plate by vigorous pipetting, fixed with 2% formaldehyde solution, and analyzed using the Attune NxT Flow Cytometer (Thermo Fischer) equipped with a 637 nm laser with 670/14 nm bandpass filter.

**B3Z T Cell Activation.** 10<sup>5</sup> RMA-S cells were seeded in a treated 96 well plate at 37°C overnight. The following day the culture media was replaced with media containing 20 µM peptide along with 10<sup>5</sup> B3Z cells in culture media and co-incubated overnight. Cells were then spun down at 500xg for 5 mins and washed with 1X PBS a total of two times. Lysis buffer containing 0.2% saponin, 500 µM CPRG reagent, 20 mM MgCl<sub>2</sub>, and 100 mM β-mercaptoethanol in 1X PBS was added to each well. After 2-4 hours absorbance 570 was recorded using a BioTek Epoch 2 microplate reader.

**Sample Preparation for CD and Tryptophan Emission Spectroscopy.** pHLLIP-OVA was solubilized to 20 µM in 5 mM sodium phosphate buffer (pH 8.0). The peptide was diluted to a final concentration of 5 µM before analysis. Liposomes were prepared by drying 1-palmitoyl-2-oleoyl-sn-glycero-3-phosphocholine (POPC) as a thin film and desiccation under vacuum for at least 24 h. Lipids were rehydrated in 5 mM sodium phosphate (pH 8.0) for at least 30 min at 37°C with periodic gentle vortexing. The resulting large multilamellar vesicles were rapidly frozen and thawed seven times and subsequently extruded through a polycarbonate membrane with 200 nm pores using a Mini-Extruder (Avanti Polar Lipids) to produce large unilamellar vesicles (LUVs). pHLLIP-

OVA was incubated with the resulting LUVs at a 1:300 ratio. pH was adjusted to the desired experimental values with HCl and the samples were incubated at RT for 30 min prior to analysis. Fluorescence emission spectra were recorded using a Fluorolog-3 spectrofluorometer (HORIBA). The excitation wavelength was set at 280 nm, and the emission spectra were measured from 300 to 450 nm. The excitation and emission slit widths were set to 5 nm.

**CD Spectroscopy.** Far-ultraviolet CD spectra were recorded on a Jasco J-815 CD spectrometer equipped with a Peltier thermally controlled cuvette holder (Jasco). Samples were measured in 0.1 cm quartz cuvette. CD intensity was expressed as mean residue molar ellipticity  $[\theta]$  calculated by the following equation:  $[\theta] = \theta_{\text{obs}}/10lc_n$  (in deg  $\text{cm}^{-2} \text{dmol}^{-1}$ )  $\theta_{\text{obs}}$  is the observed ellipticity in millidegrees,  $l$  is the optical path length in centimeters,  $c$  is the molar peptide concentration, and  $n$  is the number of amino acid residues. Spectra were recorded from 260 to 200 nm in 1 nm intervals at a 100 nm/min scan rate. Five scans were averaged for each sample. The spectrum of POPC liposomes was subtracted out from samples containing pHLP-OVA in the presence of POPC.

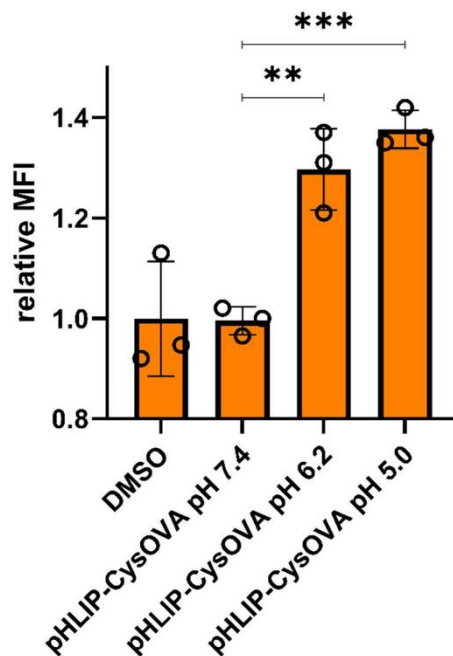
**B3Z Targeting pHLP-OVA Treated B16 Cells.** B16 cells were seeded in a treated 96-well plate at 37°C overnight. The following day the media was removed, and cells were incubated with indicated concentration of pHLP-OVA at 37°C for 5-10 min. The pH was then adjusted to a pH of 5 by using a pre-established volume of DMEM, pH 2.0 buffered with citric acid, and the plate was incubated for 10 min. After the treatment, the media was washed once with DMEM and  $10^5$  B3Z cells were added to each well. B3Z and B16 cells were co-cultured for 8 hours before being spun down at 500xg for 5 min and washed with 1X PBS a total of two times. Lysis buffer containing 0.2% saponin, 500  $\mu\text{M}$  CPRG reagent, 20 mM  $\text{MgCl}_2$ , and 100 mM  $\beta$  mercaptoethanol in 1X PBS was added to each well. After 2-4 hours absorbance 570 was recorded using a BioTek Epoch 2 microplate reader

**25-D1.16 Labeled pHLP-CysOVA treated DC2.4 Cells.** DC2.4 cells were seeded in a treated 96-well plate at 37°C overnight. The following day the media was removed, and cells were incubated with indicated concentration of pHLP-OVA at 37°C for 5-10 min. The pH was then adjusted to the desired value using a pre-established volume of DMEM,

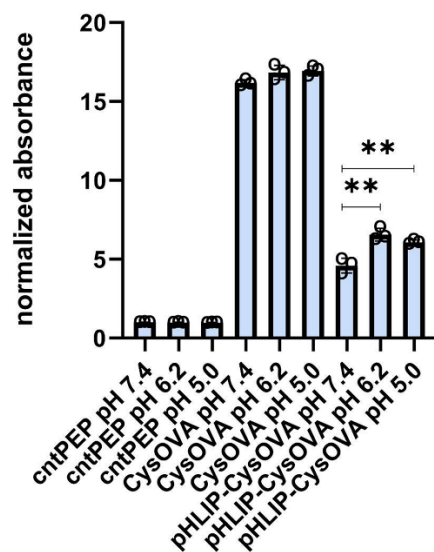
pH 2.0 buffered with citric acid, and incubated for 10 min. The media was replaced with a 1:50 dilution of the APC conjugated SIINFEKL-H-2K<sup>b</sup> specific antibody clone 25-D1.16 for 2 hours at 4°C. Cells were fixed with 2% formaldehyde solution and analyzed using the Attune NxT Flow Cytometer (Thermo Fischer) equipped with a 637 nm laser with 670/14 nm bandpass filter.

**B3Z IL-2 Secretion.** B16 cells were seeded in a treated 24-well plate at 37°C overnight. The following day cell media was removed and treatment solution with 2.5 μM of pHLIP-OVA and incubated at 37°C for 5-10 min. The pH was then adjusted to a pH of 6.2 or 5.0 by using a pre-established volume of DMEM, pH 2.0 buffered with citric acid, and the plate was incubated for 10 min. After the treatment, the media was washed once with DMEM and 10<sup>6</sup> B3Z cells were added to each well. B3Z and B16 cells were co-cultured overnight. IL-2 released by B3Z or B16 cells in cell supernatants were detected by IL-2 ELISA kits according to the manufacture's instruction.

## 3.7 Supplementary Figures



**Figures S3.1.** DC2.4 cells were incubated with peptide for 5 mins before adjusting to pH 5 for 10 mins. Cells were washed and incubated with APC labeled 25-D1.16 antibody (specific for SIINFEKL on H-2Kb) for 1 h and analyzed via flow cytometry. Data are represented as mean  $\pm$  SD of biological replicates ( $n=3$ ). P-values were determined by a two-tailed t-test (\*\*  $p < 0.01$ ).



**Figures S3.2.**  $2.5 \mu\text{M}$  pHLIP-CysOVA was incubated with B16 cells for 5 mins before adjusting to the indicated pH for 10 mins. Cells were washed and co-cultured with B3Z T cells for 8 hours before lysing and measuring  $\beta$ -galactosidase activity via the colorimetric reagent CPRG on a plate reader at 570 nm. Data are represented as mean  $\pm$  SD of biological replicates ( $n=3$ ). P-values were determined by a two-tailed t-test (\*\*  $p < 0.01$ ).

### 3.8 References

1. Manzari, M. T., Shabay, Y., Kiguchi, H., Rosen, N., Scaltriti, M., and Heller, D. A. (2021) Targeted drug delivery strategies for precision medicines, *Nat Rev Mater* 6, 351-370.
2. Rothenberg, M. L., Carbone, D. P., and Johnson, D. H. (2003) Improving the evaluation of new cancer treatments: challenges and opportunities, *Nat Rev Cancer* 3, 303-309.
3. Zhong, L., Li, Y., Xiong, L., Wang, W., Wu, M., Yuan, T., Yang, W., Tian, C., Miao, Z., Wang, T., and Yang, S. (2021) Small molecules in targeted cancer therapy: advances, challenges, and future perspectives, *Signal Transduct Target Ther* 6, 201.
4. Chari, R. V. (2008) Targeted cancer therapy: conferring specificity to cytotoxic drugs, *Acc Chem Res* 41, 98-107.
5. Erickson, H. K., Park, P. U., Widdison, W. C., Kovtun, Y. V., Garrett, L. M., Hoffman, K., Lutz, R. J., Goldmacher, V. S., and Blattler, W. A. (2006) Antibody-maytansinoid conjugates are activated in targeted cancer cells by lysosomal degradation and linker-dependent intracellular processing, *Cancer Res* 66, 4426-4433.
6. Tsuchikama, K., and An, Z. (2018) Antibody-drug conjugates: recent advances in conjugation and linker chemistries, *Protein Cell* 9, 33-46.
7. Ford, C. H., Newman, C. E., Johnson, J. R., Woodhouse, C. S., Reeder, T. A., Rowland, G. F., and Simmonds, R. G. (1983) Localisation and toxicity study of a vindesine-anti-CEA conjugate in patients with advanced cancer, *Br J Cancer* 47, 35-42.
8. Pettinato, M. C. (2021) Introduction to Antibody-Drug Conjugates, *Antibodies (Basel)* 10.
9. Walles, M., Connor, A., and Hainzl, D. (2017) ADME and Safety Aspects of Non-cleavable Linkers in Drug Discovery and Development, *Curr Top Med Chem* 17, 3463-3475.

10. Ramalho, M. J., Loureiro, J. A., Coelho, M. A. N., and Pereira, M. C. (2022) Transferrin Receptor-Targeted Nanocarriers: Overcoming Barriers to Treat Glioblastoma, *Pharmaceutics* 14.
11. Bloise, N., Okkeh, M., Restivo, E., Della Pina, C., and Visai, L. (2021) Targeting the "Sweet Side" of Tumor with Glycan-Binding Molecules Conjugated-Nanoparticles: Implications in Cancer Therapy and Diagnosis, *Nanomaterials (Basel)* 11.
12. Ebrahimnejad, P., Sodagar Taleghani, A., Asare-Addo, K., and Nokhodchi, A. (2022) An updated review of folate-functionalized nanocarriers: A promising ligand in cancer, *Drug Discov Today* 27, 471-489.
13. Master, A. M., and Sen Gupta, A. (2012) EGF receptor-targeted nanocarriers for enhanced cancer treatment, *Nanomedicine (Lond)* 7, 1895-1906.
14. Palmerston Mendes, L., Pan, J., and Torchilin, V. P. (2017) Dendrimers as Nanocarriers for Nucleic Acid and Drug Delivery in Cancer Therapy, *Molecules* 22.
15. Rosenblum, D., Joshi, N., Tao, W., Karp, J. M., and Peer, D. (2018) Progress and challenges towards targeted delivery of cancer therapeutics, *Nat Commun* 9, 1410.
16. Akhtar, M. J., Ahamed, M., Alhadlaq, H. A., Alrokayan, S. A., and Kumar, S. (2014) Targeted anticancer therapy: overexpressed receptors and nanotechnology, *Clin Chim Acta* 436, 78-92.
17. Boedtkjer, E., and Pedersen, S. F. (2020) The Acidic Tumor Microenvironment as a Driver of Cancer, *Annu Rev Physiol* 82, 103-126.
18. Anderson, M., Moshnikova, A., Engelman, D. M., Reshetnyak, Y. K., and Andreev, O. A. (2016) Probe for the measurement of cell surface pH in vivo and ex vivo, *Proc Natl Acad Sci U S A* 113, 8177-8181.
19. Reshetnyak, Y. K., Segala, M., Andreev, O. A., and Engelman, D. M. (2007) A monomeric membrane peptide that lives in three worlds: in solution, attached to, and inserted across lipid bilayers, *Biophys J* 93, 2363-2372.
20. Reshetnyak, Y. K., Andreev, O. A., Segala, M., Markin, V. S., and Engelman, D. M. (2008) Energetics of peptide (pHLIP) binding to and folding across a lipid bilayer membrane, *Proc Natl Acad Sci U S A* 105, 15340-15345.

21. Onyango, J. O., Chung, M. S., Eng, C. H., Klees, L. M., Langenbacher, R., Yao, L., and An, M. (2015) Noncanonical amino acids to improve the pH response of pHLIP insertion at tumor acidity, *Angew Chem Int Ed Engl* 54, 3658-3663.
22. An, M., Wijesinghe, D., Andreev, O. A., Reshetnyak, Y. K., and Engelman, D. M. (2010) pH-(low)-insertion-peptide (pHLIP) translocation of membrane impermeable phalloidin toxin inhibits cancer cell proliferation, *Proc Natl Acad Sci U S A* 107, 20246-20250.
23. Burns, K. E., McCleerey, T. P., and Thevenin, D. (2016) pH-Selective Cytotoxicity of pHLIP-Antimicrobial Peptide Conjugates, *Sci Rep* 6, 28465.
24. Burns, K. E., and Thevenin, D. (2015) Down-regulation of PAR1 activity with a pHLIP-based allosteric antagonist induces cancer cell death, *Biochem J* 472, 287-295.
25. Burns, K. E., Robinson, M. K., and Thevenin, D. (2015) Inhibition of cancer cell proliferation and breast tumor targeting of pHLIP-monomethyl auristatin E conjugates, *Mol Pharm* 12, 1250-1258.
26. Thevenin, D., An, M., and Engelman, D. M. (2009) pHLIP-mediated translocation of membrane-impermeable molecules into cells, *Chem Biol* 16, 754-762.
27. Gerhart, J., Thevenin, A. F., Bloch, E., King, K. E., and Thevenin, D. (2018) Inhibiting Epidermal Growth Factor Receptor Dimerization and Signaling Through Targeted Delivery of a Juxtamembrane Domain Peptide Mimic, *ACS Chem Biol* 13, 2623-2632.
28. Burns, K. E., Hensley, H., Robinson, M. K., and Thevenin, D. (2017) Therapeutic Efficacy of a Family of pHLIP-MMAF Conjugates in Cancer Cells and Mouse Models, *Mol Pharm* 14, 415-422.
29. Karabadzhak, A. G., Weerakkody, D., Wijesinghe, D., Thakur, M. S., Engelman, D. M., Andreev, O. A., Markin, V. S., and Reshetnyak, Y. K. (2012) Modulation of the pHLIP transmembrane helix insertion pathway, *Biophys J* 102, 1846-1855.
30. Adochite, R. C., Moshnikova, A., Carlin, S. D., Guerrieri, R. A., Andreev, O. A., Lewis, J. S., and Reshetnyak, Y. K. (2014) Targeting breast tumors with pH (low) insertion peptides, *Mol Pharm* 11, 2896-2905.

31. Reshetnyak, Y. K., Yao, L., Zheng, S., Kuznetsov, S., Engelman, D. M., and Andreev, O. A. (2011) Measuring tumor aggressiveness and targeting metastatic lesions with fluorescent pHLIP, *Mol Imaging Biol* 13, 1146-1156.
32. Cheng, C. J., Bahal, R., Babar, I. A., Pincus, Z., Barrera, F., Liu, C., Svoronos, A., Braddock, D. T., Glazer, P. M., Engelman, D. M., Saltzman, W. M., and Slack, F. J. (2015) MicroRNA silencing for cancer therapy targeted to the tumour microenvironment, *Nature* 518, 107-110.
33. Neefjes, J., Jongsma, M. L., Paul, P., and Bakke, O. (2011) Towards a systems understanding of MHC class I and MHC class II antigen presentation, *Nat Rev Immunol* 11, 823-836.
34. Gorentla, B. K., and Zhong, X. P. (2012) T cell Receptor Signal Transduction in T lymphocytes, *J Clin Cell Immunol* 2012, 5.
35. Huppa, J. B., and Davis, M. M. (2003) T-cell-antigen recognition and the immunological synapse, *Nat Rev Immunol* 3, 973-983.
36. Ouspenskaia, T., Law, T., Clauser, K. R., Klaeger, S., Sarkizova, S., Aguet, F., Li, B., Christian, E., Knisbacher, B. A., Le, P. M., Hartigan, C. R., Keshishian, H., Apffel, A., Oliveira, G., Zhang, W., Chen, S., Chow, Y. T., Ji, Z., Jungreis, I., Shukla, S. A., Justesen, S., Bachireddy, P., Kellis, M., Getz, G., Hacohen, N., Keskin, D. B., Carr, S. A., Wu, C. J., and Regev, A. (2022) Unannotated proteins expand the MHC-I-restricted immunopeptidome in cancer, *Nat Biotechnol* 40, 209-217.
37. Engelhard, V. H., Obeng, R. C., Cummings, K. L., Petroni, G. R., Ambakhtwala, A. L., Chianese-Bullock, K. A., Smith, K. T., Lulu, A., Varhegyi, N., Smolkin, M. E., Myers, P., Mahoney, K. E., Shabanowitz, J., Buettner, N., Hall, E. H., Haden, K., Cobbold, M., Hunt, D. F., Weiss, G., Gaughan, E., and Slingluff, C. L., Jr. (2020) MHC-restricted phosphopeptide antigens: preclinical validation and first-in-humans clinical trial in participants with high-risk melanoma, *J Immunother Cancer* 8.
38. Xie, N., Shen, G., Gao, W., Huang, Z., Huang, C., and Fu, L. (2023) Neoantigens: promising targets for cancer therapy, *Signal Transduct Target Ther* 8, 9.
39. Pearlman, A. H., Hwang, M. S., Konig, M. F., Hsiue, E. H., Douglass, J., DiNapoli, S. R., Mog, B. J., Bettegowda, C., Pardoll, D. M., Gabelli, S. B., Papadopoulos, N.,

- Kinzler, K. W., Vogelstein, B., and Zhou, S. (2021) Targeting public neoantigens for cancer immunotherapy, *Nat Cancer* 2, 487-497.
40. Lang, F., Schrors, B., Lower, M., Tureci, O., and Sahin, U. (2022) Identification of neoantigens for individualized therapeutic cancer vaccines, *Nat Rev Drug Discov* 21, 261-282.
41. Miller, J. F., and Basten, A. (1996) Mechanisms of tolerance to self, *Curr Opin Immunol* 8, 815-821.
42. Backlund, C. M., Holden, R. L., Moynihan, K. D., Garafola, D., Farquhar, C., Mehta, N. K., Maiorino, L., Pham, S., Iorgulescu, J. B., Reardon, D. A., Wu, C. J., Pentelute, B. L., and Irvine, D. J. (2022) Cell-penetrating peptides enhance peptide vaccine accumulation and persistence in lymph nodes to drive immunogenicity, *Proc Natl Acad Sci U S A* 119, e2204078119.
43. Embgenbroich, M., and Burgdorf, S. (2018) Current Concepts of Antigen Cross-Presentation, *Front Immunol* 9, 1643.
44. Niemi, J. V. L., Sokolov, A. V., and Schioth, H. B. (2022) Neoantigen Vaccines; Clinical Trials, Classes, Indications, Adjuvants and Combinatorial Treatments, *Cancers (Basel)* 14.
45. Kelly, J. J., Bloodworth, N., Shao, Q., Shabanowitz, J., Hunt, D., Meiler, J., and Pires, M. M. (2024) A Chemical Approach to Assess the Impact of Post-translational Modification on MHC Peptide Binding and Effector Cell Engagement, *ACS Chem Biol* 19, 1991-2001.
46. Pawlak, J. B., Hos, B. J., van de Graaff, M. J., Megantari, O. A., Meeuwenoord, N., Overkleeft, H. S., Filippov, D. V., Ossendorp, F., and van Kasteren, S. I. (2016) The Optimization of Bioorthogonal Epitope Ligation within MHC-I Complexes, *ACS Chem Biol* 11, 3172-3178.
47. Schumacher, T. N., Heemels, M. T., Neefjes, J. J., Kast, W. M., Melief, C. J., and Ploegh, H. L. (1990) Direct binding of peptide to empty MHC class I molecules on intact cells and in vitro, *Cell* 62, 563-567.
48. Ljunggren, H. G., Stam, N. J., Ohlen, C., Neefjes, J. J., Hoglund, P., Heemels, M. T., Bastin, J., Schumacher, T. N., Townsend, A., Karre, K., and et al. (1990) Empty MHC class I molecules come out in the cold, *Nature* 346, 476-480.

49. Dubey, P., Hendrickson, R. C., Meredith, S. C., Siegel, C. T., Shabanowitz, J., Skipper, J. C., Engelhard, V. H., Hunt, D. F., and Schreiber, H. (1997) The immunodominant antigen of an ultraviolet-induced regressor tumor is generated by a somatic point mutation in the DEAD box helicase p68, *J Exp Med* 185, 695-705.
50. van der Gracht, A. M. F., de Geus, M. A. R., Camps, M. G. M., Ruckwardt, T. J., Sarris, A. J. C., Bremmers, J., Maurits, E., Pawlak, J. B., Posthoorn, M. M., Bongers, K. M., Filippov, D. V., Overkleeft, H. S., Robillard, M. S., Ossendorp, F., and van Kasteren, S. I. (2018) Chemical Control over T-Cell Activation in Vivo Using Deprotection of trans-Cyclooctene-Modified Epitopes, *ACS Chem Biol* 13, 1569-1576.
51. Messaoudi, I., LeMaout, J., and Nikolic-Zugic, J. (1999) The mode of ligand recognition by two peptide:MHC class I-specific monoclonal antibodies, *J Immunol* 163, 3286-3294.
52. Svoronos, A. A., Bahal, R., Pereira, M. C., Barrera, F. N., Deacon, J. C., Bosenberg, M., DiMaio, D., Glazer, P. M., and Engelman, D. M. (2020) Tumor-Targeted, Cytoplasmic Delivery of Large, Polar Molecules Using a pH-Low Insertion Peptide, *Mol Pharm* 17, 461-471.
53. Joffre, O. P., Segura, E., Savina, A., and Amigorena, S. (2012) Cross-presentation by dendritic cells, *Nat Rev Immunol* 12, 557-569.
54. Zhang, Z., Rohweder, P. J., Ongpipattanakul, C., Basu, K., Bohn, M. F., Dugan, E. J., Steri, V., Hann, B., Shokat, K. M., and Craik, C. S. (2022) A covalent inhibitor of K-Ras(G12C) induces MHC class I presentation of haptened peptide neoepitopes targetable by immunotherapy, *Cancer Cell* 40, 1060-1069 e1067.
55. Zhang, A. Q., Hostetler, A., Chen, L. E., Mukkamala, V., Abraham, W., Padilla, L. T., Wolff, A. N., Maiorino, L., Backlund, C. M., Aung, A., Melo, M., Li, N., Wu, S., and Irvine, D. J. (2023) Universal redirection of CAR T cells against solid tumours via membrane-inserted ligands for the CAR, *Nat Biomed Eng* 7, 1113-1128.
56. Zhao, B., Hou, S., and Ricciardi, R. P. (2003) Chromatin repression by COUP-TFII and HDAC dominates activation by NF-kappaB in regulating major

- histocompatibility complex class I transcription in adenovirus tumorigenic cells, *Virology* 306, 68-76.
57. Dersh, D., Holly, J., and Yewdell, J. W. (2021) A few good peptides: MHC class I-based cancer immunosurveillance and immunoevasion, *Nat Rev Immunol* 21, 116-128.
  58. Sade-Feldman, M., Jiao, Y. J., Chen, J. H., Rooney, M. S., Barzily-Rokni, M., Eliane, J. P., Bjorgaard, S. L., Hammond, M. R., Vitzthum, H., Blackmon, S. M., Frederick, D. T., Hazar-Rethinam, M., Nadres, B. A., Van Severter, E. E., Shukla, S. A., Yizhak, K., Ray, J. P., Rosebrock, D., Livitz, D., Adalsteinsson, V., Getz, G., Duncan, L. M., Li, B., Corcoran, R. B., Lawrence, D. P., Stemmer-Rachamimov, A., Boland, G. M., Landau, D. A., Flaherty, K. T., Sullivan, R. J., and Hacohen, N. (2017) Resistance to checkpoint blockade therapy through inactivation of antigen presentation, *Nat Commun* 8, 1136.
  59. Calcinotto, A., Filipazzi, P., Grioni, M., Iero, M., De Milito, A., Ricupito, A., Cova, A., Canese, R., Jachetti, E., Rossetti, M., Huber, V., Parmiani, G., Generoso, L., Santinami, M., Borghi, M., Fais, S., Bellone, M., and Rivoltini, L. (2012) Modulation of microenvironment acidity reverses anergy in human and murine tumor-infiltrating T lymphocytes, *Cancer Res* 72, 2746-2756.
  60. Lardner, A. (2001) The effects of extracellular pH on immune function, *J Leukoc Biol* 69, 522-530.
  61. Tannock, I. F., and Rotin, D. (1989) Acid pH in tumors and its potential for therapeutic exploitation, *Cancer Res* 49, 4373-4384.
  62. Togashi, Y., Shitara, K., and Nishikawa, H. (2019) Regulatory T cells in cancer immunosuppression - implications for anticancer therapy, *Nat Rev Clin Oncol* 16, 356-371.

## **Chapter 4 Evaluation and Diversification of Small Molecule Inducers of MHC-I Surface Expression**

Adapted from: Kelly, J. J<sup>#</sup>; Newkirk, S, E<sup>#</sup>; Chordia, Mahendra; Pires, M. M., Evaluation and Diversification of Small Molecule Inducers of MHC-I Surface Expression. **2025** bioRxiv 01.31.635109

<sup>#</sup> authors contributed equally

### **4.1 Abstract**

Immunotherapy has emerged as a powerful strategy for combating cancer by harnessing the patient's immune system to recognize and eliminate malignant cells. The major histocompatibility complex class I (MHC-I) has a pivotal role in the recognition step. These surface proteins present cancer-specific neoantigens to CD8<sup>+</sup> T cells, which triggers activation and T cell-mediated killing. However, cancer cells can often evade immune detection by downregulating MHC-I surface expression, which renders the immune response less effective. In turn, this resistance mechanism offers an opportunity to bolster MHC-I surface expression *via* therapeutic interventions. Here, we conducted an initial comprehensive evaluation of previously purported small molecule MHC-I inducers and identified heat shock protein 90 (Hsp90) inhibitors as privileged inducers of MHC-I surface expression. With a core scaffold in hand, we employed an *in situ* click chemistry-based derivatization strategy to generate 380 novel compounds in the same family. New agents from this library showed high levels of induction, with one of the triazole-based analogs, **CiIMB-325**, also enhancing T cell activation and exhibiting lower toxicity, which could potentiate some immunotherapeutic modalities. Moreover, we demonstrated the potential of a click chemistry-based diversification strategy for the discovery of small molecules to counter immune evasion.

### **4.2 Introduction**

The immune system can, often times, be precise, efficient, and powerful in detecting and eliminating cancerous cells. One of the principal mechanisms that the immune system leverages for cancer cell detection is through the presentation of cancer-specific peptides

on the major histocompatibility complex (MHC) of the pathogenic cell.<sup>1</sup> In particular, MHC class I (MHC-I) is a membrane protein expressed on most nucleated cells and is responsible for presenting short (typically 8-12 amino acids long) peptides to CD8+ T cells.<sup>2</sup> Recognition of a peptide-MHC complex (pMHC) by a CD8+ T cell through its T cell receptor (TCR) can result in a cytotoxic response through release of a host of agents including perforin and granzyme B.<sup>3</sup> For a CD8+ T cell to be activated against a target cell (and undergo subsequent phenotypic changes), it must first recognize a 'non-self' peptide which are generated inside the cell and presented on MHC-I. The types of non-self peptides that are typically found on the surface of cancer cells are broadly known as neoantigens.<sup>4</sup>

Neoantigens are generated *via* structural alterations to the proteome of cancer cells through amino acid substitution,<sup>5</sup> post-translational modifications,<sup>6</sup> and other mechanisms.<sup>7</sup> These non-self peptides, which can be loaded on MHC-I for presentation, can potentially engage with TCRs on T cells.<sup>8</sup> Therefore, CD8+ T cells displaying the cognate TCR are well positioned to specifically recognize and respond to neoantigen-presenting cancer cells to promote an anti-cancer immune response.<sup>7</sup> In many instances, these mechanisms are central to eliminate the emergence of cancerous cells. Yet, there is considerable evidence demonstrating that cancer cells can actively avoid immune recognition by CD8+ T cells.<sup>9, 10</sup> These mechanisms of resistance include, but are not limited to, remodeling of the tumor environment to be hypoxic and immunosuppressive,<sup>11-13</sup> increasing expression of immune checkpoint proteins (e.g., programmed death-ligand (PD-L1) and cytotoxic T-lymphocyte associated protein 4 (CTLA-4),<sup>14, 15</sup> promoting the secretion of immunosuppressive cytokines,<sup>16</sup> and downregulating MHC-I molecules.<sup>17</sup> Critically, the downregulation of surface MHC-I can directly impair patient response to programmed cell death protein 1 (PD-1) blockade immunotherapy.<sup>18</sup> Given the tremendous success of cancer immunotherapy that directly relies on MHC-I/TCR engagement, there is a clear need to discover potent agents that promote the expression of MHC-I in cancer patients. By restoring or enhancing MHC-I expression, it may be possible to overcome immune resistance observed in many cancers, thus making the cancer cell more susceptible to T cell-mediated killing (**Figure 4.1**).

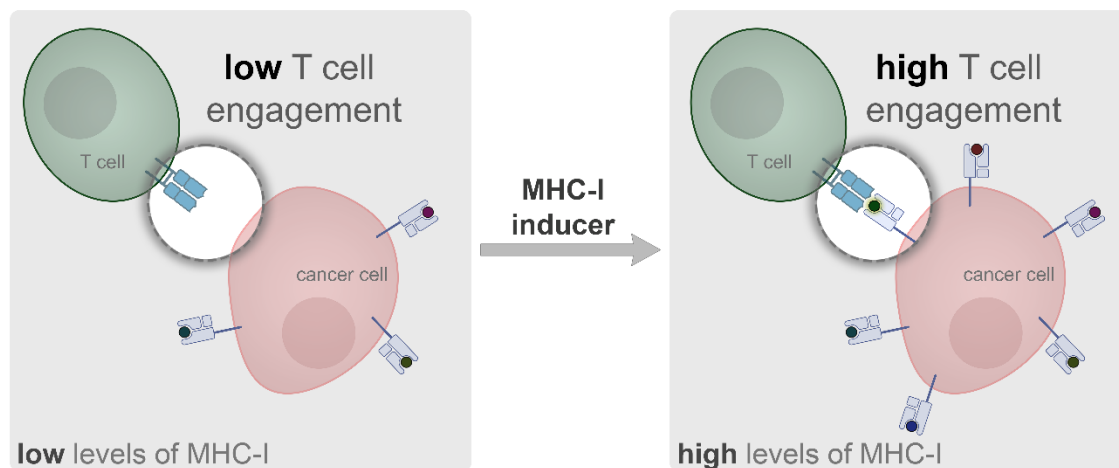


**Figure 4.1.** Schematic representation of strategy to increase MHC-I expression and CD8<sup>+</sup> T cell response. Cancer cells can downregulate the expression of MHC-I as a mechanism of evasion from a patient's immunosurveillance. The use of small molecule inducers could potentially enhance immunotherapeutic approaches that are widely used in the clinic.

The concept of using small molecules to promote the expression of MHC-I is not novel in and of itself. There have been a number of reports that identified compounds with this purported function. These compounds span a diverse set of biological functions and include DNA methyltransferase (DMNT) inhibitors,<sup>19-26</sup> histone deacetylase (HDAC) inhibitors,<sup>27-29</sup> kinase inhibitors,<sup>30</sup> heat shock protein 90 (Hsp90) inhibitors,<sup>31,32</sup> stimulator of interferon genes (STING) agonists,<sup>33-35</sup> and others.<sup>36-39</sup> Although a wider range of FDA approved agents have been screened for MHC-I induction,<sup>40,41</sup> principally, to the best of our knowledge, a definitive comparison across small molecule inducers has not been previously reported. Given the diversity of reagents across the prior reports (e.g., cell lines, antibodies, concentrations, incubation times, etc.), it is critical to first establish the best-in-class scaffold. In this work, we conducted a rigorous head-to-head screen of small molecules to compare their ability to enhance MHC-I surface expression in colorectal cancer cells. Additionally, we show that Hsp90 inhibitors can increase the presentation of cancer-specific neoantigens. With a privileged scaffold in hand, we conducted a high-

throughput diversification screen to generate a range of analogs that could be evaluated for their pharmacological properties.

### 4.3 Results and Discussion

#### 4.3.1 Screening small molecules for their MHC-I upregulation activity

To identify the best-in-class drug scaffold for MHC-I upregulation, a flow cytometry-based assay was developed. Briefly, CT26 murine colorectal cancer cells were incubated with individual members of a library of 25 small molecules that have previously been shown to increase MHC-I expression. These included DNMT, kinase, HDAC, bromodomain and extra-terminal (BET), proteasome, and Hsp90 inhibitors, as well as STING agonists and IMiDs. After cellular treatment with each individual compound, a fluorescent anti-H-2K<sup>d</sup> antibody was used to quantify MHC-I expression *via* flow cytometry (**Figure 4.2A**). As expected at this high concentration, most of these molecules showed an increase in MHC-I surface expression at a concentration of 5  $\mu$ M (**Figure S4.2**). Still, it was notable that some of the molecules did not show any enhancement above background. To identify the most potent inducers of MHC-I surface expression, a second screen was performed at a more stringent concentration of 1  $\mu$ M. Our results showed that three of the small molecules exhibited an increase in MHC-I surface expression above a two-fold cutoff (**Figure 4.2B**). The identified MHC-I enhancers were primarily in two pharmacological classes: DNMT inhibitors (decitabine **1** and guadecitabine **3**) and Hsp90 inhibitors (zelavespib **23**). After incubation of the three lead compounds at a concentration of 500 nM with CT26 cells, it was found that **23** led to higher overall expression of MHC-I on the surface compared to the two DNMT inhibitors (**Figure 4.2C**). Therefore, we decided to focus on Hsp90 inhibitors and expand our search within this class beyond zelavespib in search of the most potent MHC-I inducers.

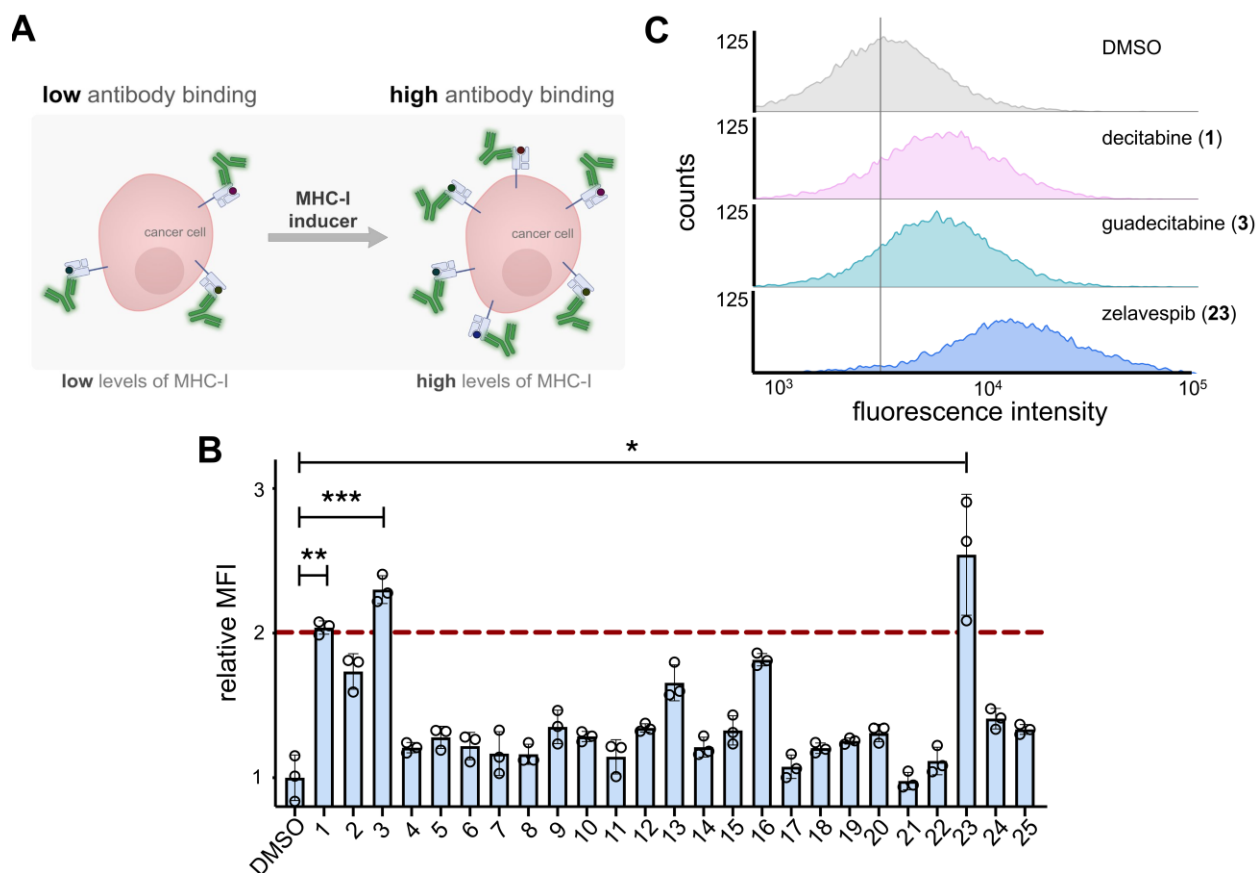


**Figure 4.2** (A) Schematic representation of fluorescent antibody readout for increased MHC-I surface expression upon treatment with small molecules inducers. (B) Flow cytometry analysis of CT26 cells treated with 1  $\mu$ M of indicated compounds. Red dashed lined indicates threshold of 2-fold increase in MHC-I surface expression relative to DMSO control. MFI is the mean fluorescence intensity of the level of fluorescence relative to the DMSO control. Data are represented as mean  $\pm$  SD ( $n=3$ ).  $p$ -values were determined by a two-tailed  $t$ -test (\*  $p < 0.05$ , \*\*  $p < 0.01$ , \*\*\*  $p < 0.001$ ). (C) Flow cytometry histograms of CT26 cells incubated with 500 nM of indicated compounds. H-2K<sup>d</sup> expression was measured by APC anti-mouse H-2K<sup>d</sup> antibody. The vertical grey line represents median fluorescence intensity of DMSO treated cells.

#### 4.3.2 Screening Hsp90 inhibitors for MHC-I Surface upregulation activity

To further explore the relationship between Hsp90 inhibitors and MHC-I surface expression, six additional Hsp90 inhibitors were examined (**Figure 4.3A**). In total within

this sub-library, three of the molecules were from the purine-based family, one from the resorcinol family, and three from the benzoquinone family of Hsp90 inhibitors. To more readily assess their potency, a concentration scan was performed in CT26 cells rather than a single concentration analysis. Our results revealed that all but two (pimipib and tanespimycin) of the Hsp90 inhibitors tested had  $EC_{50}$  values in the nanomolar range for MHC-I surface expression. Among these, it was found that radicicol, BIIB021 and geldanamycin had the lowest  $EC_{50}$  values, at 72, 92, and 144 nM, respectively. Interestingly, together these top hits covered all three primary classes of Hsp90 inhibitors; we pose that this could suggest that Hsp90 inhibition is a primary driver of the phenotypic observation of MHC-I induction. Presumably, if any off-target activity were to be observed and if it were to be the driver of the induction, there is likely to be a single class that is favored. We note that the top hits enhanced MHC-I surface expression in CT26 cells by approximately 5 to 8-fold compared to basal expression levels, a marked increase relative to the initial hit that prompted the focus on Hsp90 inhibitors (**Figure 4.3B**). To ensure that Hsp90 inhibitors could operate in other cellular contexts, we tested them in the human colorectal cancer cell line HCT116 and found them to be effective MHC-I inducers (**Figure 4.3C**). Overall, these results demonstrate that Hsp90 inhibitors are potent inducers of MHC-I surface expression, and this prompted us to further explore them in assembling a larger and more diverse structure activity relationship campaign.

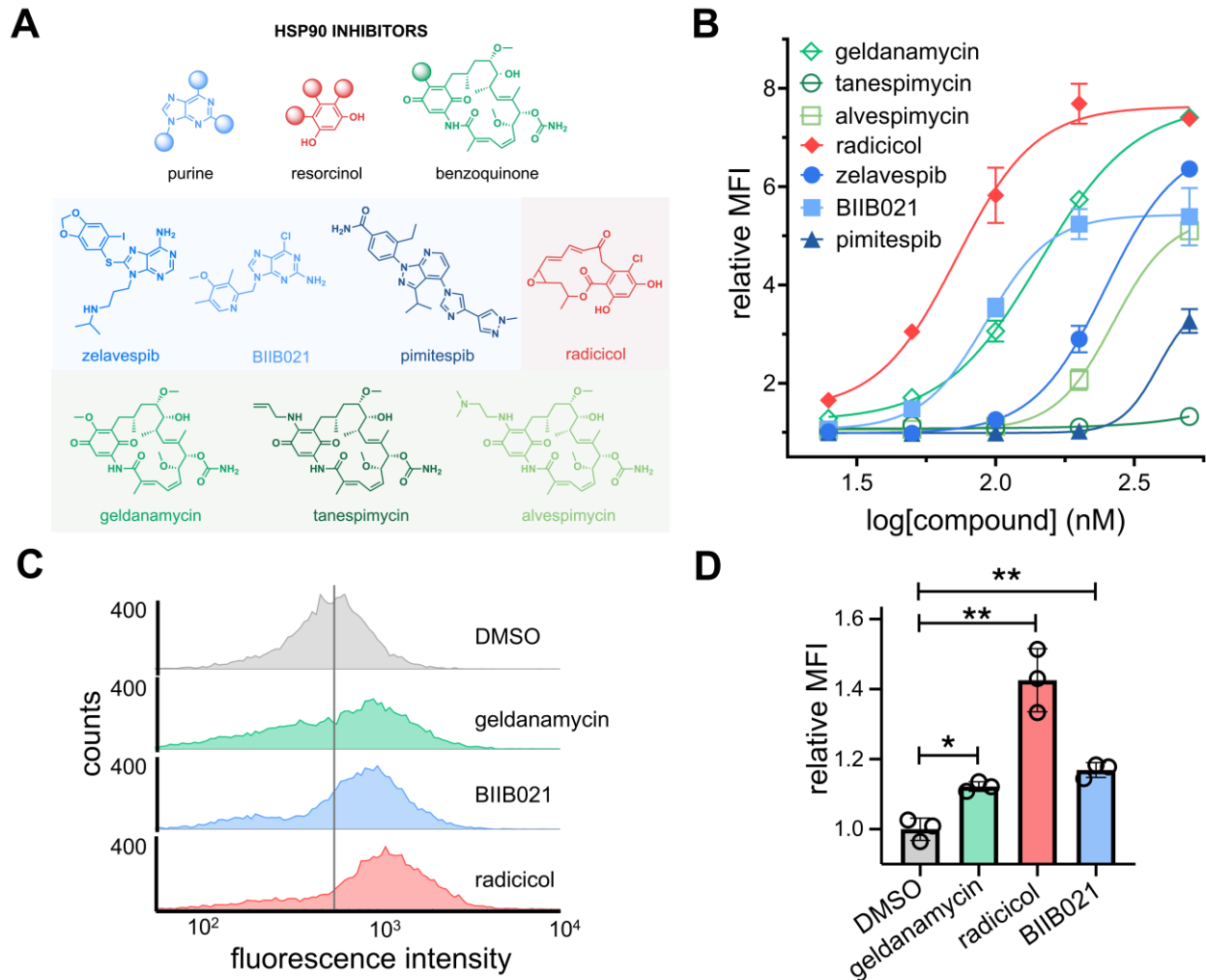


**Figure 4.3** (A) Chemical structures of seven Hsp90 inhibitors tested for their enhancement of MHC-I surface expression. (B) Dose-response analysis by flow cytometry of CT26 cells treated with varying concentrations of seven Hsp90 inhibitors. H-2K<sup>d</sup> expression was measured by APC anti-mouse H-2K<sup>d</sup> antibody. Data are represented as mean  $\pm$  SD ( $n=3$ ), and Boltzmann sigmoidal curves were fitted to the data using GraphPad Prism. EC<sub>50</sub> values are the concentration of compound needed to achieve 50% of the maximal MHC-I surface expression levels. (C) Flow cytometry histograms of HCT116 cells incubated with 200 nM of indicated compounds. HLA-A, B, C surface expression was measured by APC anti-human HLA-A, B, C antibody. The vertical grey line represents median fluorescence intensity of DMSO treated cells. (D) Flow cytometry analysis of MC38-OVA cells treated with 100 nM of indicated compound. SIINFEKL-H2-K<sup>b</sup> expression was measured by APC anti-mouse H-2K<sup>b</sup> bound to

*SIINFEKL antibody. MFI is the mean fluorescence intensity of the level of fluorescence relative to the DMSO control. Data are represented as mean  $\pm$  SD (n=3). p-values were determined by a two-tailed t-test (\*  $p < 0.05$ , \*\*  $p < 0.01$ , \*\*\*\*  $p < 0.0001$ ).*

In theory, the enhancement of MHC-I surface expression should broadly sample a greater breadth of cytosolic peptides including potential neoantigens. This is key because the efficacy of checkpoint blockage therapy relies principally on cytotoxic CD8<sup>+</sup> T cells recognizing neoantigens presented on cancer cell surfaces. We next investigated the potential upregulation of specific antigens from live cells upon their treatment with Hsp90 inhibitors (**Figure 4.3D**). To test this, we used murine MC38-OVA cells which are genetically modified to express the protein ovalbumin (OVA).<sup>42</sup> OVA contains the sequence SIINFEKL, which has been previously used as a model neoantigen. Upon the intracellular processing of OVA and the production of SIINFEKL, it is known that this peptide can be presented by H-2K<sup>b</sup> and is recognized by SIINFEKL-specific CD8<sup>+</sup> T cells.<sup>43</sup> MC38-OVA cells were treated with 100 nM of Hsp90 inhibitors for 48 hours, followed by incubation with a fluorescent antibody specific for H-2K<sup>b</sup> bound to SIINFEKL. Satisfyingly, cellular treatment with Hsp90 inhibitors led to a significant increase in the presentation of the model neoantigen SIINFEKL, indicating that Hsp90 inhibitors can potentially promote the presentation of neoantigen-specific pMHC complexes (**Figure 4.3D**).

#### **4.3.3 High-throughput click chemistry diversification strategy of Hsp90 inhibitor**

With the three top candidates in hand, we sought to further diversify a core scaffold to broadly understand how structure could potentially drive MHC-I upregulation. We posed that a large-scale sub-library around a single agent could provide us with a larger set of agents that can be tested and selected for specific biological properties (e.g., improved toxicity profile, solubility, and selectivity). From the three agents, we moved forward with BIIB021 due to its potency (with many similar structures in clinical evaluation for Hsp90 inhibition)<sup>44-46</sup> and its robust chemical structure. Given the nature of our derivatization strategy, it was important to consider the potential stability of the starting scaffold; both radicicol and geldanamycin have structural fragments that are known to have low inherent chemical stability. Also, the availability of the crystal structure of BIIB021 in complex with

Hsp90 can provide an avenue to understand how the analogs may be interacting with their target protein.<sup>47</sup>

For the generation of the library, we chose to use *in situ* click chemistry. In this format, an alkyne is installed within the core scaffold, and this parent molecule is plated into a microwell plate system with each well containing a new azide-tagged fragment. This approach presents considerable advantages for drug discovery of MHC-I inducers. Click reactions have a high level of specificity and efficiency, particularly exemplified by the Cu(I)-catalyzed azide-alkyne cycloaddition (CuAAC), which enables precise modifications and synthesizes complex molecules with minimal byproducts.<sup>48-50</sup> The versatility inherent in using a library of azides allows for the exploration of diverse molecular combinations and structural variations, essential for identifying drug candidates with optimal pharmacological properties. Moreover, it facilitates the simultaneous screening and synthesis of potential drug candidates, speeding up the identification of active compounds. Recently, this click chemistry-based strategy has been used to identify small molecule modulators of glucagon-like-peptide-1 receptor.<sup>51</sup> It has also been shown with this method that over 80% of azide molecules formed triazole products at yields of 70% or higher.<sup>52</sup>

In the context of our core purine scaffold, we needed to consider a site to install the alkyne handle. From the crystal structure of BIIB021 in complex with Hsp90, we identified the N9 position of the purine core as a solvent-exposed site that is amendable to chemical modification.<sup>47</sup> Moreover, previous reports have demonstrated that this position can be leveraged to access purine-based analogs while retaining Hsp90 inhibition.<sup>53</sup> Therefore, our envisioned approach involved modifying a precursor of BIIB021, 2-amino-6-chloropurine, with an alkyne on the N9 position in order to react it with a library of small molecule azides (**Figure 4.4A**). We reasoned that the resulting triazole ring from the click reaction would structurally mimic the pyridine ring of BIIB021 and allow us to rapidly generate hundreds of derivatives.

To build the alkyne-bearing purine, we reacted 2-amino-6-chloropurine with propargyl bromide to yield the major product 9-propargyl-2-amino-6-chloropurine. The other product was the N7 regioisomer, which was separated during purification. The identity of isolated

N9 alkyne-bearing compound was confirmed by NMR and its purity was analyzed by RP-HPLC. Next, a model *in situ* CuAAC test reaction was performed with the alkyne-modified precursor and a small subset of azide bearing molecules. To cover the potential variability in types of chemical structures found in the full library, we selected a subset of molecules that varied in size, polarity, and steric environment surrounding the azide. Of note, the reactions were performed in microwell plates in an experimental procedure that mimicked the conditions for the eventual *in situ* set of reactions. All three reactions showed a conversion rate of >90% to the triazole product (**Figure S4.3-4.5**). With the model reactions showing high levels of conversion, we reasoned that the reaction conditions were well-suited for a larger screen. The goal of utilizing a larger library was to ensure that modifications to the purine core would cover a large chemical space to broadly sample the engagement with the target. Moreover, given the nature of the phenotypic assay, we reasoned that the diversity of this library could also be important in improving other properties that are necessary for a lead candidate including high accumulation levels, low off-target effects, and reduced toxicity.

In total, 380 azide-containing small molecules were dispensed into wells containing the alkyne-bearing purine analog and the click reaction reagents. After the reaction step, contents of each well were incubated with CT26 cells, and MHC-I induction was monitored by treatment with a fluorescently tagged antibody as previously described. Critically, incubation of CT26 cells with the alkyne precursor alone or the additional click reagents did not result in any increase in MHC-I surface expression (**Figure S4.6**). This indicates that the reaction reagents have no activity on their own. The results from the 380-member screen revealed that four of the click reaction mixtures (3, 27, 325, and 335), showed an increase in MHC-I surface expression above a two-fold cutoff over the DMSO control (**Figure 4.4B**). To further confirm these results, cells were treated with each of four reaction mixtures in a more stringent concentration (theoretically 500 nM, assuming complete conversion). From these results, cell treatment with compound 325 led to the highest levels of MHC-I surface expression (**Figure S4.7**). The click product between the alkyne precursor and compound 325 of the azide library was then synthesized and purified to yield 'Click MHC-I Booster-325 (**CiIMB-325**).

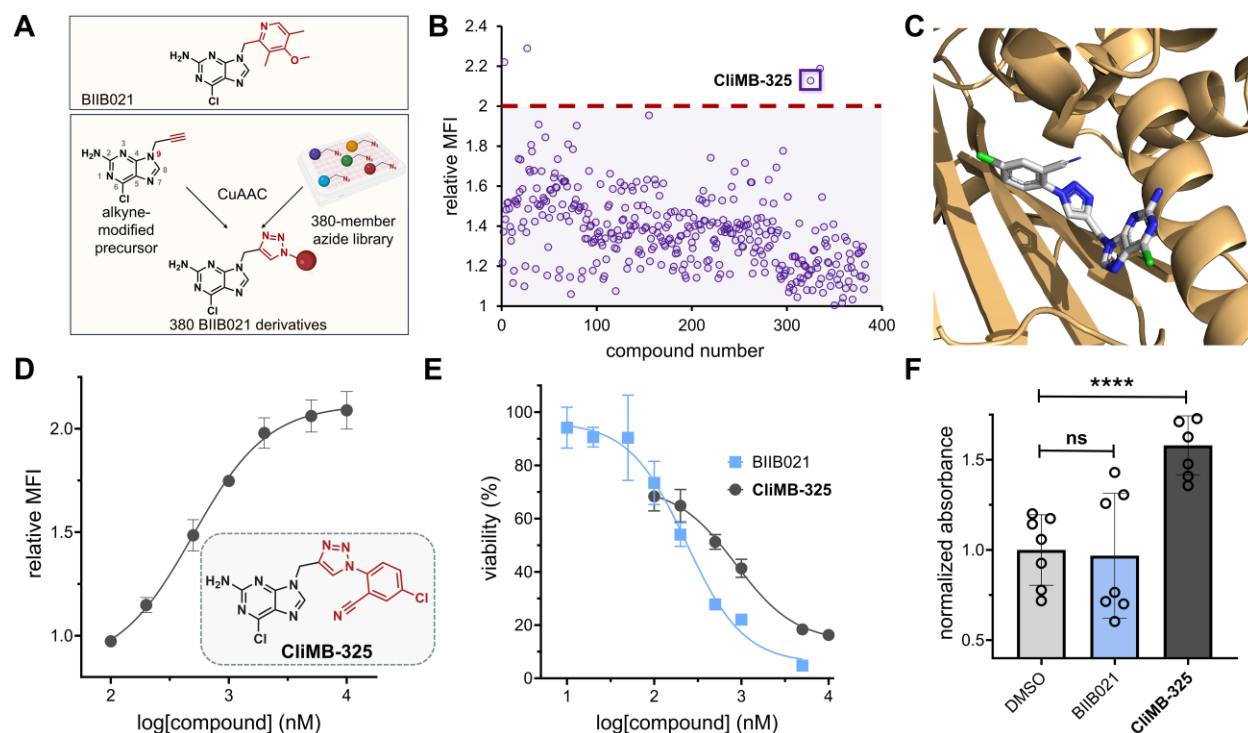


**Figure 4.4** (A) Schematic representation of BIIB021 derivatization strategy. (B) Flow cytometry analysis of CT26 cells treated with click products between 9-propargyl-2-amino-6-chloropurine and the 380-member azide library. H-2K<sup>d</sup> expression was measured by APC anti-mouse H-2K<sup>d</sup> antibody and performed in singlet. Red dashed lined indicates threshold of 2-fold increase in MHC-I surface expression relative to DMSO control. MFI is the mean fluorescence intensity of the level of fluorescence relative to the DMSO control. (C) Stick model of **ClIMB-325** (white) docked into Hsp90 (light orange) was generated using existing crystal structure data (PDB ID: 3qdd) and Rosetta. (D) Dose-response curve and chemical structure of **ClIMB-325**. CT26 cells were treated with varying concentrations of **ClIMB-325**. H-2K<sup>d</sup> expression was measured by APC anti-mouse H-2K<sup>d</sup> antibody via flow cytometry. MFI is the mean fluorescence intensity of the level of fluorescence relative to the DMSO control. Data are represented as mean  $\pm$  SD ( $n=3$ ), and Boltzmann sigmoidal curves were fitted to the data using GraphPad Prism. EC<sub>50</sub> values are the concentration of compound needed to achieve 50% of the maximal MHC-I surface expression levels. (E) Dose-response curves of CT26 cells treated with varying concentrations of **ClIMB-325** or BIIB021

determined via MTT cell viability assay. Data are represented as mean  $\pm$  SD ( $n=4$ ), and nonlinear regression curves were fitted to the data using GraphPad Prism. IC<sub>50</sub> values are the concentration of compound at which maximal cell viability is inhibited by 50%. (F) MC38-OVA cells were incubated with 100 nM BIIB021 and 1  $\mu$ M **ClIMB-325** for 48 hours. Subsequently, cells were co-cultured with B3Z T cells for six hours.  $\beta$ -galactosidase expression was then measured via the colorimetric reagent CPRG on a plate reader at 570 nm. Data are represented as mean  $\pm$  SD ( $n=7$ ).  $p$ -values were determined by a two-tailed  $t$ -test ( $ns$  = not significant, \*\*\*\*  $p < 0.0001$ ).

#### 4.3.4 ClIMB-325 enhances MHC-I surface expression and T cell activation

Finally, we sought to further characterize our novel purine-based lead agent **ClIMB-325**. By docking **ClIMB-325** into Hsp90 using RosettaLigand, we found that **ClIMB-325** binds in a similar manner to BIIB021 (PDB ID: 3qdd) with no measurable deviation in Hsp90 conformation (**Figure 4.4C**). Next, to establish its potency, a concentration scan of **ClIMB-325** was performed using CT26 cells to assess its ability to increase MHC-I expression. Our results showed that **ClIMB-325** retained MHC-I upregulation activity with an EC<sub>50</sub> of 498 nM (**Figure 4.4D**). Given the failed clinical progression of BIIB021 due to toxicity issues,<sup>44</sup> we also performed an MTT cell viability assay comparing BIIB021 with **ClIMB-325**. We found that **ClIMB-325** demonstrated a 3.7-fold improvement in toxicity over its parent compound, BIIB021, with IC<sub>50</sub> values of 861 nM and 233 nM, respectively (**Figure 4.4E**).

Given that the downregulation of MHC-I surface expression reduces T cell recognition of neoantigens, we then sought to investigate whether the upregulation of MHC-I induced by **ClIMB-325** results in enhanced T cell activation. To do so, we used the B3Z T cell hybridoma cell line, which contains OVA-specific TCRs and expresses the enzyme  $\beta$ -galactosidase under the control of an IL-2 inducible promoter. Upon B3Z recognition of the OVA-pMHC complex on OVA expressing cells, the subsequent IL-2 production promotes the expression of  $\beta$ -galactosidase.  $\beta$ -galactosidase activity can then be measured *via* hydrolysis of the reagent chlorophenol red- $\beta$ -galactopyranoside (CPRG) which leads to a color change that is reflective of T cell activation levels.<sup>54</sup> MC38-OVA cells were incubated with BIIB021 and **ClIMB-325** for 48 hours before being co-cultured

with B3Z T cells. While TCR activation in cells treated with BIIB021 did not significantly differ from the DMSO control, MC38-OVA cells treated with **CiIMB-325** exhibited a nearly 1.6-fold increase in TCR activation levels (**Figure 4.4F**). Overall, these results validate the use of a high-throughput click chemistry screen to generate bioactive compounds with MHC-I upregulation activity.

#### *4.4 Conclusion*

Here, we have identified compounds that have immunomodulatory effects on colorectal cancer cell lines. Hsp90 inhibitors were found to be among the most potent class of molecules tested that increase MHC-I surface expression as well as promote the display of cancer-specific neoantigens for CD8<sup>+</sup> T cell recognition. Leveraging an Hsp90 inhibitor core scaffold, we have also demonstrated as proof-of-concept a novel high-throughput click chemistry-based screening platform for the discovery of molecules with immunomodulatory activity. While our initial screen utilized a 380-member azide library, we plan to expand to a 1,200-member azide library to sample a wider chemical space for molecules that upregulate MHC-I. Additionally, beyond the purine-based scaffold used in this study, we intend to extend this strategy to resorcinol and benzoquinone-based scaffolds, which have also been favored for the development of new Hsp90 inhibitors.<sup>55-60</sup> Ultimately, however, we envision that our approach of modifying preexisting chemical scaffolds with alkynes for large-scale click chemistry-based derivatization can be broadly applicable for various phenotypic screens beyond MHC-I upregulation.

Counteracting cancer immune evasion mechanisms is necessary to enhance the efficacy of immunotherapy treatments. To this point, a significant portion of patients fail to respond to PD-1 blockade therapy due to the development of resistant tumors resulting from MHC-I downregulation.<sup>18</sup> This challenge underscores the need to reengage the immune system by converting immunologically 'cold' tumors back into 'hot' tumors that can be recognized and targeted for elimination. Therefore, we anticipate that developing a widely applicable approach to increase MHC-I surface expression is a promising avenue to combat resistant cancer.

## 4.5 Summary and Future Outlook

Here, we investigated how diverse classes of small molecules modulate MHC-I surface expression on cancer cells. We identified a best-in-class scaffold for enhancing MHC-I expression in colorectal cancer cells and developed a high-throughput derivatization strategy to discover additional immunomodulatory compounds. Building on this, we are expanding our scaffold library to improve our structure-activity relationship analysis and optimize efficacy. With a 4,000-member azide library in hand, we aim to scale our efforts by an order of magnitude to explore a broader chemical space and identify high-priority candidates. Finally, we will assess the *in vivo* activity of MHC-I upregulating compounds in combination with checkpoint inhibitors to evaluate potential synergy in enhancing anti-tumor immunity.

Most small molecule drugs exhibit some degree of polypharmacology, engaging multiple protein targets rather than acting exclusively on their intended target, which can lead to diverse biological effects. Even highly selective small molecules can still induce unexpected phenotypic outcomes in patients. We hypothesized here that some of the anti-cancer activity of small-molecule drugs may arise from enhancing immune system interactions with cancer cells rather than solely through their proposed primary mechanism of action. Since small molecule efficacy is primarily optimized using *in vitro* cell culture models, which typically lack immune components, the extent to which the immune system contributes to their anti-cancer effects remains incompletely understood. Obtaining a deeper understanding of these immune-modulatory effects could inform the development of combination therapies that enhance anti-tumor activity.

## 4.6 Material and Methods

**Materials.** All library compounds were purchased from either Selleck Chemicals, AK Scientific, A2B Chem, MedChemExpress, GlpBio, Cayman Chemical Company, or AmBeed. Compounds were solubilized in DMSO and stored at -20°C. Recombinant murine and human IFN- $\gamma$  were purchased from PeproTech. APC-labeled antibodies against H-2K<sup>d</sup>/H-2D<sup>d</sup>, HLA-A,B,C, and H-2K<sup>b</sup> bound to SIINFEKL were purchased from BioLegend. The library of 380 azide-containing small molecules were purchased from

Enamine (catalog # AZD-380-X-100). For the synthesis of **ClIMB-325**, 2-amino-6-chloropurine was purchased from AmBeed (catalog # A135577) and 2-azido-5-chlorobenzonitrile was purchased from Enamine (catalog # EN300-279694). Dulbecco's Modified Eagle's Medium (DMEM), Roswell Park Memorial Institute (RPMI) 1640 medium, and McCoy's 5A medium were purchased from VWR. Fetal Bovine Serum (FBS) and penicillin-streptomycin were purchased from Sigma-Aldrich.

**Mammalian Cell Culture.** CT26 cells were cultured in RPMI 1640 media supplemented with 10% fetal bovine serum, 50 IU/mL penicillin, and 50 µg/mL streptomycin. HCT116 cells were kindly provided by Dr. Anja-Katrin Bielinsky and were cultured in McCoy's 5A media supplemented with 10% fetal bovine serum, 50 IU/mL penicillin, 50 µg/mL streptomycin, and 2 mM GlutaMAX. MC38-OVA cells were kindly provided by Dr. Mirna Perusina Lanfranca and were cultured in DMEM supplemented with 10% fetal bovine serum, 50 IU/mL penicillin, 50 µg/mL streptomycin, 50 µg/mL gentamycin, and 10 µg/mL blasticidin. B3Z cells were kindly provided by Dr. Aaron Esser-Kahn and maintained in RPMI 1640 media supplemented with 10% fetal bovine serum, 50 IU/mL penicillin, and 50 µg/mL streptomycin. All cells were cultured in T75 flasks and maintained in a humidified atmosphere of 5% CO<sub>2</sub> at 37°C.

**Flow Cytometry-Based Assays.**  $1.5 \times 10^4$  cells were seeded in a treated 96-well plate along with indicated concentrations of library compounds at 37°C. After 48 hours, cells were washed once with PBS, removed using TrypLE™ Express Enzyme (Thermo Fisher), and transferred to a round-bottom 96-well plate. Transferred cells were centrifuged (1100 x g, 5 min) in a Thermo Scientific Jouan C4i centrifuge, and the cell pellets were resuspended and fixed in 4% formaldehyde solution for 20 minutes. The plate was centrifuged (1100 x g, 5 min) and pelleted cells were resuspended in a 1:100 dilution of indicated fluorescence antibodies in culture media for 1 hour at 4°C. Flow cytometry was performed using the following antibodies: APC anti-mouse H-2K<sup>d</sup>/H-2D<sup>d</sup> (clone 34-1-2S), APC anti-human HLA-A,B,C (clone W6/32), or APC anti-mouse H-2K<sup>b</sup> bound to SIINFEKL (clone 25-D1.16). Cells were analyzed using an Attune NxT Flow Cytometer (Thermo Fisher) equipped with a 637 nm laser with 670/14 nm bandpass filter.

**MTT Cell Viability Assay.**  $1.5 \times 10^4$  CT26 cells were seeded in a treated 96-well plate, either with or without compounds (BIIB021 and **ClIMB-325**) at indicated concentrations at 37°C. After 48 hours, a solution of MTT in PBS (filter sterilized through a 0.2- $\mu$ M filter) was added to each well to achieve a final concentration of 0.45 mg/mL. After incubating at 37°C for 2 hours, cells were centrifuged (1100 x g, 5 min) in a Thermo Scientific Jouan C4i centrifuge and the supernatant was removed. 100  $\mu$ L of DMSO was added to each well to dissolve the formation of formazan precipitate. The absorbance of the solution in each well was read at 570 nm using a BioTek Synergy H1 Microplate Reader. Wells containing no cells (only the added DMSO) were used as a negative control for viability, while untreated cells served as the positive control for 100% viability.

**B3Z T Cell Activation.**  $1.5 \times 10^4$  MC38-OVA cells were seeded in a treated 96 well plate, either with or without compounds (BIIB021 and **ClIMB-325**) at indicated concentrations at 37°C. After 48 hours, the culture media was replaced with media containing  $10^5$  B3Z cells, which were co-incubated with the MC38-OVA cells for 6 hours. Cells were centrifuged (1100 x g, 5 min) in a Thermo Scientific Jouan C4i centrifuge and the supernatant was removed. Lysis buffer containing 0.2% saponin, 500 mM CPRG reagent, 20 mM  $\text{MgCl}_2$ , and 100 mM  $\beta$ -mercaptoethanol in 1X PBS was added to each well. After 45 minutes, absorbance at 570 nm was recorded using a BioTek Synergy H1 Microplate Reader.

**Molecular Docking Studies.** Conformational predictions of **ClIMB-325** in Hsp90 were performed using RosettaLigand using the crystal structure of BIIB021 bound to Hsp90 (PDB ID: 3qdd). Native crystal structure was prepared for docking by removing all water molecules and co-crystallized ligands. PyMOL was used for visualization of the docking results.

## 4.7 Supplementary Figures

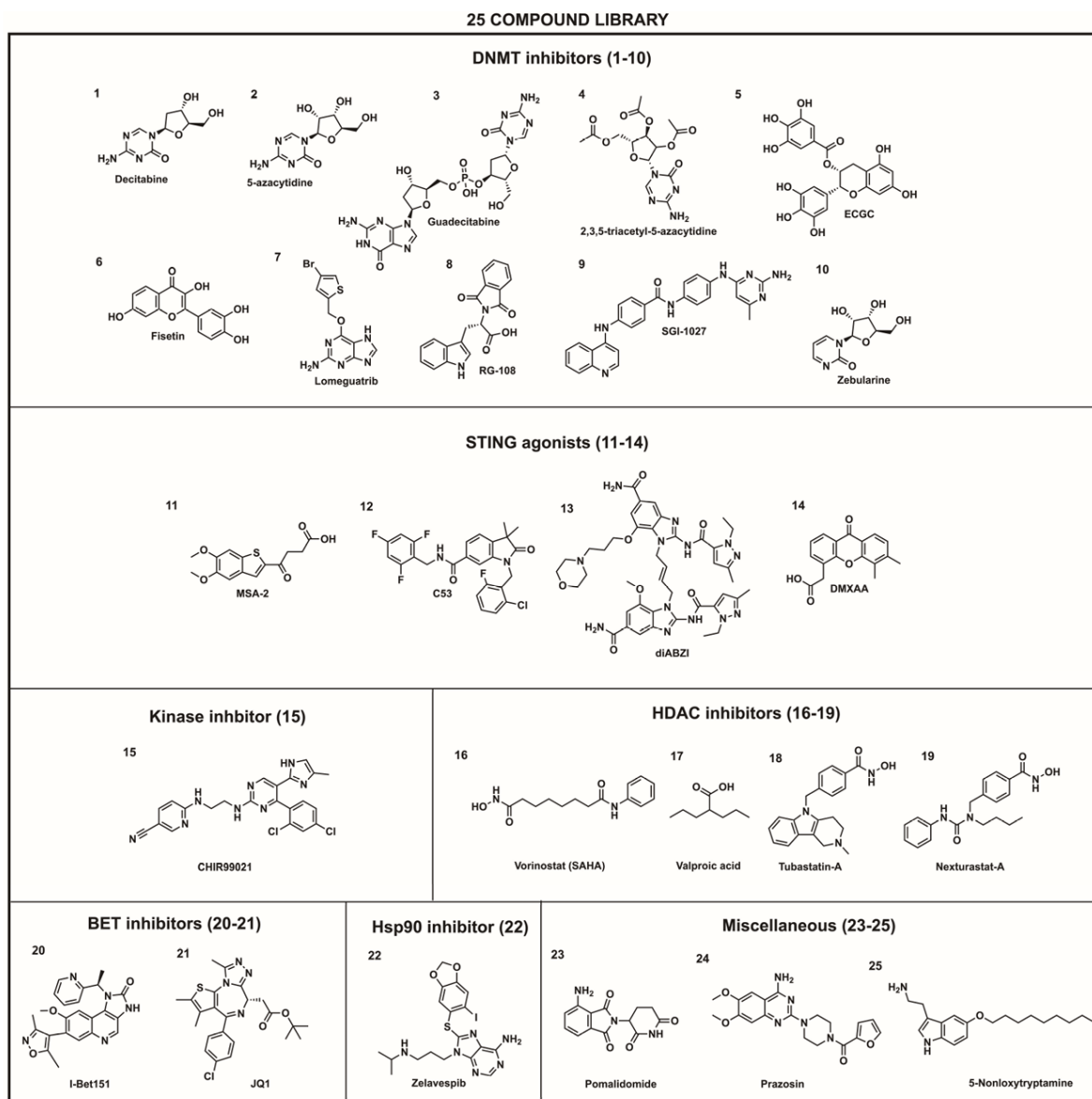


**Figure S4.1.** Structures of 25 compounds in library of small molecule MHC-I inducers, subdivided by class. Compounds 1-10 are DNMT inhibitors, 11-14 are STING agonists, 15 is a kinase inhibitor, 16-19 are HDAC inhibitors, 20-21 are BET inhibitors, 22 is an Hsp90 inhibitor, and 23-25 are miscellaneous compounds.

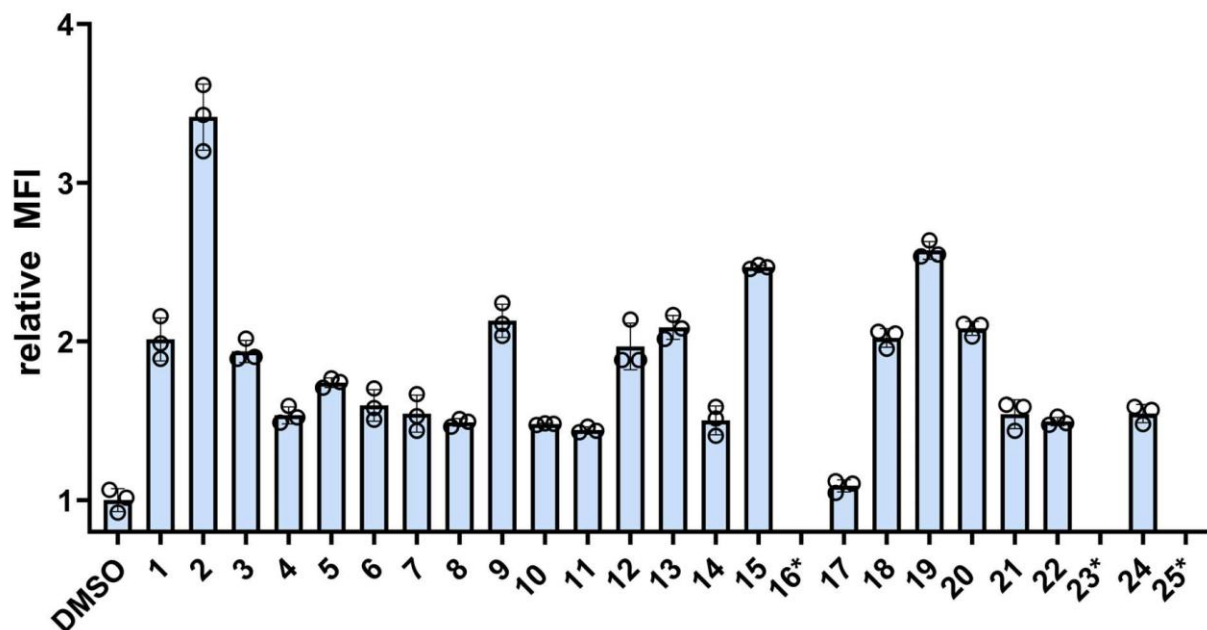


**Figure S4.2.** Flow cytometry analysis of CT26 cells treated with 25-member library at 5  $\mu\text{M}$ . H-2Kd surface expression was measured by APC-conjugated anti-mouse H-2Kd antibody. MFI means fluorescence intensity of the level of fluorescence relative to the DMSO control. Compounds containing no data bar and denoted with \* indicate that the compound was toxic to the cells at 5  $\mu\text{M}$  concentration. Data are represented as mean  $\pm$  SD ( $n=3$ ).

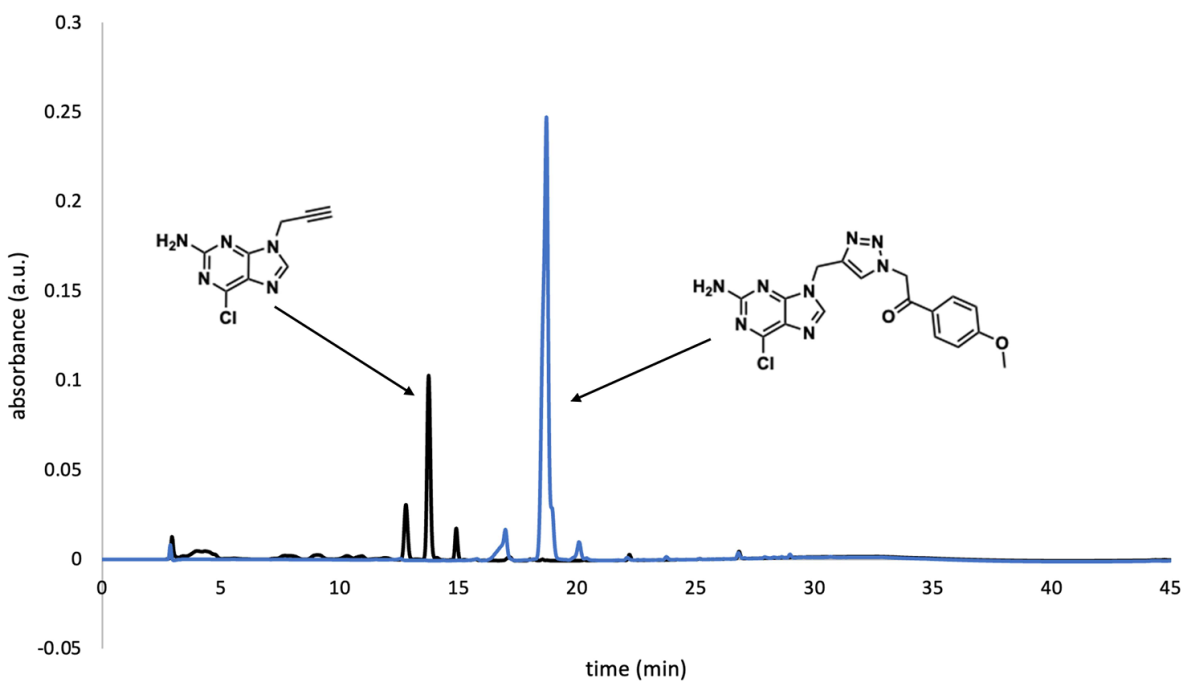


**Figure S4.3.** Analytical HPLC of reaction between 9-propargyl-2-amino-6-chloropurine and 2-azido-1-(4-methoxy-phenyl)-ethanone. 9-propargyl-2-amino-6-chloropurine and 2-azido-1-(4-methoxy-phenyl)-ethanone, each at a concentration of 10 mM, were reacted with 40 mM L-ascorbic acid and 2 mM CuSO<sub>4</sub>/THPTA in a 3:2 ratio of DMSO to water, with a total reaction volume of 100  $\mu$ L. Overlaid HPLC chromatograms of reaction mixture prior to addition of 2-azido-1-(4-methoxy-phenyl)-ethanone (black) and the full reaction mixture after incubation shaking at 37  $^{\circ}$ C for 20 h (blue) are shown.

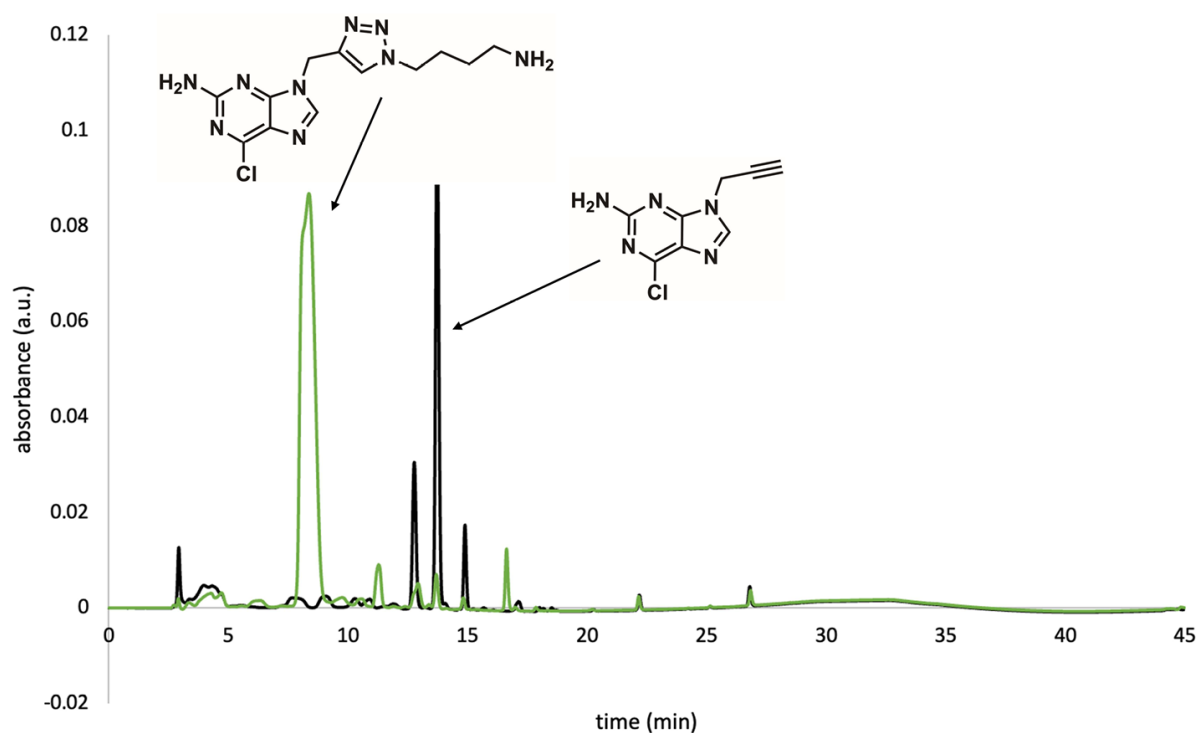


**Figure S4.4.** Analytical HPLC of reaction between 9-propargyl-2-amino-6-chloropurine and 4-azido-1-butanamine. 9-propargyl-2-amino-6-chloropurine and 4-azido-1-butanamine, each at a concentration of 10 mM, were reacted with 40 mM L-ascorbic acid and 2 mM CuSO<sub>4</sub>/THPTA in a 3:2 ratio of DMSO to water, with a total reaction volume of 100  $\mu$ L. Overlaid HPLC chromatograms of reaction mixture prior to addition of 4-azido-1 butanamine (black) and the full reaction mixture after incubation shaking at 37  $^{\circ}$ C for 20 h (green) are shown.

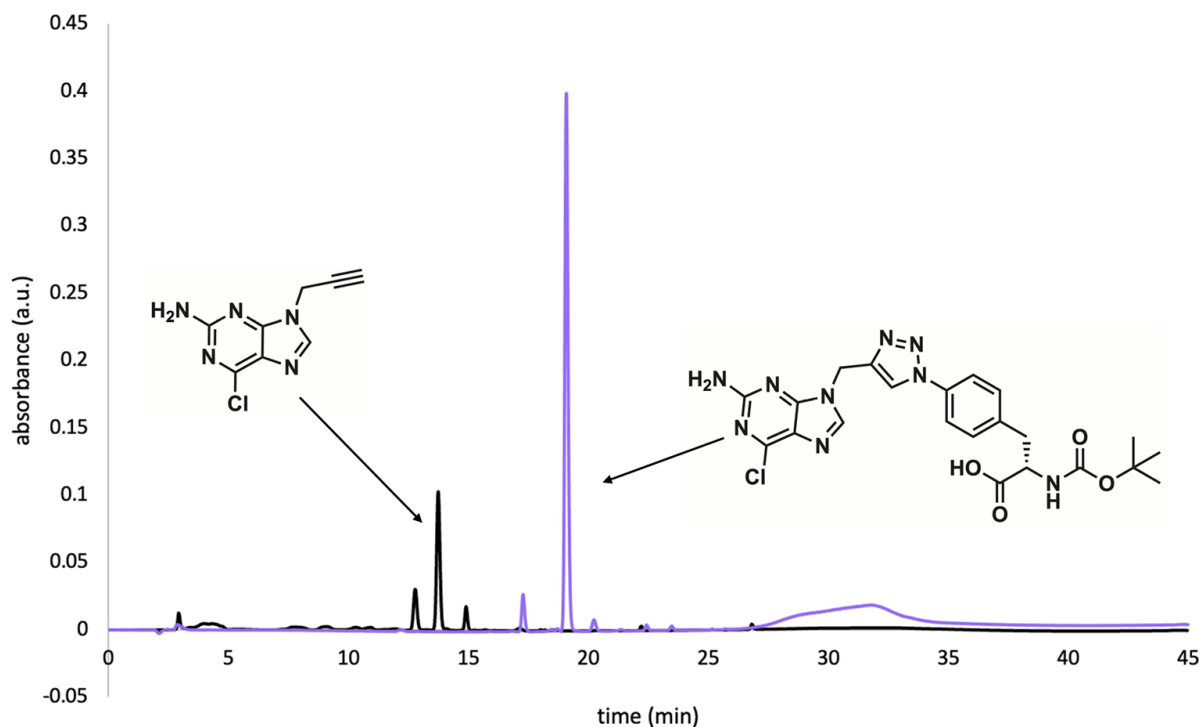


**Figure S4.5.** Analytical HPLC of reaction between 9-propargyl-2-amino-6-chloropurine and Boc-4-azido-L-phenylalanine. 9-propargyl-2-amino-6-chloropurine and Boc-4-azido-L-phenylalanine, each at a concentration of 10 mM, were reacted with 40 mM L-ascorbic acid and 2 mM CuSO<sub>4</sub>/THPTA in a 3:2 ratio of DMSO to water, with a total reaction volume of 100  $\mu$ L. Overlaid HPLC chromatograms of reaction mixture prior to addition of Boc-4 azido-L-phenylalanine (black) and the full reaction mixture after incubation shaking at 37  $^{\circ}$ C for 20 h (purple) are shown.

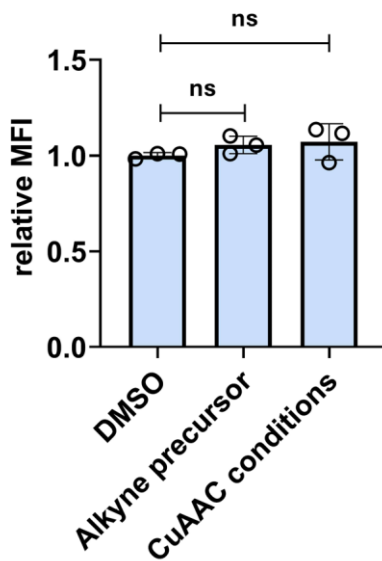


**Figure S4.6.** Flow cytometry analysis of CT26 cells treated with 1  $\mu$ M 9-propargyl-2-amino 6-chloropurine or a 1:10,000 dilution of CuAAC click reagents. H-2Kd expression was measured by APC anti-mouse H-2Kd antibody. MFI is mean fluorescence intensity of the level of fluorescence relative to the DMSO control. Data are represented as mean  $\pm$  SD ( $n=3$ ).  $P$ -values were determined by a two-tailed  $t$ -test (ns = not significant).

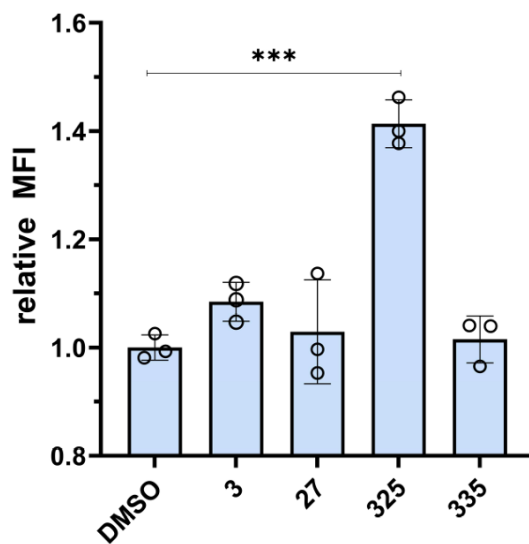
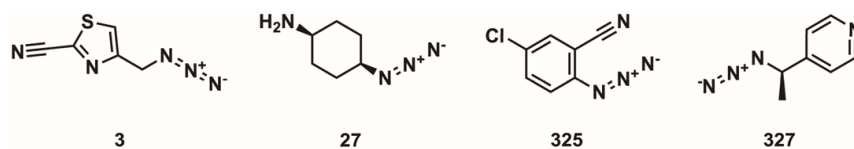


**Figure S4.7.** Structures of the four azide-containing small molecules from 380 compound library screen that resulted in the greatest fold change over background in MHC-I surface expression when reacted with 9-propargyl-2-amino-6-chloropurine. Flow cytometry analysis of CT26 cells treated with 1:20,000 dilution of click reaction mixtures containing azides 3, 27, 325, and 335. H-2K<sup>d</sup> expression was measured by APC anti-mouse H-2K<sup>d</sup> antibody. MFI means fluorescence intensity of the level of fluorescence relative to the DMSO control. Data are represented as mean  $\pm$  SD ( $n=3$ ).  $p$  values were determined by a two-tailed  $t$ -test (\*\*\*)  $p < 0.001$ .

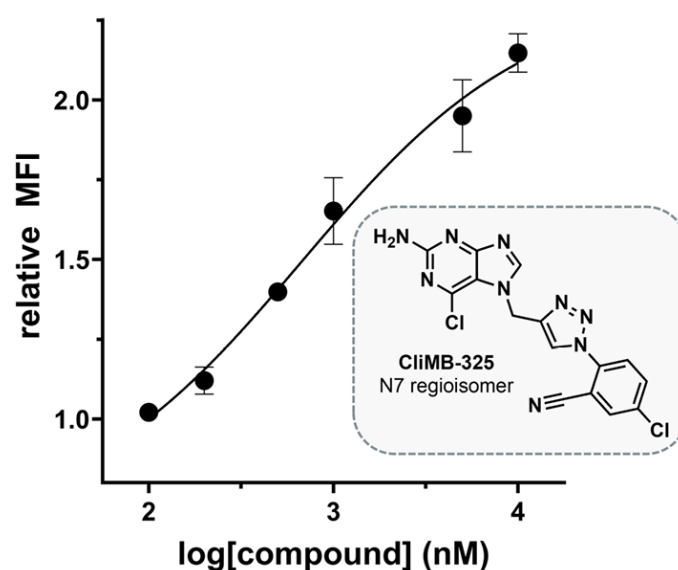


**Figure S4.8.** Dose-response curve and chemical structure of the regioisomer of ClIMB 325, formed from a reaction between the minor N7 regioisomer of the alkyne-modified BIIB021 precursor (7-propargyl-2-amino-6-chloropurine) and 2-azido-5-chlorobenzonitrile (azide 325 from 380 compound screen). CT26 cells were treated with varying concentrations of the ClIMB-325 regioisomer. H-2K<sup>d</sup> expression was measured by APC anti-mouse H-2K<sup>d</sup> antibody via flow cytometry. MFI means fluorescence intensity of the level of fluorescence relative to the DMSO control. Data are represented as mean  $\pm$  SD ( $n=3$ ), and Boltzmann sigmoidal curves were fitted to the data using GraphPad Prism.  $EC_{50}$  values are the concentration of compound needed to achieve 50% of the maximal MHC-I surface expression levels.

#### 4.8 References

1. Dersh, D.; Holly, J.; Yewdell, J. W. A few good peptides: MHC class I-based cancer immunosurveillance and immunoevasion. *Nat Rev Immunol* **2021**, *21* (2), 116-128. DOI: 10.1038/s41577-020-0390-6 From NLM Medline.
2. Neefjes, J.; Jongstra, M. L.; Paul, P.; Bakke, O. Towards a systems understanding of MHC class I and MHC class II antigen presentation. *Nat Rev Immunol* **2011**, *11* (12), 823-836. DOI: 10.1038/nri3084 From NLM Medline.
3. Huppa, J. B.; Davis, M. M. T-cell-antigen recognition and the immunological synapse. *Nat Rev Immunol* **2003**, *3* (12), 973-983. DOI: 10.1038/nri1245 From NLM Medline.
4. Boon, T.; Van Pel, A.; De Plaen, E.; Chomez, P.; Lurquin, C.; Szikora, J. P.; Sibille, C.; Mariame, B.; Van den Eynde, B.; Lethe, B.; et al. Genes coding for T-cell-defined tumour transplantation antigens: point mutations, antigenic peptides, and subgenomic expression. *Cold Spring Harbor Symp Quant Biol* **1989**, *54 Pt 1*, 587-596. DOI: 10.1101/sqb.1989.054.01.070 From NLM Medline.
5. Mardis, E. R. Neoantigens and genome instability: impact on immunogenomic phenotypes and immunotherapy response. *Genome Med* **2019**, *11* (1), 71. DOI: 10.1186/s13073-019-0684-0 From NLM Medline.
6. Kacen, A.; Javitt, A.; Kramer, M. P.; Morgenstern, D.; Tsaban, T.; Shmueli, M. D.; Teo, G. C.; da Veiga Leprevost, F.; Barnea, E.; Yu, F.; et al. Post-translational modifications reshape the antigenic landscape of the MHC I immunopeptidome in tumors. *Nat Biotechnol* **2023**, *41* (2), 239-251. DOI: 10.1038/s41587-022-01464-2 From NLM Medline.
7. Xie, N.; Shen, G.; Gao, W.; Huang, Z.; Huang, C.; Fu, L. Neoantigens: promising targets for cancer therapy. *Signal Transduct Target Ther* **2023**, *8* (1), 9. DOI: 10.1038/s41392-022-01270-x From NLM Medline.
8. Kelly, J. J.; Bloodworth, N.; Shao, Q.; Shabanowitz, J.; Hunt, D.; Meiler, J.; Pires, M. M. A Chemical Approach to Assess the Impact of Post-translational Modification on MHC Peptide Binding and Effector Cell Engagement. *ACS Chem Biol* **2024**, *19* (9), 1991-2001. DOI: 10.1021/acscchembio.4c00312 From NLM Medline.
9. Roerden, M.; Spranger, S. Cancer immune evasion, immunoeediting and intratumour heterogeneity. *Nat Rev Immunol* **2025**. DOI: 10.1038/s41577-024-01111-8 From NLM Publisher.
10. Galassi, C.; Chan, T. A.; Vitale, I.; Galluzzi, L. The hallmarks of cancer immune evasion. *Cancer Cell* **2024**, *42* (11), 1825-1863. DOI: 10.1016/j.ccell.2024.09.010 From NLM Medline.

11. Fu, Z.; Mowday, A. M.; Smaill, J. B.; Hermans, I. F.; Patterson, A. V. Tumour Hypoxia-Mediated Immunosuppression: Mechanisms and Therapeutic Approaches to Improve Cancer Immunotherapy. *Cells* **2021**, *10* (5). DOI: 10.3390/cells10051006 From NLM Medline.
12. Warburg, O. On the origin of cancer cells. *Science* **1956**, *123* (3191), 309-314. DOI: 10.1126/science.123.3191.309 From NLM Medline.
13. Li, Y.; Patel, S. P.; Roszik, J.; Qin, Y. Hypoxia-Driven Immunosuppressive Metabolites in the Tumor Microenvironment: New Approaches for Combinational Immunotherapy. *Front Immunol* **2018**, *9*, 1591. DOI: 10.3389/fimmu.2018.01591 From NLM PubMed-not-MEDLINE.
14. He, X.; Xu, C. Immune checkpoint signaling and cancer immunotherapy. *Cell Res* **2020**, *30* (8), 660-669. DOI: 10.1038/s41422-020-0343-4 From NLM Medline.
15. Dong, H.; Strome, S. E.; Salomao, D. R.; Tamura, H.; Hirano, F.; Flies, D. B.; Roche, P. C.; Lu, J.; Zhu, G.; Tamada, K.; et al. Tumor-associated B7-H1 promotes T-cell apoptosis: a potential mechanism of immune evasion. *Nat Med* **2002**, *8* (8), 793-800. DOI: 10.1038/nm730 From NLM Medline.
16. Tie, Y.; Tang, F.; Wei, Y. Q.; Wei, X. W. Immunosuppressive cells in cancer: mechanisms and potential therapeutic targets. *J Hematol Oncol* **2022**, *15* (1), 61. DOI: 10.1186/s13045-022-01282-8 From NLM Medline.
17. Taylor, B. C.; Balko, J. M. Mechanisms of MHC-I Downregulation and Role in Immunotherapy Response. *Front Immunol* **2022**, *13*, 844866. DOI: 10.3389/fimmu.2022.844866 From NLM Medline.
18. Zaretsky, J. M.; Garcia-Diaz, A.; Shin, D. S.; Escuin-Ordinas, H.; Hugo, W.; Hu-Lieskovan, S.; Torrejon, D. Y.; Abril-Rodriguez, G.; Sandoval, S.; Barthly, L.; et al. Mutations Associated with Acquired Resistance to PD-1 Blockade in Melanoma. *N Engl J Med* **2016**, *375* (9), 819-829. DOI: 10.1056/NEJMoa1604958 From NLM Medline.
19. Russo, S.; Feola, S.; Feodoroff, M.; Chiaro, J.; Antignani, G.; Fucciello, M.; D'Alessio, F.; Hamdan, F.; Pellinen, T.; Molsa, R.; et al. Low-dose decitabine enhances the efficacy of viral cancer vaccines for immunotherapy. *Mol Ther Oncol* **2024**, *32* (1), 200766. DOI: 10.1016/j.omton.2024.200766 From NLM PubMed-not-MEDLINE.
20. Fonsatti, E.; Nicolay, H. J.; Sigalotti, L.; Calabro, L.; Pezzani, L.; Colizzi, F.; Altomonte, M.; Guidoboni, M.; Marincola, F. M.; Maio, M. Functional up-regulation of human leukocyte antigen class I antigens expression by 5-aza-2'-deoxycytidine in cutaneous melanoma:

- immunotherapeutic implications. *Clin Cancer Res* **2007**, *13* (11), 3333-3338. DOI: 10.1158/1078-0432.CCR-06-3091 From NLM Medline.
21. Terracina, K. P.; Graham, L. J.; Payne, K. K.; Manjili, M. H.; Baek, A.; Damle, S. R.; Bear, H. D. DNA methyltransferase inhibition increases efficacy of adoptive cellular immunotherapy of murine breast cancer. *Cancer Immunol Immunother* **2016**, *65* (9), 1061-1073. DOI: 10.1007/s00262-016-1868-8 From NLM Medline.
22. Ma, R.; Rei, M.; Woodhouse, I.; Ferris, K.; Kirschner, S.; Chandran, A.; Gileadi, U.; Chen, J. L.; Pereira Pinho, M.; Ariosa-Morejon, Y.; et al. Decitabine increases neoantigen and cancer testis antigen expression to enhance T-cell-mediated toxicity against glioblastoma. *Neuro Oncol* **2022**, *24* (12), 2093-2106. DOI: 10.1093/neuonc/noac107 From NLM Medline.
23. Krishnadas, D. K.; Bao, L.; Bai, F.; Chencheri, S. C.; Lucas, K. Decitabine facilitates immune recognition of sarcoma cells by upregulating CT antigens, MHC molecules, and ICAM-1. *Tumour Biol* **2014**, *35* (6), 5753-5762. DOI: 10.1007/s13277-014-1764-9 From NLM Medline.
24. Son, C. H.; Lee, H. R.; Koh, E. K.; Shin, D. Y.; Bae, J. H.; Yang, K.; Park, Y. S. Combination treatment with decitabine and ionizing radiation enhances tumor cells susceptibility of T cells. *Sci Rep* **2016**, *6*, 32470. DOI: 10.1038/srep32470 From NLM Publisher.
25. Pappalardi, M. B.; Keenan, K.; Cockerill, M.; Kellner, W. A.; Stowell, A.; Sherk, C.; Wong, K.; Pathuri, S.; Briand, J.; Steidel, M.; et al. Discovery of a first-in-class reversible DNMT1-selective inhibitor with improved tolerability and efficacy in acute myeloid leukemia. *Nat Cancer* **2021**, *2* (10), 1002-1017. From NLM Medline.
26. Coral, S.; Sigalotti, L.; Gasparollo, A.; Cattarossi, I.; Visintin, A.; Cattelan, A.; Altomonte, M.; Maio, M. Prolonged upregulation of the expression of HLA class I antigens and costimulatory molecules on melanoma cells treated with 5-aza-2'-deoxycytidine (5-AZA-CdR). *J Immunother* **1999**, *22* (1), 16-24. DOI: 10.1097/00002371-199901000-00003 From NLM Medline.
27. Mora-Garcia Mde, L.; Duenas-Gonzalez, A.; Hernandez-Montes, J.; De la Cruz-Hernandez, E.; Perez-Cardenas, E.; Weiss-Steider, B.; Santiago-Osorio, E.; Ortiz-Navarrete, V. F.; Rosales, V. H.; Cantu, D.; et al. Up-regulation of HLA class-I antigen expression and antigen-specific CTL response in cervical cancer cells by the demethylating agent hydralazine and the histone deacetylase inhibitor valproic acid. *J Transl Med* **2006**, *4*, 55. DOI: 10.1186/1479-5876-4-55 From NLM PubMed-not-MEDLINE.
28. Woan, K. V.; Lienlaf, M.; Perez-Villaroel, P.; Lee, C.; Cheng, F.; Knox, T.; Woods, D. M.;

- Barrios, K.; Powers, J.; Sahakian, E.; et al. Targeting histone deacetylase 6 mediates a dual anti-melanoma effect: Enhanced antitumor immunity and impaired cell proliferation. *Mol Oncol* **2015**, *9* (7), 1447-1457. DOI: 10.1016/j.molonc.2015.04.002 From NLM Medline.
29. Narukawa, T.; Yasuda, S.; Horinaka, M.; Taniguchi, K.; Tsujikawa, T.; Morita, M.; Ukimura, O.; Sakai, T. The Novel HDAC Inhibitor OBP-801 Promotes MHC Class I Presentation Through LMP2 Upregulation, Enhancing the PD-1-Targeting Therapy in Clear Cell Renal Cell Carcinoma. *Cancers (Basel)* **2024**, *16* (23). DOI: 10.3390/cancers16234058 From NLM PubMed-not-MEDLINE.
30. Bao, Y.; Qiao, Y.; Choi, J. E.; Zhang, Y.; Mannan, R.; Cheng, C.; He, T.; Zheng, Y.; Yu, J.; Gondal, M.; et al. Targeting the lipid kinase PIKfyve upregulates surface expression of MHC class I to augment cancer immunotherapy. *Proc Natl Acad Sci U S A* **2023**, *120* (49), e2314416120. DOI: 10.1073/pnas.2314416120 From NLM Medline.
31. Haggerty, T. J.; Dunn, I. S.; Rose, L. B.; Newton, E. E.; Pandolfi, F.; Kurnick, J. T. Heat shock protein-90 inhibitors enhance antigen expression on melanomas and increase T cell recognition of tumor cells. *PLoS One* **2014**, *9* (12), e114506. DOI: 10.1371/journal.pone.0114506 From NLM Medline.
32. Caldas-Lopes, E.; Cerchietti, L.; Ahn, J. H.; Clement, C. C.; Robles, A. I.; Rodina, A.; Moulick, K.; Taldone, T.; Gozman, A.; Guo, Y.; et al. Hsp90 inhibitor PU-H71, a multimodal inhibitor of malignancy, induces complete responses in triple-negative breast cancer models. *Proc Natl Acad Sci U S A* **2009**, *106* (20), 8368-8373. DOI: 10.1073/pnas.0903392106 From NLM Medline.
33. Wang, L.; Liang, Z.; Guo, Y.; Habimana, J. D.; Ren, Y.; Amissah, O. B.; Mukama, O.; Peng, S.; Ding, X.; Lv, L.; et al. STING agonist diABZI enhances the cytotoxicity of T cell towards cancer cells. *Cell Death Dis* **2024**, *15* (4), 265. DOI: 10.1038/s41419-024-06638-1 From NLM Medline.
34. Lu, D.; Shang, G.; Li, J.; Lu, Y.; Bai, X. C.; Zhang, X. Activation of STING by targeting a pocket in the transmembrane domain. *Nature* **2022**, *604* (7906), 557-562. DOI: 10.1038/s41586-022-04559-7 From NLM Medline.
35. Pan, B. S.; Perera, S. A.; Piesvaux, J. A.; Presland, J. P.; Schroeder, G. K.; Cumming, J. N.; Trotter, B. W.; Altman, M. D.; Buevich, A. V.; Cash, B.; et al. An orally available non-nucleotide STING agonist with antitumor activity. *Science* **2020**, *369* (6506). DOI: 10.1126/science.aba6098 From NLM Medline.
36. Davis, D. A.; Shrestha, P.; Aisabor, A. I.; Stream, A.; Galli, V.; Pise-Masison, C. A.; Tagawa, T.;

- Ziegelbauer, J. M.; Franchini, G.; Yarchoan, R. Pomalidomide increases immune surface marker expression and immune recognition of oncovirus-infected cells. *Oncoimmunology* **2019**, *8* (2), e1546544. DOI: 10.1080/2162402X.2018.1546544 From NLM PubMed-not-MEDLINE.
37. Kowalewski, D. J.; Walz, S.; Backert, L.; Schuster, H.; Kohlbacher, O.; Weisel, K.; Rittig, S. M.; Kanz, L.; Salih, H. R.; Rammensee, H. G.; et al. Carfilzomib alters the HLA-presented peptidome of myeloma cells and impairs presentation of peptides with aromatic C-termini. *Blood Cancer J* **2016**, *6* (4), e411. DOI: 10.1038/bcj.2016.14 From NLM Medline.
38. Zhang, M.; Wang, G.; Ma, Z.; Xiong, G.; Wang, W.; Huang, Z.; Wan, Y.; Xu, X.; Hoyle, R. G.; Yi, C.; et al. BET inhibition triggers antitumor immunity by enhancing MHC class I expression in head and neck squamous cell carcinoma. *Mol Ther* **2022**, *30* (11), 3394-3413. DOI: 10.1016/j.ymthe.2022.07.022 From NLM Medline.
39. Stachura, P.; Liu, W.; Xu, H. C.; Wlodarczyk, A.; Stencel, O.; Pandey, P.; Vogt, M.; Bhatia, S.; Picard, D.; Remke, M.; et al. Unleashing T cell anti-tumor immunity: new potential for 5-Nonloxytryptamine as an agent mediating MHC-I upregulation in tumors. *Mol Cancer* **2023**, *22* (1), 136. DOI: 10.1186/s12943-023-01833-8 From NLM Medline.
40. Dong, H.; Wen, C.; He, L.; Zhang, J.; Xiang, N.; Liang, L.; Hu, L.; Li, W.; Liu, J.; Shi, M.; et al. Nilotinib boosts the efficacy of anti-PDL1 therapy in colorectal cancer by restoring the expression of MHC-I. *J Transl Med* **2024**, *22* (1), 769. DOI: 10.1186/s12967-024-05572-2 From NLM Medline.
41. Yu, Q.; Dong, Y.; Wang, X.; Su, C.; Zhang, R.; Xu, W.; Jiang, S.; Dang, Y.; Jiang, W. Pharmacological induction of MHC-I expression in tumor cells revitalizes T cell antitumor immunity. *JCI Insight* **2024**, *9* (17). DOI: 10.1172/jci.insight.177788 From NLM Medline.
42. Song, T. Y.; Long, M.; Zhao, H. X.; Zou, M. W.; Fan, H. J.; Liu, Y.; Geng, C. L.; Song, M. F.; Liu, Y. F.; Chen, J. Y.; et al. Tumor evolution selectively inactivates the core microRNA machinery for immune evasion. *Nat Commun* **2021**, *12* (1), 7003. DOI: 10.1038/s41467-021-27331-3 From NLM Medline.
43. Shastri, N.; Gonzalez, F. Endogenous generation and presentation of the ovalbumin peptide/Kb complex to T cells. *J Immunol* **1993**, *150* (7), 2724-2736. From NLM Medline.
44. Dickson, M. A.; Okuno, S. H.; Keohan, M. L.; Maki, R. G.; D'Adamo, D. R.; Akhurst, T. J.; Antonescu, C. R.; Schwartz, G. K. Phase II study of the HSP90-inhibitor BIIB021 in gastrointestinal stromal tumors. *Ann Oncol* **2013**, *24* (1), 252-257. DOI: 10.1093/annonc/mds275 From NLM Medline.
45. Shi, J.; Van de Water, R.; Hong, K.; Lamer, R. B.; Weichert, K. W.; Sandoval, C. M.; Kasibhatla,

- S. R.; Boehm, M. F.; Chao, J.; Lundgren, K.; et al. EC144 is a potent inhibitor of the heat shock protein 90. *J Med Chem* **2012**, *55* (17), 7786-7795. DOI: 10.1021/jm300810x From NLM Medline.
46. Hong, D.; Said, R.; Falchook, G.; Naing, A.; Moulder, S.; Tsimberidou, A. M.; Galluppi, G.; Dakappagari, N.; Storgard, C.; Kurzrock, R.; et al. Phase I study of BIIB028, a selective heat shock protein 90 inhibitor, in patients with refractory metastatic or locally advanced solid tumors. *Clin Cancer Res* **2013**, *19* (17), 4824-4831. DOI: 10.1158/1078-0432.CCR-13-0477 From NLM Medline.
47. Shin, S. C.; El-Damasy, A. K.; Lee, J. H.; Seo, S. H.; Kim, J. H.; Seo, Y. H.; Lee, Y.; Yu, J. H.; Bang, E. K.; Kim, E. E.; et al. Structural Basis for Design of New Purine-Based Inhibitors Targeting the Hydrophobic Binding Pocket of Hsp90. *Int J Mol Sci* **2020**, *21* (24). DOI: 10.3390/ijms21249377 From NLM Medline.
48. Tornøe, C. W.; Christensen, C.; Meldal, M. Peptidotriazoles on solid phase: [1,2,3]-triazoles by regiospecific copper(i)-catalyzed 1,3-dipolar cycloadditions of terminal alkynes to azides. *J Org Chem* **2002**, *67* (9), 3057-3064. DOI: 10.1021/jo011148j From NLM PubMed-not-MEDLINE.
49. Rostovtsev, V. V.; Green, L. G.; Fokin, V. V.; Sharpless, K. B. A stepwise Huisgen cycloaddition process: copper(I)-catalyzed regioselective "ligation" of azides and terminal alkynes. *Angew Chem Int Ed Engl* **2002**, *41* (14), 2596-2599. DOI: 10.1002/1521-3773(20020715)41:14<2596::AID-ANIE2596>3.0.CO;2-4 From NLM Medline.
50. Neumann, S.; Biewend, M.; Rana, S.; Binder, W. H. The CuAAC: Principles, Homogeneous and Heterogeneous Catalysts, and Novel Developments and Applications. *Macromol Rapid Commun* **2020**, *41* (1), e1900359. DOI: 10.1002/marc.201900359 From NLM Medline.
51. Xin, Y.; Liu, S.; Liu, Y.; Qian, Z.; Liu, H.; Zhang, B.; Guo, T.; Thompson, G. J.; Stevens, R. C.; Sharpless, K. B.; et al. Affinity selection of double-click triazole libraries for rapid discovery of allosteric modulators for GLP-1 receptor. *Proc Natl Acad Sci U S A* **2023**, *120* (11), e2220767120. DOI: 10.1073/pnas.2220767120 From NLM Medline.
52. Meng, G.; Guo, T.; Ma, T.; Zhang, J.; Shen, Y.; Sharpless, K. B.; Dong, J. Modular click chemistry libraries for functional screens using a diazotizing reagent. *Nature* **2019**, *574* (7776), 86-89. DOI: 10.1038/s41586-019-1589-1 From NLM PubMed-not-MEDLINE.
53. Kasibhatla, S. R.; Hong, K.; Biamonte, M. A.; Busch, D. J.; Karjian, P. L.; Sensintaffar, J. L.;

- Kamal, A.; Lough, R. E.; Brekken, J.; Lundgren, K.; et al. Rationally designed high-affinity 2-amino-6-halopurine heat shock protein 90 inhibitors that exhibit potent antitumor activity. *J Med Chem* **2007**, *50* (12), 2767-2778. DOI: 10.1021/jm050752+ From NLM Medline.
54. Karttunen, J.; Shastri, N. Measurement of ligand-induced activation in single viable T cells using the lacZ reporter gene. *Proc Natl Acad Sci U S A* **1991**, *88* (9), 3972-3976. DOI: 10.1073/pnas.88.9.3972 From NLM Medline.
55. Jung, S.; Yoon, N. G.; Yang, S.; Kim, D.; Lee, W. S.; Hong, K. B.; Lee, C.; Kang, B. H.; Lee, J. H.; Kang, S. Discovery of 2-((4-resorcinolyl)-5-aryl-1,2,3-triazol-1-yl)acetates as potent Hsp90 inhibitors with selectivity over TRAP1. *Bioorg Med Chem Lett* **2020**, *30* (2), 126809. DOI: 10.1016/j.bmcl.2019.126809 From NLM Medline.
56. Tseng, H. J.; Banerjee, S.; Qian, B.; Lai, M. J.; Wu, T. Y.; Hsu, T. I.; Lin, T. E.; Hsu, K. C.; Chuang, K. H.; Liou, J. P.; et al. Design, synthesis, and biological activity of dual monoamine oxidase A and heat shock protein 90 inhibitors, N-Methylpropargylamine-conjugated 4-isopropylresorcinol for glioblastoma. *Eur J Med Chem* **2023**, *256*, 115459. DOI: 10.1016/j.ejmech.2023.115459 From NLM Medline.
57. Park, S. Y.; Oh, Y. J.; Lho, Y.; Jeong, J. H.; Liu, K. H.; Song, J.; Kim, S. H.; Ha, E.; Seo, Y. H. Design, synthesis, and biological evaluation of a series of resorcinol-based N-benzyl benzamide derivatives as potent Hsp90 inhibitors. *Eur J Med Chem* **2018**, *143*, 390-401. DOI: 10.1016/j.ejmech.2017.11.054 From NLM Medline.
58. Liu, Y. M.; Tu, H. J.; Wu, C. H.; Lai, M. J.; Yu, S. C.; Chao, M. W.; Wu, Y. W.; Teng, C. M.; Pan, S. L.; Liou, J. P. Ring-opening of five-membered heterocycles conjugated 4-isopropylresorcinol scaffold-based benzamides as HSP90 inhibitors suppressing tumor growth in vitro and in vivo. *Eur J Med Chem* **2021**, *219*, 113428. DOI: 10.1016/j.ejmech.2021.113428 From NLM Medline.
59. Muranaka, K.; Ichikawa, S.; Matsuda, A. Rational design and synthesis of ansa-adenosines as potential antitumor agents. *Nucleic Acids Symp Ser (Oxf)* **2009**, (53), 5-6. DOI: 10.1093/nass/nrp003 From NLM Medline.
60. Patterson, J.; Palombella, V. J.; Fritz, C.; Normant, E. IPI-504, a novel and soluble HSP-90 inhibitor, blocks the unfolded protein response in multiple myeloma cells. *Cancer Chemother Pharmacol* **2008**, *61* (6), 923-932. DOI: 10.1007/s00280-007-0546-0 From NLM Medline.

## **Chapter 5 A Chemical Approach to Assess Impact of Post-Translational Modification on MHC Peptide Binding and Effector Cell Engagement**

Adapted from: Kelly, J. J.; Bloodworth, N.; Shao, Q.; Shabanowitz, J.; Hunt, D.; Meiler, J.; Pires, M. M., A Chemical Approach to Assess Impact of Post-Translational Modification on MHC Peptide Binding and Effector Cell Engagement *ACS Chem. Biol.* **2024**, 19, 9, 1991–2001.

### **5.1 Abstract**

The human major histocompatibility complex (MHC) plays a pivotal role in the presentation of peptidic fragments from proteins, which can originate from self-proteins or from nonhuman antigens, such as those produced by viruses or bacteria. To prevent cytotoxicity against healthy cells, thymocytes expressing T cell receptors (TCRs) that recognize self-peptides are removed from circulation (negative selection), thus leaving T cells that recognize nonself-peptides. Current understanding suggests that post-translationally modified (PTM) proteins and the resulting peptide fragments they generate following proteolysis are largely excluded from negative selection; this feature means that PTMs can generate nonself-peptides that potentially contribute to the development of autoreactive T cells and subsequent autoimmune diseases. Although it is well-established that PTMs are prevalent in peptides present on MHCs, the precise mechanisms by which PTMs influence the antigen presentation machinery remain poorly understood. In the present work, we introduce chemical modifications mimicking PTMs on synthetic peptides. This is the first systematic study isolating the impact of PTMs on MHC binding and also their impact on TCR recognition. Our findings reveal various ways PTMs alter antigen presentation, which could have implications for tumor neoantigen presentation.

### **5.2 Introduction**

To maintain homeostasis, the human immune system must efficiently recognize and destroy cells that have accumulated genetic mutations or have been invaded by pathogenic microorganisms.<sup>1, 2</sup> Self-identification to the immune system is a primary mechanism deployed by human cells to flag the presence of nonself-proteins or proteins produced by genetic lesions.<sup>3</sup> To this end, presentation of antigenic peptidic fragments

via the major histocompatibility complex (MHC) to surveying immune cells serves as a key system to recognize diseased cells (**Figure 5.1A**).<sup>2</sup> MHC is present in the membrane of every nucleated cell and is responsible for presenting both antigenic and endogenous protein fragments to the extracellular space. The recognition of peptide-MHC complexes (pMHCs) by T cell receptors (TCRs)<sup>4</sup> initiates an immune cell response, the nature of which depends on the type of the T cell (primarily CD4<sup>+</sup> and CD8<sup>+</sup> cells).<sup>5</sup>

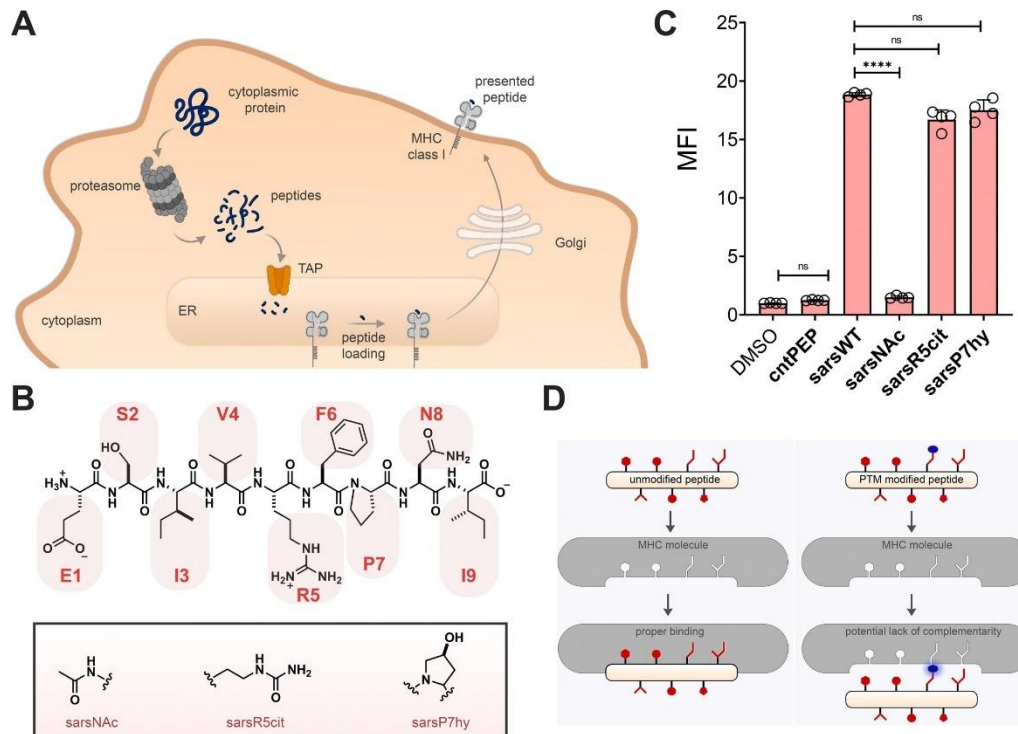


**Figure 5.1** (A) Schematic representation of the process involving the proteolytic processing of cytosolic protein into peptides. Subsequent steps lead to the loading of the peptides onto MHC molecules that are then transported to cell surface for presentation. (B) Chemical structures of sarsWT and the PTM modified variants. (C) Flow cytometry analysis of RMA-S cells treated with specific peptide (20  $\mu$ M) detected by APC conjugated antimouse H-2K<sup>b</sup> antibody. Data are represented as mean  $\pm$  SD (n = 3). P-values were determined by a two-tailed t-test (\*\*\*\* p < 0.0001, ns = not significant). (D) A general schematic representation of how the orientation of the PTM within the presented peptide could negatively impact binding to MHC molecules (right) compared to the unmodified peptide (left). Note that modifications can also occur on the termini of the peptides.

Critically, precise recognition and binding of pMHCs by TCRs must operate with a high level of fidelity since the response to self-peptides in healthy cells can result in cellular injury.<sup>6</sup> Through negative selection, thymocytes expressing TCRs that bind tightly to self-peptides are removed from circulation.<sup>4, 7</sup> In theory, changes to the primary sequence of a protein could yield autoreactive pMHC as long as the primary sequence was not part of the negative selection process. Some primary sequence changes can be permanent such as amino acid changes due to gene mutations, while others can be transient, like post-translational modifications (PTMs). In healthy states, enzymatic PTMs are added by specific sets of enzymes to modulate protein activity, localization, and interactions of the protein with other cellular components.<sup>8</sup> Because PTMs are covalent modifications, most are stable enough to persist through protease digestion and loading onto MHC molecules, potentially leading to the presentation of modified peptide during immune surveillance.<sup>9</sup>

Remarkably, human proteins containing PTMs have been shown to be excluded from negative selection, despite the potential that pMHCs with PTM-modified peptides to yield autoreactive cells.<sup>10</sup> It has been hypothesized that this exclusion is due to the relatively low abundance of PTMs in healthy and young adults in the prime phase of negative selection, compared to the unmodified parent proteins. However, thymus involution after adolescence may contribute to age-related autoimmune diseases.<sup>11, 12</sup> Additionally, various factors, such as imbalances of PTM writers and erasers in diseased states, cellular stresses, or aging, can dramatically increase the prevalence of PTMs across the proteome.<sup>13</sup> Collectively, the increased level of pMHCs bearing PTMs mean that a higher proportion of potentially autoreactive cells is present.<sup>10, 14-19</sup> In other words, when peptides with PTM modifications are presented, the immune system may perceive them as nonself, triggering a pathogenic autoimmune response.<sup>20-22</sup> A recent example of this phenomenon involved cysteine carboxyethylation by a cellular metabolite, leading to a pathogenic neoantigen presented on pMHC and resulting in autoreactive T cell responses.<sup>23</sup>

Various PTMs have been previously found in pMHCs.<sup>20, 24-30</sup> Notably, increased conversion of arginine to citrulline in the myelin sheath has been shown to lead to the development of self-reactive T cells that exacerbate the progression of autoimmune diseases such as Rheumatoid Arthritis (RA) and Multiple Sclerosis (MS).<sup>31-36</sup> Moreover,

there is mounting evidence that pMHCs presenting peptides with PTMs are prevalent in tumors.<sup>37-40</sup> A recent report revealed that PTMs can shape the antigenic landscape.<sup>40</sup> Despite the importance of PTMs in potentially generating autoreactive peptides, several aspects of PTM biology in this field remain poorly defined. One primary barrier to better understanding the impact of PTMs on pMHCs has been the complexity of assigning the role of PTMs in the context of the many steps leading to MHC presentation. These processes may include changes in a protein half-life, altered proteolytic processing to generate presentable peptides, or binding affinity of individual peptides to MHC molecules. Among these factors, peptide binding affinity to MHC molecules is a primary determinant of the peptide repertoire within pMHCs.<sup>41, 42</sup> Here, we systematically isolate the impact of PTMs on the ability of the peptides to bind to MHC molecules and be recognized by cognate T cells.

### ***5.3 Results and Discussion***

In general, PTMs can be challenging to detect in the context of complex biological systems, and the levels of PTMs can change in response to cellular cues.<sup>43</sup> Traditional cellular assays do not typically establish the ratio of PTM proteins relative to their unmodified counterparts.<sup>44</sup> These challenges are amplified when analyzing PTMs on peptides from pMHCs.<sup>45</sup> Extracting peptides from isolated MHCs involves challenging separation steps and downstream mass spectrometry analysis.<sup>46</sup> On the other hand, a top-down approach of treating cells with PTM-modified proteins also poses a challenge because exogenous proteins are not readily processed to yield peptides that are presented by MHC I molecules.<sup>47</sup> Even if the peptides get processed, the ultimate pMHC presentation involves multiple factors including peptide half-life,<sup>48</sup> uptake efficiency, or peptide binding affinity to MHC. Consequently, assessment of how various naturally occurring PTMs impact peptide binding to MHCs and recognition by TCRs has not been systematically conducted.

#### ***5.3.1 PTMs alter peptide binding affinity to MHC***

To address these challenges, we based our approach on the RMA-S cell line, which lacks the TAP importer.<sup>49, 50</sup> TAP is essential for delivering peptides from the cytosol to the endoplasmic reticulum. By incubating peptides with RMA-S cells at lower temperatures,

we allowed peptides to associate with surface-bound MHCs (**Figure S5.1**). Upon increasing the temperature, we observed the stabilization of pMHCs on the cell surface. The quantity of MHC on the cell surface correlated with the binding affinity<sup>51-56</sup> of the peptide to the MHC molecule, quantified via a fluorescently labeled anti-MHC antibody.<sup>57</sup> Given the features of this well-established cell line, we anticipated that RMA-S cells would effectively reveal the impact of PTMs on peptides that bind to MHC with high affinity. Moreover, RMA-S cells have been used extensively for isolating the affinity of a peptide for MHC.

To start, we sought to identify a peptide from SARS-CoV-2 spike protein that could be displayed on MHC molecules. We used NetMHCpan4.0,<sup>58</sup> an algorithm that estimates the propensity of peptides to bind MHC, to select a peptide sequence (ESIVRFPNI, referred to as **sarsWT**) for stabilization of the specific MHC molecule (H-2K<sup>b</sup>) on the surface of RMA-S cells. The peptide was synthesized using standard solid-phase peptide synthesis techniques. The culture medium of the RMA-S cells was supplemented with **sarsWT** at 26 °C to enable association of the peptide with surface bound MHCs. Following **sarsWT** incubation, the temperature was raised to 37 °C. Subsequently, the cells were incubated with APC conjugated antimouse H-2K<sup>b</sup> antibody and analyzed by flow cytometry where fluorescence is expected to correspond with the amount of **sarsWT** bound to the MHC. The peptide SNFVSAGI (**cntPEP**) was used as a negative control since it has been reported to not interact appreciably with H-2K<sup>b</sup>.<sup>59</sup> Various concentrations of **sarsWT** were used to optimize the RMA-S stabilization assay with the goal of increasing the number of pMHC molecules formed on the surface of the cells (**Figure S5.2**). We found an increased fluorescence signal corresponding to increasing concentrations of **sarsWT**, indicating that the peptide bound and stabilized the MHC on the surface of the cell. The amount of stable pMHCs that formed at the surface also saturated at 50 μM of peptide and showed an EC<sub>50</sub> of 1.7 μM. These results confirmed the suitability of RMA-S to report on the stabilization of the pMHC complex by **sarsWT**.

Another parameter to consider is the time in which the MHC binding peptide has to associate with the MHC to reach MHC saturation. To evaluate this time frame, the workflow described above was conducted; however, the peptide incubation time at 37 °C

was varied from 2 to 6 h (**Figure S5.3**). The results showed that the fluorescent signal increased with increased incubation periods. This is likely due to accumulation of stabilized pMHCs in the presence of excess high-affinity peptide. Nevertheless, a 6 h incubation at 37 °C provided the highest signal-to-noise ratio and was used for downstream assays.

With an optimized protocol in hand, we then synthesized a panel of peptides containing PTMs to investigate their potential impact on MHC binding (**Figure 5.1B**). We envisioned that modifying residues on **sarsWT** would be representative of how the selected modifications may impact binding of different MHC peptides. The specific PTMs chosen were a proline to hydroxyproline,<sup>60, 61</sup> arginine to citrulline<sup>62</sup>, and *N*-terminus acetylation<sup>63</sup> modifications, as they are naturally occurring PTMs. By performing the RMA-S stabilization assay, we found that the citrullination and hydroxy-proline modifications had no significant effect on MHC binding, but the *N*-terminal acetylation modification completely disrupted MHC binding (**Figure 5.1C**). Gratifyingly, there is precedence for *N*-acetylated peptides to be displaced in MHC class I.<sup>64</sup> These results demonstrate that naturally occurring PTMs can alter pMHC complex formation and influence the antigen presentation pathway depending on the interface of the peptide and the MHC molecule (**Figure 5.1D**).

### **5.3.2** *TCR recognition of pMHC is distinctly altered by PTM compared to MHC affinity*

Next, we shifted our focus to the peptide epitope SIINFELK (**ovaWT**) from the model antigen ovalbumin (OVA) to interrogate how other PTMs impact MHC binding as well as TCR recognition.<sup>65</sup> To this end, we synthesized a new library of OVA peptides containing PTMs on its serine and lysine residues and performed a concentration scan to assess MHC binding using the RMA-S stabilization assay (**Figure 5.2A**). Interestingly, there was a significant decrease in MHC binding when serine was phosphorylated despite predictions that this site does not contribute significantly to binding (**Figure 5.2B**).<sup>66</sup> Our results highlight the potential deficiency of current models to predict how PTMs could impact peptide binding to MHC molecules given how PTM products can be structurally distinct relative to the side chains of the canonical amino acids.

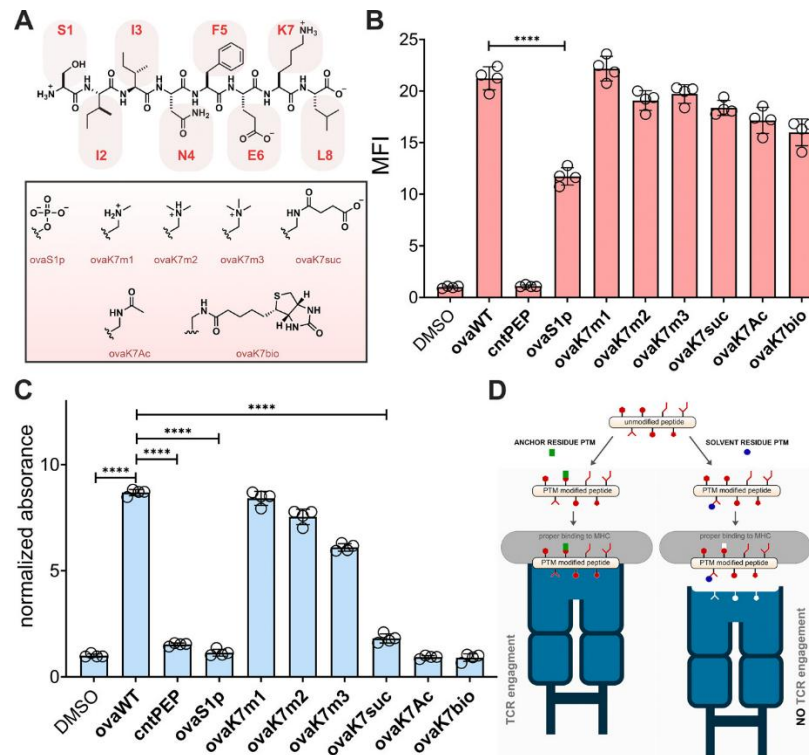


**Figure 5.2** (A) Chemical structures of **ovaWT** and the PTM modified variants. (B) Flow cytometry analysis of RMA-S cells treated with specific peptide (20  $\mu$ M) detected by APC conjugated antimouse H-2K<sup>b</sup> antibody. (C) RMA-S cells were incubated with peptide and B3Z T cells overnight at an effector to target ratio of 1:1.  $\beta$ -galactosidase expression was then measured via the colorimetric reagent CPRG on a plate reader at 570 nm. (D) Schematic representation of how PMTs can impact engagement with TCRs. Data are represented as mean  $\pm$  SD ( $n = 4$ ).  $P$ -values were determined by a two-tailed  $t$  test (\*\*\*\*  $p < 0.0001$ )

The side chain of lysine (K7) on **ovaWT** was explored next. Lysine was decorated with different types of PTMs that included three different charge states. Previously, the same lysine on SIINFEKL had been altered with various groups including fluorophores and caging groups.<sup>67-69</sup> Our data showed considerable accommodation of structural alterations to the lysine side chain (**Figure 5.2B**). With larger modifications such as biotin, binding levels are altered but the change is not significant. These findings can be explained by the solvent exposed nature of lysine on the pMHC complex and the length of the lysine side chain, which may reduce structurally unfavorable interactions with the

MHC molecule (**Figure 5.1D**).<sup>66</sup> Critically, for **ovaWT** the anchor residues that are more important for the overall binding affinity to MHC molecules (Phe5 and Leu8) are not amendable to conventional PTMs.<sup>70</sup>

We then sought to detect changes in peptide binding via a competition assay using the parent cell line (RMA) that has a competent TAP system. To this end, we performed a competition assay using the panel of OVA peptides barring PTM mark in live RMA cells. The assay was performed by coincubating RMA cells individually with PTM-modified peptides and also **ovaFI** (SIINFEK(FITC)L), in which the  $\gamma$  position of lysine is modified with fluoresceine. **ovaFI** has long been utilized by the field to interrogate binding of untagged peptides for MHC molecules. A decrease in cellular fluorescence should indicate higher association levels with MHC molecules, thereby informing on the relative affinity of the PTM-modified molecules. Critically, this assay retains MHC molecules within a physiologically relevant context and this alternative readout should complement the RMA-S MHC stabilization assay. As expected, the trend in binding affinity in the competition experiment closely mirrored our results with the RMA-S stabilization assay indicating that the RMA-S assay can accurately report on relative MHC binding affinities in a cellular context (**Figure S5.4**). As further evidence and to specifically detect PTM-modified peptides bound on MHC, **ovaWT** and **ovaK7m3** treated RMA-S cells had their MHC-bound peptides eluted and identified using mass spectrometry. The canonical binding peptide, ovaWT, was clearly detected after elution from live RMA-S cells (**Figure S5.5-S5.6**). Likewise, the **ovaK7m3** was detected by mass spectrometry and this provides direct evidence that trimethylation of K7 does not disrupt binding of this peptide to MHC (**Figure S5.7-S5.8**). While PTMs on solvent exposed residues could potentially retain binding to MHCs, their overall impact may be more strongly reflected in the pMHC engagement with TCRs. TCRs recognize T cell exposed motifs of the bound peptide within pMHCs.<sup>68, 70</sup> Therefore, PTMs at these positions may have a greater impact on T cell activation.

To assess the impact of **ovaWT** PTMs on TCR recognition, we utilized the B3Z T cell hybridoma cell line that contains an OVA specific TCR along with a NFAT-LacZ reporter gene that encodes for  $\beta$ -galactosidase on an IL-2 inducible promoter.<sup>71</sup> Upon B3Z

recognition of the OVA pMHC complex on RMA-S cells, IL-2 production promotes  $\beta$ -galactosidase expression, which can hydrolyze chlorophenol red- $\beta$ -D-galactopyranoside (CPRG), and the resulting color change is representative of activation levels. Our results showed that the PTMs have a much more significant effect on TCR recognition than on peptide binding to MHC (**Figure 5.2C**). While relatively modest disruption of TCR recognition was seen for increasing the degree of methylation on the lysine residue, near complete disruption of TCR recognition was seen for all PTMs that imparted a change in charge of either the serine or lysine residue. Additionally, the reduction in TCR recognition for both the phosphoserine and biotinylated OVA cannot be fully explained solely by their decrease in MHC binding. Instead, the PTMs that are well accommodated for MHC binding could be displayed away from the binding cleft and alter engagement with TCRs on cognate T cells (**Figure 5.2D**).

### **5.3.3** *Assessing influence of PTMs on display of disease relevant peptides*

To confirm the relevance of these findings in a broader context, we also performed the T cell activation assay on DC2.4 dendritic cells, which also express H-2K<sup>b</sup>. Unlike the RMA-S cells, peptides were incubated with DC2.4 cells at 37 °C and were expected to load onto MHC molecules if they display sufficient affinity toward H-2K<sup>b</sup>. Satisfyingly, the pattern of T cells activation with PTM modified **ovaWT** peptides showed a similar profile with DC2.4 cells as RMA-S cells (**Figure S5.9**). Our results confirmed that the impact of PTMs on T cell activation may be consistent across multiple cell types. Finally, we sought to investigate whether we could assess PTMs on a peptide that has potential pathological implications. To this end, a number of autoimmune diseases, including RA and MS, have been described to involve the citrullination of arginine.<sup>72</sup> Citrullination is carried out by peptidylarginine deiminases (PADs) and higher levels of citrullinated proteins have been found in older mice relative to young mice.<sup>73</sup> A shift in higher levels of citrullination past the full scope of negative selection could provide a pathway for autoreactivity. Using a peptide originating from a known PAD substrate myelin basic protein (RTAHYGSL, **mbpWT**) as the baseline (**Figure 5.3A**), we found that there was a statistically significant increase in peptide binding to MHC molecules upon citrullination

(Figure 5.3B). This result is consistent with the possibility that PTMs can impact presentation of peptides in the context of disease-linked peptides.

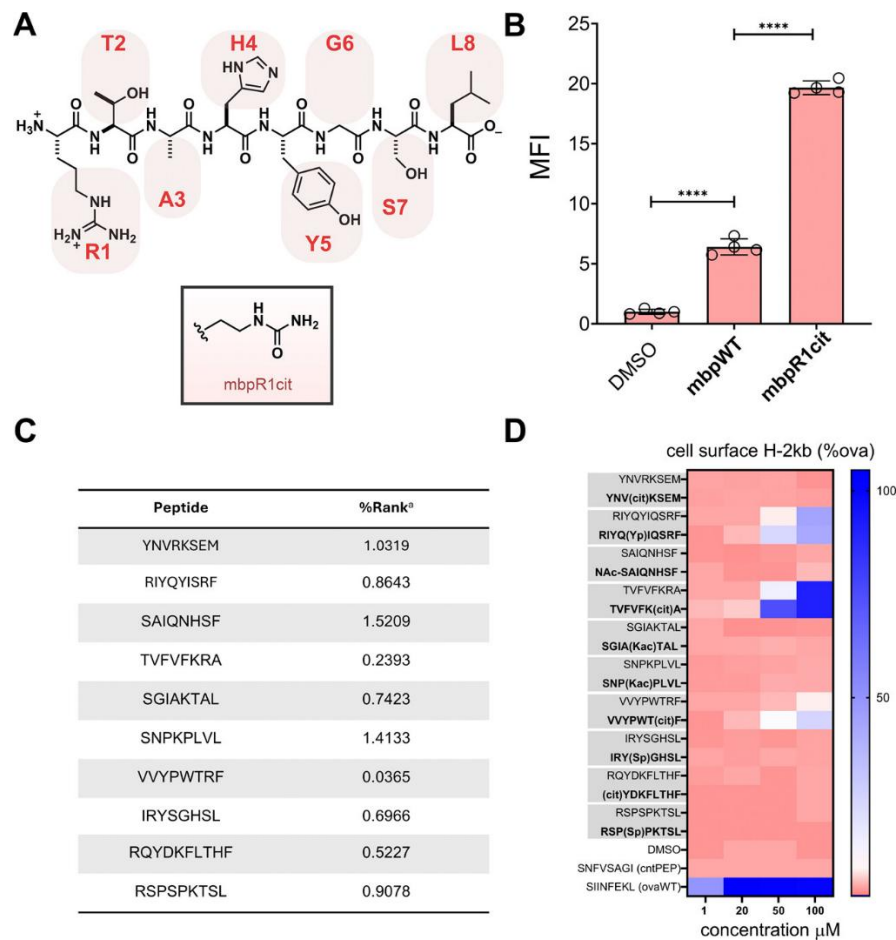


**Figure 5.3** (A) Chemical structures of *mbpWT* and the PTM modified variant. (B) Flow cytometry analysis of RMA-S cells treated with specific peptide (20  $\mu$ M) detected by APC conjugated anti-mouse H-2K<sup>b</sup> antibody. (C) NetMHCpan 4.1 predicted binding scores of tumor associated peptides. %Rank is the prediction score for comparing MHC binding across random peptides where a %Rank of 1 indicates that a peptide scored in the top 1% of random peptides. A %Rank of <2 or <0.5 are the cutoffs for weak binding or strong binding to MHC respectively. A %Rank >2 indicates nonbinders. (D) A heat map of wild-type and PTM modified peptides relative MHC binding analyzed by using the RMA-S stabilization assay. RMA-S cells were incubated with peptide at indicated concentration of peptides and detected via flow cytometry with APC conjugated antimouse H-2K<sup>b</sup> antibodies. Abbreviations: Cit (citrullination), Yp (phosphorylated

*tyrosine*), *Kac* (*lysine acetylated at the  $\gamma$  position*), *NAc* (*acetylation at the  $\alpha$  position*), and *Sp* (*phosphorylated serine*). Data are represented as mean  $\pm$  SD ( $n = 4$ ). *P*-values were determined by a two-tailed *t* test (\*\*\*\*  $p < 0.0001$ ).

We then sought to uncover if PTMs are playing a role in influencing the presentation of cancer antigens. However, only a limited number of studies have identified a wide range of PTM modified MHC peptides presented on cancer cells.<sup>39, 40</sup> Additionally, the specific impact of these PTMs on peptide-MHC binding remains unclear. To this end, we synthesized 10 PTM modified MHC peptides previously identified on cancer cells and compared their binding affinity to MHC to their respective unmodified versions.<sup>39, 40</sup> Out of this library, only 3 PTM modified peptides were found to bind to MHC at the biologically relevant concentrations, highlighting the need for secondary validation assays for peptide libraries identified through mass spectrometry screens (**Figure 5.3C,D**). Interestingly, out of the peptides that bound, the PTM versions all showed significant improvement in MHC stabilization on RMA-S cells suggesting that PTMs may enhance the presentation of cancer associated peptides (**Figure S5.10**).

#### **5.3.4 Modeling PTM influence on peptide-MHC binding affinity**

To gain additional insight into how PTMs might alter peptide binding affinity to H-2K<sup>b</sup>, we simulated peptide binding to H-2K<sup>b</sup> using ROSETTA and FlexPepDock. FlexPepDock has been previously benchmarked against MHC-I bound peptides and is capable of generating models with subangstrom accuracy.<sup>74, 75</sup> One advantage of FlexPepDock over contemporary machine learning methods is its ability to incorporate noncanonical amino acids and PTM residues by generating custom ROSETTA parameters files; this enables FlexPepDock to generate accurate models of MHC-I bound epitopes containing such residues.<sup>76, 77</sup> Furthermore, the binding energy metrics calculated by this application (the reweighted\_sc score term) can serve a surrogate for peptide binding affinity to MHC-I.<sup>78</sup> We simulated the binding of the SARS-CoV-2-derived peptides to H-2K<sup>b</sup> and generated results recapitulating experimentally derived binding affinity changes (**Figure 5.4**). ROSETTA correctly predicts decreased binding affinity for the top-scoring decoys after N-terminal acetylation (corresponding to an increase in the average reweighted\_sc term; ROSETTA energy metrics are inversely proportional to binding affinity). ROSETTA

predicts either no change or a modest increase in binding affinity for the other two PTMs assessed (**Figure 5.4A**). When the top-scoring model for each peptide is visually inspected, we noted significant alterations in the peptide backbone structure for the acetylated N-terminus peptide variant largely confined to the H-2K<sup>b</sup> N-terminus binding pocket (**Figure 5.4B**), a region that is largely responsible for dictating epitope binding specificity and cannot easily accommodate large conformational changes. Conversely, R5 citrullinated and P7 hydroxylated variants are located outside the H-2K<sup>b</sup> binding pockets and regions tolerant of larger conformational changes (**Figure 5.4C**).

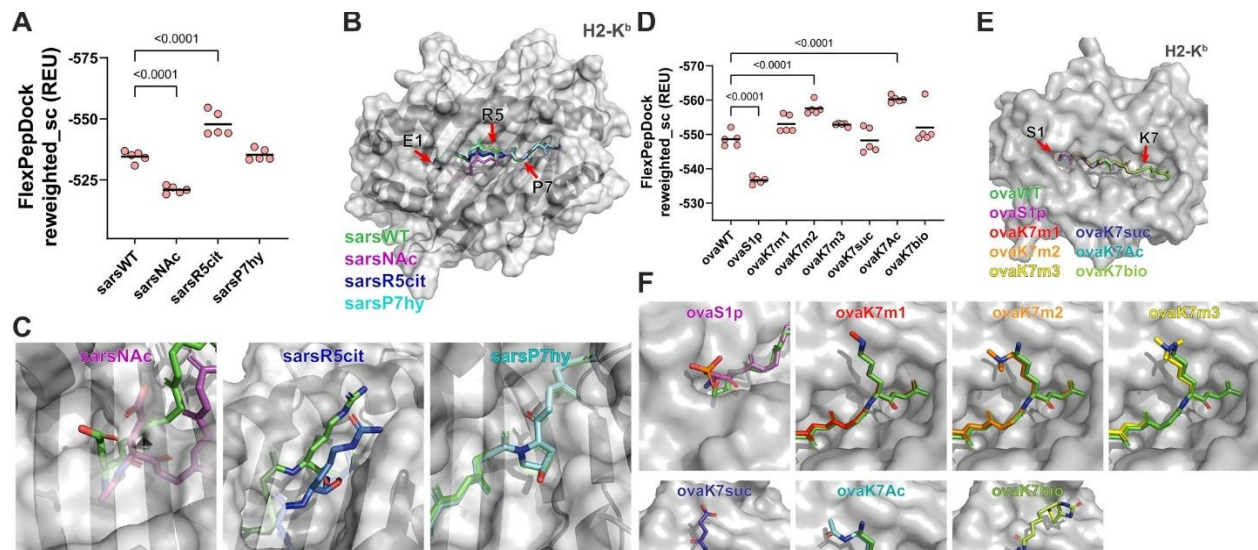


**Figure 5.4** Modeling the SARS peptide with and without PTMs using FlexPepDock. (A) N-terminal acetylation results in higher reweighted\_sc values (and thus lower likelihood of binding) compared to the wild-type peptide, consistent with experimental results (one-way ANOVA and Holm-Sidak posthoc; individual values correspond to the top 0.5% of models generated, and bars represent mean score term values). (B) Top peptide models generated for each epitope positioned in the H-2K<sup>b</sup> binding cleft. (C) Side chain modifications compared to the unmodified epitope for the SARS-CoV-2 peptide. Modeling the ovalbumin-derived peptide with and without PTMs using FlexPepDock. (D) Phosphorylation of the N-terminal serine residue generates models with higher average reweighted\_sc terms, similar to N-terminal acetylation of the SARS-CoV-2 peptide (one-way ANOVA and Holm-Sidak posthoc; individual values correspond to the top 0.5% of models generated, and bars represent mean score term values). (E) Superimposed

*peptide backbones for the top peptide models generated for each PTM. (F) Detailed side-chain configurations for the top-scoring models generated by FlexPepDock.*

We repeated this analysis on the ovalbumin-derived peptide and each PTM (**Figure 5.4D**). Phosphorylation of the N-terminus serine generates structures with higher (and therefore less favorable) score terms, again likely due to disruption of the N-terminus peptide-binding pocket (**Figure 5.4E**). Peptide models with the remaining PTMs scored either equivalently or slightly better than their wild-type counterparts. While largely consistent with experimental data, ROSETTA predicts modest increases in peptide binding favorability that are not observed experimentally. This may be a result of biases inherent in ROSETTA's scoring weights that have not been fully optimized for unusual or noncanonical amino acids such as those modeled here. Alternatively, the assay used for assessing binding affinity may be insufficiently sensitive to detect small changes above certain affinity thresholds. Modifications at the lysine in position 7 alter T cell activation *in vitro* as illustrated in **Figure 5.2C**. *In silico*, these altered residues do not interact appreciably with peptide binding pockets but instead occur in the region displayed by MHC-I to patrolling T cells (**Figure 5.4F**). Methylated and acetylated lysine alters residue charge and hydrophobicity; succinylation adds a negative charge (as opposed to lysine's normally positively charged side chain); and biotinylation results in the addition of a large aliphatic heteropolycyclic side chain very different in size and character from the native lysine residue.

Finally, we performed a similar analysis with the **mbp** peptide with and without R1 citrullination and generated *in silico* results that recapitulated experimental findings (**Figure 5.3**). Citrullination at R1 significantly increases the reweighted\_sc metrics for the models generated by ROSETTA (**Figure S5.11**). While this modification occurs at the N-terminus binding pocket, it does not appreciably alter peptide backbone configuration (**Figure S5.11**). It does, however, alter side chain hydrophobicity and charge. Given that the citrullinated variant is charge-neutral (compared to arginine's 1+ charge) and given H-2Kb's preference for hydrophobic or charge-neutral residues at binding pockets, it is reasonable to expect this modification may enhance peptide binding affinity.

Increasingly, there are efforts dedicated to developing therapeutic agents that harness a patient's immune system against cancerous lesions.<sup>79-81</sup> A prominent example involves the modulation of the programmed death-1 (PD-1) system and its cognate programmed death-ligand 1 (PD-L1). Cancers can often hijack this set of proteins to maintain growth while suppressing the patient immune response against transformed cells. Immune checkpoint inhibitors that disrupt the association of PD-1 and PD-L1 have shown potent anticancer activity by a number of mechanisms but primarily via increased T cell engagement.<sup>82, 83</sup> Neoantigens arising from genetic lesions likely provide a pool of antigens that can be presented by cancer MHCs on the cell surface during checkpoint therapy. Importantly, our results suggest that therapeutic agents that increase the presentation of peptides through an altered balance of PTM marks could potentially complement the targeting antigenic pool.

Considering the observed roles of PTMs in MHC binding and recognition by TCRs, it is conceivable that the balance of PTM addition by “writers” and PTM removal by “erasers” can be central in immunological health. Any imbalance that could be driven by age or manufactured by therapeutic interventions could result in pathological state. For example, proteins could naturally exist in high abundance of nonacetylated states on lysine side chains past the peak period of negative selection of T cells. After cancer development, there is an increased level of acetylation, but those marks need to be removed by “erasers” called Lysine Deacetylases (KDAC) to reduce an anticancer immunological response against the cancerous cells. Upon the administration of KDAC inhibitors, a larger pool of acetylated peptide would be presented. As our data showed, the acetylation of lysine that interacts with TCRs would escape negative selection and provide an anticancer immunological response. Such “cryptic” antigens could potentially be driving the pharmacological effect of some PTM modulators in cancer patients. To this end, there are a high number of ongoing studies evaluating the combination of KDAC inhibitors and PD-1/PDL-1 inhibitors across many types of difficult-to-treat tumors.<sup>84-90</sup> We are currently working toward using this strategic platform to demonstrate how KDAC inhibitors directly lead to an immunopeptidome that reveal cryptic antigens able to enhance antitumor immunological activity.

#### **5.4 Conclusion**

In conclusion, the data presented here demonstrate that naturally occurring PTMs can drastically impact the antigen presentation pathway by altering either their affinity towards MHC molecules or TCR recognition by cognate T cells. In our assays, we showed that some PTMs can disrupt peptide binding to MHC, but primarily on residues that directly engage with MHCs. Conversely, PTMs on residues whose sidechains are positioned away from the MHC binding face are more sensitive to TCR recognition due to the altered binding modality with TCRs. To the best of our knowledge, our study is the first systematic analysis of the impact that PTMs have on MHC binding in a whole cell context and how PTMs can also alter T cell activation using live target and effector cells. Provided that negative selection is age-dependent and becomes increasingly diminished past adolescence, it is evident that PTMs could be causal events that result in autoimmune diseases.

#### **5.5 Summary and Future Outlook**

In Chapter 5, we aimed to systematically determine the molecular mechanisms behind how PTMs influence antigen presentation. Two key determinants of antigen recognition by the immune system are (1) the binding affinity of peptides to MHC molecules and (2) the specific recognition of the pMHC complex by T cells through their TCRs. To isolate and assess the contributions of each factor, we used a controlled cell-based system to evaluate how PTMs influence antigen presentation and immune recognition.

Expanding this work requires a deeper understanding of how cancer cells generate PTMs that are absent in healthy tissue and how the immune system responds by generating PTM-specific T cells. The biochemical pathways underlying PTM-modified neoantigen formation in cancer remain poorly understood, making it challenging to predict which PTM-containing peptides will be displayed on MHC. Furthermore, emerging evidence suggests that PTMs may serve as privileged structures for eliciting cancer-specific T cell responses, likely because they are absent during T cell development in the thymus. Developing predictive strategies to determine whether a PTM induces sufficient physiochemical changes to generate circulating T cells could significantly advance immunotherapy approaches for targeting cancer.

## 5.6 Materials and Methods

**Materials.** All peptide related reagents and protected amino acids were purchased from Chem Impex. APC-labeled anti-mouse H-2K<sup>d</sup>/H-2D<sup>d</sup> antibody was purchased from Biologend. Pooled Human Serum and acetic acid (glacial, >99.99% trace metals basis), and penicillin-streptomycin was purchased from Sigma Aldrich. Dulbecco's Modified Eagle's Medium (DMEM) was purchased from VWR. Fetal Bovine Serum (FBS) was purchased from R&D Systems. Angiotensin II phosphate > 95% HPLC and vasoactive intestinal peptide (VIP) 1-12 human, porcine, rat was purchased from AnaSpec. Pierce™ Waters, LC/MS grade was purchased from Thermo Scientific. Methanol, Optima™ LC/MS grade was purchased from Fisher Chemical. Acetonitrile, B&J Brand™ LC-MS, for LC-MS and HPLC, >99.9% was purchased from Honeywell. Kasil 1624 potassium silicate solution was purchased from PQ Corporation. 100 μm i.d. x 360 μm o.d. Polyimide coated fused silica nano-capillary tubing and 75 μm i.d. x 360 μm o.d. Polyimide coated fused silica nano-capillary tubing were purchased from PolyMicro Technologies, Inc. Reprosil Pur 120 C18 AQ 3 μm and Reprosil Pur 120 C18 AQ 10 μm were purchased from Dr Maisch GMBH. Mode 5424 Centrifuge and Protein LoBind microcentrifuge tubes were purchased from Eppendorf. Teflon tubing, 0.012-inch i.d. x 0.060-inch o.d. was purchased from Zeus Industrial Products, Inc. P-2000 microcapillary laser puller with fused silica adapter was purchased from Sutter Instrument Co. LTQ-Orbitrap mass spectrometer was purchased from Thermo-Fisher Scientific. All other organic chemical reagents were purchased from Fisher Scientific or Sigma Aldrich and used without further purification. ALL COMPOUNDS ARE >95% PURE BY HPLC ANALYSIS.

**Mammalian Cell Culture.** RMA-S cells were a kind gift from Dr. John Sampson. RMA-S cells were maintained in RPMI 1640 media supplemented with 10% fetal bovine serum, 50 IU/mL penicillin, 50 μg/mL streptomycin, 1X MEM non-essential amino acid solution (ThermoFisher) and cultured in a humidified atmosphere of 5% CO<sub>2</sub> at 37°C. B3Z cells were kindly provided by Dr. Aaron Esser-Kahn and maintained in RPMI 1640 media supplemented with 10% fetal bovine serum, 50 IU/mL penicillin, 50 μg/mL streptomycin and cultured in a humidified atmosphere of 5% CO<sub>2</sub> at 37°C.

**RMA-S Stabilization Assay.**  $10^5$  RMA-S cells were seeded in a treated 96 well plate at 37°C overnight. The next day, RMA-S cells were moved to a 26°C incubator for 24-48 hours. Following the incubation period, cells were incubated with peptides in culture media at indicated concentrations for 1 hour at 26°C before being moved to the 37°C incubator for 6 hours. The media was then replaced with a 1:100 dilution of APC-labeled anti-mouse H-2K<sup>d</sup>/H-2D<sup>d</sup> antibody in culture media for 1 hour at 4°C. Cells were removed from the well plate by vigorous pipetting, fixed with 2% formaldehyde solution, and analyzed using the Attune NxT Flow Cytometer (Thermo Fischer) equipped with a 637 nm laser with 670/14 nm bandpass filter.

**Mild Acid Elution.**  $10^9$  RMA-S cells were treated with 20  $\mu$ M peptide at 26°C for 1 h. Cells were then warmed to 37°C for 6 h. RMA-S cells were collected by spinning down at 500 x g for 5 mins and thoroughly washed with 1X PBS Buffer pH 7.4 (Invitrogen). Next, 15 mL of mild acid elution (MAE) buffer (0.131 M citric acid, 0.066M Na<sub>2</sub>HPO<sub>4</sub>, 150 mM NaCl, 0.3  $\mu$ M Aprotinin, and 5 mM iodoacetamide at pH 3.3) was added to RMA-S cells for 2 min. RMA-S cells were then spun down at 4000 x g for 5 min and the supernatant was collected, lyophilized, and stored at -80°C until further use.

**Mass Spectrometry Analysis.** The emitter tip of the analytical column was laser-pulled to produce an opening of 2-5  $\mu$ m, and a 2 mm kasil frit was used in place of the irregular reverse phase (RP) resin. The precolumns (100  $\mu$ m i.d. x 360  $\mu$ m O.D. fused silica) were packed to 7 cm with 10  $\mu$ m C18 beads, and the analytical columns (75  $\mu$ m i.d. x 360  $\mu$ m o.d. fused silica) were packed to 10 cm with 3  $\mu$ m C18 beads. Ova samples and 100 fmol each of the internal standards (Angio and Vaso) were loaded onto the precolumn using a pressure vessel for a 15-minute desalting rinse at a flow rate of 100 nL/min with 0.1% acetic acid (AcOH) in water before connecting to the analytical column with a 2 cm Teflon tubing. Reverse phase separation was conducted at a flow rate of 100 nL/min by HPLC using 0.1% AcOH for solvent A and 0.1% AcOH in 60% acetonitrile for solvent B, and a gradient as follows: 0% to 60% solvent B in 60 minutes, 60% to 100% solvent B in 2 minutes, 100% solvent B for 4 minutes, 0% in 2 minutes, followed by a 22-minute equilibration with 100% solvent A. The peptides eluted from the analytical column were electrosprayed into an LTQ-Orbitrap mass spectrometer. MS1 spectra were acquired with

a resolution of 60,000, an AGC target of  $5e5$  and scan range of 300 to 2000  $m/z$  in the Orbitrap analyzer, followed by low resolution data dependent MS2 acquisition in the ion trap with normal scan rate. Only precursor ions with charge +2 and +3 were selected for fragmentation. The top 2 most abundant precursor ions, as well as the targeted +1 and +2 precursor masses for the **ovaWT** and **ovaK7m3** peptides, were selected for collision-activated dissociation (CAD) in the ion trap analyzer with an AGC target of  $1e4$ , a normalized collision energy of 35%, an activation time of 30 ms, and a 2.0  $m/z$  isolation window. If the same precursor ion was selected three times or was detected twice within a 20-second repeat duration, the ion was dynamically excluded for 15 seconds. The presence of **ovaWT** and **ovaK7m3** peptides was verified by manually inspecting the targeted MS2 spectra for the expected fragmentations and fragment ion masses.

**B3Z T cell activation:**  $10^5$  RMA-S cells were seeded in a treated 96 well plate at  $37^\circ\text{C}$  overnight. The following day the culture media was replaced with media containing indicated concentration of peptide along with  $10^5$  B3Z cells in culture media and co-incubated overnight. Cells were then spun down at  $500\times g$  for 5 mins and washed with 1X PBS a total of two times. Lysis buffer containing 0.2% saponin,  $500\ \mu\text{M}$  CPRG reagent,  $100\ \text{mM}$   $\text{MgCl}_2$ , and  $100\ \text{mM}$   $\beta$ -mercaptoethanol in 1X PBS was added to each well. After 2-4 hours absorbance 570 was recorded using a BioTek Epoch 2 microplate reader.

**Computational Methods:** We used the FlexPepDock refinement application in combination with ROSETTA scripts to simulate peptide docking to H-2Kb in ROSETTA 3.13.1,2 FlexPepDock refinement has successfully recapitulated peptide/MHC-I complex structures with sub-angstrom accuracy, and we have used this protocol to generate peptide/MHC-I structures for peptides containing post-translational modifications and other non-canonical amino acids. The refinement protocol requires initial templates that approximate the final peptide configuration. We identified templates by scoring sequence alignments between the peptide to model and H2-Kb bound peptides with structures available in the PDB. The H-2Kb MHC-1 model was generated using AlphFold2.5 Residues in the template peptide were sequentially mutated to match those of the peptide to model using the ROSETTA mover MutateResidue. For modeling residues with post-translational modifications, we applied either pre-existing patches with the ROSETTA

move ModifyVariantType or created de-novo parameter files and rotamer libraries as described. For each docking simulation 1000 models were created. Models were sorted by the reweighted\_sc statistic (a modified ROSETTA energy score term that doubles contributions from interface residues and triples contributions from peptide residues) and the top 0.5% scoring models selected for further analysis. We previously validated this statistic as a metric for peptide binding affinity using a variant of the FlexPepBind protocol as described by Alam et al.<sup>4,7</sup> Computations were carried out with resources provided by the Vanderbilt Advanced Computing Center for Research and Education (ACCRE). Top scoring models were rendered and visually inspected using the Pymol Molecular Graphics System v2.0 by Schrödinger, LLC.

### 5.7 Supplemental Figures

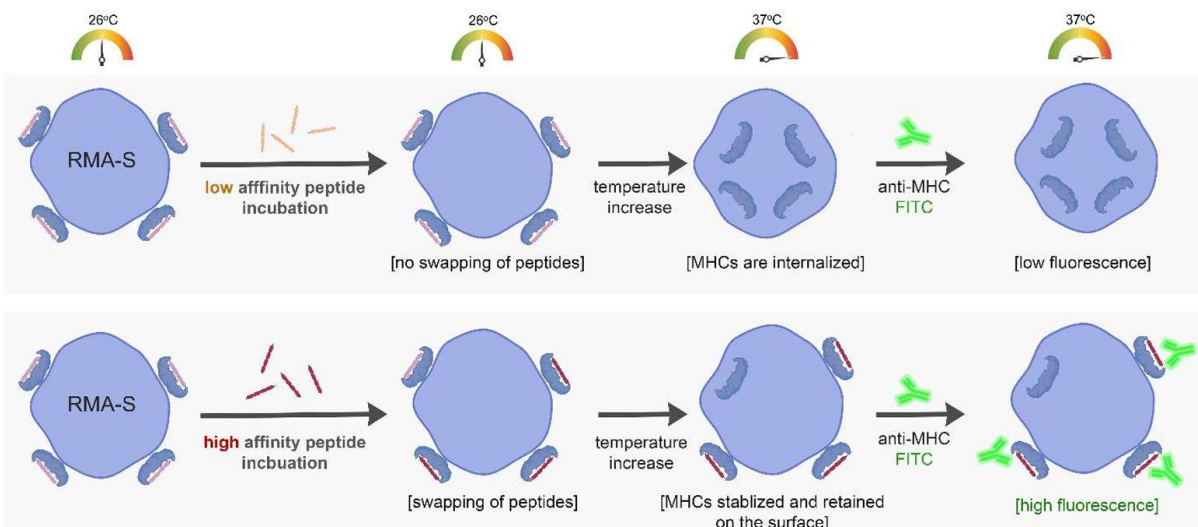


**Figure S5.1.** RMA-S stabilization assay workflow. RMA-S cells express low affinity peptides on their surface at 26 °C. When the temperature is raised to 37 °C, in the absence of a high affinity MHC binding peptide (top) the low affinity pMHC complex dissociates and the empty MHC is internalized and degraded. In the presence of a high affinity binder (bottom) the pMHC complex remains stable at 37 °C and can be detected via fluorescently labeled anti-MHC antibodies.

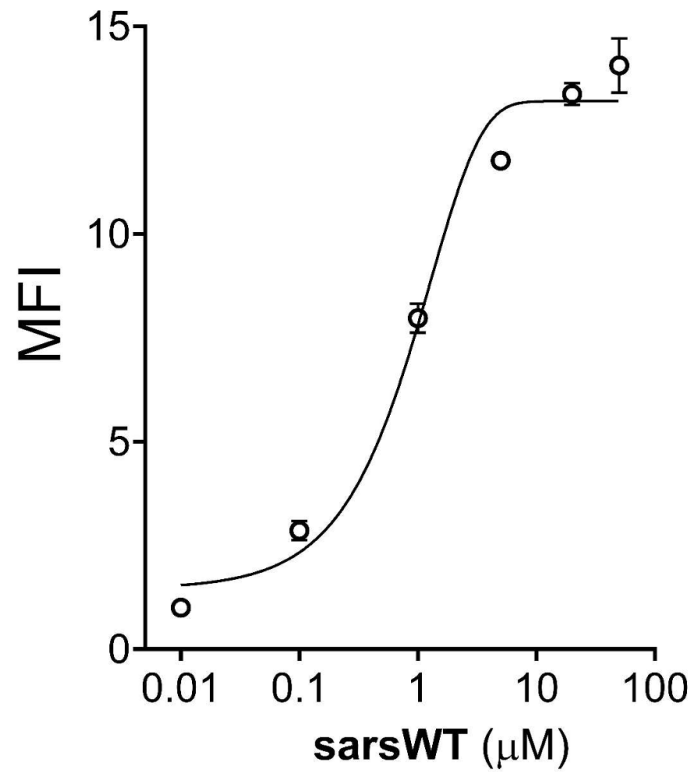


**Figure S5.2.** Flow cytometry analysis of RMA-S cells treated with indicated concentration of sarsWT detected by APC conjugated anti-mouse H-2K<sup>b</sup> antibody. Data are represented as mean  $\pm$  SD (n= 3). P-values were determined by a two-tailed t-test (\* p < 0.05, \*\* p < 0.01, \*\*\* p < 0.001, \*\*\*\* p < 0.0001, ns = not significant).

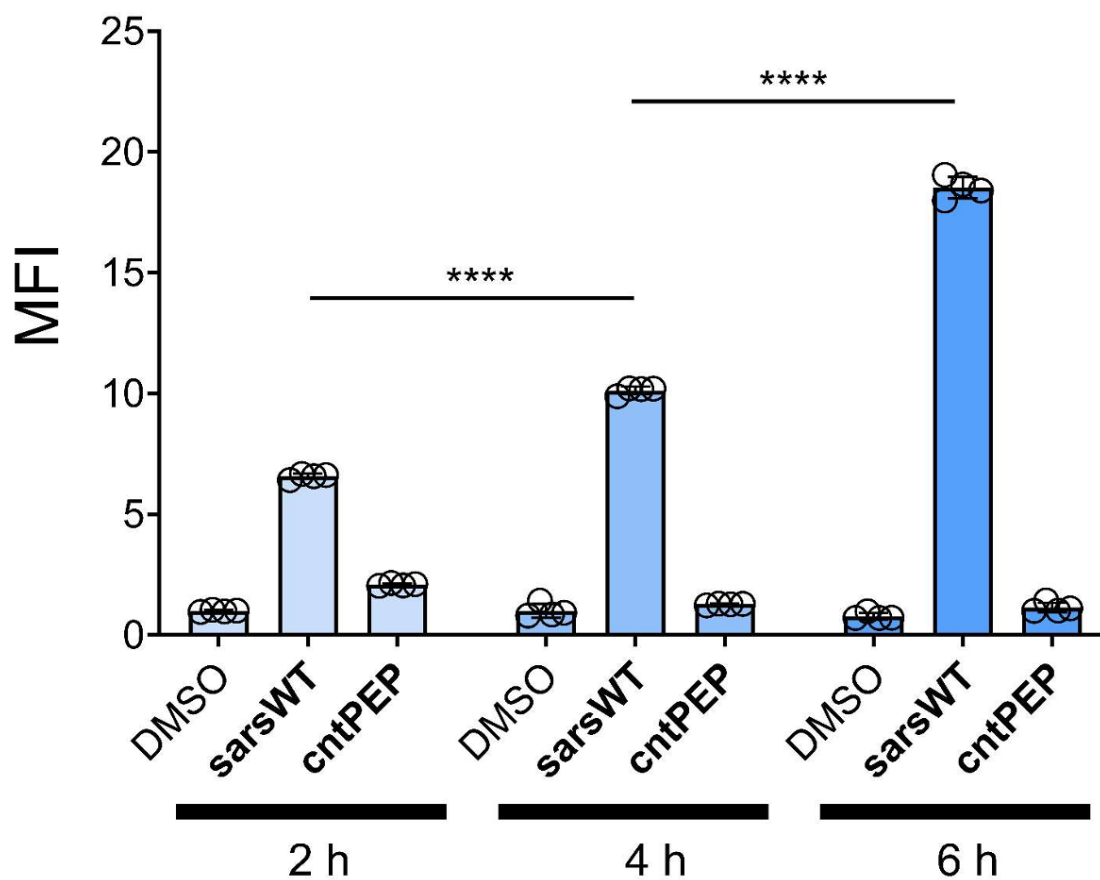


**Figure S5.3.** Flow cytometry analysis of RMA-S cells treated with of sarsWT (20  $\mu$ M) for indicated time points detected by APC conjugated anti-mouse H-2K<sup>b</sup> antibody. Data are represented as mean  $\pm$  SD ( $n=3$ ). P-values were determined by a two-tailed t-test (\*  $p < 0.05$ , \*\*  $p < 0.01$ , \*\*\*  $p < 0.001$ , \*\*\*\*  $p < 0.0001$ , ns = not significant).

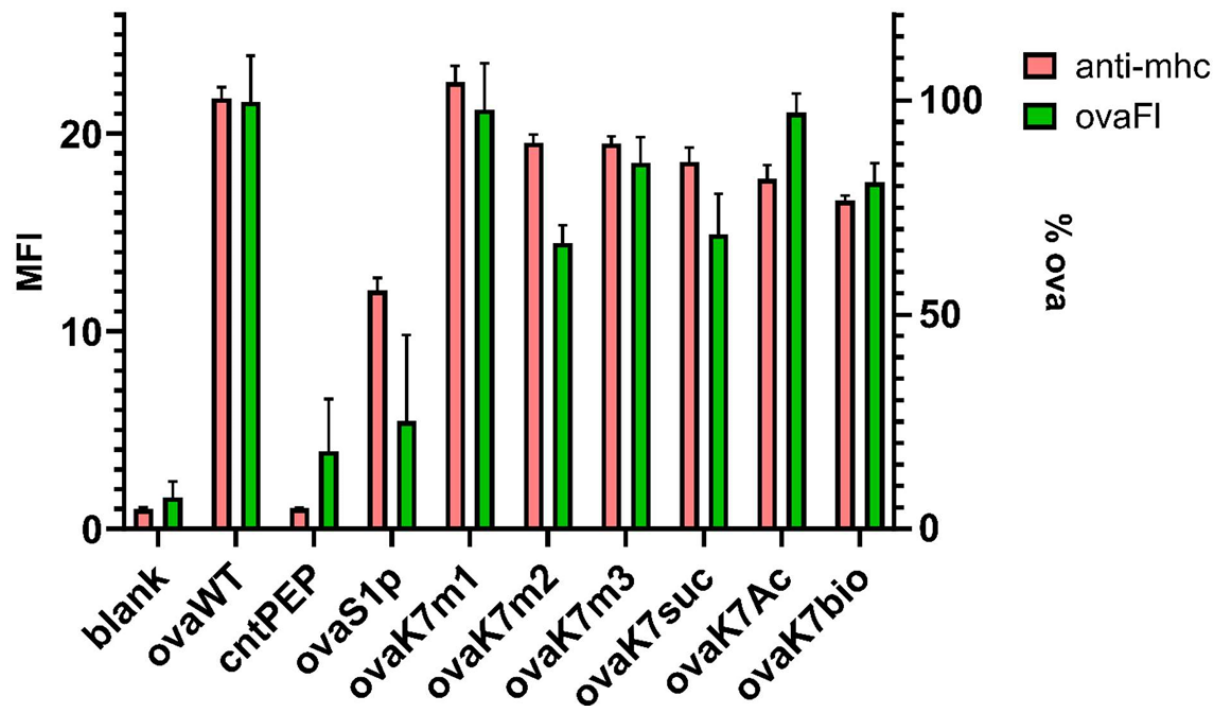


**Figure S5.4.** Flow cytometry analysis of RMA-S cells treated with indicated peptide and detected by APC conjugated anti-mouse H-2Kb antibody (red). RMA cells were co incubated with ovaFI (4  $\mu$ M) and excess of indicated peptide (32  $\mu$ M) (green). Data is represented as a percent decrease in fluorescence relative to ovaWT. Data are represented as mean  $\pm$  SD (n= 3).

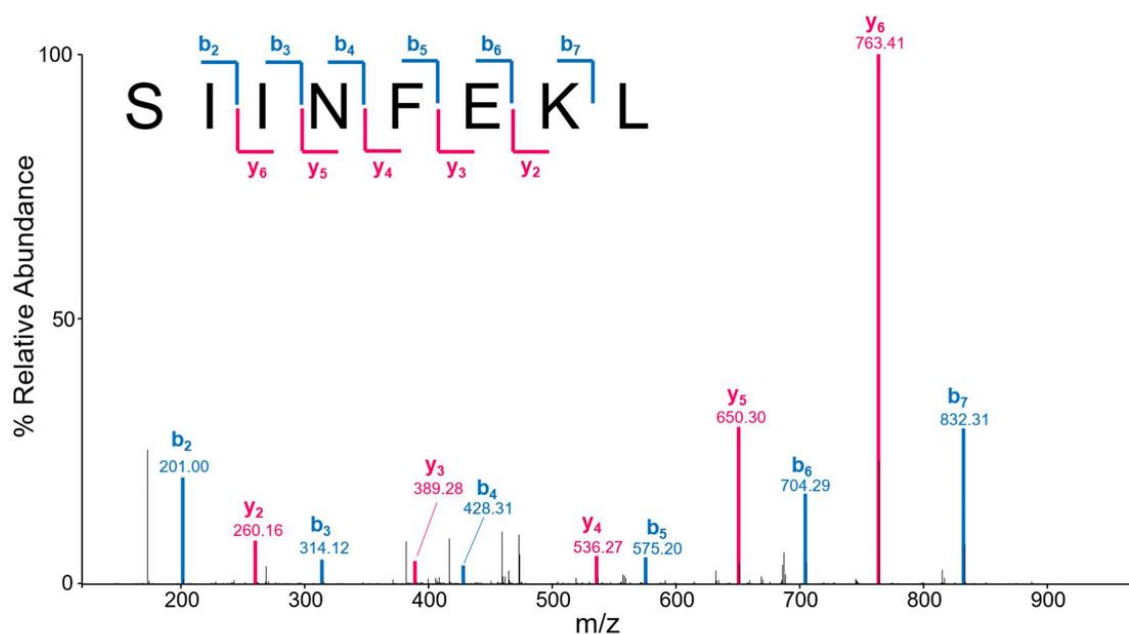


**Figure S5.6.** Collision-activated dissociation (CAD) tandem mass spectrometry (MS/MS) spectrum acquired in the ion trap showing fragment masses of ovaWT  $[M+2H]^{2+}$  precursor ion with  $m/z$  482.2744. Sequence coverage for  $b+$  ion fragments are labeled in blue, and  $y+$  ion fragments are labeled in pink. The identified ions are sufficient for complete sequence coverage.

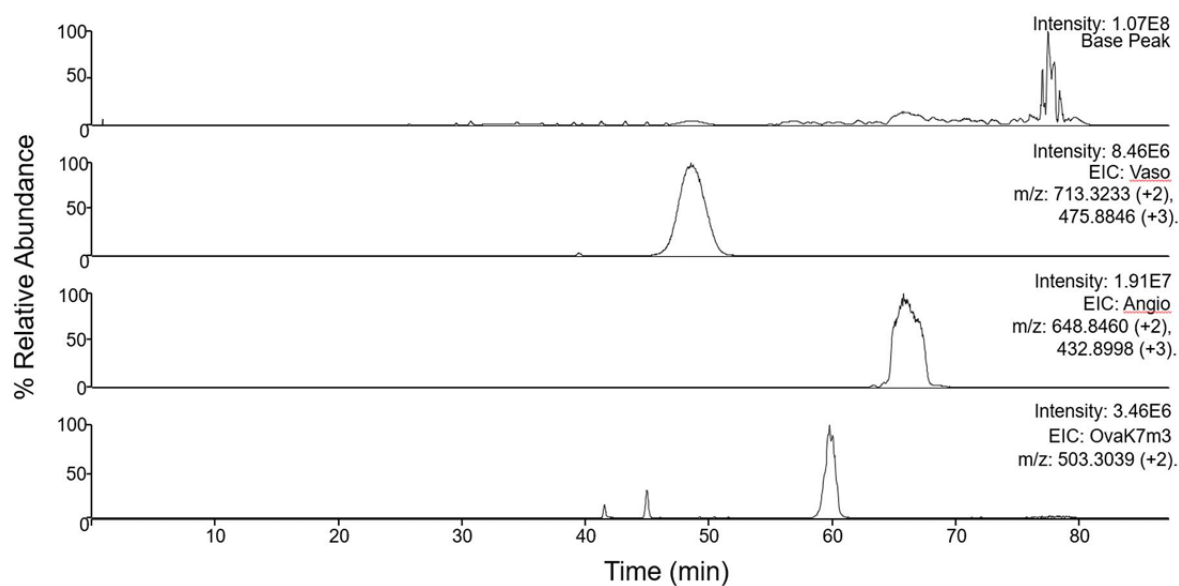


**Figure S5.7:** LC-MS analysis of ovaK7m3 and spiked internal standard peptides. Extracted ion chromatograms (EIC) are shown for the base peak and selected ion  $m/z$  corresponding to the ovaK7m3, 100 fmol each of Vaso and Angio peptides.

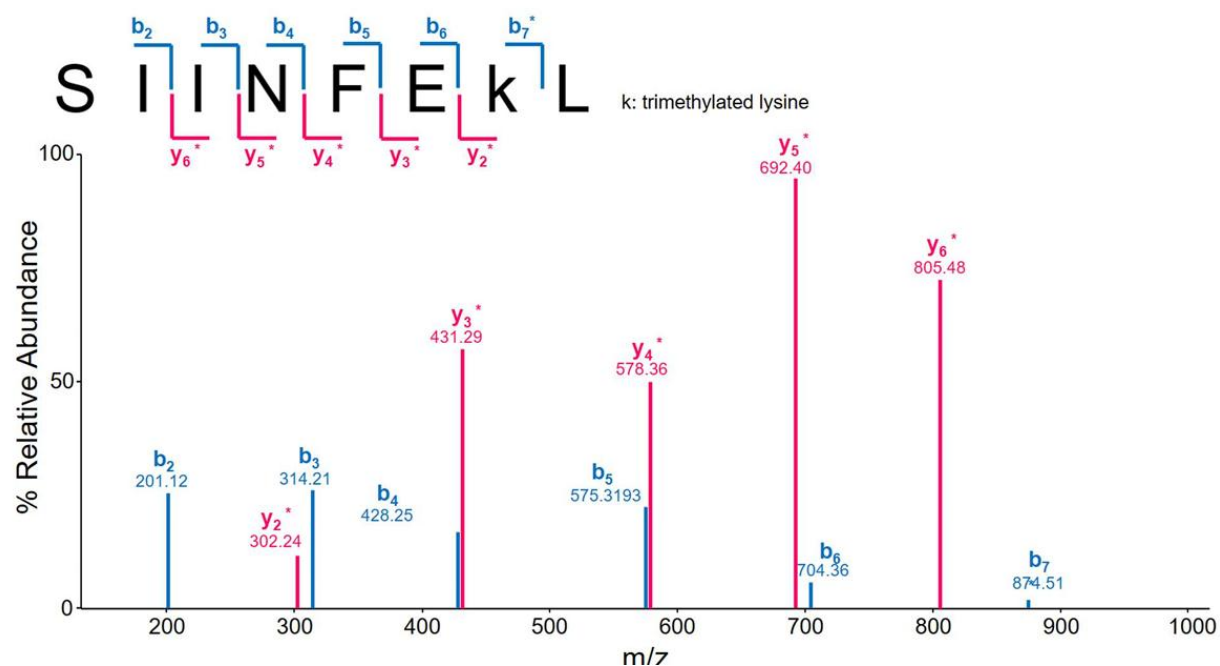


**Figure S5.8.** Collision-activated dissociation (CAD) tandem mass spectrometry (MS/MS) spectrum acquired in the ion trap showing fragment masses of ovaK7m3  $[M+2H]^{2+}$  precursor ion with  $m/z$  482.2744. Sequence coverage for  $b+$  ion fragments are labeled in blue, and  $y+$  ion fragments are labeled in pink. The identified ions are sufficient for complete sequence coverage.

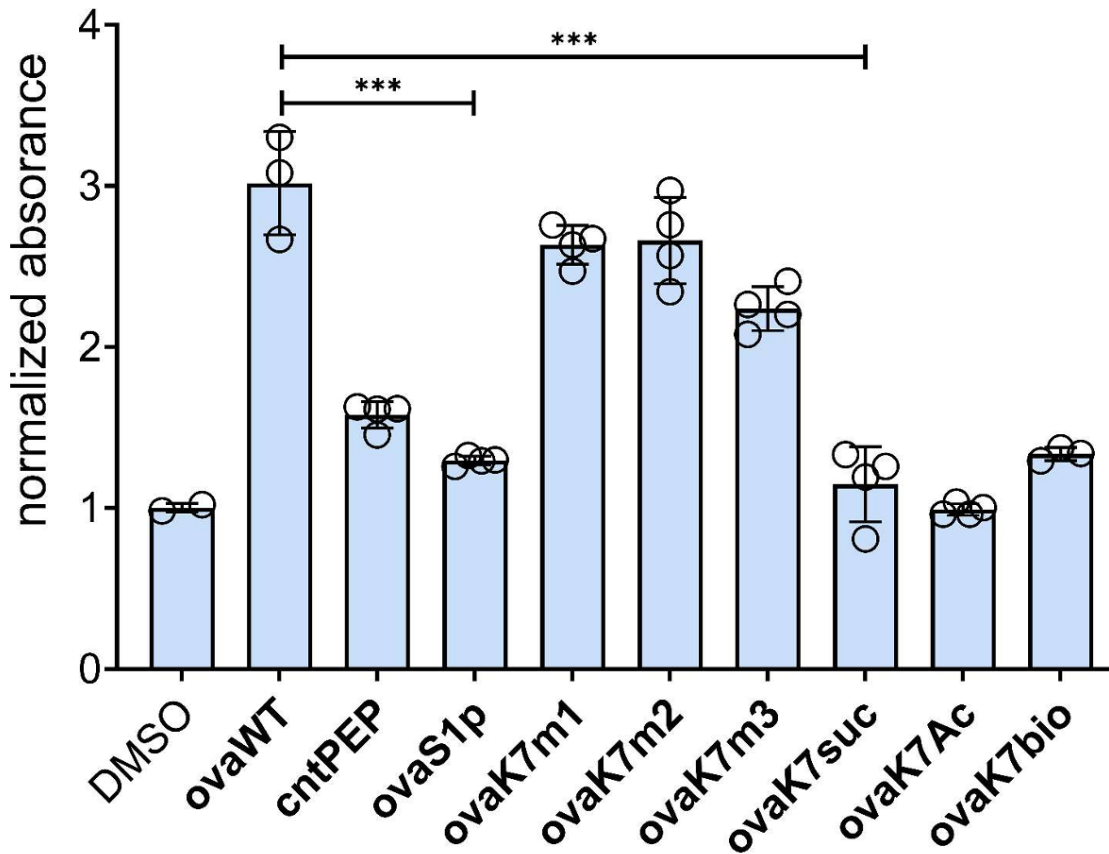


**Figure S5.9.** DC2.4 cells were incubated with peptide and B3Z T-cells overnight at an effector to target ratio of 1:1.  $\beta$ -galactosidase expression was then measured via the colorimetric reagent CPRG on a plate reader at 570 nm.

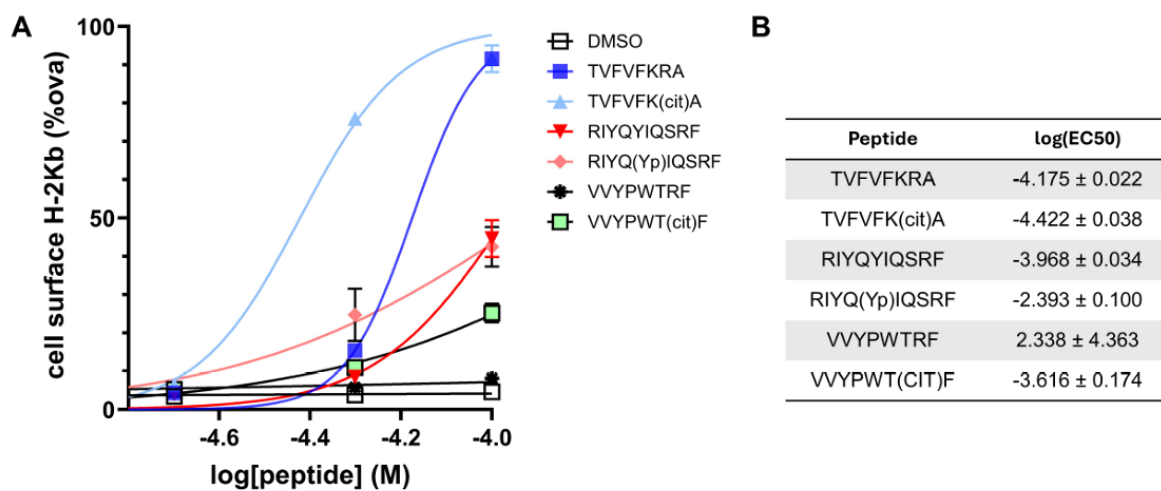


**Figure S5.10.** (A) Dose response-curve of WT and PTM modified peptides using the RMA-S stabilization assay. RMA-S cells were incubated with peptide at indicated concentration of peptides and detected via flow cytometry with APC conjugated anti mouse H-2Kb antibodies. (B) Table of log(EC50) values. Abbreviations: Cit (citrullination), Yp (phosphorylated tyrosine).

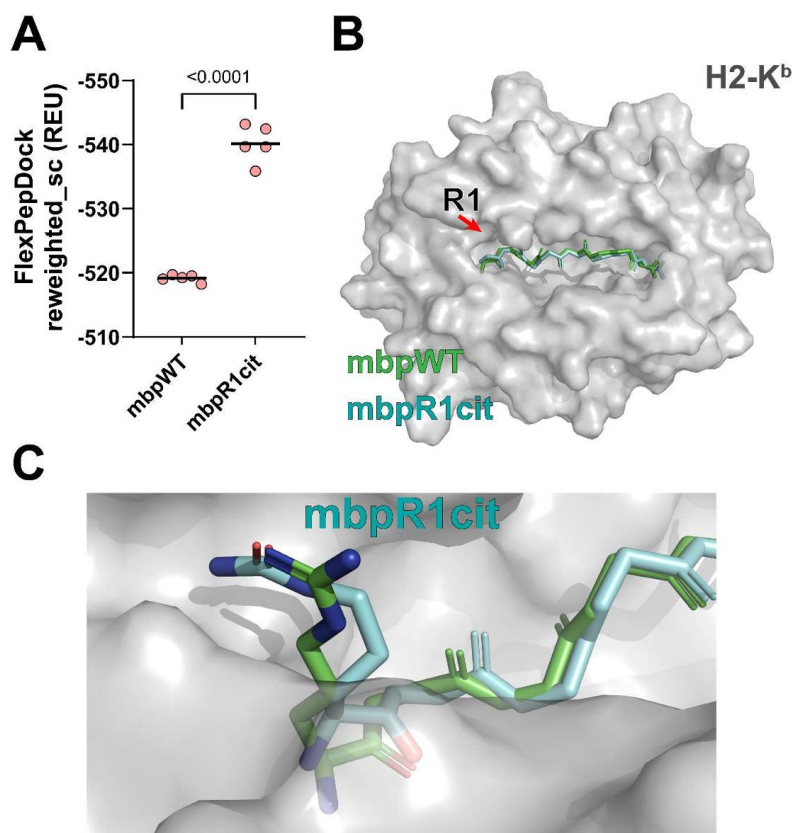


**Figure S5.11.** Modeling the peptide *mbp* with and without citrullination of the N-terminus arginine residue. (A) Arginine citrullination generates models with a higher average reweighted\_sc, consistent with experimental results showing citrullination enhances binding affinity (two-tailed student's *t* test; individual values correspond to the top 0.5% of models generated, and bars represent mean score term values). (B) Superimposed backbones for the top model generated for the *mbp*WT and *mbp*R1cit variants show little difference in overall peptide configuration. (C) Detailed side-chain configuration for both the *mbp*WT and *mbp*R1cit variant at the N-terminal arginine residue.

## 5.7 References

1. Roche, P. A., and Furuta, K. (2015) The ins and outs of MHC class II-mediated antigen processing and presentation, *Nat Rev Immunol* 15, 203-216.
2. Neefjes, J., Jongstra, M. L., Paul, P., and Bakke, O. (2011) Towards a systems understanding of MHC class I and MHC class II antigen presentation, *Nat Rev Immunol* 11, 823-836.
3. Pishesha, N., Harmand, T. J., and Ploegh, H. L. (2022) A guide to antigen processing and presentation, *Nat Rev Immunol* 22, 751-764.
4. Huppa, J. B., and Schutz, G. J. (2023) T-cell antigen recognition: catch-as-catch-can or catch-22?, *EMBO J* 42, e113507.
5. Gorentla, B. K., and Zhong, X. P. (2012) T cell Receptor Signal Transduction in T lymphocytes, *J Clin Cell Immunol* 2012, 5.
6. Jameson, S. C. (2002) Maintaining the norm: T-cell homeostasis, *Nat Rev Immunol* 2, 547-556.
7. Klein, L., Kyewski, B., Allen, P. M., and Hogquist, K. A. (2014) Positive and negative selection of the T cell repertoire: what thymocytes see (and don't see), *Nat Rev Immunol* 14, 377-391.
8. Conibear, A. C. (2020) Deciphering protein post-translational modifications using chemical biology tools, *Nat Rev Chem* 4, 674-695.
9. Sandalova, T., Sala, B. M., and Achour, A. (2022) Structural aspects of chemical modifications in the MHC-restricted immunopeptidome; Implications for immune recognition, *Front Chem* 10, 861609.
10. Raposo, B., Merky, P., Lundqvist, C., Yamada, H., Urbonaviciute, V., Niaudet, C., Viljanen, J., Kihlberg, J., Kyewski, B., Ekwall, O., Holmdahl, R., and Backlund, J. (2018) T cells specific for post-translational modifications escape intrathymic tolerance induction, *Nat Commun* 9, 353.
11. Srinivasan, J., Lancaster, J. N., Singarapu, N., Hale, L. P., Ehrlich, L. I. R., and Richie, E. R. (2021) Age-Related Changes in Thymic Central Tolerance, *Front Immunol* 12, 676236.

12. Lancaster, J. N., Keatinge-Clay, D. E., Srinivasan, J., Li, Y., Selden, H. J., Nam, S., Richie, E. R., and Ehrlich, L. I. R. (2022) Central tolerance is impaired in the middle-aged thymic environment, *Aging Cell* 21, e13624.
13. Li, W., Li, F., Zhang, X., Lin, H. K., and Xu, C. (2021) Insights into the post-translational modification and its emerging role in shaping the tumor microenvironment, *Signal Transduct Target Ther* 6, 422.
14. Michaelsson, E., Malmstrom, V., Reis, S., Engstrom, A., Burkhardt, H., and Holmdahl, R. (1994) T cell recognition of carbohydrates on type II collagen, *J Exp Med* 180, 745-749.
15. Sidney, J., Vela, J. L., Friedrich, D., Kolla, R., von Herrath, M., Wesley, J. D., and Sette, A. (2018) Low HLA binding of diabetes-associated CD8+ T-cell epitopes is increased by post translational modifications, *BMC Immunol* 19, 12.
16. McAdam, S. N., Fleckenstein, B., Rasmussen, I. B., Schmid, D. G., Sandlie, I., Bogen, B., Viner, N. J., and Sollid, L. M. (2001) T cell recognition of the dominant I-A(k)-restricted hen egg lysozyme epitope: critical role for asparagine deamidation, *J Exp Med* 193, 1239-1246.
17. Mamula, M. J., Gee, R. J., Elliott, J. I., Sette, A., Southwood, S., Jones, P. J., and Blier, P. R. (1999) Isoaspartyl post-translational modification triggers autoimmune responses to self-proteins, *J Biol Chem* 274, 22321-22327.
18. Kim, J. K., Mastronardi, F. G., Wood, D. D., Lubman, D. M., Zand, R., and Moscarello, M. A. (2003) Multiple sclerosis: an important role for post-translational modifications of myelin basic protein in pathogenesis, *Mol Cell Proteomics* 2, 453-462.
19. Doyle, H. A., and Mamula, M. J. (2012) Autoantigenesis: the evolution of protein modifications in autoimmune disease, *Curr Opin Immunol* 24, 112-118.
20. Clement, C. C., Moncrieffe, H., Lele, A., Janow, G., Becerra, A., Bauli, F., Saad, F. A., Perino, G., Montagna, C., Cobelli, N., Hardin, J., Stern, L. J., Ilowite, N., Porcelli, S. A., and Santambrogio, L. (2016) Autoimmune response to transthyretin in juvenile idiopathic arthritis, *JCI Insight* 1.
21. Clement, C. C., Nanaware, P. P., Yamazaki, T., Negroni, M. P., Ramesh, K., Morozova, K., Thangaswamy, S., Graves, A., Kim, H. J., Li, T. W., Vigano, M.,

- Soni, R. K., Gadina, M., Tse, H. Y., Galluzzi, L., Roche, P. A., Denzin, L. K., Stern, L. J., and Santambrogio, L. (2021) Pleiotropic consequences of metabolic stress for the major histocompatibility complex class II molecule antigen processing and presentation machinery, *Immunity* 54, 721-736 e710.
22. Clement, C. C., Osan, J., Buque, A., Nanaware, P. P., Chang, Y. C., Perino, G., Shetty, M., Yamazaki, T., Tsai, W. L., Urbanska, A. M., Calvo-Calle, J. M., Ramsamooj, S., Ramsamooj, S., Vergani, D., Mieli-Vergani, G., Terziroli Beretta-Piccoli, B., Gadina, M., Montagna, C., Goncalves, M. D., Sallusto, F., Galluzzi, L., Soni, R. K., Stern, L. J., and Santambrogio, L. (2022) PDIA3 epitope-driven immune autoreactivity contributes to hepatic damage in type 2 diabetes, *Sci Immunol* 7, eabl3795.
23. Zhai, Y., Chen, L., Zhao, Q., Zheng, Z. H., Chen, Z. N., Bian, H., Yang, X., Lu, H. Y., Lin, P., Chen, X., Chen, R., Sun, H. Y., Fan, L. N., Zhang, K., Wang, B., Sun, X. X., Feng, Z., Zhu, Y. M., Zhou, J. S., Chen, S. R., Zhang, T., Chen, S. Y., Chen, J. J., Zhang, K., Wang, Y., Chang, Y., Zhang, R., Zhang, B., Wang, L. J., Li, X. M., He, Q., Yang, X. M., Nan, G., Xie, R. H., Yang, L., Yang, J. H., and Zhu, P. (2023) Cysteine carboxyethylation generates neoantigens to induce HLA-restricted autoimmunity, *Science* 379, eabg2482.
24. Petersen, J., Purcell, A. W., and Rossjohn, J. (2009) Post-translationally modified T cell epitopes: immune recognition and immunotherapy, *J Mol Med (Berl)* 87, 1045-1051.
25. Marcilla, M., Alpizar, A., Lombardia, M., Ramos-Fernandez, A., Ramos, M., and Albar, J. P. (2014) Increased diversity of the HLA-B40 ligandome by the presentation of peptides phosphorylated at their main anchor residue, *Mol Cell Proteomics* 13, 462-474.
26. Bassani-Sternberg, M., Braunlein, E., Klar, R., Engleitner, T., Sinitcyn, P., Audehm, S., Straub, M., Weber, J., Slotta-Huspenina, J., Specht, K., Martignoni, M. E., Werner, A., Hein, R., D, H. B., Peschel, C., Rad, R., Cox, J., Mann, M., and Krackhardt, A. M. (2016) Direct identification of clinically relevant neoepitopes presented on native human melanoma tissue by mass spectrometry, *Nat Commun* 7, 13404.

27. Malaker, S. A., Penny, S. A., Steadman, L. G., Myers, P. T., Loke, J. C., Raghavan, M., Bai, D. L., Shabanowitz, J., Hunt, D. F., and Cobbold, M. (2017) Identification of Glycopeptides as Posttranslationally Modified Neoantigens in Leukemia, *Cancer Immunol Res* 5, 376-384.
28. Marino, F., Mommen, G. P., Jeko, A., Meiring, H. D., van Gaans-van den Brink, J. A., Scheltema, R. A., van Els, C. A., and Heck, A. J. (2017) Arginine (Di)methylated Human Leukocyte Antigen Class I Peptides Are Favorably Presented by HLA-B\*07, *J Proteome Res* 16, 34-44.
29. Mohammed, F., Stones, D. H., Zarling, A. L., Willcox, C. R., Shabanowitz, J., Cummings, K. L., Hunt, D. F., Cobbold, M., Engelhard, V. H., and Willcox, B. E. (2017) The antigenic identity of human class I MHC phosphopeptides is critically dependent upon phosphorylation status, *Oncotarget* 8, 54160-54172.
30. Mangalaparthy, K. K., Madugundu, A. K., Ryan, Z. C., Garapati, K., Peterson, J. A., Dey, G., Prakash, A., and Pandey, A. (2021) Digging deeper into the immunopeptidome: characterization of post-translationally modified peptides presented by MHC I, *J Proteins Proteom* 12, 151-160.
31. Ireland, J., Herzog, J., and Unanue, E. R. (2006) Cutting edge: unique T cells that recognize citrullinated peptides are a feature of protein immunization, *J Immunol* 177, 1421-1425.
32. Huseby, E. S., Sather, B., Huseby, P. G., and Goverman, J. (2001) Age-dependent T cell tolerance and autoimmunity to myelin basic protein, *Immunity* 14, 471-481.
33. Malmstrom, V., Catrina, A. I., and Klareskog, L. (2017) The immunopathogenesis of seropositive rheumatoid arthritis: from triggering to targeting, *Nat Rev Immunol* 17, 60-75.
34. Curran, A. M., Naik, P., Giles, J. T., and Darrah, E. (2020) PAD enzymes in rheumatoid arthritis: pathogenic effectors and autoimmune targets, *Nat Rev Rheumatol* 16, 301-315.
35. Yang, L., Tan, D., and Piao, H. (2016) Myelin Basic Protein Citrullination in Multiple Sclerosis: A Potential Therapeutic Target for the Pathology, *Neurochem Res* 41, 1845-1856.

36. Hill, J. A., Southwood, S., Sette, A., Jevnikar, A. M., Bell, D. A., and Cairns, E. (2003) Cutting edge: the conversion of arginine to citrulline allows for a high-affinity peptide interaction with the rheumatoid arthritis-associated HLA-DRB1\*0401 MHC class II molecule, *J Immunol* 171, 538-541.
37. Ramarathinam, S. H., Croft, N. P., Illing, P. T., Faridi, P., and Purcell, A. W. (2018) Employing proteomics in the study of antigen presentation: an update, *Expert Rev Proteomics* 15, 637-645.
38. Jaeger, A. M., Stopfer, L. E., Ahn, R., Sanders, E. A., Sandel, D. A., Freed-Pastor, W. A., Rideout, W. M., 3rd, Naranjo, S., Fessenden, T., Nguyen, K. B., Winter, P. S., Kohn, R. E., Westcott, P. M. K., Schenkel, J. M., Shanahan, S. L., Shalek, A. K., Spranger, S., White, F. M., and Jacks, T. (2022) Deciphering the immunopeptidome in vivo reveals new tumour antigens, *Nature* 607, 149-155.
39. Yi, X., Liao, Y., Wen, B., Li, K., Dou, Y., Savage, S. R., and Zhang, B. (2021) caAtlas: An immunopeptidome atlas of human cancer, *iScience* 24, 103107.
40. Kacen, A., Javitt, A., Kramer, M. P., Morgenstern, D., Tsaban, T., Shmueli, M. D., Teo, G. C., da Veiga Leprevost, F., Barnea, E., Yu, F., Admon, A., Eisenbach, L., Samuels, Y., Schueler-Furman, O., Levin, Y., Nesvizhskii, A. I., and Merbl, Y. (2023) Post-translational modifications reshape the antigenic landscape of the MHC I immunopeptidome in tumors, *Nat Biotechnol* 41, 239-251.
41. Garstka, M. A., Fish, A., Celie, P. H., Joosten, R. P., Janssen, G. M., Berlin, I., Hoppes, R., Stadnik, M., Janssen, L., Ovaa, H., van Veelen, P. A., Perrakis, A., and Neefjes, J. (2015) The first step of peptide selection in antigen presentation by MHC class I molecules, *Proc Natl Acad Sci U S A* 112, 1505-1510.
42. Sette, A., Vitiello, A., Reheman, B., Fowler, P., Nayarsina, R., Kast, W. M., Melief, C. J., Oseroff, C., Yuan, L., Ruppert, J., Sidney, J., del Guercio, M. F., Southwood, S., Kubo, R. T., Chesnut, R. W., Grey, H. M., and Chisari, F. V. (1994) The relationship between class I binding affinity and immunogenicity of potential cytotoxic T cell epitopes, *J Immunol* 153, 5586-5592.
43. Deribe, Y. L., Pawson, T., and Dikic, I. (2010) Post-translational modifications in signal integration, *Nat Struct Mol Biol* 17, 666-672.

44. Zhao, Y., and Jensen, O. N. (2009) Modification-specific proteomics: strategies for characterization of post-translational modifications using enrichment techniques, *Proteomics* 9, 4632-4641.
45. Solleder, M., Guillaume, P., Racle, J., Michaux, J., Pak, H. S., Muller, M., Coukos, G., Bassani-Sternberg, M., and Gfeller, D. (2020) Mass Spectrometry Based Immunopeptidomics Leads to Robust Predictions of Phosphorylated HLA Class I Ligands, *Mol Cell Proteomics* 19, 390-404.
46. Hassan, C., Kester, M. G., Oudgenoeg, G., de Ru, A. H., Janssen, G. M., Drijfhout, J. W., Spaapen, R. M., Jimenez, C. R., Heemskerk, M. H., Falkenburg, J. H., and van Veelen, P. A. (2014) Accurate quantitation of MHC-bound peptides by application of isotopically labeled peptide MHC complexes, *J Proteomics* 109, 240-244.
47. Colbert, J. D., Cruz, F. M., and Rock, K. L. (2020) Cross-presentation of exogenous antigens on MHC I molecules, *Curr Opin Immunol* 64, 1-8.
48. Lee, J. M., Hammaren, H. M., Savitski, M. M., and Baek, S. H. (2023) Control of protein stability by post-translational modifications, *Nat Commun* 14, 201.
49. Ljunggren, H. G., Stam, N. J., Ohlen, C., Neefjes, J. J., Hoglund, P., Heemels, M. T., Bastin, J., Schumacher, T. N., Townsend, A., Karre, K., and et al. (1990) Empty MHC class I molecules come out in the cold, *Nature* 346, 476-480.
50. Schumacher, T. N., Heemels, M. T., Neefjes, J. J., Kast, W. M., Melief, C. J., and Ploegh, H. L. (1990) Direct binding of peptide to empty MHC class I molecules on intact cells and in vitro, *Cell* 62, 563-567.
51. Saito, Y., Peterson, P. A., and Matsumura, M. (1993) Quantitation of peptide anchor residue contributions to class I major histocompatibility complex molecule binding, *J Biol Chem* 268, 21309-21317.
52. Ross, P., Holmes, J. C., Gojanovich, G. S., and Hess, P. R. (2012) A cell-based MHC stabilization assay for the detection of peptide binding to the canine classical class I molecule, DLA-88, *Vet Immunol Immunopathol* 150, 206-212.
53. Apostolopoulos, V., Haurum, J. S., and McKenzie, I. F. (1997) MUC1 peptide epitopes associated with five different H-2 class I molecules, *Eur J Immunol* 27, 2579-2587.

54. Cerundolo, V., Elliott, T., Elvin, J., Bastin, J., Rammensee, H. G., and Townsend, A. (1991) The binding affinity and dissociation rates of peptides for class I major histocompatibility complex molecules, *Eur J Immunol* 21, 2069-2075.
55. De Silva, A. D., Boesteanu, A., Song, R., Nagy, N., Harhaj, E., Harding, C. V., and Joyce, S. (1999) Thermolabile H-2Kb molecules expressed by transporter associated with antigen processing-deficient RMA-S cells are occupied by low-affinity peptides, *J Immunol* 163, 4413-4420.
56. Feltkamp, M. C., Vierboom, M. P., Kast, W. M., and Melief, C. J. (1994) Efficient MHC class I-peptide binding is required but does not ensure MHC class I-restricted immunogenicity, *Mol Immunol* 31, 1391-1401.
57. Elvin, J., Potter, C., Elliott, T., Cerundolo, V., and Townsend, A. (1993) A method to quantify binding of unlabeled peptides to class I MHC molecules and detect their allele specificity, *J Immunol Methods* 158, 161-171.
58. Jurtz, V., Paul, S., Andreatta, M., Marcatili, P., Peters, B., and Nielsen, M. (2017) NetMHCpan-4.0: Improved Peptide-MHC Class I Interaction Predictions Integrating Eluted Ligand and Peptide Binding Affinity Data, *J Immunol* 199, 3360-3368.
59. Dubey, P., Hendrickson, R. C., Meredith, S. C., Siegel, C. T., Shabanowitz, J., Skipper, J. C., Engelhard, V. H., Hunt, D. F., and Schreiber, H. (1997) The immunodominant antigen of an ultraviolet-induced regressor tumor is generated by a somatic point mutation in the DEAD box helicase p68, *J Exp Med* 185, 695-705.
60. Kjellen, P., Brunsberg, U., Broddefalk, J., Hansen, B., Vestberg, M., Ivarsson, I., Engstrom, A., Svejgaard, A., Kihlberg, J., Fugger, L., and Holmdahl, R. (1998) The structural basis of MHC control of collagen-induced arthritis; binding of the immunodominant type II collagen 256-270 glycopeptide to H-2Aq and H-2Ap molecules, *Eur J Immunol* 28, 755-767.
61. Rosloniec, E. F., Whittington, K. B., Zaller, D. M., and Kang, A. H. (2002) HLA-DR1 (DRB1\*0101) and DR4 (DRB1\*0401) use the same anchor residues for binding an immunodominant peptide derived from human type II collagen, *J Immunol* 168, 253-259.

62. Huizinga, T. W., Amos, C. I., van der Helm-van Mil, A. H., Chen, W., van Gaalen, F. A., Jawaheer, D., Schreuder, G. M., Wener, M., Breedveld, F. C., Ahmad, N., Lum, R. F., de Vries, R. R., Gregersen, P. K., Toes, R. E., and Criswell, L. A. (2005) Refining the complex rheumatoid arthritis phenotype based on specificity of the HLA-DRB1 shared epitope for antibodies to citrullinated proteins, *Arthritis Rheum* 52, 3433-3438.
63. Yague, J., Alvarez, I., Rognan, D., Ramos, M., Vazquez, J., and de Castro, J. A. (2000) An N-acetylated natural ligand of human histocompatibility leukocyte antigen (HLA)-B39. Classical major histocompatibility complex class I proteins bind peptides with a blocked NH<sub>2</sub> terminus in vivo, *J Exp Med* 191, 2083-2092.
64. Sun, M., Liu, J., Qi, J., Tefsen, B., Shi, Y., Yan, J., and Gao, G. F. (2014) Nalpha-terminal acetylation for T cell recognition: molecular basis of MHC class I-restricted nalpha-acetylpeptide presentation, *J Immunol* 192, 5509-5519.
65. Shastri, N., and Gonzalez, F. (1993) Endogenous generation and presentation of the ovalbumin peptide/Kb complex to T cells, *J Immunol* 150, 2724-2736.
66. Koch, C. P., Perna, A. M., Pillong, M., Todoroff, N. K., Wrede, P., Folkers, G., Hiss, J. A., and Schneider, G. (2013) Scrutinizing MHC-I binding peptides and their limits of variation, *PLoS Comput Biol* 9, e1003088.
67. Swee, L. K., Guimaraes, C. P., Sehwat, S., Spooner, E., Barrasa, M. I., and Ploegh, H. L. (2013) Sortase-mediated modification of alphaDEC205 affords optimization of antigen presentation and immunization against a set of viral epitopes, *Proc Natl Acad Sci U S A* 110, 1428-1433.
68. Fremont, D. H., Stura, E. A., Matsumura, M., Peterson, P. A., and Wilson, I. A. (1995) Crystal structure of an H-2Kb-ovalbumin peptide complex reveals the interplay of primary and secondary anchor positions in the major histocompatibility complex binding groove, *Proc Natl Acad Sci U S A* 92, 2479-2483.
69. van der Gracht, A. M. F., de Geus, M. A. R., Camps, M. G. M., Ruckwardt, T. J., Sarris, A. J. C., Bremmers, J., Maurits, E., Pawlak, J. B., Posthoorn, M. M., Bongers, K. M., Filippov, D. V., Overkleeft, H. S., Robillard, M. S., Ossendorp, F., and van Kasteren, S. I. (2018) Chemical Control over T-Cell Activation in Vivo Using

- Deprotection of trans-Cyclooctene-Modified Epitopes, *ACS Chem Biol* 13, 1569-1576.
70. Deres, K., Beck, W., Faath, S., Jung, G., and Rammensee, H. G. (1993) MHC/peptide binding studies indicate hierarchy of anchor residues, *Cell Immunol* 151, 158-167.
71. Karttunen, J., and Shastri, N. (1991) Measurement of ligand-induced activation in single viable T cells using the lacZ reporter gene, *Proc Natl Acad Sci U S A* 88, 3972-3976.
72. Curran, A. M., Girgis, A. A., Jang, Y., Crawford, J. D., Thomas, M. A., Kawalerski, R., Coller, J., Bingham, C. O., 3rd, Na, C. H., and Darrah, E. (2023) Citrullination modulates antigen processing and presentation by revealing cryptic epitopes in rheumatoid arthritis, *Nat Commun* 14, 1061.
73. Martinod, K., Witsch, T., Erpenbeck, L., Savchenko, A., Hayashi, H., Cherpokova, D., Gallant, M., Mauler, M., Cifuni, S. M., and Wagner, D. D. (2017) Peptidylarginine deiminase 4 promotes age-related organ fibrosis, *J Exp Med* 214, 439-458.
74. Raveh, B., London, N., and Schueler-Furman, O. (2010) Sub-angstrom modeling of complexes between flexible peptides and globular proteins, *Proteins* 78, 2029-2040.
75. Liu, T., Pan, X., Chao, L., Tan, W., Qu, S., Yang, L., Wang, B., and Mei, H. (2014) Subangstrom accuracy in pHLA-I modeling by Rosetta FlexPepDock refinement protocol, *J Chem Inf Model* 54, 2233-2242.
76. Tivon, B., Gabizon, R., Somsen, B. A., Cossar, P. J., Ottmann, C., and London, N. (2021) Covalent flexible peptide docking in Rosetta, *Chem Sci* 12, 10836-10847.
77. Bloodworth, N., Barbaro, N. R., Moretti, R., Harrison, D. G., and Meiler, J. (2022) Rosetta FlexPepDock to predict peptide-MHC binding: An approach for non-canonical amino acids, *PLoS One* 17, e0275759.
78. Alam, N., and Schueler-Furman, O. (2017) Modeling Peptide-Protein Structure and Binding Using Monte Carlo Sampling Approaches: Rosetta FlexPepDock and FlexPepBind, *Methods Mol Biol* 1561, 139-169.
79. Tumei, P. C., Harview, C. L., Yearley, J. H., Shintaku, I. P., Taylor, E. J., Robert, L., Chmielowski, B., Spasic, M., Henry, G., Ciobanu, V., West, A. N., Carmona, M., Kivork, C., Seja, E., Cherry, G., Gutierrez, A. J., Grogan, T. R., Mateus, C.,

- Tomasic, G., Glaspy, J. A., Emerson, R. O., Robins, H., Pierce, R. H., Elashoff, D. A., Robert, C., and Ribas, A. (2014) PD-1 blockade induces responses by inhibiting adaptive immune resistance, *Nature* 515, 568-571.
80. Topalian, S. L., Hodi, F. S., Brahmer, J. R., Gettinger, S. N., Smith, D. C., McDermott, D. F., Powderly, J. D., Carvajal, R. D., Sosman, J. A., Atkins, M. B., Leming, P. D., Spigel, D. R., Antonia, S. J., Horn, L., Drake, C. G., Pardoll, D. M., Chen, L., Sharfman, W. H., Anders, R. A., Taube, J. M., McMiller, T. L., Xu, H., Korman, A. J., Jure-Kunkel, M., Agrawal, S., McDonald, D., Kollia, G. D., Gupta, A., Wigginton, J. M., and Sznol, M. (2012) Safety, activity, and immune correlates of anti-PD-1 antibody in cancer, *N Engl J Med* 366, 2443-2454.
81. Marin-Acevedo, J. A., Dholaria, B., Soyano, A. E., Knutson, K. L., Chumsri, S., and Lou, Y. (2018) Next generation of immune checkpoint therapy in cancer: new developments and challenges, *J Hematol Oncol* 11, 39.
82. Gubin, M. M., Zhang, X., Schuster, H., Caron, E., Ward, J. P., Noguchi, T., Ivanova, Y., Hundal, J., Arthur, C. D., Krebber, W. J., Mulder, G. E., Toebes, M., Vesely, M. D., Lam, S. S., Korman, A. J., Allison, J. P., Freeman, G. J., Sharpe, A. H., Pearce, E. L., Schumacher, T. N., Abersold, R., Rammensee, H. G., Melief, C. J., Mardis, E. R., Gillanders, W. E., Artyomov, M. N., and Schreiber, R. D. (2014) Checkpoint blockade cancer immunotherapy targets tumour-specific mutant antigens, *Nature* 515, 577-581.
83. Riaz, N., Morris, L., Havel, J. J., Makarov, V., Desrichard, A., and Chan, T. A. (2016) The role of neoantigens in response to immune checkpoint blockade, *Int Immunol* 28, 411-419.
84. Zhang, P., Du, Y., Bai, H., Wang, Z., Duan, J., Wang, X., Zhong, J., Wan, R., Xu, J., He, X., Wang, D., Fei, K., Yu, R., Tian, J., and Wang, J. (2022) Optimized dose selective HDAC inhibitor tucidinostat overcomes anti-PD-L1 antibody resistance in experimental solid tumors, *BMC Med* 20, 435.
85. Truong, A. S., Zhou, M., Krishnan, B., Utsumi, T., Manocha, U., Stewart, K. G., Beck, W., Rose, T. L., Milowsky, M. I., He, X., Smith, C. C., Bixby, L. M., Perou, C. M., Wobker, S. E., Bailey, S. T., Vincent, B. G., and Kim, W. Y. (2021) Entinostat

- induces antitumor immune responses through immune editing of tumor neoantigens, *J Clin Invest* 131.
86. Baretta, M., and Yarchoan, M. (2021) Epigenetic modifiers synergize with immune-checkpoint blockade to enhance long-lasting antitumor efficacy, *J Clin Invest* 131.
87. Burke, B., Eden, C., Perez, C., Belshoff, A., Hart, S., Plaza-Rojas, L., Delos Reyes, M., Prajapati, K., Voelkel-Johnson, C., Henry, E., Gupta, G., and Guevara-Patino, J. (2020) Inhibition of Histone Deacetylase (HDAC) Enhances Checkpoint Blockade Efficacy by Rendering Bladder Cancer Cells Visible for T Cell-Mediated Destruction, *Front Oncol* 10, 699.
88. Llopiz, D., Ruiz, M., Villanueva, L., Iglesias, T., Silva, L., Egea, J., Lasarte, J. J., Pivette, P., Trochon-Joseph, V., Vasseur, B., Dixon, G., Sangro, B., and Sarobe, P. (2019) Enhanced anti-tumor efficacy of checkpoint inhibitors in combination with the histone deacetylase inhibitor Belinostat in a murine hepatocellular carcinoma model, *Cancer Immunol Immunother* 68, 379-393.
89. Gameiro, S. R., Malamas, A. S., Tsang, K. Y., Ferrone, S., and Hodge, J. W. (2016) Inhibitors of histone deacetylase 1 reverse the immune evasion phenotype to enhance T-cell mediated lysis of prostate and breast carcinoma cells, *Oncotarget* 7, 7390-7402.
90. Woods, D. M., Sodre, A. L., Villagra, A., Sarnaik, A., Sotomayor, E. M., and Weber, J. (2015) HDAC Inhibition Upregulates PD-1 Ligands in Melanoma and Augments Immunotherapy with PD-1 Blockade, *Cancer Immunol Res* 3, 1375-1385.

## **Chapter 6 Impact of Non-Enzymatic Modification to Peptides on MHC Peptide Binding and TCR Engagement**

Adapted from: Joey J. Kelly, Tian Zhang, and Marcos M. Pires., Impact of Non-Enzymatic Modification to Peptides on MHC Peptide Binding and TCR Engagement. **2025**. Manuscript in preparation.

### **6.1 Abstract**

The adaptive immune system relies on the presentation of antigenic peptides by major histocompatibility complex class I (MHC-I) molecules to cytotoxic T cells, enabling the identification and elimination of infected or transformed cells. These peptides are typically derived from intracellular proteins and undergo a rigorous selection process to ensure self-tolerance. However, post-translational modifications (PTMs) and non-enzymatic chemical modifications can introduce structural and chemical modifications to peptides, potentially affecting immune recognition. In this study, we investigated the impact of non-enzymatic PTMs on antigen presentation and T cell recognition. Using the well-characterized model epitope SIINFEKL, we synthesized and analyzed variants incorporating common non-enzymatically derived PTMs to assess their impact on MHC-I binding interactions as well as T cell recognition. Additionally, we developed an enrichment strategy using an alkyne-modified probe to identify sites of non-enzymatic acylation prone to MHC-I display. These findings underscore the significance of non-enzymatic PTMs in altering the immunopeptidome and modulating immune responses.

### **6.2 Introduction**

The adaptive immune system represents a formidable defensive system against infected and transformed cells. Principally, adaptive immunity relies on the ability of immune cells to recognize and respond to specific antigens, which are often presented as peptides on the surface of host cells. Major histocompatibility complex (MHC) molecules, and the peptides they present, are pivotal to the orchestration of immune defense.<sup>1, 2</sup> MHC molecules are grouped into two main classes: class I and class II.<sup>3</sup> While both classes

are critical for immune function, MHC class I (MHC-I) molecules are the primary vehicle in presenting peptides to cytotoxic T cells.<sup>4</sup>

MHC-I molecules are expressed on the surface of nearly all nucleated cells in the human body. MHC-I molecules bind and present a diverse array of peptides derived from the protease digestion of intracellular proteins.<sup>5</sup> Once displayed on the surface of the host cells within MHC-I, this complex is primed to engage with cytotoxic T cells, a subset of T lymphocytes specialized in identifying and eliminating peptides that are not recognized to be “self”.<sup>6</sup> The designation of self vs non-self is paramount to the proper function of the adaptive immune system. The repertoire of T cells circulating in an adult represents the output that follows a negative selection process in the thymus, which starts in early childhood and effectively wanes towards the end of adolescence.<sup>7</sup> Through this process, T cells whose T cell receptors (TCRs) have propensity to bind self-peptides are killed and removed from future propagation. As a result, the remaining T cells in circulation can potentially bind to any peptides that were not included in the negative selection process.<sup>8</sup>

We typically assign non-self-antigens as peptides derived from pathogens (e.g., bacteria, fungi, and viruses) or transformed cells derived from genetic lesions that yielded new primary sequences. But more broadly, non-self-peptides can be any peptide sequence that has altered chemical composition.<sup>9</sup> Crucially, the presented peptides on MHC-I molecules are not static; they are highly dynamic and subject to variation based on the chemical changes to the proteome.<sup>10</sup> The amino acid sequence of the presented peptide is critical for this recognition. Even a single amino acid alteration can drastically affect the TCR's ability to recognize the peptide, potentially rendering the immune response ineffective.<sup>11, 12</sup> Therefore, it is of paramount importance to evaluate the impact of amino acid modifications on the peptides presented by MHC-I molecules, as these changes can profoundly influence the efficiency of immune surveillance and response.

Amino acid modifications on presented peptides can occur through various mechanisms. Pre-translational modifications often occur via a genetic mutation that swaps an amino acid for another canonical amino acid. Because the human genome (except for cancerous lesions) is relatively stable, pre-translational modifications are mostly represented in the negative selection and do not constitute a non-self-peptidic antigen.<sup>13</sup> In contrast, post-

translational modifications (PTMs) are not necessarily covered in the negative selection.<sup>14</sup> To this end, it was recently revealed that most PTMs are poorly selected against due to their low abundance through the thymus lifetime.<sup>15</sup> PTMs, such as phosphorylation, glycosylation, and ubiquitination, can alter the structure and function of proteins, including those that are later processed into peptides for presentation.<sup>16, 17</sup> These modifications can affect the peptide binding affinity for MHC-I molecules or its recognition by TCRs, ultimately influencing the immune response.<sup>18-22</sup> We recently systematically assessed the impact of PTMs on the binding affinity and T cell recognition by synthetically accessing these modified peptides and comparing them with their unmodified counterparts.<sup>23</sup> PTMs are chemical marks that are installed and removed by enzymatic process, which are often orchestrated in a regulated balanced manner.<sup>24</sup> In diseased states, the PTM balance can be altered and result in immunopathological conditions.<sup>25-29</sup>

A less appreciated form of post-translational modification of proteins involves chemical change by non-enzymatic chemical entities. While some of these modifications are native and regulated (e.g., some forms of cysteine oxidation during oxidative bursts), other chemical alterations are not tightly regulated, and, therefore, can yield a pool of non-self peptides.<sup>30-34</sup> Most significantly, whereas most enzymatic PTMs can be reversed by erasers, the reversal of non-enzymatic PTMs have not been reported to be natively reversed.<sup>35</sup> By in large, the chemical entities that result in non-enzymatic PTMs are electrophilic species that react with nucleophilic amino acids (e.g., cysteine, arginine, lysine, histidine, tyrosine, and to a less extent aspartic acid and glutamic acid). The source of the electrophilic species also varies, and this has implications for the source of the immunological response. There are well known examples of reactive species naturally formed in healthy cells such as reactive oxygen species (ROS), reactive nitrogen species (RNS), oxidative phosphorylation byproducts (starting with methyl oxyglacal), and non-native short chain fatty acids that are activated to acetyl-co-enzyme A adducts.<sup>36</sup>

In the absence of the inclusion of these chemical modifications during the negative selection, these modified proteins (and the non-self peptides they generate) can potentially be the source of auto-immunity pathologies.<sup>37</sup> The implications of the amino acid modifications on peptide presentation are vast. Firstly, such modifications can affect

the stability of the peptide-MHC complex. The binding affinity between a peptide and MHC-I molecule is a critical determinant of whether the peptide will be effectively presented to T cells. Amino acid modifications can either enhance or disrupt this binding, thereby influencing the stability of the complex and the likelihood of T cell recognition.<sup>38, 39</sup> Secondly, these modifications can directly impact the interaction between the presented peptide and the T cell receptor (TCR) of cytotoxic T cells. TCRs are finely tuned to recognize specific peptide-HLA combinations. Any alteration in the peptide sequence due to amino acid modifications can potentially disrupt this recognition, inhibiting the immune response against the infected or transformed cell.<sup>40, 41</sup> Furthermore, the presence of modified peptides can lead to the activation of autoimmune responses, where the immune system mistakenly targets healthy, self-cells.<sup>42</sup> This is particularly relevant in the context of autoimmune diseases where the immune system erroneously recognizes self-peptides with amino acid modifications as foreign, leading to chronic inflammation and tissue damage.<sup>43-47</sup> Here, we determine the effects of non-enzymatic PTMs on the stability of the pMHC complex and T cell recognition, as well as develop a novel enrichment strategy to identify sites of non-enzymatic modification displayed on MHC.

### 6.3 Results and Discussion

To investigate how non-enzymatic PTMs influence peptide affinity for MHC molecules, we employed RMA-S cells. These cells lack the transporter associated with antigen processing (TAP), leading to reduced surface expression on H-2K<sup>b</sup>.<sup>48, 49</sup> However, incubation with high-affinity peptides stabilizes H-2K<sup>b</sup> molecules, restoring their surface expression. Previous studies have demonstrated a strong correlation between the abundance of surface MHC complexes and peptide affinity for H-2K<sup>b</sup>.<sup>50-52</sup>

To investigate the effects of non-enzymatic PTMs on peptide affinity for MHC, we used the model epitope SIINFEKL (**ovaWT**) from the protein ovalbumin. **ovaWT** is widely used in antigen presentation studies due to its well-characterized interactions with H-2K<sup>b</sup>, allowing us to assess how non-enzymatic PTMs influence antigen presentation.<sup>53</sup> One of the residues we investigated was the lysine residue of **ovaWT** as lysine is among the most frequently modified amino acids. One major driver of non-enzymatic PTMs is oxidative stress, which can lead to lysine modifications such as side-chain formylation

and the conversion of the  $\gamma$ -amine to aminoadipic acid or homocitrulline.<sup>54, 55</sup> Another significant class of lysine PTMs arise from reactions with reactive sugar metabolites, forming stable covalent adducts.<sup>56, 57</sup> To examine these modifications, we synthesized **ovaWT** variants incorporating a formylated lysine side chain (**ovaK7<sub>formyl</sub>**), aminoadipic acid (**ovaK7<sub>aad</sub>**), homocitrulline (**ovaK7<sub>hcit</sub>**), and a lactic acid adduct (**ovaK7<sub>lac</sub>**).

Additionally, **ovaWT** contains an asparagine residue which is commonly presented on MHC-I after its undergone deamidation.<sup>58</sup> Deamidation often occurs through the formation of a succinimide intermediate, leading to the conversion of asparagine to aspartate or the formation of an iso-aspartate bond in the peptide backbone.<sup>59</sup> Notably, deamidation can also result from enzymatic activity, as N-glycosidase enzymes remove glycosylated asparagine residues, contributing to the presentation of deamidated peptides on MHC molecules.<sup>60</sup> To assess the impact of deamidation on **ovaWT**, we synthesized peptide variants in which asparagine was replaced with aspartate (**ovaN4D**) or an iso-aspartate bond (**ovaN4D<sub>iso</sub>**)

Lastly, cysteine is another nucleophilic residue prone to non-enzymatic PTMs. However, because **ovaWT** does not naturally contain a cysteine residue, we introduced a cysteine at position six (**ovaE6C**) to assess its impact on MHC binding. This modification allowed us to investigate how PTMs at different peptide positions affect H-2K<sup>b</sup> binding while minimizing disruptions to known “anchor point” residues essential for affinity.<sup>61</sup> Notably, **ovaE6C** exhibited enhanced MHC binding compared to **ovaWT**. Cysteine is highly susceptible to oxidation, leading to the irreversible formation of a sulfonic acid PTM.<sup>62</sup> To examine this modification, we synthesized a sulfonic acid-modified variant (**ovaE6C<sub>so3</sub>**). Additionally, cysteine-containing peptides have been reported to form disulfide bonds with free molecules, altering their immunogenic properties.<sup>33, 63</sup> To explore this, we synthesized variants featuring glutathione disulfide modification (**ovaE6C<sub>GSH</sub>**). Beyond oxidation, cysteine is also highly reactive toward electrophilic metabolites such as fumarate and itaconate.<sup>64, 65</sup> To investigate these modifications, we synthesized peptides modified with fumarate (**ovaE6C<sub>fum</sub>**) and itaconate (**ovaE6C<sub>ita</sub>**).

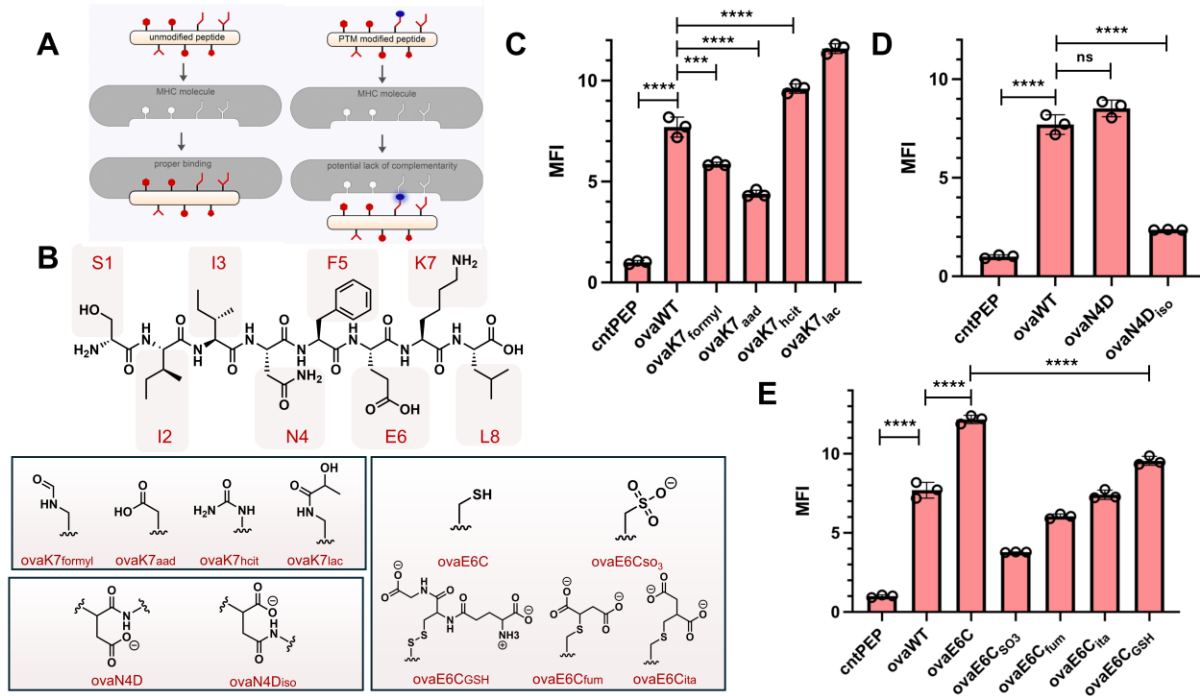


**Figure 6.1** (A) Schematic representation of how chemical modifications can negatively influence binding to MHC-I molecules (right). (B) Chemical structures of ovaWT and the PTM modified variants. Flow cytometry analysis of RMA-S cells treated with indicated peptide (5  $\mu$ M) detected by APC conjugated anti-mouse H-2Kb antibody for lysine modifications (C) asparagine modifications (D) or cysteine modifications (E). Data is represented as mean  $\pm$  SD (N=3). Adjusted p-values were determined by a one-way ANOVA with multiple comparisons (\*\*\*  $p < 0.001$ , \*\*\*\*  $p < 0.0001$ , ns = not significant).

### 6.3.1 Impact of modifications on MHC-I affinity

With these peptides in hand, we examined how the modifications affect **ovaWT** binding to H-2K<sup>b</sup>. RMA-S cells were incubated with 5  $\mu$ M peptide, revealing that the lysine modifications had minimal impact on MHC affinity. This result was expected, as position 7 of **ovaWT** is a solvent-exposed site with limited interactions with the H-2K<sup>b</sup> molecule (**Figure 6.1C**). While such residues are less critical for MHC binding, they are more likely to influence T cell recognition. For asparagine modifications, **ovaN4D** had no significant effect on MHC affinity compared to **ovaWT**. However, **ovaN4D<sub>iso</sub>** showed a marked decrease in MHC surface expression on RMA-S cells, suggesting that structural alteration to the peptide backbone can significantly disrupt peptide binding (**Figure 6.1D**). We next

assessed how cysteine modifications influence MHC binding relative to **ovaE6C**. Oxidation to sulfonic acid (**ovaE6C<sub>SO3</sub>**) resulted in the greatest reduction in affinity. Surprisingly, conjugation to glutathione (**ovaE6C<sub>GSH</sub>**) had no significant effect, indicating that even large structural modifications at this position can be well tolerated for MHC presentation (**Figure 6.1E**).

### 6.3.2 Impact of modifications on TCR recognition

Next, we evaluated how non-enzymatic PTMs affect T cell recognition of their target ligand. RMA-S cells were incubated with 5  $\mu$ M peptide and then co-cultured with B3Z T cells. B3Z T cells express a TCR specific to **ovaWT** presented by H-2K<sup>b</sup> and contain a  $\beta$ -galactosidase reporter gene under the control of an IL-2 inducible promoter. Upon recognition of its cognate ligand, B3Z activation induces  $\beta$ -galactosidase expression, which can be quantified on a plate reader via the enzymatic conversion of chlorophenol red  $\beta$ -D galactopyranoside (CPRG) to chlorophenol red.<sup>66</sup>

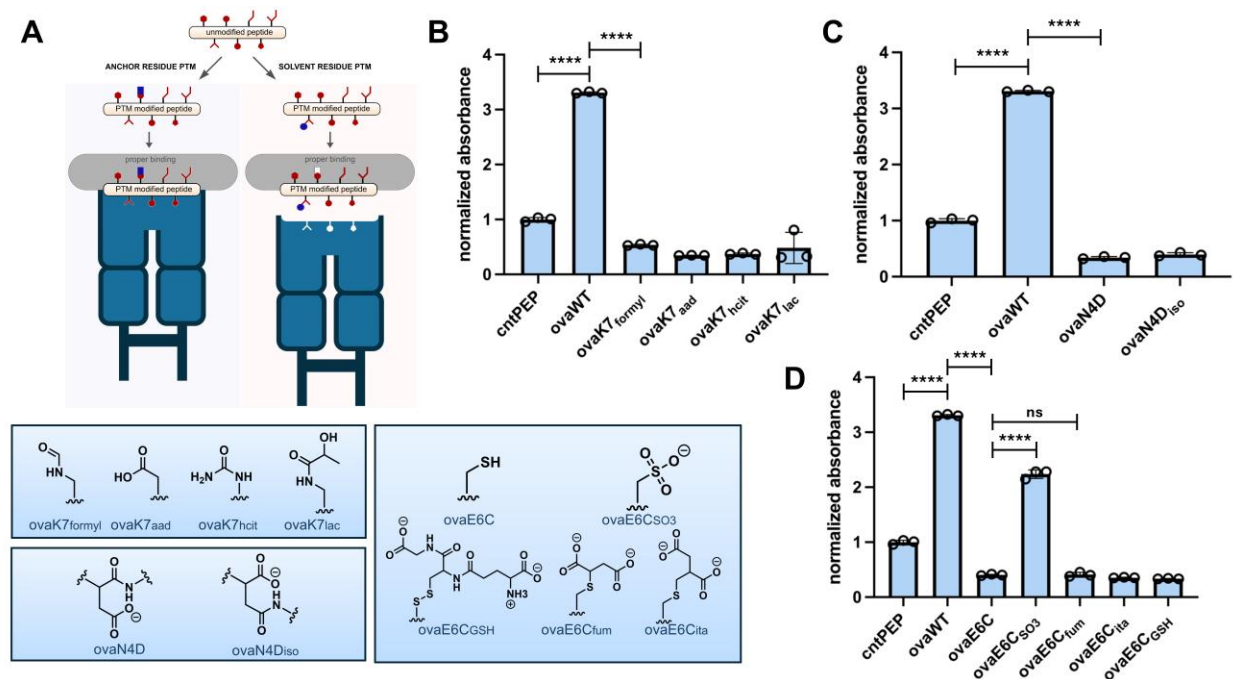


**Figure 6.2** (A) Schematic representation of how chemical modifications can influence TCR recognition. (B) RMA-S cells were incubated with indicated peptide and B3Z T cells overnight at an effector to target ratio of 1:1.  $\beta$ -galactosidase expression was then

measured via the conversion of the colorimetric reagent CPRG on a plate reader at 570 nm.  $\beta$ -galactosidase expression was determined for peptides with lysine modifications (C) asparagine modifications (D) or cysteine modifications (E). Adjusted *p*-values were determined by a one-way ANOVA with multiple comparisons (\*\*\*\*  $p < 0.0001$ , *ns* = not significant).

As previously mentioned, position 7 of **ovaWT** is a solvent-exposed residue that plays a key role in TCR interactions. As expected, despite its minimal effects on H-2K<sup>b</sup> affinity, modifications this position completely abrogated T cell activation (**Figure 6.2B**). This is likely due to the loss of the lysine side chain's positive charge, as previous studies have shown that charge alterations at TCR-contact residues can eliminate recognition.<sup>23, 67</sup> Similarly, both asparagine modifications abolished T cell activation, further supporting the notion that charge-altering modifications significantly impact TCR recognition (**Figure 6.2C**).

Since **ovaE6C** introduces a structural change relative to **ovaWT**, we did not anticipate significant insights into how cysteine modifications influence T cell activation. Indeed, **ovaE6C** did not enhance activation compared to the control peptide. However, unexpectedly, the sulfonic acid-modified variant **ovaE6C<sub>so3</sub>** restored T cell activation (**Figure 6.2D**). We attribute this response to the sulfonic acid moiety structurally mimicking the original glutamate residue. This finding suggests that negatively charged oxidized PTMs can functionally mimic negatively charged residues, potentially contributing to cross-reactivity of T cells. Overall, these results provide proof-of-concept that non-enzymatic PTMs can dramatically influence the antigen presentation via MHC molecules and modulate T cell responses.

### **6.3.3 Identification of acylation sites displayed on MHC-I**

We next aimed to identify targets of non-enzymatic modifications by developing an enrichment strategy to isolate modified peptides. A targeted pull-down approach was necessary because unbiased methods often fail to detect low-abundance modifications in complex cellular environments.<sup>68</sup> To achieve selective capture, we propose to first tag sites of non-enzymatic acylation sites using an alkyne-modified chemical probe (**1**), previously developed for labeling such modifications.<sup>69</sup> Then, we would isolate MHC-

associated peptides from cells by mild-acid elution,<sup>70, 71</sup> followed by a reaction with biotin-azide through copper-catalyzed azide-alkyne cycloaddition (CuAAC). This would allow for the subsequent capture of modified peptides on streptavidin-functionalized beads and identification of the acylation sites by LC-MS/MS. Non-enzymatic lysine acylation occurs from the nucleophilic attack of the lysine side-chain amine on a coenzyme A thioester intermediate, leading to modifications such as acetylation, succinylation, crotonylation, butyrylation, and malonylation.<sup>72-74</sup> Therefore, we anticipate that this strategy would enable the identification of non-enzymatic acylation sites displayed on MHC-I.

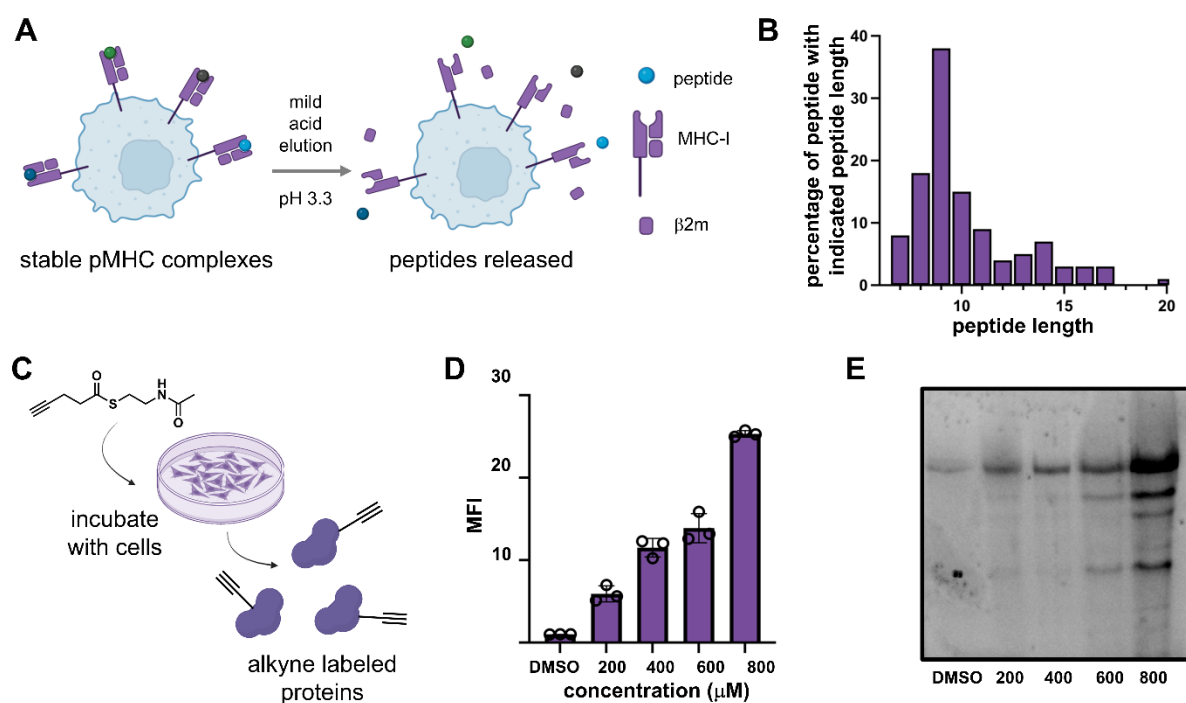


**Figure 6.3** (A) Schematic representing release of MHC-binding peptides from MAE treatment. (B) Distribution of peptide lengths identified from a MAE treated sample of  $10^9$  MDA-MB-231 cells. (C) Schematic representation of protein labeling strategy with **1**. (D) Flow cytometry analysis of **1** treated MDA-MB-231 cells. MDA-MB-231 were treated with indicated concentrations of **1** before being treated with FAM- $N_3$  in a solution of  $CuSO_4$ , ascorbic acid, and THPTA. Data is represented as mean  $\pm$  SD (N=3). P-values were determined by a two-tailed t-test (\*  $p < 0.05$ , \*\*  $p < 0.01$ , \*\*\*  $p < 0.001$ , \*\*\*\*  $p < 0.0001$ , ns = not significant). (E) Fluorescent SDS-PAGE analysis of MDA-MB-231

*cells treated with 1 followed by incubation with FAM-N<sub>3</sub>, CuSO<sub>4</sub>, ascorbic acid, and THPTA.*

We first confirmed that mild-acid elution allowed us to isolate MHC-associated peptides from MDA-MB-231 cells (**Figure 6.3A**). Cells were treated with a citric acid buffer at pH 3.3 and the supernatant underwent centrifugation and purification on an Oasis-HLB column prior to filtration with a molecular weight cutoff Amicon ultrafilter device then analyzed via LC-MS/MS. Here, we found that 80% of peptides recovered were centered around 8-12 amino acids in length, which is in agreement with the known lengths preferred by presentation by MHC-I molecules (**Figure 6.3B**).<sup>75</sup>

Next, we evaluated if whether **1** could label acylation sites. To confirm cellular incorporation, MDA-MB-231 cells were treated with increasing concentrations of **1**, followed by reaction with FAM-azide, and then cellular fluorescence was measured by flow cytometry (**Figure 6.3C**). We observed a concentration-dependent increase in labeling efficiency, indicating successful probe uptake (**Figure 6.3D**). To further validate that **1** effectively labeled protein targets, we performed fluorescent gel analysis using lysates from **1** treated cells after FAM-azide labeling (**Figure 6.3E**), confirming effective incorporation onto protein targets. With this, we are well-suited to capture and enrich MHC-associated peptides modified with **1** to identify sites of non-enzymatic acylation that are displayed on MHC.

#### **6.4 Conclusion**

In this study, we investigated the impact of non-enzymatic PTMs on MHC-I antigen presentation and T cell recognition. Our results demonstrate that non-enzymatic PTMs can significantly alter peptide binding affinity to MHC-I molecules and modulate TCR recognition. These findings highlight the potential for non-enzymatic PTMs to influence immune surveillance by modifying the immunopeptidome in ways that could either enhance or disrupt antigen presentation. Furthermore, our analysis of cancer-associated peptides revealed that non-enzymatic PTMs can affect MHC-I stability. This suggests that such modifications may contribute to immune evasion or, conversely, create novel antigenic targets for immune recognition.

Additionally, we are developing an enrichment strategy to identify non-enzymatic acylation sites displayed on MHC-I. This is particularly important because modified MHC-associated peptides can evade negative selection, enabling them to initiate an immune response. Identifying these modified MHC-associated peptides could provide insights into the development of neoantigens for cancer immunotherapy and their role in autoimmune disease

One major source of non-enzymatic acylation occurs from short-chain fatty acids (SCFAs), which can be incorporated into coenzyme A and modify lysine residues. SCFAs are produced by the gut microbiota through the fermentation of dietary fibers and are presented in millimolar concentrations in the gut lumen, where they have been shown to induce acylation in human proteins.<sup>76, 77</sup> Moreover, recent studies suggest that SCFAs may contribute to the progression of irritable bowel syndrome (IBS).<sup>78</sup> Given their ability to modify proteins, including sequences displayed on MHC-I, investigating SCFA-induced modifications could help elucidate mechanisms underlying inflammatory conditions such as IBS.

### ***6.5 Summary and Future Outlook***

In Chapter 6, we examined how non-enzymatic modifications to peptides by reactive species influence the antigen presentation pathway. These modifications may play a crucial role in the presentation of cancer-specific neoantigens, given the tumor microenvironment's high levels of reactive oxygen species and other reactive metabolites due to accelerated tumor growth. These conditions create ideal conditions for generating unique neoantigens, which could be exploited for cancer-specific immune responses. Identifying these modified neoantigens could enable the development of novel immunotherapies by improving neoantigen prediction and enhancing T cell recognition. Additionally, identifying modified neoantigens may help describe the progression of inflammatory autoimmune conditions.

More broadly, there is growing recognition that exogenous metabolites can shape immune responses. For example, haptenated antigens presented on MHC molecules have been implicated in  $\beta$ -lactam allergy development. This suggests that exposure to other electrophilic species, such as pesticides or environmental toxins, could similarly

induce immune responses by modifying peptides and altering antigen presentation. Additionally, pioneering work by the Craik lab has shown that haptens modifying cancer-specific mutations can be leveraged for immunotherapy. Given the increasing prevalence of covalent drugs as a therapeutic modality, it is plausible that covalent modifications contribute to immune responses over time by promoting the display of modified peptides on MHC. A deeper investigation into the mechanisms by which covalent drug modifications influence antigen presentation could reveal new insights into unintended immunogenicity or even novel therapeutic strategies.

## 6.6 Materials and Methods

**Materials.** All peptide related reagents and protected amino acids were purchased from Chem Impex. APC-labeled anti-mouse H-2K<sup>d</sup>/H-2D<sup>d</sup> antibody was purchased from Biolegend. Pooled Human Serum and acetic acid (glacial, >99.99% trace metals basis), and penicillin-streptomycin was purchased from Sigma Aldrich. Dulbecco's Modified Eagle's Medium (DMEM) was purchased from VWR. Fetal Bovine Serum (FBS) was purchased from R&D Systems.

**Mammalian Cell Culture.** RMA-S cells were a kind gift from Dr. John Sampson. RMA-S cells were maintained in RPMI 1640 media supplemented with 10% fetal bovine serum, 50 IU/mL penicillin, 50 µg/mL streptomycin, 1X MEM non-essential amino acid solution (ThermoFisher) and cultured in a humidified atmosphere of 5% CO<sub>2</sub> at 37°C. B3Z cells were kindly provided by Dr. Aaron Esser-Kahn and maintained in RPMI 1640 media supplemented with 10% fetal bovine serum, 50 IU/mL penicillin, 50 µg/mL streptomycin and cultured in a humidified atmosphere of 5% CO<sub>2</sub> at 37°C. MDA-MB-231 cells were maintained in DMEM media supplemented with 10% fetal bovine serum, 50 IU/mL penicillin, 50 µg/mL streptomycin and cultured in a humidified atmosphere of 5% CO<sub>2</sub> at 37°C.

**RMA-S Stabilization Assay.** 10<sup>5</sup> RMA-S cells were seeded in a treated 96 well plate at 37°C overnight. The next day, RMA-S cells were moved to a 26°C incubator for 24-48 hours. Following the incubation period, cells were incubated with peptides in culture

media at indicated concentrations for 1 hour at 26°C before being moved to the 37°C incubator for 6 hours. The media was then replaced with a 1:100 dilution of APC-labeled anti-mouse H-2K<sup>d</sup>/H-2D<sup>d</sup> antibody in culture media for 1 hour at 4°C. Cells were removed from the well plate by vigorous pipetting, fixed with 2% formaldehyde solution, and analyzed using the Attune NxT Flow Cytometer (Thermo Fischer) equipped with a 637 nm laser with 670/14 nm bandpass filter.

**B3Z T cell activation:** 10<sup>5</sup> RMA-S cells were seeded in a treated 96 well plate at 37°C overnight. The following day the culture media was replaced with media containing indicated concentration of peptide along with 10<sup>5</sup> B3Z cells in culture media and co-incubated overnight. Cells were then spun down at 500xg for 5 mins and washed with 1X PBS a total of two times. Lysis buffer containing 0.2% saponin, 500 μM CPRG reagent, 100 mM MgCl<sub>2</sub>, and 100 mM β-mercaptoethanol in 1X PBS was added to each well. After 2-4 hours absorbance 570 was recorded using a BioTek Epoch 2 microplate reader.

**Mild Acid Elution.** 10<sup>9</sup> MDA-MB-231 cells thoroughly washed with 1X PBS Buffer pH 7.4 (Invitrogen). Next, 15 mL of mild acid elution (MAE) buffer (0.131 M citric acid, 0.066M Na<sub>2</sub>HPO<sub>4</sub>, 150 mM NaCl, 0.3 μM Aprotinin, and 5 mM iodoacetamide at pH 3.3) was added to MDA-MB-231 cells for 2 min. MDA-MB-231 cells were then spun down at 4000 x g for 5 min and the supernatant was collected. Next, the supernatant was filtered through an Oasis HLB column (Waters). The supernatant was then filtered through a 15 mL Amicon 3 kDa cutoff centrifuge filter before being lyophilized and stored at -80°C.

## 6.7 References

1. Neefjes, J., Jongsma, M. L., Paul, P., and Bakke, O. (2011) Towards a systems understanding of MHC class I and MHC class II antigen presentation, *Nat Rev Immunol* 11, 823-836.
2. Pishesha, N., Harmand, T. J., and Ploegh, H. L. (2022) A guide to antigen processing and presentation, *Nat Rev Immunol* 22, 751-764.
3. Roche, P. A., and Furuta, K. (2015) The ins and outs of MHC class II-mediated antigen processing and presentation, *Nat Rev Immunol* 15, 203-216.
4. Rock, K. L., Reits, E., and Neefjes, J. (2016) Present Yourself! By MHC Class I and MHC Class II Molecules, *Trends Immunol* 37, 724-737.
5. Hulpke, S., and Tampe, R. (2013) The MHC I loading complex: a multitasking machinery in adaptive immunity, *Trends Biochem Sci* 38, 412-420.
6. Vyas, J. M., Van der Veen, A. G., and Ploegh, H. L. (2008) The known unknowns of antigen processing and presentation, *Nat Rev Immunol* 8, 607-618.
7. Ashby, K. M., and Hogquist, K. A. (2024) A guide to thymic selection of T cells, *Nat Rev Immunol* 24, 103-117.
8. Klein, L., Kyewski, B., Allen, P. M., and Hogquist, K. A. (2014) Positive and negative selection of the T cell repertoire: what thymocytes see (and don't see), *Nat Rev Immunol* 14, 377-391.
9. Xie, N., Shen, G., Gao, W., Huang, Z., Huang, C., and Fu, L. (2023) Neoantigens: promising targets for cancer therapy, *Signal Transduct Target Ther* 8, 9.
10. Truong, H. V., and Sgourakis, N. G. (2021) Dynamics of MHC-I molecules in the antigen processing and presentation pathway, *Curr Opin Immunol* 70, 122-128.
11. Schumacher, T. N., Scheper, W., and Kvistborg, P. (2019) Cancer Neoantigens, *Annu Rev Immunol* 37, 173-200.
12. Saito, N. G., Chang, H. C., and Paterson, Y. (1999) Recognition of an MHC class I-restricted antigenic peptide can be modulated by para-substitution of its buried tyrosine residues in a TCR-specific manner, *J Immunol* 162, 5998-6008.
13. Palmer, E. (2003) Negative selection--clearing out the bad apples from the T-cell repertoire, *Nat Rev Immunol* 3, 383-391.

14. Zhai, Y., and Zhu, P. (2023) Post-translationally modified neoantigens: Promising targets for diagnostic strategy of autoimmune diseases, *Clin Transl Med* 13, e1373.
15. Raposo, B., Merky, P., Lundqvist, C., Yamada, H., Urbonaviciute, V., Niaudet, C., Viljanen, J., Kihlberg, J., Kyewski, B., Ekwall, O., Holmdahl, R., and Backlund, J. (2018) T cells specific for post-translational modifications escape intrathymic tolerance induction, *Nat Commun* 9, 353.
16. Andersen, M. H., Bonfill, J. E., Neisig, A., Arsequell, G., Sondergaard, I., Neefjes, J., Zeuthen, J., Elliott, T., and Haurum, J. S. (1999) Phosphorylated peptides can be transported by TAP molecules, presented by class I MHC molecules, and recognized by phosphopeptide-specific CTL, *Journal of Immunology* 163, 3812-3818.
17. Haurum, J. S., Hoier, I. B., Arsequell, G., Neisig, A., Valencia, G., Zeuthen, J., Neefjes, J., and Elliott, T. (1999) Presentation of cytosolic glycosylated peptides by human class I major histocompatibility complex molecules in vivo, *J Exp Med* 190, 145-150.
18. Petersen, J., Wurzbacher, S. J., Williamson, N. A., Ramarathinam, S. H., Reid, H. H., Nair, A. K., Zhao, A. Y., Nastovska, R., Rudge, G., Rossjohn, J., and Purcell, A. W. (2009) Phosphorylated self-peptides alter human leukocyte antigen class I-restricted antigen presentation and generate tumor-specific epitopes, *Proc Natl Acad Sci U S A* 106, 2776-2781.
19. Mohammed, F., Cobbold, M., Zarling, A. L., Salim, M., Barrett-Wilt, G. A., Shabanowitz, J., Hunt, D. F., Engelhard, V. H., and Willcox, B. E. (2008) Phosphorylation-dependent interaction between antigenic peptides and MHC class I: a molecular basis for the presentation of transformed self, *Nat Immunol* 9, 1236-1243.
20. Malaker, S. A., Penny, S. A., Steadman, L. G., Myers, P. T., Loke, J. C., Raghavan, M., Bai, D. L., Shabanowitz, J., Hunt, D. F., and Cobbold, M. (2017) Identification of Glycopeptides as Posttranslationally Modified Neoantigens in Leukemia, *Cancer Immunol Res* 5, 376-384.
21. Corthay, A., Bäcklund, J., Broddefalk, J., Michaëlsson, E., Goldschmidt, T. J., Kihlberg, J., and Holmdahl, R. (1998) Epitope glycosylation plays a critical role

- for T cell recognition of type II collagen in collagen-induced arthritis, *Eur J Immunol* 28, 2580-2590.
22. Bäcklund, J., Treschow, A., Bockermann, R., Holm, B., Holm, L., Issazadeh-Navikas, S., Kihlberg, J., and Holmdahl, R. (2002) Glycosylation of type II collagen is of major importance for T cell tolerance and pathology in collagen-induced arthritis, *Eur J Immunol* 32, 3776-3784.
  23. Kelly, J. J., Bloodworth, N., Shao, Q., Shabanowitz, J., Hunt, D., Meiler, J., and Pires, M. M. (2024) A Chemical Approach to Assess the Impact of Post-translational Modification on MHC Peptide Binding and Effector Cell Engagement, *ACS Chem Biol* 19, 1991-2001.
  24. Conibear, A. C. (2020) Deciphering protein post-translational modifications using chemical biology tools, *Nat Rev Chem* 4, 674-695.
  25. Doyle, H. A., and Mamula, M. J. (2012) Autoantigenesis: the evolution of protein modifications in autoimmune disease, *Current Opinion in Immunology* 24, 112-118.
  26. Kim, J. K., Mastronardi, F. G., Wood, D. D., Lubman, D. M., Zand, R., and Moscarello, M. A. (2003) Multiple sclerosis - An important role for post-translational modifications of myelin basic protein in pathogenesis, *Mol Cell Proteomics* 2, 453-462.
  27. Mamula, M. J., Gee, R. J., Elliott, J. I., Sette, A., Southwood, S., Jones, P. J., and Blier, P. R. (1999) Isoaspartyl post-translational modification triggers autoimmune responses to self-proteins, *J Biol Chem* 274, 22321-22327.
  28. Sidney, J., Vela, J. L., Friedrich, D., Kolla, R., von Herrath, M., Wesley, J. D., and Sette, A. (2018) Low HLA binding of diabetes-associated CD8+T-cell epitopes is increased by post translational modifications, *Bmc Immunol* 19.
  29. Li, W., Li, F. F., Zhang, X., Lin, H. K., and Xu, C. (2022) Insights into the post-translational modification and its emerging role in shaping the tumor microenvironment (vol 7, 31, 2022), *Signal Transduct Tar* 7.
  30. Maksimovic, I., and David, Y. (2021) Non-enzymatic Covalent Modifications as a New Chapter in the Histone Code, *Trends in Biochemical Sciences* 46, 718-730.
  31. Herzog, J., Maekawa, Y., Cirrito, T. P., Illian, B. S., and Unanue, E. R. (2005) Activated antigen-presenting cells select and present chemically modified

- peptides recognized by unique CD4 T cells, *P Natl Acad Sci USA* 102, 7928-7933.
32. Mannering, S. I., Harrison, L. C., Williamson, N. A., Morris, J. S., Thearle, D. J., Jensen, K. P., Kay, T. W. H., Rossjohn, J., Falk, B. A., Nepom, G. T., and Purcell, A. W. (2005) The insulin A-chain epitope recognized by human T cells is posttranslationally modified, *Journal of Experimental Medicine* 202, 1191-1197.
  33. Chen, W. S., Yewdell, J. W., Levine, R. L., and Bennink, J. R. (1999) Modification of cysteine residues in vitro and in vivo affects the immunogenicity and antigenicity of major histocompatibility complex class I-restricted viral determinants, *Journal of Experimental Medicine* 189, 1757-1764.
  34. Meadows, L., Wang, W., denHaan, J. M. M., Blokland, E., Reinhardus, C., Drijfhout, J. W., Shabanowitz, J., Pierce, R., Agulnik, A. I., Bishop, C. E., Hunt, D. F., Goulmy, E., and Engelhard, V. H. (1997) The HLA-A\*0201-restricted H-Y antigen contains a posttranslationally modified cysteine that significantly affects T cell recognition, *Immunity* 6, 273-281.
  35. Harmel, R., and Fiedler, D. (2018) Features and regulation of non-enzymatic post-translational modifications, *Nat Chem Biol* 14, 244-252.
  36. Piedrafita, G., Keller, M. A., and Ralser, M. (2015) The Impact of Non-Enzymatic Reactions and Enzyme Promiscuity on Cellular Metabolism during (Oxidative) Stress Conditions, *Biomolecules* 5, 2101-2122.
  37. Haro, I., Sanmarti, R., and Gomara, M. J. (2022) Implications of Post-Translational Modifications in Autoimmunity with Emphasis on Citrullination, Homocitrullination and Acetylation for the Pathogenesis, Diagnosis and Prognosis of Rheumatoid Arthritis, *Int J Mol Sci* 23.
  38. Kacen, A., Javitt, A., Kramer, M. P., Morgenstern, D., Tsaban, T., Shmueli, M. D., Teo, G. C., da Veiga Leprevost, F., Barnea, E., Yu, F., Admon, A., Eisenbach, L., Samuels, Y., Schueler-Furman, O., Levin, Y., Nesvizhskii, A. I., and Merbl, Y. (2023) Post-translational modifications reshape the antigenic landscape of the MHC I immunopeptidome in tumors, *Nat Biotechnol* 41, 239-251.
  39. Karle, A. C., Oostingh, G. J., Mutschlechner, S., Ferreira, F., Lackner, P., Bohle, B., Fischer, G. F., Vogt, A. B., and Duschl, A. (2012) Nitration of the Pollen Allergen

- Bet v 1.0101 Enhances the Presentation of Bet v 1-Derived Peptides by HLA-DR on Human Dendritic Cells, *Plos One* 7.
40. Sandalova, T., Sala, B. M., and Achour, A. (2022) Structural aspects of chemical modifications in the MHC-restricted immunopeptidome; Implications for immune recognition, *Front Chem* 10.
  41. Madhurantakam, C., Duru, A. D., Sandalova, T., Webb, J. R., and Achour, A. (2012) Inflammation-Associated Nitrotyrosination Affects TCR Recognition through Reduced Stability and Alteration of the Molecular Surface of the MHC Complex, *Plos One* 7.
  42. Lande, R., Pietraforte, I., Mennella, A., Palazzo, R., Spinelli, F. R., Giannakakis, K., Spadaro, F., Falchi, M., Ricciari, V., Stefanantoni, K., Conrad, C., Alessandri, C., Conti, F., and Frasca, L. (2021) Complementary Effects of Carbamylated and Citrullinated LL37 in Autoimmunity and Inflammation in Systemic Lupus Erythematosus, *Int J Mol Sci* 22.
  43. Arentz-Hansen, H., Körner, R., Molberg, O., Quarsten, H., Vader, W., Kooy, Y. M. C., Lundin, K. E. A., Koning, F., Roepstorff, P., Sollid, L. M., and McAdam, S. N. (2000) The intestinal T cell response to  $\alpha$ -gliadin in adult celiac disease is focused on a single deamidated glutamine targeted by tissue transglutaminase, *Journal of Experimental Medicine* 191, 603-612.
  44. Doyle, H. A., Zhou, J., Wolff, M. J., Harvey, B. P., Roman, R. M., Gee, R. J., Koski, R. A., and Mamula, M. J. (2006) Isoaspartyl post-translational modification triggers anti-tumor T and B lymphocyte immunity, *J Biol Chem* 281, 32676-32683.
  45. Li, H. Y. S., and Carayanniotis, G. (2006) Iodination of tyrosyls in thyroglobulin generates neoantigenic determinants that cause thyroiditis, *Journal of Immunology* 176, 4479-4483.
  46. Hutchings, P. R., Cooke, A., Dawe, K., Champion, B. R., Geysen, M., Valerio, R., and Roitt, I. M. (1992) A Thyroxine-Containing Peptide Can Induce Murine Experimental Autoimmune-Thyroiditis, *Journal of Experimental Medicine* 175, 869-872.
  47. Kolypetri, P., Carayanniotis, K., Rahman, S., Georghiou, P. E., Magafa, V., Cordopatis, P., and Carayanniotis, G. (2014) The Thyroxine-Containing

- Thyroglobulin Peptide (aa 2549-2560) Is a Target Epitope in Iodide-Accelerated Spontaneous Autoimmune Thyroiditis, *Journal of Immunology* 193, 96-101.
48. Schumacher, T. N., Heemels, M. T., Neefjes, J. J., Kast, W. M., Melief, C. J., and Ploegh, H. L. (1990) Direct binding of peptide to empty MHC class I molecules on intact cells and in vitro, *Cell* 62, 563-567.
49. Ljunggren, H. G., Stam, N. J., Ohlen, C., Neefjes, J. J., Hoglund, P., Heemels, M. T., Bastin, J., Schumacher, T. N., Townsend, A., Karre, K., and et al. (1990) Empty MHC class I molecules come out in the cold, *Nature* 346, 476-480.
50. Elvin, J., Potter, C., Elliott, T., Cerundolo, V., and Townsend, A. (1993) A method to quantify binding of unlabeled peptides to class I MHC molecules and detect their allele specificity, *J Immunol Methods* 158, 161-171.
51. Cerundolo, V., Elliott, T., Elvin, J., Bastin, J., Rammensee, H. G., and Townsend, A. (1991) The binding affinity and dissociation rates of peptides for class I major histocompatibility complex molecules, *Eur J Immunol* 21, 2069-2075.
52. Saito, Y., Peterson, P. A., and Matsumura, M. (1993) Quantitation of peptide anchor residue contributions to class I major histocompatibility complex molecule binding, *J Biol Chem* 268, 21309-21317.
53. Shastri, N., and Gonzalez, F. (1993) Endogenous Generation and Presentation of the Ovalbumin Peptide/K(B) Complex to T-Cells, *Journal of Immunology* 150, 2724-2736.
54. Lin, H., Levison, B. S., Buffa, J. A., Huang, Y., Fu, X., Wang, Z., Gogonea, V., DiDonato, J. A., and Hazen, S. L. (2017) Myeloperoxidase-mediated protein lysine oxidation generates 2-aminoadipic acid and lysine nitrile in vivo, *Free Radic Biol Med* 104, 20-31.
55. Cook, K. W., Xue, W., Symonds, P., Daniels, I., Gijon, M., Boocock, D., Coveney, C., Miles, A. K., Shah, S., Atabani, S., Choudhury, R. H., Vaghela, P., Weston, D., Metheringham, R. L., Brentville, V. A., and Durrant, L. G. (2021) Homocitrullination of lysine residues mediated by myeloid-derived suppressor cells in the tumor environment is a target for cancer immunotherapy, *J Immunother Cancer* 9.
56. Wisniewski, J. R., Zougman, A., and Mann, M. (2008) N-Formylation of lysine is a widespread post-translational modification of nuclear proteins occurring at

- residues involved in regulation of chromatin function, *Nucleic Acids Res* 36, 570-577.
57. Zhang, D., Gao, J. J., Zhu, Z. J., Mao, Q. Y., Xu, Z. Q., Singh, P. K., Rimayi, C. C., Moreno-Yruela, C., Xu, S. L., Li, G. Y., Sin, Y. C., Chen, Y., Olsen, C. A., Snyder, N. W., Dai, L. Z., Li, L. J., and Zhao, Y. M. (2025) Lysine <sc>l</sc>-lactylation is the dominant lactylation isomer induced by glycolysis, *Nat Chem Biol* 21.
  58. Mangalaparathi, K. K., Madugundu, A. K., Ryan, Z. C., Garapati, K., Peterson, J. A., Dey, G., Prakash, A., and Pandey, A. (2021) Digging deeper into the immunopeptidome: characterization of post-translationally modified peptides presented by MHC I, *J Proteins Proteom* 12, 151-160.
  59. Kato, K., Nakayoshi, T., Kurimoto, E., and Oda, A. (2020) Mechanisms of Deamidation of Asparagine Residues and Effects of Main-Chain Conformation on Activation Energy, *Int J Mol Sci* 21.
  60. Mei, S. T., Ayala, R., Ramarathinam, S. H., Illing, P. T., Faridi, P., Song, J. N., Purcell, A. W., and Croft, N. P. (2020) Immunopeptidomic Analysis Reveals That Deamidated HLA-bound Peptides Arise Predominantly from Deglycosylated Precursors, *Mol Cell Proteomics* 19, 1236-1247.
  61. Falk, K., Rotzschke, O., Stevanovic, S., Jung, G., and Rammensee, H. G. (1991) Allele-Specific Motifs Revealed by Sequencing of Self-Peptides Eluted from Mhc Molecules, *Nature* 351, 290-296.
  62. Paulsen, C. E., and Carroll, K. S. (2013) Cysteine-Mediated Redox Signaling: Chemistry, Biology, and Tools for Discovery, *Chem Rev* 113, 4633-4679.
  63. Haque, M. A., Hawes, J. W., and Blum, J. S. (2001) Cysteinylation of MHC class II ligands: Peptide endocytosis and reduction within APC influences T cell recognition, *Journal of Immunology* 166, 4543-4551.
  64. Guberovic, I., and Frezza, C. (2024) Functional implications of fumarate-induced cysteine succination, *Trends in Biochemical Sciences* 49, 775-790.
  65. Mills, E. L., Ryan, D. G., Prag, H. A., Dikovskaya, D., Menon, D., Zaslona, Z., Jedrychowski, M. P., Costa, A. S. H., Higgins, M., Hams, E., Szpyt, J., Runtsch, M. C., King, M. S., McGouran, J. F., Fischer, R., Kessler, B. M., McGettrick, A. F., Hughes, M. M., Carroll, R. G., Booty, L. M., Knatko, E. V., Meakin, P. J., Ashford, M. L. J., Modis, L. K., Brunori, G., Sévin, D. C., Fallon, P. G., Caldwell,

- S. T., Kunji, E. R. S., Chouchani, E. T., Frezza, C., Dinkova-Kostova, A. T., Hartley, R. C., Murphy, M. P., and O'Neill, L. A. (2018) Itaconate is an anti-inflammatory metabolite that activates Nrf2 via alkylation of KEAP1, *Nature* 556, 113-+.
66. Karttunen, J., and Shastri, N. (1991) Measurement of Ligand-Induced Activation in Single Viable T-Cells Using the LacZ Reporter Gene, *P Natl Acad Sci USA* 88, 3972-3976.
67. van der Gracht, A. M. F., de Geus, M. A. R., Camps, M. G. M., Ruckwardt, T. J., Sarris, A. J. C., Bremmers, J., Maurits, E., Pawlak, J. B., Posthoorn, M. M., Bongers, K. M., Filippov, D. V., Overkleeft, H. S., Robillard, M. S., Ossendorp, F., and van Kasteren, S. I. (2018) Chemical Control over T-Cell Activation Using Deprotection of Cyclooctene-Modified Epitopes, *Acs Chemical Biology* 13, 1569-1576.
68. Stopfer, L. E., D'Souza, A. D., and White, F. M. (2021) 1,2,3, MHC: a review of mass-spectrometry-based immunopeptidomics methods for relative and absolute quantification of pMHCs, *Immuno-oncol Technol* 11, 100042.
69. Kulkarni, R. A., Worth, A. J., Zengeya, T. T., Shrimp, J. H., Garlick, J. M., Roberts, A. M., Montgomery, D. C., Sourbier, C., Gibbs, B. K., Mesaros, C., Tsai, Y. C., Das, S., Chan, K. C., Zhou, M., Andresson, T., Weissman, A. M., Linehan, W. M., Blair, I. A., Snyder, N. W., and Meier, J. L. (2017) Discovering Targets of Non-enzymatic Acylation by Thioester Reactivity Profiling, *Cell Chem Biol* 24, 231-242.
70. Sugawara, S., Abo, T., and Kumagai, K. (1987) A Simple Method to Eliminate the Antigenicity of Surface Class-I Mhc Molecules from the Membrane of Viable Cells by Acid Treatment at Ph3, *Journal of Immunological Methods* 100, 83-90.
71. Bassani-Sternberg, M., Braunlein, E., Klar, R., Engleitner, T., Sinitcyn, P., Audehm, S., Straub, M., Weber, J., Slotta-Huspenina, J., Specht, K., Martignoni, M. E., Werner, A., Hein, R., D, H. B., Peschel, C., Rad, R., Cox, J., Mann, M., and Krackhardt, A. M. (2016) Direct identification of clinically relevant neoepitopes presented on native human melanoma tissue by mass spectrometry, *Nat Commun* 7, 13404.

72. James, A. M., Hoogewijs, K., Logan, A., Hall, A. R., Ding, S. J., Fearnley, I. M., and Murphy, M. P. (2017) Non-enzymatic-acetylation of Lysine Residues by AcetylCoA Often Occurs via a Proximal -acetylated Thiol Intermediate Sensitive to Glyoxalase II, *Cell Rep* 18, 2105-2112.
73. Baldensperger, T., and Glomb, M. A. (2021) Pathways of Non-enzymatic Lysine Acylation, *Front Cell Dev Biol* 9.
74. Wagner, G. R., and Payne, R. M. (2013) Widespread and Enzyme-independent - Acetylation and -Succinylation of Proteins in the Chemical Conditions of the Mitochondrial Matrix, *J Biol Chem* 288, 29036-29045.
75. Rammensee, H., Bachmann, J., Emmerich, N. P., Bachor, O. A., and Stevanovic, S. (1999) SYFPEITHI: database for MHC ligands and peptide motifs, *Immunogenetics* 50, 213-219.
76. Zhang, X., Ning, Z., Mayne, J., Yang, Y., Deeke, S. A., Walker, K., Farnsworth, C. L., Stokes, M. P., Couture, J. F., Mack, D., Stintzi, A., and Figeys, D. (2020) Widespread protein lysine acetylation in gut microbiome and its alterations in patients with Crohn's disease, *Nat Commun* 11, 4120.
77. Cummings, J. H., Pomare, E. W., Branch, W. J., Naylor, C. P., and Macfarlane, G. T. (1987) Short chain fatty acids in human large intestine, portal, hepatic and venous blood, *Gut* 28, 1221-1227.
78. Jiang, W. X., Wu, J. L., Zhu, S. F., Xin, L. Y., Yu, C. H., and Shen, Z. (2022) The Role of Short Chain Fatty Acids in Irritable Bowel Syndrome, *J Neurogastroenterol* 28, 540-548.

## **Chapter 7 Measurement of Accumulation of Antibiotics to *Staphylococcus aureus* in Phagosomes of Live Macrophages**

Adapted from: Kelly, J. J.<sup>#</sup>; Dalesandro, B. E.<sup>#</sup>; Lui, Z.; Chordia, M. D.; Ongwae, G.E.; Pires, M. M., Systematic Evaluation of the Permeability of Antibiotics to the Peptidoglycan of Intracellular *Staphylococcus aureus*. **2024**. Angew. Chem. Int. Ed. 63, e202313870

<sup>#</sup>authors contributed equally

### **7.1 Abstract**

*Staphylococcus aureus* (*S. aureus*) has evolved the ability to persist after uptake into host immune cells. This intracellular niche enables *S. aureus* to potentially escape host immune responses and survive the lethal actions of antibiotics. While the elevated tolerance of *S. aureus* to small-molecule antibiotics is likely to be multifactorial, we pose that there may be contributions related to permeation of antibiotics into phagocytic vacuoles, which would require translocation across two mammalian bilayers. To empirically test this, we adapted our recently developed permeability assay to determine the accumulation of FDA-approved antibiotics into phagocytic vacuoles of live macrophages. Bioorthogonal reactive handles were metabolically anchored within the surface of *S. aureus*, and complementary tags were chemically added to antibiotics. Following phagocytosis of tagged *S. aureus* cells, we were able to specifically analyze the arrival of antibiotics within the phagosomes of infected macrophages. Our findings enabled the determination of permeability differences between extra- and intracellular *S. aureus*, thus providing a roadmap to dissect the contribution of antibiotic permeability to intracellular pathogens.

### **7.2 Introduction**

*Staphylococcus aureus* (*S. aureus*) is a significant human pathogen that can cause a wide range of infections from mild skin infections to severe diseases such as sepsis and pneumonia.<sup>1-3</sup> The increasing incidence of drug-resistant *S. aureus* infections, particularly methicillin-resistant *S. aureus* (MRSA), is a major concern.<sup>4-6</sup> MRSA is resistant to many commonly used antibiotics; this resistance poses a significant challenge in effectively

treating MRSA infections and can lead to more severe illness, prolonged hospital stays, and increased healthcare costs. Overall, the increasing incidence of drug-resistant *S. aureus* infections highlights the importance of understanding the factors that impact the efficacy of therapeutics against bacterial pathogens.

In addition to genetic alterations that result in drug resistant phenotypes, *S. aureus* has evolved another mode of persistence in a host organism. Host immune cells, such as macrophages and neutrophils, phagocytose bacteria as an anti-bacterial response.<sup>7-11</sup> In turn, immune cells have a variety of potent mechanisms to kill phagocytosed bacteria including the release of reactive oxygen and nitrogen species (ROS and RNS), the production of antimicrobial peptides and enzymes, and the acidification of the phagosome.<sup>12</sup> Yet, some pathogens continue to remain viable despite these challenging environments.<sup>11, 13-18</sup> *S. aureus* that survive inside immune cells can serve as potential reservoirs that can seed reoccurring infections and can persist for days<sup>9, 10, 19</sup> a feature that has been demonstrated both in vitro and in vivo.<sup>20-22</sup>

Mechanistically, antibiotic tolerance by intracellular *S. aureus* has been previously ascribed to a phenotypic switch to small colony variants.<sup>7, 23, 24</sup> An alternative or complementary mechanism that can promote the persistence of *S. aureus* within immune cells is reduced accumulation of antibiotics to the subcellular organelle housing these cells (Figure 7.1A). Antibiotics must traverse two membrane bilayers (immune cell plasma membrane and phagosome bilayer) to reach the target pathogen relative to extracellular *S. aureus* cells. These additional barriers could potentially diminish the effective concentration of the therapeutic agent within the phagosome, leading to less effective antibacterial activity. Herein, we developed an assay to directly measure the permeability of the antibiotic to the surface of *S. aureus* present in the phagosomes of macrophages (Figure 7.1B). We demonstrated that structural modifications of antibiotics can dictate the abundance of agents within phagocytic vacuoles. Uniquely, these measurements are reflective of antibiotic accumulation at the target bacteria cells and not a total measurement of antibiotic levels in the immune cell.

### 7.3 Results and Discussion

Prior efforts to assess levels of antibiotics in host mammalian cells have most commonly been approximated by their antibacterial activity (minimum inhibitor concentration, MIC).<sup>22, 25, 26</sup> The main challenges in using MIC determinations as a proxy for the concentration of the antibiotics in the phagosome are that tolerant phenotypes (induced following phagocytosis) can alter MIC values regardless of drug concentration and/or phagosome pH can alter drug efficacy.<sup>27</sup> Aside from MIC determination, antibiotic concentration measurements have also been made based on the inherent fluorescence of those agents, such as in the case of quinolones or by introducing a radioactive isotope.<sup>28, 29</sup> These methods pose clear challenges and limitations including the overall throughput and confounding antibacterial/ permeation effects. Moreover, these analyses revealed the antibiotic concentration of the entire immune cell rather than the phagocytic vacuole. The concentration of the antibiotic inside the phagosome could potentially differ from that in the general cytosol; thus, the whole cell concentration may not properly describe the effective level that reaches the target bacterial cells.

Appreciating that intracellular residence can lower the efficacy of antibiotics, a group at Genentech developed an antibody-antibiotic conjugate that eliminated intracellular *S. aureus* in an in vivo model of infection. More specifically, a rifamycin derivative was conjugated to an antibody directed at the wall-teichoic acids (WTA) of *S. aureus*, whereby rifamycin was released upon cleavage by intracellular proteases.<sup>21</sup> Another clever strategy involved the use of a proline-based cell penetrating peptide that was conjugated to kanamycin that targeted intracellular bacteria.<sup>30</sup> Similarly, vancomycin was conjugated to an arginine-based cell penetrating peptide, which led to its potentiation.<sup>31</sup> Antimicrobial peptides have also been designed to directly target intracellular bacterial pathogens.<sup>32</sup> Together, these efforts highlight diverse and promising approaches to targeting intracellular pathogens.<sup>33, 34</sup> We set out to isolate the impact of intracellular residence to the accessibility of antibiotics by systematically determining the permeability of a panel of antibiotics to the cell wall of intracellular *S. aureus*.

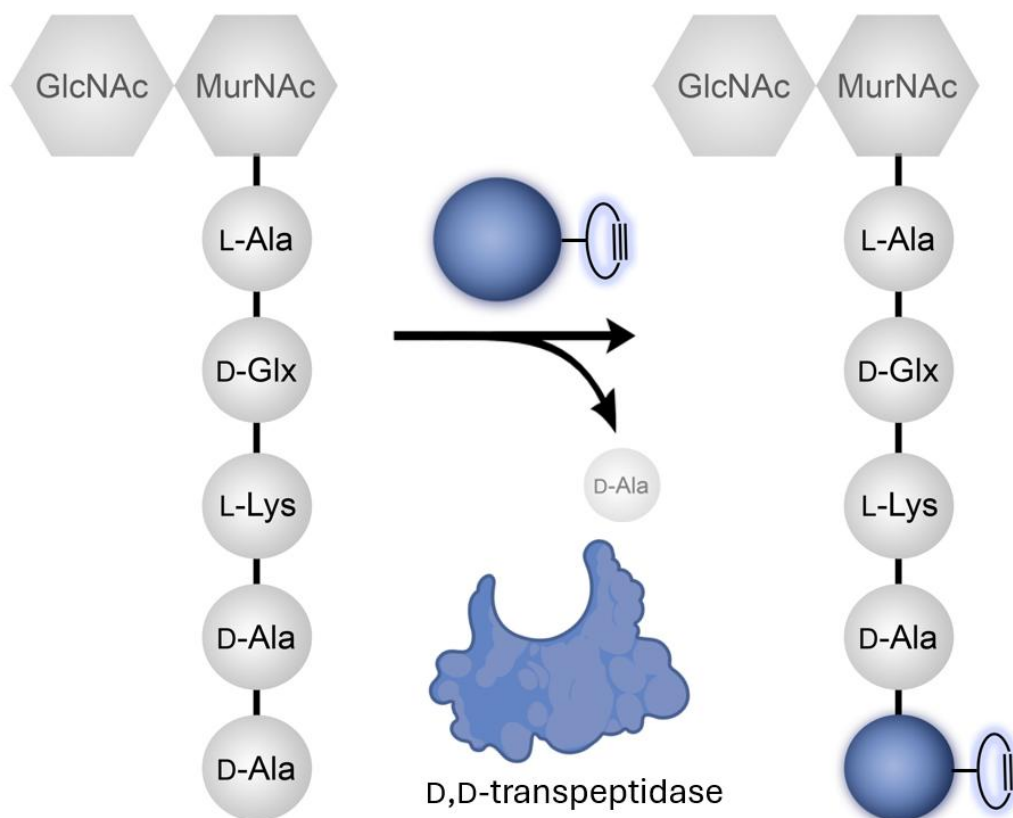


**Figure 7.1** Mode of incorporation of single amino acids into the 5<sup>th</sup> position of the peptidoglycan stem peptide

To measure the accumulation of antibiotics, we combined an assay our laboratory recently developed aimed at systematically assessing how flexibility and size of large biopolymers impact their ability to reach the peptidoglycan (PG) surface of *S. aureus* cells<sup>35, 36</sup> to with one that we developed measure the permeability of molecules into mycobacteria.<sup>37</sup> In this new iteration (**Figure 7.1**), a strained alkyne dibenzocyclooctyne (DBCO) is metabolically installed within the PG of *S. aureus*. DBCO-tagged bacterial cells are then incubated with macrophages to promote their uptake. Treatment of cells with azide-modified antibiotics (azAbx) post infection was expected to result in the reaction between the DBCO and azAbx via strain promoted alkyne-azide cycloaddition (SPAAC).<sup>38-40</sup> A chase step with an azide modified fluorophore imprints a signal that is reflective of unmodified DBCO epitopes. Cellular fluorescence measurement should then

enable a fluorescent, live-cell analysis of antibiotic accumulation, whereby cellular fluorescence inversely correlates with antibiotic accumulation levels (**Figure 7.2**).

The site-specific metabolic installation of a bioorthogonal reactive handle within the PG of *S. aureus* is central to the overall assay. For Gram-positive bacteria, the cell wall is primarily comprised of a thick layer of PG that displays various surface proteins and extracellular matrices; these biomacromolecules are essential to maintain the overall integrity of the cell.<sup>41</sup> PG is composed of repeating disaccharide units, N-acetylglucosamine (GlcNAc) and N acetylmuramic acid (MurNAc), covalently linked to a short stem peptide (L-Ala-D-Glu-L-Lys-D-Ala-D-Ala). The stem peptide strands are crosslinked together by transpeptidase (TP) enzymes to create a dense, mesh-like scaffold that surrounds the cell as a single molecule.<sup>42-44</sup> Given that the PG is a critical component to the fitness of the pathogen, many antibiotics target PG biosynthesis enzymes.<sup>45, 46</sup> Our lab<sup>36, 47-57</sup> and others<sup>58-61</sup> have extensively demonstrated the ability to metabolically remodel bacterial PG with synthetic analogs of PG precursors. For most of these modifications, the viability and overall cellular structure of the PG remain unaffected. Further, we demonstrated that such analogs can be incorporated in vivo into the cell wall of *S. aureus* infected *C. elegans*<sup>49</sup> and various diverse bacterial species residing in the gut microbiome of a mouse model.<sup>55</sup>

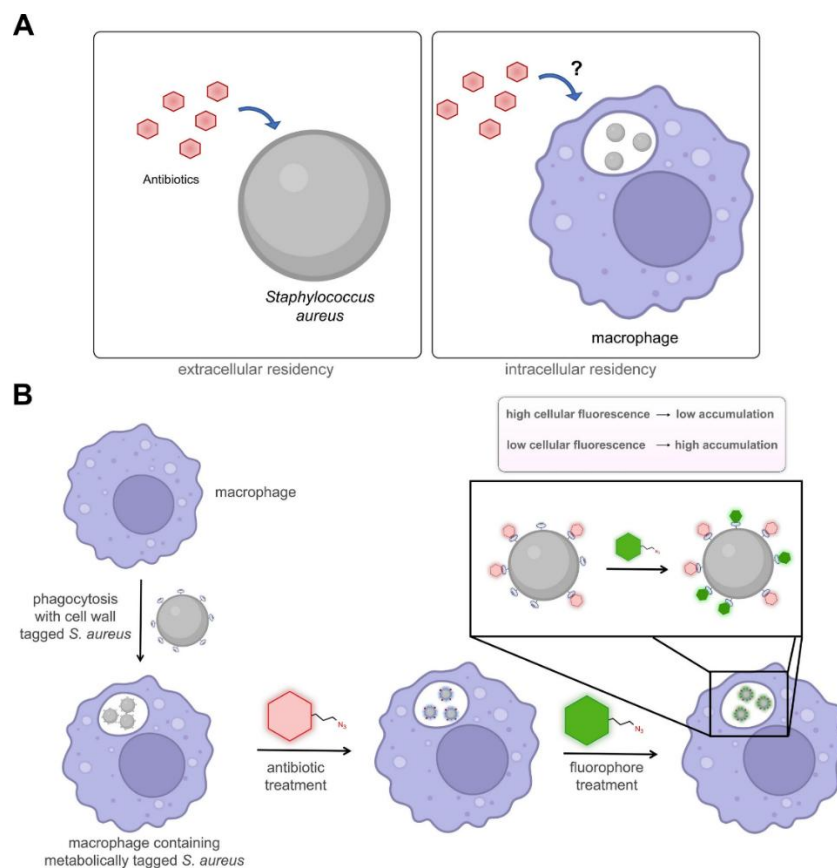


**Figure 7.2** (A) Cartoon representation of antibiotic permeability to extracellular *S. aureus* (left) and intracellular *S. aureus* (right). (B) Workflow of the assay for measuring accumulation of antibiotics using a competition towards tags within the cell wall of *S. aureus*.

### 7.3.1 Optimizing **D-DapD** labeling conditions for *S. aureus*

To start, we prepared DBCO-tagged PGs by synthesizing the unnatural amino acid, D-diaminopropanoic acid (Dap) and conjugated its sidechain with DBCO to yield **D-DapD**. Incubation of this amino acid in the growth media of *S. aureus* results in the exchange of the terminal D-alanine on the PG stem peptide with the supplemented unnatural amino acid (**Figure S7.1**). *S. aureus* cells were incubated with culture media containing **D-DapD** (or its stereocontrol, **L-DapD**) overnight to allow for incorporation throughout the PG matrix. The modified L-amino acid is not expected to be metabolically processed by the cell wall transpeptidases, and, therefore, no tagging should occur. Bacterial cells were washed to remove unincorporated metabolic tags, followed by incubation with azide-

modified rhodamine 110 (R110az), and cellular fluorescence measurement by flow cytometry (**Figure 7.3A**). Satisfyingly, the fluorescence associated with *S. aureus* cells metabolically labeled with **D-DapD** were significantly higher than DMSO treated cells (**Figure 7.3B**). Cells treated with the stereocontrol, **L-DapD**, exhibited similar fluorescence levels to DMSO treated cells indicating that the DapD was incorporated in the PG scaffold of *S. aureus* in a stereoselective manner. Additionally, incubation with **D-DapD** did not perturb cell growth (**Figure 7.3C**). Confocal microscopy showed that the fluorescence pattern was consistent with PG incorporation as the fluorescence remained peripheral and septal (**Figure 7.3D**).

We further confirmed DBCO installation on the PG of *S. aureus* by isolating the entire PG scaffold (sacculi) from cells that had been treated with **D-DapD** followed by R110az. Sacculi isolation was performed using standard methods that disrupt the whole cell, leaving discrete and intact units of sacculi that are similar in size.<sup>62</sup> Isolation of sacculi with the DBCO tag was not performed due to the chemical instability of the triple bond of DBCO in the isolation conditions (acid, high temperatures). Instead, we isolated the stable triazole product formed after the SPAAC reaction. Flow cytometry analysis of the fluorescently tagged sacculi (SaccuFlow<sup>62</sup>) was performed wherein the sacculi was found to be highly fluorescent (**Figure S7.2**). Sacculi isolated from DMSO-treated *S. aureus* cells displayed minimal fluorescence levels. As expected, confocal microscopy analysis revealed that the fluorescently labeled sacculi were similar in size and shape compared to whole cell *S. aureus* while also retaining similar labeling patterns (**Figure 7.3D**). Together, these results established that tagging of the sacculi was successful and the DBCO sites could be specifically labeled by treatment with an azide-modified fluorophore.

We next set out to test labeling conditions to optimize the dynamic range of the assay. Following the same workflow as described before, *S. aureus* cells were grown over night in the presence of increasing concentrations of **D-DapD**, washed, treated with R110az, and analyzed by flow cytometry. As expected, the cellular fluorescence levels of *S. aureus* grown with **D-DapD** increased in a concentration dependent manner (**Figure S7.3A**); this indicates that more **D-DapD** was covalently linked into the growing PG scaffold as more amino acid was supplemented into the growth media. From these results, the **D-DapD**

concentration of 500  $\mu\text{M}$  was selected for subsequent experiments. We next evaluated the impact of fluorophore concentration on the cellular fluorescence levels. *S. aureus* cells were labeled **D-DapD** followed by incubation with increasing concentrations of R110az, which resulted in increasing cellular fluorescence levels, as expected (**Figure S7.3B**). The selected parameters of **D-DapD** and R110az concentrations were based on the large dynamic range that these conditions afforded while reducing reagent consumption and the exposure to non-native molecules. To ensure the timeframe of the assay on the surface of *S. aureus* will enable completion of the SPAAC reaction, a time course of R110az labeling was performed, which indicated that the R110az reaction mostly plateaued within 30 minutes (**Figure S7.3C**). Lastly, to investigate the permeation effects of the fluorophore itself, we examined two additional azide fluorophores: fluorescein azide (Flaz) and coumarin azide (Coaz). These dyes have different physiochemical properties (charges/molecular weight) than R110az and could potentially result in superior signal-to-noise ratios. Although inferior to R110az, both were demonstrated to be compatible (**Figure S7.3D**) as indicated by significant fluorescence signals over cells in the absence of the metabolic label.

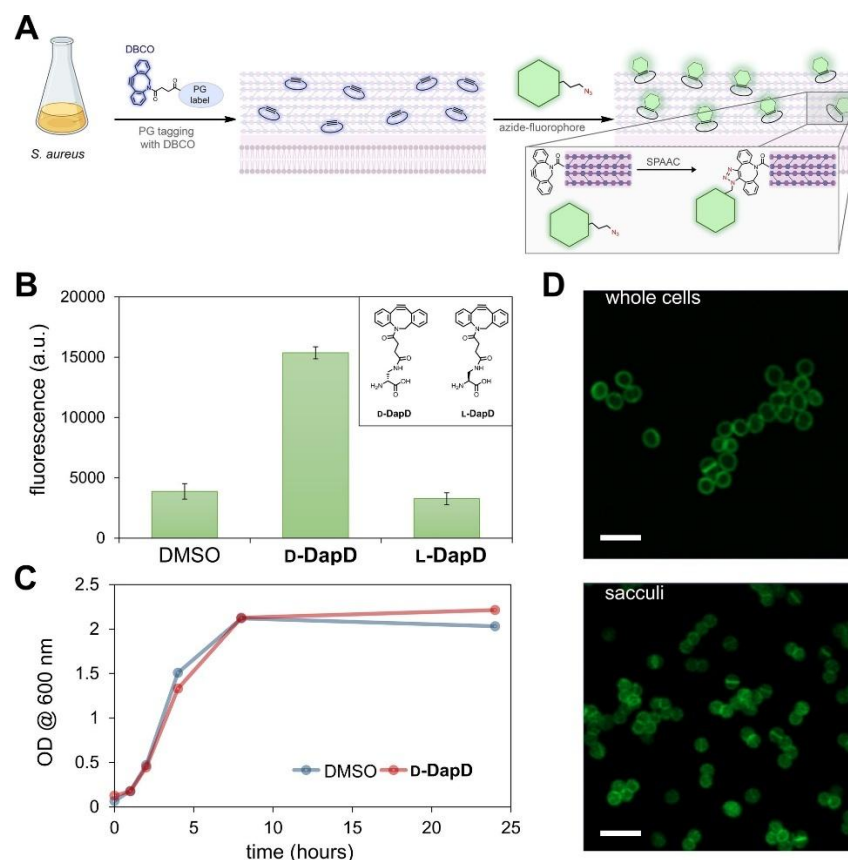


**Figure 7.3** (A) Workflow schematic of the PG labeling with a DBCO-displaying agent followed by treatment with an azide-tagged fluorophore. (B) *S. aureus* was incubated overnight with 500  $\mu$ M of **D-DapD** or **L-DapD** in tryptic soy broth (TSB) at 37° PBS and incubated for an additional 30 min with 25  $\mu$ M of R110az in PBS at 37°C. The next day cells were washed 3x with C. Cells were then fixed with 2% formaldehyde in PBS and 10,000 events per sample were analyzed via flow cytometry. (C) Measurement of OD 600 over time for *S. aureus* cells treated with either DMSO or 500  $\mu$ M of **D-DapD** in TSB. (D) Confocal microscopy analysis of *S. aureus* cells (top) and isolated sacculi (bottom) after treatment with 500  $\mu$ M of **D-DapD** in tryptic soy broth. Cells were washed 3x with PBS and incubated for an additional 30 min at 37°C with 25  $\mu$ M of R110az in PBS before fixation with 2% formaldehyde in PBS. Scale bar=5  $\mu$ m. Data are represented as mean  $\pm$  SD of biological replicates (n=3)

### 7.3.2 Assessing accessibility of antibiotics to cell surface of *S. aureus*

We then evaluated the ability of the assay to report on the accessibility of FDA-approved antibiotics modified with azide tags to the PG of *S. aureus* in phagocytic vacuoles. We synthesized an azAbx panel to make them compatible with our assay workflow (**Figure 7.4**). Azides were installed on parts of the antibiotic that were found to minimally perturb their structure. The azAbx included were rifamycin, erythromycin, linezolid, and ciprofloxacin, which are treatment options for *S. aureus* infections.<sup>63-66</sup> The selected antibiotics have chemical compositions that range in hydrophobicity, polarity, size, and charge to examine how these factors affect their ultimate accumulation into phagosomes. Furthermore, we also tested two variations of ciprofloxacin: one containing the azide modification on the piperazine group that has an overall net negative charge and another that has an additional ester modification to return the molecule to a net neutral charge. This modification was done to evaluate the impact of net charge on the permeability of antibiotics to the phagosome. In the pulse step, DBCO-tagged cells were treated with the azAbx. Antibiotics that reach the PG are expected to form a stable and irreversible bond with DBCO. In the chase step, R110az reacts with the remaining intact DBCO sites on the PG. Therefore, antibiotics that readily reach bacterial pathogens should result in low cellular fluorescence levels (**Figure 7.2B**).

To establish the baseline reactivity level of the azAbx without a membrane-permeability barrier, *S. aureus* cells were metabolically tagged with **D-DapD** and incubated with each individual member of the azAbx library. All azAbx were tested at 25  $\mu\text{M}$  based on our findings using R110az. Following incubation with the azAbx, cells were washed, treated with R110az, and cellular fluorescence was analyzed by flow cytometry (**Figure 7.5A**). From the data observed, it was found that nonpolar antibiotics, such as linezolid and rifamycin, were able to sieve through the PG and fully react with the DBCO modified PG within 2 h, as indicated by a low fluorescence signal. The small size of linezolid and the flexible backbone of rifamycin could be, at least in part, the reason for these observations. Conversely, the increased rigidity and polarity of ciprofloxacin and erythromycin could play a role in hindering the permeation of these molecules through the PG; to this end, full reaction was not observed until nearly 8 h (**Figure 7.5A**). When extracellular *S. aureus*

was treated with untagged antibiotics, we observed no change in cellular fluorescence levels (**Figure S7.5**). These results suggest that the change in fluorescence observed in Figure 7.4A are not related to bacterial cell lysis/death. Interestingly, a similar pattern of permeation was observed for the two ciprofloxacin derivatives, indicating that masking the net negative charge of ciprofloxacin-N had negligible effects in terms of reaching DBCO sites within PG of 3 *S. aureus*.

To further ensure whether that the SPAAC reaction between the azAbx and **D-DapD** was complete within the timeframe of the assay, we modified amine-terminated beads to display DBCO epitopes (**Figure S7.4A**). As these beads are compatible with flow cytometry, this approach provides a parallel workflow to the live cell analysis but without the potential barrier of the matrix-like PG scaffold. Our results showed that the antibiotics in this panel readily react in the absence of a complex cell wall structure, as indicated by background fluorescence levels observed for all five azAbx within 2 h (**Figure S7.4B**). These results clearly suggest that the PG itself could pose as a permeation barrier. Sieving through the crosslinked PG has been ascribed to play a role in the activity of antimicrobial peptides<sup>67</sup> and components of the human immune system (e.g., lysozyme and antibodies).<sup>68, 69</sup> Early work showed that molecular sieving was operative within isolated sacculi with synthetic polymers<sup>70, 71</sup> but systematic studies had not been carried out in live bacterial cells using antibiotics. Sieving within the PG scaffold is likely to be dependent on multiple factors, including the level of crosslinking, which can vary across strains and species.<sup>72</sup> Given that the estimated crosslinking levels in *S. aureus* can range from 80 to 90%, it is probable that sieving could be particularly prominent.<sup>73, 74</sup>

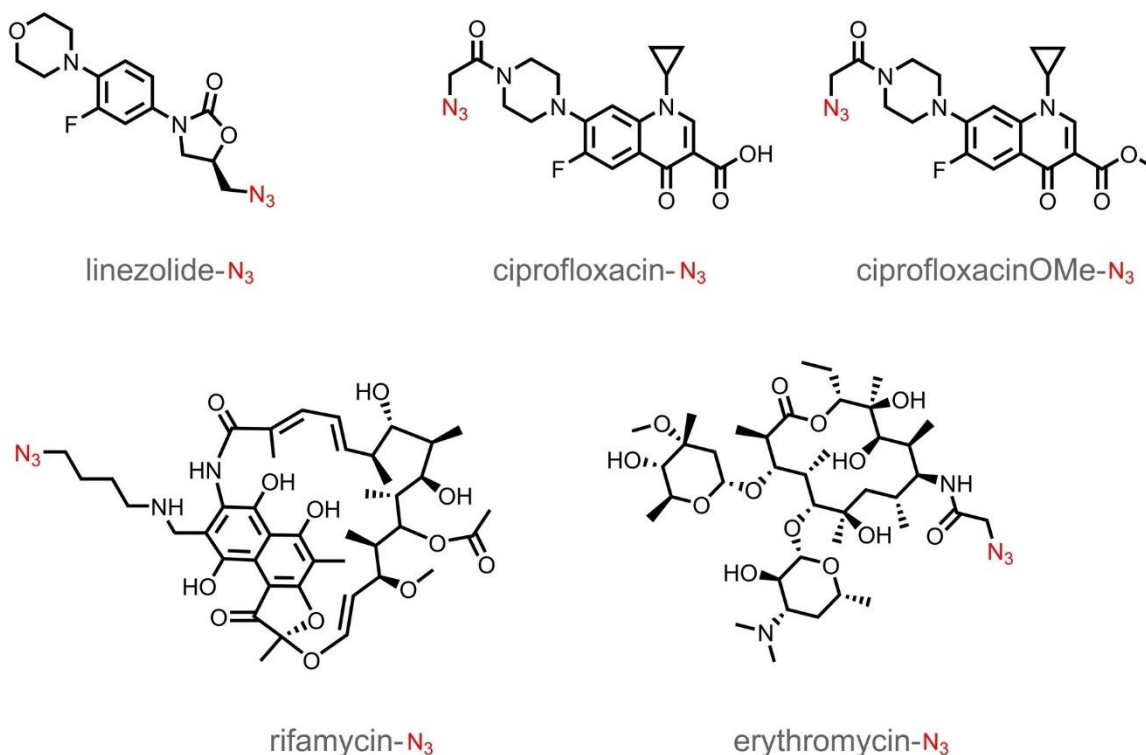


**Figure 7.4** Chemical structures of azide modified antibiotics.

### 7.3.3 Investigating accumulation of antibiotics to MRSA

To demonstrate the adoptability of the assay across other strains of *S. aureus*, we also performed a similar analysis with MRSA. Satisfyingly, treatment of USA300 *S. aureus* with **D-DapD** resulted in a high fluorescence signal when incubated with R110az, indicating that **D-DapD** was incorporated into the PG layer of a methicillin-resistant strain and readily reacted with an azide molecule (Figure 4B). Further, we went on to investigate azAbx accessibility to USA300 PG. After incubating **D-DapD** labeled USA300 with the azAbx, a similar pattern was observed for all azAbx compared to methicillin sensitive *S. aureus* (25923, MSSA), as evidenced by a significant decrease in fluorescence signal compared to DMSO treated cells (Figure 4C) after incubation with the azAbx for 4 h. This indicates that the azAbx were able to sieve through the USA300 PG layer.

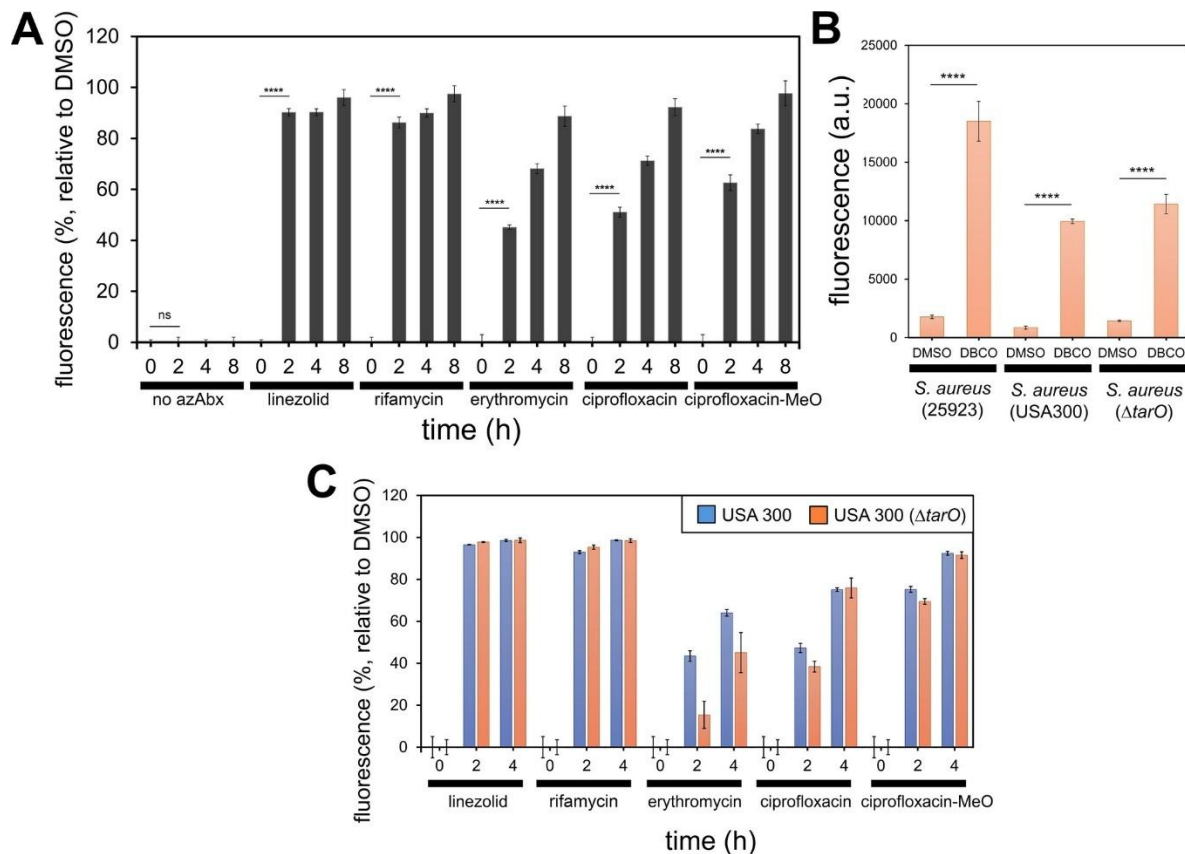


**Figure 7.5** (A) *S. aureus* was incubated overnight with 500  $\mu\text{M}$  of **D-DapD** in TSB at 37°C. The next day cells were washed 3x with PBS and incubated with 25  $\mu\text{M}$  azAbx in PBS for indicated time points at 37°C. Following the azAbx incubation, the cells were resuspended in 25  $\mu\text{M}$  of R110az in PBS for 30 min at 37°C and fixed with 2% formaldehyde in PBS before 10,000 events per sample were analyzed via flow cytometry. (B) *S. aureus* 25923, USA 300, and a WTA deletion strain,  $\Delta\text{tarO}$ , were incubated overnight with 500  $\mu\text{M}$  of **D-DapD** in TSB at 37°C. Cells were then fixed with 2% formaldehyde in PBS and 10,000 events per sample were analyzed via flow cytometry. (C) *S. aureus* cells (USA300 and  $\Delta\text{tarO}$ ) were incubated with 500  $\mu\text{M}$  of **D-DapD** overnight, washed 3x with PBS, and followed by incubation with 25  $\mu\text{M}$  of azAbx in PBS for indicated time points. Following azAbx incubation, the cells were resuspended in 25  $\mu\text{M}$  of R110az in PBS for 30 min, fixed in 2% formaldehyde in PBS, and 10,000 events per sample were analyzed via flow cytometry. Data are represented as mean  $\pm$  SD of biological replicates ( $n=3$ ).  $P$ -values were determined by a two-tailed  $T$ -test (\*\*\*\*  $p < 0.0001$ , ns = not significant).

Further, we aimed to investigate the contribution that PG-anchored, brush-like polysaccharides play on permeability. The surface of *S. aureus* is coated with wall teichoic acids (WTAs), that are anionic glycopolymers known to sterically hinder biomolecules from reaching the surface of the PG.<sup>21, 36, 69</sup> Our group recently described how WTA can be a major determinant of surface accessibility to large polymers (polyprolines and PEG-based), which was determined by also using a combination of PG tags and SPAAC.<sup>36</sup> Analogously, we tested whether WTAs may alter the accessibility of azAbx, which are considerably smaller, to the PG layer. Our data showed no significant difference between the USA300 parental strain and tarO deletion strain, which cannot biosynthesize WTA on the surface of *S. aureus* (**Figure 7.5 B,C**). These results indicate that WTAs do not appear to hinder permeation of smaller molecules to the PG matrix. To the best of our knowledge, this had not been shown before.

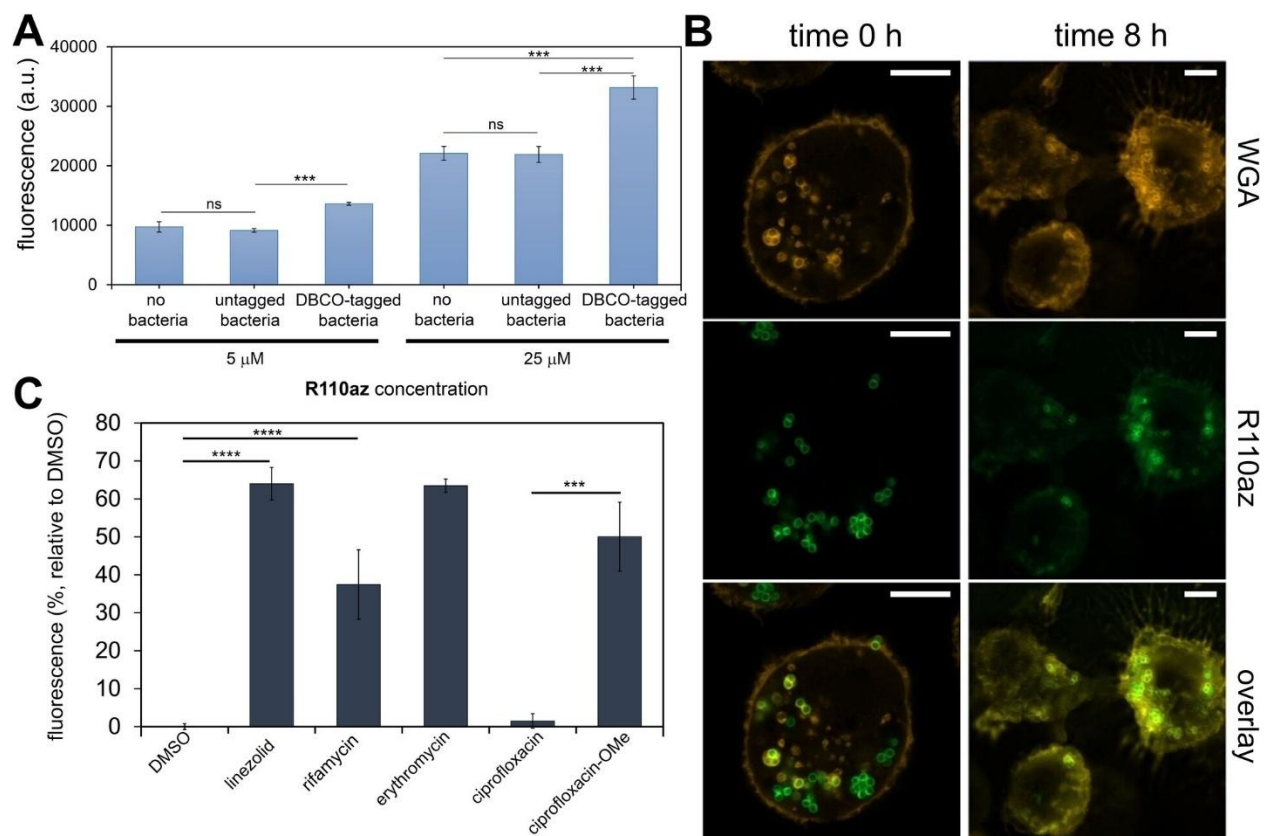


**Figure 7.6 (A)** *S. aureus* was grown overnight with 500  $\mu$ M of *D-DapD* in TSB at 37°C.

The following day the *S. aureus* was washed 3 x with PBS and infected J774A macrophages in DMEM containing no antibiotics at an MOI of 100 for 1 h in a humidified

incubator at 37°C and 5% CO<sub>2</sub>. Following bacterial uptake, macrophages were incubated with varying concentrations of R110az in PBS for 30 min, fixed with 4% formaldehyde in PBS, and 10,000 events per sample were analyzed via flow cytometry. (B) Confocal analysis of **D-DapD** infected J774A macrophages. *S. aureus* was labeled overnight with 500 μM of **D-DapD** and then immediately reacted with 25 μM of R110az. Fluorescently labeled *S. aureus* was infected into J774A macrophages at MOI 100 in a humidified incubator at 37°C and 5% CO<sub>2</sub>. Immediately following bacterial uptake, time 0 h samples were fixed and analyzed by confocal microscopy. Time 8 h samples were resuspended in PBS for 8 h, fixed with 4% formaldehyde in PBS, and analyzed by confocal microscopy. Macrophage membranes were labeled with 5 mg/mL wheat germ agglutinin (WGA) tetramethylrodamine. Scale bar = 10 μm. (C) *S. aureus* was grown overnight with 500 μM of **D-DapD** in TSB at 37°C. The following day the *S. aureus* was washed 3x with PBS and infected J774A macrophages in DMEM containing no antibiotics at an MOI of 100 for 1 h in a humidified incubator at 37°C and 5% CO<sub>2</sub>. After that, the azAbx library was incubated with bacteria infected macrophages for 8 h before being incubated with 25 μM R110az, fixed with 4% formaldehyde in PBS, and 10,000 events per sample were analyzed by flow cytometry. Data are represented as mean ± SD of biological replicates (n=3). P-values were determined by a two-tailed t-test (\*p<0.05, \*\*\*p<0.001, ns = not significant).

#### 7.3.4 Measuring antibiotic permeability to intracellular pathogens

Finally, the accumulation levels of the molecules in the azAbx panel were tested. After macrophage phagocytosis of **D-DapD** labeled *S. aureus*, cells were incubated with the azAbx panel over an 8 h period (**Figure 7.6C**). When internalized *S. aureus* labeled with **D-DapD** was incubated with linezolid and erythromycin, fluorescence levels were similar to those of extracellular *S. aureus*; these results are suggestive that these antibiotics can readily reach phagocytic vacuoles. Conversely, ciprofloxacin appeared unable to access the phagosome, as evidenced by indistinguishable fluorescence levels between ciprofloxacin incubated cells and those in the absence of an azAbx. We reason that the net negative charge of ciprofloxacin-N3 could play a role in reducing the permeability of this antibiotic across the membrane bilayers. To test this, a derivative was also made in

which the carboxylic acid was masked as a methyl ester. Our data showed that a marked improvement in permeability was observed, as the fluorescence for intracellular *S. aureus* treated with ciprofloxacin-MeO was significantly lower than those treated with ciprofloxacin.

The masking of the carboxylic acid of ciprofloxacin (and other fluoroquinolones) as an ester has been explored in the past.<sup>75, 76</sup> Moreover, our results may indicate that performing phenotypic susceptibility testing via MIC against intra cellular pathogens may be biased by the inability of an antibiotic to reach the phagosome. We demonstrated that masking groups known to hinder membrane permeability, i.e. ciprofloxacin-MeO, improved antibiotic accumulation to the phagosome, emphasizing the need to develop strategies to improve the permeability profiles of existing antibiotic classes. Therefore, our results highlight the importance of taking antibiotic accessibility to the phagosome into consideration when evaluating drug effectiveness against intra cellular pathogens. Furthermore, we successfully demonstrated the applicability of our assay to empirically analyze the permeability of antibiotics to the surface of intracellular *S. aureus*. We anticipate that this platform can serve as foundational precedence to address the permeability of other classes of antibiotics to aid in developing effective treatments for persisting intracellular *S. aureus* infections.

Additionally, we applied our assay workflow to another intracellular pathogen, *Streptococcus pyogenes* (*S. pyogenes*), to establish that our concept can be translated to other bacterial pathogens. As such, *S. pyogenes* was labeled overnight with **D-DapD** and incorporation levels were assayed by incubation with R110az. Our results demonstrated a significant increase in cellular fluorescence compared to unlabeled *S. pyogenes*, indicating successful metabolic labeling and SPAAC on the surface of *S. pyogenes* (**Figure S7.7A**). As expected, azide-tagged linezolid treatment led to a reduction in cellular fluorescence. Next, **D-DapD** labeled *S. pyogenes* were incubated with macrophages to enable cell uptake. Cells treated with linezolid led to a decrease in cellular fluorescence, indicating that the mammalian cell and phagosome bilayer did not hinder linezolid permeation to intracellular *S. pyogenes* (**Figure S7.7B**). Overall, our

results indicate that our assay workflow can be applied to other intracellular pathogens to aid in the assessment of antibiotics accumulation in phagocytic vacuoles.

#### *7.4 Conclusion*

We demonstrated that the assay we developed is a suitable approach to assess the permeability of antibiotics to the surface of extracellular Gram-positive pathogens and in the phagocytic vacuoles of macrophages. A select group of FDA-approved antibiotics were successfully modified with an azide handle to covalently react with DBCO moieties embedded within the PG of *S. aureus* to give a direct read out of antibiotic accumulation. Understanding the ability of antibiotics to penetrate both the mammalian cell membrane and phagosome is critical in terms of treating intracellular *S. aureus* infections. With our approach, we were able to identify that the overall efficacy of certain classes of antibiotics against intracellular *S. aureus* may be largely impacted by the membrane barrier provided by the phagocytic cell. Therefore, it is critical to consider additional membrane components when it comes to treating intracellular bacterial infections. We anticipate our assay will be valuable in distinguishing the root cause of antibiotic resistance in intracellular pathogens.

#### *7.5 Summary and Future Outlook*

The stagnation in antibiotic development over the past few decades has severely limited our ability to combat antibiotic resistant bacteria. To address this challenge, it is critical to accelerate the discovery of new antibiotics that can circumvent resistance mechanisms. One major strategy employed by opportunistic pathogens, such as *S. aureus*, to evade antibiotic and immune pressure is intracellular survival within host cells. This presents a significant barrier to antibiotic development, as the extent to which antibiotics reach their bacterial targets in this environment remains poorly understood.

Chapter 7 describes the novel application of our lab's recently developed Peptidoglycan Accessibility Click-Mediated Assessment (PAC-MAN) to quantify the accumulation of azide-modified antibiotics in intracellular pathogens. Using this approach, we demonstrated that a prodrug derivative of ciprofloxacin significantly enhances its

intracellular accumulation in *S. aureus*. We anticipate that this technique will facilitate the development of more effective antibiotics for intracellular bacterial infections.

To further elucidate the molecular determinants governing the accumulation of compounds in intracellular pathogens, we aim to expand this assay to incorporate a diverse library of azide-modified compounds. This approach will enable us to identify the chemical properties that enhance intracellular accumulation to *S. aureus*. Ultimately, these insights will inform the rational design of antibiotic leads with improved efficacy against resistant bacteria.

### 7.6 Materials and Methods

**Materials.** All peptide related reagents and protected amino acids were purchased from Chem-Impex. DBCO-NHS (Catalog # BP-22231) was purchased from Broad Pharm. Deacetamide Linezolid Azide was purchased from Toronto Research Chemicals (Cat #: D195600). Dulbecco's Modified Eagle's Medium (DMEM) was purchased from VWR. Fetal Bovine Serum (FBS) was purchased from R&D Systems. Penicillin-Streptomycin was purchased from Sigma-Aldrich. All other organic chemical reagents were purchased from Fisher Scientific or Sigma Aldrich and used without further purification.

**Bacterial Cell Culture.** Bacterial cells were cultured in specified media in an aerobic environment while shaking at 250 rpm at 37°C. *Staphylococcus aureus* (*S. aureus*) ATCC 25923 and *S. aureus* USA 300 were grown in Tryptic Soy Broth (TSB). BLS2 organisms should be manipulated using proper protective equipment.

**Mammalian Cell Culture.** J774A.1 cells were cultured in Dulbecco's modified Eagle's medium (DMEM) supplemented with 10% (v/v) FBS, 50 IU/mL penicillin, 50 µg/mL streptomycin, and 2 mM L-glutamine in a humidified atmosphere of 5% CO<sub>2</sub> at 37°C.

**Labeling of Whole Bacterial Cells with D-DapD.** *S. aureus* was grown over-night to stationary phase in TSB while shaking (250 rpm) at 37°C. Bacterial cells from the overnight growth were used to inoculate TSB (1:100) supplemented with 500 µM **D-DapD** (or indicated concentration) and incubated at 37°C with shaking (250 rpm) for 16 h. The bacteria were harvested, washed three times with 1X phosphate buffered saline (PBS). The bacterial cells were resuspended in 1X PBS supplemented with 25 µM (or indicated

concentration) of either 6-azido-rhodamine 110 (R110az, Lumiprobe #D5230), 6-azido-fluorescein (Flaz, Lumiprobe #D1530), or 3-azido-7-hydroxy coumarin (Coaz, Sigma Aldrich #909513) in 1X PBS and incubated at 37°C for 30 min. The bacteria were spun down to remove excess dye, immediately fixed with a 2% formaldehyde solution in 1X PBS, and analyzed using the Attune NxT Flow Cytometer (Thermo Fisher) equipped with a 488 nm laser with 530/30 nm bandpass filter. The data were analyzed using Attune Nxt software.

**Peptidoglycan Isolation of *S. aureus*.** *S. aureus* ATCC 25923 was grown over-night to stationary phase in TSB medium. A 2 mL culture volume containing either DMSO or 500  $\mu$ M **D-DapD** in TSB medium was inoculated (1:100) from the stationary phase cultures and allowed to grow for 16 h while shaking (250 rpm) 37°C. The cultures were harvested, resuspended in 25  $\mu$ M of R110az in 1X PBS for 30 min at 37°C, and washed thrice with 1X PBS. The samples were boiled at 100 °C for 25 min and centrifuged at 14,000 g for 5 min at 4°C. The cells were placed in 2 mL of 2% (w/v) sodium dodecyl sulfate (SDS) and boiled for 30 min followed by centrifugation at 14,000 g for 5 min at 4°C. Cells were then washed 6 times with DI water to remove the SDS. After washing, cells were resuspended in 2 mL of 20 mM Tris buffer (pH 8.0). Pellets were treated with 800  $\mu$ g DNase for 24 h followed by 800  $\mu$ g trypsin for another 24 h at 37°C while shaking (115 rpm). Pellets were boiled for 25 min followed by centrifugation at 14,000 g for 5 min at 4°C. The pellet was harvested by centrifugation at 16,000 g for 5 min, resuspended in 1X PBS, and further diluted for analysis by flow cytometry and confocal imaging.

**Azide- Antibiotic (Abx) competition of Whole Bacterial Cells with D-DapD.** *S. aureus* was grown over-night to stationary phase in TSB while shaking (250 rpm) at 37°C. Bacterial cells from the overnight growth were used to inoculate TSB (1:100) supplemented with 500  $\mu$ M **D-DapD** and incubated at 37°C with shaking (250 rpm) for 16 h. The bacteria were harvested, washed three times with 1X PBS. The bacterial cells were resuspended in 1X PBS supplemented with 25  $\mu$ M of azide- Abx for the indicated amount of time at 37°C. The bacteria were spun down to remove excess antibiotics and were resuspended in 1X PBS supplemented with 25  $\mu$ M 6-azido-rhodamine 110 (R110az, Lumiprobe #D5230) in 1X PBS and incubated at 37°C for 30 min. The bacteria were spun

down to remove excess dye, immediately fixed with a 2% formaldehyde solution in 1X PBS, and analyzed using the Attune NxT Flow Cytometer (Thermo Fisher) equipped with a 488 nm laser with 530/30 nm bandpass filter. The data were analyzed using Attune Nxt software.

**Confocal Microscopy Analysis of Whole Bacterial Cells and Bacterial Sacculi.** Glass microscope slides were spotted with a 1% agarose pad and 2  $\mu$ L of the fixed bacterial samples were deposited onto the agarose. Samples were covered with a micro cover glass and imaged using a Zeiss 880/990 multiphoton Airyscan microscopy system (63x oil-immersion lens) equipped with a 488 nm laser. Images were obtained and analyzed via Zeiss Zen software. We acknowledge the Keck Center for Cellular Imaging and for the usage of the Zeiss 880/980 multiphoton Airyscan microscopy system (PI- AP: NIH-OD025156).

**DBCO Modification of Polystyrene Beads.** 100  $\mu$ L amino functionalized polystyrene beads (5% w/v, 5 mg) were spun down at 21000 g for 10 min in a 1.7 mL ebb tube and washed with 1 mL deionized water before use. The beads were then spun down and resuspended in 1 mL 20 mM sodium borate buffer pH 9 with 2  $\mu$ g/mL DBCO-NHS and reacted in 37°C for 2 h with shaking. The resulting beads were spun down at 21000 g for 10 min, washed once and resuspended in sodium borate buffer. 20  $\mu$ L acetic anhydride was added to the suspension and reacted in 37°C for 2h with shaking. The resulting product was then spun down and washed twice with 1 mL PBS and resuspend in 1 mL PBS for further use. Control beads were acetylated with acetic anhydride directly after wash with deionized water in the same conditions.

**Competition with Azide-Abx on DBCO Modified Polystyrene Beads.** DBCO modified and acetylated polystyrene beads were 1 to 1 diluted in PBS before adding to the assay. To a 96-well plate added 5  $\mu$ L beads each well to 25  $\mu$ M of each azide-abx in the library with a final volume of 100  $\mu$ L in multiplicity of 12. The plate was incubated in 37°C for 2 h, 4 h, 6 h, 8 h. At each time point, 3 wells of the beads in each group were transferred to a 0.45 mm MultiScreen HV Filter Plate (Sigma, Cat # MSHVN4510) and vacuum filtered. The beads were then washed with 200 mL PBS two times to remove the residue azide-abx and resuspended in 100  $\mu$ L PBS until next reaction. After collection of the last time

point, 100  $\mu$ L of 25 mM **Fi-Az** was added to each well and the plate was then incubated in 37°C for 30 min. The samples were then vacuum filtered and washed twice with 200  $\mu$ L PBS and then resuspended in 200  $\mu$ L PBS. The samples were then analyzed by Attune™ NxT Flow Cytometer (Thermo Fisher) equipped with a 488 nm laser with 530/30 nm bandpass filter. The data were analyzed using Attune Nxt software.

**Azide- Abx Competition to Intracellular *S. aureus*.** *S. aureus* ATCC 25923 was grown to stationary phase in TSB while shaking (250 rpm) at 37 °C. Bacterial cells from the overnight growth were used to inoculate TSB (1:100) supplemented with 500  $\mu$ M **D-DapD** and incubated at 37 °C with shaking (250 rpm) for 16 h. The bacteria were harvested, washed three times with 1X PBS. The bacterial cells were resuspended with 1X PBS to the original culture volume. J774A.1 cells were cultured as described above. On the day prior to the experiment, J774A.1 cells were seeded into a 48- well plate and allowed to adhere. On the day of the experiment, J774A.1 cells were washed with 1X PBS by centrifuging 5 min at 100 *g*. The washed J774A cells were then mixed with **D-DapD** labeled *S. aureus* (MOI 100) in DMEM + 10% FBS containing no antibiotics. The cell mixture was then incubated at 37 °C for 1 hour to induce phagocytosis. The cell mixture was centrifuged for 5 min at 100 *g* and media was replaced with DMEM + 10% FBS + 300  $\mu$ g/mL gentamycin and incubated at 4°C for 30 min. The cells were washed three times with 1X PBS and incubated with either a solution containing 25  $\mu$ M R110az (for no Abx competition samples) or 25  $\mu$ M azide- Abx + 300  $\mu$ g/mL gentamycin in 1X PBS for indicated amounts of time at 37°C. The Abx medium was removed, and the cells were incubated with a solution of 25  $\mu$ M R110az in 1X PBS for 30 min at 37°C. The cells were washed thrice with 1X PBS and fixed for 30 min with 4% formaldehyde in 1X PBS. Samples were then removed from the well plate by scraping and analyzed *via* flow cytometry as described above.

**Confocal Analysis of *S. aureus* Infection of Macrophages.** *S. aureus* was grown overnight to stationary phase in TSB while shaking (250 rpm) at 37 °C. Bacterial cells from the overnight growth were used to inoculate TSB (1:100) supplemented with 500  $\mu$ M **D-DapD** and incubated at 37 °C with shaking (250 rpm) for 16 h. The bacteria were harvested, washed three times with 1X PBS. The bacterial cells were resuspended in 1X

PBS supplemented with 25  $\mu\text{M}$  of R110az in 1X PBS and incubated at 37°C for 30 min. The bacteria were washed thrice and resuspended in 1X PBS to the original culture volume. J774A.1 cells were cultured as described above. On the day prior to the experiment, J774A.1 cells were seeded into 35 mm glass bottom microwell dishes and allowed to adhere. On the day of the experiment, J774A.1 cells were washed with 1X PBS by centrifuging 5 min at 100  $g$ . The washed J774A cells were then mixed with **D-DapD** labeled *S. aureus* (MOI 100) in DMEM + 10% FBS containing no antibiotics. The cell mixture was then incubated at 37°C for 1 hour to induce phagocytosis. The cell mixture was centrifuged for 5 min at 100  $g$  and media was replaced with DMEM + 10% FBS + 300  $\mu\text{g}/\text{mL}$  gentamycin and incubated at 4°C for 30 min. The cells were washed thrice with 1X PBS and fixed for 30 min with 4% formaldehyde in 1X PBS. J774A.1 macrophages were then treated with 5  $\mu\text{g}/\text{mL}$  of TMR-tagged Wheat Germ Agglutinin (Vector Laboratories, RI-1022) for 30 min at 4°C and imaged using a Zeiss 880/990 multiphoton Airyscan microscopy system (63x oil-immersion lens) equipped with 488 nm and 550 nm lasers. Images were obtained and analyzed via Zeiss Zen software. We acknowledge the Keck Center for Cellular Imaging and for the usage of the Zeiss 880/980 multiphoton Airyscan microscopy system (PI- AP: NIH-OD025156).

### 7.7 Supplementary Figures

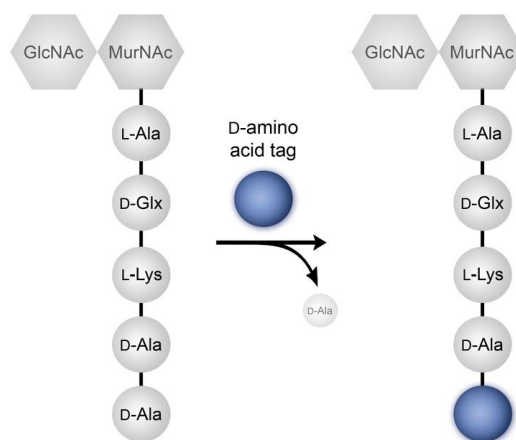


**Figure S7.1.** Mode of incorporation of single amino acids into the 5th position of the peptidoglycan stem peptide.

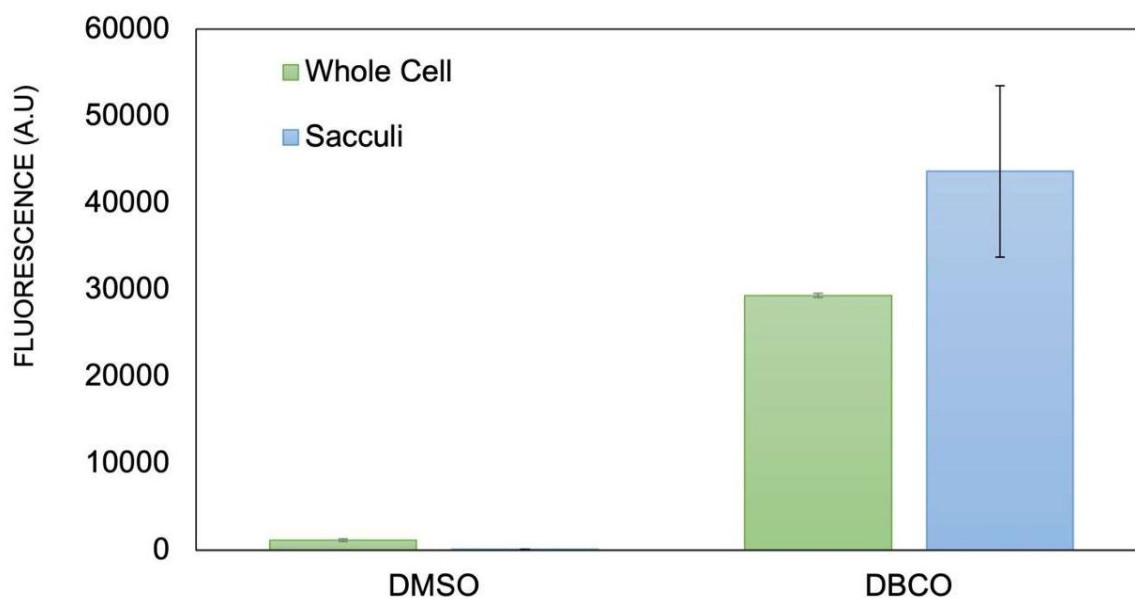


**Figure S7.2. Flow cytometry analysis of whole bacterial cells and isolated bacterial sacculi.** *S. aureus* 25922 were labeled overnight with 500  $\mu\text{M}$  of D-DapD followed by incubation with 25  $\mu\text{M}$  of R110az. Whole cell samples were analyzed by flow cytometry. Following incubation with R110az, both DMSO-treated and DBCO-treated *S. aureus* sacculi were isolated and analyzed by flow cytometry. 10,000 events were recorded for each condition. Data are represented as mean  $\pm$  SD of biological replicates ( $n=3$ )

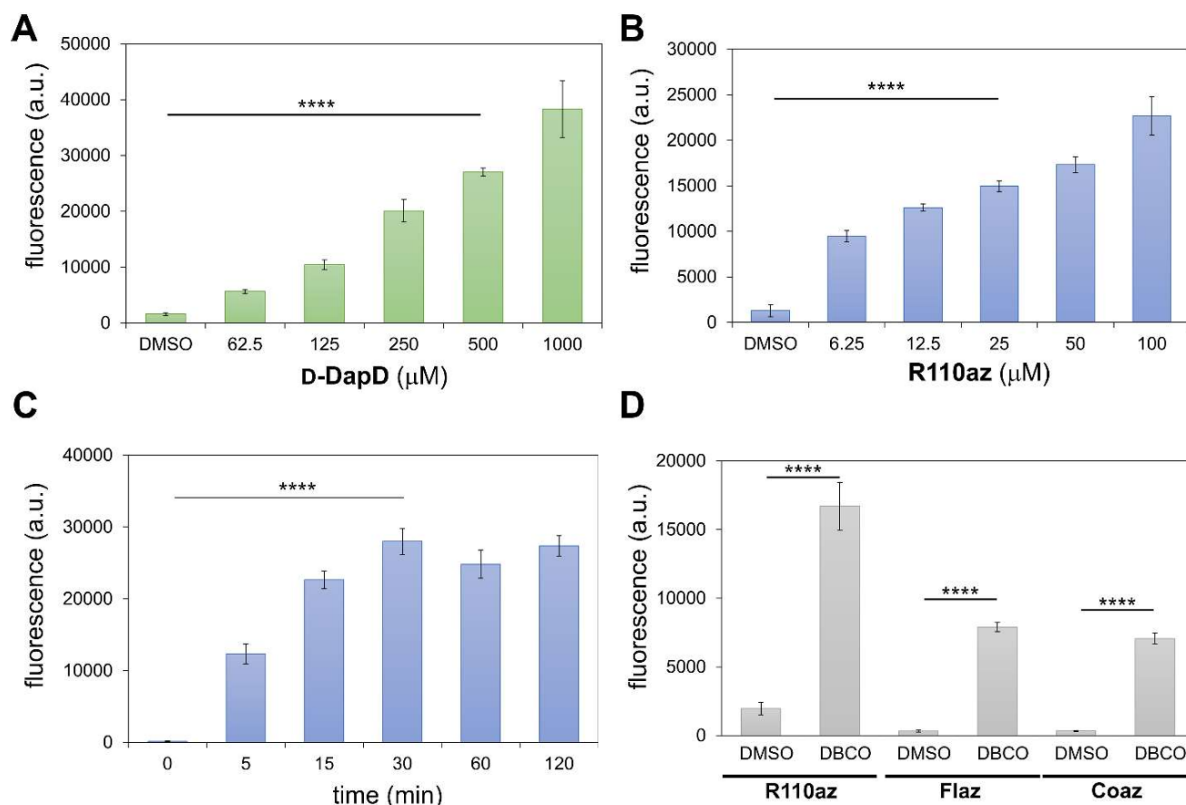


**Figure S7.3. *in vitro* S. aureus labeling optimization.** A) Flow cytometry analysis of *S. aureus* incubated over-night with increasing concentrations of D-DapD, followed by incubation with 25  $\mu\text{M}$  R110az for 30 min. B) Flow cytometry analysis of *S. aureus* incubated over-night with 500  $\mu\text{M}$  D-DapD, followed by incubation with increasing concentrations of R110az for 30 min. C) Flow cytometry analysis of *S. aureus* incubated over-night with 500  $\mu\text{M}$  D-DapD, followed by incubation with 25  $\mu\text{M}$  R110az over time. D) Flow cytometry analysis of *S. aureus* incubated overnight with 500  $\mu\text{M}$  D-DapD, followed by incubation with R110az, 6-azido-fluorescein azide (Flaz), and 3-azido-7-hydroxy coumarin azide (Coaz). 10,000 events were recorded for each condition. Data are represented as mean  $\pm$  SD of biological replicates ( $n=3$ ).  $P$ -values were determined by a two-tailed  $t$ -test (\*\*\* $p < 0.001$ , \*\*\*\* $p < 0.0001$ , ns = not significant).

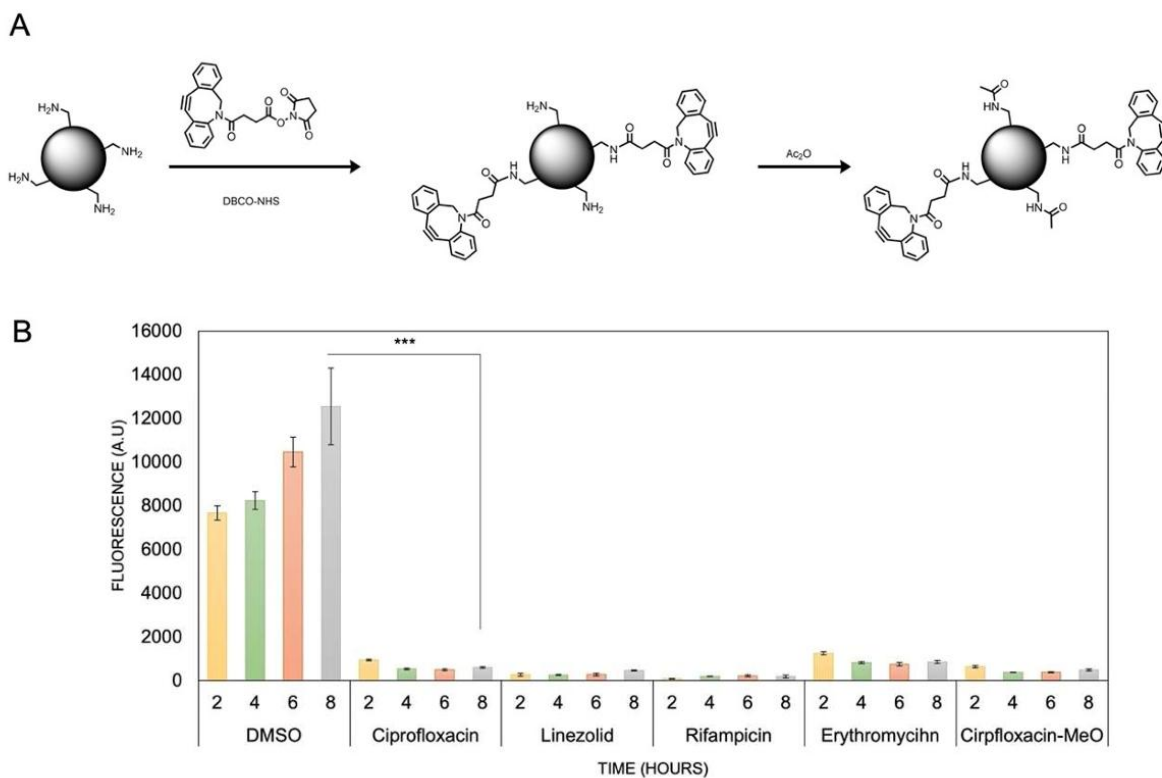


**Figure S7.4. Synthesis of DBCO- modified polystyrene beads and azAbx competition to DBCO- modified polystyrene beads.** A) Amine functionalized polystyrene beads were reacted with DBCO-NHS to form DBCO functionalized flow cytometer beads. The beads were further reacted with acetic anhydride to cap the remaining free amines. B) DBCO functionalized beads were incubated with 25  $\mu$ M of azAbx over time, followed by incubation with 25  $\mu$ M of Flaz for 30 min. Data are represented as mean  $\pm$  SD of biological replicates ( $n=3$ ). 10,000 events were recorded for each condition.  $P$ -values were determined by a two-tailed  $t$ -test (\*\* $p < 0.001$ , \*\*\*\* $p < 0.0001$ , ns = not significant).

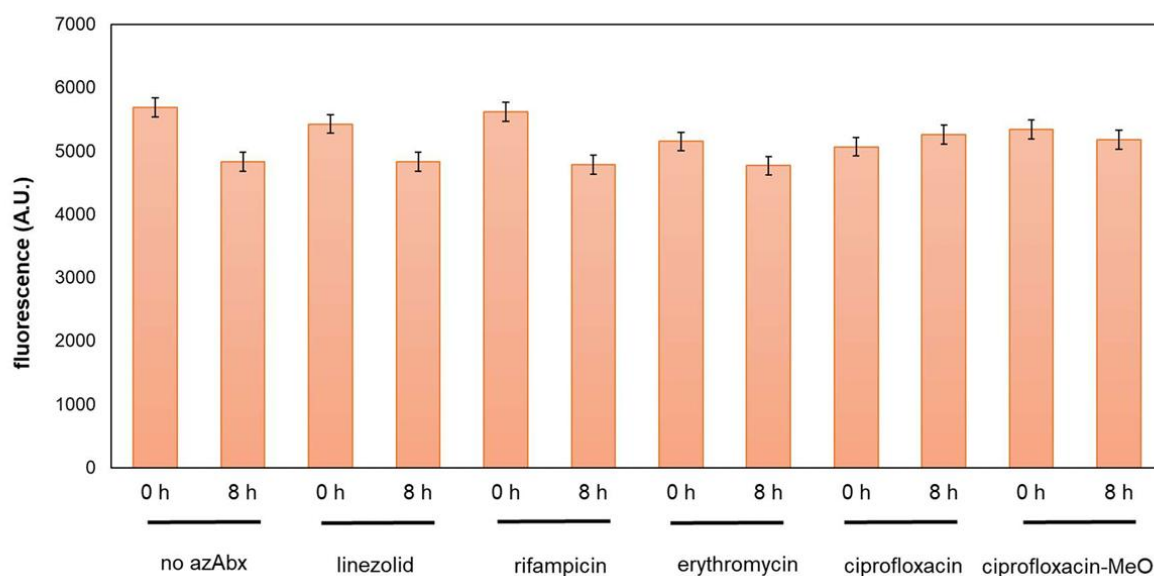


**Figure S7.5. Non-azide Abx competition to DBCO-modified *S. aureus*.** *S. aureus* cells were incubated with 500  $\mu\text{M}$  of D-DapD overnight followed by incubation with 25  $\mu\text{M}$  of unmodified (non-azide) Abx for indicated time points. Following the unmodified Abx incubation, the cells were resuspended in 25  $\mu\text{M}$  of R110az for 30 min and analyzed by flow cytometry. 10,000 events were recorded for each condition. Data are represented as mean  $\pm$  SD of biological replicates ( $n=3$ ).

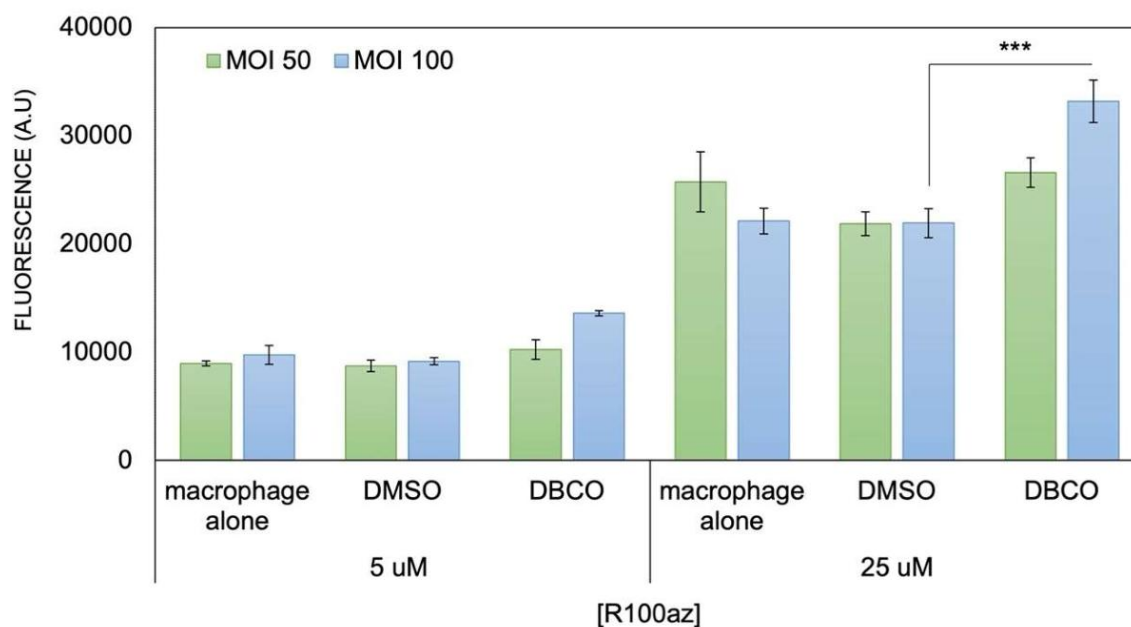


**Figure S7.6. Multiplicity of Infection (MOI) Assay.** *S. aureus* was grown overnight with 500  $\mu$ M of D-DapD and infected into J774A macrophages at MOI 50 and MOI 100. Following bacterial uptake, varying concentrations of R110az were incubated for 30 min, and cells were analyzed by flow cytometry. 10,000 events were recorded for each condition. Data are represented as mean  $\pm$  SD of biological replicates ( $n=3$ ). *P*-values were determined by a two-tailed *t*-test (\*\*\* $p < 0.001$ , \*\*\*\* $p < 0.0001$ , ns = not significant).

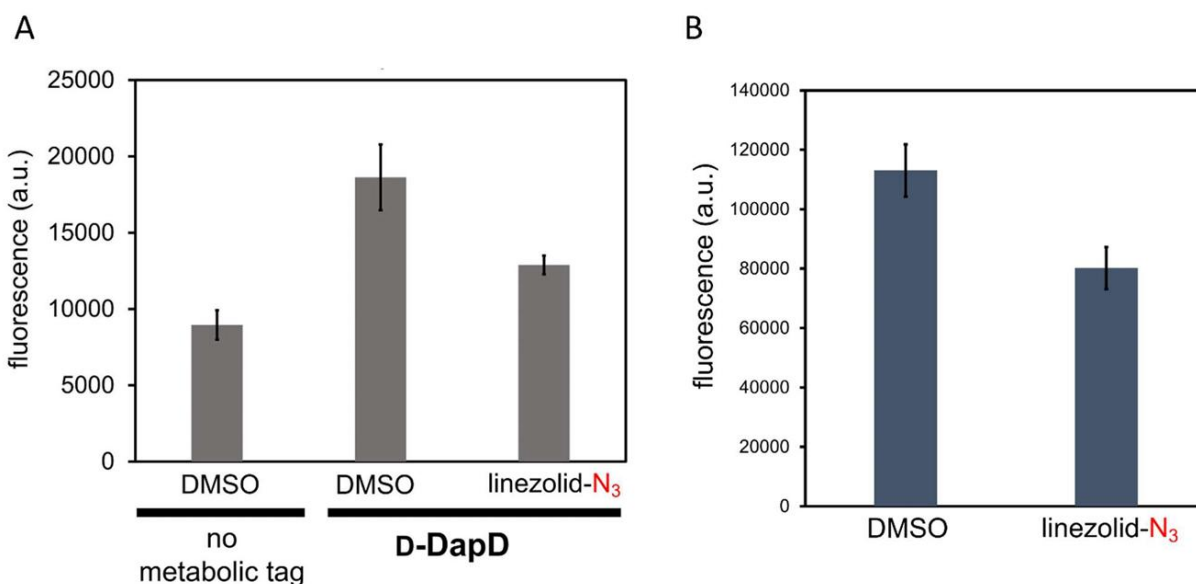


**Figure S7.7. Application of Assay Workflow to *S. pyogenes*.** A) Flow cytometry analysis of *S. pyogenes* incubated over-night with D-DapD or DMSO, followed by incubation with either DMSO or linezolid-N<sub>3</sub>, and then incubated with 25  $\mu$ M R110az for 30 min. B) *S. pyogenes* was grown overnight with 500  $\mu$ M of D-DapD and infected into J774A macrophages at MOI 100. Following bacterial uptake, DMSO or linezolid-N<sub>3</sub> was incubated with the macrophages for 2 hours. The cells were then treated with R110az for 30 min, and cells were analyzed by flow cytometry. 10,000 events were recorded for each condition. Data are represented as mean  $\pm$  SD of biological replicates ( $n=3$ ). *P*-values were determined by a two-tailed *t*-test (\*\* $p < 0.001$ , \*\*\*\* $p < 0.0001$ , ns = not significant).

COMPOUND	MIC (mg/l)	COMPOUND	MIC (mg/l)
CIPROFLOXACIN-N <sub>3</sub>	16	CIPROFLOXACIN	2 <sup>a</sup>
LINEZOLID-N <sub>3</sub>	16	LINEZOLID	4 <sup>b</sup>
RIFAMYCIN-N <sub>3</sub>	2	RIFAMYCIN	0.1 <sup>c</sup>
ERYTHROMYCIN-N <sub>3</sub>	>32	ERYTHROMYCIN	0.4 <sup>c</sup>

**Table S1. Minimum Inhibitory Concentration (MIC) of azAbx library.** *S. aureus* 25923 was grown overnight and diluted with TSB to OD600 = 0.2 and was regrown to OD600 = 1.0. Cultures were diluted to 10<sup>6</sup> CFU/mL in cation-adjusted MH broth. 100 μL was inoculated into each well of a U-bottom 96-well plate containing 100 μL of serially diluted azAbx solution. After incubation for 24 hours at 37°C, MIC values were determined by the lowest concentration of azAbx resulting in no bacterial growth visible to the naked eye based on three biological replicates.

*a* *Antibiotics (Basel)*. 2021 Sep 24;10(10):1159. doi: 10.3390/antibiotics10101159.

*b* *Antimicrob Agents Chemother*. 1996 Apr;40(4):839-45. doi: 10.1128/AAC.40.4.839.

*c* *Antimicrob Agents Chemother*. 1981 Jun;19(6):1050-5. doi: 10.1128/AAC.19.6.1050.

## 7.8 References

1. DeLeo, F. R., Otto, M., Kreiswirth, B. N., and Chambers, H. F. (2010) Community-associated methicillin-resistant *Staphylococcus aureus*, *Lancet* 375, 1557-1568.
2. Naimi, T. S., LeDell, K. H., Como-Sabetti, K., Borchardt, S. M., Boxrud, D. J., Etienne, J., Johnson, S. K., Vandenesch, F., Fridkin, S., O'Boyle, C., Danila, R. N., and Lynfield, R. (2003) Comparison of community- and health care-associated methicillin-resistant *Staphylococcus aureus* infection, *JAMA* 290, 2976-2984.
3. Klevens, R. M., Morrison, M. A., Nadle, J., Petit, S., Gershman, K., Ray, S., Harrison, L. H., Lynfield, R., Dumyati, G., Townes, J. M., Craig, A. S., Zell, E. R., Fosheim, G. E., McDougal, L. K., Carey, R. B., Fridkin, S. K., and Active Bacterial Core surveillance, M. I. (2007) Invasive methicillin-resistant *Staphylococcus aureus* infections in the United States, *JAMA* 298, 1763-1771.
4. Boucher, H. W., Talbot, G. H., Bradley, J. S., Edwards, J. E., Gilbert, D., Rice, L. B., Scheld, M., Spellberg, B., and Bartlett, J. (2009) Bad bugs, no drugs: no ESKAPE! An update from the Infectious Diseases Society of America, *Clin Infect Dis* 48, 1-12.
5. Boucher, H. W., and Corey, G. R. (2008) Epidemiology of methicillin-resistant *Staphylococcus aureus*, *Clin Infect Dis* 46 Suppl 5, S344-349.
6. Lowy, F. D. (2003) Antimicrobial resistance: the example of *Staphylococcus aureus*, *J Clin Invest* 111, 1265-1273.
7. Tuchscher, L., Medina, E., Hussain, M., Volker, W., Heitmann, V., Niemann, S., Holzinger, D., Roth, J., Proctor, R. A., Becker, K., Peters, G., and Löffler, B. (2011) *Staphylococcus aureus* phenotype switching: an effective bacterial strategy to escape host immune response and establish a chronic infection, *EMBO Mol Med* 3, 129-141.
8. Schnaith, A., Kashkar, H., Leggio, S. A., Addicks, K., Kronke, M., and Krut, O. (2007) *Staphylococcus aureus* subvert autophagy for induction of caspase-independent host cell death, *J Biol Chem* 282, 2695-2706.
9. Kubica, M., Guzik, K., Koziel, J., Zarebski, M., Richter, W., Gajkowska, B., Golda, A., Maciag-Gudowska, A., Brix, K., Shaw, L., Foster, T., and Potempa, J. (2008) A potential new pathway for *Staphylococcus aureus* dissemination: the silent

- survival of *S. aureus* phagocytosed by human monocyte-derived macrophages, *PLoS One* 3, e1409.
10. Hamza, T., and Li, B. (2014) Differential responses of osteoblasts and macrophages upon *Staphylococcus aureus* infection, *BMC Microbiol* 14, 207.
  11. Rogers, D. E. (1956) Studies on bacteriemia. I. Mechanisms relating to the persistence of bacteriemia in rabbits following the intravenous injection of staphylococci, *J Exp Med* 103, 713-742.
  12. Pidwill, G. R., Gibson, J. F., Cole, J., Renshaw, S. A., and Foster, S. J. (2020) The Role of Macrophages in *Staphylococcus aureus* Infection, *Front Immunol* 11, 620339.
  13. Peyrusson, F., Varet, H., Nguyen, T. K., Legendre, R., Sismeiro, O., Coppee, J. Y., Wolz, C., Tenson, T., and Van Bambeke, F. (2020) Intracellular *Staphylococcus aureus* persists upon antibiotic exposure, *Nat Commun* 11, 2200.
  14. Thwaites, G. E., and Gant, V. (2011) Are bloodstream leukocytes Trojan Horses for the metastasis of *Staphylococcus aureus*?, *Nat Rev Microbiol* 9, 215-222.
  15. Gresham, H. D., Lowrance, J. H., Caver, T. E., Wilson, B. S., Cheung, A. L., and Lindberg, F. P. (2000) Survival of *Staphylococcus aureus* inside neutrophils contributes to infection, *J Immunol* 164, 3713-3722.
  16. Garzoni, C., and Kelley, W. L. (2011) Return of the Trojan horse: intracellular phenotype switching and immune evasion by *Staphylococcus aureus*, *EMBO Mol Med* 3, 115-117.
  17. Fraunholz, M., and Sinha, B. (2012) Intracellular *Staphylococcus aureus*: live-in and let die, *Front Cell Infect Microbiol* 2, 43.
  18. Anwar, S., Prince, L. R., Foster, S. J., Whyte, M. K., and Sabroe, I. (2009) The rise and rise of *Staphylococcus aureus*: laughing in the face of granulocytes, *Clin Exp Immunol* 157, 216-224.
  19. Flannagan, R. S., Heit, B., and Heinrichs, D. E. (2016) Intracellular replication of *Staphylococcus aureus* in mature phagolysosomes in macrophages precedes host cell death, and bacterial escape and dissemination, *Cell Microbiol* 18, 514-535.
  20. Sandberg, A., Hessler, J. H., Skov, R. L., Blom, J., and Frimodt-Moller, N. (2009) Intracellular activity of antibiotics against *Staphylococcus aureus* in a mouse peritonitis model, *Antimicrob Agents Chemother* 53, 1874-1883.

21. Lehar, S. M., Pillow, T., Xu, M., Staben, L., Kajihara, K. K., Vandlen, R., DePalatis, L., Raab, H., Hazenbos, W. L., Morisaki, J. H., Kim, J., Park, S., Darwish, M., Lee, B. C., Hernandez, H., Loyet, K. M., Lupardus, P., Fong, R., Yan, D., Chalouni, C., Luis, E., Khalfin, Y., Plise, E., Cheong, J., Lyssikatos, J. P., Strandh, M., Koefoed, K., Andersen, P. S., Flygare, J. A., Wah Tan, M., Brown, E. J., and Mariathasan, S. (2015) Novel antibody-antibiotic conjugate eliminates intracellular *S. aureus*, *Nature* 527, 323-328.
22. Barcia-Macay, M., Seral, C., Mingeot-Leclercq, M. P., Tulkens, P. M., and Van Bambeke, F. (2006) Pharmacodynamic evaluation of the intracellular activities of antibiotics against *Staphylococcus aureus* in a model of THP-1 macrophages, *Antimicrob Agents Chemother* 50, 841-851.
23. Rowe, S. E., Wagner, N. J., Li, L., Beam, J. E., Wilkinson, A. D., Radlinski, L. C., Zhang, Q., Miao, E. A., and Conlon, B. P. (2020) Reactive oxygen species induce antibiotic tolerance during systemic *Staphylococcus aureus* infection, *Nat Microbiol* 5, 282-290.
24. Tuchscher, L., Heitmann, V., Hussain, M., Viemann, D., Roth, J., von Eiff, C., Peters, G., Becker, K., and Loffler, B. (2010) *Staphylococcus aureus* small-colony variants are adapted phenotypes for intracellular persistence, *J Infect Dis* 202, 1031-1040.
25. Seral, C., Van Bambeke, F., and Tulkens, P. M. (2003) Quantitative analysis of gentamicin, azithromycin, telithromycin, ciprofloxacin, moxifloxacin, and oritavancin (LY333328) activities against intracellular *Staphylococcus aureus* in mouse J774 macrophages, *Antimicrob Agents Chemother* 47, 2283-2292.
26. Seral, C., Barcia-Macay, M., Mingeot-Leclercq, M. P., Tulkens, P. M., and Van Bambeke, F. (2005) Comparative activity of quinolones (ciprofloxacin, levofloxacin, moxifloxacin and garenoxacin) against extracellular and intracellular infection by *Listeria monocytogenes* and *Staphylococcus aureus* in J774 macrophages, *J Antimicrob Chemother* 55, 511-517.
27. Lemaire, S., Tulkens, P. M., and Van Bambeke, F. (2011) Contrasting effects of acidic pH on the extracellular and intracellular activities of the anti-gram-positive fluoroquinolones moxifloxacin and delafloxacin against *Staphylococcus aureus*, *Antimicrob Agents Chemother* 55, 649-658.

28. Hand, W. L., and King-Thompson, N. L. (1990) Uptake of antibiotics by human polymorphonuclear leukocyte cytoplasts, *Antimicrob Agents Chemother* 34, 1189-1193.
29. Hand, W. L., King-Thompson, N., and Holman, J. W. (1987) Entry of roxithromycin (RU 965), imipenem, cefotaxime, trimethoprim, and metronidazole into human polymorphonuclear leukocytes, *Antimicrob Agents Chemother* 31, 1553-1557.
30. Brezden, A., Mohamed, M. F., Nepal, M., Harwood, J. S., Kuriakose, J., Seleem, M. N., and Chmielewski, J. (2016) Dual Targeting of Intracellular Pathogenic Bacteria with a Cleavable Conjugate of Kanamycin and an Antibacterial Cell-Penetrating Peptide, *J Am Chem Soc* 138, 10945-10949.
31. Antonoplis, A., Zang, X., Huttner, M. A., Chong, K. K. L., Lee, Y. B., Co, J. Y., Amieva, M. R., Kline, K. A., Wender, P. A., and Cegelski, L. (2018) A Dual-Function Antibiotic-Transporter Conjugate Exhibits Superior Activity in Sterilizing MRSA Biofilms and Killing Persister Cells, *J Am Chem Soc* 140, 16140-16151.
32. Buccini, D. F., Cardoso, M. H., and Franco, O. L. (2020) Antimicrobial Peptides and Cell-Penetrating Peptides for Treating Intracellular Bacterial Infections, *Front Cell Infect Microbiol* 10, 612931.
33. Rohrig, C., Huemer, M., Lorge, D., Luterbacher, S., Phothaworn, P., Schefer, C., Sobieraj, A. M., Zinsli, L. V., Mairpady Shambat, S., Leimer, N., Keller, A. P., Eichenseher, F., Shen, Y., Korbsrisate, S., Zinkernagel, A. S., Loessner, M. J., and Schmelcher, M. (2020) Targeting Hidden Pathogens: Cell-Penetrating Enzybiotics Eradicate Intracellular Drug-Resistant Staphylococcus aureus, *mBio* 11.
34. Zeiders, S. M., and Chmielewski, J. (2021) Antibiotic-cell-penetrating peptide conjugates targeting challenging drug-resistant and intracellular pathogenic bacteria, *Chem Biol Drug Des* 98, 762-778.
35. Ferraro, N. J., and Pires, M. M. (2022) Genetic Determinants of Surface Accessibility in Staphylococcus aureus, *Bioconjug Chem* 33, 767-772.
36. Ferraro, N. J., Kim, S., Im, W., and Pires, M. M. (2021) Systematic Assessment of Accessibility to the Surface of Staphylococcus aureus, *ACS Chem Biol* 16, 2527-2536.
37. Liu, Z., Lepori, I., Chordia, M. D., Dalesandro, B. E., Guo, T., Dong, J., Siegrist, M. S., and Pires, M. M. (2023) A Metabolic-Tag-Based Method for Assessing the

- Permeation of Small Molecules Across the Mycomembrane in Live Mycobacteria, *Angew Chem Int Ed Engl* 62, e202217777.
38. Agard, N. J., Prescher, J. A., and Bertozzi, C. R. (2004) A strain-promoted [3 + 2] azide-alkyne cycloaddition for covalent modification of biomolecules in living systems, *J Am Chem Soc* 126, 15046-15047.
  39. Jewett, J. C., Sletten, E. M., and Bertozzi, C. R. (2010) Rapid Cu-free click chemistry with readily synthesized biarylazacyclooctynones, *J Am Chem Soc* 132, 3688-3690.
  40. Baskin, J. M., Prescher, J. A., Laughlin, S. T., Agard, N. J., Chang, P. V., Miller, I. A., Lo, A., Codelli, J. A., and Bertozzi, C. R. (2007) Copper-free click chemistry for dynamic in vivo imaging, *Proc Natl Acad Sci U S A* 104, 16793-16797.
  41. Sharif, S., Singh, M., Kim, S. J., and Schaefer, J. (2009) Staphylococcus aureus peptidoglycan tertiary structure from carbon-13 spin diffusion, *J Am Chem Soc* 131, 7023-7030.
  42. Vollmer, W. (2008) Structural variation in the glycan strands of bacterial peptidoglycan, *FEMS Microbiol Rev* 32, 287-306.
  43. Vollmer, W., and Bertsche, U. (2008) Murein (peptidoglycan) structure, architecture and biosynthesis in Escherichia coli, *Biochim Biophys Acta* 1778, 1714-1734.
  44. Vollmer, W., Joris, B., Charlier, P., and Foster, S. (2008) Bacterial peptidoglycan (murein) hydrolases, *FEMS Microbiol Rev* 32, 259-286.
  45. Salamaga, B., Kong, L., Pasquina-Lemonche, L., Lafage, L., von Und Zur Muhlen, M., Gibson, J. F., Grybchuk, D., Tooke, A. K., Panchal, V., Culp, E. J., Tatham, E., O'Kane, M. E., Catley, T. E., Renshaw, S. A., Wright, G. D., Plevka, P., Bullough, P. A., Han, A., Hobbs, J. K., and Foster, S. J. (2021) Demonstration of the role of cell wall homeostasis in Staphylococcus aureus growth and the action of bactericidal antibiotics, *Proc Natl Acad Sci U S A* 118.
  46. Reed, P., Atilano, M. L., Alves, R., Hoiczky, E., Sher, X., Reichmann, N. T., Pereira, P. M., Roemer, T., Filipe, S. R., Pereira-Leal, J. B., Ligoxygakis, P., and Pinho, M. G. (2015) Staphylococcus aureus Survives with a Minimal Peptidoglycan Synthesis Machine but Sacrifices Virulence and Antibiotic Resistance, *PLoS Pathog* 11, e1004891.

47. Pidgeon, S. E., and Pires, M. M. (2017) Vancomycin-Dependent Response in Live Drug-Resistant Bacteria by Metabolic Labeling, *Angew Chem Int Ed Engl* *56*, 8839-8843.
48. Pidgeon, S. E., and Pires, M. M. (2017) Cell Wall Remodeling by a Synthetic Analog Reveals Metabolic Adaptation in Vancomycin Resistant Enterococci, *ACS Chem Biol* *12*, 1913-1918.
49. Pidgeon, S. E., and Pires, M. M. (2017) Cell Wall Remodeling of *Staphylococcus aureus* in Live *Caenorhabditis elegans*, *Bioconjug Chem* *28*, 2310-2315.
50. Pidgeon, S. E., Apostolos, A. J., Nelson, J. M., Shaku, M., Rimal, B., Islam, M. N., Crick, D. C., Kim, S. J., Pavelka, M. S., Kana, B. D., and Pires, M. M. (2019) L,D-Transpeptidase Specific Probe Reveals Spatial Activity of Peptidoglycan Cross-Linking, *ACS Chem Biol* *14*, 2185-2196.
51. Fura, J. M., Kearns, D., and Pires, M. M. (2015) D-Amino Acid Probes for Penicillin Binding Protein-based Bacterial Surface Labeling, *J Biol Chem* *290*, 30540-30550.
52. Dalesandro, B. E., and Pires, M. M. (2021) Induction of Endogenous Antibody Recruitment to the Surface of the Pathogen *Enterococcus faecium*, *ACS Infect Dis* *7*, 1116-1125.
53. Apostolos, A. J., Nelson, J. M., Silva, J. R. A., Lameira, J., Achimovich, A. M., Gahlmann, A., Alves, C. N., and Pires, M. M. (2020) Facile Synthesis and Metabolic Incorporation of m-DAP Bioisosteres Into Cell Walls of Live Bacteria, *ACS Chem Biol* *15*, 2966-2975.
54. Apostolos, A. J., Ocius, K. L., Koyasseril-Yehiya, T. M., Santamaria, C., Silva, J. R. A., Lameira, J., Alves, C. N., Siegrist, M. S., and Pires, M. M. (2022) Metabolic Processing of Selenium-Based Bioisosteres of meso-Diaminopimelic Acid in Live Bacteria, *Biochemistry* *61*, 1404-1414.
55. Apostolos, A. J., Chordia, M. D., Kolli, S. H., Dalesandro, B. E., Rutkowski, M. R., and Pires, M. M. (2022) Real-time non-invasive fluorescence imaging of gut commensal bacteria to detect dynamic changes in the microbiome of live mice, *Cell Chem Biol*.
56. Apostolos, A. J., Pidgeon, S. E., and Pires, M. M. (2020) Remodeling of Cross-bridges Controls Peptidoglycan Cross-linking Levels in Bacterial Cell Walls, *ACS Chem Biol* *15*, 1261-1267.

57. Apostolos, A. J., Kelly, J. J., Ongwae, G. M., and Pires, M. M. (2022) Structure Activity Relationship of the Stem Peptide in Sortase A Mediated Ligation from *Staphylococcus aureus*, *Chembiochem* 23, e202200412.
58. Welsh, M. A., Taguchi, A., Schaefer, K., Van Tyne, D., Lebreton, F., Gilmore, M. S., Kahne, D., and Walker, S. (2017) Identification of a Functionally Unique Family of Penicillin-Binding Proteins, *J Am Chem Soc* 139, 17727-17730.
59. Ngadjeua, F., Braud, E., Saidjalolov, S., Iannazzo, L., Schnappinger, D., Ehrh, S., Hugonnet, J. E., Mengin-Lecreulx, D., Patin, D., Etheve-Quelquejeu, M., Fonvielle, M., and Arthur, M. (2018) Critical Impact of Peptidoglycan Precursor Amidation on the Activity of L,d-Transpeptidases from *Enterococcus faecium* and *Mycobacterium tuberculosis*, *Chemistry* 24, 5743-5747.
60. Gautam, S., Kim, T., and Spiegel, D. A. (2015) Chemical probes reveal an extraseptal mode of cross-linking in *Staphylococcus aureus*, *J Am Chem Soc* 137, 7441-7447.
61. Gautam, S., Kim, T., Shoda, T., Sen, S., Deep, D., Luthra, R., Ferreira, M. T., Pinho, M. G., and Spiegel, D. A. (2015) An Activity-Based Probe for Studying Crosslinking in Live Bacteria, *Angew Chem Int Ed Engl* 54, 10492-10496.
62. Apostolos, A. J., Ferraro, N. J., Dalesandro, B. E., and Pires, M. M. (2021) SaccuFlow: A High-Throughput Analysis Platform to Investigate Bacterial Cell Wall Interactions, *ACS Infect Dis* 7, 2483-2491.
63. Wu, C. Y., and Lee, P. I. (2007) Antibiotic-lock therapy and erythromycin for treatment of catheter-related *Candida parapsilosis* and *Staphylococcus aureus* infections, *J Antimicrob Chemother* 60, 706-707.
64. Rayner, C., and Munckhof, W. J. (2005) Antibiotics currently used in the treatment of infections caused by *Staphylococcus aureus*, *Intern Med J* 35 Suppl 2, S3-16.
65. Gidari, A., Sabbatini, S., Schiaroli, E., Perito, S., Francisci, D., Baldelli, F., and Monari, C. (2020) Tedizolid-Rifampicin Combination Prevents Rifampicin-Resistance on in vitro Model of *Staphylococcus aureus* Mature Biofilm, *Front Microbiol* 11, 2085.
66. Baldoni, D., Haschke, M., Rajacic, Z., Zimmerli, W., and Trampuz, A. (2009) Linezolid alone or combined with rifampin against methicillin-resistant *Staphylococcus aureus* in experimental foreign-body infection, *Antimicrob Agents Chemother* 53, 1142-1148.

67. Lienkamp, K., Kumar, K. N., Som, A., Nusslein, K., and Tew, G. N. (2009) "Doubly selective" antimicrobial polymers: how do they differentiate between bacteria?, *Chemistry* 15, 11710-11714.
68. Guariglia-Oropeza, V., and Helmann, J. D. (2011) Bacillus subtilis sigma(V) confers lysozyme resistance by activation of two cell wall modification pathways, peptidoglycan O-acetylation and D-alanylation of teichoic acids, *J Bacteriol* 193, 6223-6232.
69. Gautam, S., Kim, T., Lester, E., Deep, D., and Spiegel, D. A. (2016) Wall teichoic acids prevent antibody binding to epitopes within the cell wall of Staphylococcus aureus, *ACS Chem Biol* 11, 25-30.
70. Sara, M., and Sleytr, U. B. (1987) Molecular sieving through S layers of Bacillus stearothermophilus strains, *J Bacteriol* 169, 4092-4098.
71. Demchick, P., and Koch, A. L. (1996) The permeability of the wall fabric of Escherichia coli and Bacillus subtilis, *J Bacteriol* 178, 768-773.
72. Lovering, A. L., Safadi, S. S., and Strynadka, N. C. (2012) Structural perspective of peptidoglycan biosynthesis and assembly, *Annu Rev Biochem* 81, 451-478.
73. Vollmer, W., and Seligman, S. J. (2010) Architecture of peptidoglycan: more data and more models, *Trends Microbiol* 18, 59-66.
74. Gally, D., and Archibald, A. R. (1993) Cell wall assembly in Staphylococcus aureus: proposed absence of secondary crosslinking reactions, *J Gen Microbiol* 139, 1907-1913.
75. Pais, J. P., Policarpo, M., Pires, D., Francisco, A. P., Madureira, A. M., Testa, B., Anes, E., and Constantino, L. (2022) Fluoroquinolone Derivatives in the Treatment of Mycobacterium tuberculosis Infection, *Pharmaceuticals (Basel)* 15.
76. Su, F. Y., Srinivasan, S., Lee, B., Chen, J., Convertine, A. J., West, T. E., Ratner, D. M., Skerrett, S. J., and Stayton, P. S. (2018) Macrophage-targeted drugamers with enzyme-cleavable linkers deliver high intracellular drug dosing and sustained drug pharmacokinetics against alveolar pulmonary infections, *J Control Release* 287, 1-11.

## Chapter 8 Summary and Future Outlook

The emergence of cancer immunotherapy has transformed patient treatment. However, significant challenges remain in identifying conserved, cancer-specific antigens as well as overcoming immune evasion mechanisms. To this end, neoantigens presented on MHC represent a promising class of tumor-specific antigens to target. However, cancer cells often escape detection by suppressing neoantigen expression or by downregulating MHC presentation, thereby diminishing T cell-mediated responses. These evasion strategies underscore the urgent need to further understand the molecular mechanisms governing antigen presentation. Additionally, it provides opportunities to develop therapeutic strategies to enhance neoantigen display, restore MHC expression, and improve immune recognition to drive more effective anti-tumor responses.

Chapter 1 explores the biological role of antigen presentation through MHC-I and MHC-II in response to infectious disease and cancer. MHC-I presentation enables the immune system to detect intracellular antigens, including viral peptides and tumor-associated neoantigens, allowing for the elimination of unhealthy or infected cells. In contrast, MHC-II antigen presentation plays a crucial role in initiating and regulating adaptive immune responses by displaying extracellular antigens to CD4<sup>+</sup> T cells. Enhancing these processes has shown great promise in advancing cancer treatment options. The presence of cancer-specific neoantigens on MHC molecules provides a unique therapeutic opportunity, as these antigens are absent on healthy cells and are selectively recognized by immune cells. This combination allows for the targeted elimination of cancer cells while minimizing off-target toxicity.

A comprehensive understanding of the biological pathways governing antigen processing and presentation, as well as T cell response to pMHC complexes, is essential for improving immunotherapy strategies. These efforts have driven major advances in immune checkpoint blockade, adoptive T cell therapy, and cancer vaccine development. However, key challenges remain, including the identification of patient-specific neoantigens and the underlying molecular mechanisms resulting in their presentation on MHC molecules. Overcoming these obstacles requires deeper investigation into the

factors influencing neoantigen presentation on MHC and improved methods for neoantigen detection.

A key advancement in MHC-targeted therapies was the identification of the peptide sequences presented by MHC-I molecules. In Chapter 2, we outlined the evolution of techniques used to characterize MHC-associated peptides. Notably, we discussed how PTM-modified MHC-associated peptides represent a distinct and biologically relevant class of antigens, as their evasion of thymic negative selection enables them to modulate immune responses. Recent advances in mass spectrometry have greatly expanded the catalog of identified PTM-modified MHC-associated peptides. However, studies on their functional impact on antigen presentation have largely focused on a limited subset of PTMs, such as phosphorylation, glycosylation, and citrullination. The broader implications of PTMs on antigen display and immune recognition remain largely unexplored. Therefore, there is a significant need for more comprehensive investigations into their role in adaptive immunity.

Furthermore, an emerging understanding of how reactive chemical species influence immune signaling is shedding light on mechanisms that drive autoimmunity and allergic responses. Concurrently, these insights provide a foundation for developing cancer-specific immunotherapies that exploit covalent ligands that target cancer-specific protein mutations. To fully harness the therapeutic of PTM modified antigens, future research must integrate structural, functional, and immunological approaches to systematically elucidate how diverse PTMs influence antigen presentation and immune recognition.

In Chapter 3, we explored the use of pHLIP to selectively deliver immunogenic peptides to cancer cells and enhanced T cell recognition. Tumors often exhibit heterogenous neoantigen expression which complicates immune-mediated clearance. Also, the lack of widely shared neoantigens across individuals in a population further restricts the development of universal therapies. To address this, we pursued an alternative strategy of targeting cancer cells directly for delivery with an immunogenic peptide. By exploiting the acidic tumor microenvironment, a feature commonly conserved among various types of tumors, we facilitated the presentation of antigenic peptides on MHC-I molecules and ultimately improving T cell engagement.

One of the key advantages of pHILIP as a delivery platform is its ability to transport peptides that are larger and more polar than conventional MHC-I ligands. This versatility makes it a promising tool for delivering a diverse range of neoantigens. However, extending this strategy to MHC haplotypes beyond H-2K<sup>b</sup> will require investigation into which sites on peptides of interest are available for modification to install a cysteine for disulfide bond formation. Establishing a broadly applicable system for neoantigen delivery could significantly enhance the personalization of cancer immunotherapies allowing for more precise immune targeting across different tumor types.

In Chapter 4, we investigated the potential of using small molecules to modulate MHC-I surface expression in cancer cells. Through this work, we identified a promising scaffold that enhances MHC-I expression in colorectal cancer cells and developed a high-throughput derivatization platform to systematically generate and evaluate additional immunomodulatory compounds. Moving forward, we plan to expand our library of derivatives to better understand the structure-activity relationship between our molecules and MHC-I upregulation as well as optimize our compounds biological properties. We aim to do this by scaling our screening efforts to our 4,000-member azide library. Additionally, we aim to assess our compound's ability to upregulate MHC-I expression in vivo as well as determine if they enhance the efficacy of checkpoint inhibitors for immunotherapy applications.

A broader consideration for this project is that most small molecule drugs exhibit some degree of polypharmacology, the phenomenon where compounds interact with multiple protein targets, which often leads to unexplored biological effects. We hypothesized that certain small molecule anticancer agents may exert their cytotoxic effect by altering immune interactions with tumors in ways that extend beyond their expected primary mechanism of action. Since small molecules are typically optimized for efficacy in in vitro models that lack most immune system components, their impact on the immune response remains largely unknown. Gaining a deeper understanding of these effects could inform the development of combination therapies that enhance anti-tumor immunity.

Chapter 5 focuses on the role of PTMs in modifying antigen presentation. The immune system's recognition of antigenic peptides depends on two critical factors. One being the

binding affinity of peptides to MHC molecules and the other being their subsequent recognition by T cell receptors. To dissect these contributions, we employed a cell-based system to investigate how PTMs alter antigen presentation and influence T cell recognition.

Further exploration in this area will require a more detailed understanding of how cancer cells generate PTMs that are absent in healthy tissue and how these modifications shape immune responses. The biochemical pathways governing PTM-modified neoantigen formation remains poorly characterized making it difficult to predict which peptides will be displayed on MHC. Additionally, emerging evidence suggests that PTMs may serve as privileged targets for immune activation, likely due to their limited presence in the thymus during T cell development. Moreover, developing predictive models to assess whether a PTM sufficiently alters peptide structure to generate a robust T cell response could have significant implications for cancer immunotherapy.

Chapter 6 examined how non-enzymatic modifications induced by reactive species influence antigen presentation. The tumor microenvironment is characterized by elevated levels of reactive oxygen species and other reactive metabolites which are likely to give rise to unique neoantigens that serve as selective immune targets. Identifying and characterizing these modified antigens may improve neoantigen prediction models and advance the design of novel cancer immunotherapies. Additionally, these findings could provide insight into the role modified antigens play in inflammatory autoimmune diseases.

More broadly, it is becoming increasingly clear that exogenous metabolites shape immune response. For instance, hapten-modified peptides presented on MHC molecules are known to play a role in  $\beta$ -lactam allergies, suggesting that exposure to electrophilic environment agents may similarly alter antigen presentation and trigger an immune response. Furthermore, pioneering work from the Craik lab has demonstrated that hapten modification of a cancer-specific mutation can be leveraged for immunotherapy. Given the increasing use of covalent drugs, it is plausible that these compounds contribute to the immune response over time by modifying peptides presented on MHC. Investigating these interactions could not only provide insights into unintended immune responses but also reveal novel therapeutic strategies.

Beyond immunotherapy, antibiotic resistance remains a pressing global challenge that is exacerbated by the lack of new antibiotic development. One major strategy used by bacterial pathogens such as *Staphylococcus aureus* to evade both antibiotic and immune pressure is through intracellular persistence within host cells. However, our understanding of how well antibiotics penetrate and accumulate within these intracellular bacteria remains poorly understood and poses a significant barrier to drug development.

In Chapter 7, we applied our lab's recently developed Peptidoglycan Accessibility Click-Mediated Assessment (PAC-MAN) assay to quantify intracellular antibiotic accumulation. Using this method, we demonstrated that a prodrug derivative of ciprofloxacin significantly enhances its intracellular accumulation to *S. aureus*. We anticipate that this approach will facilitate the rational design of antibiotics with improved efficacy against intracellular pathogens. To further elucidate the molecular determinants governing intracellular antibiotic accumulation, we plan to expand our assay to screen a diverse library of azide-modified molecules. This will enable us to identify chemical properties that enhance accumulation to intracellular *S. aureus* and guide the development of next-generation antibiotics capable of overcoming resistance mechanisms.

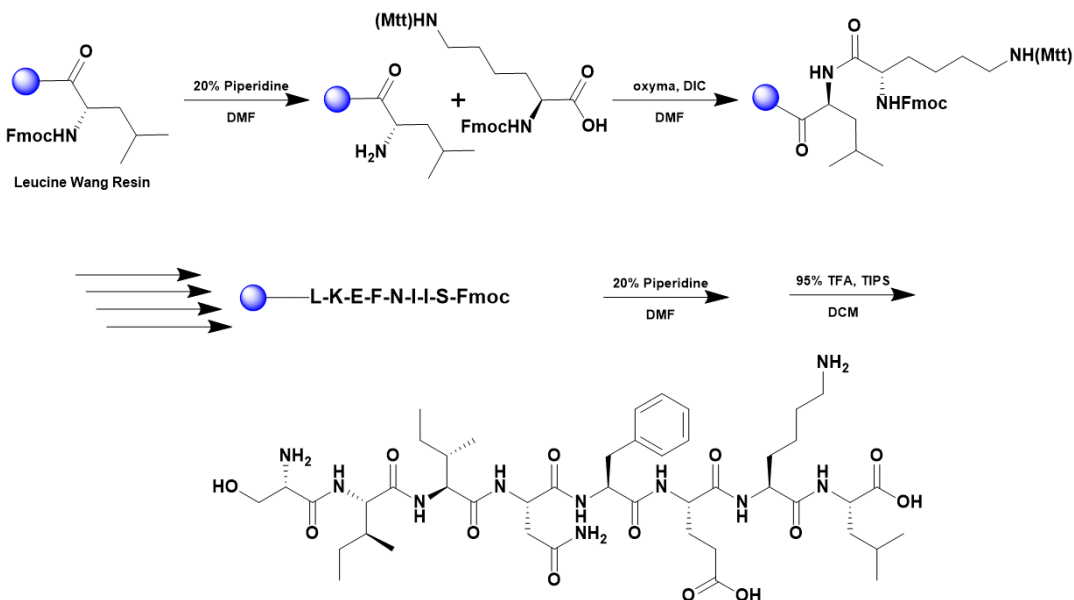
Taken together, the work presented in this dissertation advances our understanding of antigen presentation, immune modulation, and antibiotic accumulation. These studies provide a foundation for future efforts to refine cancer immunotherapy strategies, explore novel immunomodulatory compounds, and develop more effective treatments for drug-resistant infections.

## Appendix

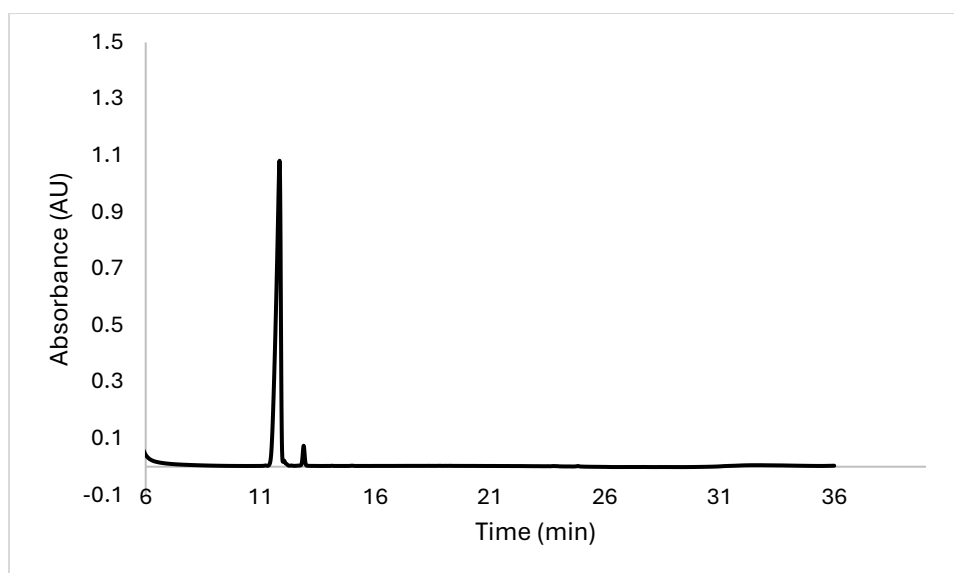
\*Note: Unless otherwise indicated, all chromatographs for HPLC analysis were observed at 220 nm.

### A.3 Synthesis and Characterization of Compounds in Chapter 3

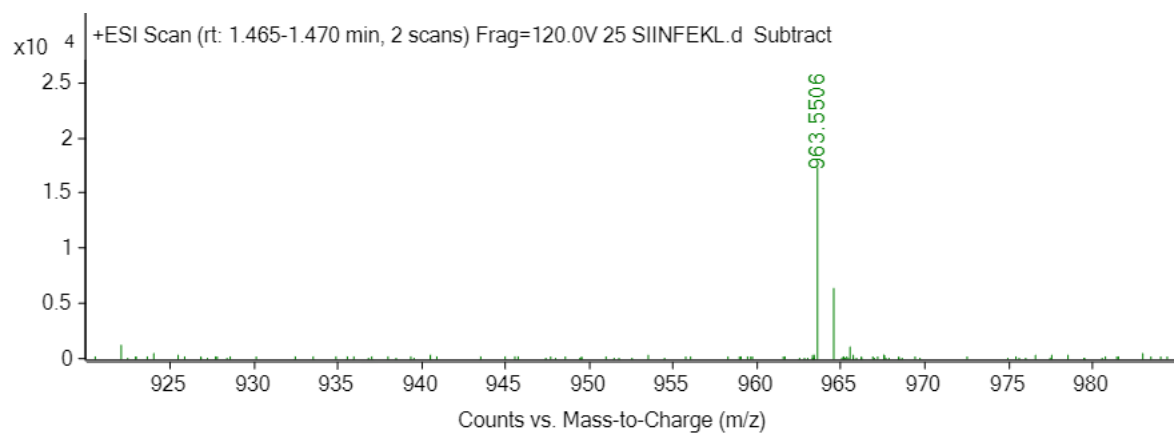
#### Scheme S1. Synthesis of SIINFKEL



A 25 mL vessel of CEM discover bio manual peptide synthesizer was charged with 0.25 mmol of leucine wang resin. The Fmoc group was removed by using a 20% piperidine solution in DMF (10 mL). Using Synergy software, the deprotection protocol was run. The piperidine solution was drained and the resin was washed with DMF (4 x 10 mL). Fmoc-L-lysine(Boc)-OH (5 eq, 1.25 mM) along with Oxyma (5 eq, 1.25 mM) and DIC (5 eq, 1.35 mmol) in DMF was added to the reaction vessel and the coupling protocol was run. The amino acid solution was drained, and the resin was washed with DMF (2 x 10 mL). The fmoc removal and coupling procedure was repeated as before using the same equivalencies for the remaining amino acids. To remove the peptide from resin, a TFA cocktail solution (95% TFA, 2.5% TIPS, and 2.5% DCM) was added to the resin and agitated for 2 hours. The resin was filtered, and the resulting solution was concentrated in vacuo. The peptide was triturated with cold diethyl ether and purified using reverse phase HPLC using H<sub>2</sub>O/CH<sub>3</sub>CN. The sample was analyzed for purity using a Waters 1525 Binary HPLC Pump using a Phenomenex Luna 5u C8(2) 100A (250 x 4.60 mm) column; gradient eluted with H<sub>2</sub>O/CH<sub>3</sub>CN. Molecular weight was confirmed using high resolution electrospray ionization mass spectrometry (HRMS, ESI/MS) analyses obtained on an Agilent 6545B Q-TOF LC/MS equipped with 1260 infinity II LC system with auto sampler. The final peptide product was lyophilized and stored at -20°C until further use.



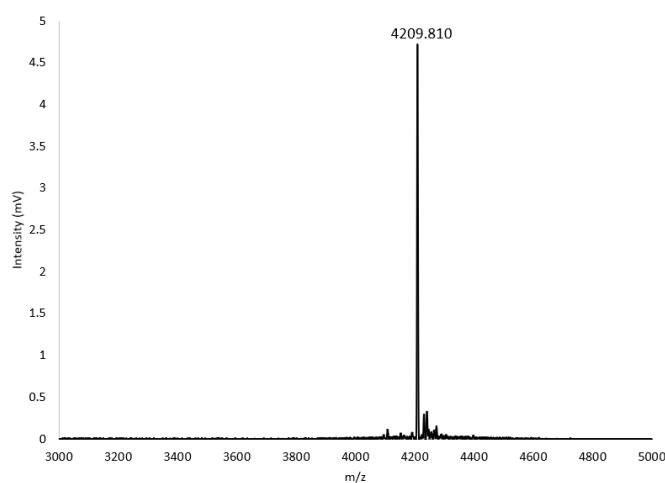
ESI-MS calculated  $[M+H^+]$ : 963.5515, found 963.5506.



## Scheme S2. Synthesis of pHLIP

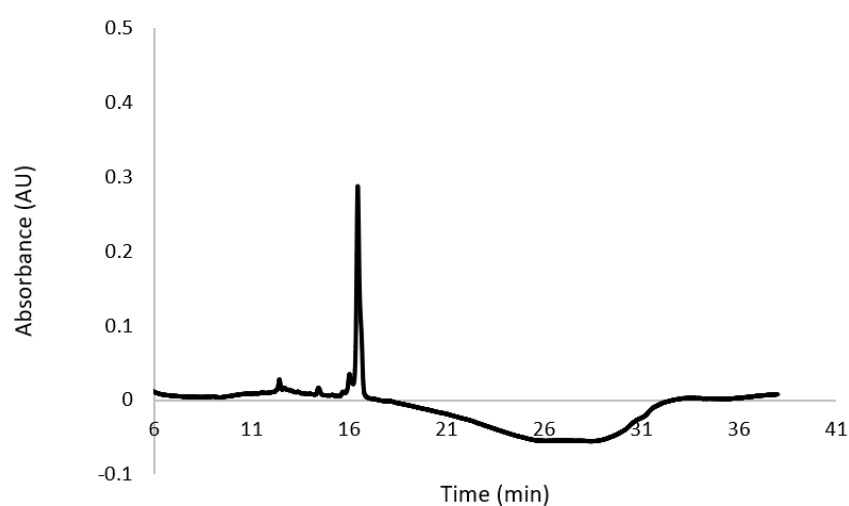
pHLIP (GGEQNPIYWARYADWLF<sup>T</sup>TPL<sup>L</sup>LLLDLALLVDADEGTCG) was prepared by Fmoc solid-phase peptide synthesis using rink amide resin (CEM, 0.19 mmol/g loading capacity) on a CEM Liberty Blue™ microwave peptide synthesizer. Each amino acid solubilized at 0.2 M in DMF was coupled using DIC or HBTU as the activator and oxyma or DIEA as the activator base. After each coupling step, Fmoc protecting groups were removed with 6% piperazine and 0.1 M HOBt in DMF. The peptide was cleaved from resin using a cocktail of trifluoroacetic acid (TFA)/phenol/water/thioanisole/1,2-ethanedithiol (82.5/5/5/5/2.5, v/v) for 2 h at room temperature. The solution was filtered to remove the resin and concentrated prior to precipitation with ice cold diethyl ether. pHLIP was purified by reverse-phase high-performance liquid chromatography (RP-HPLC) on a Phenomenex Luna Omega, 5µm, 250 mm × 21.2 mm C18 column; flow rate of 5 mL/min; phase A being water with 0.1% TFA; phase B being acetonitrile with 0.1% TFA; 60 min gradient from 95:5 to 0:100 A:B). Peptide identity was confirmed by matrix-assisted laser desorption ionization time-of-flight (MALDI-TOF) mass spectrometry (Shimadzu 8020).

MALDI-TOF calculated [M+H<sup>+</sup>]:4210.72, found 4209.81.

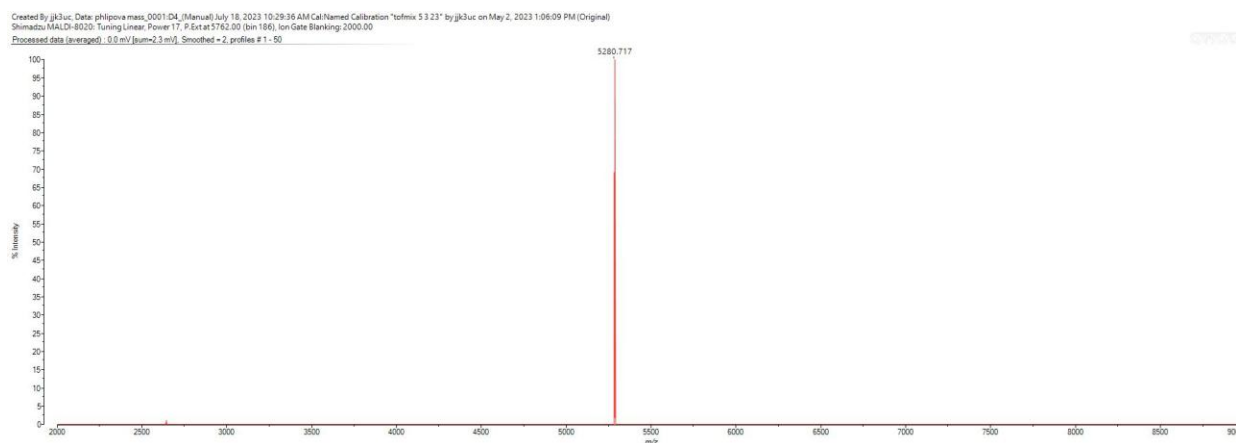


### Scheme S3. Synthesis of pHLIP-CysOVA

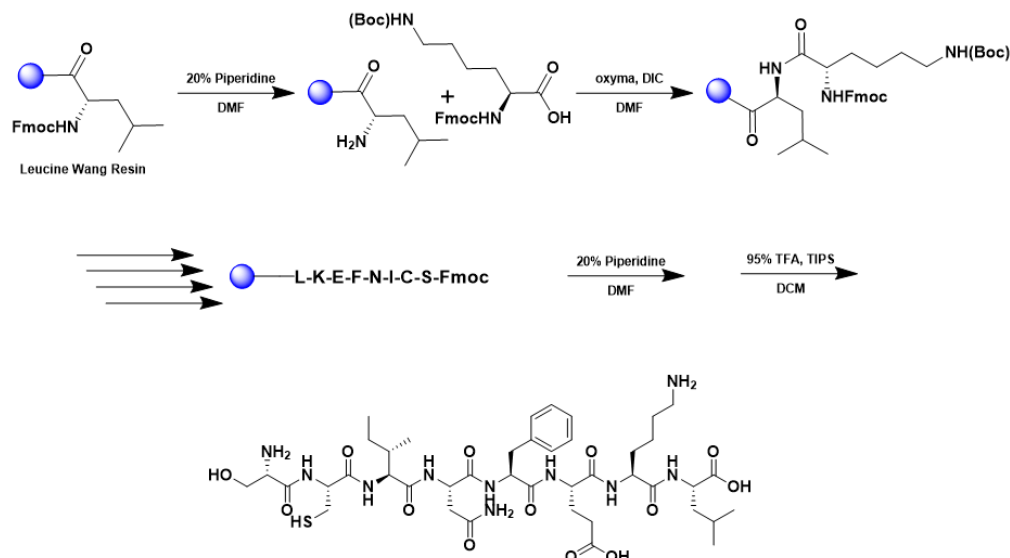
The pHLIP peptide was dissolved to 1 mM in DMSO followed by the addition of 1.5 mM CysOVA in DMSO. The samples were thoroughly mixed before adding 1 M tris buffer pH 8.0 for 4 h. The resulting pHLIP-CysOVA was purified using a Waters 1525 Binary HPLC Pump using a Phenomenex Luna 5u C8(2) 100A (250 x 4.60 mm) column; gradient eluted with H<sub>2</sub>O/CH<sub>3</sub>CN. Molecular weight was confirmed via a Shimadzu MALDI-TOF Mass Spectrometer (MALDI-8020).



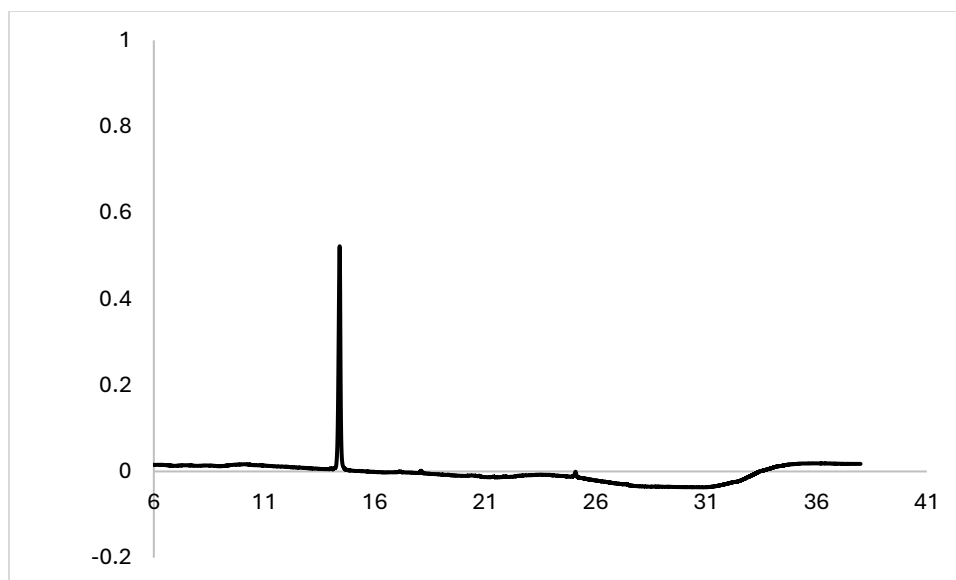
MALDI-TOF calculated  $[M+H]^+$ : 5277, found 5280.



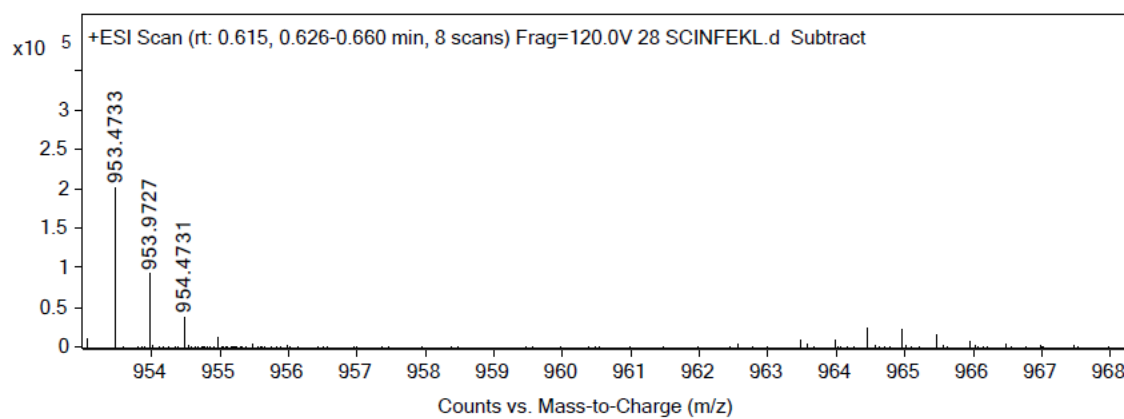
## Scheme S4. Synthesis SCINFEKL



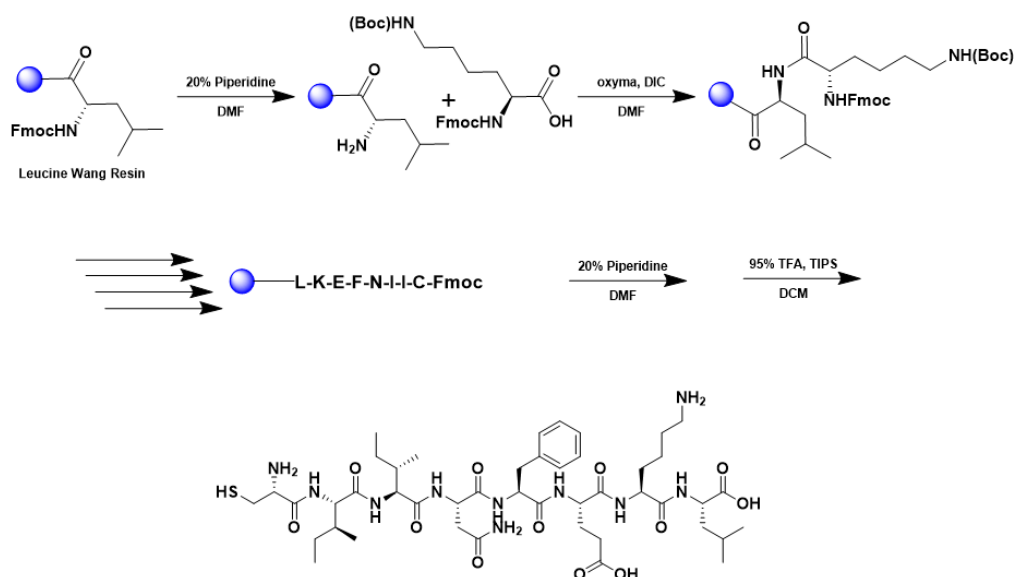
A 25 mL vessel of CEM discover bio manual peptide synthesizer was charged with 0.25 mmol of leucine wang resin. The Fmoc group was removed by using a 20% piperidine solution in DMF (10 mL). Using Synergy software, the deprotection protocol was run. The piperidine solution was drained and the resin was washed with DMF (4 x 10 mL). Fmoc-L-lysine(Boc)-OH (5 eq, 1.25 mM) along with Oxyma (5 eq, 1.25 mM) and DIC (5 eq, 1.35 mmol) in DMF was added to the reaction vessel and the coupling protocol was run. The amino acid solution was drained, and the resin was washed with DMF (2 x 10 mL). The fmoc removal and coupling procedure was repeated as before using the same equivalencies for the remaining amino acids. To remove the peptide from resin, a TFA cocktail solution (95% TFA, 2.5% TIPS, and 2.5% DCM) was added to the resin and agitated for 2 hours. The resin was filtered, and the resulting solution was concentrated in vacuo. The peptide was triturated with cold diethyl ether and purified using reverse phase HPLC using H<sub>2</sub>O/CH<sub>3</sub>CN. The sample was analyzed for purity using a Waters 1525 Binary HPLC Pump using a Phenomenex Luna 5u C8(2) 100A (250 x 4.60 mm) column; gradient eluted with H<sub>2</sub>O/CH<sub>3</sub>CN. Molecular weight was confirmed using high resolution electrospray ionization mass spectrometry (HRMS, ESI/MS) analyses obtained on an Agilent 6545B Q-TOF LC/MS equipped with 1260 infinity II LC system with auto sampler. The final peptide product was lyophilized and stored at -20°C until further use.



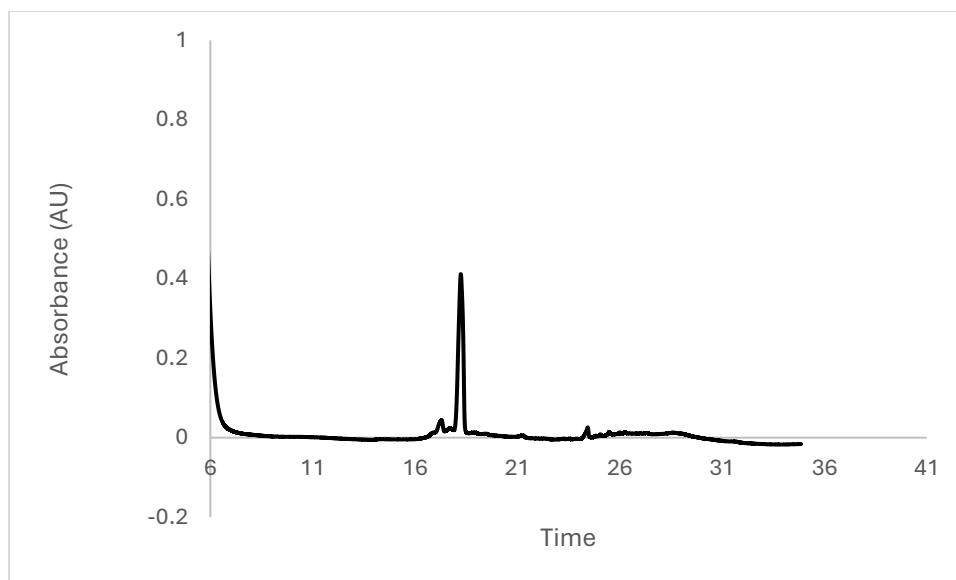
ESI-MS calculated  $[M+H]^+$ : 953.4761, found 953.4733.



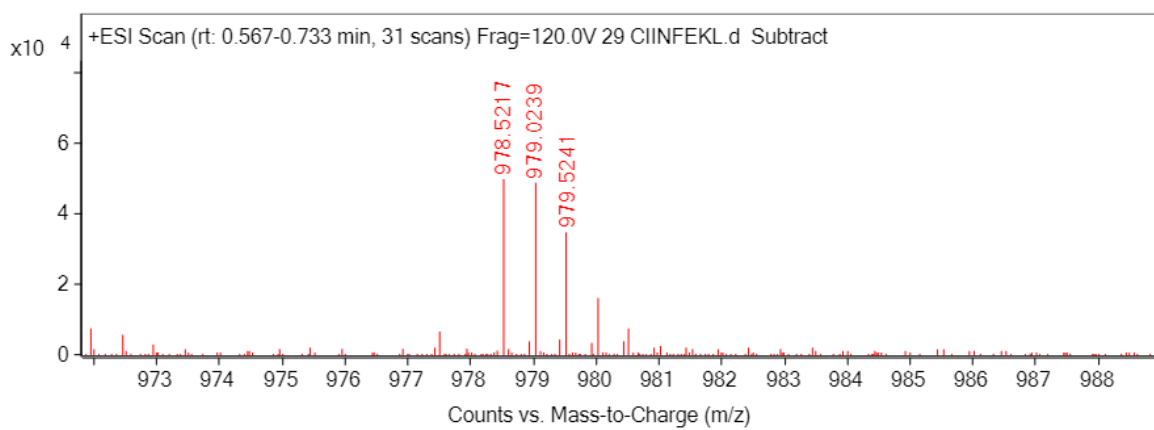
## Scheme S5. Synthesis CIINFKEL



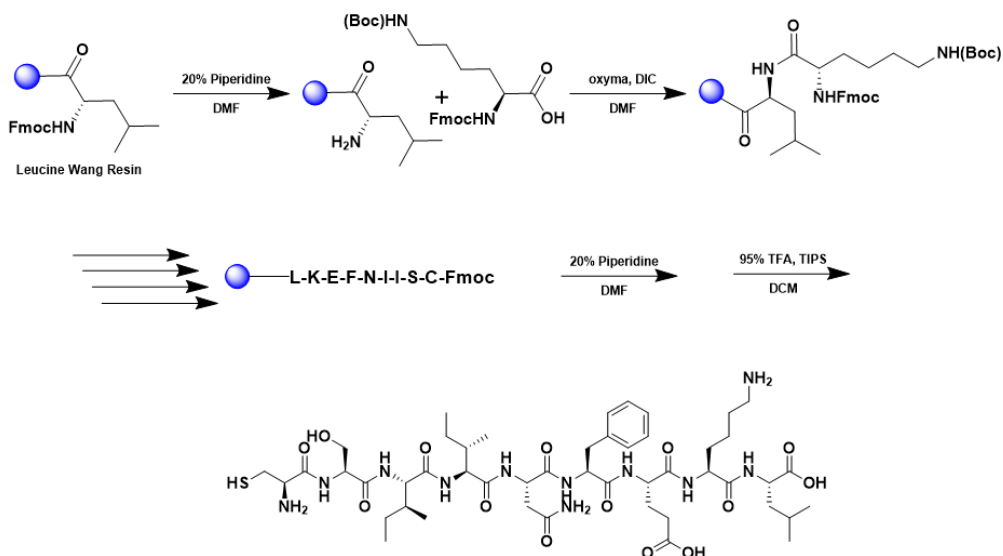
A 25 mL vessel of CEM discover bio manual peptide synthesizer was charged with 0.25 mmol of leucine wang resin. The Fmoc group was removed by using a 20% piperidine solution in DMF (10 mL). Using Synergy software, the deprotection protocol was run. The piperidine solution was drained and the resin was washed with DMF (4 x 10 mL). Fmoc-L-lysine(Boc)-OH (5 eq, 1.25 mM) along with Oxyma (5 eq, 1.25 mM) and DIC (5 eq, 1.35 mmol) in DMF was added to the reaction vessel and the coupling protocol was run. The amino acid solution was drained, and the resin was washed with DMF (2 x 10 mL). The fmoc removal and coupling procedure was repeated as before using the same equivalencies for the remaining amino acids. To remove the peptide from resin, a TFA cocktail solution (95% TFA, 2.5% TIPS, and 2.5% DCM) was added to the resin and agitated for 2 hours. The resin was filtered, and the resulting solution was concentrated in vacuo. The peptide was triturated with cold diethyl ether and purified using reverse phase HPLC using H<sub>2</sub>O/CH<sub>3</sub>CN. The sample was analyzed for purity using a Waters 1525 Binary HPLC Pump using a Phenomenex Luna 5u C8(2) 100A (250 x 4.60 mm) column; gradient eluted with H<sub>2</sub>O/CH<sub>3</sub>CN. Molecular weight was confirmed using high resolution electrospray ionization mass spectrometry (HRMS, ESI/MS) analyses obtained on an Agilent 6545B Q-TOF LC/MS equipped with 1260 infinity II LC system with auto sampler. The final peptide product was lyophilized and stored at -20°C until further use.



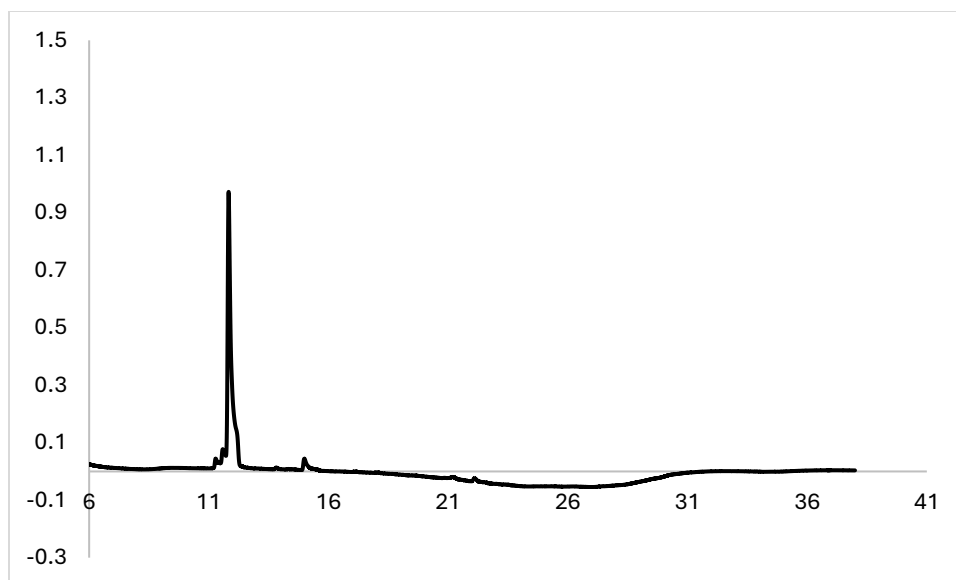
ESI-MS calculated  $[M+H^+]$ : 979.5258, found 979.5241.



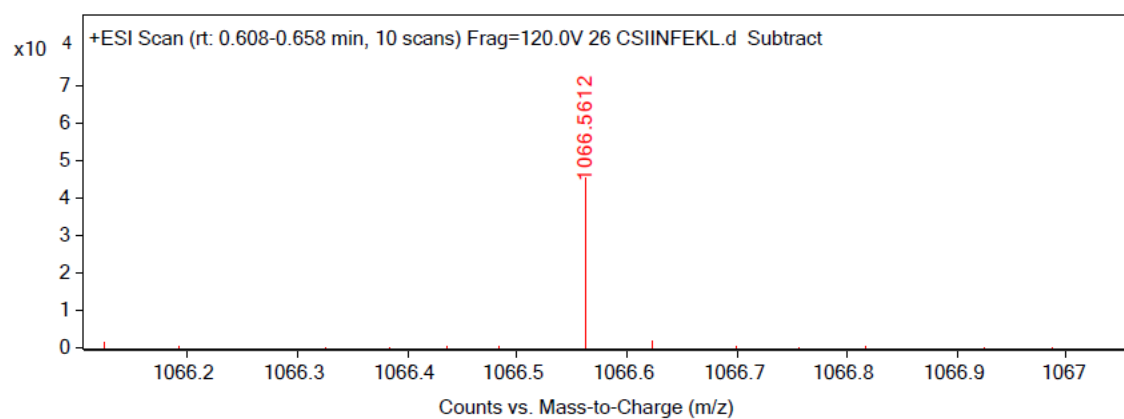
## Scheme S6. Synthesis CSIINFEKL



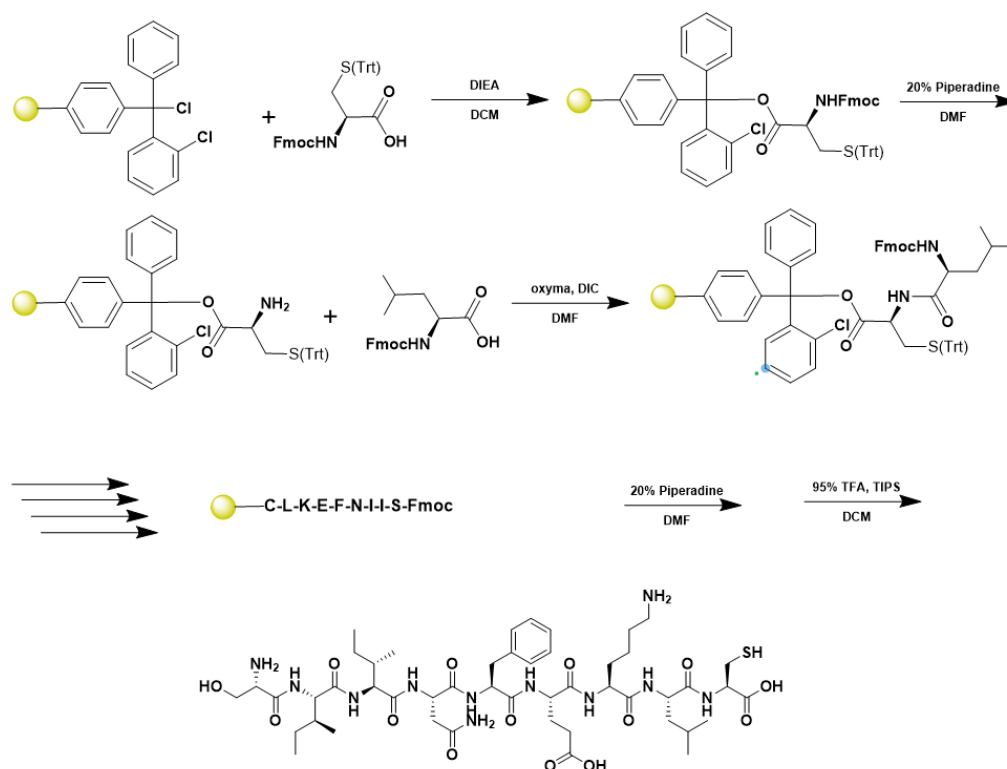
A 25 mL vessel of CEM discover bio manual peptide synthesizer was charged with 0.25 mmol of leucine wang resin. The Fmoc group was removed by using a 20% piperidine solution in DMF (10 mL). Using Synergy software, the deprotection protocol was run. The piperidine solution was drained and the resin was washed with DMF (4 x 10 mL). Fmoc-L-lysine(Boc)-OH (5 eq, 1.25 mM) along with Oxyma (5 eq, 1.25 mM) and DIC (5 eq, 1.35 mmol) in DMF was added to the reaction vessel and the coupling protocol was run. The amino acid solution was drained, and the resin was washed with DMF (2 x 10 mL). The fmoc removal and coupling procedure was repeated as before using the same equivalencies for the remaining amino acids. To remove the peptide from resin, a TFA cocktail solution (95% TFA, 2.5% TIPS, and 2.5% DCM) was added to the resin and agitated for 2 hours. The resin was filtered, and the resulting solution was concentrated in vacuo. The peptide was triturated with cold diethyl ether and purified using reverse phase HPLC using H<sub>2</sub>O/CH<sub>3</sub>CN. The sample was analyzed for purity using a Waters 1525 Binary HPLC Pump using a Phenomenex Luna 5u C8(2) 100A (250 x 4.60 mm) column; gradient eluted with H<sub>2</sub>O/CH<sub>3</sub>CN. Molecular weight was confirmed using high resolution electrospray ionization mass spectrometry (HRMS, ESI/MS) analyses obtained on an Agilent 6545B Q-TOF LC/MS equipped with 1260 infinity II LC system with auto sampler. The final peptide product was lyophilized and stored at -20°C until further use.



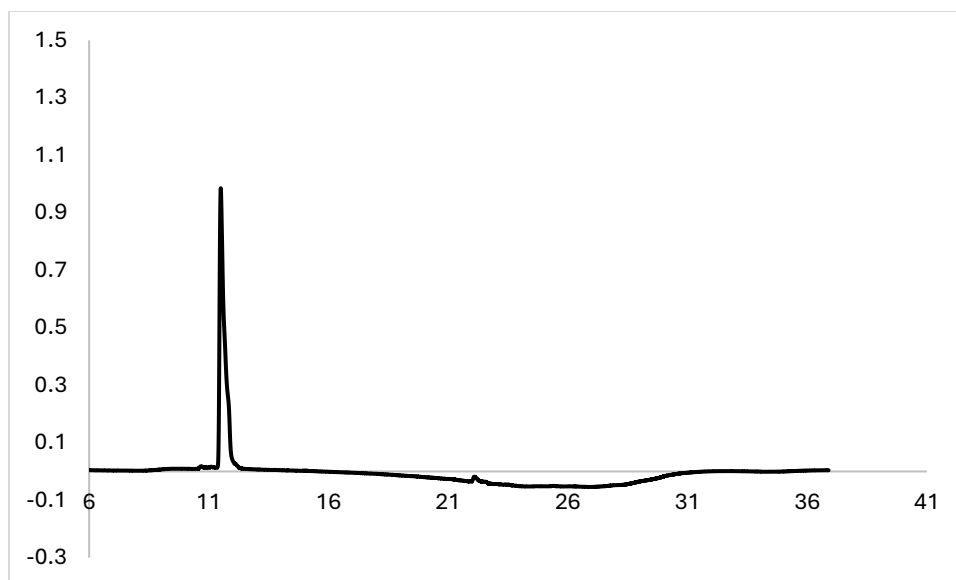
ESI-MS calculated  $[M+H^+]$ : 1066.5602, found 1066.5612.



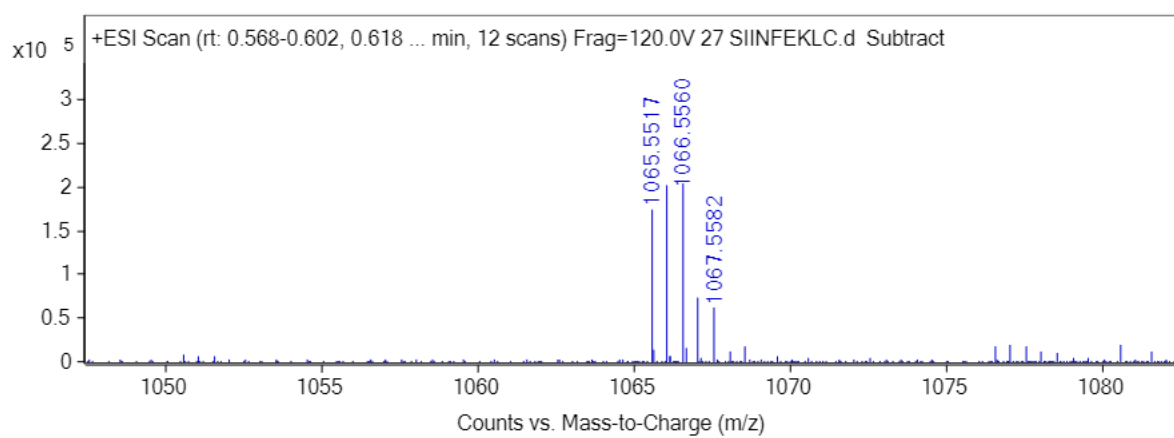
## Scheme S7. Synthesis SIINFKELC



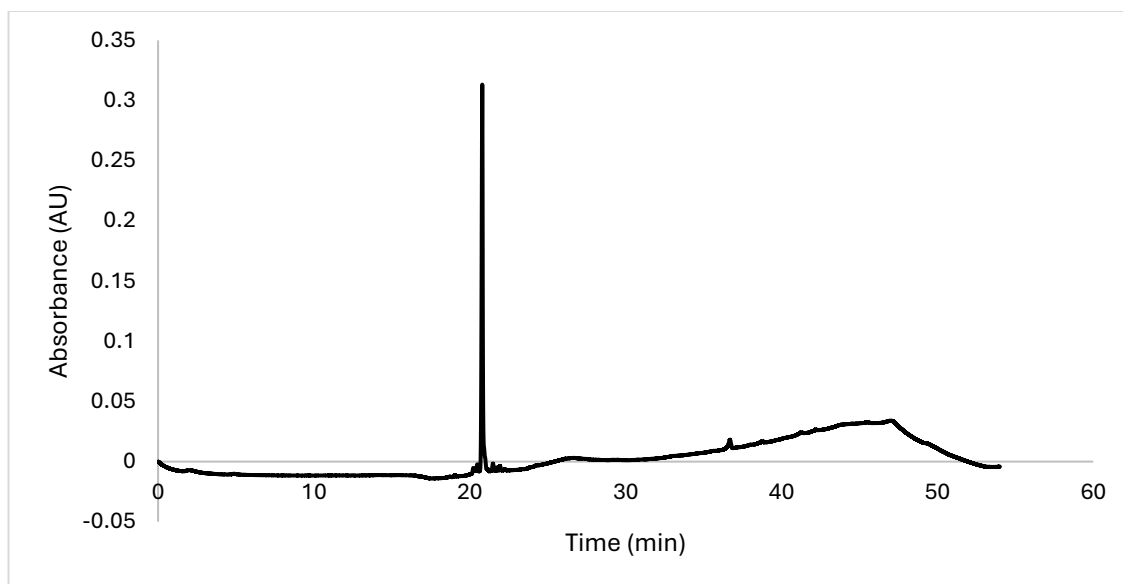
A 25 mL peptide synthesis vessel charged with 2-chlorotrityl chloride resin (0.25mmol) was added Fmoc-L-Cys(Trt)-OH (1.1 eq, 0.275 mmol) and DIEA (3 eq, 0.75 mmol) in dry DCM. The resin was agitated for 1 h at ambient temperature and washed with MeOH and DCM (3 x each). The Fmoc group was removed by using a 20% piperidine solution in DMF for 30 min at ambient temperature, then washed as before. Fmoc-L-leucine-OH (5 eq, 1.25 mM) along with Oxyma (5 eq, 1.25 mM) and DIC (5 eq, 1.35 mmol) in DMF was added to the reaction vessel and agitated for 2 h at ambient temperature. The Fmoc removal and coupling procedure was repeated as before using the same equivalencies for the remaining amino acids. To remove the peptide from resin, a TFA cocktail solution (95% TFA, 2.5% TIPS, and 2.5% DCM) was added to the resin and agitated for 2 hours. The resin was filtered, and the resulting solution was concentrated in vacuo. The peptide was triturated with cold diethyl ether and purified using reverse phase HPLC using H<sub>2</sub>O/CH<sub>3</sub>CN. The sample was analyzed for purity using a Waters 1525 Binary HPLC Pump using a Phenomenex Luna 5u C8(2) 100A (250 x 4.60 mm) column; gradient eluted with H<sub>2</sub>O/CH<sub>3</sub>CN. Molecular weight was confirmed using high resolution electrospray ionization mass spectrometry (HRMS, ESI/MS) analyses obtained on an Agilent 6545B Q-TOF LC/MS equipped with 1260 infinity II LC system with auto sampler. The final peptide product was lyophilized and stored at -20°C until further use.



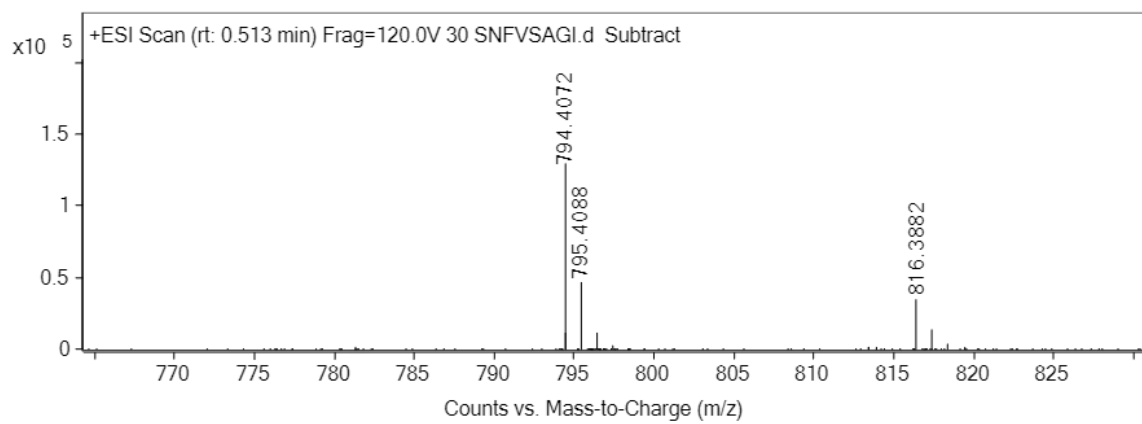
ESI-MS calculated  $[M+H^+]$ : 1066.5602, found 1066.5560.







ESI-MS calculated  $[M+H^+]$ : 794.4043, found 794.4072.



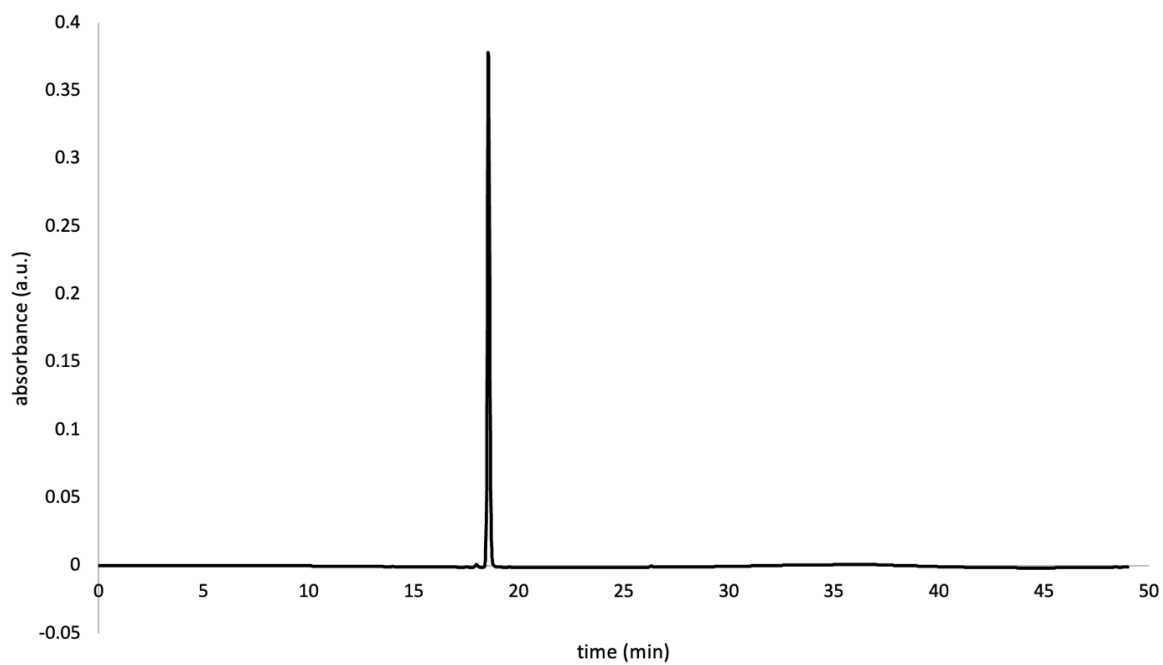
#### A.4 Synthesis and Characterization of Compounds in Chapter 4

Scheme 1. Synthesis of 9-propargyl-2-amino-6-chloropurine



9-propargyl-2-amino-6-chloropurine was synthesized based on literature procedure.<sup>1</sup> 2-amino-6-chloropurine (3.0 g, 1 eq) was suspended in DMF (50 mL) followed by addition of anhydrous K<sub>2</sub>CO<sub>3</sub> (2.934 g, 1.2 eq) and stirring under N<sub>2</sub> atmosphere for 1 hour. After this time, propargyl bromide (1.894 g, 0.9 eq) was added and stirred for 48 hours under N<sub>2</sub> atmosphere at room temperature. DMF was evaporated at 60°C under high vacuum to afford a yellowish-white powder. A 1:2 ratio of minor and major compound was produced as determined by NMR. The crude material was purified by reverse-phase preparative high-performance liquid chromatography (RP-HPLC) equipped with Waters 1525 with a 2489 UV/Visible Detector monitoring at 311 nm wavelength, on a Phenomenex Luna Omega 5 μM Polar C18 250 x 21.2 mm column using gradient elution with using H<sub>2</sub>O/MeOH with 0.1% TFA at 10 mL/min. The HPLC fractions of the major compound were concentrated under reduced pressure using a rotary evaporator, then lyophilized to dryness using a Labconco Freezone 4.5 L (-84°C) lyophilizer and characterized by NMR which matched with the reported compound.<sup>2</sup> This product was analyzed for purity using RP analytical HPLC equipped with Waters 1525 with a 2489 UV/Visible Detector monitoring at 311 nm wavelength, on a Phenomenex Luna 5 μM C18(2) 250 x mm column using gradient elution with using H<sub>2</sub>O/MeOH with 0.1% TFA at 1 mL/min. The major product was used for click chemistry.

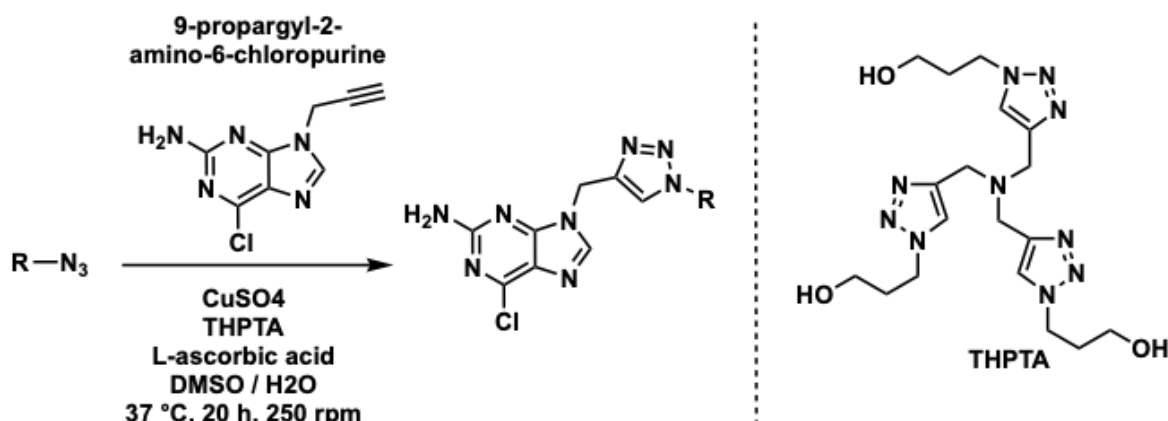
## Analytical HPLC chromatogram of 9-propargyl-2-amino-6-chloropurine



## NMR of 9-propargyl-2-amino-6-chloropurine

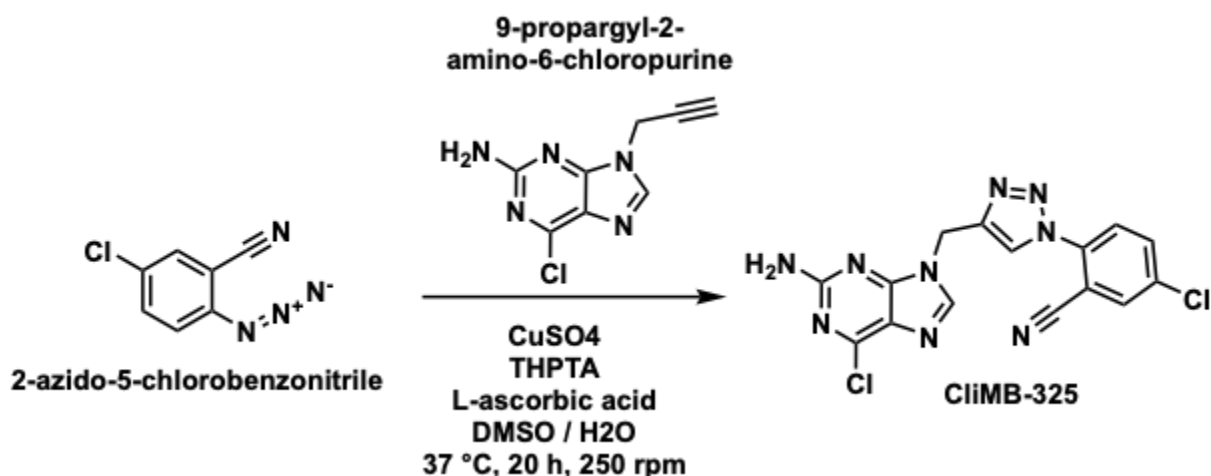
**6-chloro-9-(prop-2-yn-1-yl)-9H-purin-2-amine.** White solid<sup>2</sup>; <sup>1</sup>H NMR (600 MHz, DMSO-*d*<sub>6</sub>)  $\delta$  8.18 (s, 1H, 8-H), 7.02 (brs, 2H, -NH<sub>2</sub>), 4.93 (d, 2H, J=1 Hz, -CH<sub>2</sub>), 3.48 (t, 1H, J = 1 Hz, C $\equiv$ CH).

## Scheme 2. High-Throughput Synthesis of Triazole-Containing BIIB021 Derivatives

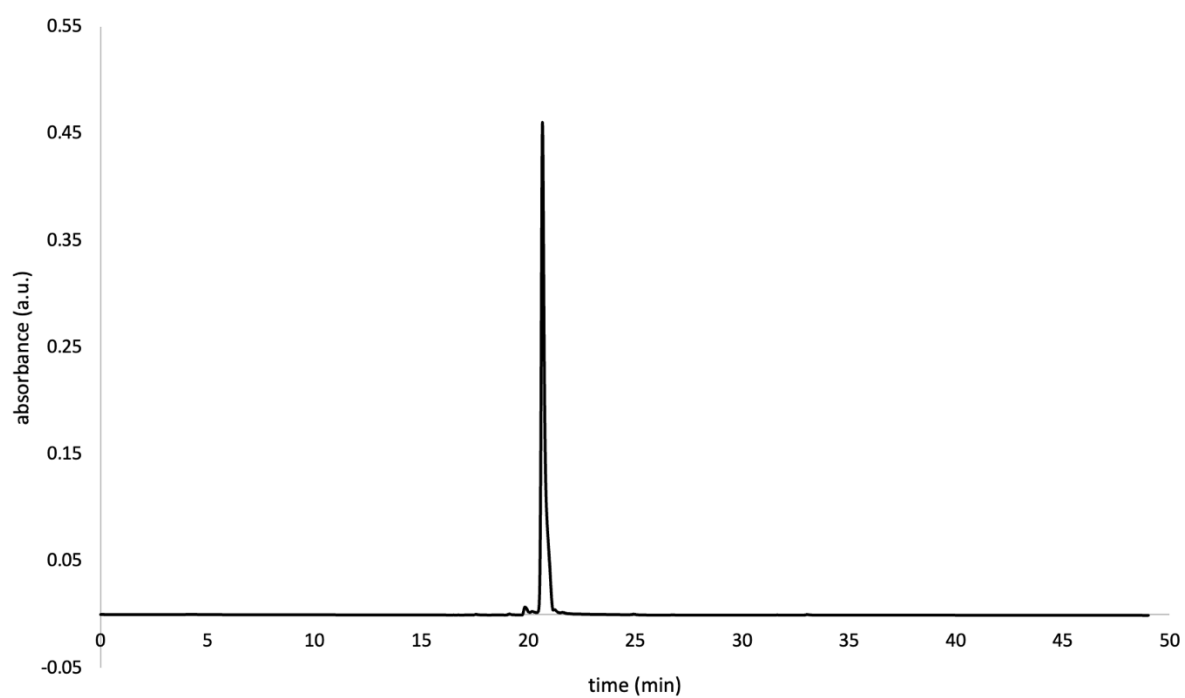


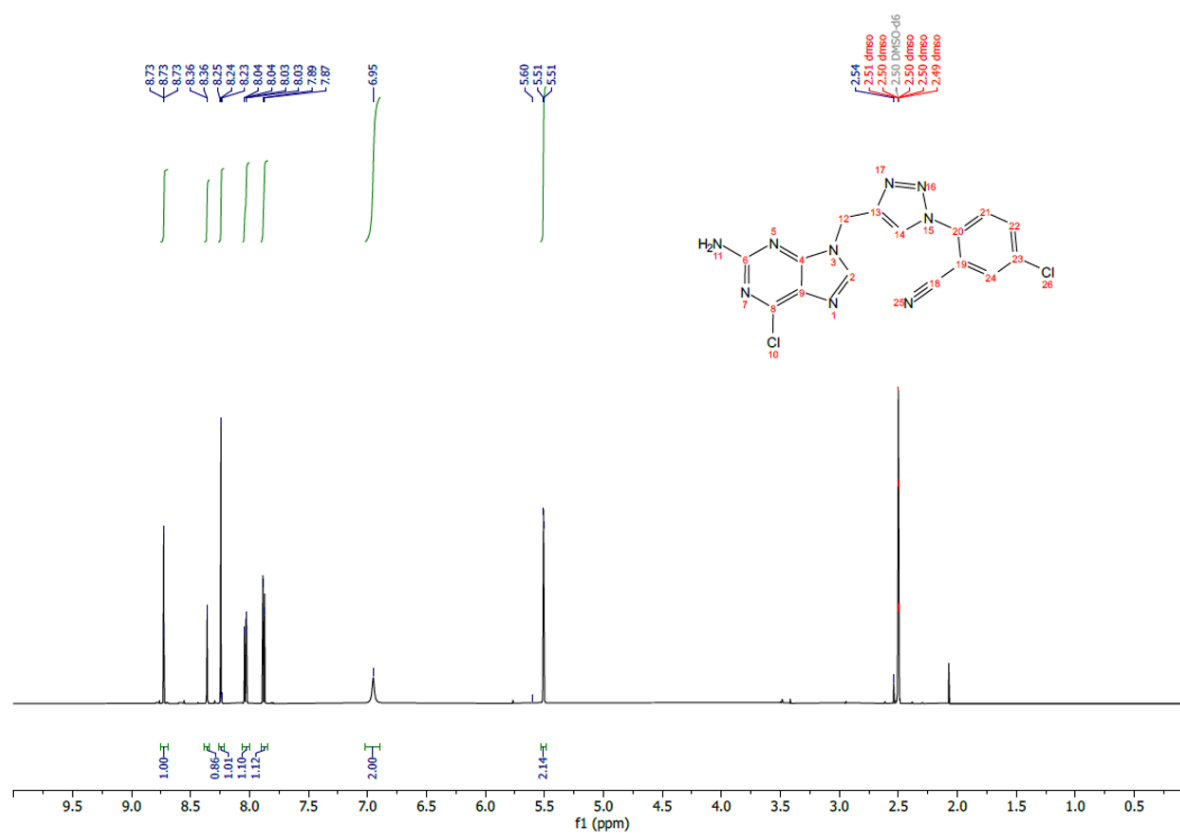
Triazole analogs were synthesized based on literature procedure.<sup>3</sup> Azide solutions from the azide library in Plates 1-5 were initially at a concentration of 100 mM in DMSO. Azides were added in each well of a 96-well plate at a concentration of 10 mM. To each well of this newly loaded plate, L-ascorbic acid solution was added to a concentration of 40 mM along with 10 mM of 9-propargyl-2-amino-6-chloropurine (synthesis shown in *Scheme 1*) and 2 mM of  $CuSO_4$ /THPTA in a solution of DMSO and water at a 3:2 ratio to a total volume of 100  $\mu$ L. The plates were sealed and swirled at 250 rpm and 37°C for 20 hours to afford the corresponding triazole product in each well.

## Scheme 3. Synthesis of CliMB-325.



In a 50 mL conical tube, the following reagents were added: 10 mM of 2-azido-5-chlorobenzonitrile (azide #325 from 380 screen), 40 mM of aqueous L-ascorbic acid, 10 mM of 9-propargyl-2-amino-6-chloropurine (synthesis shown in *Scheme 1*), 2 mM of aqueous CuSO<sub>4</sub>/THPTA solution, in a 3:2 ratio of DMSO to water at a total volume of 15 mL. The tube was swirled at 250 rpm and 37°C for 20 hours to yield **CliMB-325**. The compound was purified by reverse-phase preparative high-performance liquid chromatography (RP-HPLC) equipped with Waters 1525 with a 2489 UV/Visible Detector monitoring at 311 nm wavelength, on a Phenomenex Luna Omega 5 μM Polar C18 250 x 21.2 mm column using gradient elution with using H<sub>2</sub>O/MeCN with 0.1% TFA at 10 mL/min. The HPLC fractions of the desired purified product were concentrated under reduced pressure using a rotary evaporator, then lyophilized to dryness using a Labconco Freezone 4.5 L (-84°C) lyophilizer. The product was analyzed for purity using RP analytical HPLC equipped with Waters 1525 with a 2489 UV/Visible Detector monitoring at 311 nm wavelength, on a Phenomenex Luna 5 μM C18(2) 250 x mm column using gradient elution with using H<sub>2</sub>O/MeCN with 0.1% TFA at 1 mL/min. The final product was stored at -20°C until further use, and stocks were made at 10 mM in DMSO.

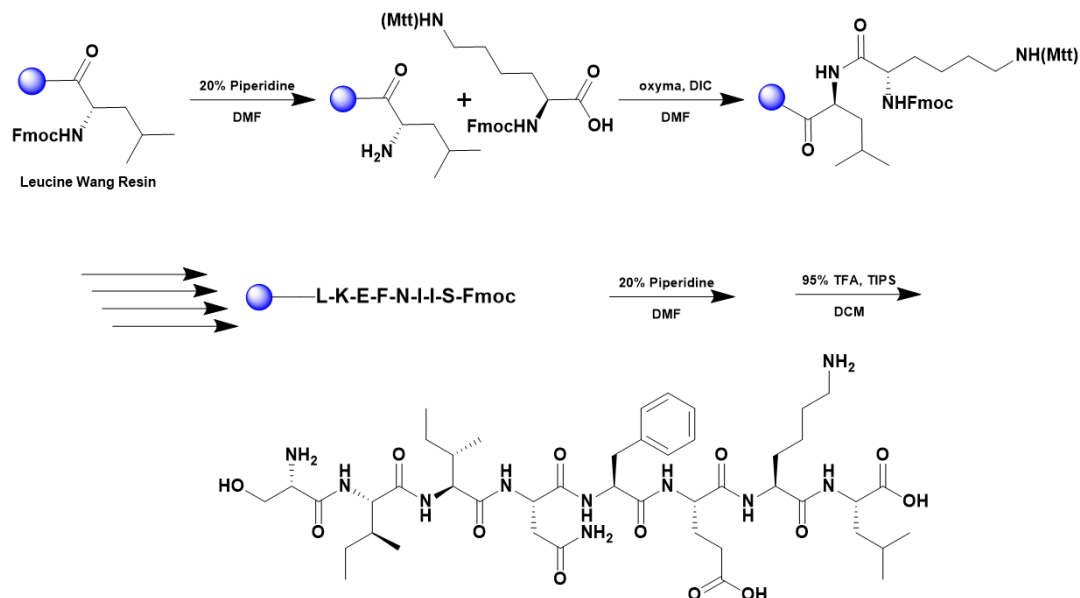
Analytical HPLC Chromatogram of **ClIMB-325**

$^1\text{H}$  NMR of ClIMB-325

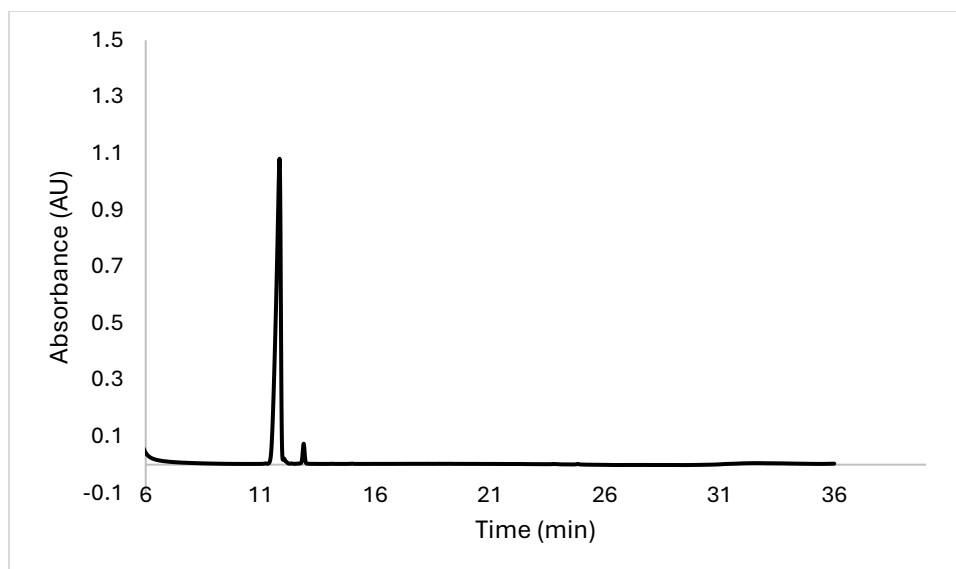


## A.5 Synthesis and Characterization of Compounds in Chapter 5

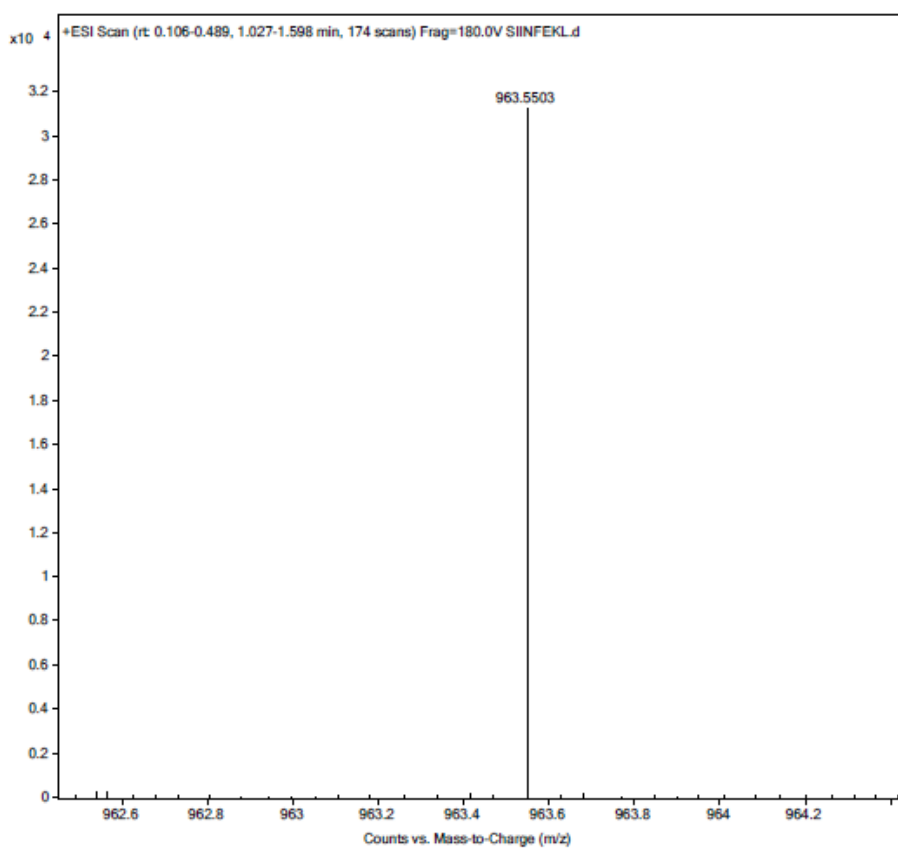
## Scheme S1. Synthesis of SIINFKEL



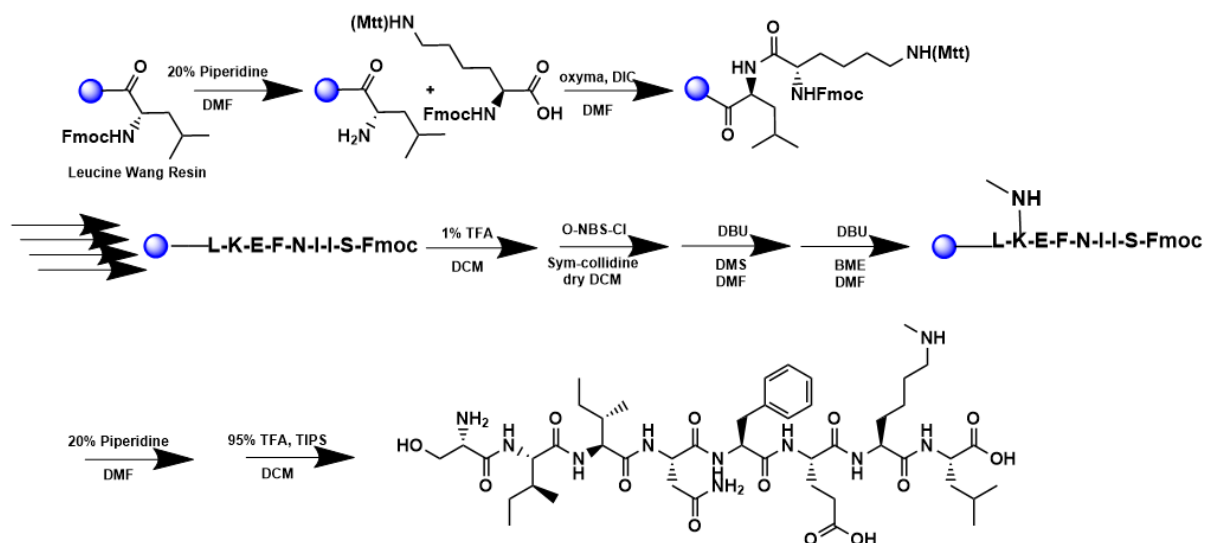
A 25 mL vessel of CEM discover bio manual peptide synthesizer was charged with 0.25 mmol of leucine wang resin. The Fmoc group was removed by using a 20% piperidine solution in DMF (10 mL). Using Synergy software, the deprotection protocol was run. The piperidine solution was drained and the resin was washed with DMF (4 x 10 mL). Fmoc-L-lysine(Mtt)-OH (5 eq, 1.25 mM) along with Oxyma (5 eq, 1.25 mM) and DIC (5 eq, 1.35 mmol) in DMF was added to the reaction vessel and the coupling protocol was run. The amino acid solution was drained, and the resin was washed with DMF (2 x 10 mL). The fmoc removal and coupling procedure was repeated as before using the same equivalencies for the remaining amino acids. To remove the peptide from resin, a TFA cocktail solution (95% TFA, 2.5% TIPS, and 2.5% DCM) was added to the resin and agitated for 2 hours. The resin was filtered, and the resulting solution was concentrated in vacuo. The peptide was triturated with cold diethyl ether and purified using reverse phase HPLC using H<sub>2</sub>O/CH<sub>3</sub>CN. The sample was analyzed for purity using a Waters 1525 Binary HPLC Pump using a Phenomenex Luna 5u C8(2) 100A (250 x 4.60 mm) column; gradient eluted with H<sub>2</sub>O/CH<sub>3</sub>CN. Molecular weight was confirmed using high resolution electrospray ionization mass spectrometry (HRMS, ESI/MS) analyses obtained on an Agilent 6545B Q-TOF LC/MS equipped with 1260 infinity II LC system with auto sampler. The final peptide product was lyophilized and stored at -20°C until further use.



ESI-MS calculated  $[M+H^+]$ : 963.5515, found 963.5503.

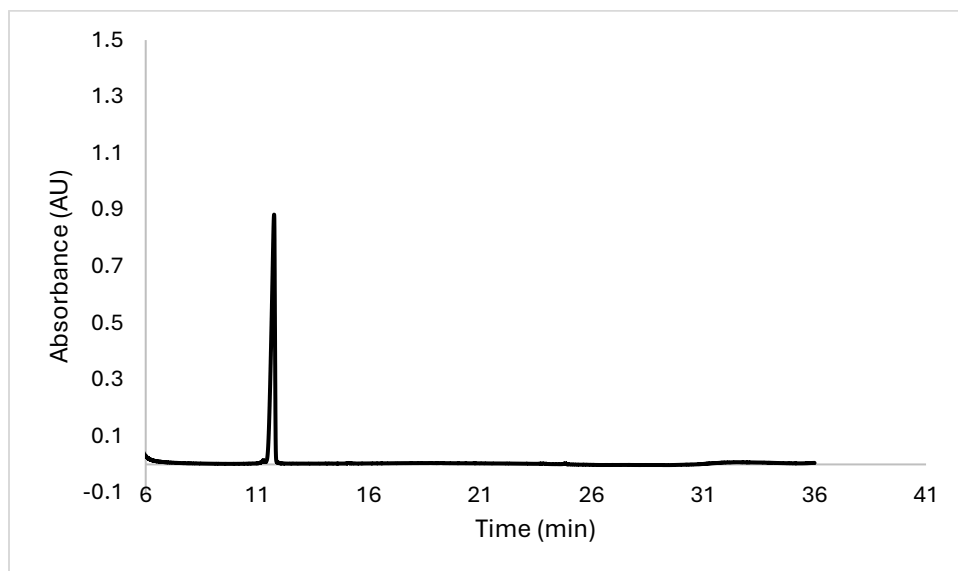


## Scheme S2. Synthesis of Monomethyl Lysine SIINFKEL

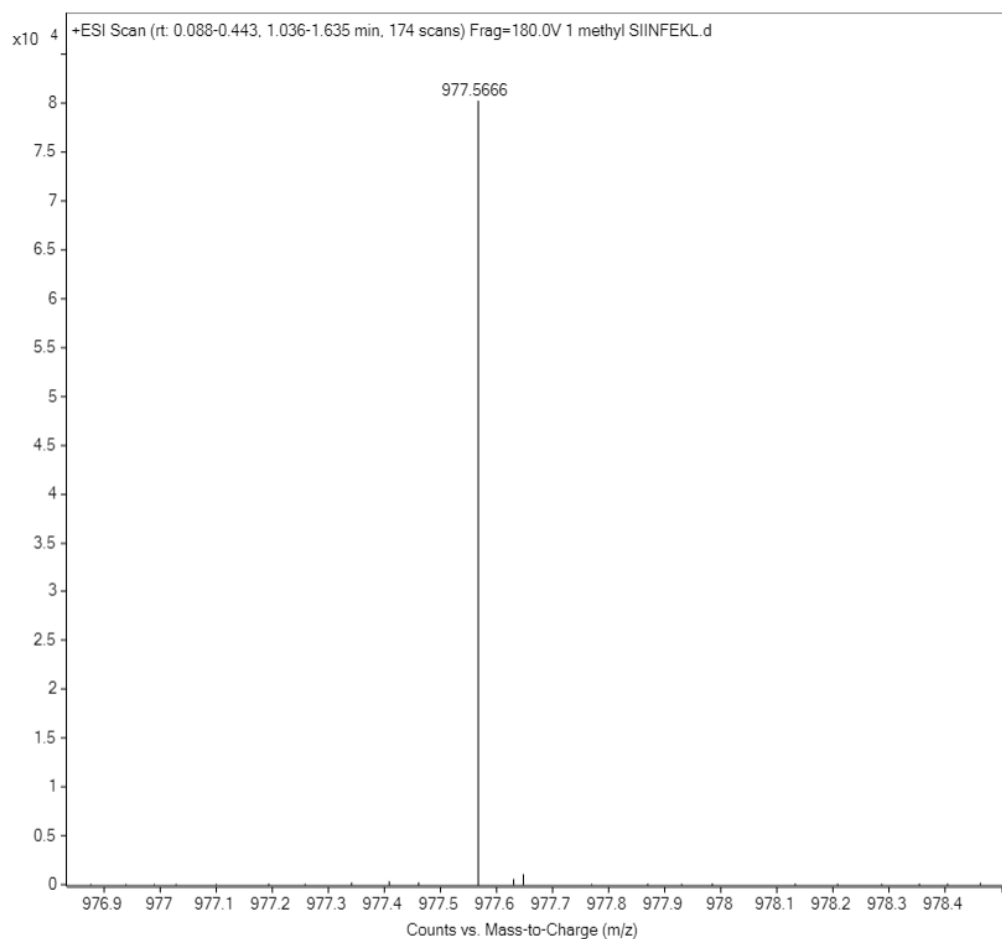


A 25 mL vessel of CEM discover bio manual peptide synthesizer was charged with 0.25 mmol of leucine wang resin. The Fmoc group was removed by using a 20% piperidine solution in DMF (10 mL). Using Synergy software, the deprotection protocol was run. The piperidine solution was drained and the resin was washed with DMF (4 x 10 mL). Fmoc-L-lysine(Mtt)-OH (5 eq, 1.25 mM) along with Oxyma (5 eq, 1.25 mM) and DIC (5 eq, 1.35 mmol) in DMF was added to the reaction vessel and the coupling protocol was run. The amino acid solution was drained, and the resin was washed with DMF (2 x 10 mL). The fmoc removal and coupling procedure was repeated as before using the same equivalencies for the remaining amino acids. The MTT protecting group was removed by the addition of 1% TFA, 2.5% TIPS, in 10 mL DCM for 15 min, washed and repeated 5 more times. O-NBS-Cl (4 eq, 1 mM) was added along with sym-collidine (10 eq, 2.5 mM) in dry DCM and treated with resin for 15 mins while agitated for a total of 2x. The solution was drained and DBU (3 eq, 0.75 mM) and DMS (10 eq, 2.5 mM) in DMF was added and agitated for 5 mins. The solution was drained and BME (10 eq, 2.5 mM) and DBU (5 eq, 1.25 mM) we added in DMF, and the solution was agitated for 30 mins. To remove the peptide from resin, a TFA cocktail solution (95% TFA, 2.5% TIPS, and 2.5% DCM) was added to the resin and agitated for 2 hours. The resin was filtered, and the resulting solution was concentrated in vacuo. The peptide was trituated with cold diethyl ether and purified using reverse phase HPLC using H<sub>2</sub>O/CH<sub>3</sub>CN. The sample was analyzed for purity using a Waters 1525 Binary HPLC Pump using a Phenomenex Luna 5u C8(2) 100A (250 x 4.60 mm) column; gradient eluted with H<sub>2</sub>O/CH<sub>3</sub>CN. Molecular weight was confirmed using high resolution electrospray ionization mass spectrometry (HRMS, ESI/MS) analyses obtained on an Agilent 6545B Q-TOF LC/MS equipped with 1260

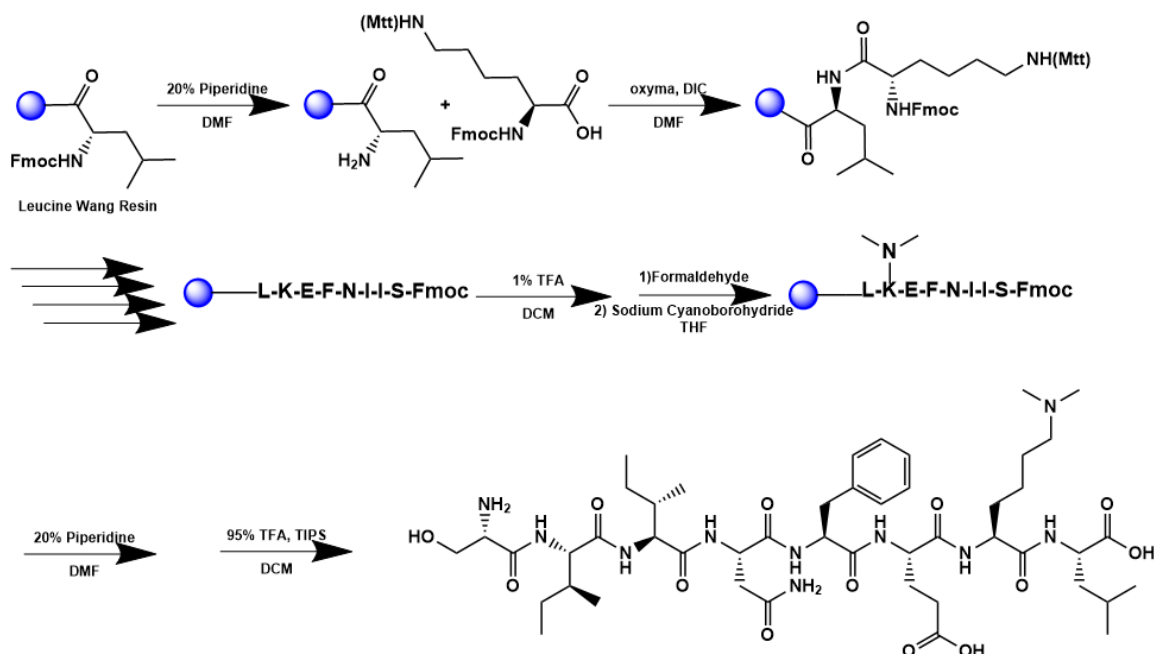
infinity II LC system with auto sampler. The final peptide product was lyophilized and stored at  $-20^{\circ}\text{C}$  until further use.



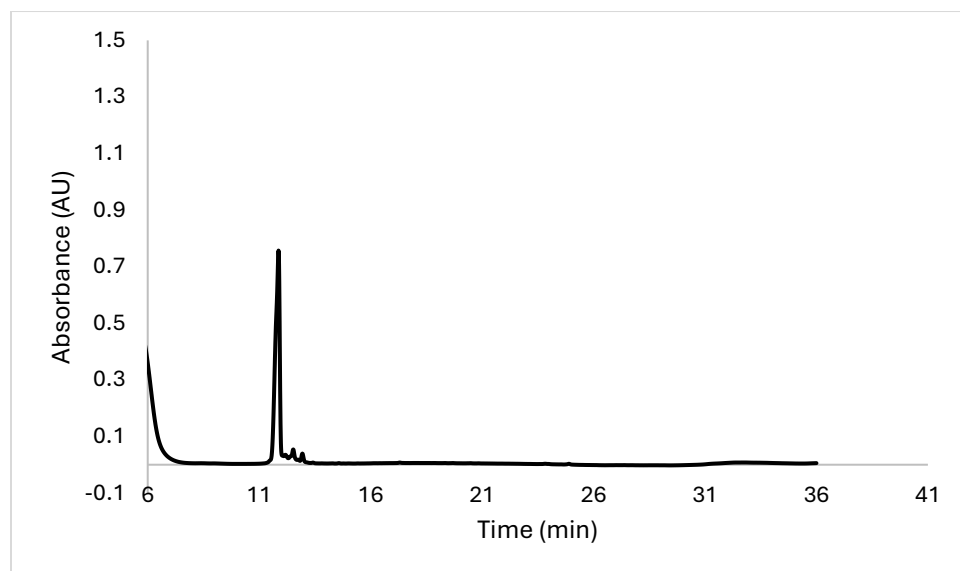
ESI-MS calculated  $[M+H^+]$ : 977.5671, found 977.5666.



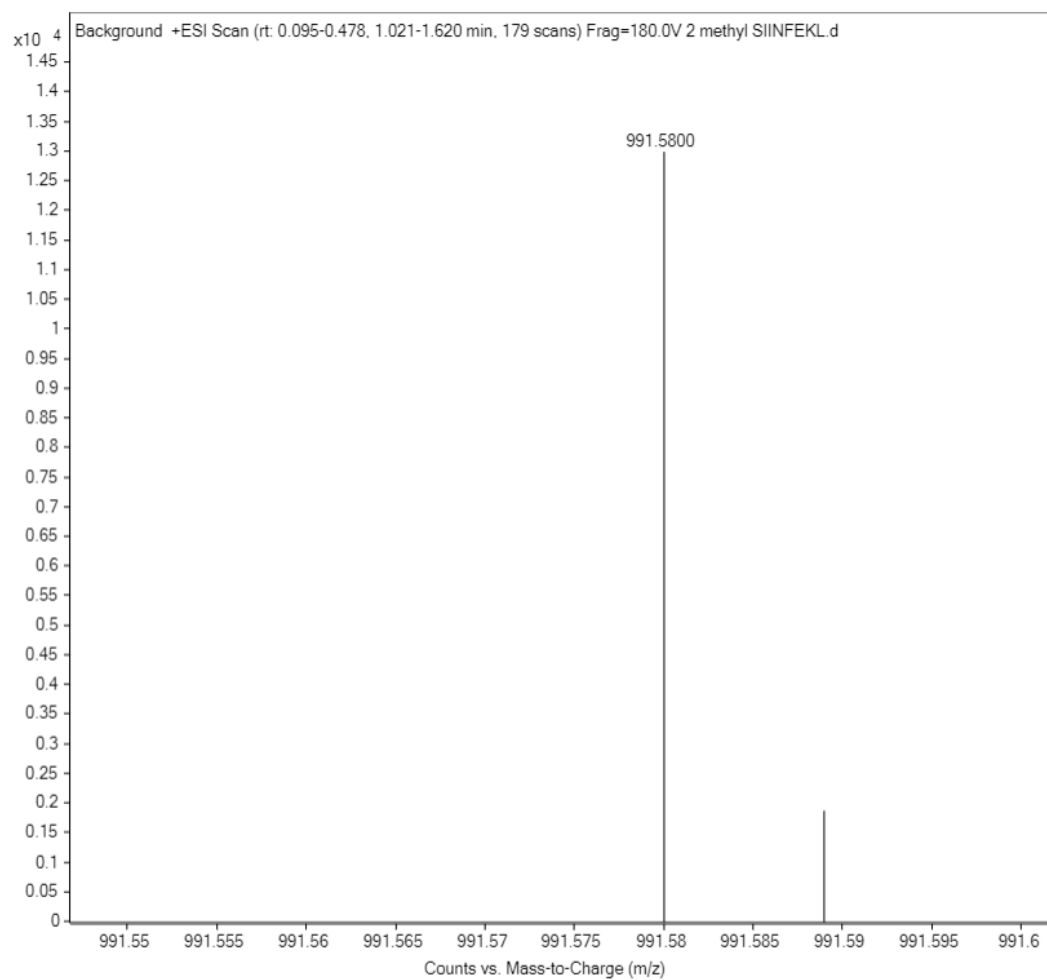
### Scheme S3. Synthesis of Dimethyl Lysine SIINFKEL



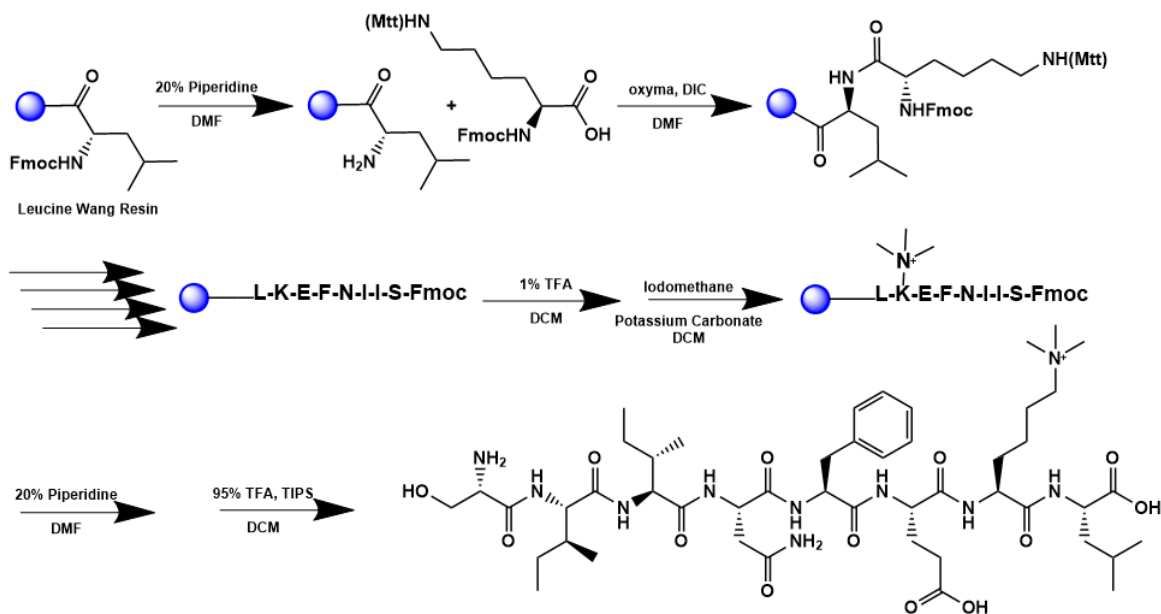
A 25 mL vessel of CEM discover bio manual peptide synthesizer was charged with 0.25 mmol of leucine wang resin. The Fmoc group was removed by using a 20% piperidine solution in DMF (10 mL). Using Synergy software, the deprotection protocol was run. The piperidine solution was drained and the resin was washed with DMF (4 x 10 mL). Fmoc-L-lysine(Mtt)-OH (5 eq, 1.25 mM) along with Oxyma (5 eq, 1.25 mM) and DIC (5 eq, 1.35 mmol) in DMF was added to the reaction vessel and the coupling protocol was run. The amino acid solution was drained, and the resin was washed with DMF (2 x 10 mL). The fmoc removal and coupling procedure was repeated as before using the same equivalencies for the remaining amino acids. The MTT protecting group was removed by the addition of 1% TFA, 2.5% TIPS, in 10 mL DCM for 15 min, washed and repeated 5 more times. Peptide solution was reacted with formaldehyde (10 eq, 12.5 mM) in THF at pH 3 for 15 mins. Sodium cyanoborohydride (20 eq, 25 mM) was added to reaction vessel and reacted for 3 hours and washed 3x with DCM and methanol. To remove the peptide from resin, a TFA cocktail solution (95% TFA, 2.5% TIPS, and 2.5% DCM) was added to the resin and agitated for 2 hours. The resin was filtered, and the resulting solution was concentrated in vacuo. The peptide was triturated with cold diethyl ether and purified using reverse phase HPLC using H<sub>2</sub>O/CH<sub>3</sub>CN. The sample was analyzed for purity using a Waters 1525 Binary HPLC Pump using a Phenomenex Luna 5u C8(2) 100A (250 x 4.60 mm) column; gradient eluted with H<sub>2</sub>O/CH<sub>3</sub>CN. Molecular weight was confirmed using high resolution electrospray ionization mass spectrometry (HRMS, ESI/MS) analyses obtained on an Agilent 6545B Q-TOF LC/MS equipped with 1260 infinity II LC system with auto sampler. The final peptide product was lyophilized and stored at -20°C until further use.



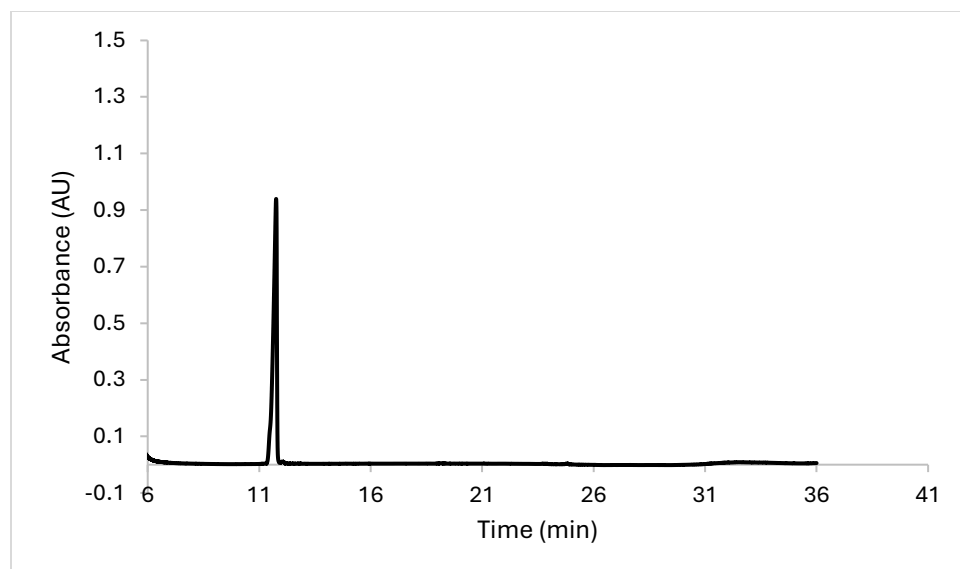
ESI-MS calculated  $[M+H^+]$ : 991.5828, found 991.5800.



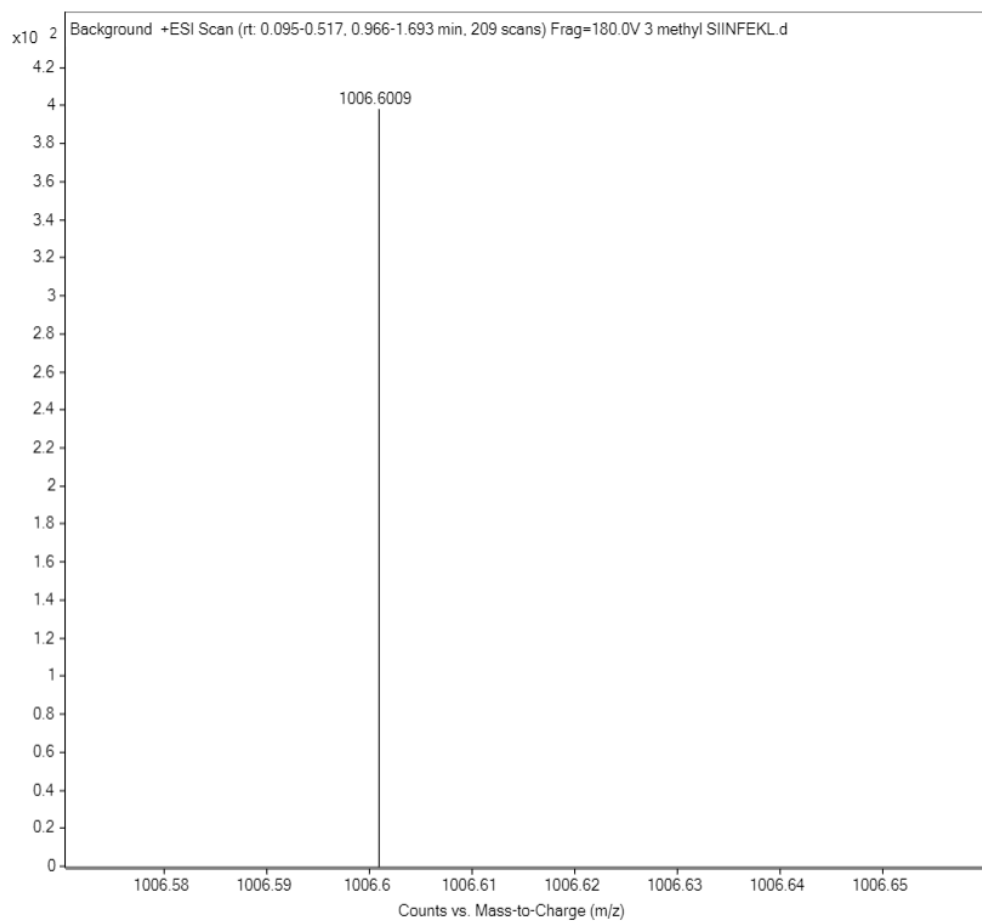
### Scheme S4. Synthesis of Trimethyl Lysine SIINFKEL



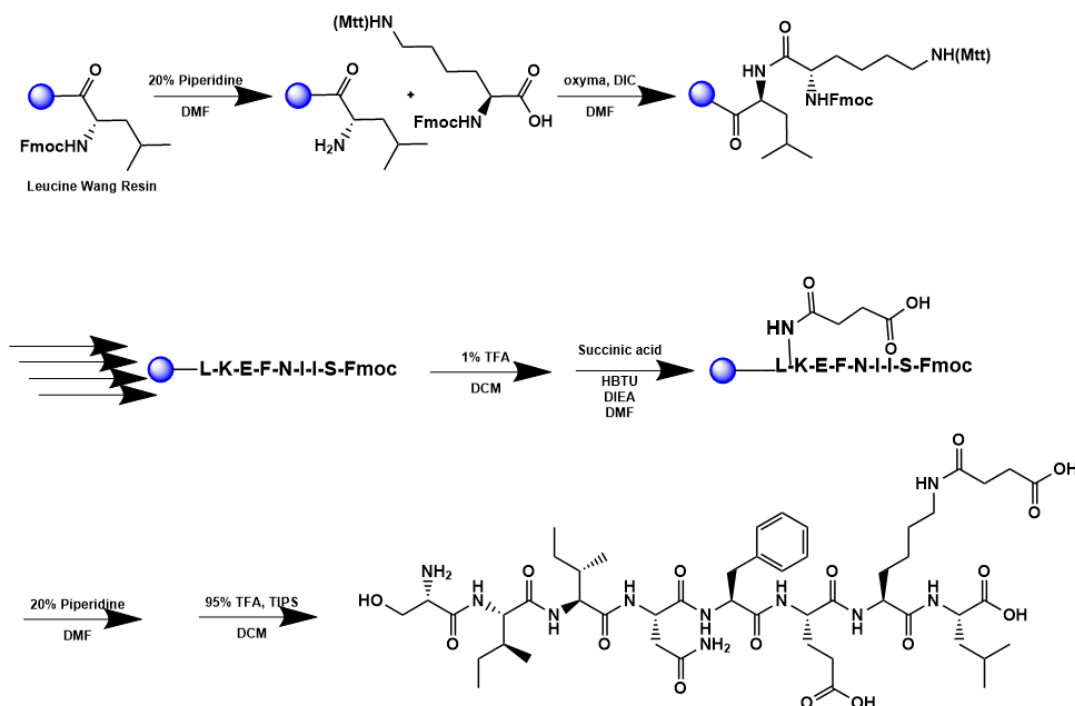
A 25 mL vessel of CEM discover bio manual peptide synthesizer was charged with 0.25 mmol of leucine wang resin. The Fmoc group was removed by using a 20% piperidine solution in DMF (10 mL). Using Synergy software, the deprotection protocol was run. The piperidine solution was drained and the resin was washed with DMF (4 x 10 mL). Fmoc-L-lysine(Mtt)-OH (5 eq, 1.25 mM) along with Oxyma (5 eq, 1.25 mM) and DIC (5 eq, 1.35 mmol) in DMF was added to the reaction vessel and the coupling protocol was run. The amino acid solution was drained, and the resin was washed with DMF (2 x 10 mL). The fmoc removal and coupling procedure was repeated as before using the same equivalencies for the remaining amino acids. The MTT protecting group was removed by the addition of 1% TFA, 2.5% TIPS, in 10 mL DCM for 15 min, washed and repeated 5 more times. Resin was transferred to a round bottom flask and stirred in a solution of iodomethane (50 eq, 12.5 mM) and potassium carbonate (10 eq, 2.5 mM) in DCM and heated to 90°C overnight and repeated three times with fresh reagent. To remove the peptide from resin, a TFA cocktail solution (95% TFA, 2.5% TIPS, and 2.5% DCM) was added to the resin and agitated for 2 hours. The resin was filtered, and the resulting solution was concentrated in vacuo. The peptide was triturated with cold diethyl ether and purified using reverse phase HPLC using H<sub>2</sub>O/CH<sub>3</sub>CN. The sample was analyzed for purity using a Waters 1525 Binary HPLC Pump using a Phenomenex Luna 5u C8(2) 100A (250 x 4.60 mm) column; gradient eluted with H<sub>2</sub>O/CH<sub>3</sub>CN. Molecular weight was confirmed using high resolution electrospray ionization mass spectrometry (HRMS, ESI/MS) analyses obtained on an Agilent 6545B Q-TOF LC/MS equipped with 1260 infinity II LC system with auto sampler. The final peptide product was lyophilized and stored at -20°C until further use.



ESI-MS calculated  $[M+H]^+$ : 1006.6063, found 1006.6009.

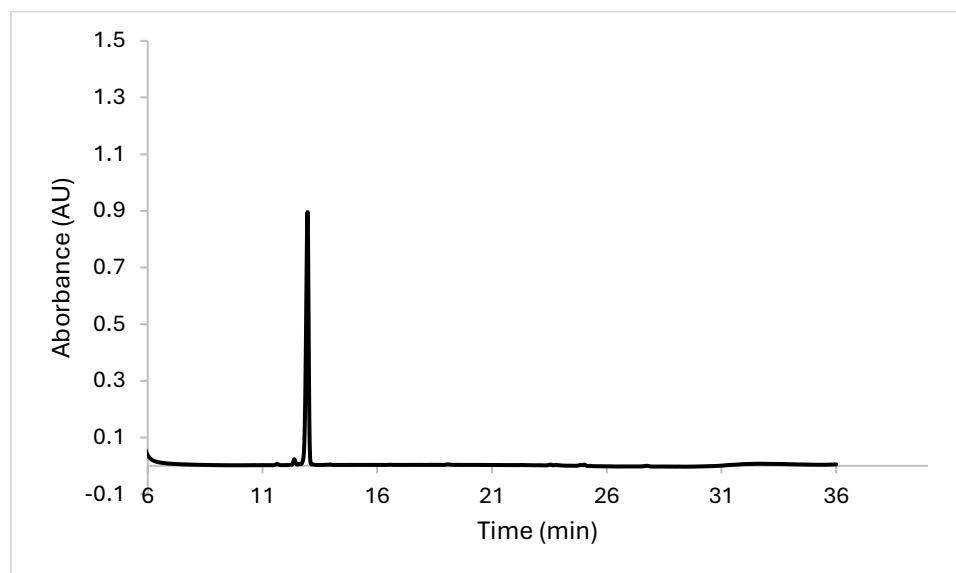


### Scheme S5. Synthesis of Succinyl Lysine SIINFKEL

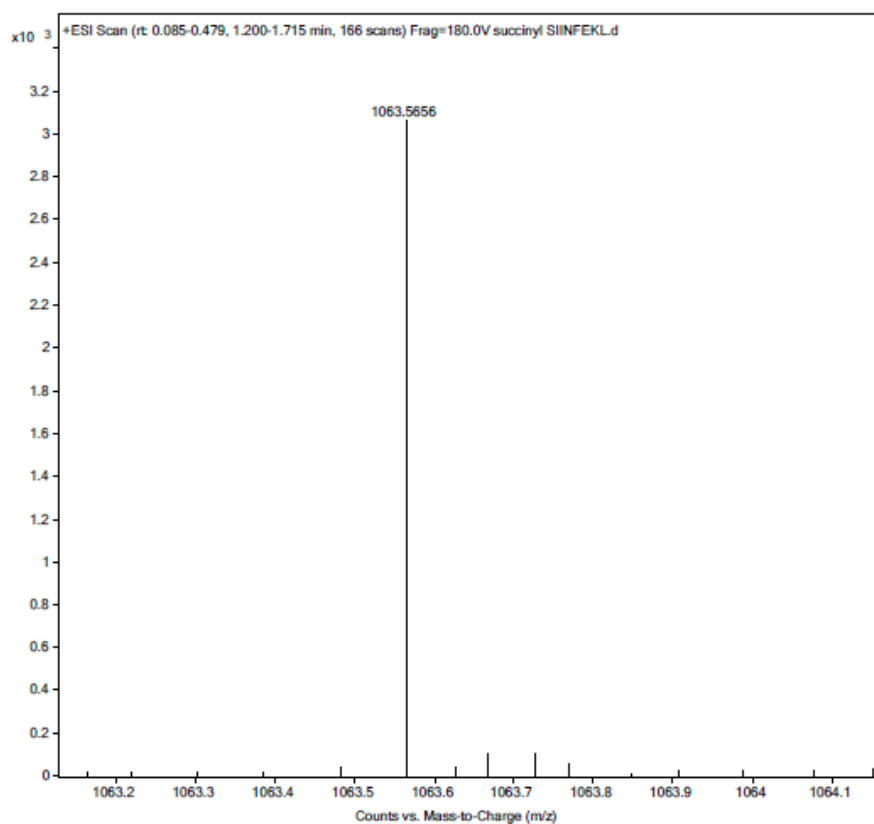


A 25 mL vessel of CEM discover bio manual peptide synthesizer was charged with 0.25 mmol of leucine wang resin. The Fmoc group was removed by using a 20% piperidine solution in DMF (10 mL). Using Synergy software, the deprotection protocol was run. The piperidine solution was drained and the resin was washed with DMF (4 x 10 mL). Fmoc-L-lysine(Mtt)-OH (5 eq, 1.25 mM) along with Oxyma (5 eq, 1.25 mM) and DIC (5 eq, 1.35 mmol) in DMF was added to the reaction vessel and the coupling protocol was run. The amino acid solution was drained, and the resin was washed with DMF (2 x 10 mL). The fmoc removal and coupling procedure was repeated as before using the same equivalencies for the remaining amino acids. The Mtt protecting group of L-Lysine(Mtt)-OH was removed by adding 10 mL of a TFA cocktail solution (1% TFA, 2% TIPS in DCM) to the resin and agitating for 10 minutes protected from light. The solution was drained, and this procedure was repeated five additional times. Succinic acid (8 eq, 2 mM) along with Oxyma (5 eq, 1.25 mM) and DIC (5 eq, 1.25 mmol) in DMF was added to the reaction vessel and agitated at room temperature for 2 hours. To remove the peptide from resin, a TFA cocktail solution (95% TFA, 2.5% TIPS, and 2.5% DCM) was added to the resin and agitated for 2 hours. The resin was filtered, and the resulting solution was concentrated in vacuo. The peptide was triturated with cold diethyl ether and purified using reverse phase HPLC using H<sub>2</sub>O/CH<sub>3</sub>CN. The sample was analyzed for purity using a Waters 1525 Binary HPLC Pump using a Phenomenex Luna 5u C8(2) 100A (250 x 4.60 mm) column; gradient eluted with H<sub>2</sub>O/CH<sub>3</sub>CN. Molecular weight was confirmed using high resolution electrospray ionization mass spectrometry (HRMS, ESI/MS) analyses

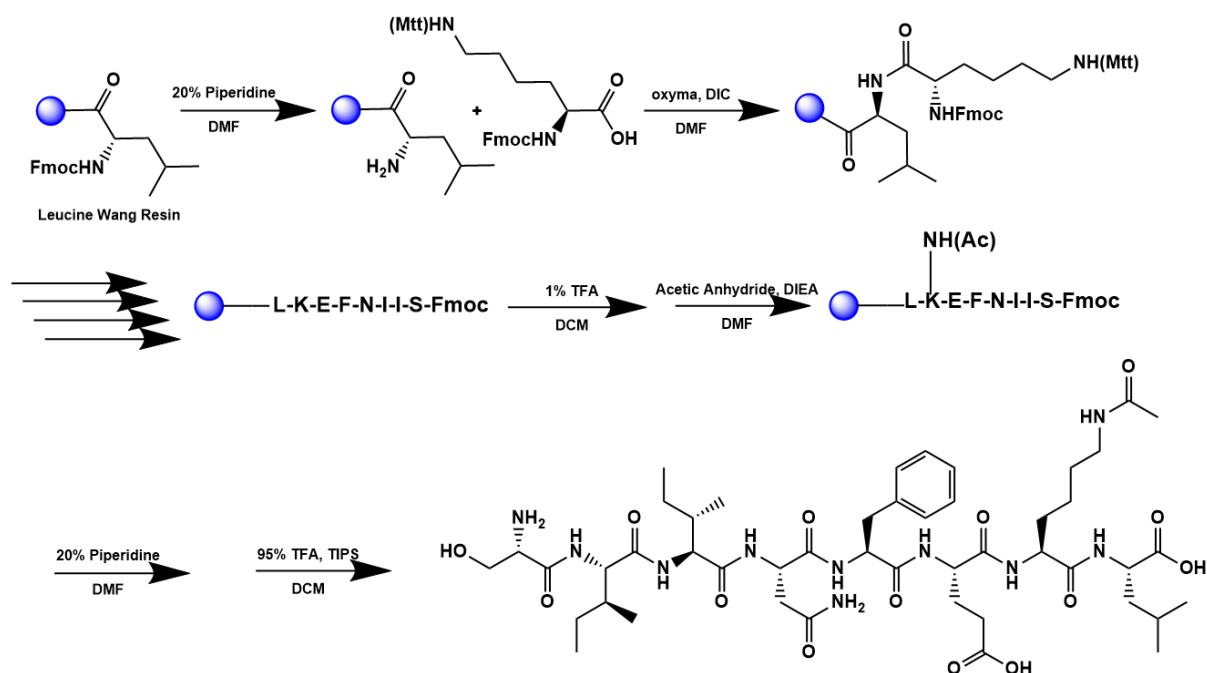
obtained on an Agilent 6545B Q-TOF LC/MS equipped with 1260 infinity II LC system with auto sampler. The final peptide product was lyophilized and stored at  $-20^{\circ}\text{C}$  until further use.



ESI-MS calculated  $[M+H^+]$ : 1063.5675, found 1063.5656.

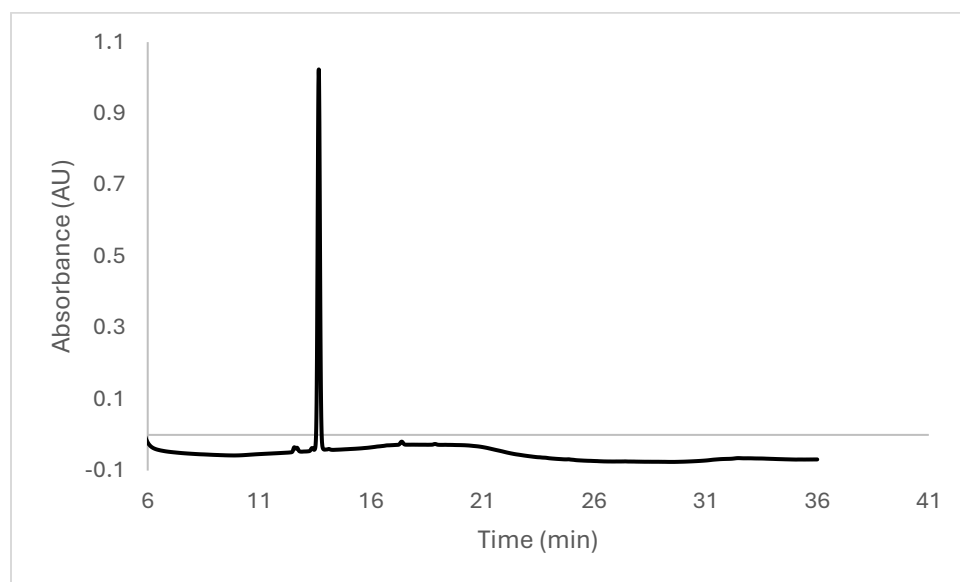


## Scheme S6. Synthesis of Acetyl Lysine SIINFKEL

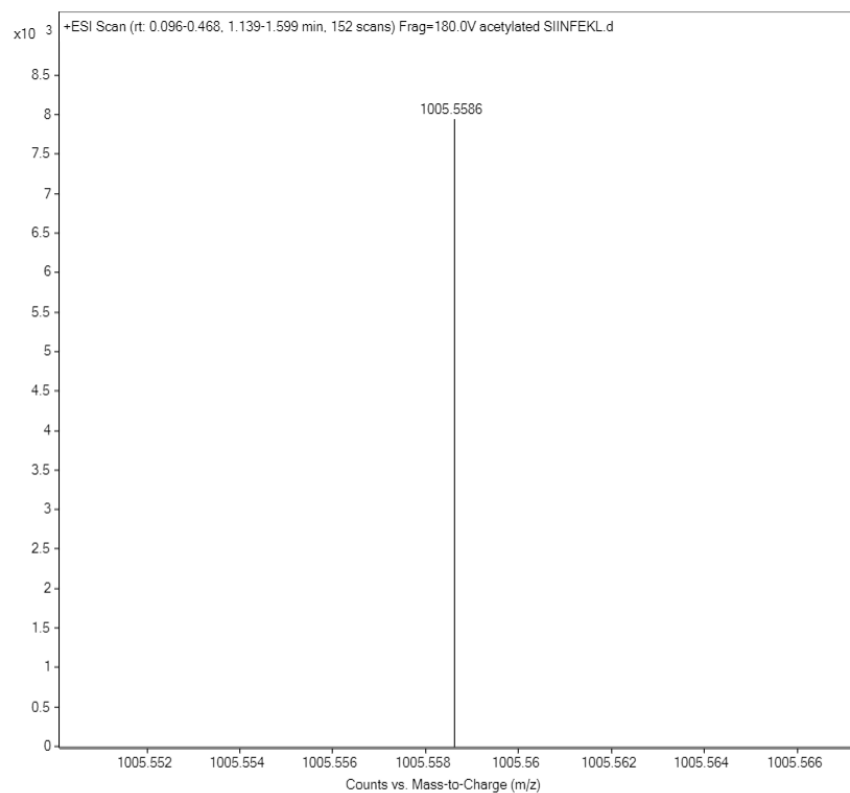


A 25 mL vessel of CEM discover bio manual peptide synthesizer was charged with 0.25 mmol of leucine wang resin. The Fmoc group was removed by using a 20% piperidine solution in DMF (10 mL). Using Synergy software, the deprotection protocol was run. The piperidine solution was drained and the resin was washed with DMF (4 x 10 mL). Fmoc-L-lysine(Mtt)-OH (5 eq, 1.25 mM) along with Oxyma (5 eq, 1.25 mM) and DIC (5 eq, 1.35 mmol) in DMF was added to the reaction vessel and the coupling protocol was run. The amino acid solution was drained, and the resin was washed with DMF (2 x 10 mL). The fmoc removal and coupling procedure was repeated as before using the same equivalencies for the remaining amino acids. The Mtt protecting group of lysine was removed by adding 10 mL of a TFA cocktail solution (1% TFA, 2% TIPS in DCM) to the resin and agitating for 10 minutes. The solution was drained, and this procedure was repeated five additional times. The resin was transferred to a 25 mL synthetic vessel and the lysine side chain of the peptide was acetylated agitating the resin for 1 hour in a solution of 5% acetic anhydride (0.5 mL), 8.5% DIEA (0.85 mL), and 86.5% DMF (8.65 mL). To remove the peptide from resin, a TFA cocktail solution (95% TFA, 2.5% TIPS, and 2.5% DCM) was added to the resin and agitated for 2 hours. The resin was filtered, and the resulting solution was concentrated in vacuo. The peptide was triturated with cold diethyl ether and purified using reverse phase HPLC using H<sub>2</sub>O/CH<sub>3</sub>CN. The sample was analyzed for purity using a Waters 1525 Binary HPLC Pump using a Phenomenex Luna 5u C8(2) 100A (250 x 4.60 mm) column; gradient eluted with H<sub>2</sub>O/CH<sub>3</sub>CN. Molecular weight was confirmed using high resolution electrospray ionization mass spectrometry (HRMS, ESI/MS) analyses obtained on an Agilent 6545B

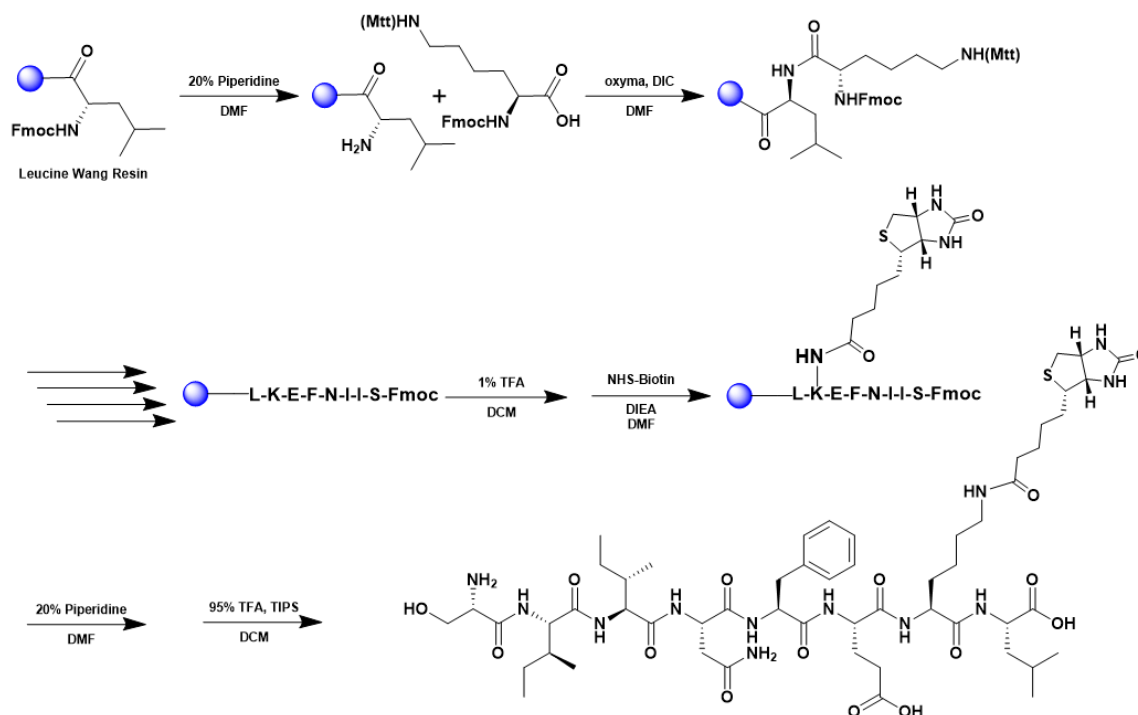
Q-TOF LC/MS equipped with 1260 infinity II LC system with auto sampler. The final peptide product was lyophilized and stored at -20°C until further use.



ESI-MS calculated  $[M+H]^+$ : 1005.5620, found 1005.5586.

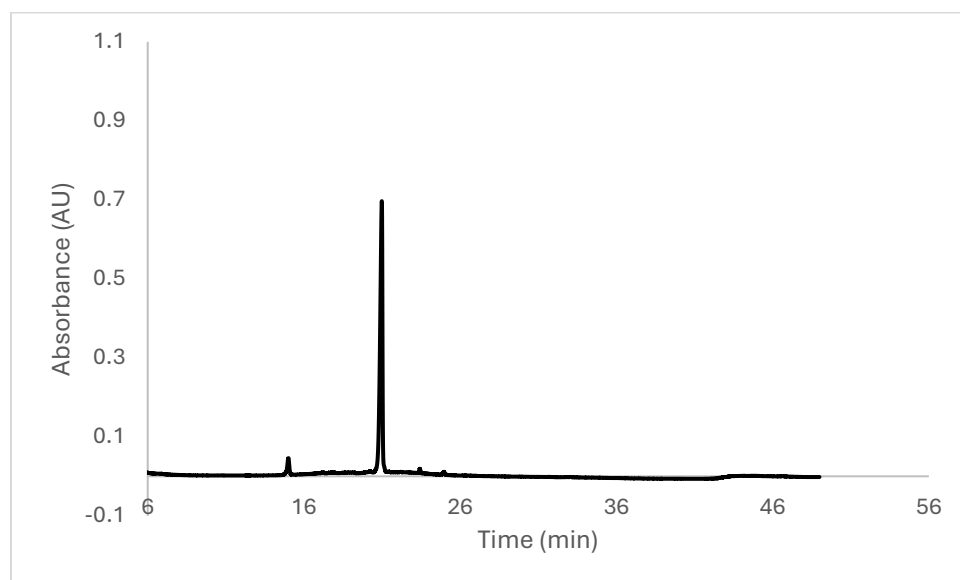


### Scheme S7. Synthesis of Biotinylated Lysine SIINFKEL

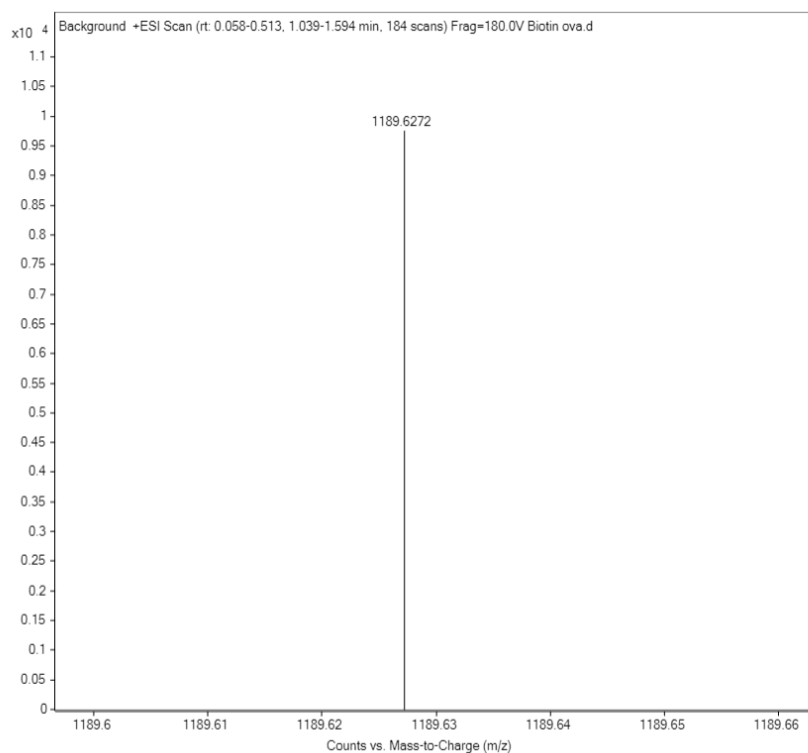


A 25 mL vessel of CEM discover bio manual peptide synthesizer was charged with 0.25 mmol of leucine wang resin. The Fmoc group was removed by using a 20% piperidine solution in DMF (10 mL). Using Synergy software, the deprotection protocol was run. The piperidine solution was drained and the resin was washed with DMF (4 x 10 mL). Fmoc-L-lysine(Mtt)-OH (5 eq, 1.25 mM) along with Oxyma (5 eq, 1.25 mM) and DIC (5 eq, 1.35 mmol) in DMF was added to the reaction vessel and the coupling protocol was run. The amino acid solution was drained, and the resin was washed with DMF (2 x 10 mL). The fmoc removal and coupling procedure was repeated as before using the same equivalencies for the remaining amino acids. The Mtt protecting group of lysine was removed by adding 10 mL of a TFA cocktail solution (1% TFA, 2% TIPS in DCM) to the resin and agitating for 10 minutes. The solution was drained, and this procedure was repeated five additional times. Biotin N-hydroxy succinimide ester (10 eq, 2.5 mM) and DIEA (4 eq, 1 mM) in DMF were reacted with peptide for 2 h while agitated. To remove the peptide from resin, a TFA cocktail solution (95% TFA, 2.5% TIPS, and 2.5% DCM) was added to the resin and agitated for 2 hours. The resin was filtered, and the resulting solution was concentrated in vacuo. The peptide was triturated with cold diethyl ether and purified using reverse phase HPLC using H<sub>2</sub>O/CH<sub>3</sub>CN. The sample was analyzed for purity using a Waters 1525 Binary HPLC Pump using a Phenomenex Luna 5u C8(2) 100A (250 x 4.60 mm) column; gradient eluted with H<sub>2</sub>O/CH<sub>3</sub>CN. Molecular weight was confirmed using high resolution electrospray ionization mass spectrometry (HRMS,

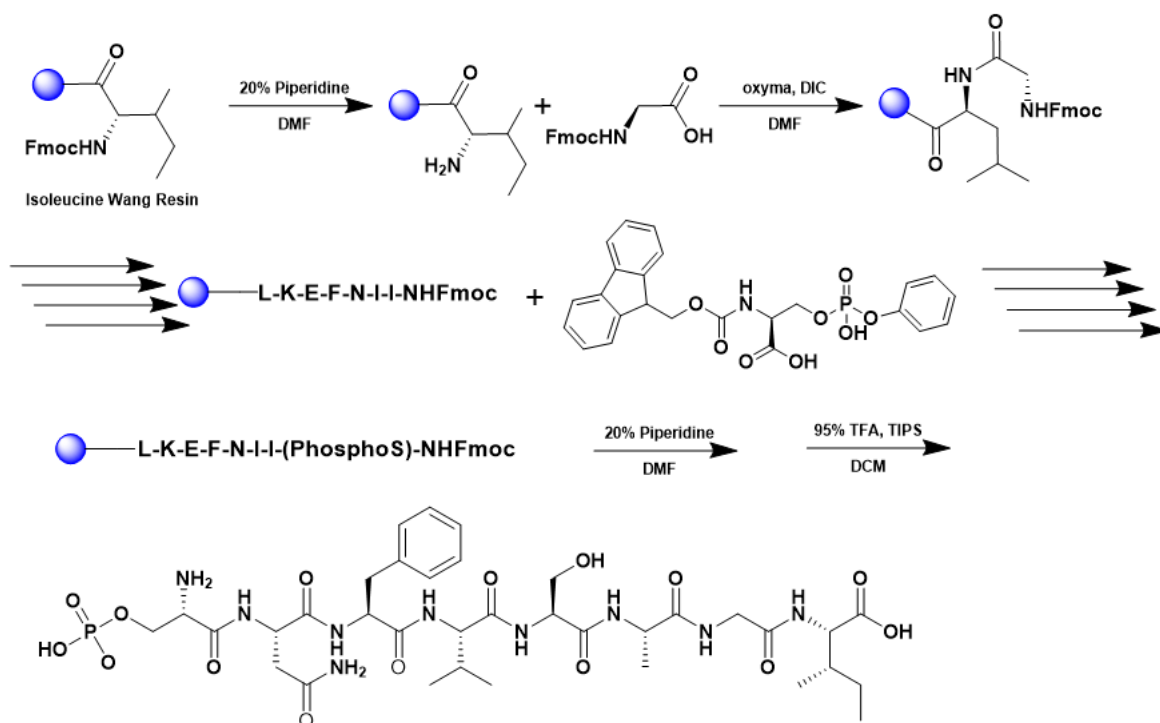
ESI/MS) analyses obtained on an Agilent 6545B Q-TOF LC/MS equipped with 1260 infinity II LC system with auto sampler. The final peptide product was lyophilized and stored at -20°C until further use.



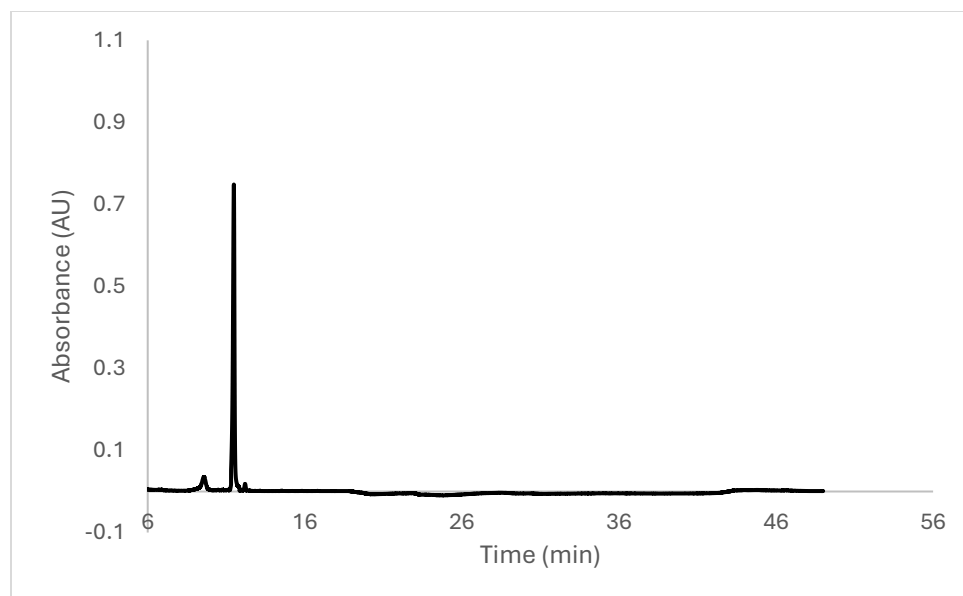
ESI-MS calculated  $[M+H]^+$ : 1189.6291, found 1189.6272.



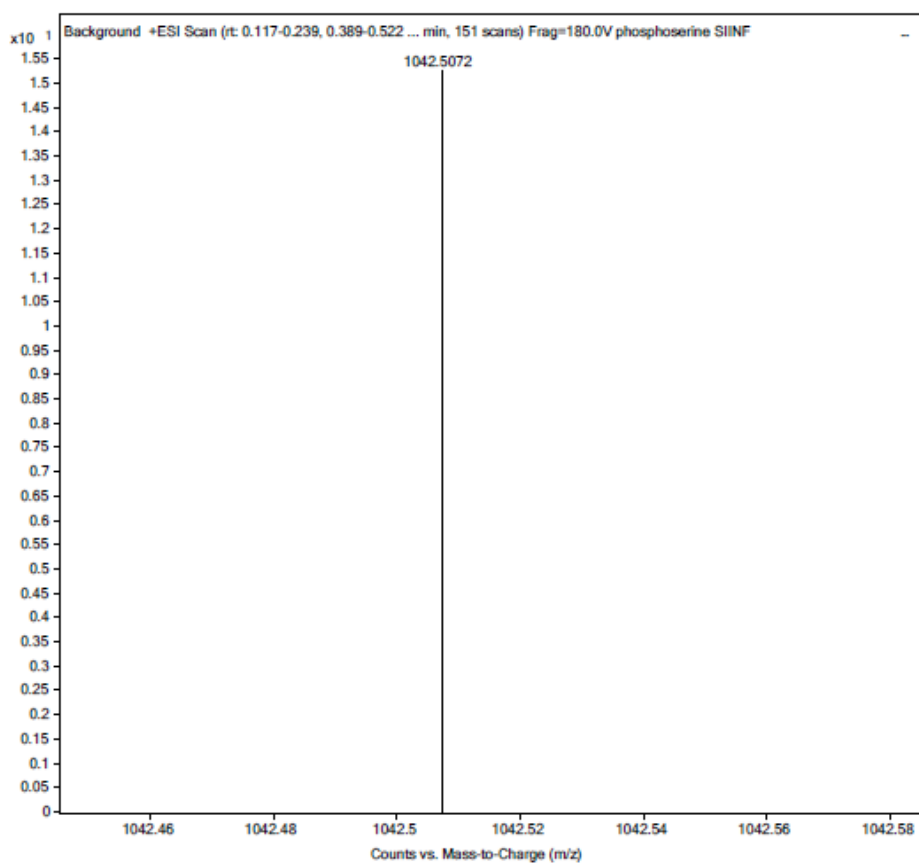
## Scheme S8. Synthesis of Phosphoserine SIINFKEL



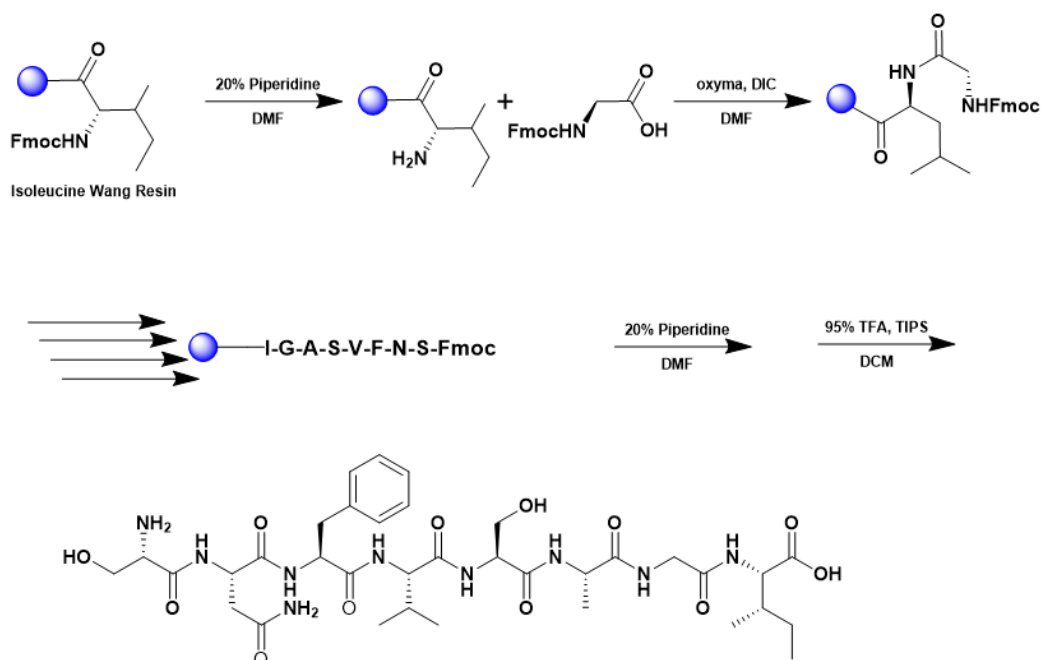
A 25 mL vessel of CEM discover bio manual peptide synthesizer was charged with 0.25 mmol of leucine wang resin. The Fmoc group was removed by using a 20% piperidine solution in DMF (10 mL). Using Synergy software, the deprotection protocol was run. The piperidine solution was drained and the resin was washed with DMF (4 x 10 mL). Fmoc-L-lysine(Mtt)-OH (5 eq, 1.25 mM) along with Oxyma (5 eq, 1.25 mM) and DIC (5 eq, 1.35 mmol) in DMF was added to the reaction vessel and the coupling protocol was run. The amino acid solution was drained, and the resin was washed with DMF (2 x 10 mL). The fmoc removal and coupling procedure was repeated as before using the same equivalencies for the remaining amino acids. To remove the peptide from resin, a TFA cocktail solution (95% TFA, 2.5% TIPS, and 2.5% DCM) was added to the resin and agitated for 2 hours. The resin was filtered, and the resulting solution was concentrated in vacuo. The peptide was triturated with cold diethyl ether and purified using reverse phase HPLC using H<sub>2</sub>O/CH<sub>3</sub>CN. The sample was analyzed for purity using a Waters 1525 Binary HPLC Pump using a Phenomenex Luna 5u C8(2) 100A (250 x 4.60 mm) column; gradient eluted with H<sub>2</sub>O/CH<sub>3</sub>CN. Molecular weight was confirmed using high resolution electrospray ionization mass spectrometry (HRMS, ESI/MS) analyses obtained on an Agilent 6545B Q-TOF LC/MS equipped with 1260 infinity II LC system with auto sampler. The final peptide product was lyophilized and stored at -20°C until further use.



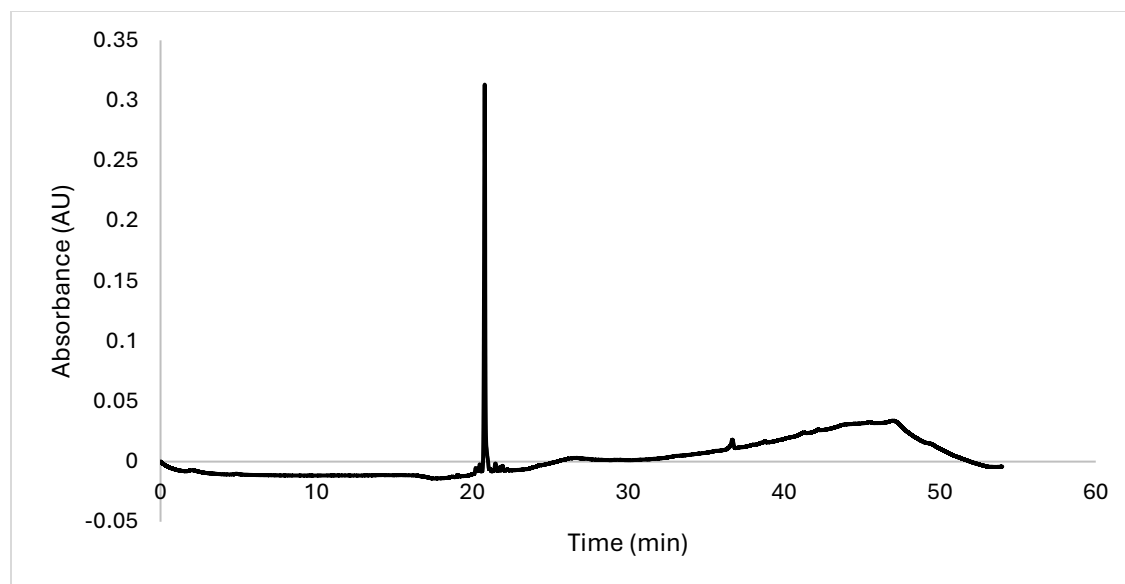
ESI-MS calculated  $[M+H^+]$ : 1042.5100, found 1042.5072.



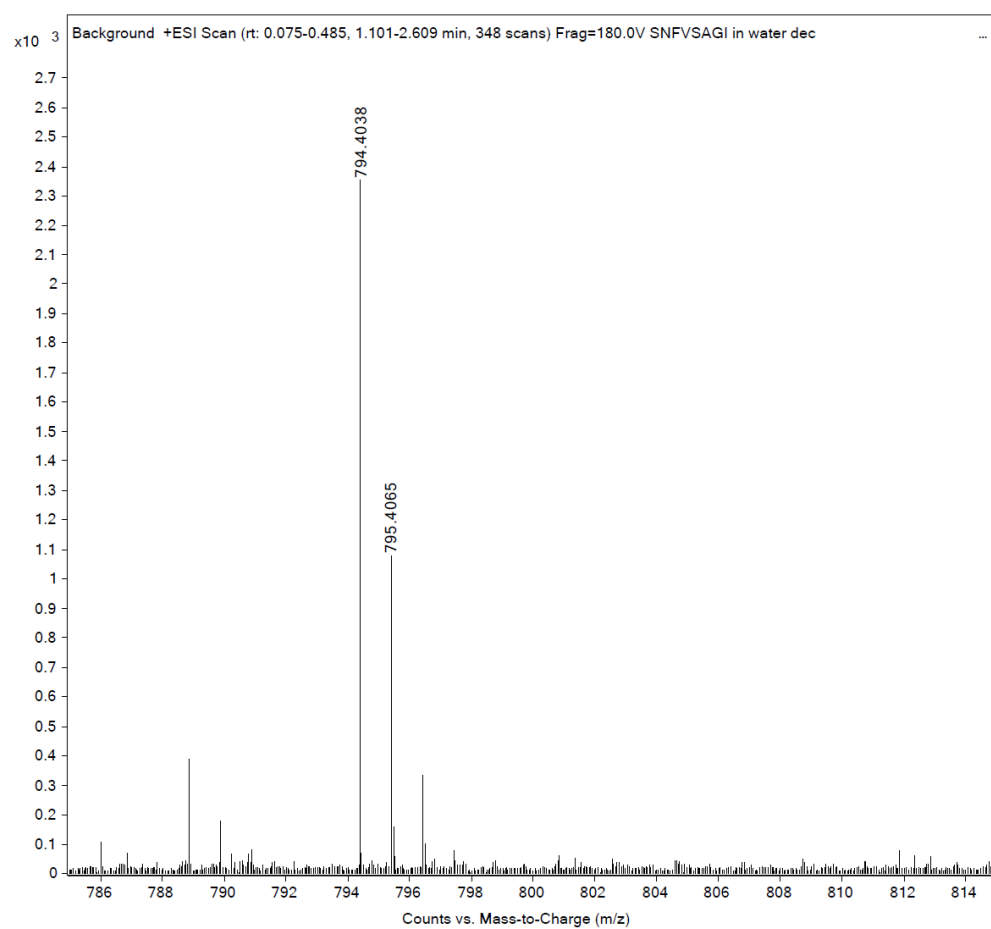
### Scheme S9. Synthesis of SNFVSAGI



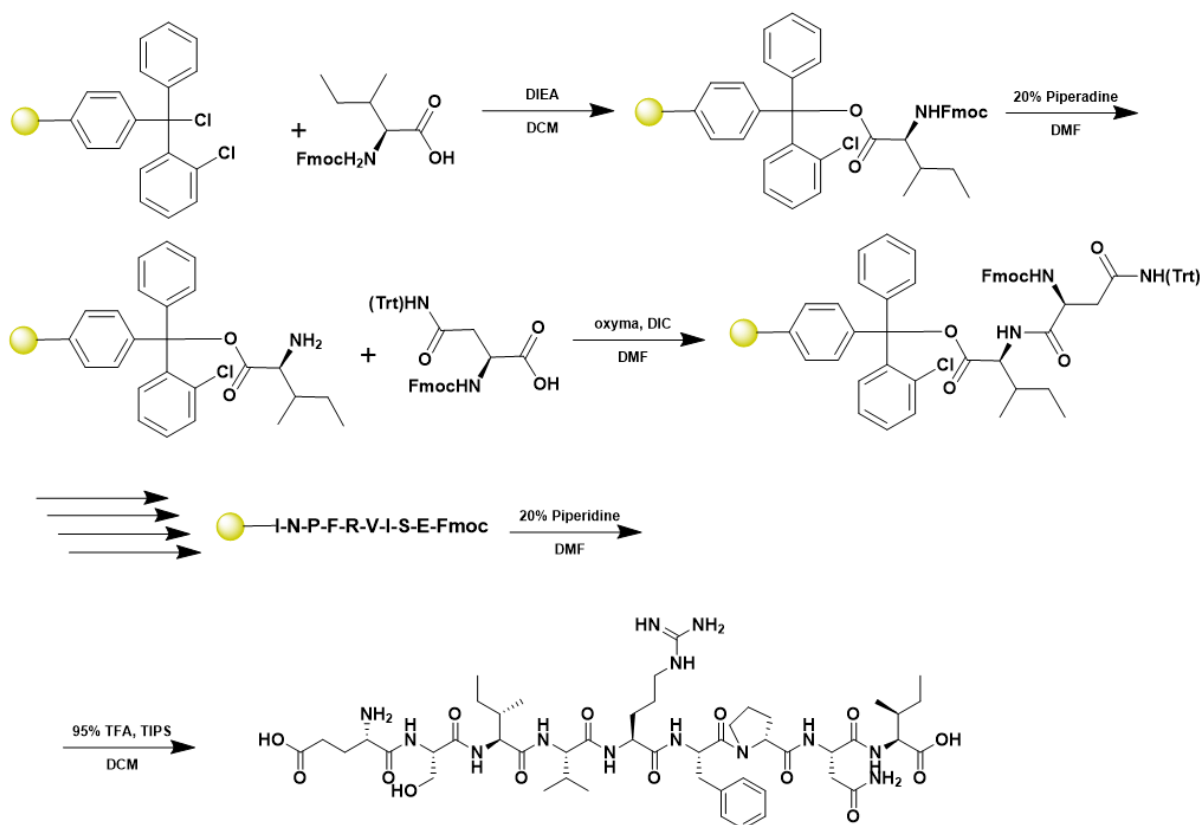
A 25 mL vessel of CEM discover bio manual peptide synthesizer was charged with 0.25 mmol of isoleucine wang resin. The Fmoc group was removed by using a 20% piperidine solution in DMF (10 mL). Using Synergy software, the deprotection protocol was run. The piperidine solution was drained and the resin was washed with DMF (4 x 10 mL). Fmoc-L-glycine (5 eq, 1.25 mM) along with Oxyma (5 eq, 1.25 mM) and DIC (5 eq, 1.35 mmol) in DMF was added to the reaction vessel and the coupling protocol was run. The amino acid solution was drained, and the resin was washed with DMF (2 x 10 mL). The fmoc removal and coupling procedure was repeated as before using the same equivalencies for the remaining amino acids. To remove the peptide from resin, a TFA cocktail solution (95% TFA, 2.5% TIPS, and 2.5% DCM) was added to the resin and agitated for 2 hours. The resin was filtered, and the resulting solution was concentrated in vacuo. The peptide was triturated with cold diethyl ether and purified using reverse phase HPLC using H<sub>2</sub>O/CH<sub>3</sub>CN. The sample was analyzed for purity using a Waters 1525 Binary HPLC Pump using a Phenomenex Luna 5u C8(2) 100A (250 x 4.60 mm) column; gradient eluted with H<sub>2</sub>O/CH<sub>3</sub>CN. Molecular weight was confirmed using high resolution electrospray ionization mass spectrometry (HRMS, ESI/MS) analyses obtained on an Agilent 6545B Q-TOF LC/MS equipped with 1260 infinity II LC system with auto sampler. The final peptide product was lyophilized and stored at -20°C until further use.



ESI-MS calculated  $[M+H]^+$ : 794.4048, found 794.4038

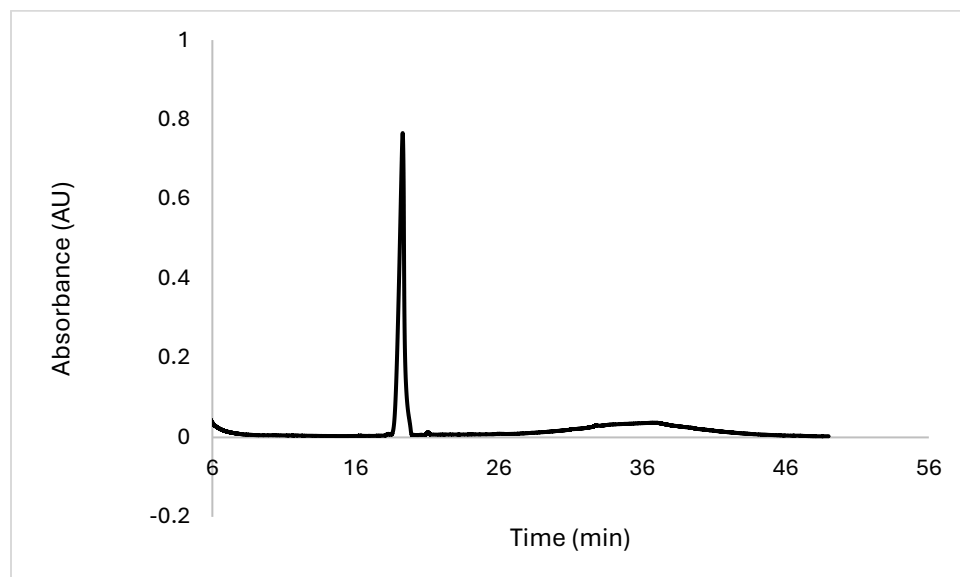


## Scheme S10. Synthesis of ESIVRFPNI

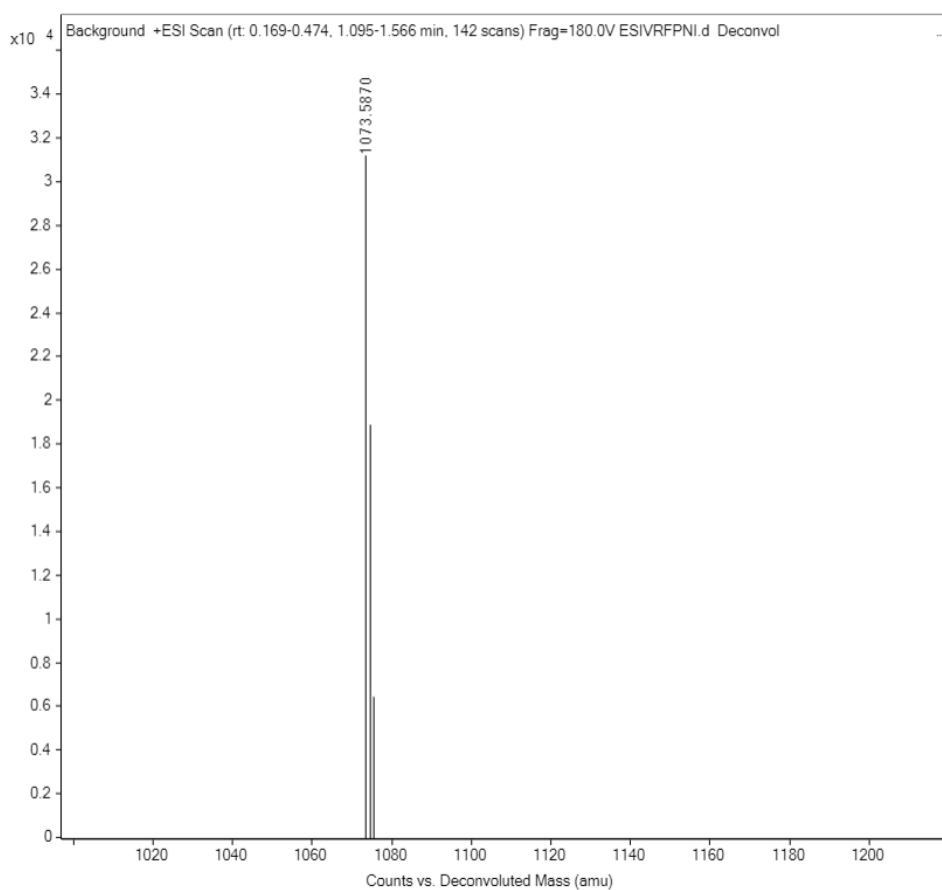


A 25 mL peptide synthesis vessel charged with 2-hlorotrityl chloride resin (0.25mmol) was added Fmoc-L-isoleucine-OH (1.1 eq, 0.275 mmol) and DIEA (3 eq, 0.75 mmol) in dry DCM. The resin was agitated for 1 h at ambient temperature and washed with MeOH and DCM (3 x each). The Fmoc group was removed by using a 20% piperidine solution in DMF for 30 min at ambient temperature, then washed as before. Fmoc-L-asparagine(Trt)-OH (5 eq, 1.25 mM) along with Oxyma (5 eq, 1.25 mM) and DIC (5 eq, 1.35 mmol) in DMF was added to the reaction vessel and agitated for 2 h at ambient temperature. The Fmoc removal and coupling procedure was repeated as before using the same equivalencies for the remaining amino acids. To remove the peptide from resin, a TFA cocktail solution (95% TFA, 2.5% TIPS, and 2.5% DCM) was added to the resin and agitated for 2 hours. The resin was filtered, and the resulting solution was concentrated in vacuo. The peptide was triturated with cold diethyl ether and purified using reverse phase HPLC using H<sub>2</sub>O/CH<sub>3</sub>CN. The sample was analyzed for purity using a Waters 1525 Binary HPLC Pump using a Phenomenex Luna 5u C8(2) 100A (250 x 4.60 mm) column; gradient eluted with H<sub>2</sub>O/CH<sub>3</sub>CN. Molecular weight was confirmed using high resolution electrospray ionization mass spectrometry (HRMS, ESI/MS) analyses obtained on an

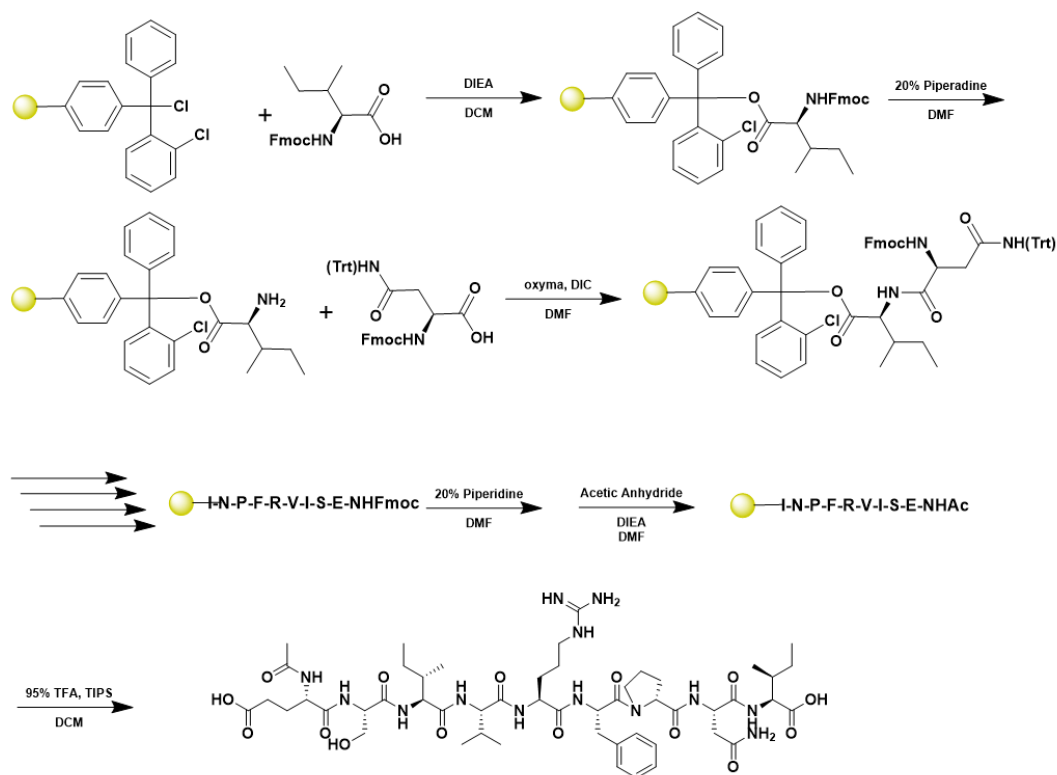
Agilent 6545B Q-TOF LC/MS equipped with 1260 infinity II LC system with auto sampler. The final peptide product was lyophilized and stored at -20°C until further use.



ESI-MS calculated [M]: 1073.5869, found 1073.5870

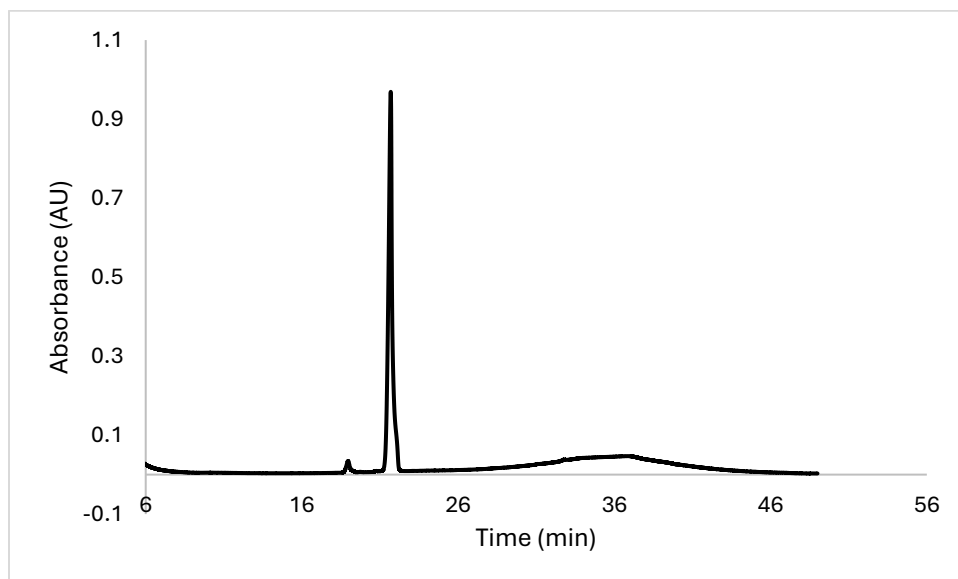


## Scheme S11. Synthesis of N-Acetyl ESIVRFPNI

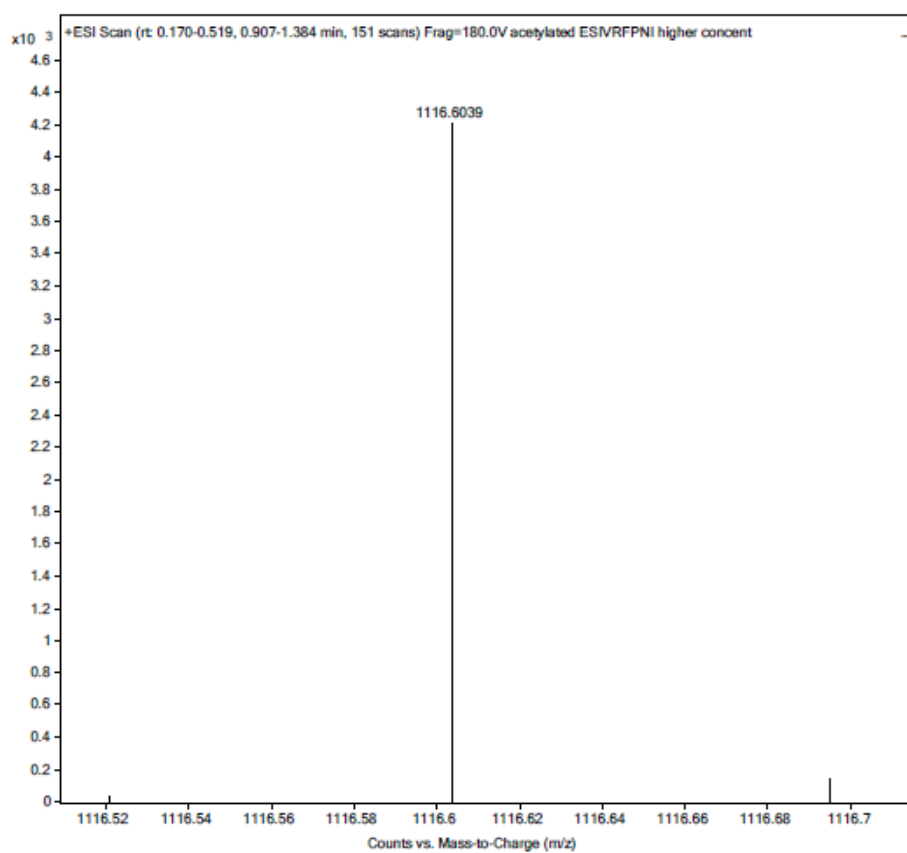


A 25 mL peptide synthesis vessel charged with 2-hlorotrytil chloride resin (0.25mmol) was added Fmoc-L-isoleucine-OH (1.1 eq, 0.275 mmol) and DIEA (3 eq, 0.75 mmol) in dry DCM. The resin was agitated for 1 h at ambient temperature and washed with MeOH and DCM (3 x each). The Fmoc group was removed by using a 20% piperidine solution in DMF for 30 min at ambient temperature, then washed as before. Fmoc-L-asparagine(Trt)-OH (5 eq, 1.25 mM) along with Oxyma (5 eq, 1.25 mM) and DIC (5 eq, 1.35 mmol) in DMF was added to the reaction vessel and agitated for 2 h at ambient temperature. The Fmoc removal and coupling procedure was repeated as before using the same equivalencies for the remaining amino acids. The final amino acid was Fmoc deprotected as described before and was acetylated by agitating the resin for 1 hour in a solution of 5% acetic anhydride (0.5 mL), 8.5% DIEA (0.85 mL), and 86.5% DMF (8.65 mL). To remove the peptide from resin, a TFA cocktail solution (95% TFA, 2.5% TIPS, and 2.5% DCM) was added to the resin and agitated for 2 hours. The resin was filtered, and the resulting solution was concentrated in vacuo. The peptide was trituated with cold diethyl ether and purified using reverse phase HPLC using H<sub>2</sub>O/CH<sub>3</sub>CN. The sample was analyzed for purity using a Waters 1525 Binary HPLC Pump using a Phenomenex Luna 5u C8(2) 100A (250 x 4.60 mm) column; gradient eluted with H<sub>2</sub>O/CH<sub>3</sub>CN. Molecular weight was confirmed using high resolution electrospray ionization mass spectrometry (HRMS, ESI/MS) analyses obtained on an Agilent 6545B Q-TOF LC/MS equipped with

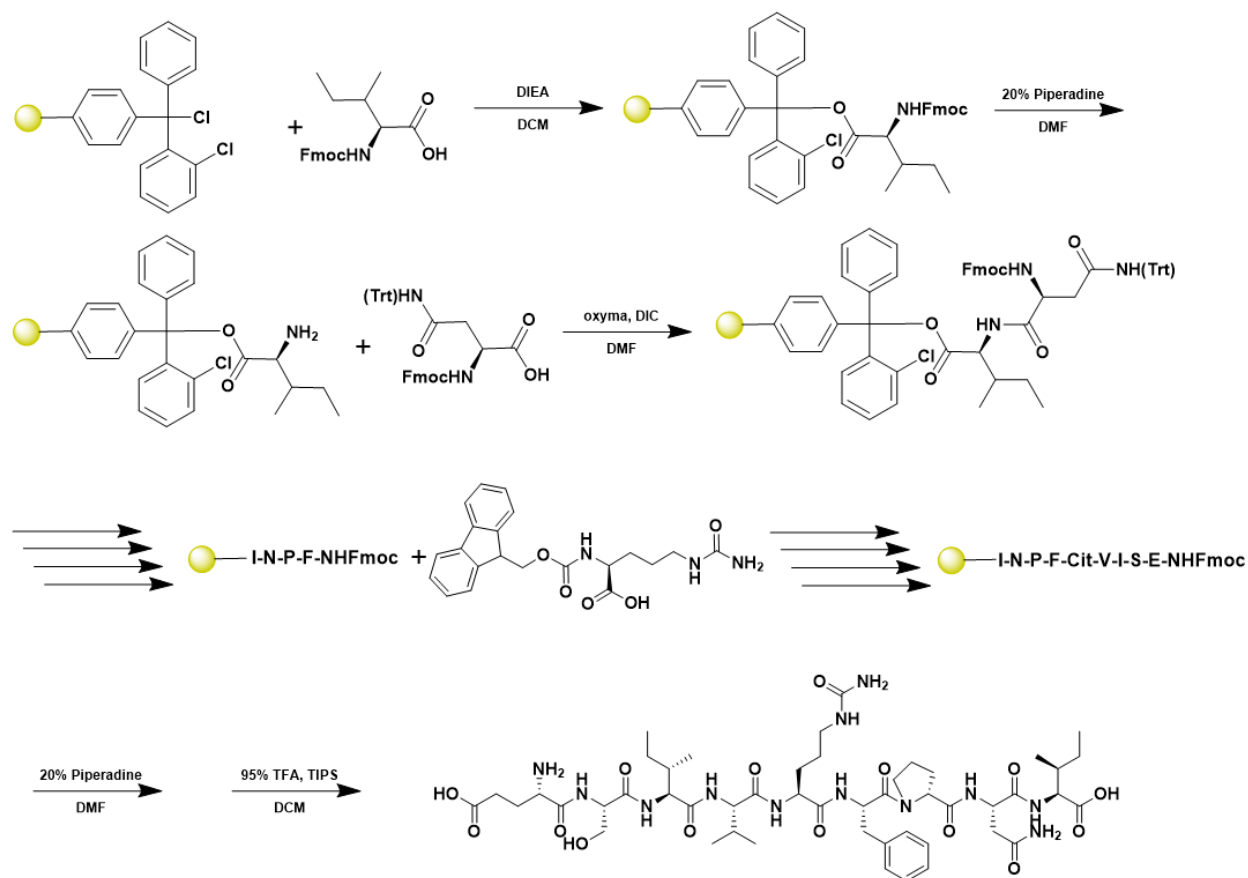
1260 infinity II LC system with auto sampler. The final peptide product was lyophilized and stored at  $-20^{\circ}\text{C}$  until further use.



ESI-MS calculated [M]: 1116.6048, found 1116.6039

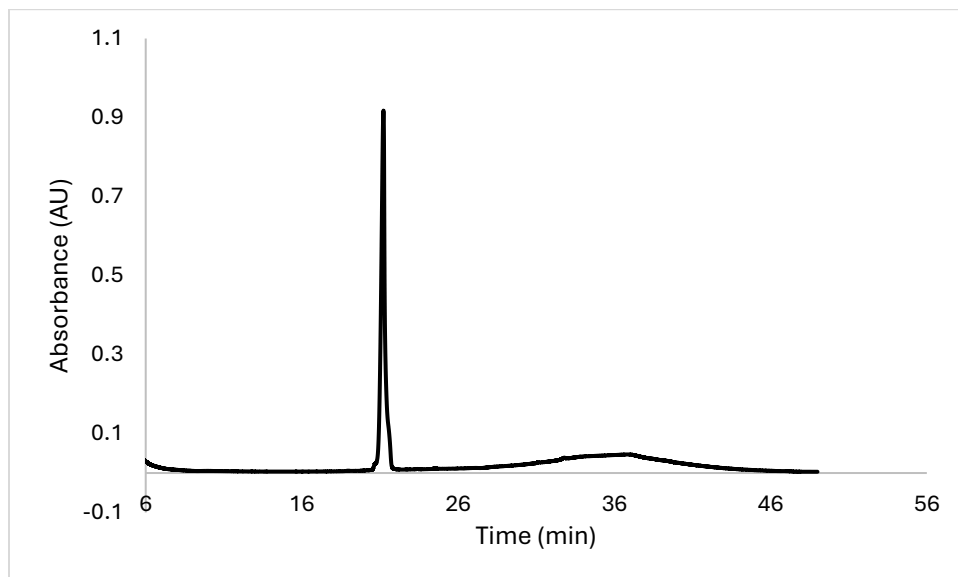


## Scheme S12. Synthesis of Citrullinated ESIVRFPNI

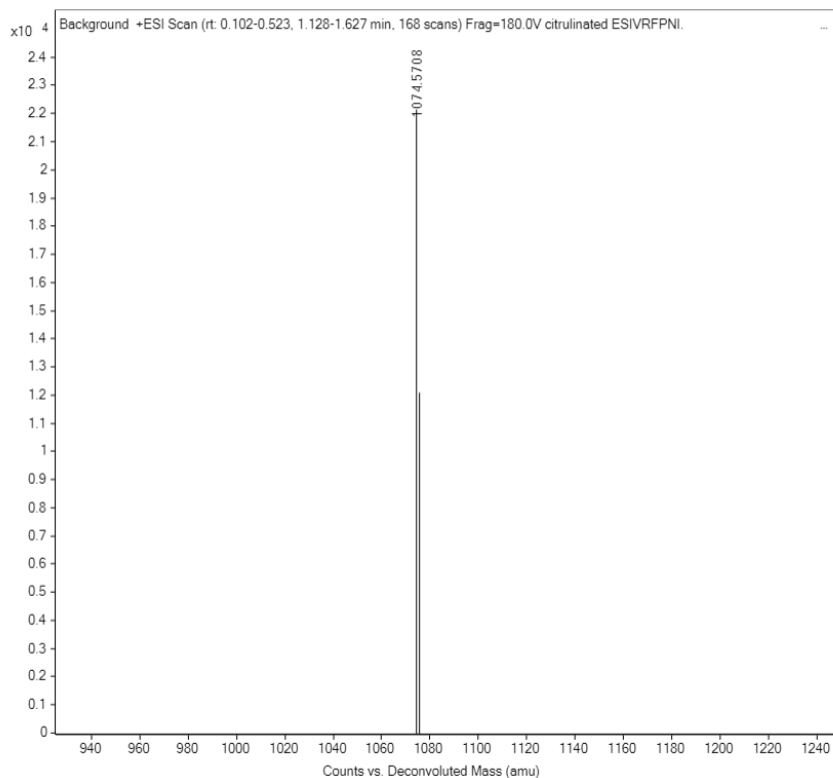


A 25 mL peptide synthesis vessel charged with 2-hlorotrityl chloride resin (0.25mmol) was added Fmoc-L-isoleucine-OH (1.1 eq, 0.275 mmol) and DIEA (3 eq, 0.75 mmol) in dry DCM. The resin was agitated for 1 h at ambient temperature and washed with MeOH and DCM (3 x each). The Fmoc group was removed by using a 20% piperidine solution in DMF for 30 min at ambient temperature, then washed as before. Fmoc-L-asparagine(Trt)-OH (5 eq, 1.25 mM) along with Oxyma (5 eq, 1.25 mM) and DIC (5 eq, 1.35 mmol) in DMF was added to the reaction vessel and agitated for 2 h at ambient temperature. The Fmoc removal and coupling procedure was repeated as before using the same equivalencies for the remaining amino acids. For the 5<sup>th</sup> position of the amino acid, Fmoc was deprotected as described above and Fmoc-L-citrulline (5 eq, 1.25 mM) along with Oxyma (5 eq, 1.25 mM) and DIC (5 eq, 1.35 mmol) in DMF was added to the reaction vessel. To remove the peptide from resin, a TFA cocktail solution (95% TFA, 2.5% TIPS, and 2.5% DCM) was added to the resin and agitated for 2 hours. The resin was filtered, and the resulting solution was concentrated in vacuo. The peptide was triturated with cold diethyl ether and purified using reverse phase HPLC using H<sub>2</sub>O/CH<sub>3</sub>CN. The sample was analyzed for purity using a Waters 1525 Binary HPLC Pump using a Phenomenex Luna 5u C8(2) 100A (250 x 4.60 mm) column; gradient eluted with H<sub>2</sub>O/CH<sub>3</sub>CN. Molecular

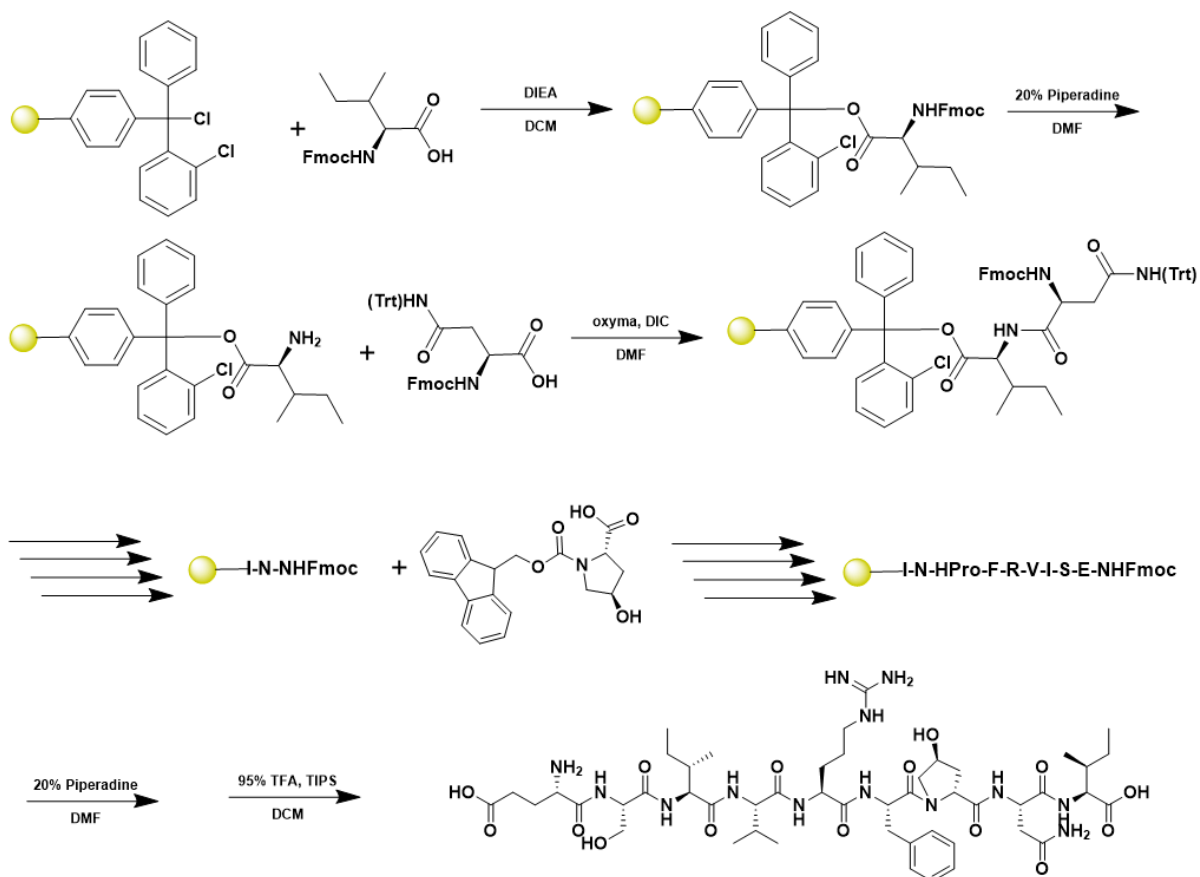
weight was confirmed using high resolution electrospray ionization mass spectrometry (HRMS, ESI/MS) analyses obtained on an Agilent 6545B Q-TOF LC/MS equipped with 1260 infinity II LC system with auto sampler. The final peptide product was lyophilized and stored at  $-20^{\circ}\text{C}$  until further use.



ESI-MS calculated [M]: 1074.5710, found 1074.5708

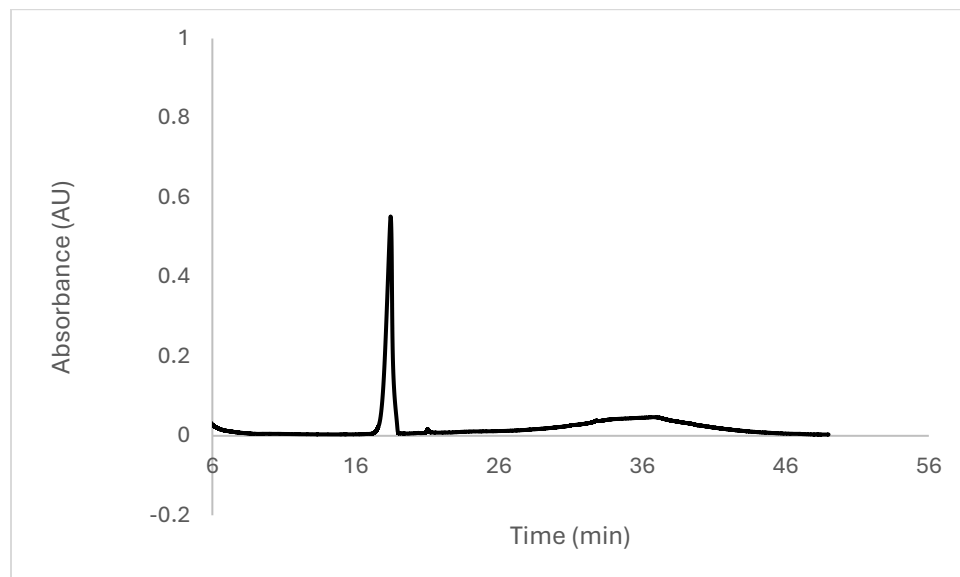


## Scheme S13. Synthesis of Hydroxy Proline ESIVRFPNI

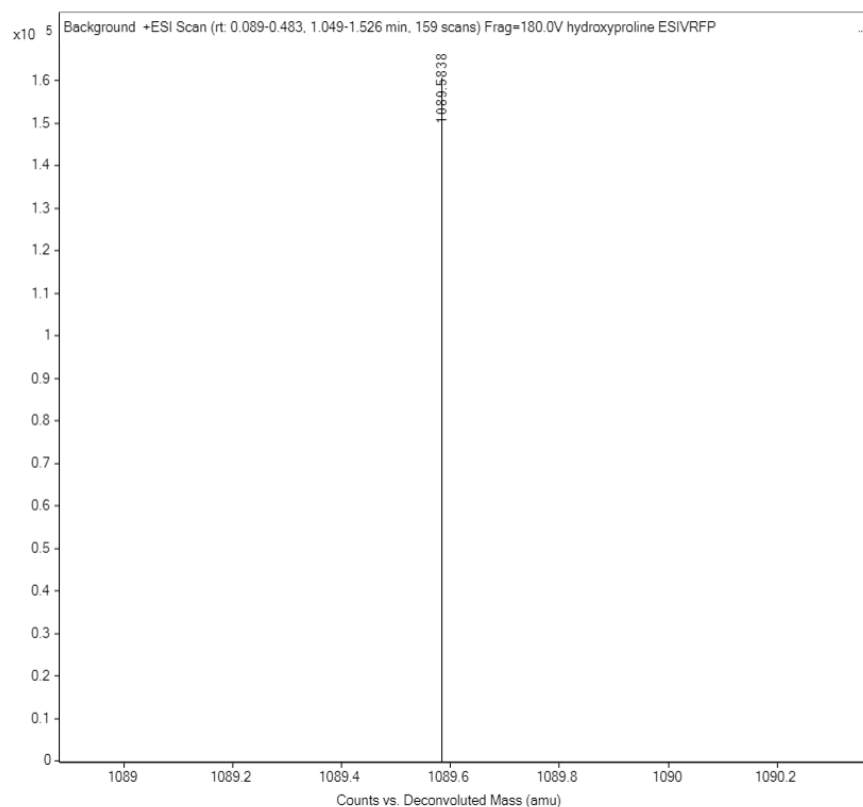


A 25 mL peptide synthesis vessel charged with 2-chlorotrityl chloride resin (0.25mmol) was added Fmoc-L-isoleucine-OH (1.1 eq, 0.275 mmol) and DIEA (3 eq, 0.75 mmol) in dry DCM. The resin was agitated for 1 h at ambient temperature and washed with MeOH and DCM (3 x each). The Fmoc group was removed by using a 20% piperidine solution in DMF for 30 min at ambient temperature, then washed as before. Fmoc-L-asparagine(Trt)-OH (5 eq, 1.25 mM) along with Oxyma (5 eq, 1.25 mM) and DIC (5 eq, 1.35 mmol) in DMF was added to the reaction vessel and agitated for 2 h at ambient temperature. The Fmoc removal and coupling procedure was repeated as before using the same equivalencies for the remaining amino acids. For the 6<sup>th</sup> position of the amino acid, Fmoc was deprotected as described above and Fmoc-L-trans-4-hydroxyproline (5 eq, 1.25 mM) was added along with Oxyma (5 eq, 1.25 mM) and DIC (5 eq, 1.35 mmol) in DMF the reaction vessel. To remove the peptide from resin, a TFA cocktail solution (95% TFA, 2.5% TIPS, and 2.5% DCM) was added to the resin and agitated for 2 hours. The resin was filtered, and the resulting solution was concentrated in vacuo. The peptide was triturated with cold diethyl ether and purified using reverse phase HPLC using H<sub>2</sub>O/CH<sub>3</sub>CN. The sample was analyzed for purity using a Waters 1525 Binary HPLC Pump using a Phenomenex Luna 5u C8(2) 100A (250 x 4.60 mm) column; gradient eluted with

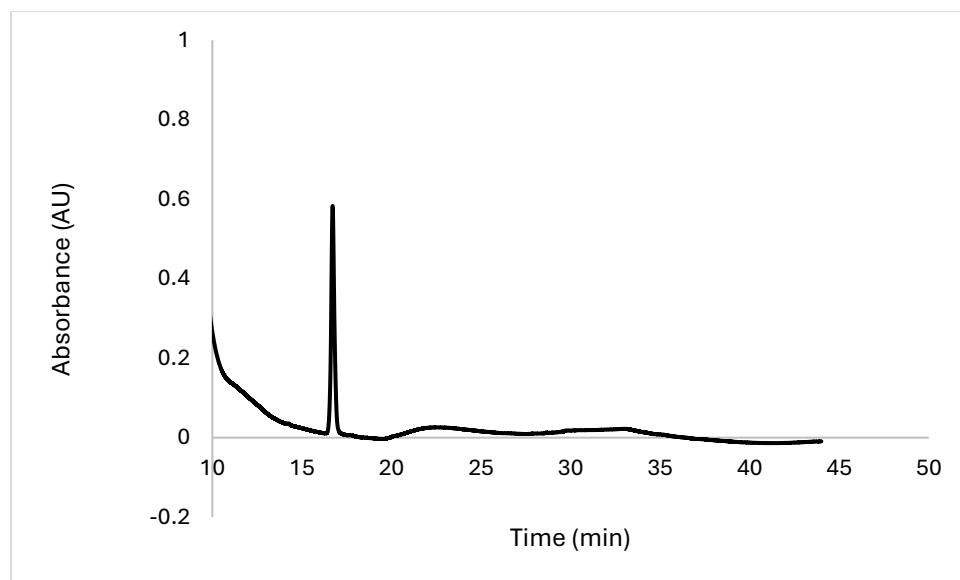
H<sub>2</sub>O/CH<sub>3</sub>CN. Molecular weight was confirmed using high resolution electrospray ionization mass spectrometry (HRMS, ESI/MS) analyses obtained on an Agilent 6545B Q-TOF LC/MS equipped with 1260 infinity II LC system with auto sampler. The final peptide product was lyophilized and stored at -20°C until further use.



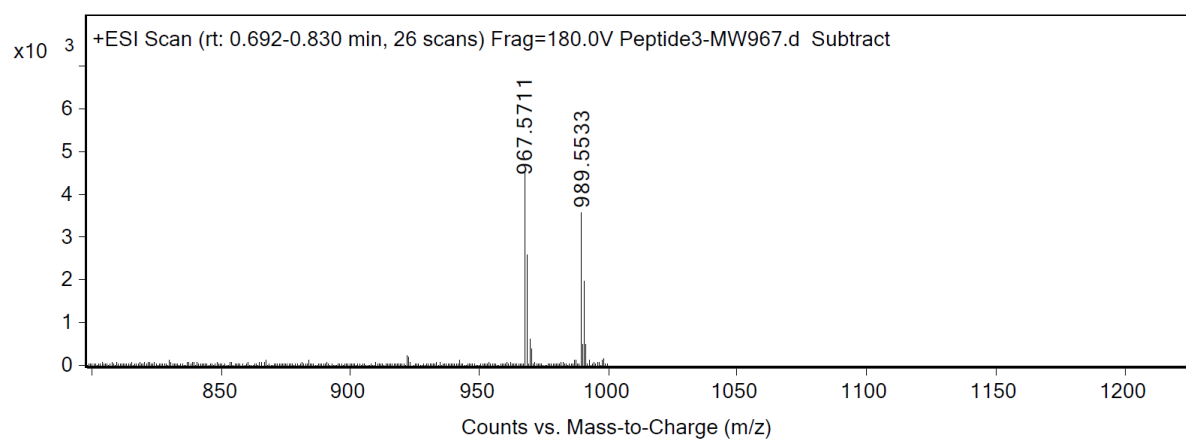
ESI-MS calculated [M]: 1089.5819, found 1089.5838





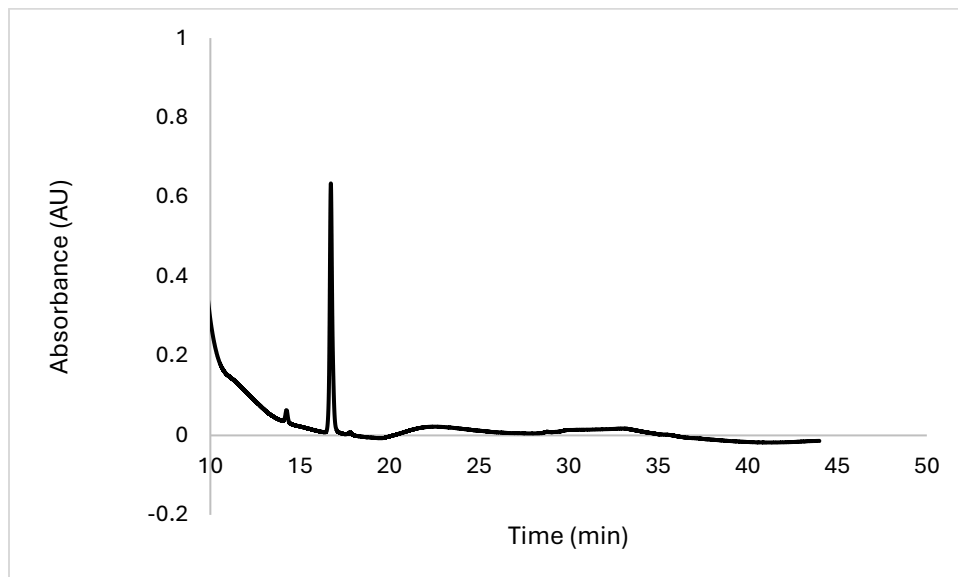


ESI-MS calculated [M]: 967.5715, found 967.5711

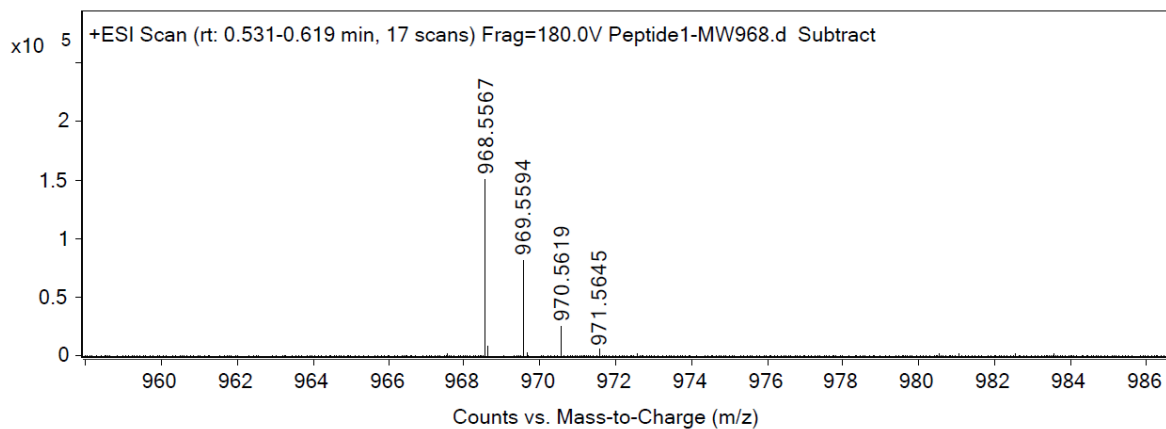




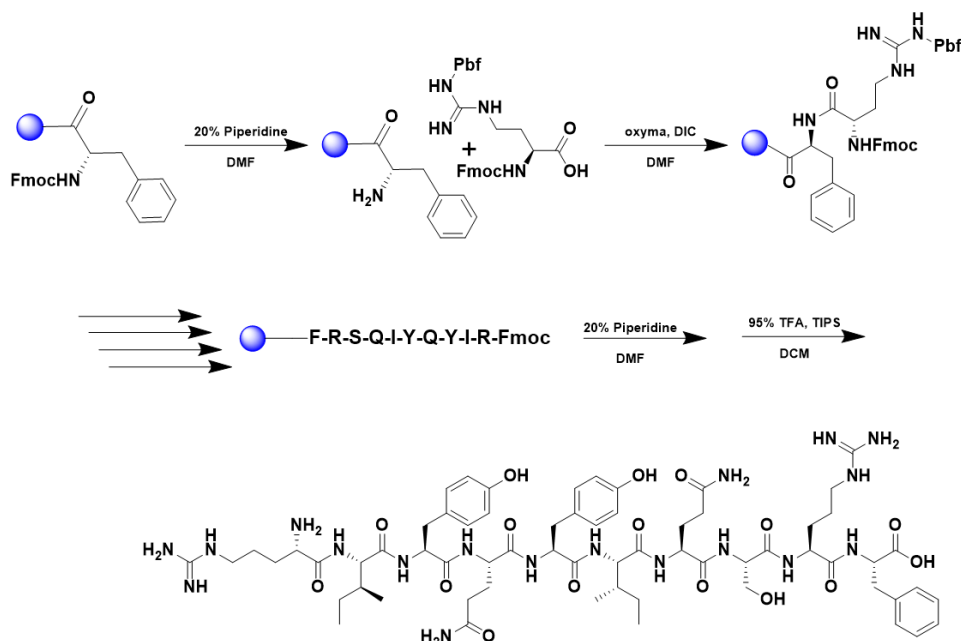
with auto sampler. The final peptide product was lyophilized and stored at  $-20^{\circ}\text{C}$  until further use.



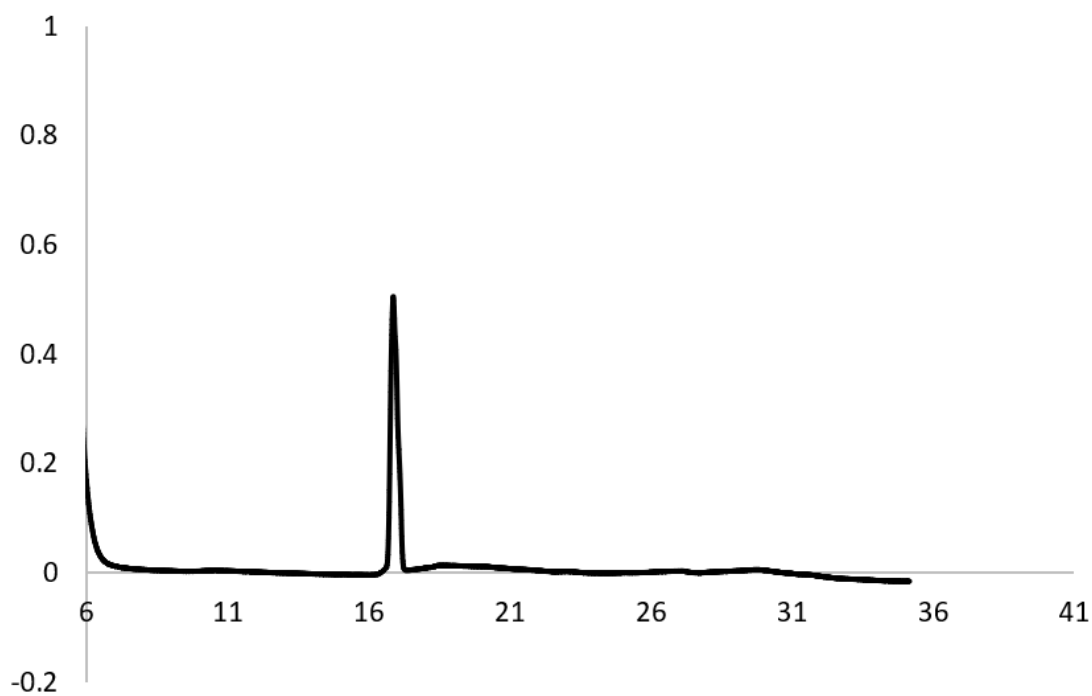
ESI-MS calculated [M]: 967.5555, found 967.5567



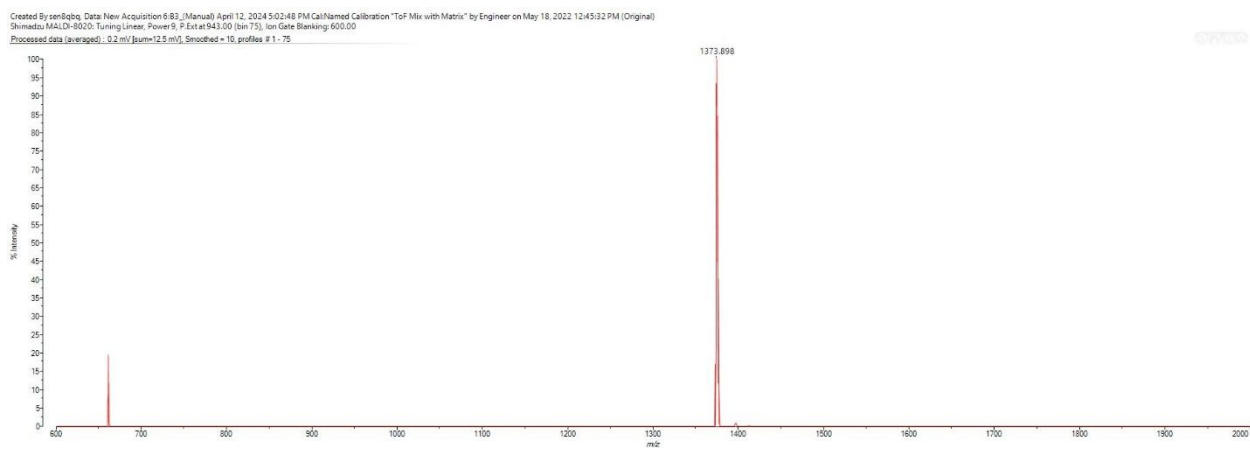
## Scheme S16. Synthesis of RIYQIQR



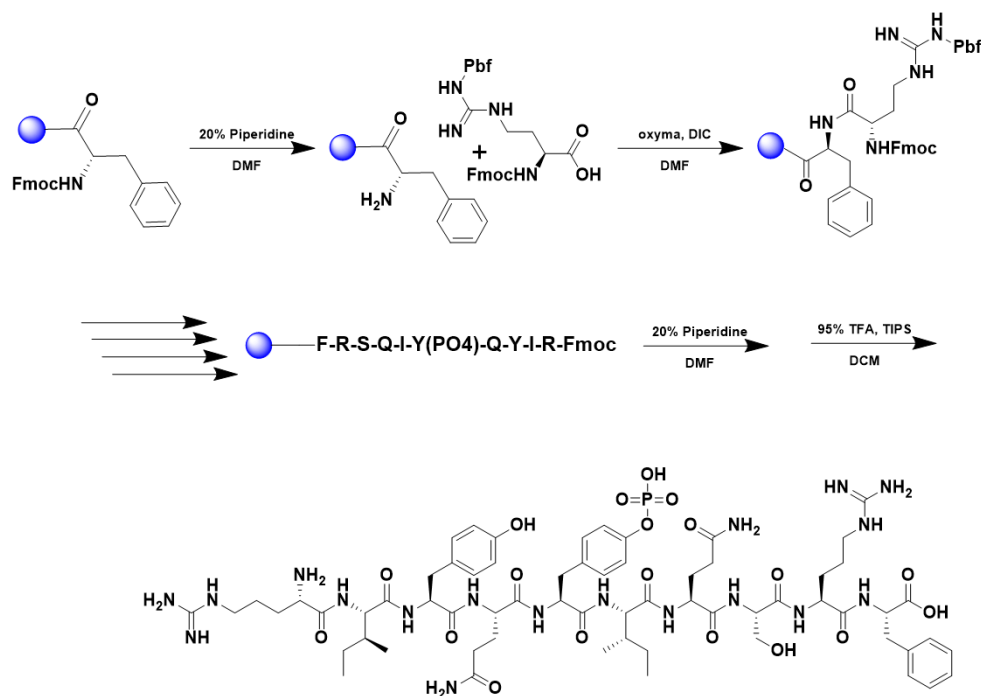
A 25 mL vessel of CEM discover bio manual peptide synthesizer was charged with 0.25 mmol of phenylalanine wang resin. The Fmoc group was removed by using a 20% piperidine solution in DMF (10 mL). Using Synergy software, the deprotection protocol was run. The piperidine solution was drained and the resin was washed with DMF (4 x 10 mL). Fmoc-L-arginine(Pbf)-OH (5 eq, 1.25 mM) along with Oxyma (5 eq, 1.25 mM) and DIC (5 eq, 1.35 mmol) in DMF was added to the reaction vessel and the coupling protocol was run. The amino acid solution was drained, and the resin was washed with DMF (2 x 10 mL). The fmoc removal and coupling procedure was repeated as before using the same equivalencies for the remaining amino acids. To remove the peptide from resin, a TFA cocktail solution (95% TFA, 2.5% TIPS, and 2.5% DCM) was added to the resin and agitated for 2 hours. The resin was filtered, and the resulting solution was concentrated in vacuo. The peptide was triturated with cold diethyl ether and purified using reverse phase HPLC using H<sub>2</sub>O/CH<sub>3</sub>CN. The sample was analyzed for purity using a Waters 1525 Binary HPLC Pump using a Phenomenex Luna 5u C8(2) 100A (250 x 4.60 mm) column; gradient eluted with H<sub>2</sub>O/CH<sub>3</sub>CN. Molecular weight was confirmed using high resolution electrospray ionization mass spectrometry (HRMS, ESI/MS) analyses obtained on an Agilent 6545B Q-TOF LC/MS equipped with 1260 infinity II LC system with auto sampler. The final peptide product was lyophilized and stored at -20°C until further use.



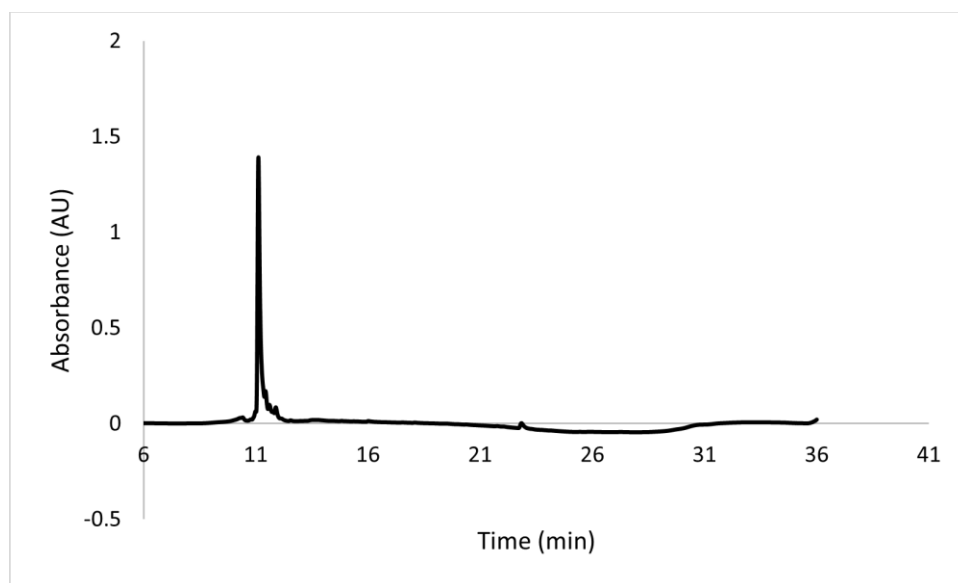
MALDI-TOF MS calculated [M]: 1373.7325, found 1373.898



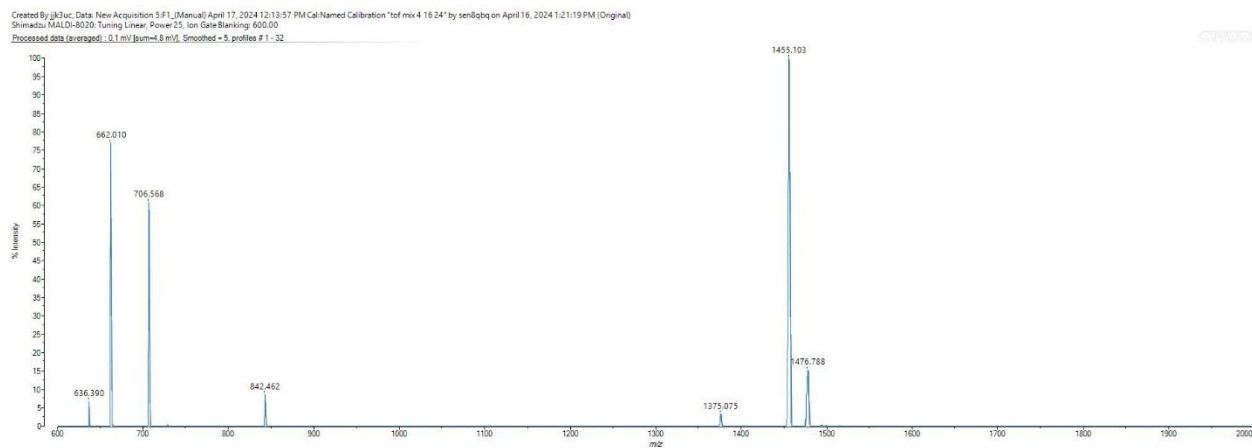
## Scheme S17. Synthesis of RIYQ(YPO4)IQSRF



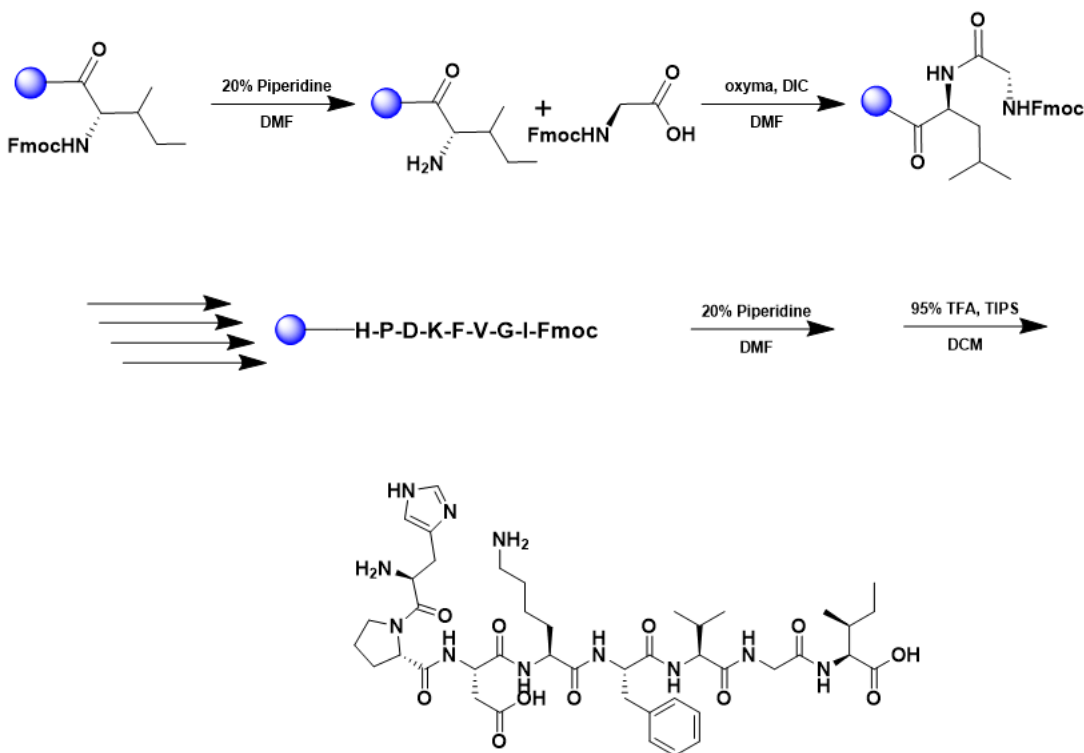
A 25 mL vessel of CEM discover bio manual peptide synthesizer was charged with 0.25 mmol of phenylalanine wang resin. The Fmoc group was removed by using a 20% piperidine solution in DMF (10 mL). Using Synergy software, the deprotection protocol was run. The piperidine solution was drained and the resin was washed with DMF (4 x 10 mL). Fmoc-L-arginine(Pbf)-OH (5 eq, 1.25 mM) along with Oxyma (5 eq, 1.25 mM) and DIC (5 eq, 1.35 mmol) in DMF was added to the reaction vessel and the coupling protocol was run. The amino acid solution was drained, and the resin was washed with DMF (2 x 10 mL). The fmoc removal and coupling procedure was repeated as before using the same equivalencies for the remaining amino acids. To remove the peptide from resin, a TFA cocktail solution (95% TFA, 2.5% TIPS, and 2.5% DCM) was added to the resin and agitated for 2 hours. The resin was filtered, and the resulting solution was concentrated in vacuo. The peptide was triturated with cold diethyl ether and purified using reverse phase HPLC using H<sub>2</sub>O/CH<sub>3</sub>CN. The sample was analyzed for purity using a Waters 1525 Binary HPLC Pump using a Phenomenex Luna 5u C8(2) 100A (250 x 4.60 mm) column; gradient eluted with H<sub>2</sub>O/CH<sub>3</sub>CN. Molecular weight was confirmed using high resolution electrospray ionization mass spectrometry (HRMS, ESI/MS) analyses obtained on an Agilent 6545B Q-TOF LC/MS equipped with 1260 infinity II LC system with auto sampler. The final peptide product was lyophilized and stored at -20°C until further use.



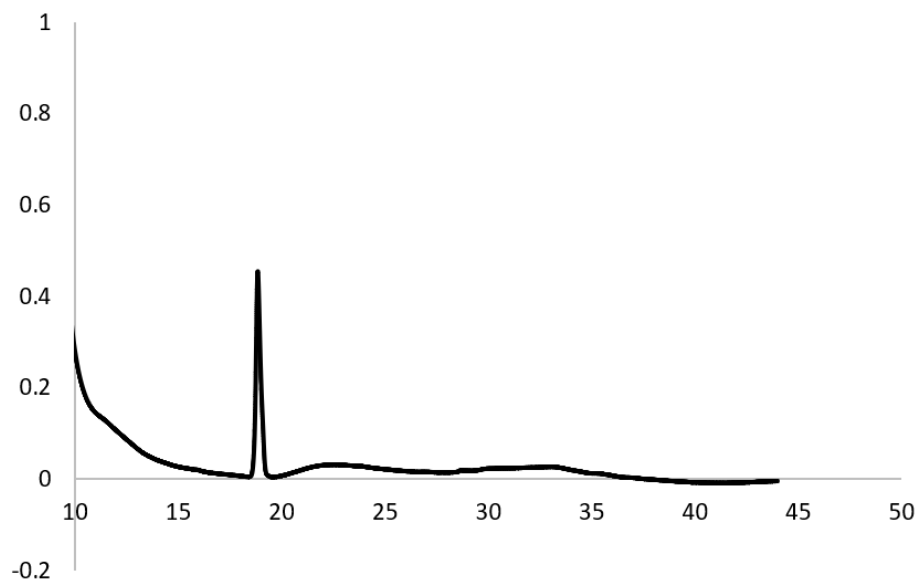
MALDI-TOF MS calculated [M]: 1452.6910, found 1455.103



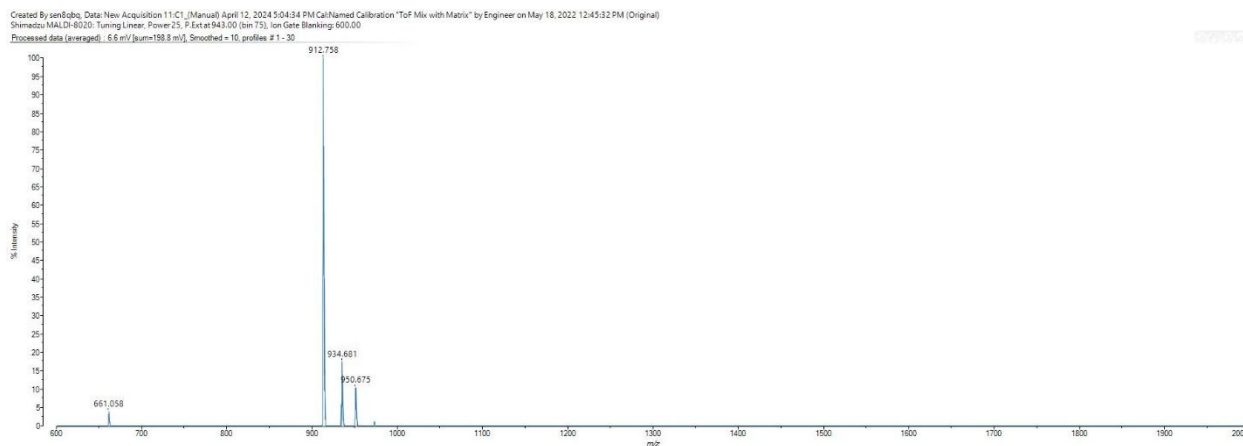
## Scheme S18. Synthesis of HPDKFVGI



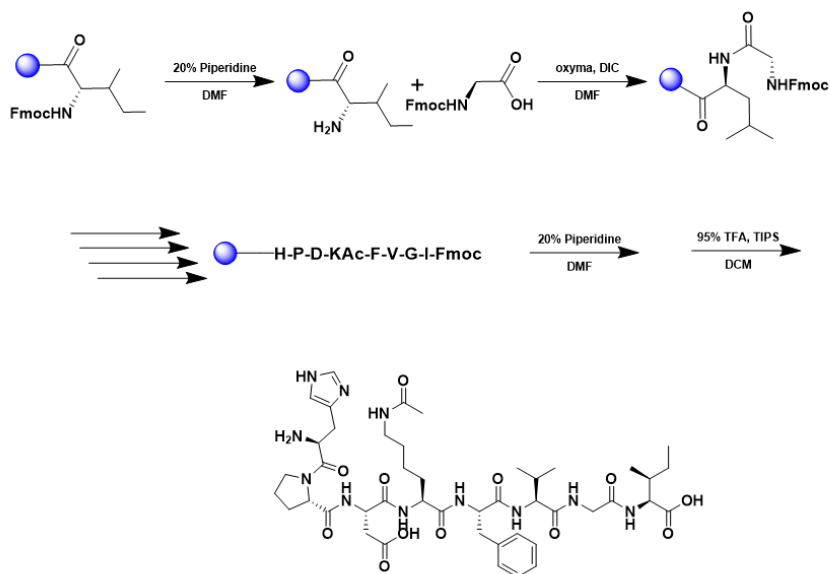
A 25 mL vessel of CEM discover bio manual peptide synthesizer was charged with 0.25 mmol of isoleucine wang resin. The Fmoc group was removed by using a 20% piperidine solution in DMF (10 mL). Using Synergy software, the deprotection protocol was run. The piperidine solution was drained and the resin was washed with DMF (4 x 10 mL). Fmoc-L-glycine (5 eq, 1.25 mM) along with Oxyma (5 eq, 1.25 mM) and DIC (5 eq, 1.35 mmol) in DMF was added to the reaction vessel and the coupling protocol was run. The amino acid solution was drained, and the resin was washed with DMF (2 x 10 mL). The fmoc removal and coupling procedure was repeated as before using the same equivalencies for the remaining amino acids. To remove the peptide from resin, a TFA cocktail solution (95% TFA, 2.5% TIPS, and 2.5% DCM) was added to the resin and agitated for 2 hours. The resin was filtered, and the resulting solution was concentrated in vacuo. The peptide was triturated with cold diethyl ether and purified using reverse phase HPLC using H<sub>2</sub>O/CH<sub>3</sub>CN. The sample was analyzed for purity using a Waters 1525 Binary HPLC Pump using a Phenomenex Luna 5u C8(2) 100A (250 x 4.60 mm) column; gradient eluted with H<sub>2</sub>O/CH<sub>3</sub>CN. Molecular weight was confirmed using high resolution electrospray ionization mass spectrometry (HRMS, ESI/MS) analyses obtained on an Agilent 6545B Q-TOF LC/MS equipped with 1260 infinity II LC system with auto sampler. The final peptide product was lyophilized and stored at -20°C until further use.



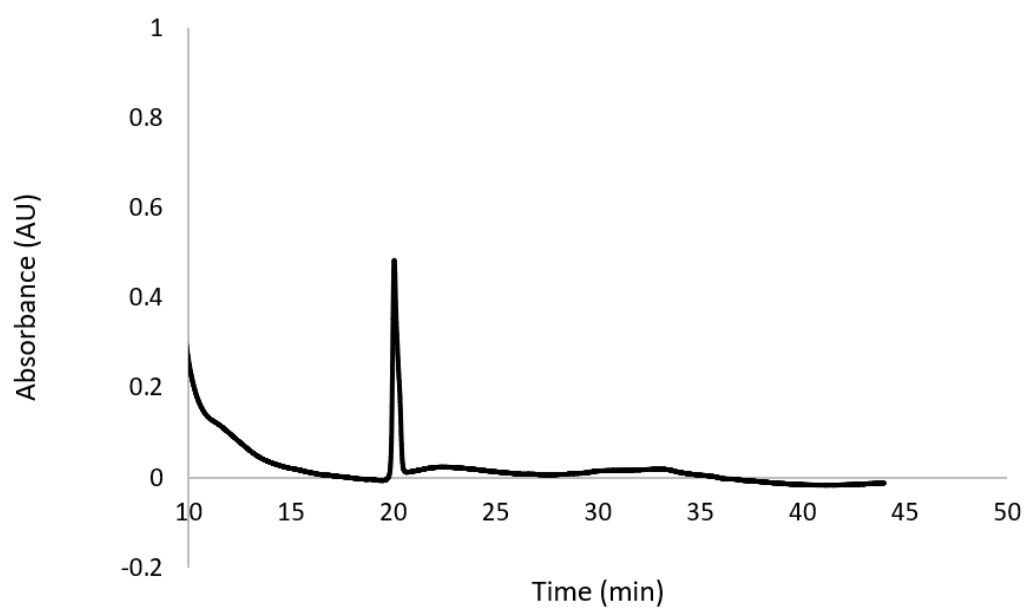
MALDI-TOF MS calculated [M]: 912.4938, found 912.758



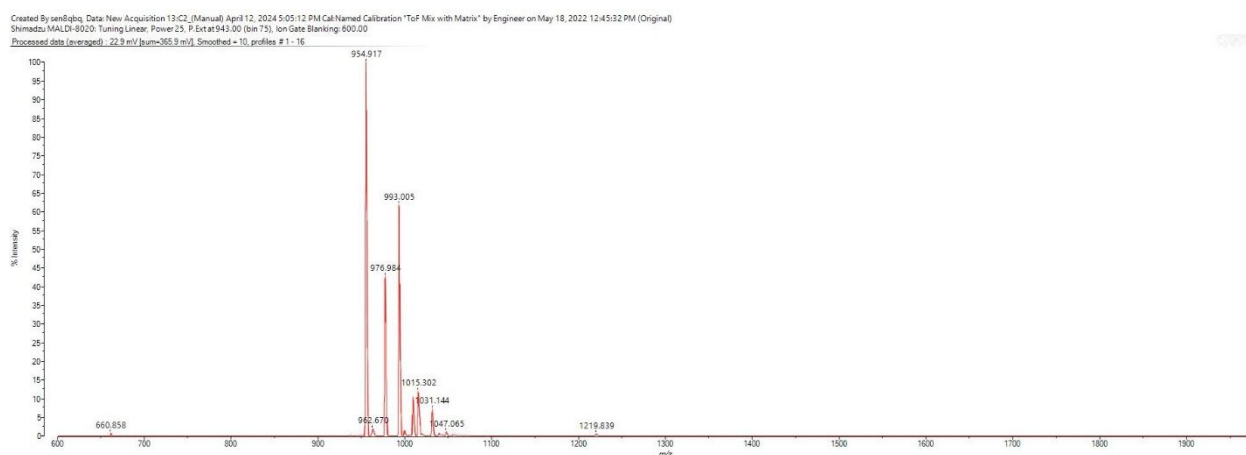
## Scheme S19. Synthesis of HPD(Kac)FVGI



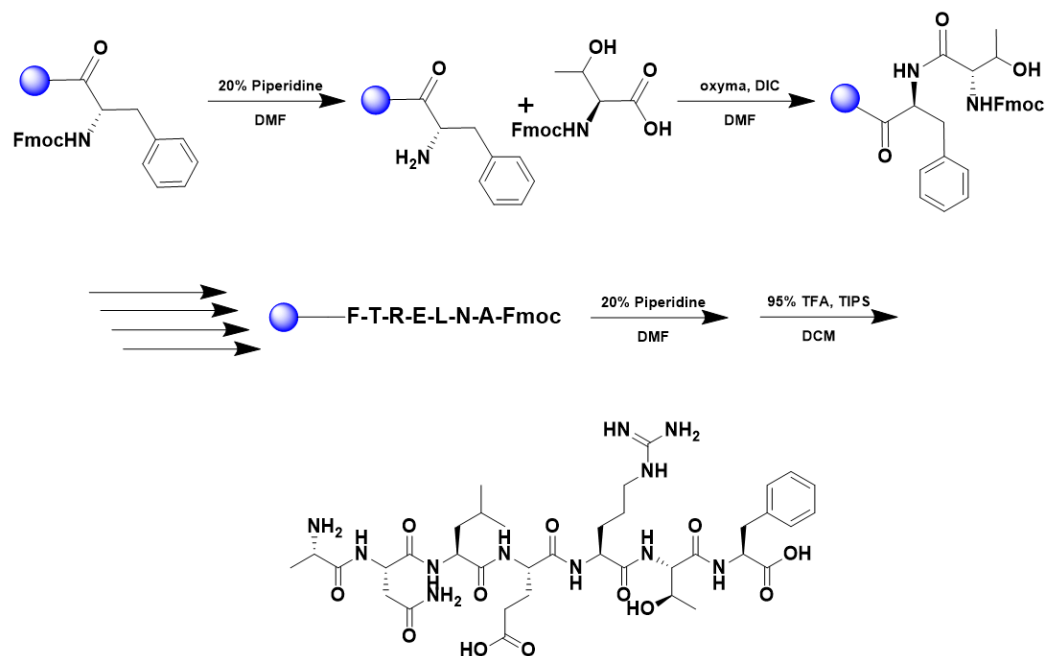
A 25 mL vessel of CEM discover bio manual peptide synthesizer was charged with 0.25 mmol of isoleucine wang resin. The Fmoc group was removed by using a 20% piperidine solution in DMF (10 mL). Using Synergy software, the deprotection protocol was run. The piperidine solution was drained and the resin was washed with DMF (4 x 10 mL). Fmoc-L-glycine (5 eq, 1.25 mM) along with Oxyma (5 eq, 1.25 mM) and DIC (5 eq, 1.35 mmol) in DMF was added to the reaction vessel and the coupling protocol was run. The amino acid solution was drained, and the resin was washed with DMF (2 x 10 mL). The fmoc removal and coupling procedure was repeated as before using the same equivalencies for the remaining amino acids. To remove the peptide from resin, a TFA cocktail solution (95% TFA, 2.5% TIPS, and 2.5% DCM) was added to the resin and agitated for 2 hours. The resin was filtered, and the resulting solution was concentrated in vacuo. The peptide was triturated with cold diethyl ether and purified using reverse phase HPLC using H<sub>2</sub>O/CH<sub>3</sub>CN. The sample was analyzed for purity using a Waters 1525 Binary HPLC Pump using a Phenomenex Luna 5u C8(2) 100A (250 x 4.60 mm) column; gradient eluted with H<sub>2</sub>O/CH<sub>3</sub>CN. Molecular weight was confirmed using high resolution electrospray ionization mass spectrometry (HRMS, ESI/MS) analyses obtained on an Agilent 6545B Q-TOF LC/MS equipped with 1260 infinity II LC system with auto sampler. The final peptide product was lyophilized and stored at -20°C until further use.



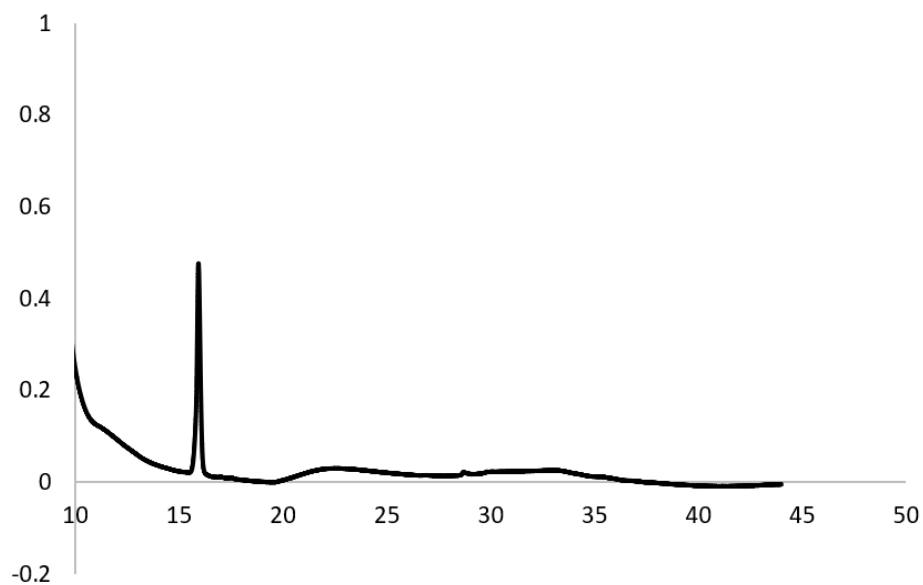
MALDI-TOF MS calculated [M]: 954.5044, found 954.917



## Scheme S20. Synthesis of ANLERTF



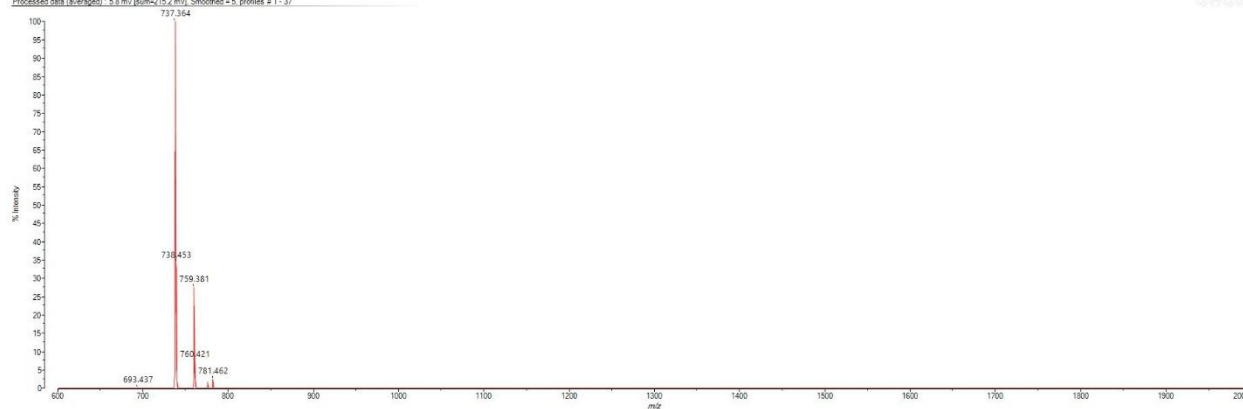
A 25 mL vessel of CEM discover bio manual peptide synthesizer was charged with 0.25 mmol of phenylalanine wang resin. The Fmoc group was removed by using a 20% piperidine solution in DMF (10 mL). Using Synergy software, the deprotection protocol was run. The piperidine solution was drained and the resin was washed with DMF (4 x 10 mL). Fmoc-L-threonine(tBu)-OH (5 eq, 1.25 mM) along with Oxyma (5 eq, 1.25 mM) and DIC (5 eq, 1.35 mmol) in DMF was added to the reaction vessel and the coupling protocol was run. The amino acid solution was drained, and the resin was washed with DMF (2 x 10 mL). The fmoc removal and coupling procedure was repeated as before using the same equivalencies for the remaining amino acids. To remove the peptide from resin, a TFA cocktail solution (95% TFA, 2.5% TIPS, and 2.5% DCM) was added to the resin and agitated for 2 hours. The resin was filtered, and the resulting solution was concentrated in vacuo. The peptide was triturated with cold diethyl ether and purified using reverse phase HPLC using H<sub>2</sub>O/CH<sub>3</sub>CN. The sample was analyzed for purity using a Waters 1525 Binary HPLC Pump using a Phenomenex Luna 5u C8(2) 100A (250 x 4.60 mm) column; gradient eluted with H<sub>2</sub>O/CH<sub>3</sub>CN. Molecular weight was confirmed using high resolution electrospray ionization mass spectrometry (HRMS, ESI/MS) analyses obtained on an Agilent 6545B Q-TOF LC/MS equipped with 1260 infinity II LC system with auto sampler. The final peptide product was lyophilized and stored at -20°C until further use.



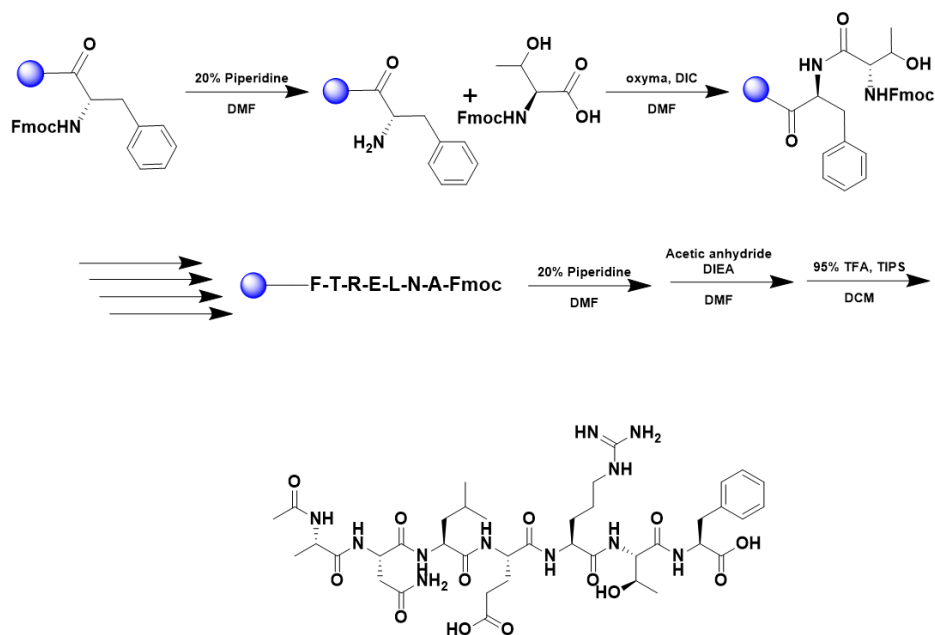
MALDI-TOF MS calculated [M]: 737.4345, found 737.364

Created By: jk2, Date: New Acquisition 652 (Manual) April 17, 2024 12:14:37 PM Cal:Named Calibration "tof mix 4 16 24" by xen@bq on April 16, 2024 1:21:19 PM (Original)  
Shimadzu MALDI-8020; Tuning: Linear, Power: 15, Ion Gate: Blanking, 600.00

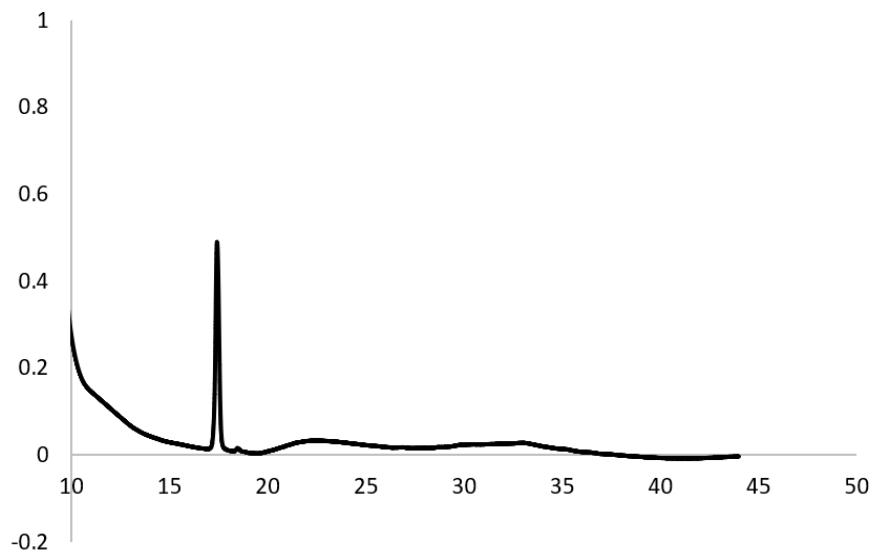
Processed data (averaged): 5.8 mV (sum=2152 mV), Smoothed=5, profiles #1 - 37



## Scheme S21. Synthesis of NAc-ANLERTF



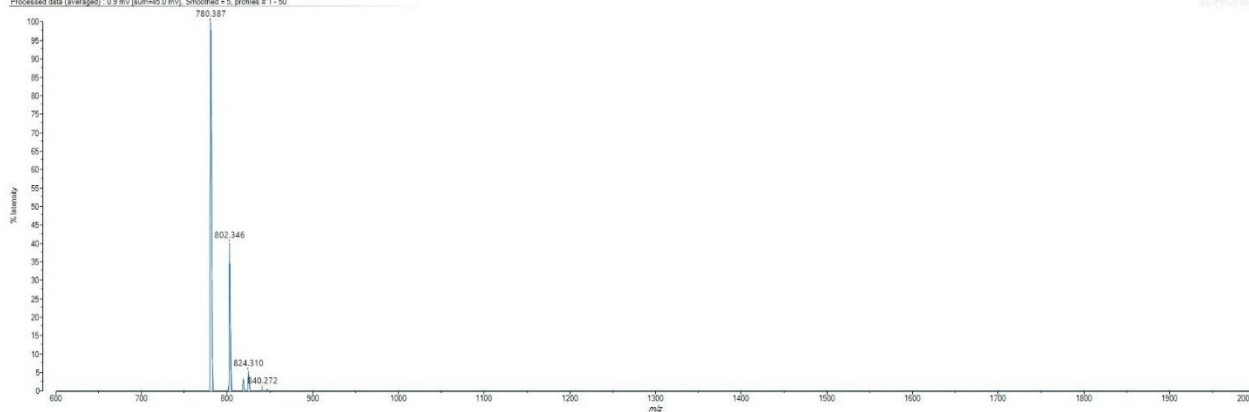
A 25 mL vessel of CEM discover bio manual peptide synthesizer was charged with 0.25 mmol of phenylalanine wang resin. The Fmoc group was removed by using a 20% piperidine solution in DMF (10 mL). Using Synergy software, the deprotection protocol was run. The piperidine solution was drained and the resin was washed with DMF (4 x 10 mL). Fmoc-L-threonine (5 eq, 1.25 mM) along with Oxyma (5 eq, 1.25 mM) and DIC (5 eq, 1.35 mmol) in DMF was added to the reaction vessel and the coupling protocol was run. The amino acid solution was drained, and the resin was washed with DMF (2 x 10 mL). The final amino acid was Fmoc deprotected as described before and was acetylated by agitating the resin for 1 hour in a solution of 5% acetic anhydride (0.5 mL), 8.5% DIEA (0.85 mL), and 86.5% DMF (8.65 mL). To remove the peptide from resin, a TFA cocktail solution (95% TFA, 2.5% TIPS, and 2.5% DCM) was added to the resin and agitated for 2 hours. The resin was filtered, and the resulting solution was concentrated in vacuo. The peptide was triturated with cold diethyl ether and purified using reverse phase HPLC using H<sub>2</sub>O/CH<sub>3</sub>CN. The sample was analyzed for purity using a Waters 1525 Binary HPLC Pump using a Phenomenex Luna 5u C8(2) 100A (250 x 4.60 mm) column; gradient eluted with H<sub>2</sub>O/CH<sub>3</sub>CN. Molecular weight was confirmed using high resolution electrospray ionization mass spectrometry (HRMS, ESI/MS) analyses obtained on an Agilent 6545B Q-TOF LC/MS equipped with 1260 infinity II LC system with auto sampler. The final peptide product was lyophilized and stored at -20°C until further use.



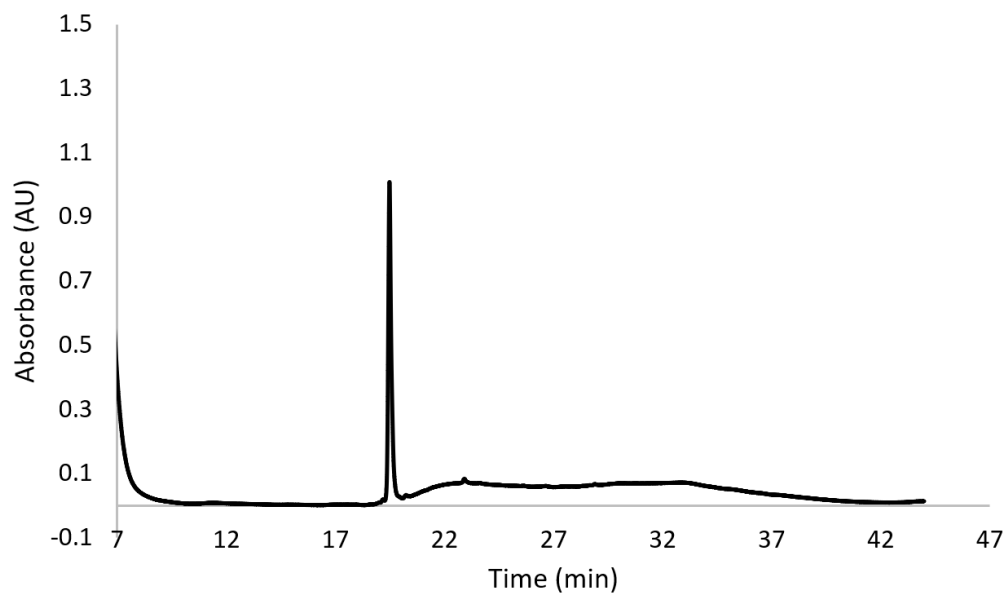
MALDI-TOF MS calculated [M]: 780.4450, found 780.387

Created By J8346; Data: New Acquisition 7:53; (Manual) April 17, 2024 12:15:07 PM Cal:Named Calibration "tof mix 4 16 24" by sen8q6q on April 16, 2024 1:21:19 PM (Original)  
 Shimadzu MALDI-8020; Tuning:Linear; Power:15; Ion Gate:Blanking; 600.00

Processed data (averaged): 0.9 mV (sum=45.0 mV); Smoothed = 5; profiles # 1 - 50



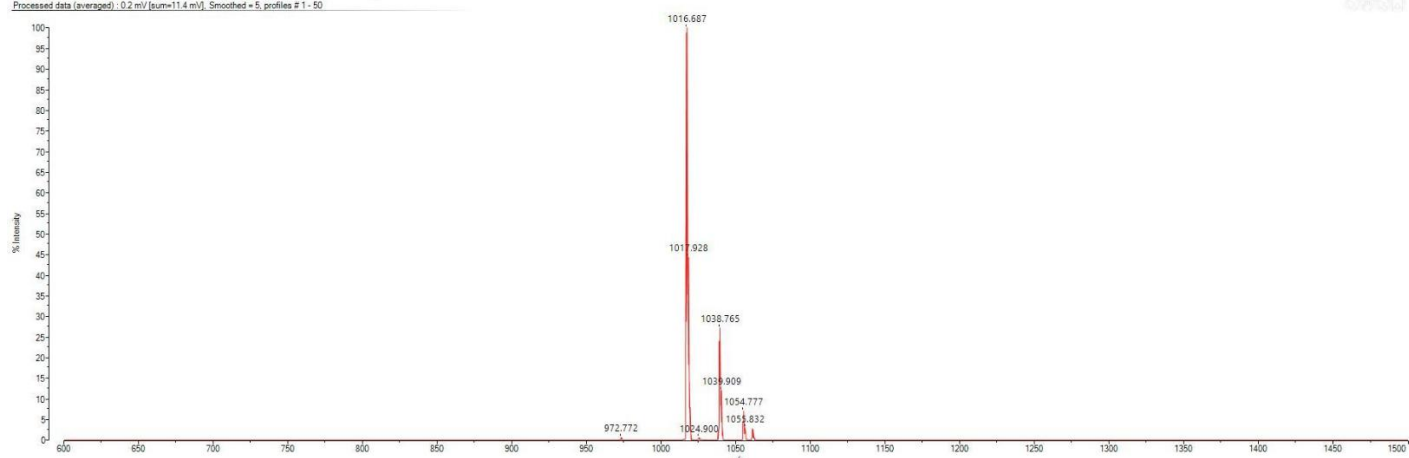




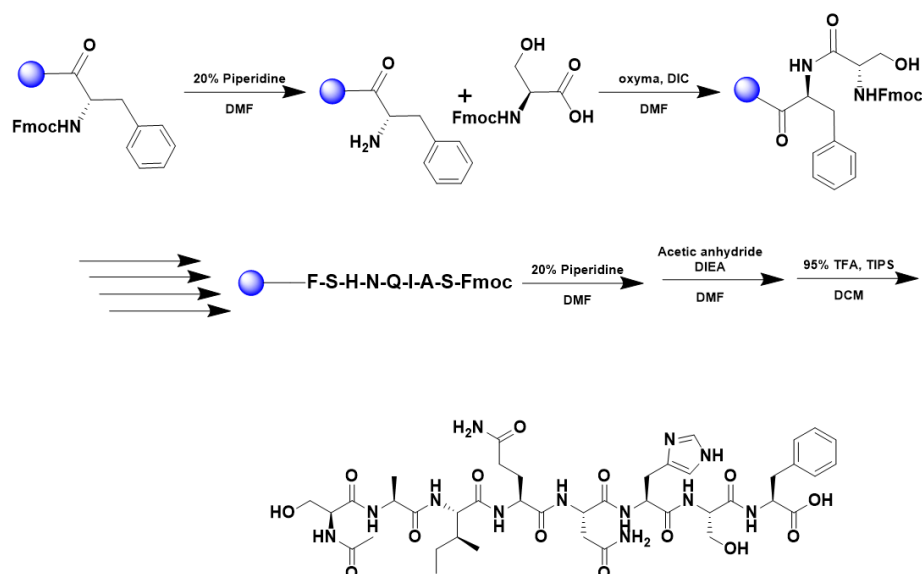
MALDI-TOF MS calculated [M]: 1016.4246, found 1016.687

Created By jk3uc. Data: New Acquisition 1A1\_1 (Manual) January 23, 2024 5:02:41 PM Cal: Named Calibration "tofmix 5 3 23" by jk3uc on May 2, 2023 1:06:09 PM (Original)  
Shimadzu MALDI-8020; Tuning Linear, Power 10, P.Ext at 1016.00 (bin 78), Ion Gate Blanking: 600.00

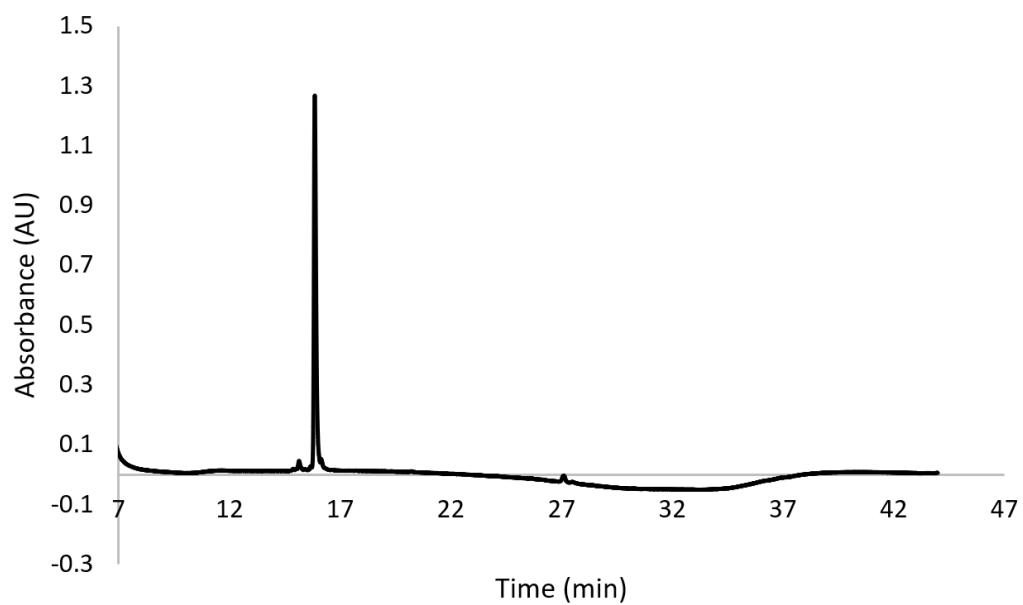
Processed data (averaged): 0.2 mL (sum=11.4 mV), Smoothed = 5, profiles # 1 - 50



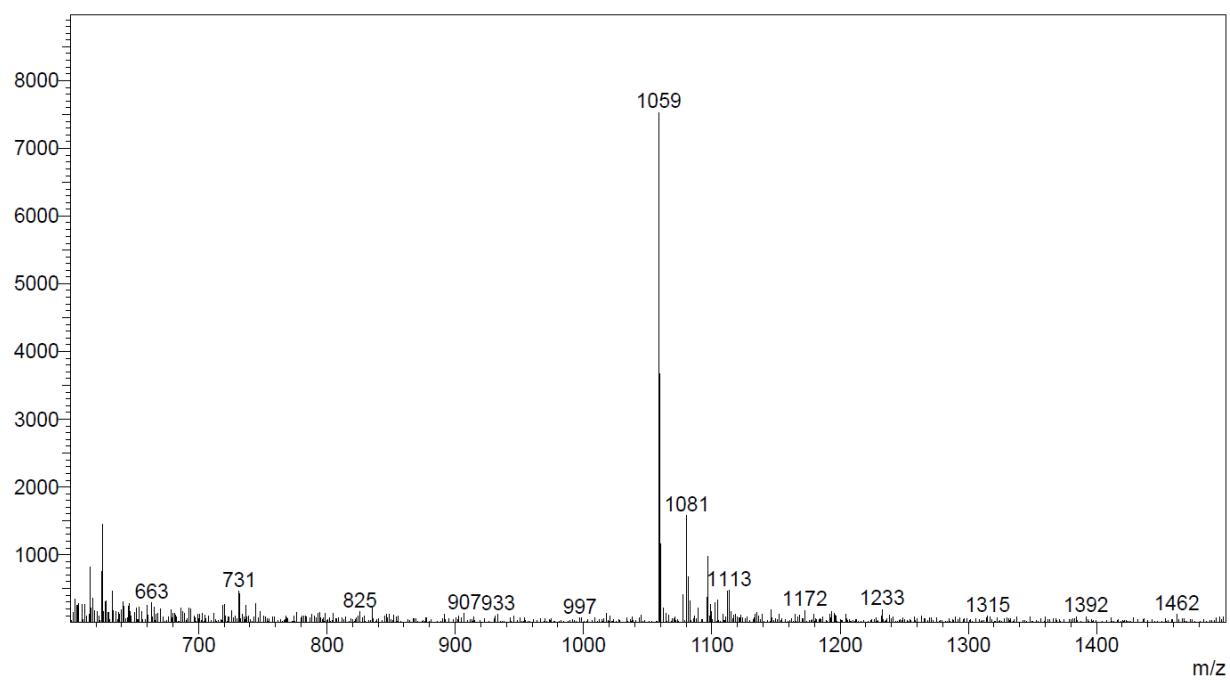
## Scheme S23. Synthesis of NAc-SAIQNHSF



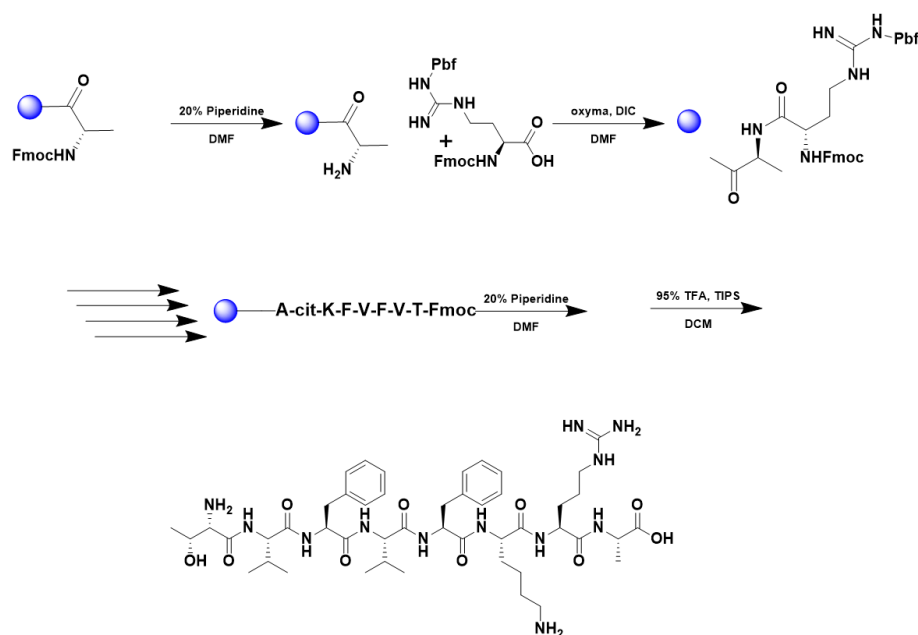
A 25 mL vessel of CEM discover bio manual peptide synthesizer was charged with 0.25 mmol of phenylalanine wang resin. The Fmoc group was removed by using a 20% piperidine solution in DMF (10 mL). Using Synergy software, the deprotection protocol was run. The piperidine solution was drained and the resin was washed with DMF (4 x 10 mL). Fmoc-L-serine-OH (5 eq, 1.25 mM) along with Oxyma (5 eq, 1.25 mM) and DIC (5 eq, 1.35 mmol) in DMF was added to the reaction vessel and the coupling protocol was run. The amino acid solution was drained, and the resin was washed with DMF (2 x 10 mL). The final amino acid was Fmoc deprotected as described before and was acetylated by agitating the resin for 1 hour in a solution of 5% acetic anhydride (0.5 mL), 8.5% DIEA (0.85 mL), and 86.5% DMF (8.65 mL). To remove the peptide from resin, a TFA cocktail solution (95% TFA, 2.5% TIPS, and 2.5% DCM) was added to the resin and agitated for 2 hours. The resin was filtered, and the resulting solution was concentrated in vacuo. The peptide was triturated with cold diethyl ether and purified using reverse phase HPLC using H<sub>2</sub>O/CH<sub>3</sub>CN. The sample was analyzed for purity using a Waters 1525 Binary HPLC Pump using a Phenomenex Luna 5u C8(2) 100A (250 x 4.60 mm) column; gradient eluted with H<sub>2</sub>O/CH<sub>3</sub>CN. Molecular weight was confirmed using high resolution electrospray ionization mass spectrometry (HRMS, ESI/MS) analyses obtained on an Agilent 6545B Q-TOF LC/MS equipped with 1260 infinity II LC system with auto sampler. The final peptide product was lyophilized and stored at -20°C until further use.



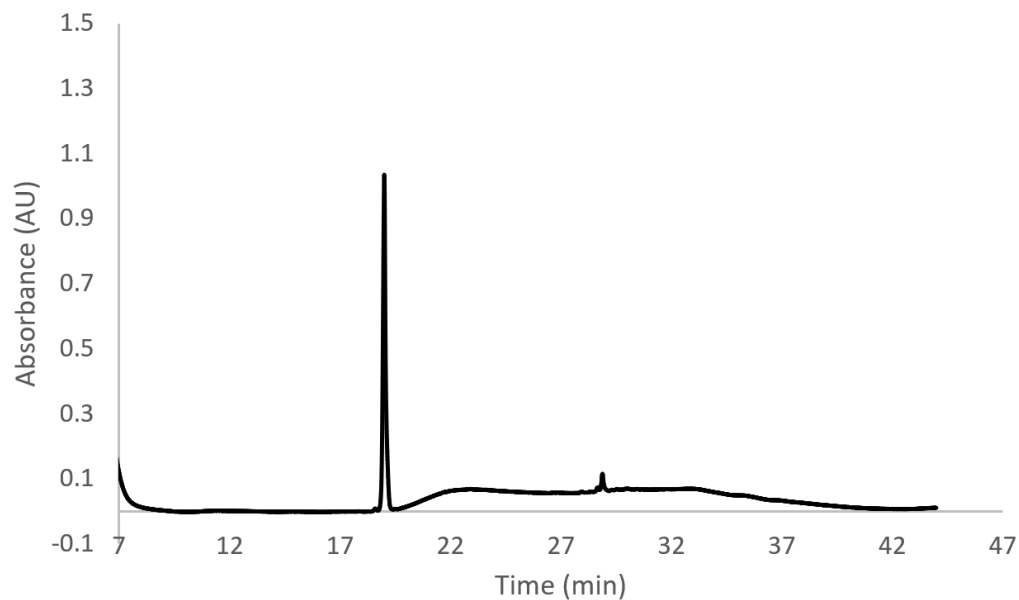
ESI-MS calculated [M]: 1059.4351, found 1059.



## Scheme S24. Synthesis of TVFVFKRA



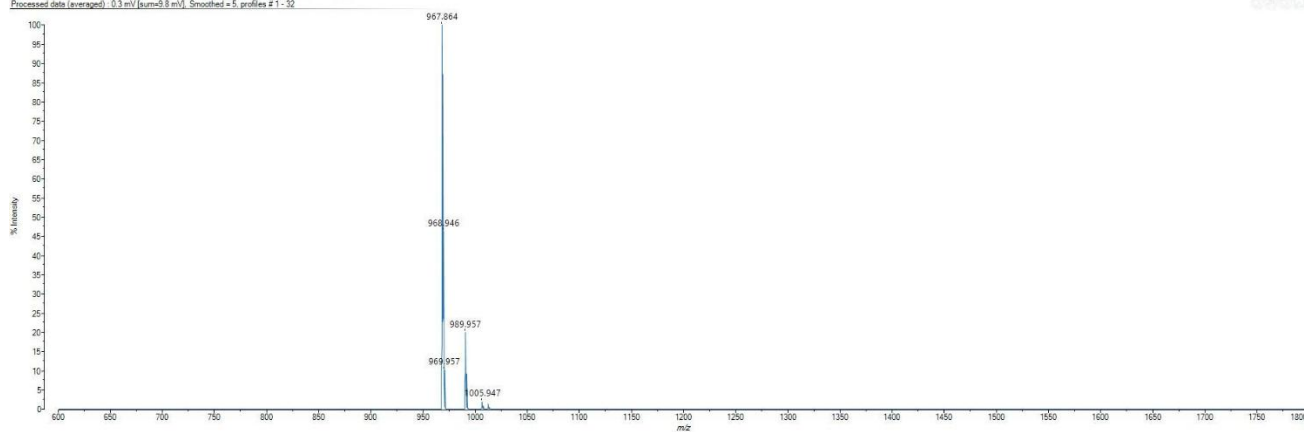
A 25 mL vessel of CEM discover bio manual peptide synthesizer was charged with 0.25 mmol of alanine wang resin. The Fmoc group was removed by using a 20% piperidine solution in DMF (10 mL). Using Synergy software, the deprotection protocol was run. The piperidine solution was drained and the resin was washed with DMF (4 x 10 mL). Fmoc-L-arginine(Pbf)-OH (5 eq, 1.25 mM) along with Oxyma (5 eq, 1.25 mM) and DIC (5 eq, 1.35 mmol) in DMF was added to the reaction vessel and the coupling protocol was run. The amino acid solution was drained, and the resin was washed with DMF (2 x 10 mL). The fmoc removal and coupling procedure was repeated as before using the same equivalencies for the remaining amino acids. To remove the peptide from resin, a TFA cocktail solution (95% TFA, 2.5% TIPS, and 2.5% DCM) was added to the resin and agitated for 2 hours. The resin was filtered, and the resulting solution was concentrated in vacuo. The peptide was triturated with cold diethyl ether and purified using reverse phase HPLC using H<sub>2</sub>O/CH<sub>3</sub>CN. The sample was analyzed for purity using a Waters 1525 Binary HPLC Pump using a Phenomenex Luna 5u C8(2) 100A (250 x 4.60 mm) column; gradient eluted with H<sub>2</sub>O/CH<sub>3</sub>CN. Molecular weight was confirmed using high resolution electrospray ionization mass spectrometry (HRMS, ESI/MS) analyses obtained on an Agilent 6545B Q-TOF LC/MS equipped with 1260 infinity II LC system with auto sampler. The final peptide product was lyophilized and stored at -20°C until further use.



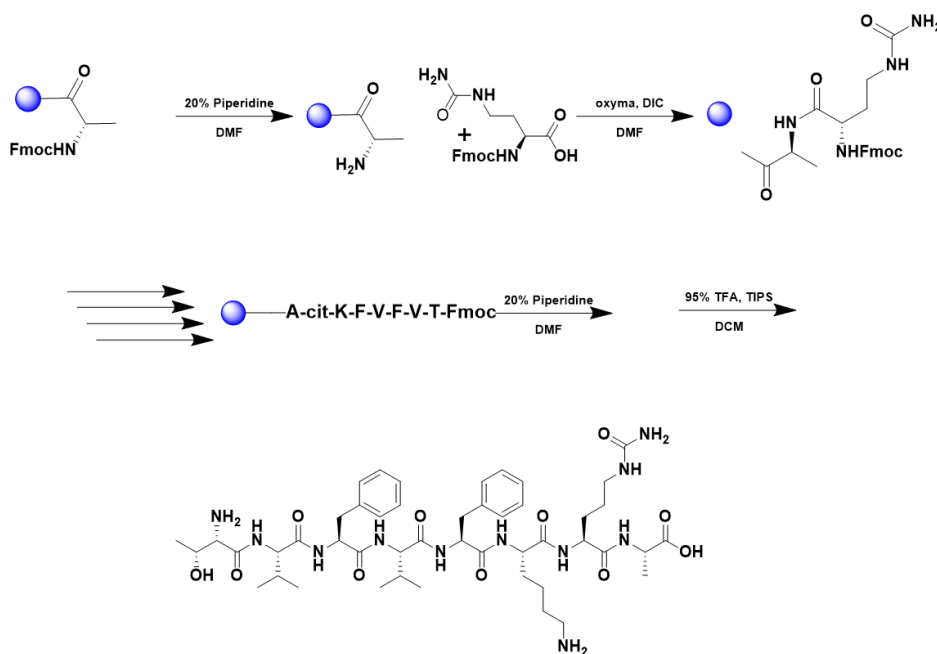
MALDI-TOF MS calculated [M]: 967.5651, found 967.864

Created By jk3uc, Date: New Acquisition 2.11\_Manual January 18, 2024 5:21:51 PM Cal Name: Calibration "tofmix 5.3.23" by jk3uc on May 2, 2023 1:06:09 PM (Original)  
Shimadzu MALDI-6020: Tuning Linear, Power 10, P.Ext at 966.00 (bin 76), Ion Gate Blanking: 600.00

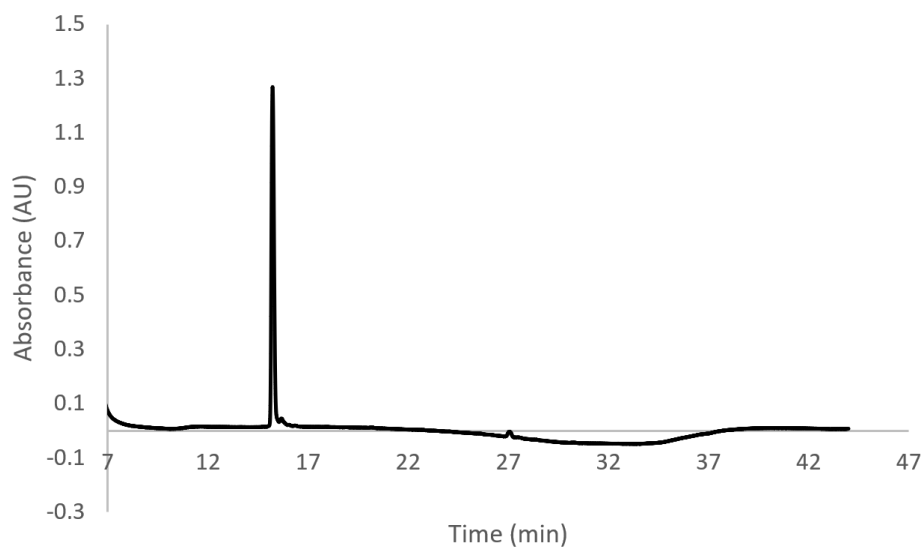
Processed data (averaged): 0.3 mV (sum=9.8 mV), Smoothed = 5, profiles # 1 - 32



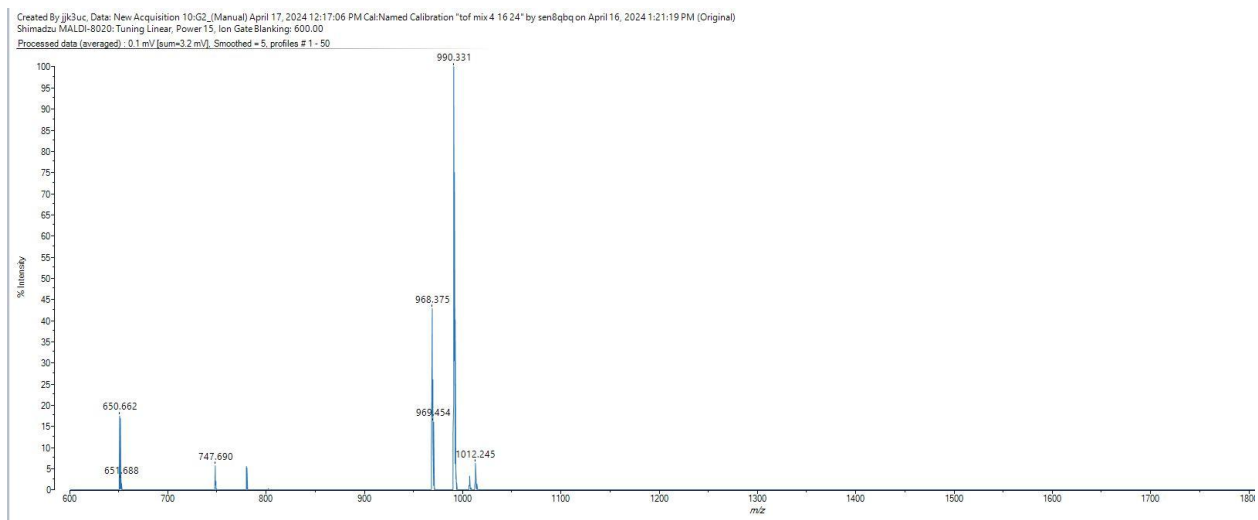
## Scheme S25. Synthesis of TVFVFK(cit)A



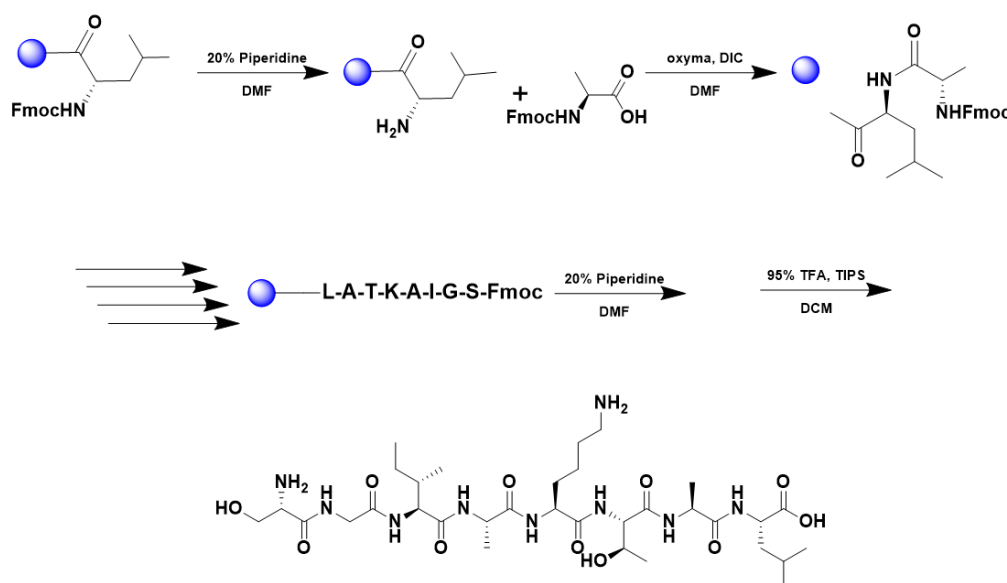
A 25 mL vessel of CEM discover bio manual peptide synthesizer was charged with 0.25 mmol of alanine wang resin. The Fmoc group was removed by using a 20% piperidine solution in DMF (10 mL). Using Synergy software, the deprotection protocol was run. The piperidine solution was drained and the resin was washed with DMF (4 x 10 mL). Fmoc-L-citrulline (5 eq, 1.25 mM) along with Oxyma (5 eq, 1.25 mM) and DIC (5 eq, 1.35 mmol) in DMF was added to the reaction vessel and the coupling protocol was run. The amino acid solution was drained, and the resin was washed with DMF (2 x 10 mL). The fmoc removal and coupling procedure was repeated as before using the same equivalencies for the remaining amino acids. To remove the peptide from resin, a TFA cocktail solution (95% TFA, 2.5% TIPS, and 2.5% DCM) was added to the resin and agitated for 2 hours. The resin was filtered, and the resulting solution was concentrated in vacuo. The peptide was triturated with cold diethyl ether and purified using reverse phase HPLC using H<sub>2</sub>O/CH<sub>3</sub>CN. The sample was analyzed for purity using a Waters 1525 Binary HPLC Pump using a Phenomenex Luna 5u C8(2) 100A (250 x 4.60 mm) column; gradient eluted with H<sub>2</sub>O/CH<sub>3</sub>CN. Molecular weight was confirmed using high resolution electrospray ionization mass spectrometry (HRMS, ESI/MS) analyses obtained on an Agilent 6545B Q-TOF LC/MS equipped with 1260 infinity II LC system with auto sampler. The final peptide product was lyophilized and stored at -20°C until further use.



MALDI-TOF MS calculated [M]: 968.5525, found 968.375



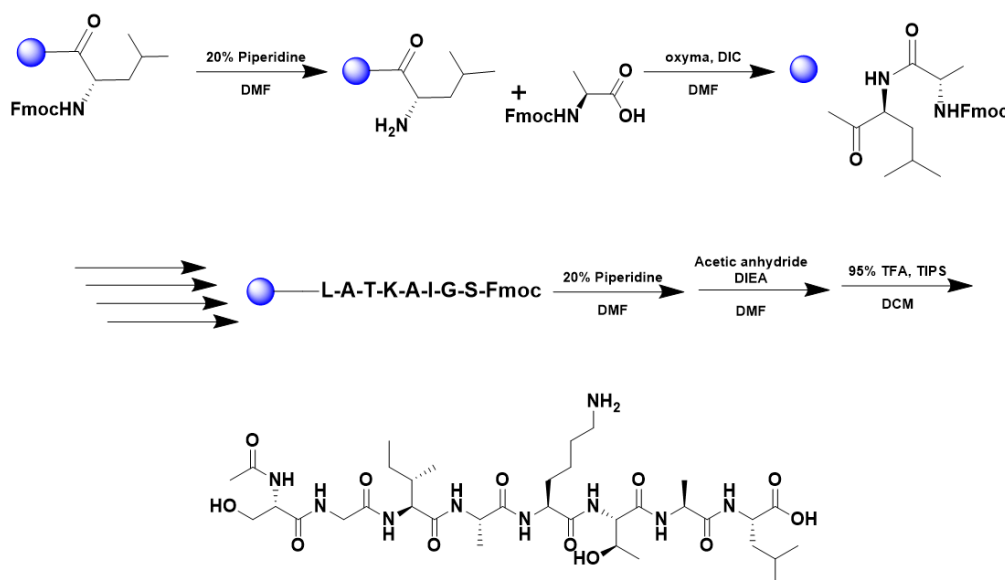
## Scheme S26. Synthesis of SGIAKTAL



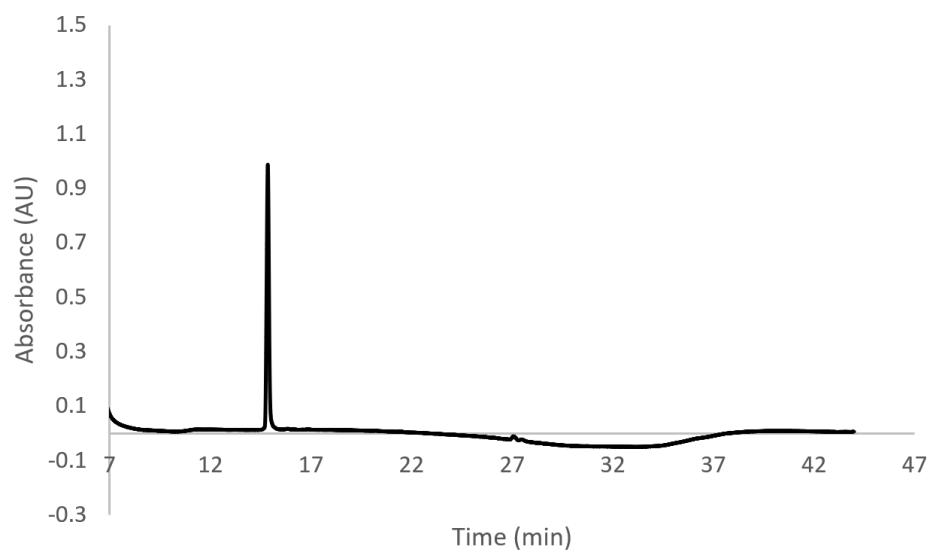
A 25 mL vessel of CEM discover bio manual peptide synthesizer was charged with 0.25 mmol of isoleucine wang resin. The Fmoc group was removed by using a 20% piperidine solution in DMF (10 mL). Using Synergy software, the deprotection protocol was run. The piperidine solution was drained and the resin was washed with DMF (4 x 10 mL). Fmoc-L-alanine (5 eq, 1.25 mM) along with Oxyma (5 eq, 1.25 mM) and DIC (5 eq, 1.35 mmol) in DMF was added to the reaction vessel and the coupling protocol was run. The amino acid solution was drained, and the resin was washed with DMF (2 x 10 mL). The fmoc removal and coupling procedure was repeated as before using the same equivalencies for the remaining amino acids. To remove the peptide from resin, a TFA cocktail solution (95% TFA, 2.5% TIPS, and 2.5% DCM) was added to the resin and agitated for 2 hours. The resin was filtered, and the resulting solution was concentrated in vacuo. The peptide was triturated with cold diethyl ether and purified using reverse phase HPLC using H<sub>2</sub>O/CH<sub>3</sub>CN. The sample was analyzed for purity using a Waters 1525 Binary HPLC Pump using a Phenomenex Luna 5u C8(2) 100A (250 x 4.60 mm) column; gradient eluted with H<sub>2</sub>O/CH<sub>3</sub>CN. Molecular weight was confirmed using high resolution electrospray ionization mass spectrometry (HRMS, ESI/MS) analyses obtained on an Agilent 6545B Q-TOF LC/MS equipped with 1260 infinity II LC system with auto sampler. The final peptide product was lyophilized and stored at -20°C until further use.



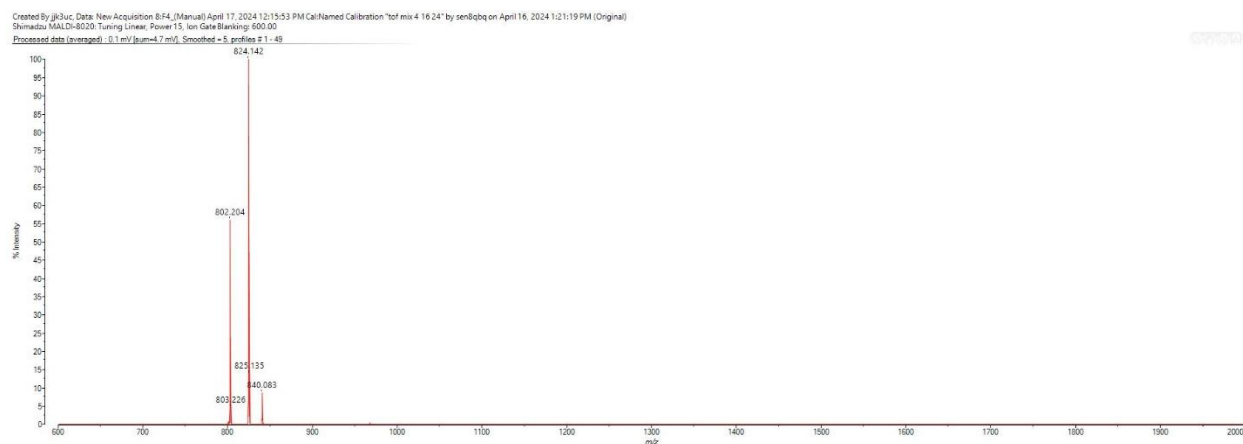
## Scheme S27. Synthesis of SGIA(Kac)TAL



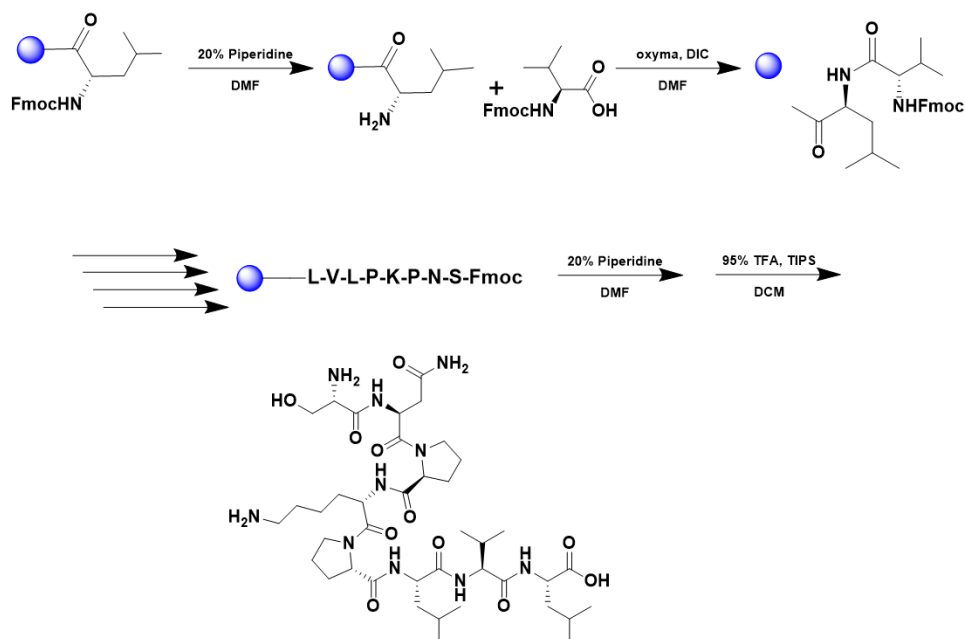
A 25 mL vessel of CEM discover bio manual peptide synthesizer was charged with 0.25 mmol of isoleucine wang resin. The Fmoc group was removed by using a 20% piperidine solution in DMF (10 mL). Using Synergy software, the deprotection protocol was run. The piperidine solution was drained and the resin was washed with DMF (4 x 10 mL). Fmoc-L-alanine (5 eq, 1.25 mM) along with Oxyma (5 eq, 1.25 mM) and DIC (5 eq, 1.35 mmol) in DMF was added to the reaction vessel and the coupling protocol was run. The amino acid solution was drained, and the resin was washed with DMF (2 x 10 mL). The fmoc removal and coupling procedure was repeated as before using the same equivalencies for the remaining amino acids. To remove the peptide from resin, a TFA cocktail solution (95% TFA, 2.5% TIPS, and 2.5% DCM) was added to the resin and agitated for 2 hours. The resin was filtered, and the resulting solution was concentrated in vacuo. The peptide was triturated with cold diethyl ether and purified using reverse phase HPLC using H<sub>2</sub>O/CH<sub>3</sub>CN. The sample was analyzed for purity using a Waters 1525 Binary HPLC Pump using a Phenomenex Luna 5u C8(2) 100A (250 x 4.60 mm) column; gradient eluted with H<sub>2</sub>O/CH<sub>3</sub>CN. Molecular weight was confirmed using high resolution electrospray ionization mass spectrometry (HRMS, ESI/MS) analyses obtained on an Agilent 6545B Q-TOF LC/MS equipped with 1260 infinity II LC system with auto sampler. The final peptide product was lyophilized and stored at -20°C until further use.



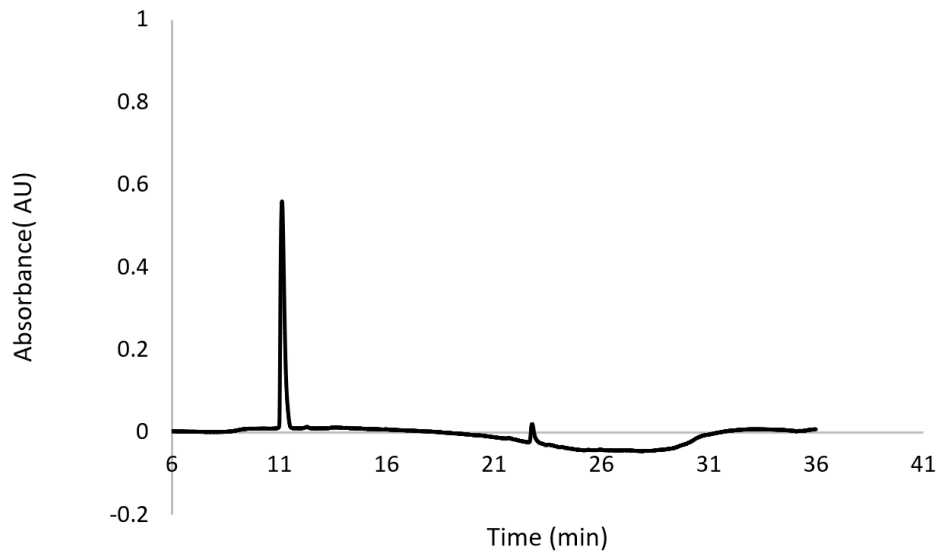
MALDI-TOF MS calculated [M]: 802.4669, found 802.204



## Scheme S28. Synthesis of SNPKPLVL

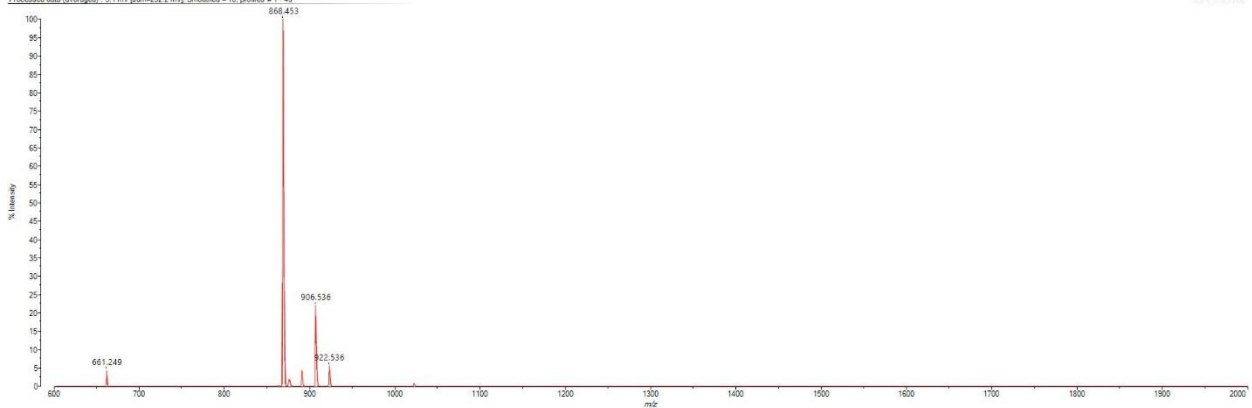


A 25 mL vessel of CEM discover bio manual peptide synthesizer was charged with 0.25 mmol of leucine wang resin. The Fmoc group was removed by using a 20% piperidine solution in DMF (10 mL). Using Synergy software, the deprotection protocol was run. The piperidine solution was drained and the resin was washed with DMF (4 x 10 mL). Fmoc-L-valine (5 eq, 1.25 mM) along with Oxyma (5 eq, 1.25 mM) and DIC (5 eq, 1.35 mmol) in DMF was added to the reaction vessel and the coupling protocol was run. The amino acid solution was drained, and the resin was washed with DMF (2 x 10 mL). The fmoc removal and coupling procedure was repeated as before using the same equivalencies for the remaining amino acids. To remove the peptide from resin, a TFA cocktail solution (95% TFA, 2.5% TIPS, and 2.5% DCM) was added to the resin and agitated for 2 hours. The resin was filtered, and the resulting solution was concentrated in vacuo. The peptide was triturated with cold diethyl ether and purified using reverse phase HPLC using H<sub>2</sub>O/CH<sub>3</sub>CN. The sample was analyzed for purity using a Waters 1525 Binary HPLC Pump using a Phenomenex Luna 5u C8(2) 100A (250 x 4.60 mm) column; gradient eluted with H<sub>2</sub>O/CH<sub>3</sub>CN. Molecular weight was confirmed using high resolution electrospray ionization mass spectrometry (HRMS, ESI/MS) analyses obtained on an Agilent 6545B Q-TOF LC/MS equipped with 1260 infinity II LC system with auto sampler. The final peptide product was lyophilized and stored at -20°C until further use.

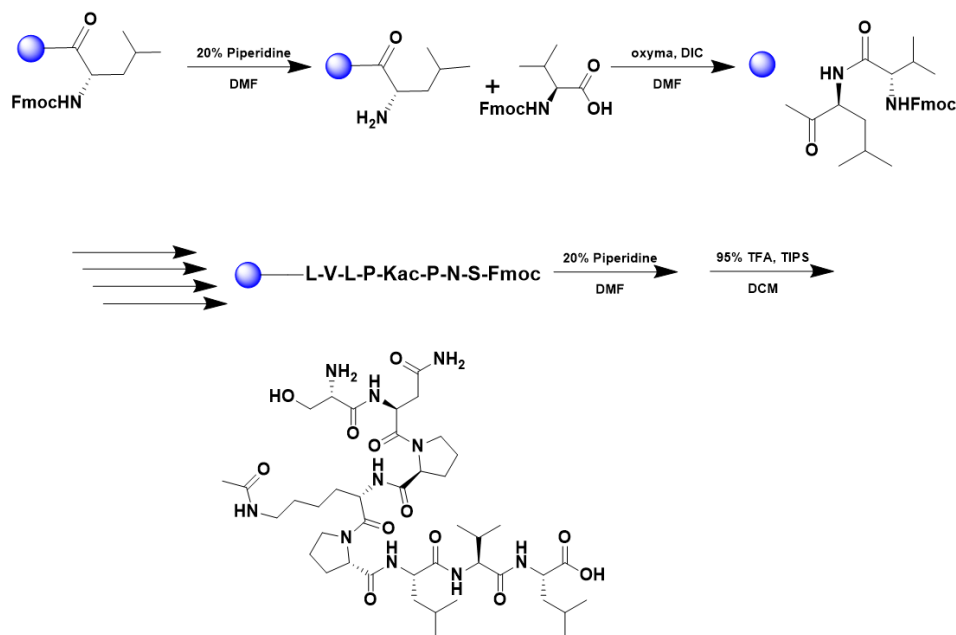


MALDI-TOF MS calculated [M]: 867.5299, found 868.453

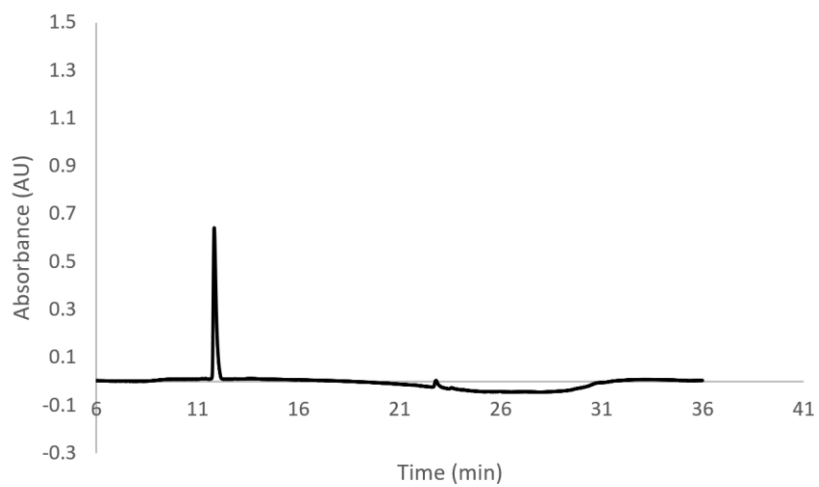
Created By sen@sqz\_Data: New Acquisition 313 (Manual) April 12, 2024 5:01:39 PM Cal: Named Calibration "ToF Mix with Matrix" by Engineer on May 18, 2022 12:45:32 PM (Original)  
 Shimadzu MALDI-2020; Tuning Linear; Power 9; P Ext at 943.00 (bin 75); Ion Gate Blanking: 600.00  
 Processed data (averaged) - 5.1 mL (pH=2.2 mV), Smoothed = 10, profiles # 1 - 49



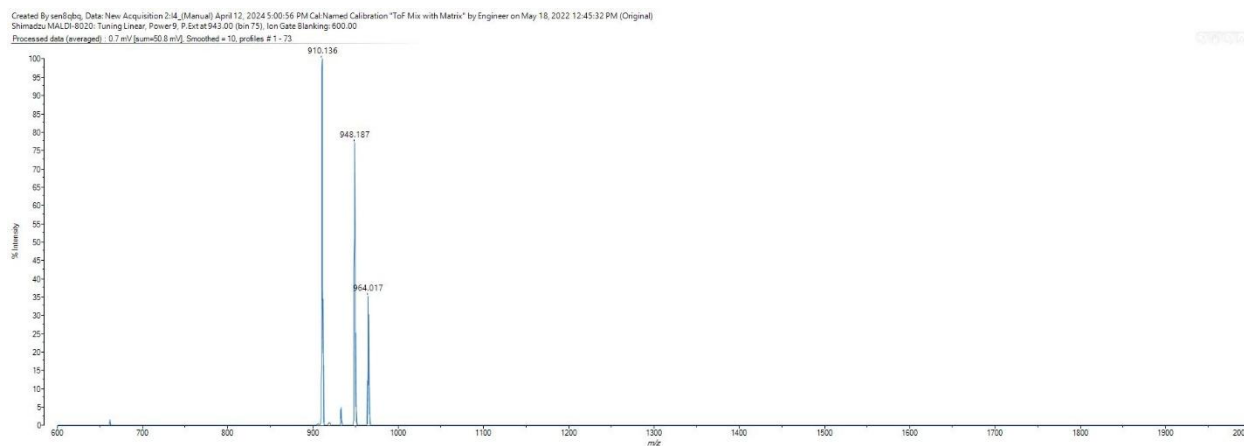
## Scheme S29. Synthesis of SNP(Kac)PLVL



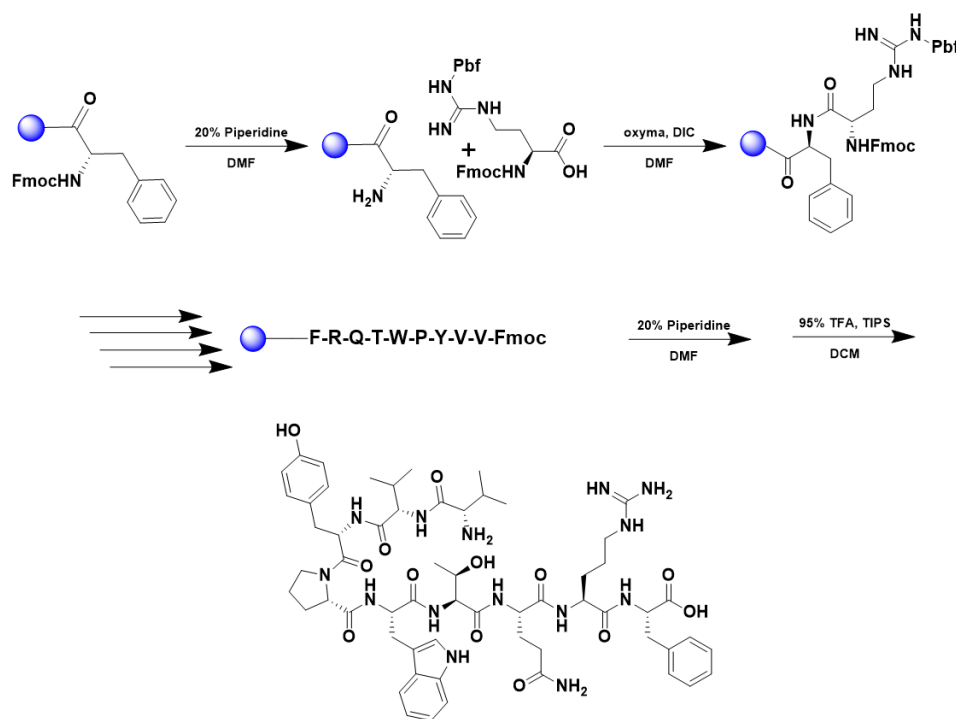
A 25 mL vessel of CEM discover bio manual peptide synthesizer was charged with 0.25 mmol of leucine wang resin. The Fmoc group was removed by using a 20% piperidine solution in DMF (10 mL). Using Synergy software, the deprotection protocol was run. The piperidine solution was drained and the resin was washed with DMF (4 x 10 mL). Fmoc-L-valine (5 eq, 1.25 mM) along with Oxyma (5 eq, 1.25 mM) and DIC (5 eq, 1.35 mmol) in DMF was added to the reaction vessel and the coupling protocol was run. The amino acid solution was drained, and the resin was washed with DMF (2 x 10 mL). The fmoc removal and coupling procedure was repeated as before using the same equivalencies for the remaining amino acids. To remove the peptide from resin, a TFA cocktail solution (95% TFA, 2.5% TIPS, and 2.5% DCM) was added to the resin and agitated for 2 hours. The resin was filtered, and the resulting solution was concentrated in vacuo. The peptide was triturated with cold diethyl ether and purified using reverse phase HPLC using H<sub>2</sub>O/CH<sub>3</sub>CN. The sample was analyzed for purity using a Waters 1525 Binary HPLC Pump using a Phenomenex Luna 5u C8(2) 100A (250 x 4.60 mm) column; gradient eluted with H<sub>2</sub>O/CH<sub>3</sub>CN. Molecular weight was confirmed using high resolution electrospray ionization mass spectrometry (HRMS, ESI/MS) analyses obtained on an Agilent 6545B Q-TOF LC/MS equipped with 1260 infinity II LC system with auto sampler. The final peptide product was lyophilized and stored at -20°C until further use.



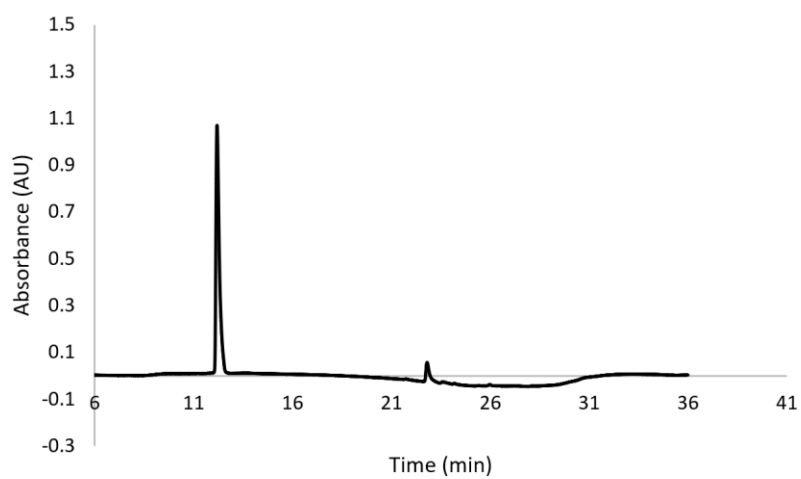
MALDI-TOF MS calculated [M]: 911.5190, found 910.136



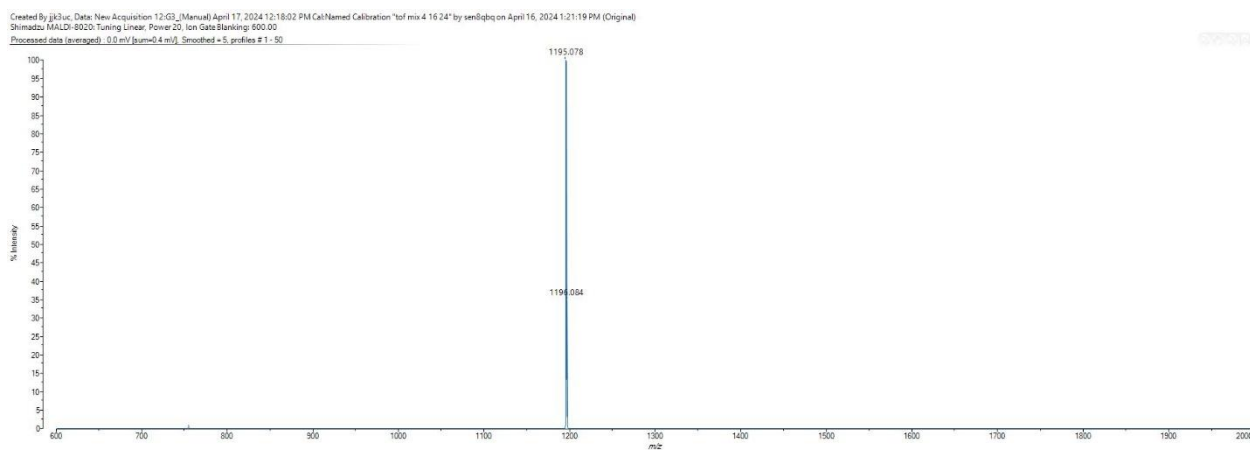
## Scheme S30. Synthesis of VVYPWTQRF



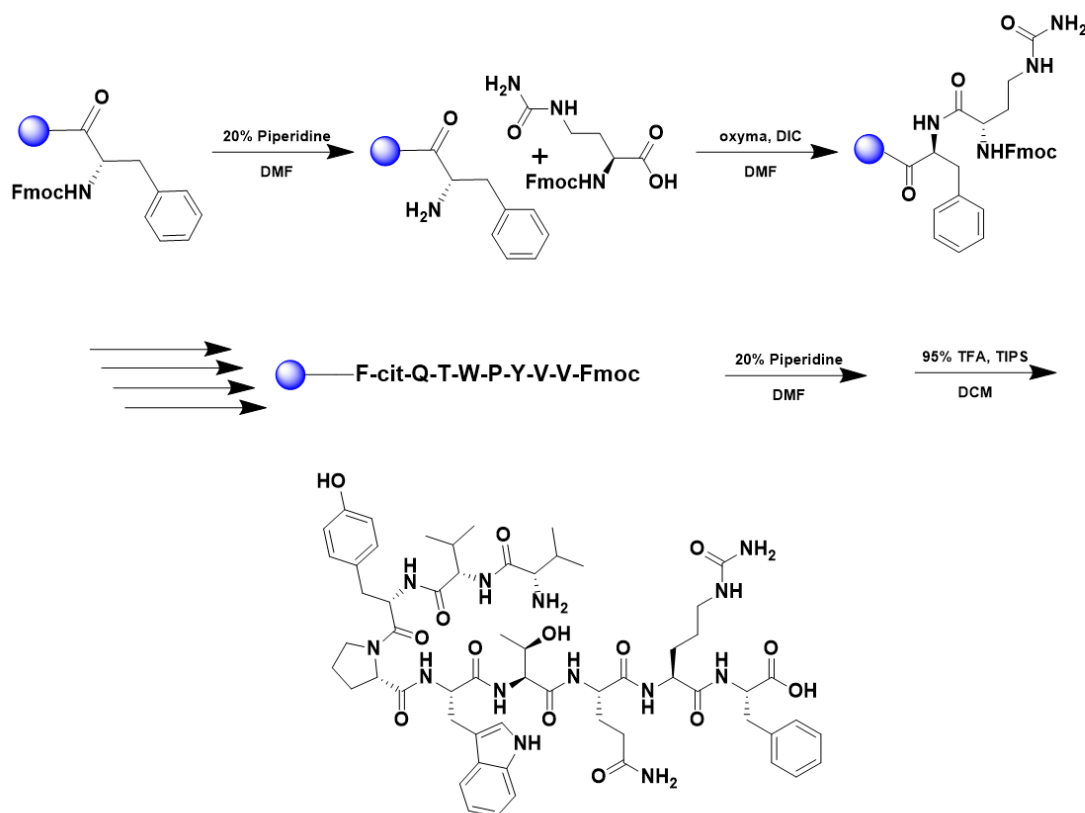
A 25 mL vessel of CEM discover bio manual peptide synthesizer was charged with 0.25 mmol of phenylalanine wang resin. The Fmoc group was removed by using a 20% piperidine solution in DMF (10 mL). Using Synergy software, the deprotection protocol was run. The piperidine solution was drained and the resin was washed with DMF (4 x 10 mL). Fmoc-L-arginine(Pbf)-OH (5 eq, 1.25 mM) along with Oxyma (5 eq, 1.25 mM) and DIC (5 eq, 1.35 mmol) in DMF was added to the reaction vessel and the coupling protocol was run. The amino acid solution was drained, and the resin was washed with DMF (2 x 10 mL). The fmoc removal and coupling procedure was repeated as before using the same equivalencies for the remaining amino acids. To remove the peptide from resin, a TFA cocktail solution (95% TFA, 2.5% TIPS, and 2.5% DCM) was added to the resin and agitated for 2 hours. The resin was filtered, and the resulting solution was concentrated in vacuo. The peptide was triturated with cold diethyl ether and purified using reverse phase HPLC using H<sub>2</sub>O/CH<sub>3</sub>CN. The sample was analyzed for purity using a Waters 1525 Binary HPLC Pump using a Phenomenex Luna 5u C8(2) 100A (250 x 4.60 mm) column; gradient eluted with H<sub>2</sub>O/CH<sub>3</sub>CN. Molecular weight was confirmed using high resolution electrospray ionization mass spectrometry (HRMS, ESI/MS) analyses obtained on an Agilent 6545B Q-TOF LC/MS equipped with 1260 infinity II LC system with auto sampler. The final peptide product was lyophilized and stored at -20°C until further use.



MALDI-TOF MS calculated [M]: 1195.6259, found 1195.078

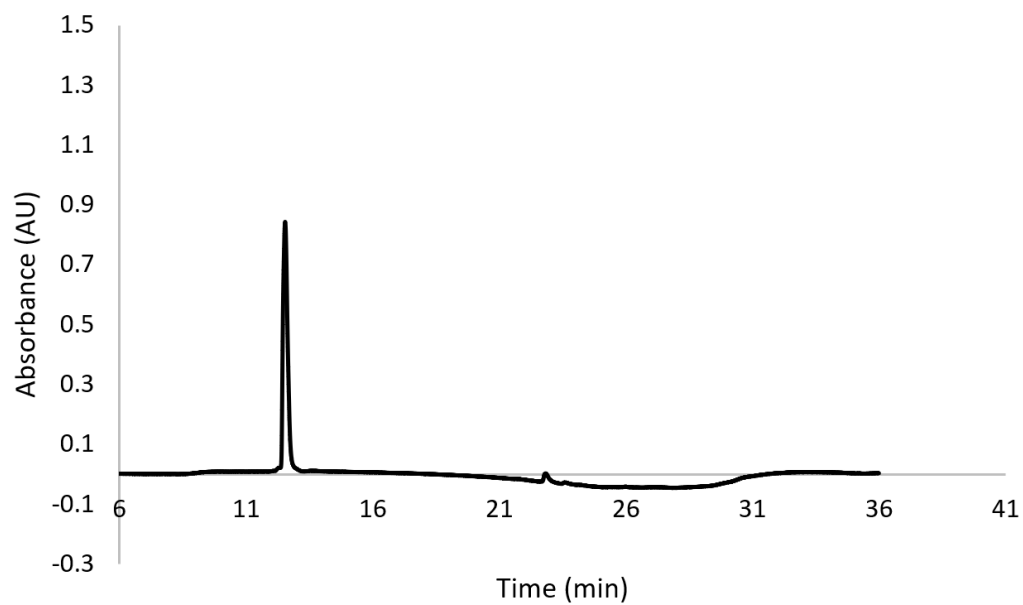


## Scheme S31. Synthesis of VVYPWTQ(cit)F

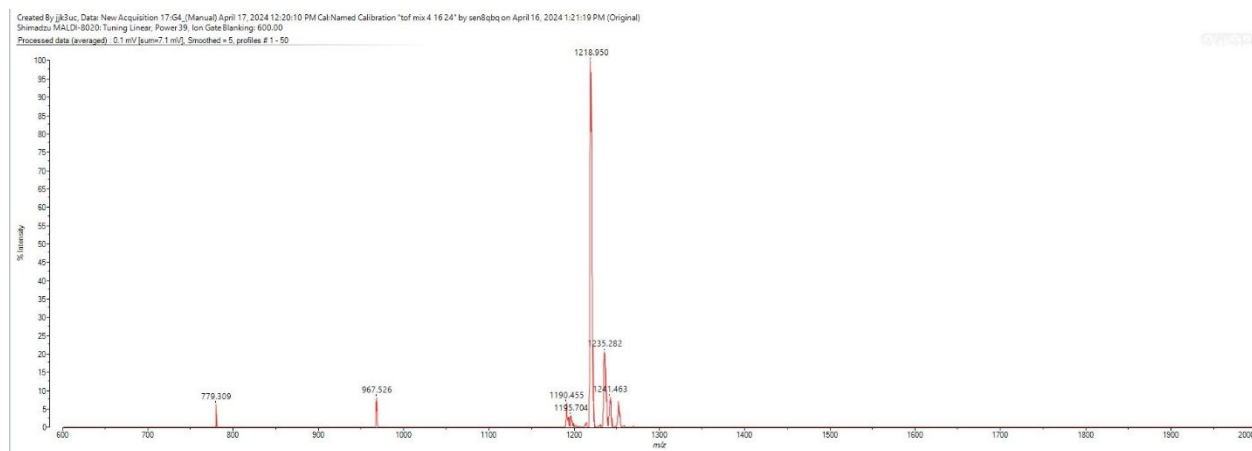


A 25 mL vessel of CEM discover bio manual peptide synthesizer was charged with 0.25 mmol of phenylalanine wang resin. The Fmoc group was removed by using a 20% piperidine solution in DMF (10 mL). Using Synergy software, the deprotection protocol was run. The piperidine solution was drained and the resin was washed with DMF (4 x 10 mL). Fmoc-L-citrulline (5 eq, 1.25 mM) along with Oxyma (5 eq, 1.25 mM) and DIC (5 eq, 1.35 mmol) in DMF was added to the reaction vessel and the coupling protocol was run. The amino acid solution was drained, and the resin was washed with DMF (2 x 10 mL). The fmoc removal and coupling procedure was repeated as before using the same equivalencies for the remaining amino acids. To remove the peptide from resin, a TFA cocktail solution (95% TFA, 2.5% TIPS, and 2.5% DCM) was added to the resin and agitated for 2 hours. The resin was filtered, and the resulting solution was concentrated in vacuo. The peptide was triturated with cold diethyl ether and purified using reverse phase HPLC using H<sub>2</sub>O/CH<sub>3</sub>CN. The sample was analyzed for purity using a Waters 1525 Binary HPLC Pump using a Phenomenex Luna 5u C8(2) 100A (250 x 4.60 mm) column; gradient eluted with H<sub>2</sub>O/CH<sub>3</sub>CN. Molecular weight was confirmed using high resolution electrospray ionization mass spectrometry (HRMS, ESI/MS) analyses obtained on an Agilent 6545B Q-TOF LC/MS equipped with 1260 infinity II LC system

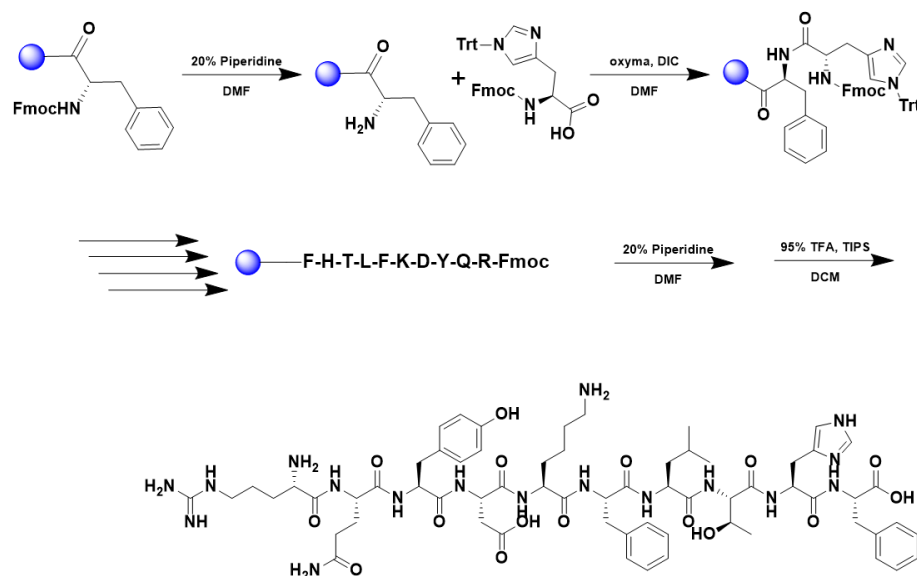
with auto sampler. The final peptide product was lyophilized and stored at  $-20^{\circ}\text{C}$  until further use.



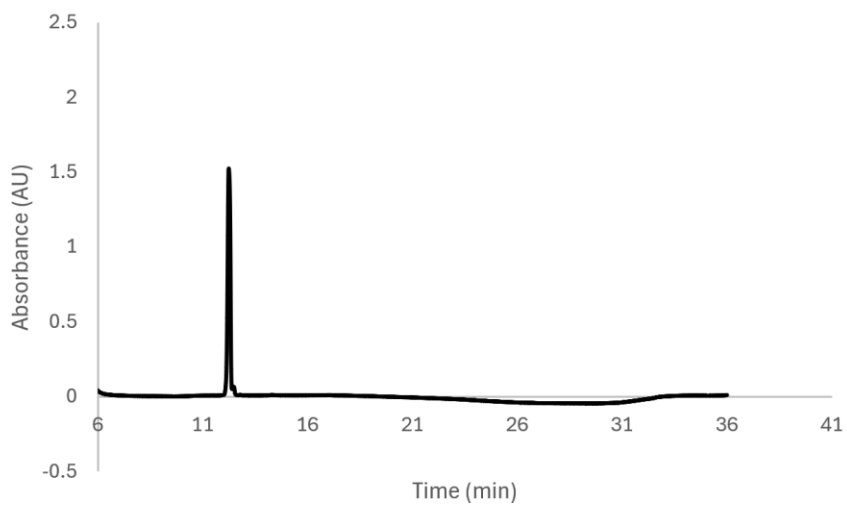
MALDI-TOF MS calculated [M]: 1196.6099, found 1195.704



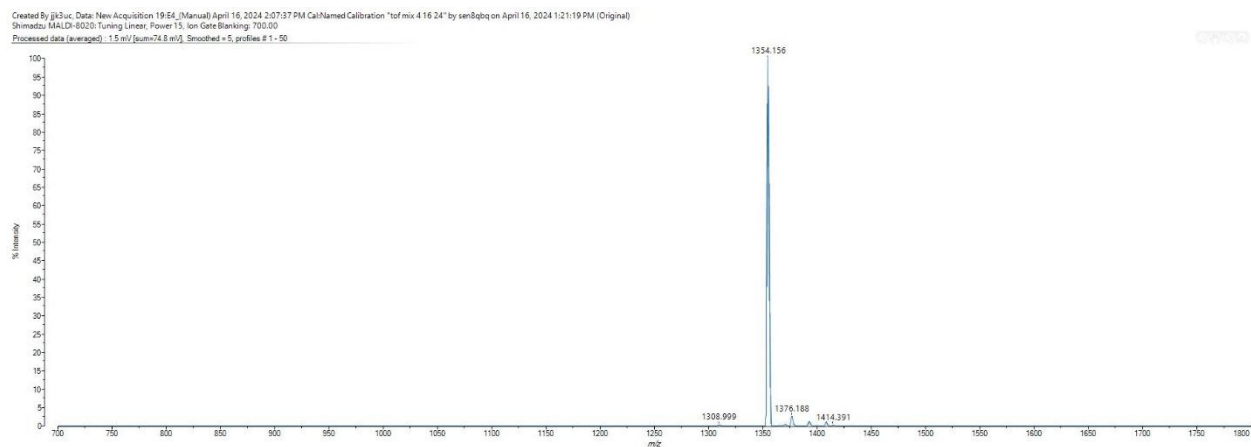
## Scheme S32. Synthesis of RQYDKFLTHF



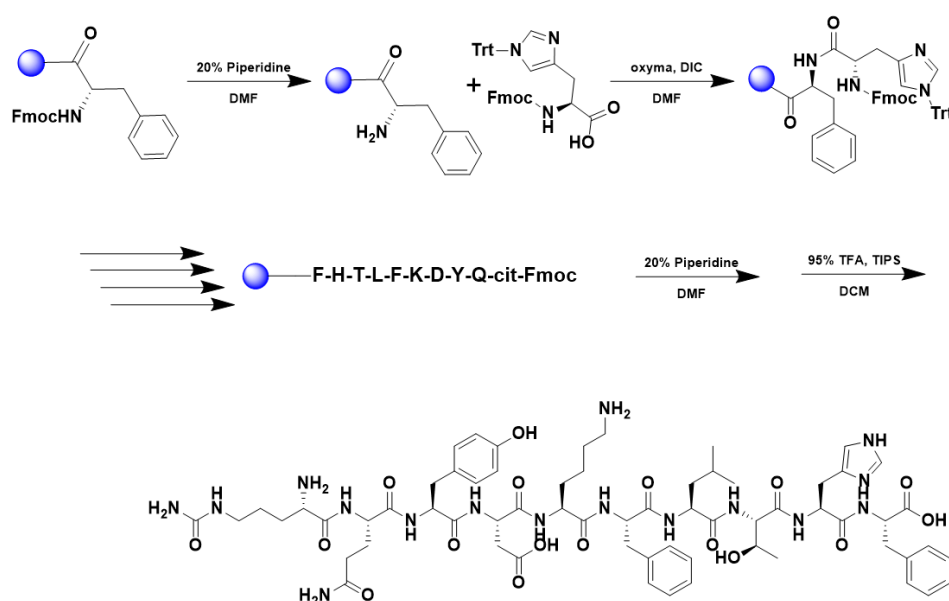
A 25 mL vessel of CEM discover bio manual peptide synthesizer was charged with 0.25 mmol of phenylalanine wang resin. The Fmoc group was removed by using a 20% piperidine solution in DMF (10 mL). Using Synergy software, the deprotection protocol was run. The piperidine solution was drained and the resin was washed with DMF (4 x 10 mL). Fmoc-L-histidine(Trt)-OH (5 eq, 1.25 mM) along with Oxyma (5 eq, 1.25 mM) and DIC (5 eq, 1.35 mmol) in DMF was added to the reaction vessel and the coupling protocol was run. The amino acid solution was drained, and the resin was washed with DMF (2 x 10 mL). The fmoc removal and coupling procedure was repeated as before using the same equivalencies for the remaining amino acids. To remove the peptide from resin, a TFA cocktail solution (95% TFA, 2.5% TIPS, and 2.5% DCM) was added to the resin and agitated for 2 hours. The resin was filtered, and the resulting solution was concentrated in vacuo. The peptide was triturated with cold diethyl ether and purified using reverse phase HPLC using H<sub>2</sub>O/CH<sub>3</sub>CN. The sample was analyzed for purity using a Waters 1525 Binary HPLC Pump using a Phenomenex Luna 5u C8(2) 100A (250 x 4.60 mm) column; gradient eluted with H<sub>2</sub>O/CH<sub>3</sub>CN. Molecular weight was confirmed using high resolution electrospray ionization mass spectrometry (HRMS, ESI/MS) analyses obtained on an Agilent 6545B Q-TOF LC/MS equipped with 1260 infinity II LC system with auto sampler. The final peptide product was lyophilized and stored at -20°C until further use.



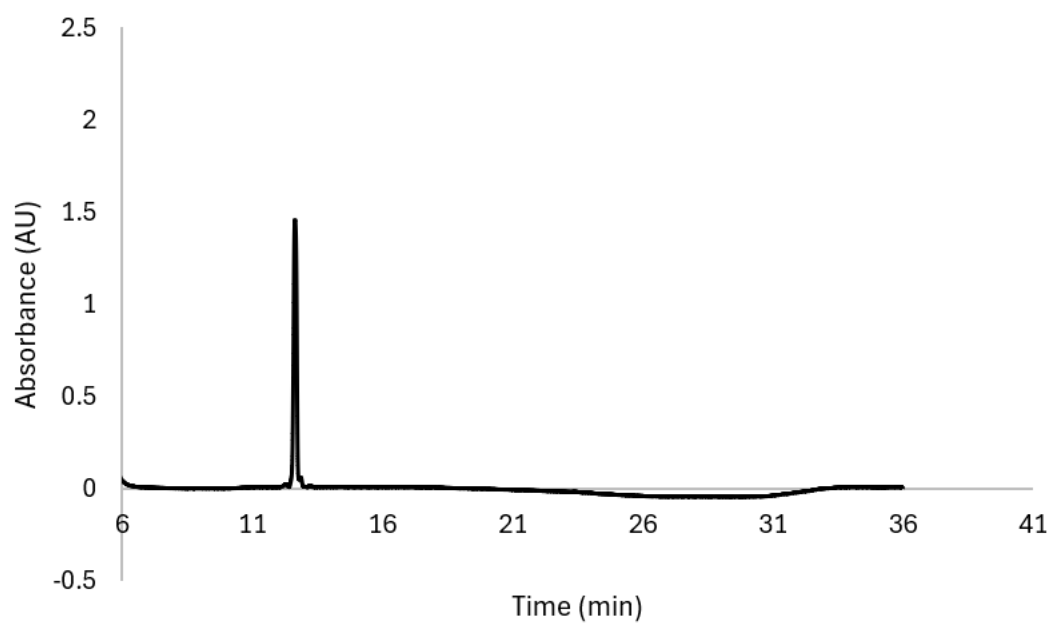
MALDI-TOF MS calculated [M]: 1354.6903, found 1354.156



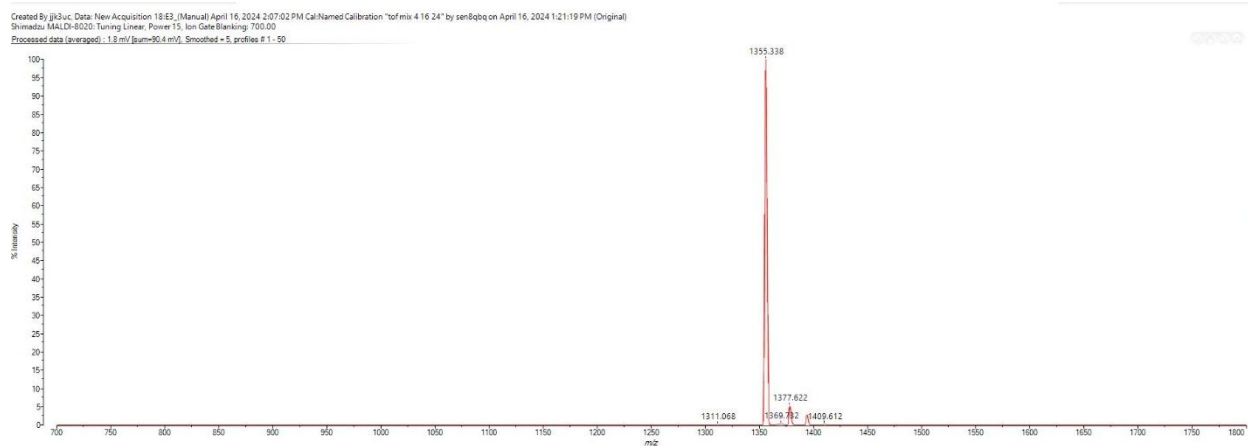
## Scheme S33. Synthesis of citQYDKFLTHF



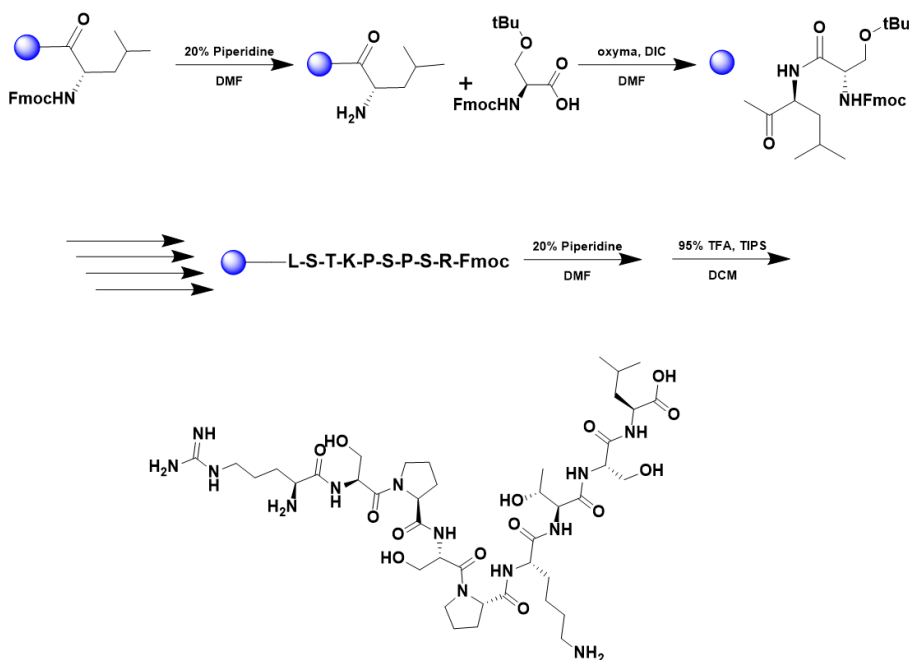
A 25 mL vessel of CEM discover bio manual peptide synthesizer was charged with 0.25 mmol of phenylalanine wang resin. The Fmoc group was removed by using a 20% piperidine solution in DMF (10 mL). Using Synergy software, the deprotection protocol was run. The piperidine solution was drained and the resin was washed with DMF (4 x 10 mL). Fmoc-L-histidine(Trt)-OH (5 eq, 1.25 mM) along with Oxyma (5 eq, 1.25 mM) and DIC (5 eq, 1.35 mmol) in DMF was added to the reaction vessel and the coupling protocol was run. The amino acid solution was drained, and the resin was washed with DMF (2 x 10 mL). The fmoc removal and coupling procedure was repeated as before using the same equivalencies for the remaining amino acids. To remove the peptide from resin, a TFA cocktail solution (95% TFA, 2.5% TIPS, and 2.5% DCM) was added to the resin and agitated for 2 hours. The resin was filtered, and the resulting solution was concentrated in vacuo. The peptide was triturated with cold diethyl ether and purified using reverse phase HPLC using H<sub>2</sub>O/CH<sub>3</sub>CN. The sample was analyzed for purity using a Waters 1525 Binary HPLC Pump using a Phenomenex Luna 5u C8(2) 100A (250 x 4.60 mm) column; gradient eluted with H<sub>2</sub>O/CH<sub>3</sub>CN. Molecular weight was confirmed using high resolution electrospray ionization mass spectrometry (HRMS, ESI/MS) analyses obtained on an Agilent 6545B Q-TOF LC/MS equipped with 1260 infinity II LC system with auto sampler. The final peptide product was lyophilized and stored at -20°C until further use.



MALDI-TOF MS calculated [M]: 1355.6743, found 1355.338

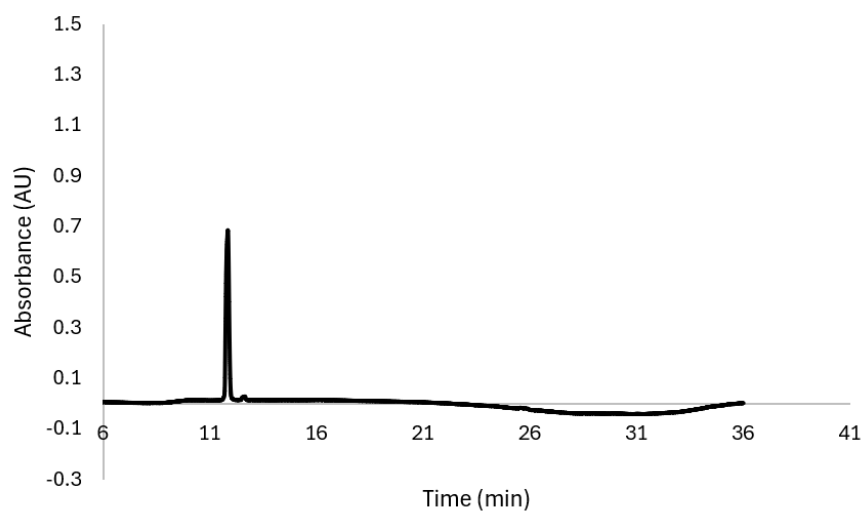


## Scheme S34. Synthesis of RSPSPKTSL

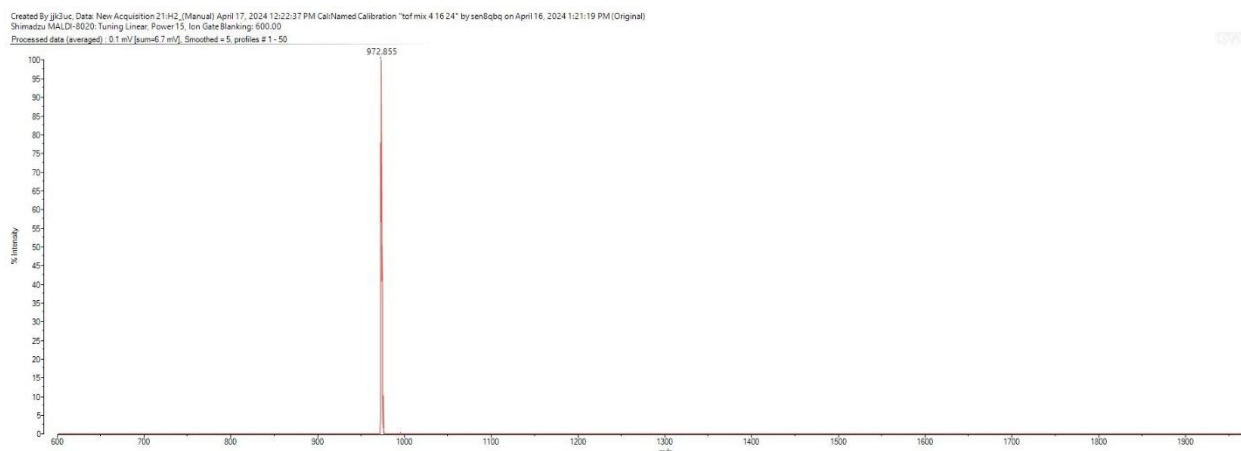


A 25 mL vessel of CEM discover bio manual peptide synthesizer was charged with 0.25 mmol of leucine wang resin. The Fmoc group was removed by using a 20% piperidine solution in DMF (10 mL). Using Synergy software, the deprotection protocol was run. The piperidine solution was drained and the resin was washed with DMF (4 x 10 mL). Fmoc-L-serine(tBu)-OH (5 eq, 1.25 mM) along with Oxyma (5 eq, 1.25 mM) and DIC (5 eq, 1.35 mmol) in DMF was added to the reaction vessel and the coupling protocol was run. The amino acid solution was drained, and the resin was washed with DMF (2 x 10 mL). The fmoc removal and coupling procedure was repeated as before using the same equivalencies for the remaining amino acids. To remove the peptide from resin, a TFA cocktail solution (95% TFA, 2.5% TIPS, and 2.5% DCM) was added to the resin and agitated for 2 hours. The resin was filtered, and the resulting solution was concentrated in vacuo. The peptide was triturated with cold diethyl ether and purified using reverse phase HPLC using H<sub>2</sub>O/CH<sub>3</sub>CN. The sample was analyzed for purity using a Waters 1525 Binary HPLC Pump using a Phenomenex Luna 5u C8(2) 100A (250 x 4.60 mm) column; gradient eluted with H<sub>2</sub>O/CH<sub>3</sub>CN. Molecular weight was confirmed using high resolution electrospray ionization mass spectrometry (HRMS, ESI/MS) analyses obtained on an Agilent 6545B Q-TOF LC/MS equipped with 1260 infinity II LC system with auto sampler. The final peptide product was lyophilized and stored at -20°C until further use.1. Nagapradeep, N., and Verma, S. (2011) Characterization of an unprecedented organomercury adduct via Hg(II)-mediated cyclization of N9-propargylguanine, *Chem Commun (Camb)* 47, 1755-1757.

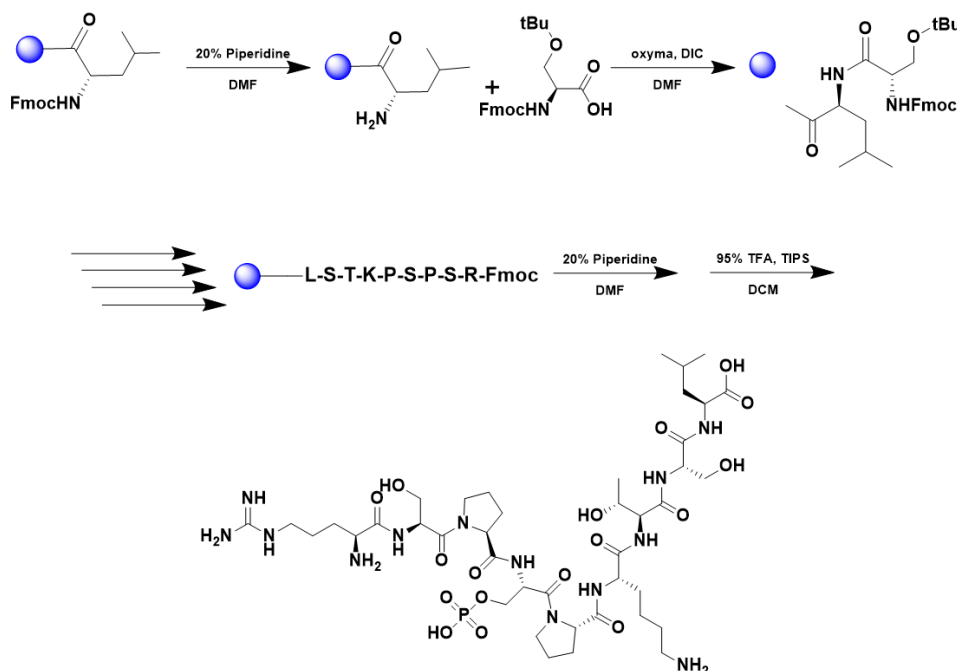
2. Zhao, J. W., Wu, Z. H., Guo, J. W., Huang, M. J., You, Y. Z., Liu, H. M., and Huang, L. H. (2019) Synthesis and anti-gastric cancer activity evaluation of novel triazole nucleobase analogues containing steroidal/coumarin/quinoline moieties, *Eur J Med Chem* 181, 111520.
3. Xin, Y., Liu, S., Liu, Y., Qian, Z., Liu, H., Zhang, B., Guo, T., Thompson, G. J., Stevens, R. C., Sharpless, K. B., Dong, J., and Shui, W. (2023) Affinity selection of double-click triazole libraries for rapid discovery of allosteric modulators for GLP-1 receptor, *Proc Natl Acad Sci U S A* 120, e2220767120.



MALDI-TOF MS calculated [M]: 972.5473, found 972.855

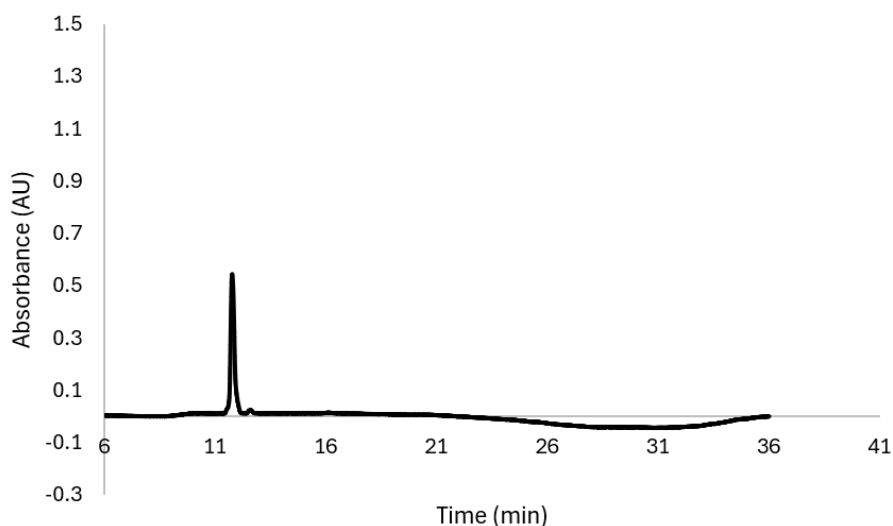


### Scheme S35. Synthesis of RSP(SPO4)PKTSL



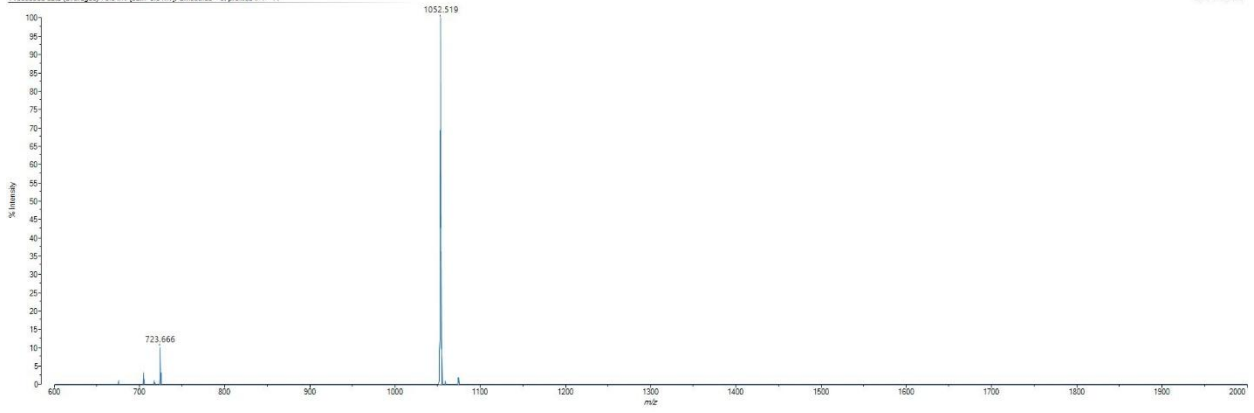
A 25 mL vessel of CEM discover bio manual peptide synthesizer was charged with 0.25 mmol of leucine wang resin. The Fmoc group was removed by using a 20% piperidine solution in DMF (10 mL). Using Synergy software, the deprotection protocol was run. The piperidine solution was drained and the resin was washed with DMF (4 x 10 mL).

Fmoc-L-serine(tBu)-OH (5 eq, 1.25 mM) along with Oxyma (5 eq, 1.25 mM) and DIC (5 eq, 1.35 mmol) in DMF was added to the reaction vessel and the coupling protocol was run. The amino acid solution was drained, and the resin was washed with DMF (2 x 10 mL). The fmoc removal and coupling procedure was repeated as before using the same equivalencies for the remaining amino acids. To remove the peptide from resin, a TFA cocktail solution (95% TFA, 2.5% TIPS, and 2.5% DCM) was added to the resin and agitated for 2 hours. The resin was filtered, and the resulting solution was concentrated in vacuo. The peptide was triturated with cold diethyl ether and purified using reverse phase HPLC using H<sub>2</sub>O/CH<sub>3</sub>CN. The sample was analyzed for purity using a Waters 1525 Binary HPLC Pump using a Phenomenex Luna 5u C8(2) 100A (250 x 4.60 mm) column; gradient eluted with H<sub>2</sub>O/CH<sub>3</sub>CN. Molecular weight was confirmed using high resolution electrospray ionization mass spectrometry (HRMS, ESI/MS) analyses obtained on an Agilent 6545B Q-TOF LC/MS equipped with 1260 infinity II LC system with auto sampler. The final peptide product was lyophilized and stored at -20°C until further use.



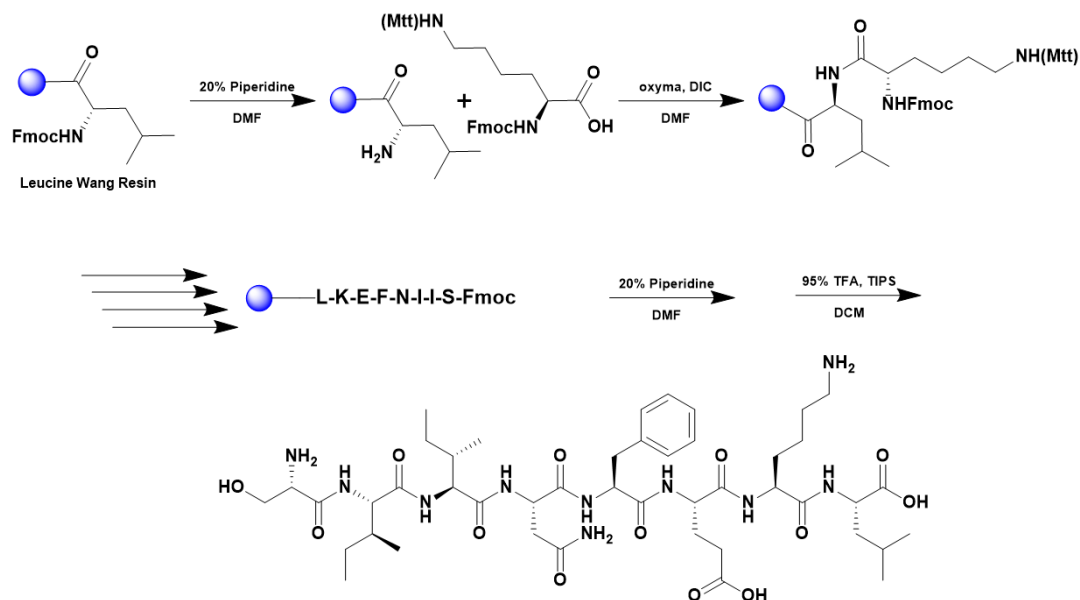
MALDI-TOF MS calculated [M]: 1051.5058, found 1052.519

Created By jk3uc, Date: New Acquisition 28:H3\_(Manual) April 17, 2024 12:25:00 PM Cal:Named Calibration "tof mix 4 16 24" by sen8qbg on April 16, 2024 1:21:19 PM (Original)  
Shimadzu MALDI-8020; Tuning: Linear, Power: 60, Ion Gate: Blanking, 6000.00  
Processed data (averaged): 0.0 mV (pump: 0.3 mL), Smoothed = 5, profiles # 1 - 11



## A.6 Synthesis and Characterization of Compounds in Chapter 6

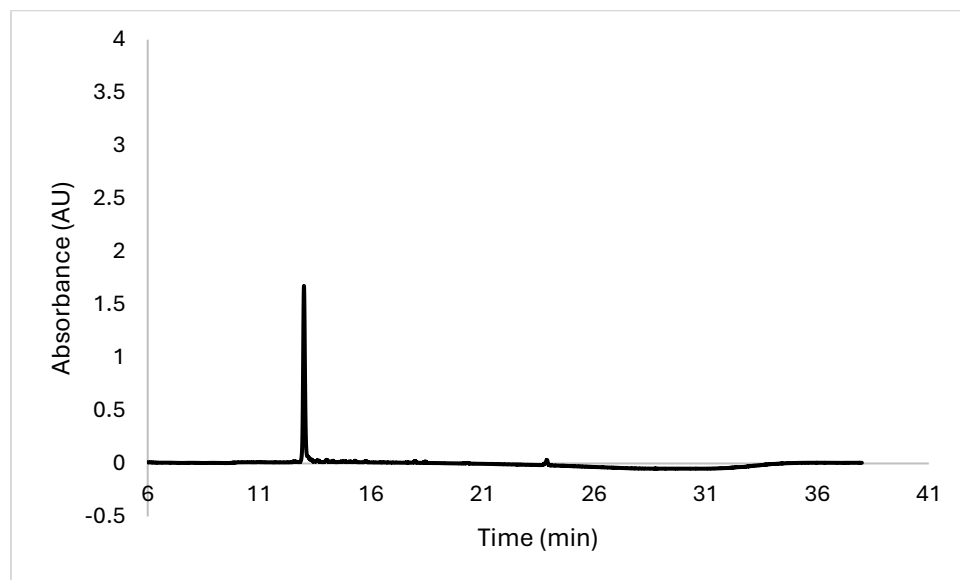
## Scheme S1. Synthesis of ovaWT



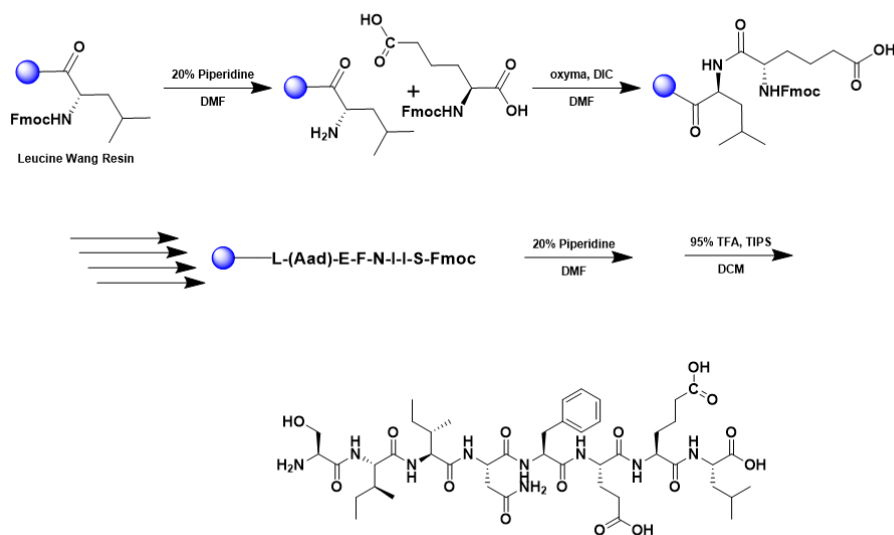
A 25 mL vessel of CEM discover bio manual peptide synthesizer was charged with 0.25 mmol of leucine wang resin. The Fmoc group was removed by using a 20% piperidine solution in DMF (10 mL). Using Synergy software, the deprotection protocol was run. The piperidine solution was drained and the resin was washed with DMF (4 x 10 mL). Fmoc-L-lysine(Mtt)-OH (5 eq, 1.25 mM) along with Oxyma (5 eq, 1.25 mM) and DIC (5 eq, 1.35 mmol) in DMF was added to the reaction vessel and the coupling protocol was run. The amino acid solution was drained, and the resin was washed with DMF (2 x 10 mL). The fmoc removal and coupling procedure was repeated as before using the same equivalencies for the remaining amino acids. To remove the peptide from resin, a TFA cocktail solution (95% TFA, 2.5% TIPS, and 2.5% DCM) was added to the resin and agitated for 2 hours. The resin was filtered, and the resulting solution was concentrated in vacuo. The peptide was triturated with cold diethyl ether and purified using reverse phase HPLC using H<sub>2</sub>O/CH<sub>3</sub>CN. The sample was analyzed for purity using a Waters 1525 Binary HPLC Pump using a Phenomenex Luna 5u C8(2) 100A (250 x 4.60 mm) column; gradient eluted with H<sub>2</sub>O/CH<sub>3</sub>CN. Molecular weight was confirmed using high resolution electrospray ionization mass spectrometry (HRMS, ESI/MS) analyses obtained on an Agilent 6545B Q-TOF LC/MS equipped with 1260 infinity II LC system with auto sampler. The final peptide product was lyophilized and stored at -20°C until further use.



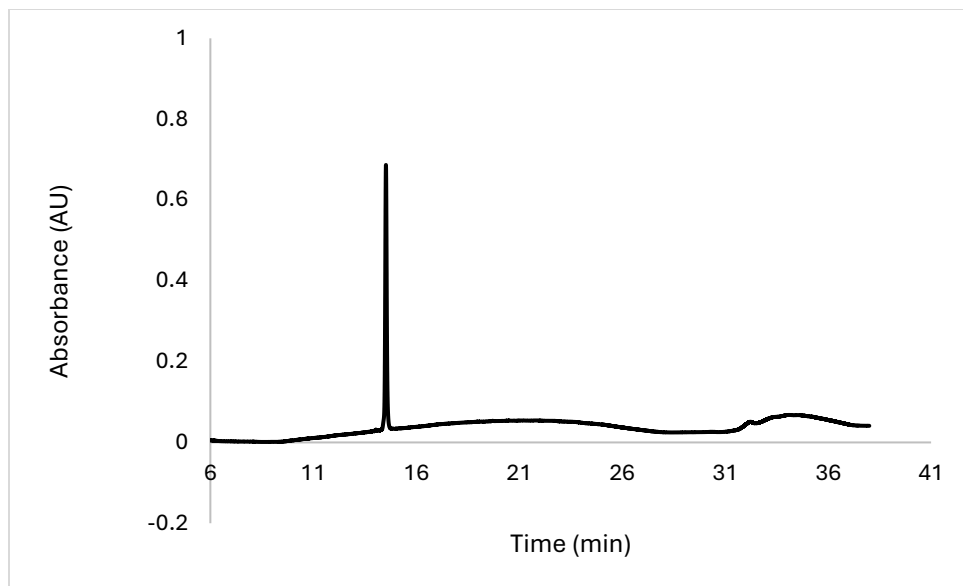
using the same equivalencies for the remaining amino acids. To remove the peptide from resin, a TFA cocktail solution (95% TFA, 2.5% TIPS, and 2.5% DCM) was added to the resin and agitated for 2 hours. The resin was filtered, and the resulting solution was concentrated in vacuo. The peptide was triturated with cold diethyl ether and purified using reverse phase HPLC using H<sub>2</sub>O/CH<sub>3</sub>CN. The sample was analyzed for purity using a Waters 1525 Binary HPLC Pump using a Phenomenex Luna 5u C8(2) 100A (250 x 4.60 mm) column; gradient eluted with H<sub>2</sub>O/CH<sub>3</sub>CN. Molecular weight was confirmed using high resolution electrospray ionization mass spectrometry (HRMS, ESI/MS) analyses obtained on an Agilent 6545B Q-TOF LC/MS equipped with 1260 infinity II LC system with auto sampler. The final peptide product was lyophilized and stored at -20°C until further use.



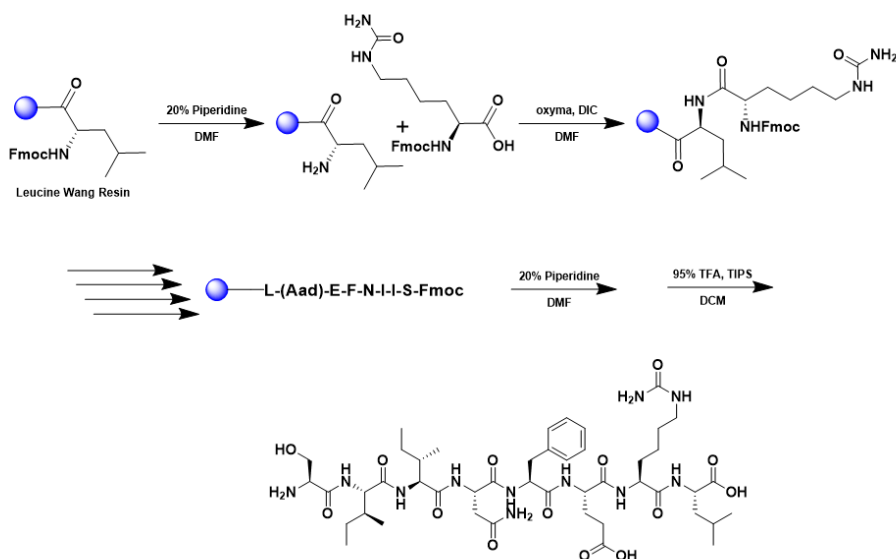
## Scheme S3. Synthesis of ovaK7aad



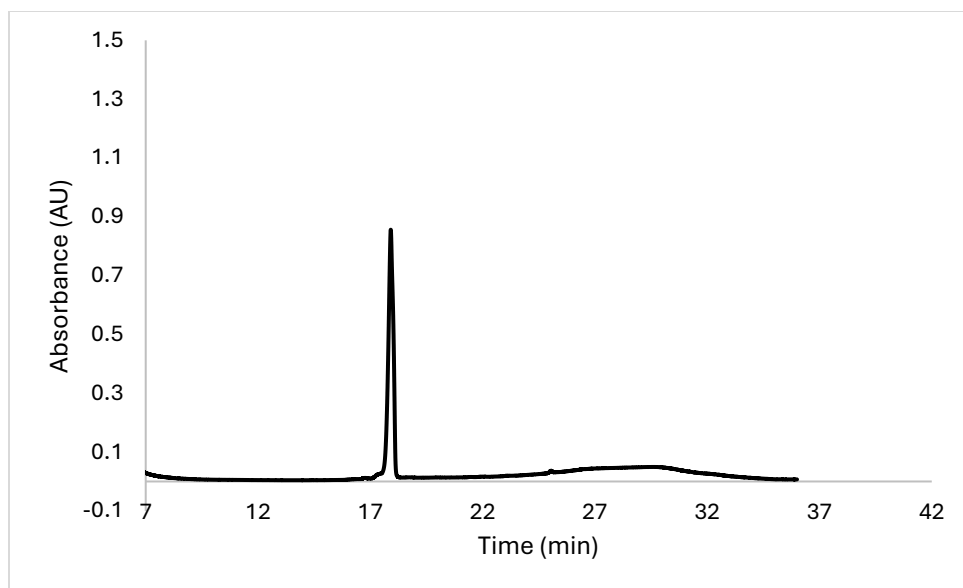
A 25 mL vessel of CEM discover bio manual peptide synthesizer was charged with 0.25 mmol of leucine wang resin. The Fmoc group was removed by using a 20% piperidine solution in DMF (10 mL). Using Synergy software, the deprotection protocol was run. The piperidine solution was drained and the resin was washed with DMF (4 x 10 mL). Fmoc-L- $\alpha$ -amino acid  $\delta$ -tert-butyl ester (5 eq, 1.25 mM) along with Oxyma (5 eq, 1.25 mM) and DIC (5 eq, 1.35 mmol) in DMF was added to the reaction vessel and the coupling protocol was run. The amino acid solution was drained, and the resin was washed with DMF (2 x 10 mL). The fmoc removal and coupling procedure was repeated as before using the same equivalencies for the remaining amino acids. For the 7<sup>th</sup> position of the amino acid, Fmoc was deprotected as described above and Fmoc-L- $\alpha$ -amino acid (5 eq, 1.25 mM) along with Oxyma (5 eq, 1.25 mM) and DIC (5 eq, 1.35 mmol) in DMF was added to the reaction vessel. To remove the peptide from resin, a TFA cocktail solution (95% TFA, 2.5% TIPS, and 2.5% DCM) was added to the resin and agitated for 2 hours. The resin was filtered, and the resulting solution was concentrated in vacuo. The peptide was triturated with cold diethyl ether and purified using reverse phase HPLC using H<sub>2</sub>O/CH<sub>3</sub>CN. The sample was analyzed for purity using a Waters 1525 Binary HPLC Pump using a Phenomenex Luna 5u C8(2) 100A (250 x 4.60 mm) column; gradient eluted with H<sub>2</sub>O/CH<sub>3</sub>CN. Molecular weight was confirmed using high resolution electrospray ionization mass spectrometry (HRMS, ESI/MS) analyses obtained on an Agilent 6545B Q-TOF LC/MS equipped with 1260 infinity II LC system with auto sampler. The final peptide product was lyophilized and stored at -20°C until further use.



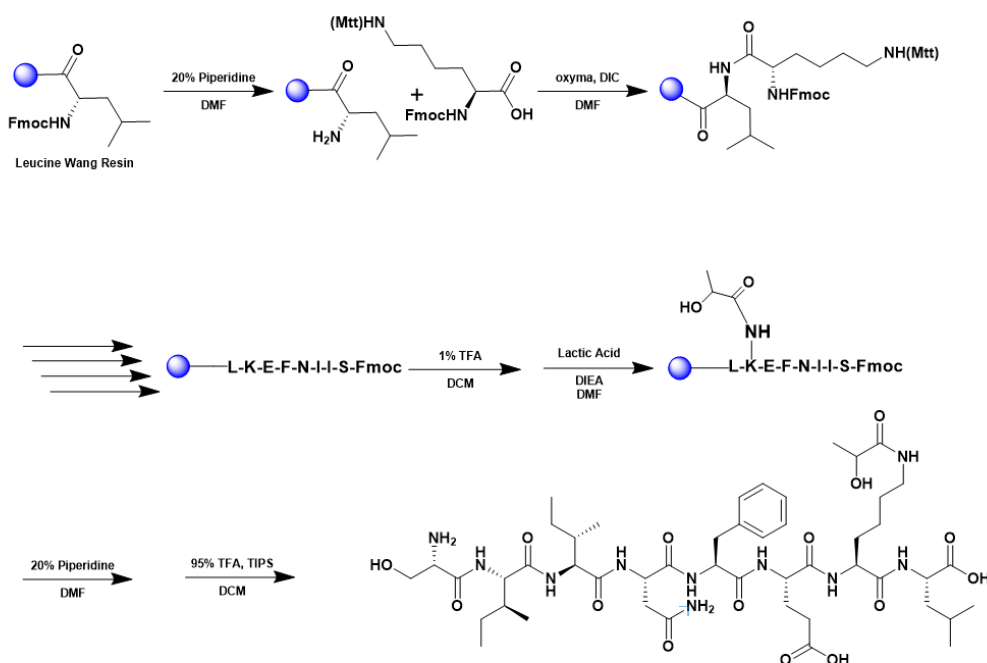
## Scheme S5. Synthesis of ovaK7hcit



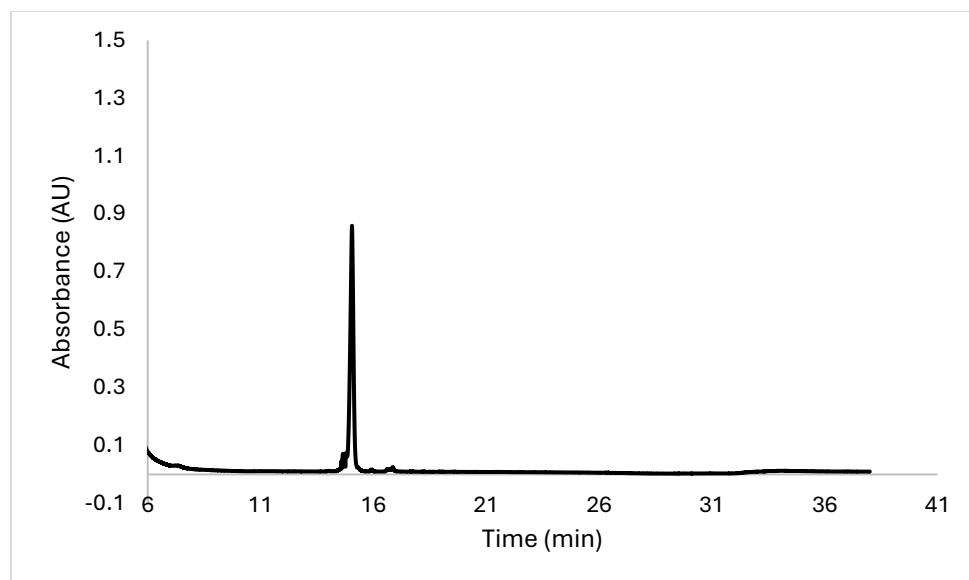
A 25 mL vessel of CEM discover bio manual peptide synthesizer was charged with 0.25 mmol of leucine wang resin. The Fmoc group was removed by using a 20% piperidine solution in DMF (10 mL). Using Synergy software, the deprotection protocol was run. The piperidine solution was drained and the resin was washed with DMF (4 x 10 mL). Fmoc-L-homocitrulline-OH (5 eq, 1.25 mM) along with Oxyma (5 eq, 1.25 mM) and DIC (5 eq, 1.35 mmol) in DMF was added to the reaction vessel and the coupling protocol was run. The amino acid solution was drained, and the resin was washed with DMF (2 x 10 mL). The fmoc removal and coupling procedure was repeated as before using the same equivalencies for the remaining amino acids. For the 7<sup>th</sup> position of the amino acid, Fmoc was deprotected as described above and Fmoc-L-homocitrulline (5 eq, 1.25 mM) along with Oxyma (5 eq, 1.25 mM) and DIC (5 eq, 1.35 mmol) in DMF was added to the reaction vessel. To remove the peptide from resin, a TFA cocktail solution (95% TFA, 2.5% TIPS, and 2.5% DCM) was added to the resin and agitated for 2 hours. The resin was filtered, and the resulting solution was concentrated in vacuo. The peptide was triturated with cold diethyl ether and purified using reverse phase HPLC using H<sub>2</sub>O/CH<sub>3</sub>CN. The sample was analyzed for purity using a Waters 1525 Binary HPLC Pump using a Phenomenex Luna 5u C8(2) 100A (250 x 4.60 mm) column; gradient eluted with H<sub>2</sub>O/CH<sub>3</sub>CN. Molecular weight was confirmed using high resolution electrospray ionization mass spectrometry (HRMS, ESI/MS) analyses obtained on an Agilent 6545B Q-TOF LC/MS equipped with 1260 infinity II LC system with auto sampler. The final peptide product was lyophilized and stored at -20°C until further use.



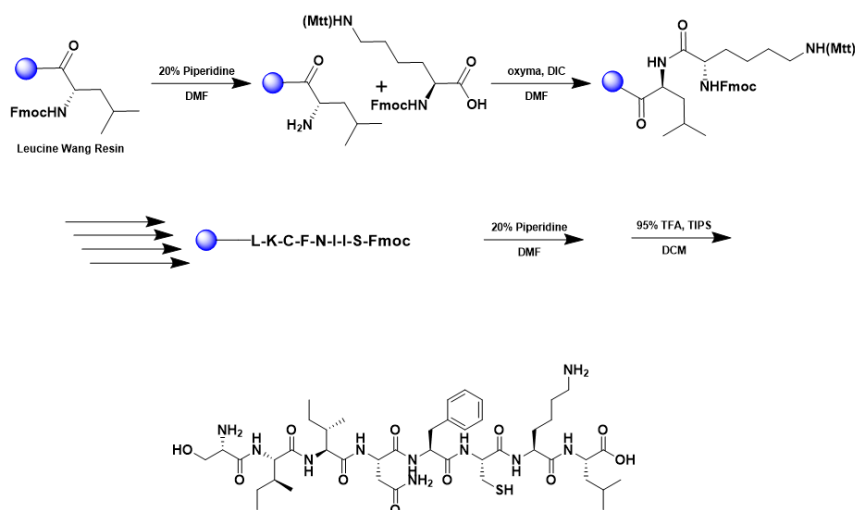
## Scheme S6. Synthesis of ovaK7lac



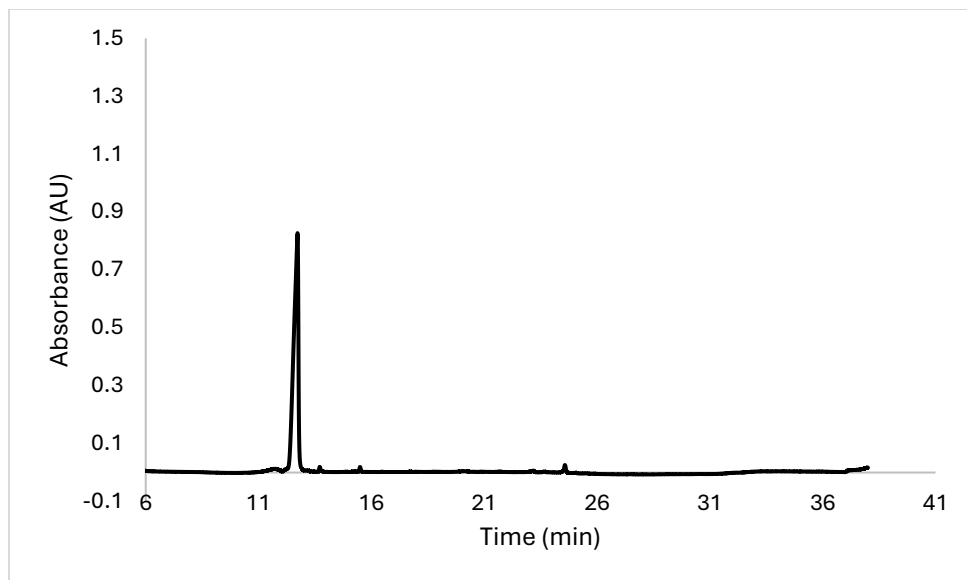
A 25 mL vessel of CEM discover bio manual peptide synthesizer was charged with 0.25 mmol of leucine wang resin. The Fmoc group was removed by using a 20% piperidine solution in DMF (10 mL). Using Synergy software, the deprotection protocol was run. The piperidine solution was drained and the resin was washed with DMF (4 x 10 mL). Fmoc-L-lysine(Mtt)-OH (5 eq, 1.25 mM) along with Oxyma (5 eq, 1.25 mM) and DIC (5 eq, 1.35 mmol) in DMF was added to the reaction vessel and the coupling protocol was run. The amino acid solution was drained, and the resin was washed with DMF (2 x 10 mL). The fmoc removal and coupling procedure was repeated as before using the same equivalencies for the remaining amino acids. The MTT protecting group was removed by the addition of 1% TFA, 2.5% TIPS, in 10 mL DCM for 15 min, washed and repeated 5 more times. Lactic acid (5 eq, 1.25 mM) along with Oxyma (5 eq, 1.25 mM) and DIC (5 eq, 1.25 mM) in DMF was added to the reaction vessel and agitated at ambient temperature for 2 hours. To remove the peptide from resin, a TFA cocktail solution (95% TFA, 2.5% TIPS, and 2.5% DCM) was added to the resin and agitated for 2 hours. The resin was filtered, and the resulting solution was concentrated in vacuo. The peptide was trituated with cold diethyl ether and purified using reverse phase HPLC using H<sub>2</sub>O/CH<sub>3</sub>CN. The sample was analyzed for purity using a Waters 1525 Binary HPLC Pump using a Phenomenex Luna 5u C8(2) 100A (250 x 4.60 mm) column; gradient eluted with H<sub>2</sub>O/CH<sub>3</sub>CN. Molecular weight was confirmed using high resolution electrospray ionization mass spectrometry (HRMS, ESI/MS) analyses obtained on an Agilent 6545B Q-TOF LC/MS equipped with 1260 infinity II LC system with auto sampler. The final peptide product was lyophilized and stored at -20°C until further use.



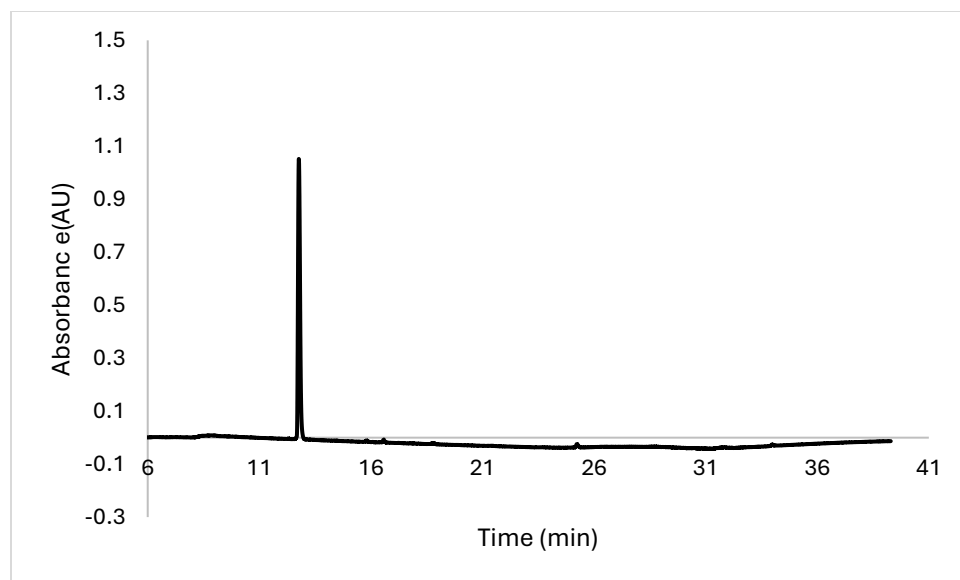
## Scheme S7. Synthesis of ovaE6C



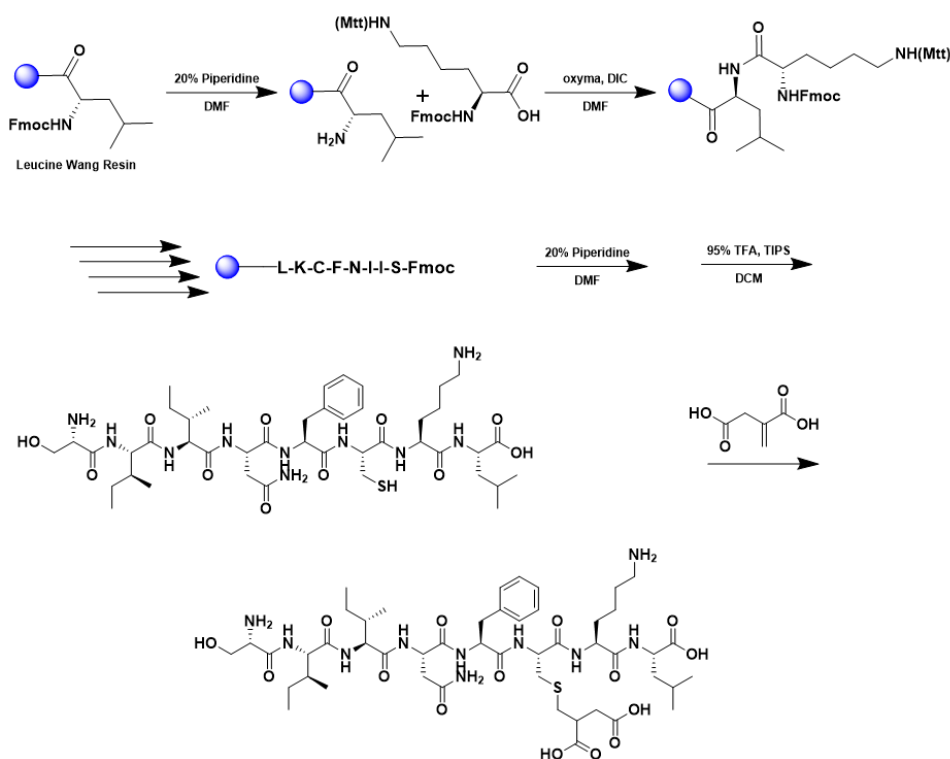
A 25 mL vessel of CEM discover bio manual peptide synthesizer was charged with 0.25 mmol of leucine wang resin. The Fmoc group was removed by using a 20% piperidine solution in DMF (10 mL). Using Synergy software, the deprotection protocol was run. The piperidine solution was drained and the resin was washed with DMF (4 x 10 mL). Fmoc-L-lysine(Mtt)-OH (5 eq, 1.25 mM) along with Oxyma (5 eq, 1.25 mM) and DIC (5 eq, 1.35 mmol) in DMF was added to the reaction vessel and the coupling protocol was run. The amino acid solution was drained, and the resin was washed with DMF (2 x 10 mL). The fmoc removal and coupling procedure was repeated as before using the same equivalencies for the remaining amino acids. To remove the peptide from resin, a TFA cocktail solution (95% TFA, 2.5% TIPS, and 2.5% DCM) was added to the resin and agitated for 2 hours. The resin was filtered, and the resulting solution was concentrated in vacuo. The peptide was triturated with cold diethyl ether and purified using reverse phase HPLC using H<sub>2</sub>O/CH<sub>3</sub>CN. The sample was analyzed for purity using a Waters 1525 Binary HPLC Pump using a Phenomenex Luna 5u C8(2) 100A (250 x 4.60 mm) column; gradient eluted with H<sub>2</sub>O/CH<sub>3</sub>CN. Molecular weight was confirmed using high resolution electrospray ionization mass spectrometry (HRMS, ESI/MS) analyses obtained on an Agilent 6545B Q-TOF LC/MS equipped with 1260 infinity II LC system with auto sampler. The final peptide product was lyophilized and stored at -20°C until further use.



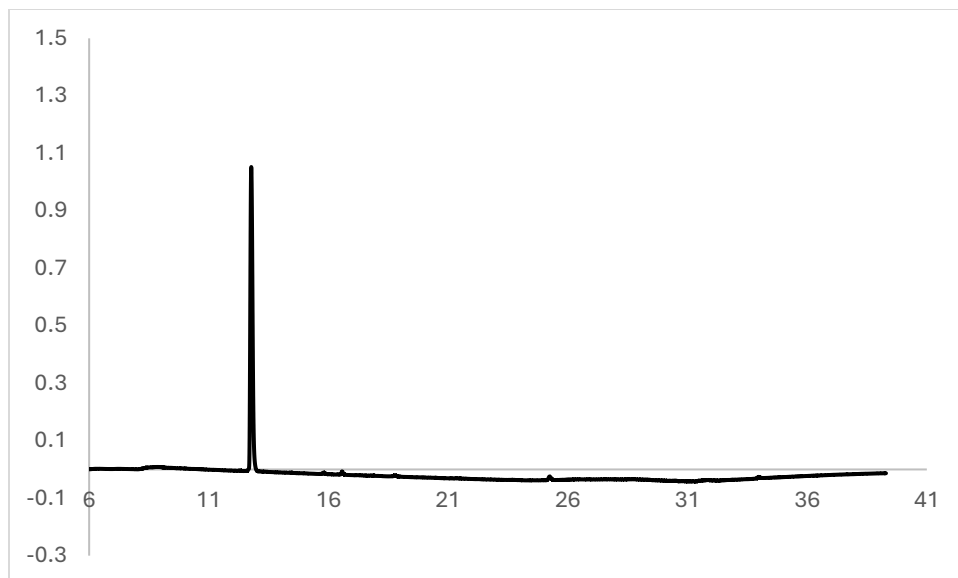


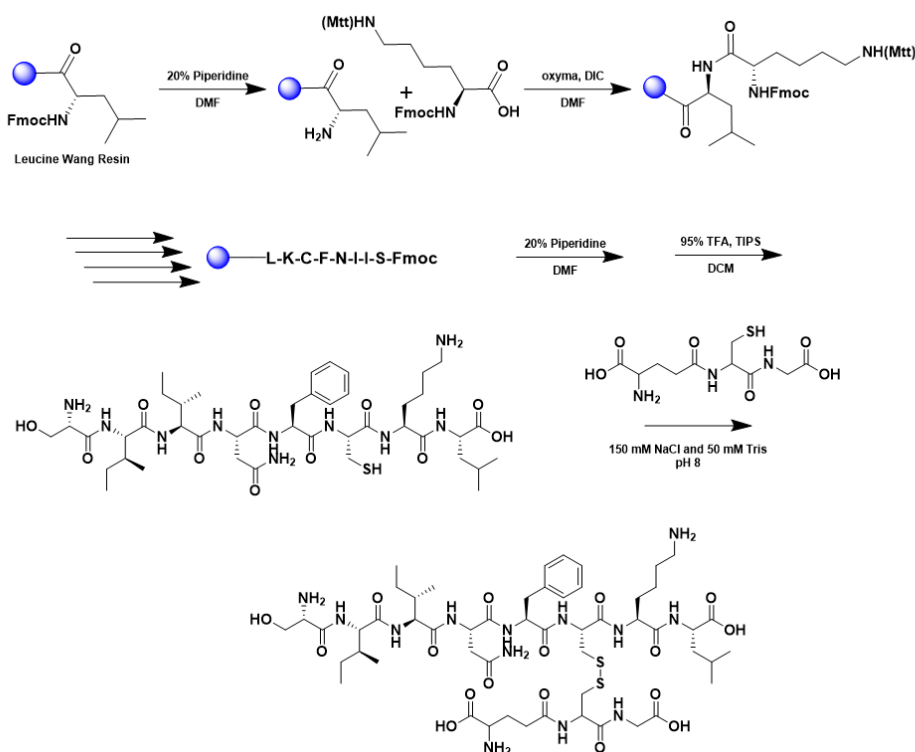


## Scheme S9. Synthesis of ovaE6Cita

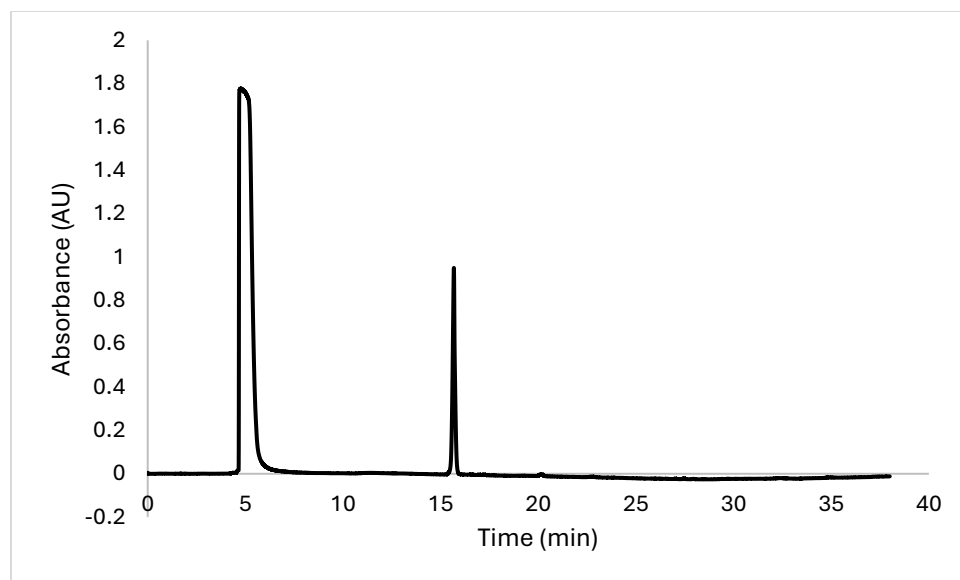


A 25 mL vessel of CEM discover bio manual peptide synthesizer was charged with 0.25 mmol of leucine wang resin. The Fmoc group was removed by using a 20% piperidine solution in DMF (10 mL). Using Synergy software, the deprotection protocol was run. The piperidine solution was drained and the resin was washed with DMF (4 x 10 mL). Fmoc-L-lysine(Mtt)-OH (5 eq, 1.25 mM) along with Oxyma (5 eq, 1.25 mM) and DIC (5 eq, 1.35 mmol) in DMF was added to the reaction vessel and the coupling protocol was run. The amino acid solution was drained, and the resin was washed with DMF (2 x 10 mL). The fmoc removal and coupling procedure was repeated as before using the same equivalencies for the remaining amino acids. To remove the peptide from resin, a TFA cocktail solution (95% TFA, 2.5% TIPS, and 2.5% DCM) was added to the resin and agitated for 2 hours. The resin was filtered, and the resulting solution was concentrated in vacuo. The peptide was triturated with cold diethyl ether and purified using reverse phase HPLC using H<sub>2</sub>O/CH<sub>3</sub>CN. The sample was analyzed for purity using a Waters 1525 Binary HPLC Pump using a Phenomenex Luna 5u C8(2) 100A (250 x 4.60 mm) column; gradient eluted with H<sub>2</sub>O/CH<sub>3</sub>CN. Molecular weight was confirmed using high resolution electrospray ionization mass spectrometry (HRMS, ESI/MS) analyses obtained on an Agilent 6545B Q-TOF LC/MS equipped with 1260 infinity II LC system with auto sampler. The final peptide product was lyophilized and stored at -20°C. Purified peptide (1 mM) and itaconic acid (4 mM) were mixed in 150 mM NaCl and 20 mM Tris pH 8 for 4 hours and purified as described before.

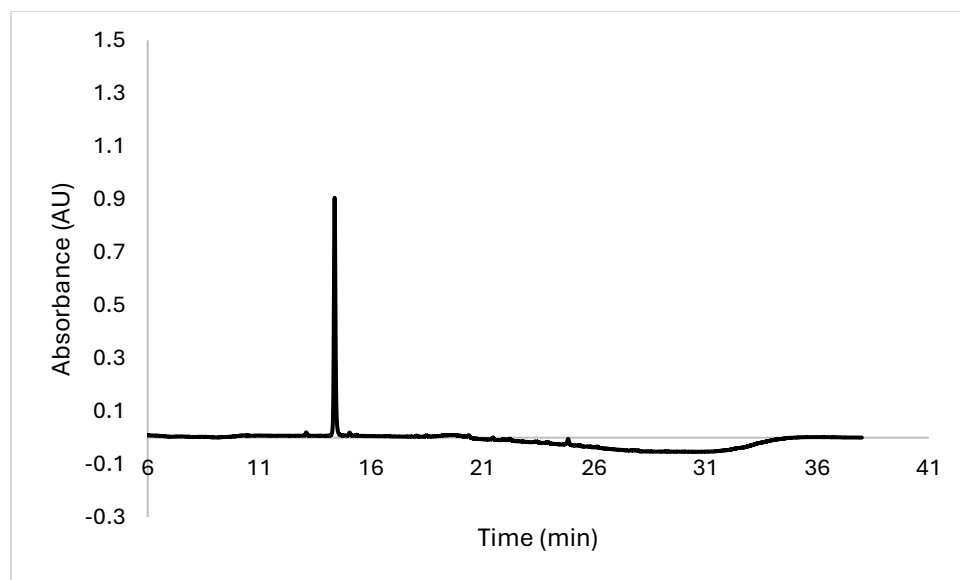


Scheme S10. Synthesis of ovaE6C<sub>GSH</sub>

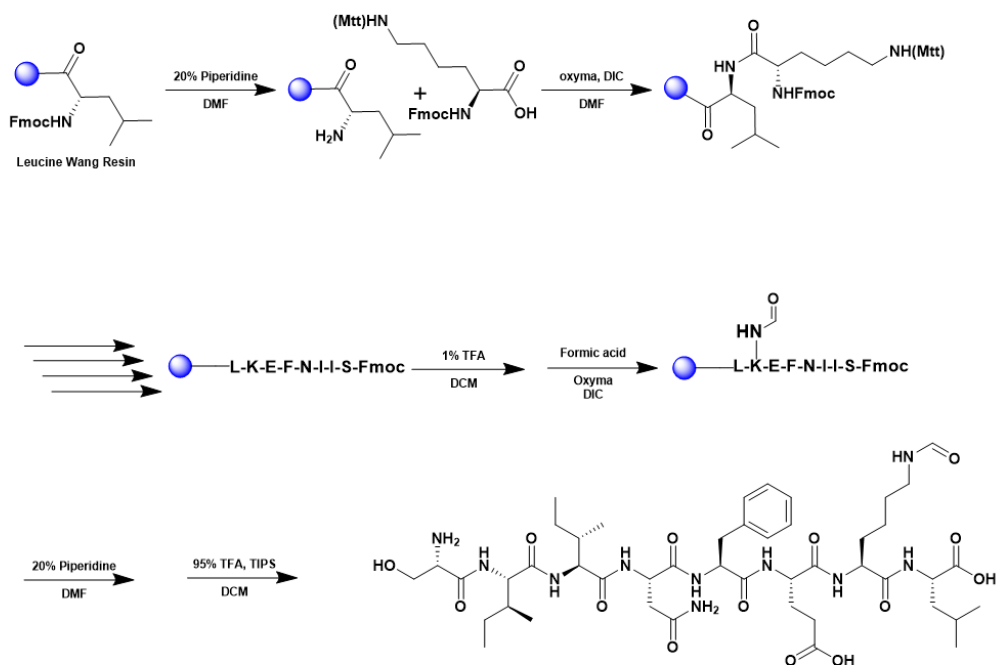
A 25 mL vessel of CEM discover bio manual peptide synthesizer was charged with 0.25 mmol of leucine wang resin. The Fmoc group was removed by using a 20% piperidine solution in DMF (10 mL). Using Synergy software, the deprotection protocol was run. The piperidine solution was drained and the resin was washed with DMF (4 x 10 mL). Fmoc-L-lysine(Mtt)-OH (5 eq, 1.25 mM) along with Oxyma (5 eq, 1.25 mM) and DIC (5 eq, 1.35 mmol) in DMF was added to the reaction vessel and the coupling protocol was run. The amino acid solution was drained, and the resin was washed with DMF (2 x 10 mL). The fmoc removal and coupling procedure was repeated as before using the same equivalencies for the remaining amino acids. To remove the peptide from resin, a TFA cocktail solution (95% TFA, 2.5% TIPS, and 2.5% DCM) was added to the resin and agitated for 2 hours. The resin was filtered, and the resulting solution was concentrated in vacuo. The peptide was triturated with cold diethyl ether and purified using reverse phase HPLC using H<sub>2</sub>O/CH<sub>3</sub>CN. The sample was analyzed for purity using a Waters 1525 Binary HPLC Pump using a Phenomenex Luna 5u C8(2) 100A (250 x 4.60 mm) column; gradient eluted with H<sub>2</sub>O/CH<sub>3</sub>CN. Molecular weight was confirmed using high resolution electrospray ionization mass spectrometry (HRMS, ESI/MS) analyses obtained on an Agilent 6545B Q-TOF LC/MS equipped with 1260 infinity II LC system with auto sampler. The final peptide product was lyophilized and stored at -20°C. Purified peptide was treated in a 1:1.5 ratio of peptide to reduced glutathione in 50 mM tris and 150 mM NaCl buffer at pH 8. The product was repurified via HPLC and the lyophilized product was stored at -20°C.



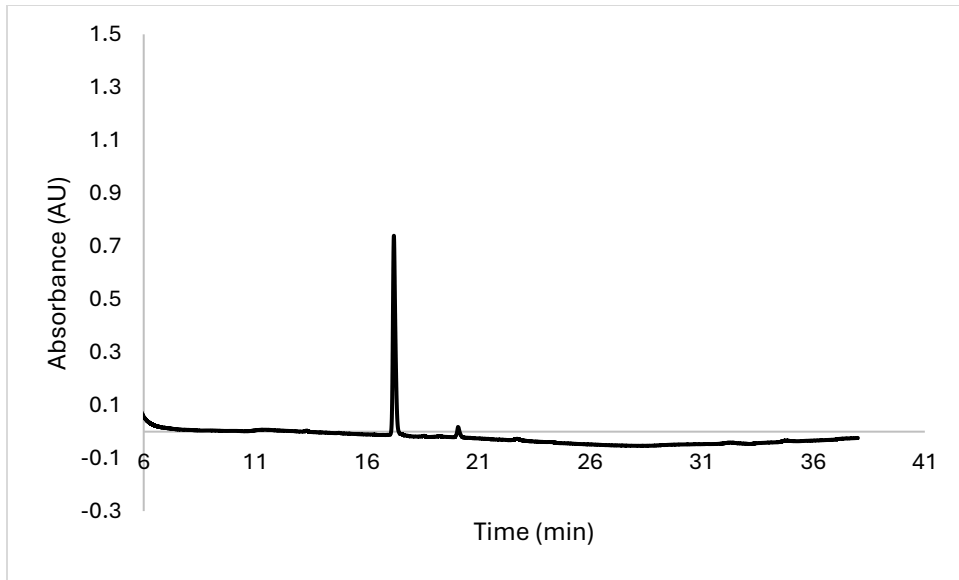




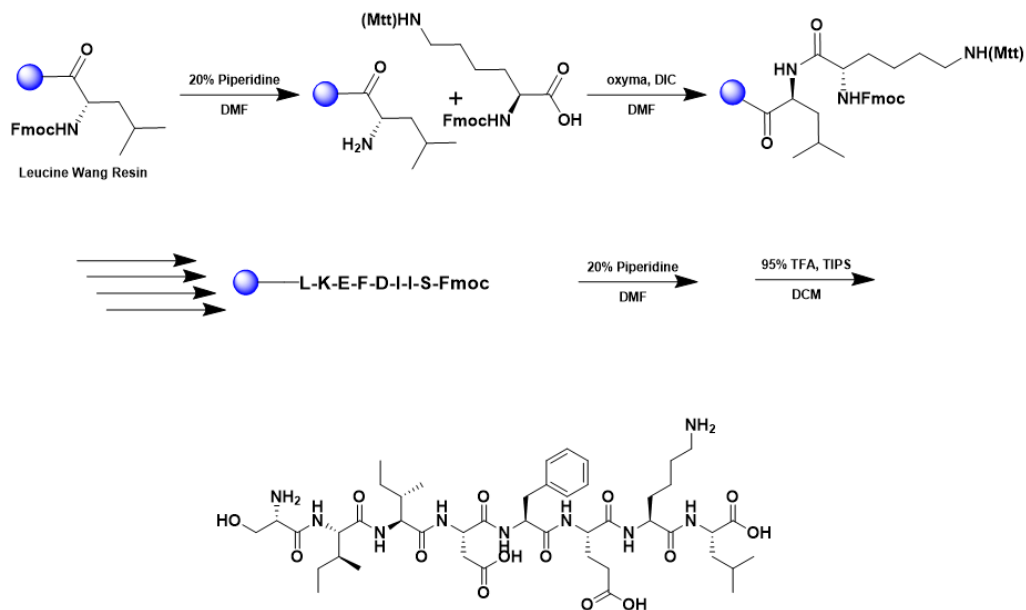
## Scheme S12. Synthesis of ovaK7formyl



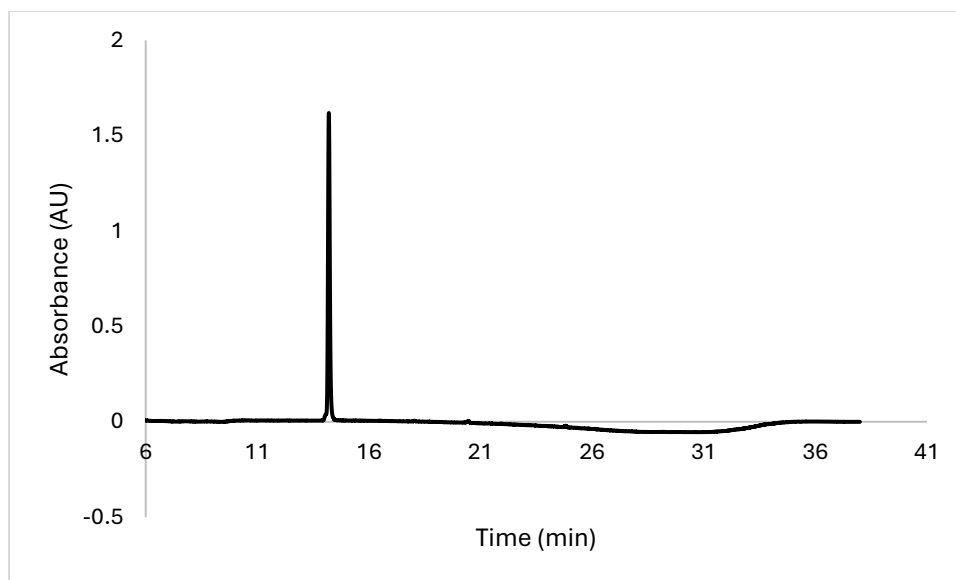
A 25 mL vessel of CEM discover bio manual peptide synthesizer was charged with 0.25 mmol of leucine wang resin. The Fmoc group was removed by using a 20% piperidine solution in DMF (10 mL). Using Synergy software, the deprotection protocol was run. The piperidine solution was drained and the resin was washed with DMF (4 x 10 mL). Fmoc-L-lysine(Mtt)-OH (5 eq, 1.25 mM) along with Oxyma (5 eq, 1.25 mM) and DIC (5 eq, 1.35 mmol) in DMF was added to the reaction vessel and the coupling protocol was run. The amino acid solution was drained, and the resin was washed with DMF (2 x 10 mL). The fmoc removal and coupling procedure was repeated as before using the same equivalencies for the remaining amino acids. The MTT protecting group was removed by the addition of 1% TFA, 2.5% TIPS, in 10 mL DCM for 15 min, washed and repeated 5 more times. Formic acid (5 eq, 1.25 mM) and DIC (5 eq, 1.35 mmol) in DMF was added to the reaction vessel and the coupling protocol was run. To remove the peptide from resin, a TFA cocktail solution (95% TFA, 2.5% TIPS, and 2.5% DCM) was added to the resin and agitated for 2 hours. The resin was filtered, and the resulting solution was concentrated in vacuo. The peptide was triturated with cold diethyl ether and purified using reverse phase HPLC using H<sub>2</sub>O/CH<sub>3</sub>CN. The sample was analyzed for purity using a Waters 1525 Binary HPLC Pump using a Phenomenex Luna 5u C8(2) 100A (250 x 4.60 mm) column; gradient eluted with H<sub>2</sub>O/CH<sub>3</sub>CN. Molecular weight was confirmed using high resolution electrospray ionization mass spectrometry (HRMS, ESI/MS) analyses obtained on an Agilent 6545B Q-TOF LC/MS equipped with 1260 infinity II LC system with auto sampler. The final peptide product was lyophilized and stored at -20°C until further use.



## Scheme S13. Synthesis of ovaN4D

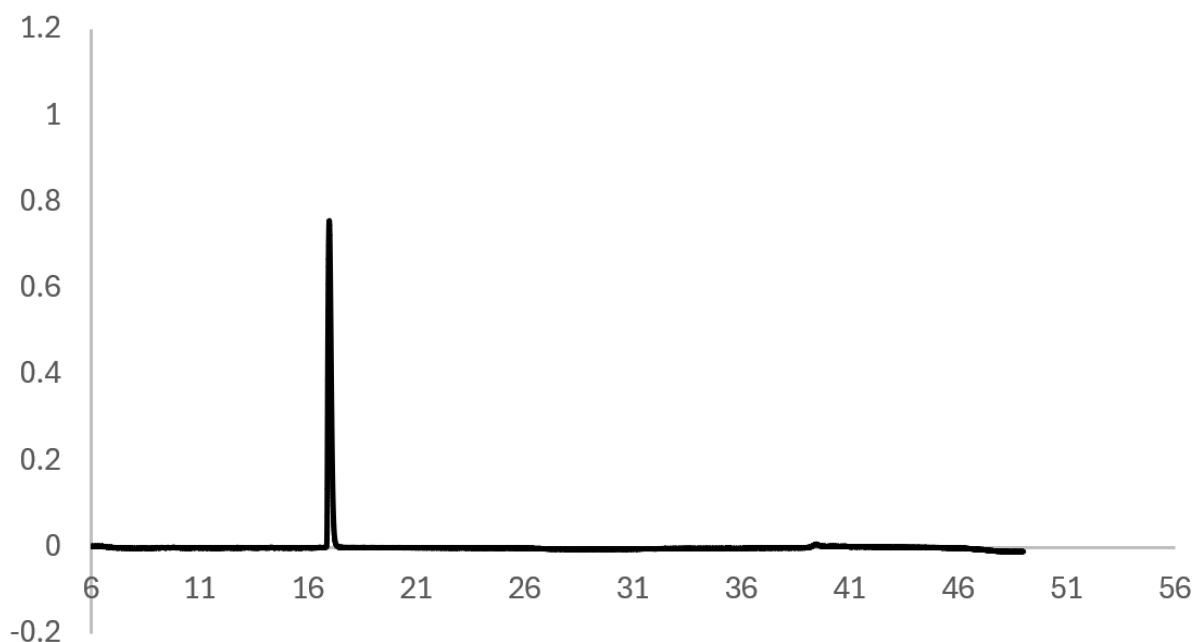


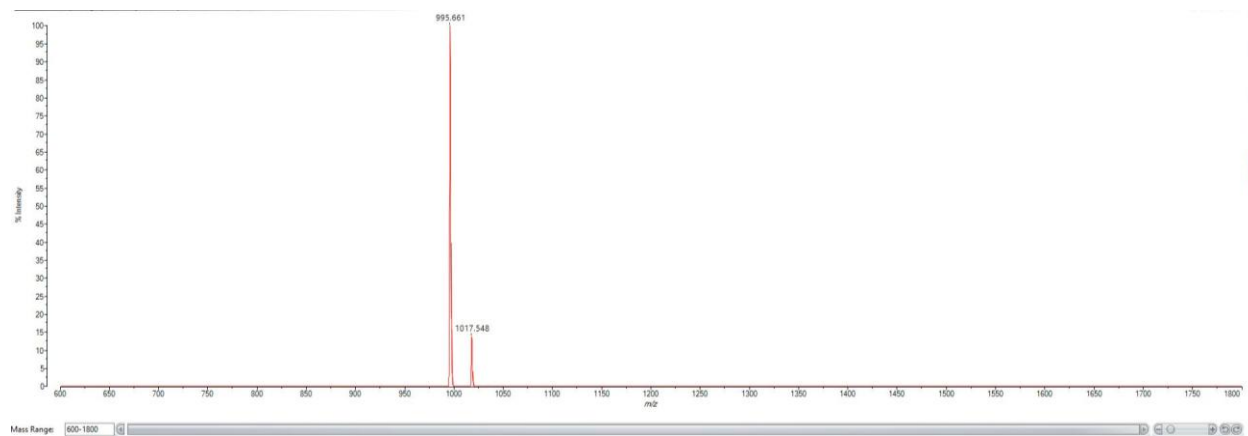
A 25 mL vessel of CEM discover bio manual peptide synthesizer was charged with 0.25 mmol of leucine wang resin. The Fmoc group was removed by using a 20% piperidine solution in DMF (10 mL). Using Synergy software, the deprotection protocol was run. The piperidine solution was drained and the resin was washed with DMF (4 x 10 mL). Fmoc-L-lysine(Mtt)-OH (5 eq, 1.25 mM) along with Oxyma (5 eq, 1.25 mM) and DIC (5 eq, 1.35 mmol) in DMF was added to the reaction vessel and the coupling protocol was run. The amino acid solution was drained, and the resin was washed with DMF (2 x 10 mL). The fmoc removal and coupling procedure was repeated as before using the same equivalencies for the remaining amino acids. To remove the peptide from resin, a TFA cocktail solution (95% TFA, 2.5% TIPS, and 2.5% DCM) was added to the resin and agitated for 2 hours. The resin was filtered, and the resulting solution was concentrated in vacuo. The peptide was triturated with cold diethyl ether and purified using reverse phase HPLC using H<sub>2</sub>O/CH<sub>3</sub>CN. The sample was analyzed for purity using a Waters 1525 Binary HPLC Pump using a Phenomenex Luna 5u C8(2) 100A (250 x 4.60 mm) column; gradient eluted with H<sub>2</sub>O/CH<sub>3</sub>CN. Molecular weight was confirmed using high resolution electrospray ionization mass spectrometry (HRMS, ESI/MS) analyses obtained on an Agilent 6545B Q-TOF LC/MS equipped with 1260 infinity II LC system with auto sampler. The final peptide product was lyophilized and stored at -20°C.



**Scheme S14. Synthesis of INFDFPKL**

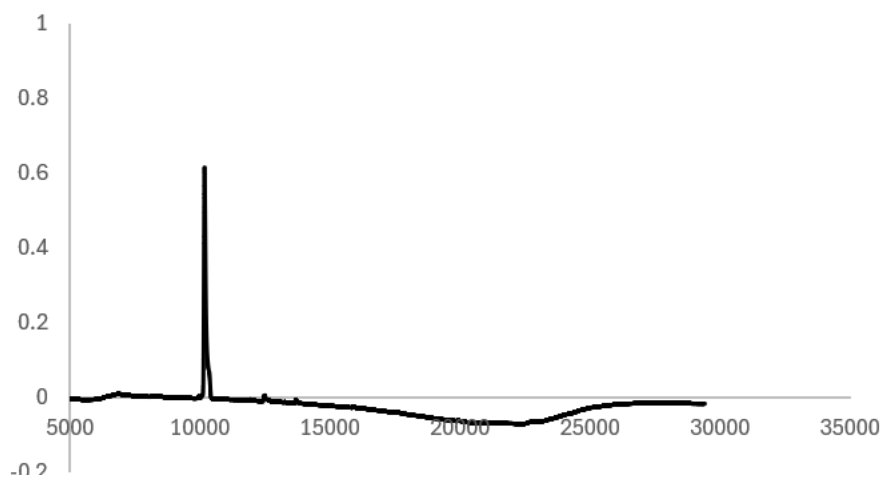
A 25 mL vessel of CEM discover bio manual peptide synthesizer was charged with 0.25 mmol of leucine wang resin. The Fmoc group was removed by using a 20% piperidine solution in DMF (10 mL). Using Synergy software, the deprotection protocol was run. The piperidine solution was drained and the resin was washed with DMF (4 x 10 mL). Fmoc-L-lysine(boc)-OH (5 eq, 1.25 mM) along with Oxyma (5 eq, 1.25 mM) and DIC (5 eq, 1.35 mmol) in DMF was added to the reaction vessel and the coupling protocol was run. The amino acid solution was drained, and the resin was washed with DMF (2 x 10 mL). The fmoc removal and coupling procedure was repeated as before using the same equivalencies for the remaining amino acids. To remove the peptide from resin, a TFA cocktail solution (95% TFA, 2.5% TIPS, and 2.5% DCM) was added to the resin and agitated for 2 hours. The resin was filtered, and the resulting solution was concentrated in vacuo. The peptide was triturated with cold diethyl ether and purified using reverse phase HPLC using H<sub>2</sub>O/CH<sub>3</sub>CN. The sample was analyzed for purity using a Waters 1525 Binary HPLC Pump using a Phenomenex Luna 5u C8(2) 100A (250 x 4.60 mm) column; gradient eluted with H<sub>2</sub>O/CH<sub>3</sub>CN. Molecular weight was confirmed using high resolution electrospray ionization mass spectrometry (HRMS, ESI/MS) analyses obtained on an Agilent 6545B Q-TOF LC/MS equipped with 1260 infinity II LC system with auto sampler. The final peptide product was lyophilized and stored at -20°C.

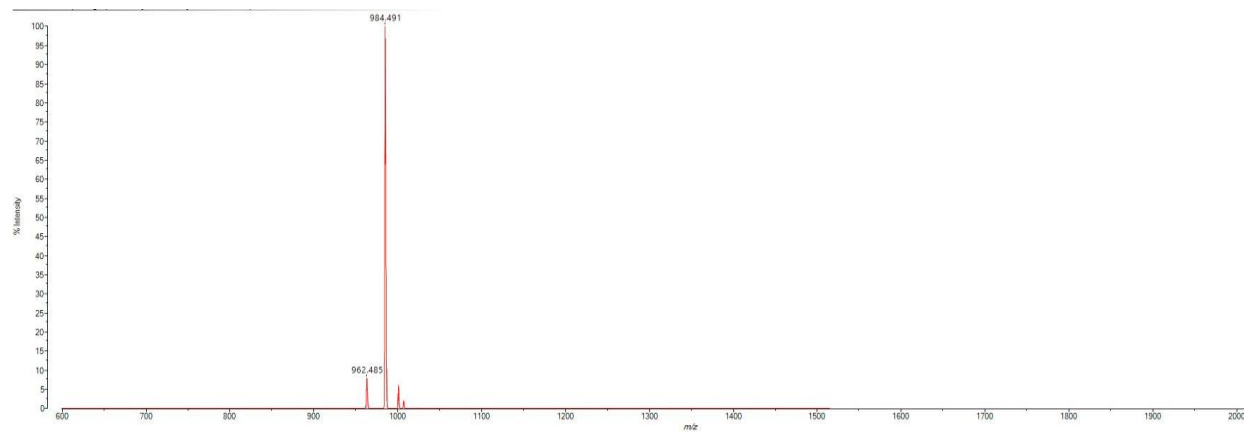




**Scheme S15. Synthesis of TALENLSTL**

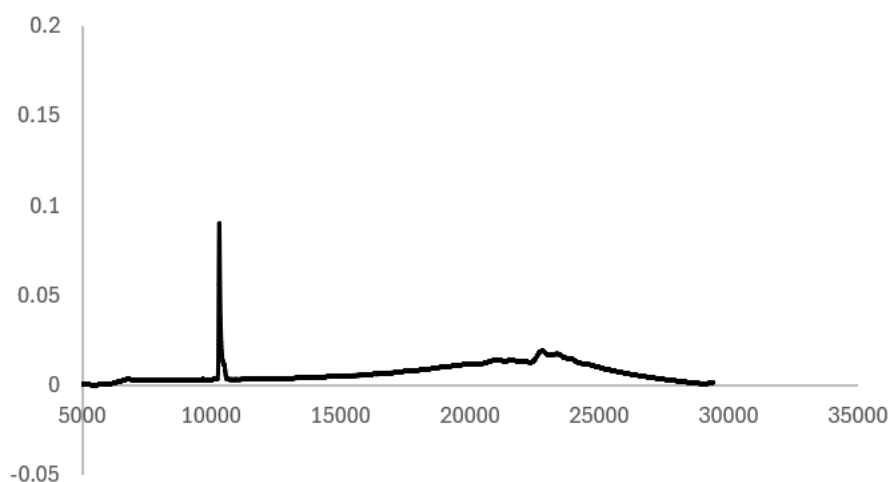
A 25 mL vessel of CEM discover bio manual peptide synthesizer was charged with 0.25 mmol of leucine wang resin. The Fmoc group was removed by using a 20% piperidine solution in DMF (10 mL). Using Synergy software, the deprotection protocol was run. The piperidine solution was drained and the resin was washed with DMF (4 x 10 mL). Fmoc-L-threonine(tBu)-OH (5 eq, 1.25 mM) along with Oxyma (5 eq, 1.25 mM) and DIC (5 eq, 1.35 mmol) in DMF was added to the reaction vessel and the coupling protocol was run. The amino acid solution was drained, and the resin was washed with DMF (2 x 10 mL). The fmoc removal and coupling procedure was repeated as before using the same equivalencies for the remaining amino acids. To remove the peptide from resin, a TFA cocktail solution (95% TFA, 2.5% TIPS, and 2.5% DCM) was added to the resin and agitated for 2 hours. The resin was filtered, and the resulting solution was concentrated in vacuo. The peptide was triturated with cold diethyl ether and purified using reverse phase HPLC using H<sub>2</sub>O/CH<sub>3</sub>CN. The sample was analyzed for purity using a Waters 1525 Binary HPLC Pump using a Phenomenex Luna 5u C8(2) 100A (250 x 4.60 mm) column; gradient eluted with H<sub>2</sub>O/CH<sub>3</sub>CN. Molecular weight was confirmed using high resolution electrospray ionization mass spectrometry (HRMS, ESI/MS) analyses obtained on an Agilent 6545B Q-TOF LC/MS equipped with 1260 infinity II LC system with auto sampler. The final peptide product was lyophilized and stored at -20°C.

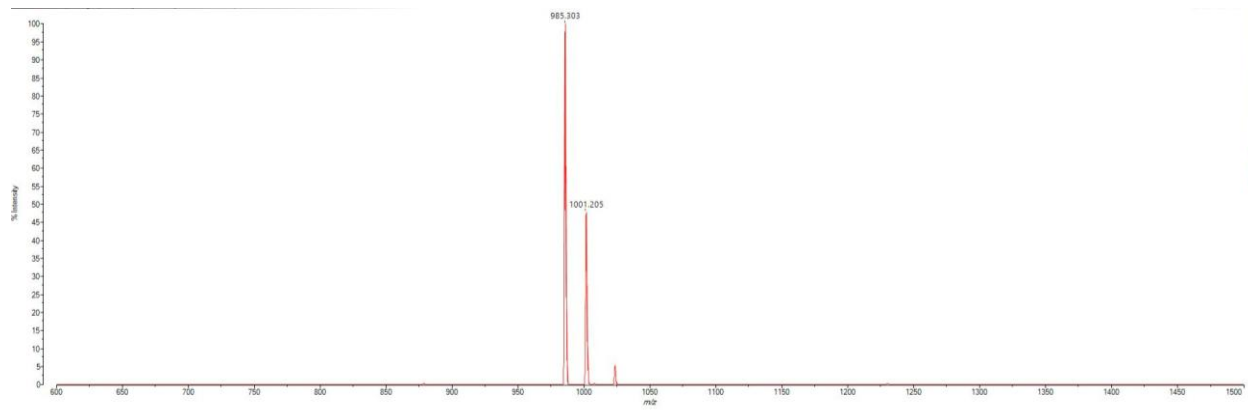




**Scheme S16. Synthesis of TALEDLSTL**

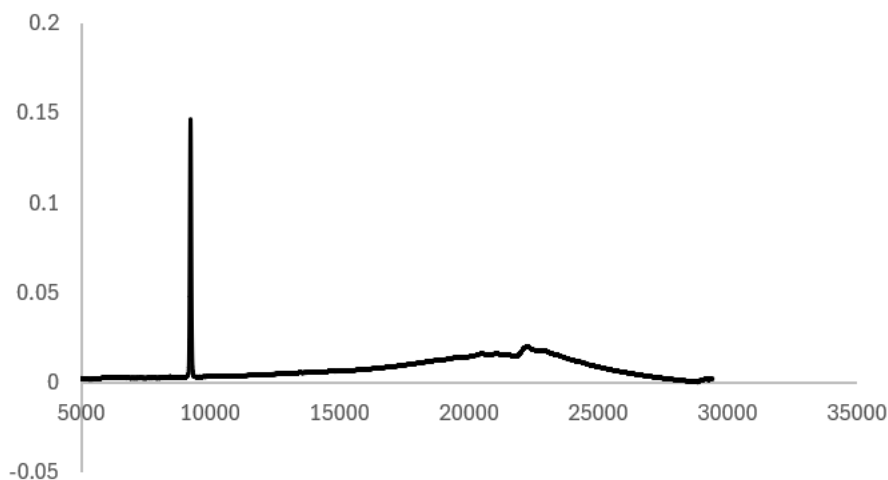
A 25 mL vessel of CEM discover bio manual peptide synthesizer was charged with 0.25 mmol of leucine wang resin. The Fmoc group was removed by using a 20% piperidine solution in DMF (10 mL). Using Synergy software, the deprotection protocol was run. The piperidine solution was drained and the resin was washed with DMF (4 x 10 mL). Fmoc-L-threonine(tBu)-OH (5 eq, 1.25 mM) along with Oxyma (5 eq, 1.25 mM) and DIC (5 eq, 1.35 mmol) in DMF was added to the reaction vessel and the coupling protocol was run. The amino acid solution was drained, and the resin was washed with DMF (2 x 10 mL). The fmoc removal and coupling procedure was repeated as before using the same equivalencies for the remaining amino acids. To remove the peptide from resin, a TFA cocktail solution (95% TFA, 2.5% TIPS, and 2.5% DCM) was added to the resin and agitated for 2 hours. The resin was filtered, and the resulting solution was concentrated in vacuo. The peptide was triturated with cold diethyl ether and purified using reverse phase HPLC using H<sub>2</sub>O/CH<sub>3</sub>CN. The sample was analyzed for purity using a Waters 1525 Binary HPLC Pump using a Phenomenex Luna 5u C8(2) 100A (250 x 4.60 mm) column; gradient eluted with H<sub>2</sub>O/CH<sub>3</sub>CN. Molecular weight was confirmed using high resolution electrospray ionization mass spectrometry (HRMS, ESI/MS) analyses obtained on an Agilent 6545B Q-TOF LC/MS equipped with 1260 infinity II LC system with auto sampler. The final peptide product was lyophilized and stored at -20°C.

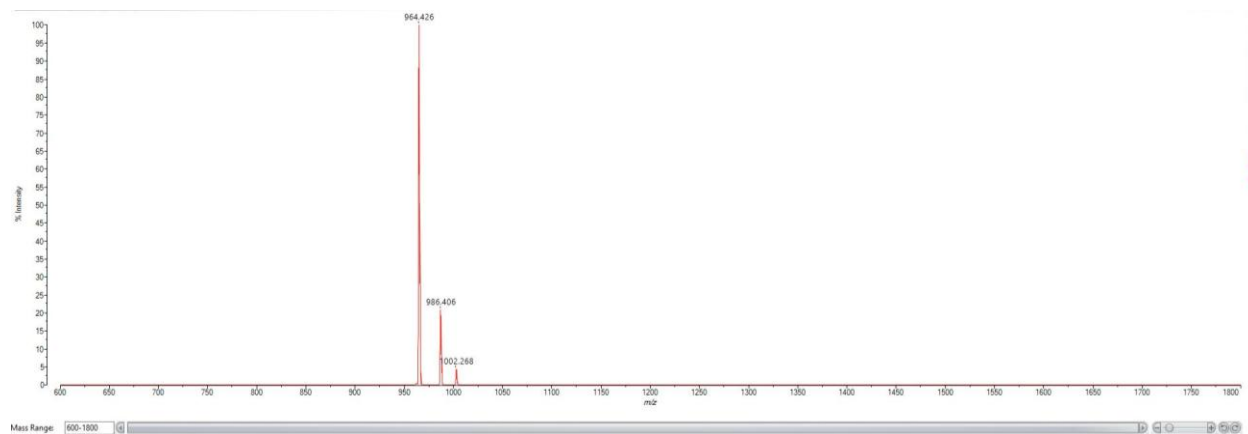




**Scheme S17. Synthesis of TALED(iso)LSTL**

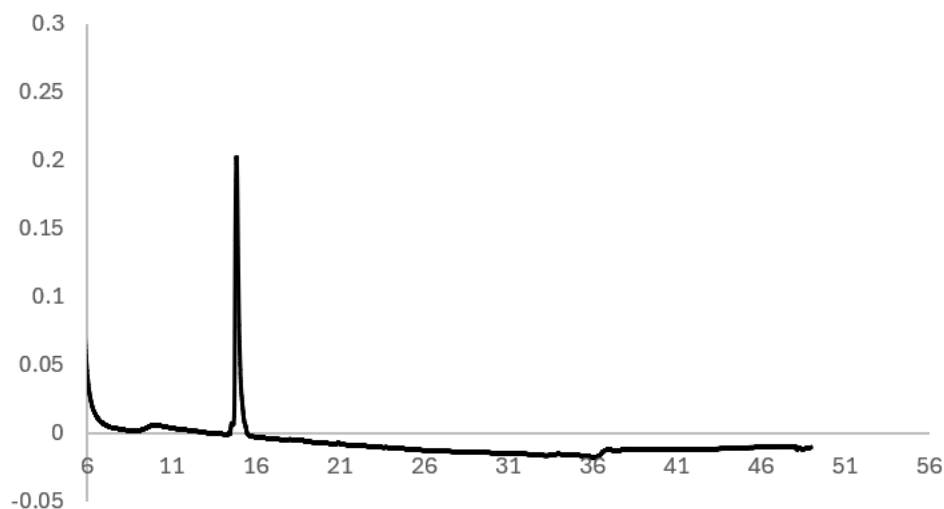
A 25 mL vessel of CEM discover bio manual peptide synthesizer was charged with 0.25 mmol of leucine wang resin. The Fmoc group was removed by using a 20% piperidine solution in DMF (10 mL). Using Synergy software, the deprotection protocol was run. The piperidine solution was drained and the resin was washed with DMF (4 x 10 mL). Fmoc-L-threonine(tBu)-OH (5 eq, 1.25 mM) along with Oxyma (5 eq, 1.25 mM) and DIC (5 eq, 1.35 mmol) in DMF was added to the reaction vessel and the coupling protocol was run. The amino acid solution was drained, and the resin was washed with DMF (2 x 10 mL). The fmoc removal and coupling procedure was repeated as before using the same equivalencies for the remaining amino acids. To remove the peptide from resin, a TFA cocktail solution (95% TFA, 2.5% TIPS, and 2.5% DCM) was added to the resin and agitated for 2 hours. The resin was filtered, and the resulting solution was concentrated in vacuo. The peptide was triturated with cold diethyl ether and purified using reverse phase HPLC using H<sub>2</sub>O/CH<sub>3</sub>CN. The sample was analyzed for purity using a Waters 1525 Binary HPLC Pump using a Phenomenex Luna 5u C8(2) 100A (250 x 4.60 mm) column; gradient eluted with H<sub>2</sub>O/CH<sub>3</sub>CN. Molecular weight was confirmed using high resolution electrospray ionization mass spectrometry (HRMS, ESI/MS) analyses obtained on an Agilent 6545B Q-TOF LC/MS equipped with 1260 infinity II LC system with auto sampler. The final peptide product was lyophilized and stored at -20°C.

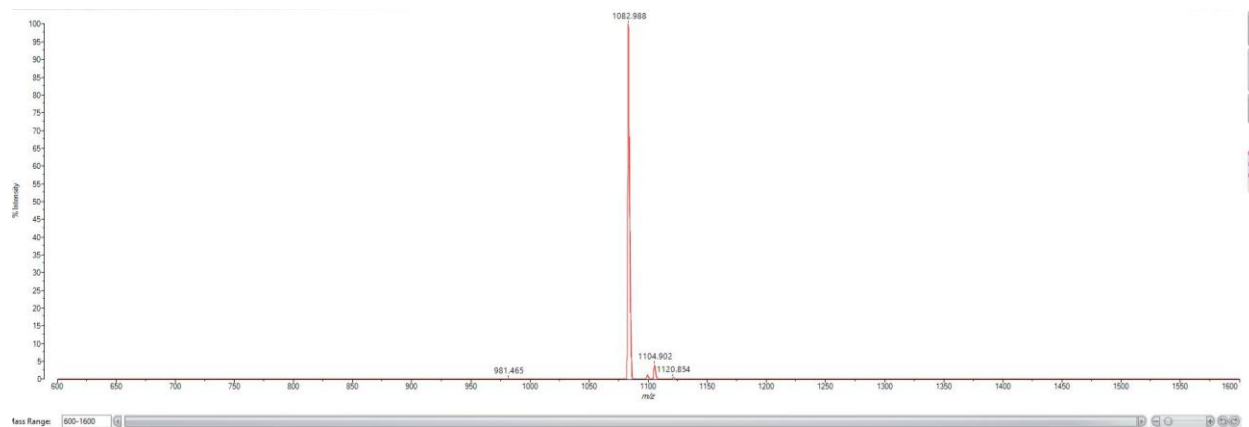




**Scheme S18. Synthesis of KGMNYTVRL**

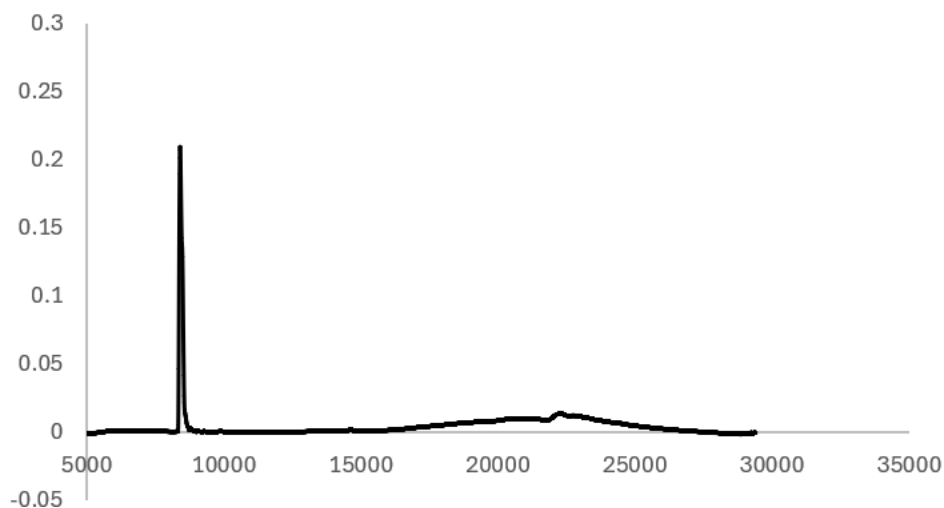
A 25 mL vessel of CEM discover bio manual peptide synthesizer was charged with 0.25 mmol of leucine wang resin. The Fmoc group was removed by using a 20% piperidine solution in DMF (10 mL). Using Synergy software, the deprotection protocol was run. The piperidine solution was drained and the resin was washed with DMF (4 x 10 mL). Fmoc-L-arginine(Pbf)-OH (5 eq, 1.25 mM) along with Oxyma (5 eq, 1.25 mM) and DIC (5 eq, 1.35 mmol) in DMF was added to the reaction vessel and the coupling protocol was run. The amino acid solution was drained, and the resin was washed with DMF (2 x 10 mL). The fmoc removal and coupling procedure was repeated as before using the same equivalencies for the remaining amino acids. To remove the peptide from resin, a TFA cocktail solution (95% TFA, 2.5% TIPS, and 2.5% DCM) was added to the resin and agitated for 2 hours. The resin was filtered, and the resulting solution was concentrated in vacuo. The peptide was triturated with cold diethyl ether and purified using reverse phase HPLC using H<sub>2</sub>O/CH<sub>3</sub>CN. The sample was analyzed for purity using a Waters 1525 Binary HPLC Pump using a Phenomenex Luna 5u C8(2) 100A (250 x 4.60 mm) column; gradient eluted with H<sub>2</sub>O/CH<sub>3</sub>CN. Molecular weight was confirmed using high resolution electrospray ionization mass spectrometry (HRMS, ESI/MS) analyses obtained on an Agilent 6545B Q-TOF LC/MS equipped with 1260 infinity II LC system with auto sampler. The final peptide product was lyophilized and stored at -20°C.

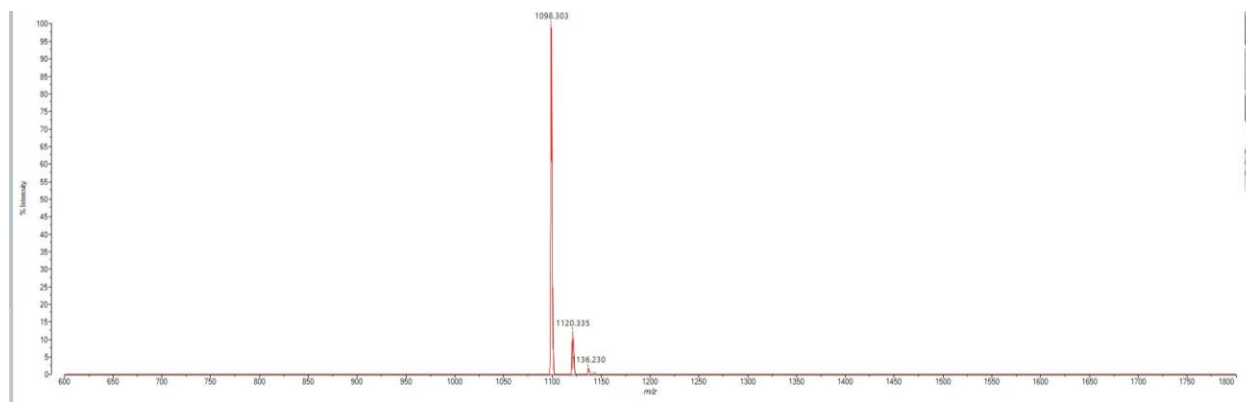




**Scheme S19. Synthesis of sulfoxide KGMNYTVRL**

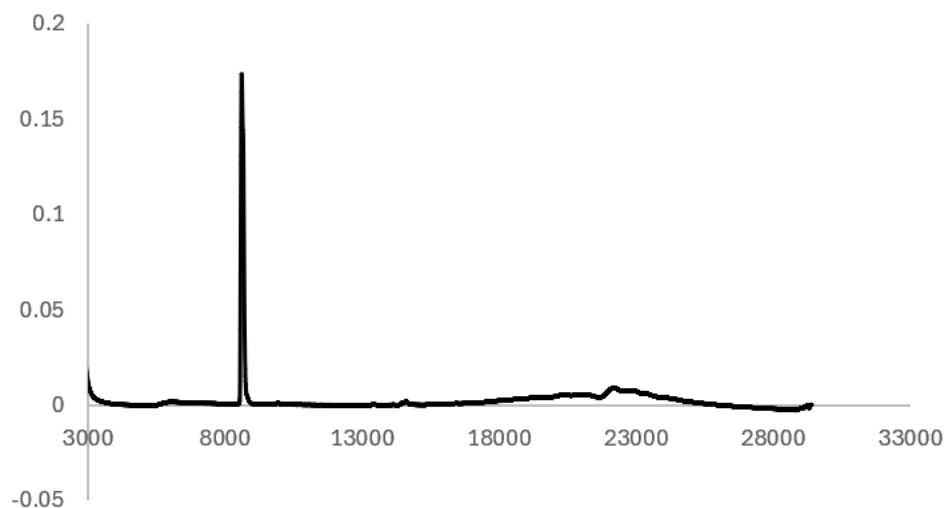
A 25 mL vessel of CEM discover bio manual peptide synthesizer was charged with 0.25 mmol of leucine wang resin. The Fmoc group was removed by using a 20% piperidine solution in DMF (10 mL). Using Synergy software, the deprotection protocol was run. The piperidine solution was drained and the resin was washed with DMF (4 x 10 mL). Fmoc-L-arginine(Pbf)-OH (5 eq, 1.25 mM) along with Oxyma (5 eq, 1.25 mM) and DIC (5 eq, 1.35 mmol) in DMF was added to the reaction vessel and the coupling protocol was run. The amino acid solution was drained, and the resin was washed with DMF (2 x 10 mL). The fmoc removal and coupling procedure was repeated as before using the same equivalencies for the remaining amino acids. For the sulfoxide modification, Fmoc-L-methionine sulfoxide (Chem Impex catalog # 03724) (5 eq, 1.25 mM) along with Oxyma (5 eq, 1.25 mM) and DIC (5 eq, 1.35 mmol) in DMF was added to the reaction vessel and the coupling protocol was run. To remove the peptide from resin, a TFA cocktail solution (95% TFA, 2.5% TIPS, and 2.5% DCM) was added to the resin and agitated for 2 hours. The resin was filtered, and the resulting solution was concentrated in vacuo. The peptide was triturated with cold diethyl ether and purified using reverse phase HPLC using H<sub>2</sub>O/CH<sub>3</sub>CN. The sample was analyzed for purity using a Waters 1525 Binary HPLC Pump using a Phenomenex Luna 5u C8(2) 100A (250 x 4.60 mm) column; gradient eluted with H<sub>2</sub>O/CH<sub>3</sub>CN. Molecular weight was confirmed using high resolution electrospray ionization mass spectrometry (HRMS, ESI/MS) analyses obtained on an Agilent 6545B Q-TOF LC/MS equipped with 1260 infinity II LC system with auto sampler. The final peptide product was lyophilized and stored at -20°C.

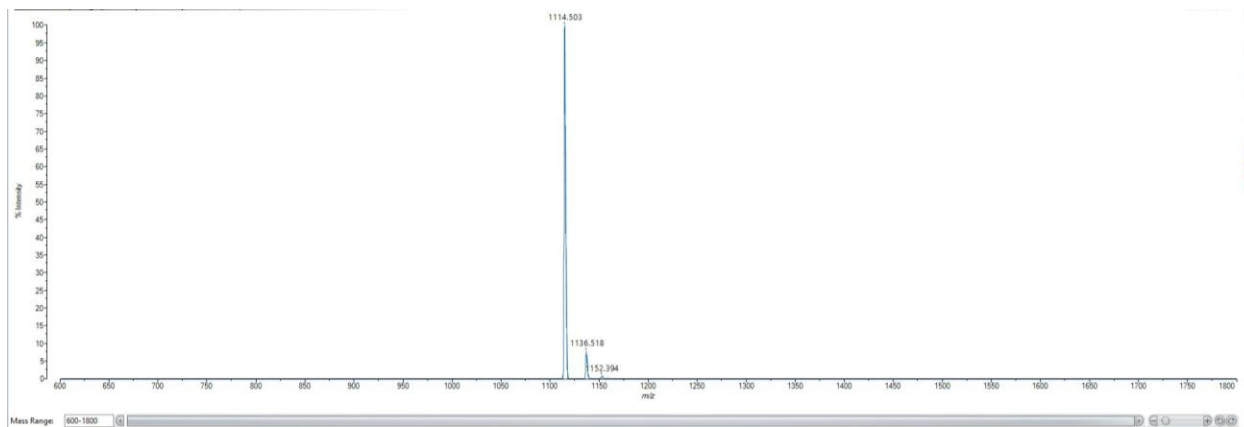




**Scheme S20. Synthesis of sulfone KGMNYTVRL**

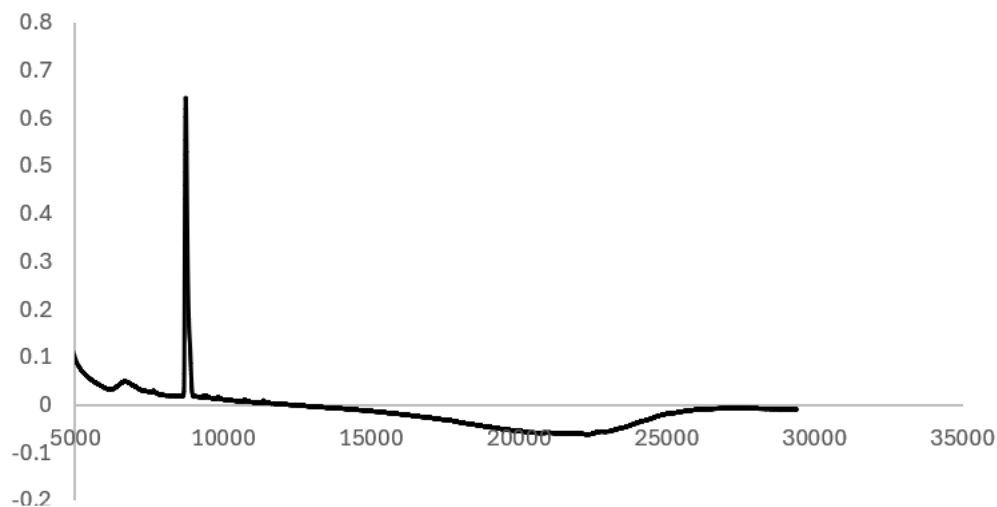
A 25 mL vessel of CEM discover bio manual peptide synthesizer was charged with 0.25 mmol of leucine wang resin. The Fmoc group was removed by using a 20% piperidine solution in DMF (10 mL). Using Synergy software, the deprotection protocol was run. The piperidine solution was drained and the resin was washed with DMF (4 x 10 mL). Fmoc-L-arginine(Pbf)-OH (5 eq, 1.25 mM) along with Oxyma (5 eq, 1.25 mM) and DIC (5 eq, 1.35 mmol) in DMF was added to the reaction vessel and the coupling protocol was run. The amino acid solution was drained, and the resin was washed with DMF (2 x 10 mL). The fmoc removal and coupling procedure was repeated as before using the same equivalencies for the remaining amino acids. For the sulfoxide modification, Fmoc-L-methionine sulfone (Chem Impex catalog # 03725) (5 eq, 1.25 mM) along with Oxyma (5 eq, 1.25 mM) and DIC (5 eq, 1.35 mmol) in DMF was added to the reaction vessel and the coupling protocol was run. To remove the peptide from resin, a TFA cocktail solution (95% TFA, 2.5% TIPS, and 2.5% DCM) was added to the resin and agitated for 2 hours. The resin was filtered, and the resulting solution was concentrated in vacuo. The peptide was trituated with cold diethyl ether and purified using reverse phase HPLC using H<sub>2</sub>O/CH<sub>3</sub>CN. The sample was analyzed for purity using a Waters 1525 Binary HPLC Pump using a Phenomenex Luna 5u C8(2) 100A (250 x 4.60 mm) column; gradient eluted with H<sub>2</sub>O/CH<sub>3</sub>CN. Molecular weight was confirmed using high resolution electrospray ionization mass spectrometry (HRMS, ESI/MS) analyses obtained on an Agilent 6545B Q-TOF LC/MS equipped with 1260 infinity II LC system with auto sampler. The final peptide product was lyophilized and stored at -20°C.

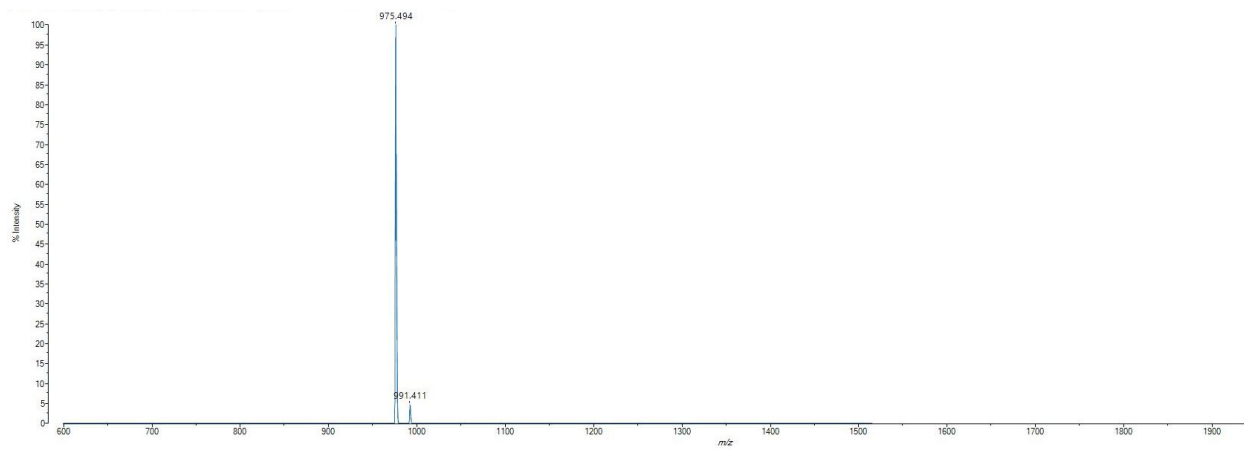




**Scheme S21. Synthesis of SAPENAVRM**

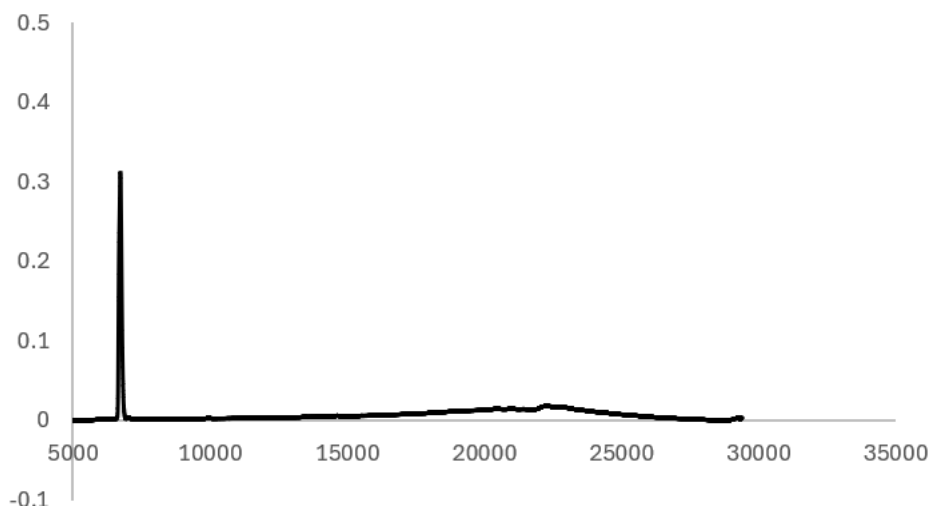
A 25 mL vessel of CEM discover bio manual peptide synthesizer was charged with 0.25 mmol of methionine wang resin. The Fmoc group was removed by using a 20% piperidine solution in DMF (10 mL). Using Synergy software, the deprotection protocol was run. The piperidine solution was drained and the resin was washed with DMF (4 x 10 mL). Fmoc-L-arginine(Pbf)-OH (5 eq, 1.25 mM) along with Oxyma (5 eq, 1.25 mM) and DIC (5 eq, 1.35 mmol) in DMF was added to the reaction vessel and the coupling protocol was run. The amino acid solution was drained, and the resin was washed with DMF (2 x 10 mL). The fmoc removal and coupling procedure was repeated as before using the same equivalencies for the remaining amino acids. To remove the peptide from resin, a TFA cocktail solution (95% TFA, 2.5% TIPS, and 2.5% DCM) was added to the resin and agitated for 2 hours. The resin was filtered, and the resulting solution was concentrated in vacuo. The peptide was triturated with cold diethyl ether and purified using reverse phase HPLC using H<sub>2</sub>O/CH<sub>3</sub>CN. The sample was analyzed for purity using a Waters 1525 Binary HPLC Pump using a Phenomenex Luna 5u C8(2) 100A (250 x 4.60 mm) column; gradient eluted with H<sub>2</sub>O/CH<sub>3</sub>CN. Molecular weight was confirmed using high resolution electrospray ionization mass spectrometry (HRMS, ESI/MS) analyses obtained on an Agilent 6545B Q-TOF LC/MS equipped with 1260 infinity II LC system with auto sampler. The final peptide product was lyophilized and stored at -20°C.

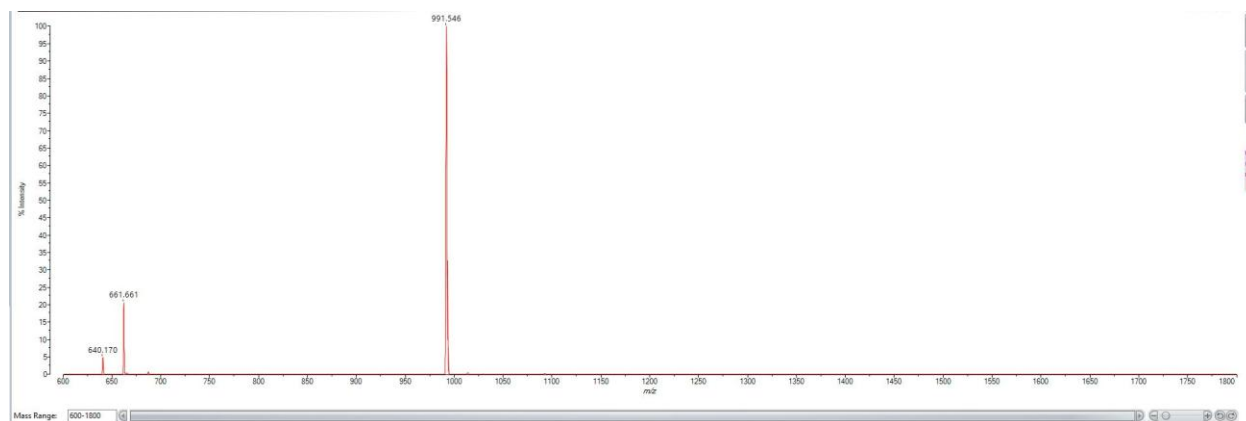




**Scheme S22. Synthesis of sulfoxide SAPENAVRM**

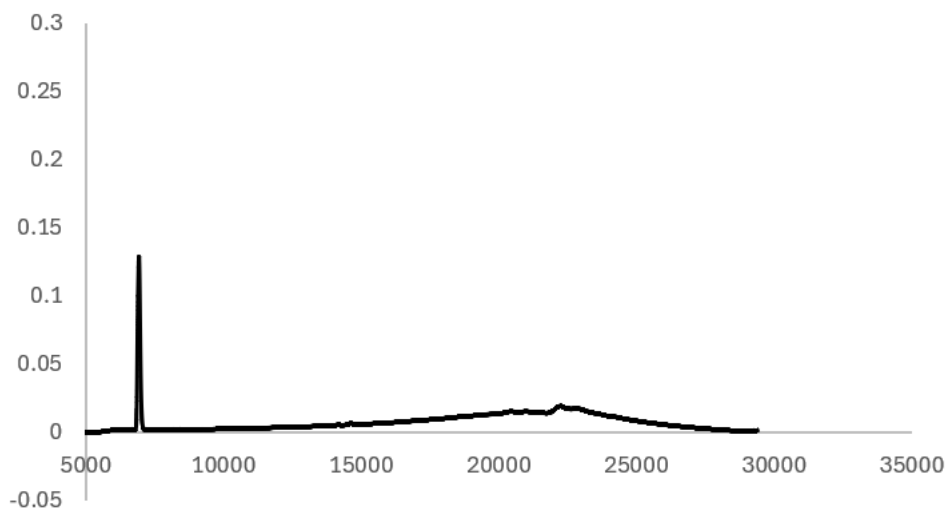
A 25 mL vessel of CEM discover bio manual peptide synthesizer was charged with 0.25 mmol of leucine wang resin. The Fmoc group was removed by using a 20% piperidine solution in DMF (10 mL). Using Synergy software, the deprotection protocol was run. The piperidine solution was drained and the resin was washed with DMF (4 x 10 mL). Fmoc-L-arginine(Pbf)-OH (5 eq, 1.25 mM) along with Oxyma (5 eq, 1.25 mM) and DIC (5 eq, 1.35 mmol) in DMF was added to the reaction vessel and the coupling protocol was run. The amino acid solution was drained, and the resin was washed with DMF (2 x 10 mL). The fmoc removal and coupling procedure was repeated as before using the same equivalencies for the remaining amino acids. For the sulfoxide modification, Fmoc-L-methionine sulfoxide (Chem Impex catalog # 03724) (5 eq, 1.25 mM) along with Oxyma (5 eq, 1.25 mM) and DIC (5 eq, 1.35 mmol) in DMF was added to the reaction vessel and the coupling protocol was run. To remove the peptide from resin, a TFA cocktail solution (95% TFA, 2.5% TIPS, and 2.5% DCM) was added to the resin and agitated for 2 hours. The resin was filtered, and the resulting solution was concentrated in vacuo. The peptide was triturated with cold diethyl ether and purified using reverse phase HPLC using H<sub>2</sub>O/CH<sub>3</sub>CN. The sample was analyzed for purity using a Waters 1525 Binary HPLC Pump using a Phenomenex Luna 5u C8(2) 100A (250 x 4.60 mm) column; gradient eluted with H<sub>2</sub>O/CH<sub>3</sub>CN. Molecular weight was confirmed using high resolution electrospray ionization mass spectrometry (HRMS, ESI/MS) analyses obtained on an Agilent 6545B Q-TOF LC/MS equipped with 1260 infinity II LC system with auto sampler. The final peptide product was lyophilized and stored at -20°C.

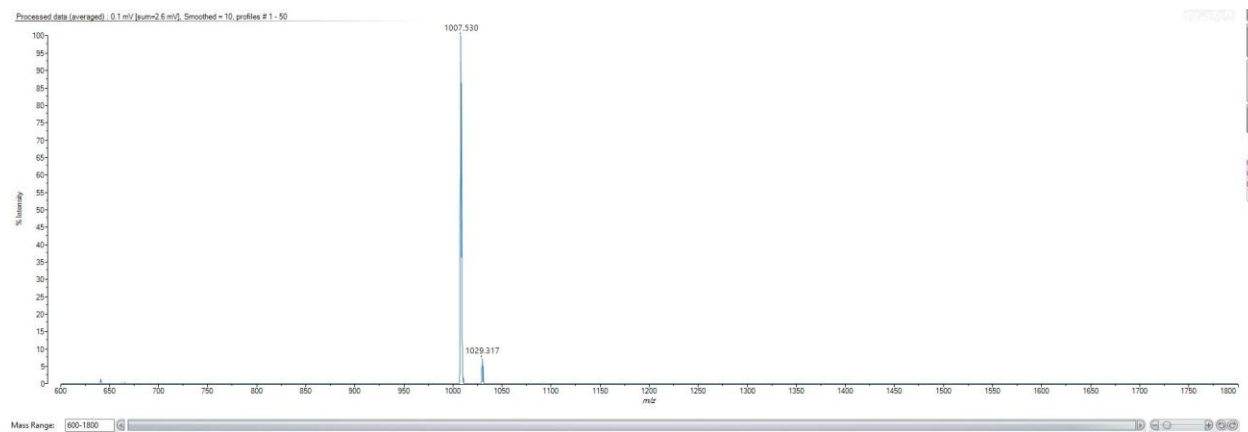




**Scheme S23. Synthesis of sulfone SAPENAVRM**

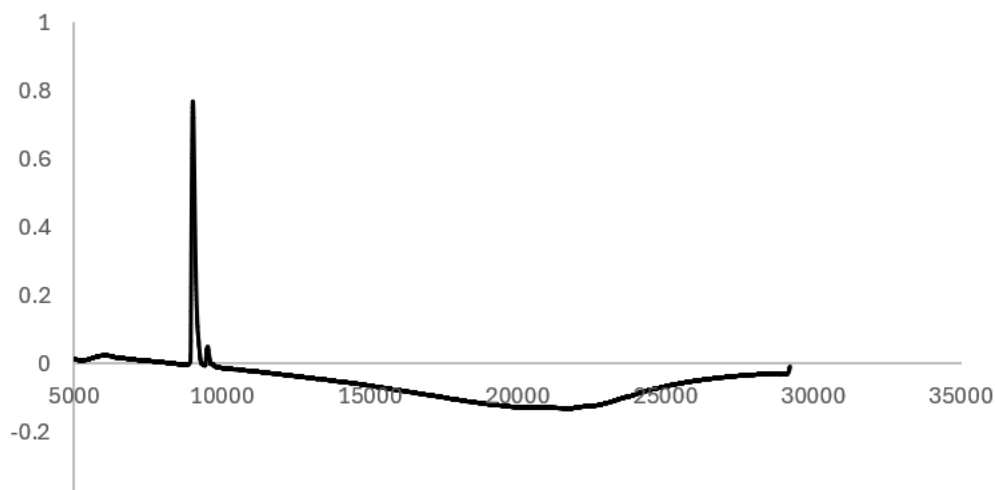
A 25 mL vessel of CEM discover bio manual peptide synthesizer was charged with 0.25 mmol of leucine wang resin. The Fmoc group was removed by using a 20% piperidine solution in DMF (10 mL). Using Synergy software, the deprotection protocol was run. The piperidine solution was drained and the resin was washed with DMF (4 x 10 mL). Fmoc-L-arginine(Pbf)-OH (5 eq, 1.25 mM) along with Oxyma (5 eq, 1.25 mM) and DIC (5 eq, 1.35 mmol) in DMF was added to the reaction vessel and the coupling protocol was run. The amino acid solution was drained, and the resin was washed with DMF (2 x 10 mL). The fmoc removal and coupling procedure was repeated as before using the same equivalencies for the remaining amino acids. For the sulfoxide modification, Fmoc-L-methionine sulfone (Chem Impex catalog # 03725) (5 eq, 1.25 mM) along with Oxyma (5 eq, 1.25 mM) and DIC (5 eq, 1.35 mmol) in DMF was added to the reaction vessel and the coupling protocol was run. To remove the peptide from resin, a TFA cocktail solution (95% TFA, 2.5% TIPS, and 2.5% DCM) was added to the resin and agitated for 2 hours. The resin was filtered, and the resulting solution was concentrated in vacuo. The peptide was triturated with cold diethyl ether and purified using reverse phase HPLC using H<sub>2</sub>O/CH<sub>3</sub>CN. The sample was analyzed for purity using a Waters 1525 Binary HPLC Pump using a Phenomenex Luna 5u C8(2) 100A (250 x 4.60 mm) column; gradient eluted with H<sub>2</sub>O/CH<sub>3</sub>CN. Molecular weight was confirmed using high resolution electrospray ionization mass spectrometry (HRMS, ESI/MS) analyses obtained on an Agilent 6545B Q-TOF LC/MS equipped with 1260 infinity II LC system with auto sampler. The final peptide product was lyophilized and stored at -20°C.

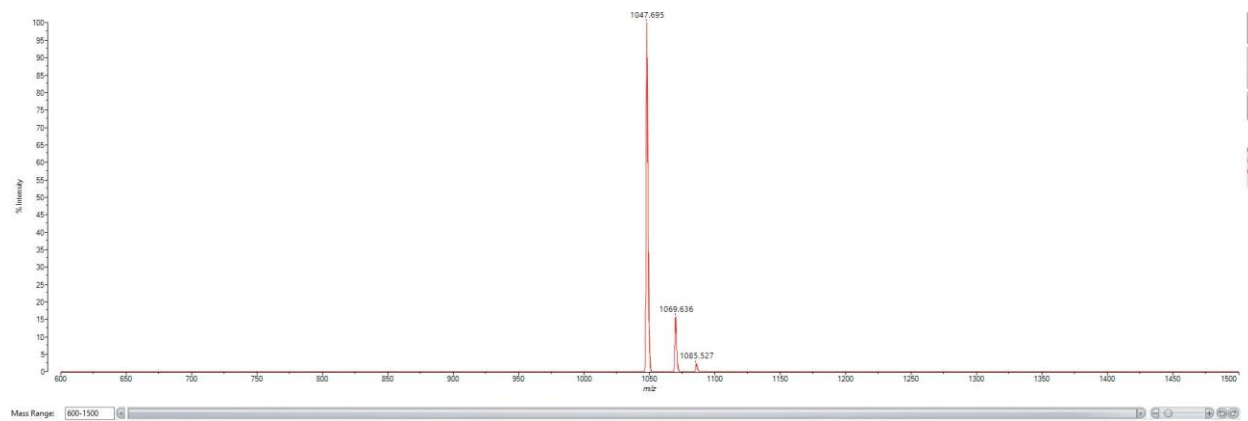




**Scheme S24. Synthesis of CGYEFTSKL**

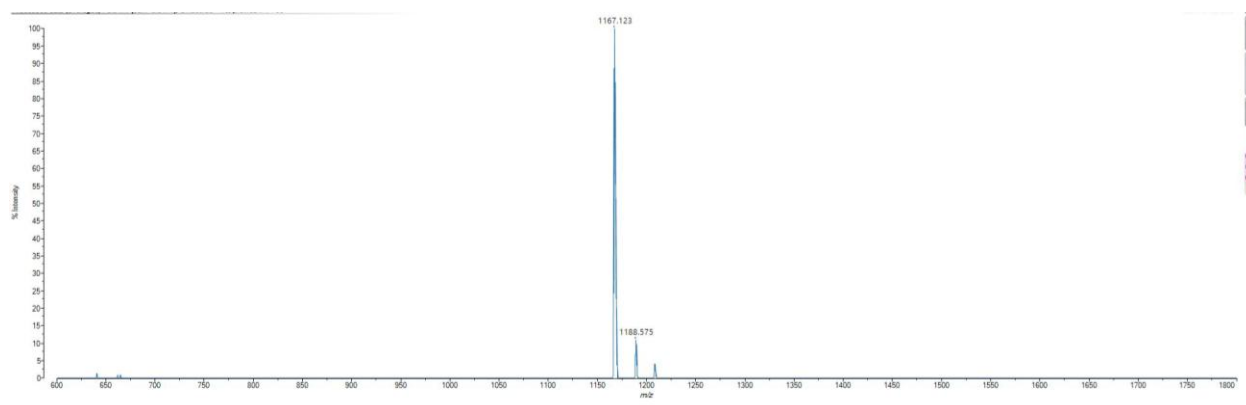
A 25 mL vessel of CEM discover bio manual peptide synthesizer was charged with 0.25 mmol of leucine wang resin. The Fmoc group was removed by using a 20% piperidine solution in DMF (10 mL). Using Synergy software, the deprotection protocol was run. The piperidine solution was drained and the resin was washed with DMF (4 x 10 mL). Fmoc-L-lysine(boc)-OH (5 eq, 1.25 mM) along with Oxyma (5 eq, 1.25 mM) and DIC (5 eq, 1.35 mmol) in DMF was added to the reaction vessel and the coupling protocol was run. The amino acid solution was drained, and the resin was washed with DMF (2 x 10 mL). The fmoc removal and coupling procedure was repeated as before using the same equivalencies for the remaining amino acids. To remove the peptide from resin, a TFA cocktail solution (95% TFA, 2.5% TIPS, and 2.5% DCM) was added to the resin and agitated for 2 hours. The resin was filtered, and the resulting solution was concentrated in vacuo. The peptide was triturated with cold diethyl ether and purified using reverse phase HPLC using H<sub>2</sub>O/CH<sub>3</sub>CN. The sample was analyzed for purity using a Waters 1525 Binary HPLC Pump using a Phenomenex Luna 5u C8(2) 100A (250 x 4.60 mm) column; gradient eluted with H<sub>2</sub>O/CH<sub>3</sub>CN. Molecular weight was confirmed using high resolution electrospray ionization mass spectrometry (HRMS, ESI/MS) analyses obtained on an Agilent 6545B Q-TOF LC/MS equipped with 1260 infinity II LC system with auto sampler. The final peptide product was lyophilized and stored at -20°C.





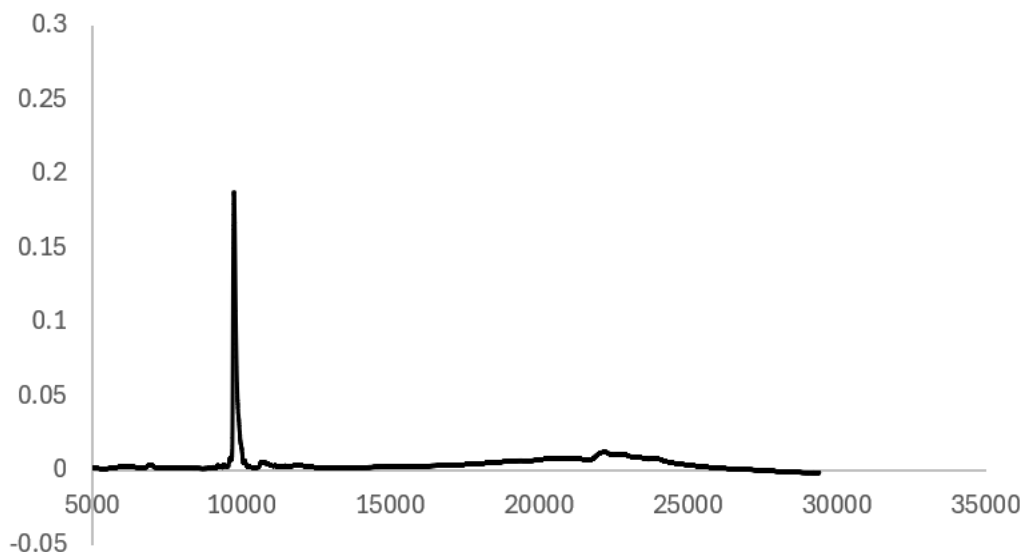
### Scheme S25. Synthesis of cysteinylated CGYEFTSKL

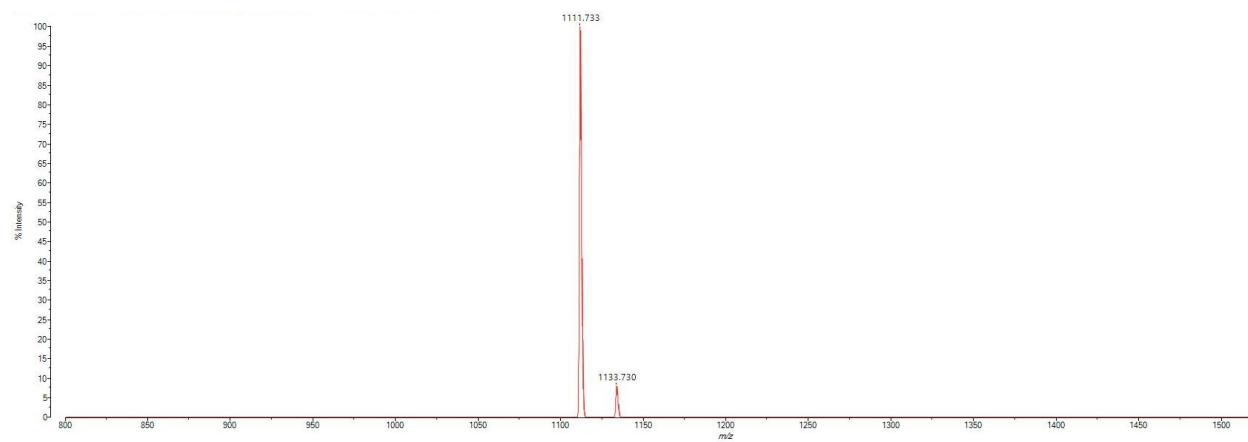
A 25 mL vessel of CEM discover bio manual peptide synthesizer was charged with 0.25 mmol of leucine wang resin. The Fmoc group was removed by using a 20% piperidine solution in DMF (10 mL). Using Synergy software, the deprotection protocol was run. The piperidine solution was drained and the resin was washed with DMF (4 x 10 mL). Fmoc-L-lysine(boc)-OH (5 eq, 1.25 mM) along with Oxyma (5 eq, 1.25 mM) and DIC (5 eq, 1.35 mmol) in DMF was added to the reaction vessel and the coupling protocol was run. The amino acid solution was drained, and the resin was washed with DMF (2 x 10 mL). The fmoc removal and coupling procedure was repeated as before using the same equivalencies for the remaining amino acids. To remove the peptide from resin, a TFA cocktail solution (95% TFA, 2.5% TIPS, and 2.5% DCM) was added to the resin and agitated for 2 hours. The resin was filtered, and the resulting solution was concentrated in vacuo. The peptide was triturated with cold diethyl ether and purified using reverse phase HPLC using H<sub>2</sub>O/CH<sub>3</sub>CN. The sample was analyzed for purity using a Waters 1525 Binary HPLC Pump using a Phenomenex Luna 5u C8(2) 100A (250 x 4.60 mm) column; gradient eluted with H<sub>2</sub>O/CH<sub>3</sub>CN. Molecular weight was confirmed using high resolution electrospray ionization mass spectrometry (HRMS, ESI/MS) analyses obtained on an Agilent 6545B Q-TOF LC/MS equipped with 1260 infinity II LC system with auto sampler. The final peptide product was lyophilized and stored at -20°C.



**Scheme S26. Synthesis of VAYEYLCHL**

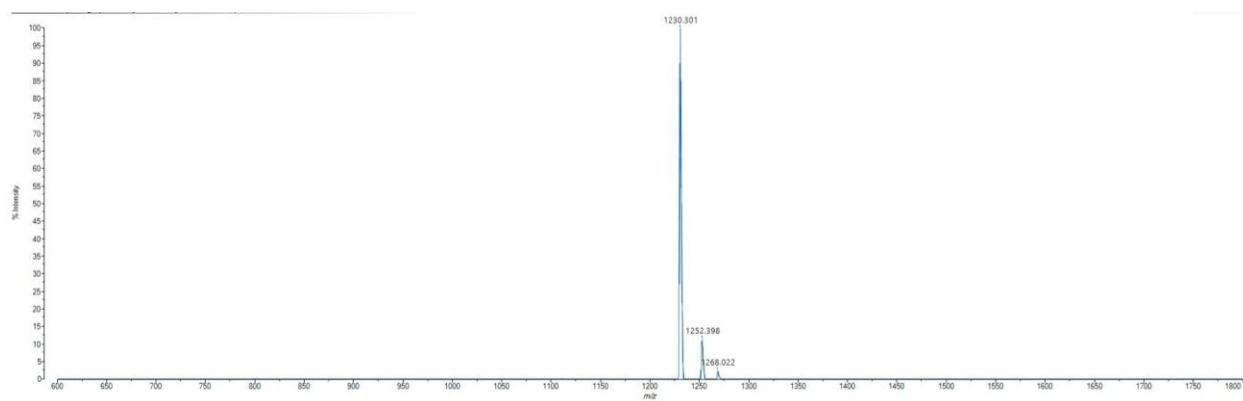
A 25 mL vessel of CEM discover bio manual peptide synthesizer was charged with 0.25 mmol of leucine wang resin. The Fmoc group was removed by using a 20% piperidine solution in DMF (10 mL). Using Synergy software, the deprotection protocol was run. The piperidine solution was drained and the resin was washed with DMF (4 x 10 mL). Fmoc-L-histidine(trt)-OH (5 eq, 1.25 mM) along with Oxyma (5 eq, 1.25 mM) and DIC (5 eq, 1.35 mmol) in DMF was added to the reaction vessel and the coupling protocol was run. The amino acid solution was drained, and the resin was washed with DMF (2 x 10 mL). The fmoc removal and coupling procedure was repeated as before using the same equivalencies for the remaining amino acids. To remove the peptide from resin, a TFA cocktail solution (95% TFA, 2.5% TIPS, and 2.5% DCM) was added to the resin and agitated for 2 hours. The resin was filtered, and the resulting solution was concentrated in vacuo. The peptide was triturated with cold diethyl ether and purified using reverse phase HPLC using H<sub>2</sub>O/CH<sub>3</sub>CN. The sample was analyzed for purity using a Waters 1525 Binary HPLC Pump using a Phenomenex Luna 5u C8(2) 100A (250 x 4.60 mm) column; gradient eluted with H<sub>2</sub>O/CH<sub>3</sub>CN. Molecular weight was confirmed using high resolution electrospray ionization mass spectrometry (HRMS, ESI/MS) analyses obtained on an Agilent 6545B Q-TOF LC/MS equipped with 1260 infinity II LC system with auto sampler. The final peptide product was lyophilized and stored at -20°C.





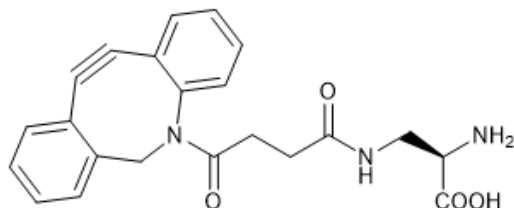
**Scheme S27. Synthesis of cysteinylated VAYEYLCHL**

A 25 mL vessel of CEM discover bio manual peptide synthesizer was charged with 0.25 mmol of leucine wang resin. The Fmoc group was removed by using a 20% piperidine solution in DMF (10 mL). Using Synergy software, the deprotection protocol was run. The piperidine solution was drained and the resin was washed with DMF (4 x 10 mL). Fmoc-L-histidine(trt)-OH (5 eq, 1.25 mM) along with Oxyma (5 eq, 1.25 mM) and DIC (5 eq, 1.35 mmol) in DMF was added to the reaction vessel and the coupling protocol was run. The amino acid solution was drained, and the resin was washed with DMF (2 x 10 mL). The fmoc removal and coupling procedure was repeated as before using the same equivalencies for the remaining amino acids. To remove the peptide from resin, a TFA cocktail solution (95% TFA, 2.5% TIPS, and 2.5% DCM) was added to the resin and agitated for 2 hours. The resin was filtered, and the resulting solution was concentrated in vacuo. The peptide was triturated with cold diethyl ether and purified using reverse phase HPLC using H<sub>2</sub>O/CH<sub>3</sub>CN. The sample was analyzed for purity using a Waters 1525 Binary HPLC Pump using a Phenomenex Luna 5u C8(2) 100A (250 x 4.60 mm) column; gradient eluted with H<sub>2</sub>O/CH<sub>3</sub>CN. Molecular weight was confirmed using high resolution electrospray ionization mass spectrometry (HRMS, ESI/MS) analyses obtained on an Agilent 6545B Q-TOF LC/MS equipped with 1260 infinity II LC system with auto sampler. The final peptide product was lyophilized and stored at -20°C.

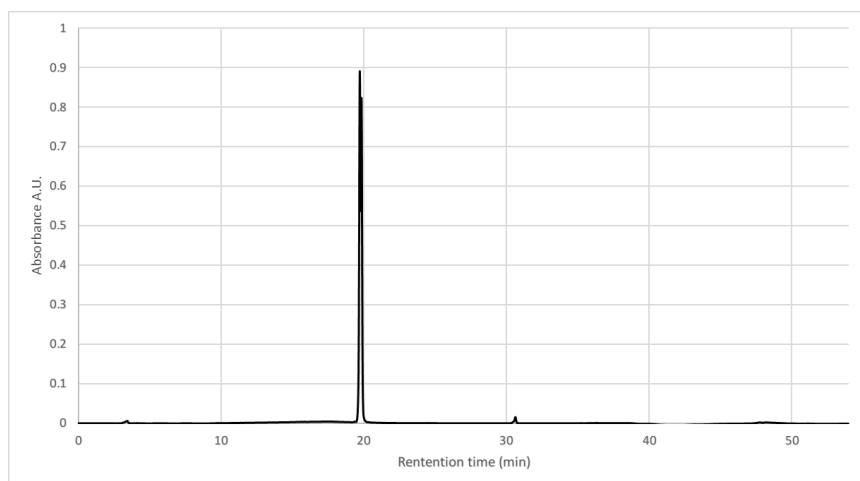


### A.7 Synthesis and Characterization of Compounds in Chapter 7

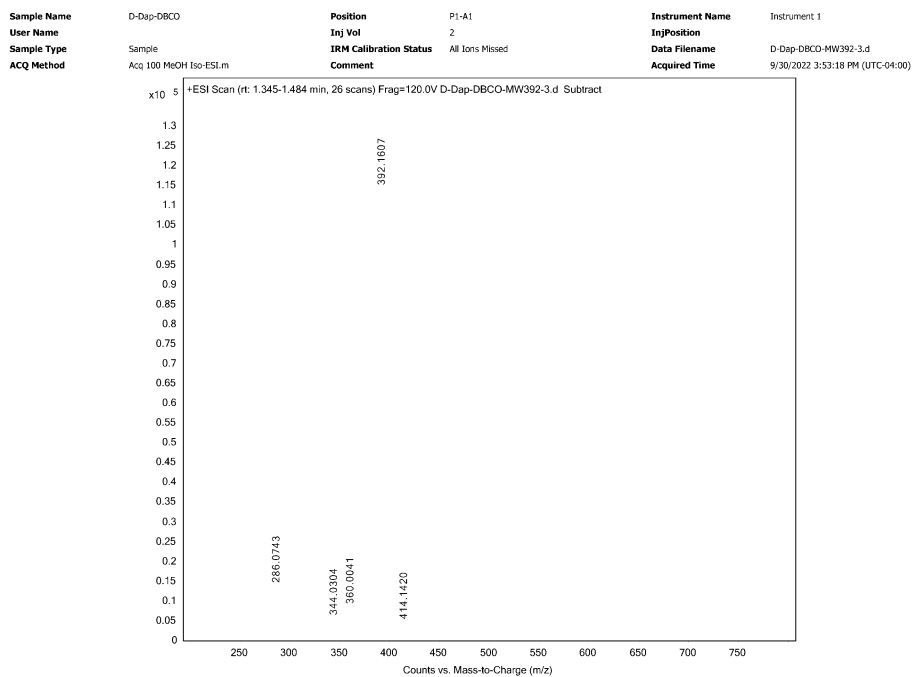
#### Scheme S1. Synthesis of D-DapD



To a 25 mL peptide synthesis vessel with 100 mg 2-Chlorotrityl chloride resin (0.142 mmol) resuspended in 15 mL dry dichloromethane, was added  $\alpha$ -Boc-N $\beta$ -Fmoc-D-2,3-diaminopropionic acid (D-Dap, 67 mg, 1.1 eq, 0.16 mmol), and DIEA (4.4 eq, 0.11 mL, 0.62 mmol). The resin was shaken for 1 hour at room temperature and washed with methanol and dichloromethane (3 times and 15 mL each). Fmoc protecting group was removed with 6M piperazine in N, N-Dimethylformamide (DMF, 15 mL) for 30 min at room temperature and washed as before. DBCO was coupled on the side chain of D-Dap on resin. 25-30 mg DBCO-NHS was dissolved in 1 mL dry DMF and added to the 25 mL peptide synthesis vessel with 100 mg equivalent 2-Chlorotrityl chloride resin with D-Dap resuspended in 2 mL DMF. The resin was shaken overnight at room temperature and washed with methanol and dichloromethane (3 times and 15 mL each). The resin was then added 20% trifluoroacetic acid (TFA) in dichloromethane after wash and shaken in room temperature for 1 h. The liquid phase was filtered and concentrated with nitrogen flow and added icy ether to precipitate the peptide. The ether layer was decanted, and the resulting solid was washed with icy ether and air dried. The crude material was purified with reverse phased high performance liquid chromatography (RP-HPLC) using a 40 to 100% linear gradient of methanol in H<sub>2</sub>O/MeOH with 0.1% TFA to yield **D-DapD**. The sample was analyzed for purity using a Waters 1525 with a Phenomenex Luna 5 $\mu$  C8(2) 100 Å (250 x 4.6 mm) column; gradient elution with H<sub>2</sub>O/CH<sub>3</sub>CN. Molecular weight was confirmed using an Agilent LC-QTOF (Agilent 1260 Infinity II Prime LC with Agilent 6545B QTOF).



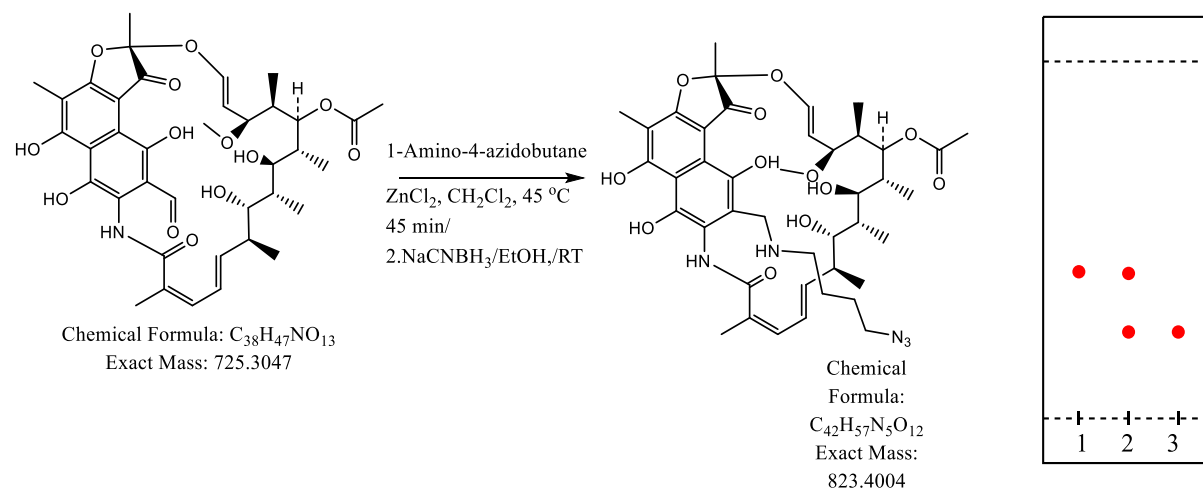
Calculated (M+H)<sup>+</sup>, 392.1605, found: (M+H)<sup>+</sup> 392.1607.



\*Note: <sup>1</sup>H and <sup>13</sup>C-NMR spectra for all new compounds and intermediates for characterization were acquired on a Varian 600MHz spectrophotometer. All NMR spectra were analyzed using MestreNova software. Residual solvent signal from CDCl<sub>3</sub>, CD<sub>3</sub>OD and DMSO-d<sub>6</sub> referenced to tetramethylsilane (TMS) were used as reference standards for defining chemical shifts of <sup>1</sup>H or <sup>13</sup>C spectra of compounds. Chemical



### Scheme S2. Synthesis of Rifampicin-azidobutane



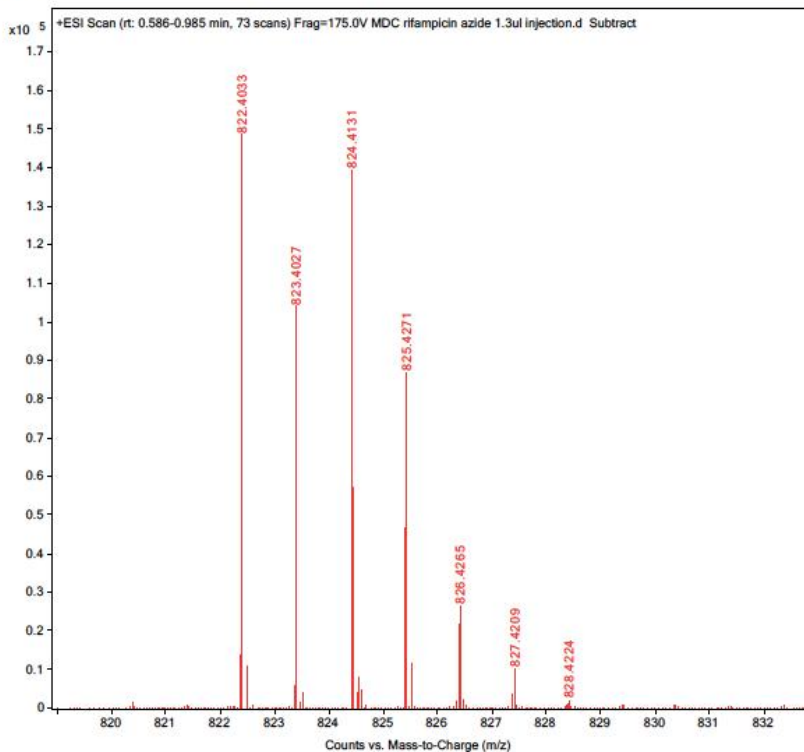
Rifampicine aldehyde (72.5mg, 0.1 mmol) dissolved in 5.0mL of anhydrous methylene chloride in 50 mL RB flask equipped with reflux condenser, to this solution was added 1-amino-4-azidobutane (17.1 mg, 0.15 mmol), followed by  $ZnCl_2$  (11.0mg, at room temperature and the mixture was refluxed at 45 °C in an oil bath for 45 minutes. The mixture was the allowed cooled to room temperature. The solvents were evaporated, and crude material as is used for reduction of iminium. The crude material was dissolved in ethanol (200% proof, 2.5mL), sodium cyanoborohydride (10.7 mg, 0.17mmol) was added to it and stirred the mixture at room temperature for 2 hr. TLC analysis of crude material indicated complete conversion starting material ( $R_t \sim 0.4$ ) to polar new compound ( $R_t \sim 0.2$ ) in EtOAc:methanol (95:5) . The volatiles were removed under vacuo using rotary evaporator. The remaining residue was dissolved in EtOAc and purified by column

chromatography over silica gel using gradient ranging from ethyl acetate to 3% methanol EtOAc. Fractions showing homogeneity on TLC were combined and concentrated under reduced pressure to yield red solid (65.1 mg, 79%). Further purification with reverse phase HPLC (80:20; Water;Methanol) afforded pure compound used for assay.

Molecular weight was confirmed using an Agilent LC-QTOF (Agilent 1260 Infinity II Prime LC with Agilent 6545B QTOF).

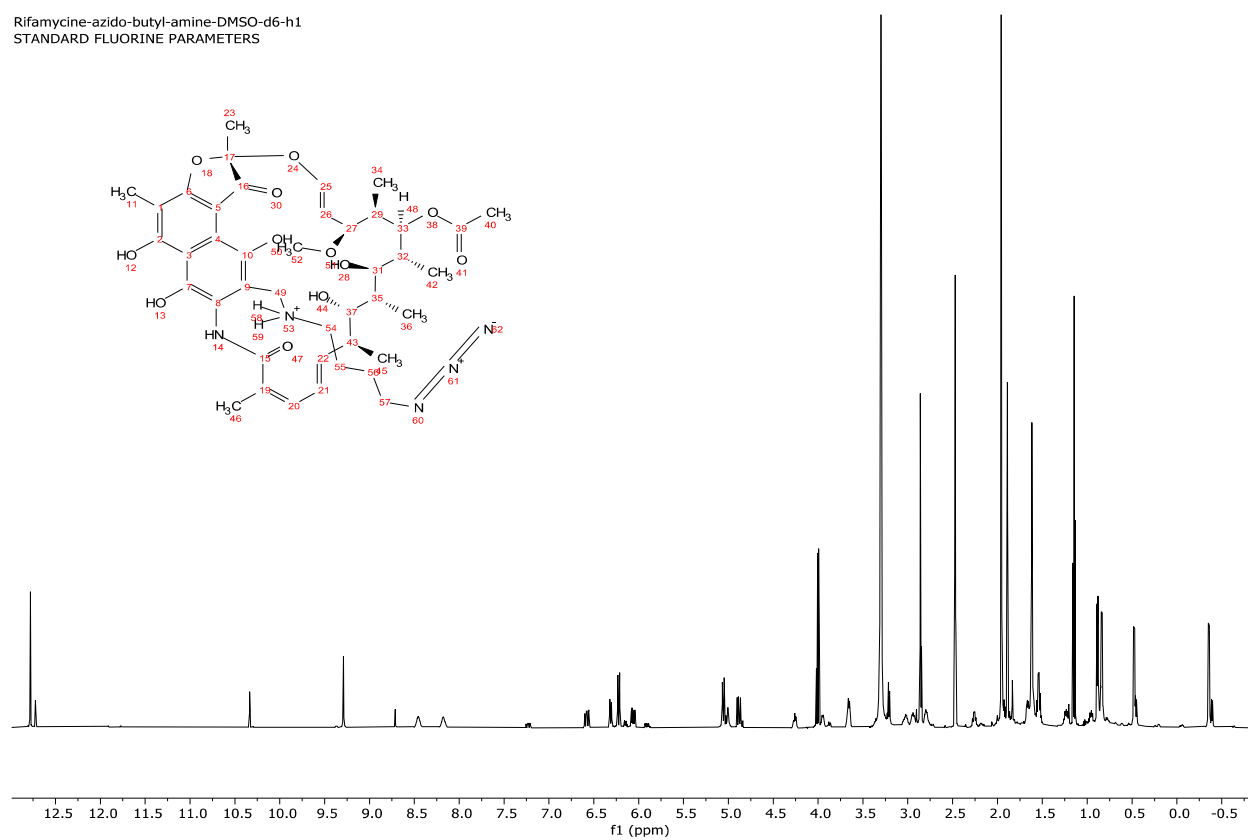
Calculated m/z, 824.534, found m/z, 824.4131

<b>Sample Name</b>	MDC Rifampicin azide	<b>Position</b>	P1-A4	<b>Instrument Name</b>	Instrument 1
<b>User Name</b>		<b>Inj Vol</b>	1	<b>InjPosition</b>	
<b>Sample Type</b>	Sample	<b>IRM Calibration Status</b>	Success	<b>Data Filename</b>	MDC rifampicin azide 1.3ul Injection.d
<b>ACQ Method</b>	Acq_80_20 MeOH_H2O Iso.m	<b>Comment</b>		<b>Acquired Time</b>	8/26/2022 2:37:15 PM (UTC-04:00)

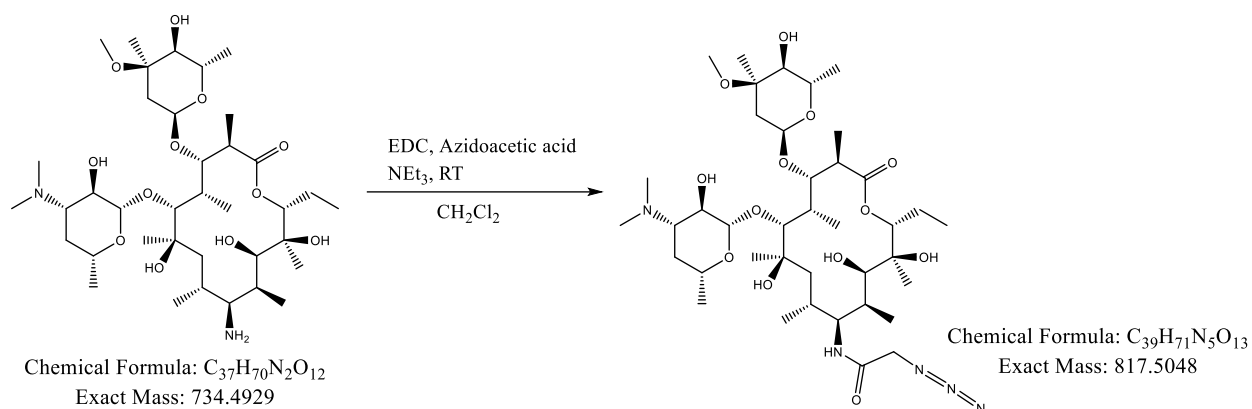


# <sup>1</sup>H-NMR

Rifamycine-azido-butyl-amine-DMSO-d6-h1  
STANDARD FLUORINE PARAMETERS



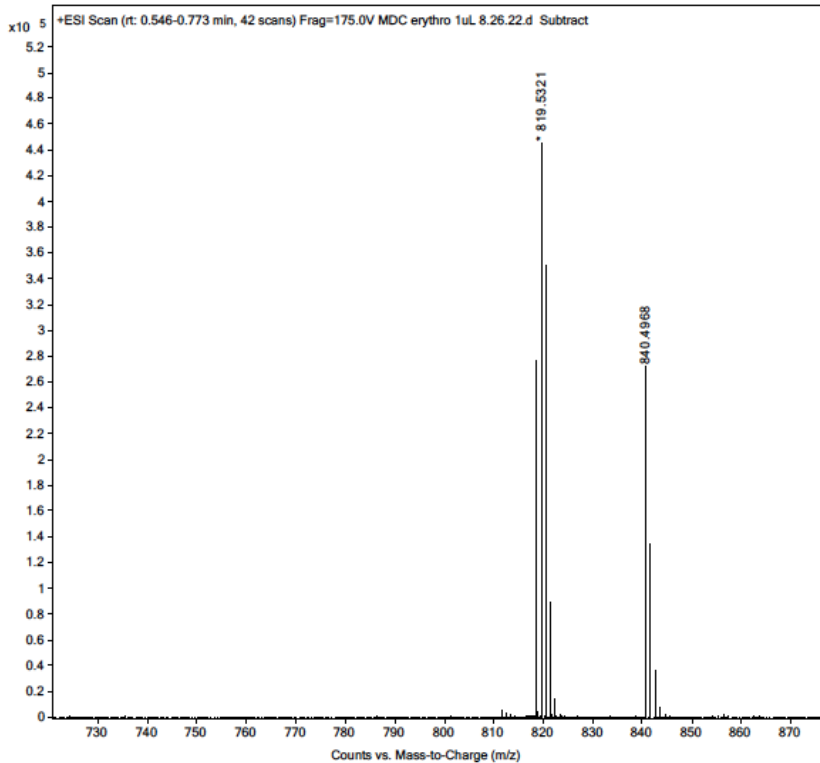
### Scheme S3. Synthesis of Erythromycin-azidoacetamide

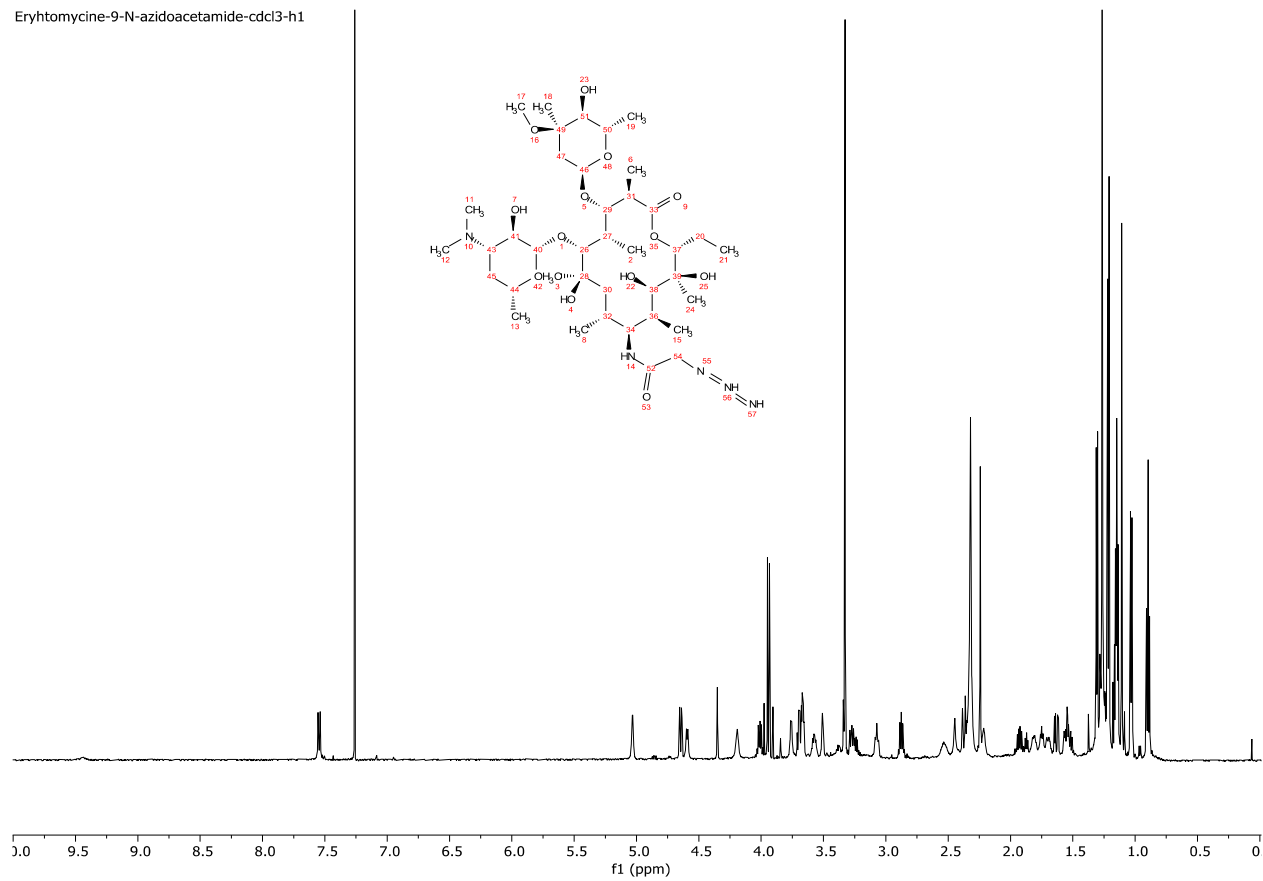


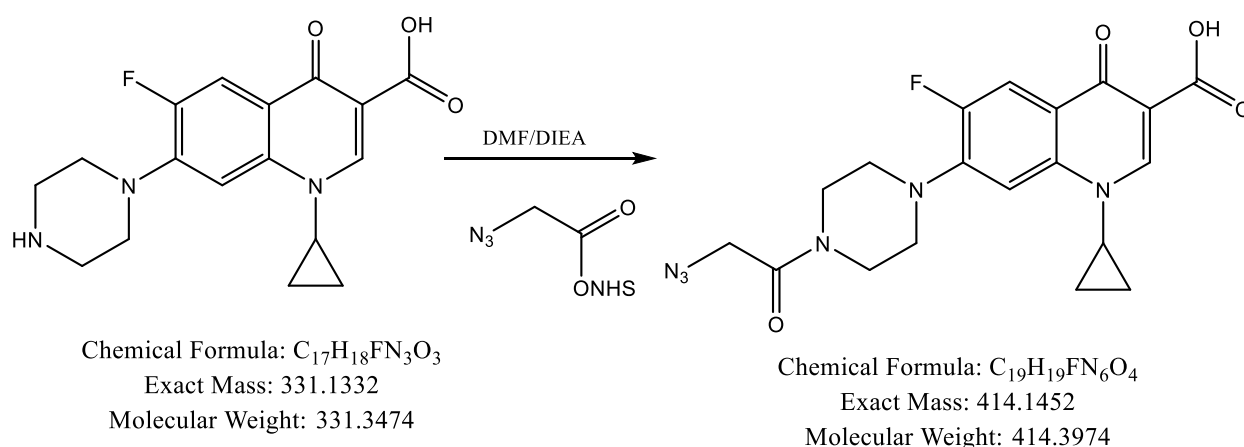
Erythromycin (25.1 mg, 0.034mmol) was dissolved in methylene chloride (5 mL), subsequently azido acetic acid (3.9 mg, 0.0386 mmol), EDC (11.5 mg) and triethyl amine (25.0ul) were added and mixture was stirred at room temperature for overnight (16hr). Next day, the solvents were evaporated under reduced pressure using rotary evaporator, the leftover crude material was purified by gradient reverse phase HPLC (C8, Water:MeOH; 95:5). The homogenous fractions collected at 205nm, were concentrated to yield pure compound. Molecular weight was confirmed using an Agilent LC-QTOF (Agilent 1260 Infinity II Prime LC with Agilent 6545B QTOF).

Calculated (M+D)<sup>+</sup>, 819.5208, found (M+D)<sup>+</sup>, 819.5321

<b>Sample Name</b>	MDC erythromycin azide	<b>Position</b>	P1-A3	<b>Instrument Name</b>	Instrument 1
<b>User Name</b>		<b>Inj Vol</b>	1	<b>Inj Position</b>	
<b>Sample Type</b>	Sample	<b>IRM Calibration Status</b>	Success	<b>Data Filename</b>	MDC erythro 1uL 8.26.22.d
<b>ACQ Method</b>	Acq 80_20 MeOH_H2O Iso.m	<b>Comment</b>		<b>Acquired Time</b>	8/26/2022 12:29:12 PM (UTC-04:00)



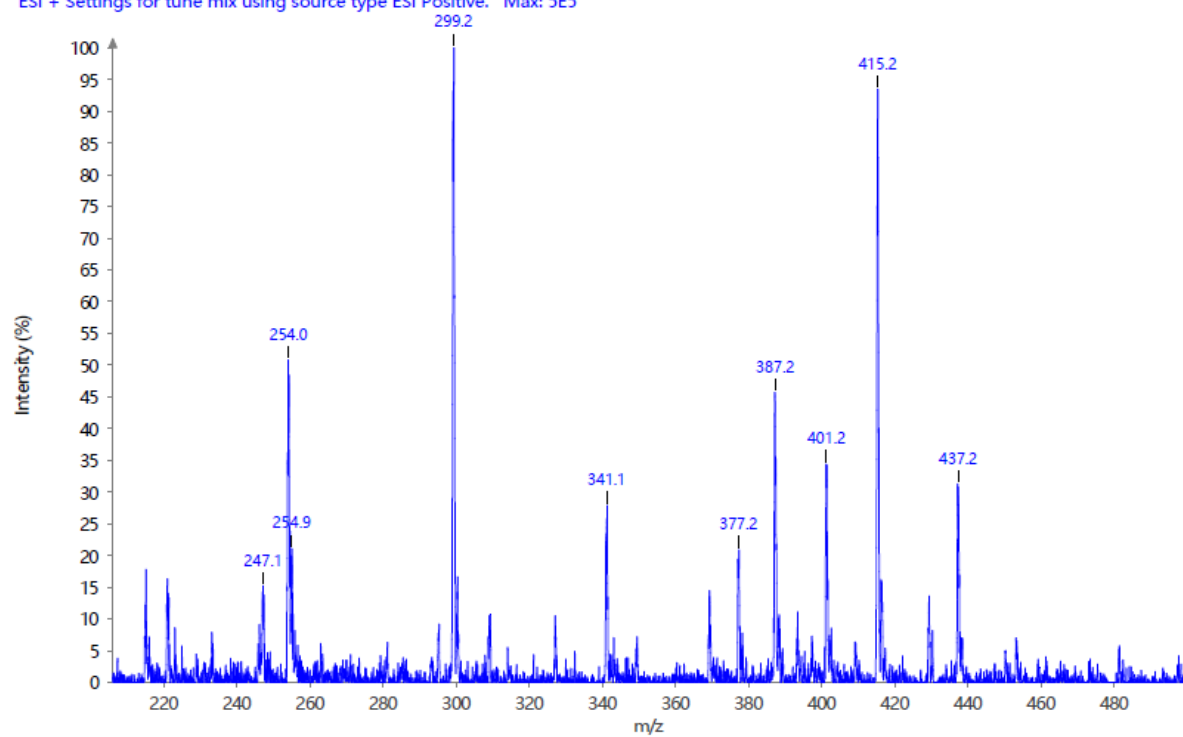
$^1\text{H-NMR}$ Erythromycin-9-N-azidoacetamide- $\text{cdCl}_3\text{-h}_1$ 

**Scheme S4.** Synthesis of N-azidoacetyl-Ciprofloxacin

Ciprofloxacin (33.1mg, 0.1 mmol) suspended in anhydrous DMF (1.0mL), to which first DIEA (50uL) was added the stirred for minute prior to addition of Azido-N-hydroxy succinate (20.3mg, 0.102mmol) and the mixture was stirred at room temperature for overnight. Some white fine solid remained undissolved in the mixture. 15.0mL of ethyl acetate was added to reaction mixture followed by 10.0mL of water. The ethyl acetate layer was pale yellow colored while water layer was brownish colored. The ethyl acetate layer was separated, the aq. Layer was once more extracted with ethyl acetate 5.0mL. The combined ethyl acetate layer wash washed with brine, dried over  $MgSO_4$  and concentrated on rotary evaporator under reduced pressure. The left-over residue was triturated with ether to obtained white solid.  $^1H$ -NMR of white solid indicated presence of unreacted azido acetic acid. The solid was dissolved in 0.5 mL DMSO and diluted with water to total volume of 10 mL. The analytical HPLC showed desired compound at  $R_t$  = min. Preparative HPLC using Water: $CH_3CN$  gradient (95:5 from 5 min. 25 min, 100% B for 5 min., total of 35 min run) purified to homogeneity by collected peak at  $R_t$ =23.4 min. (monitored at 280 and 320nm) as fractions. Combined fractions were concentrated first on rotary evaporator and then by lyophilized to obtain off white solid (14.7mg). Molecular weight was confirmed using an Advion Expression® CMS mass spectrometer.

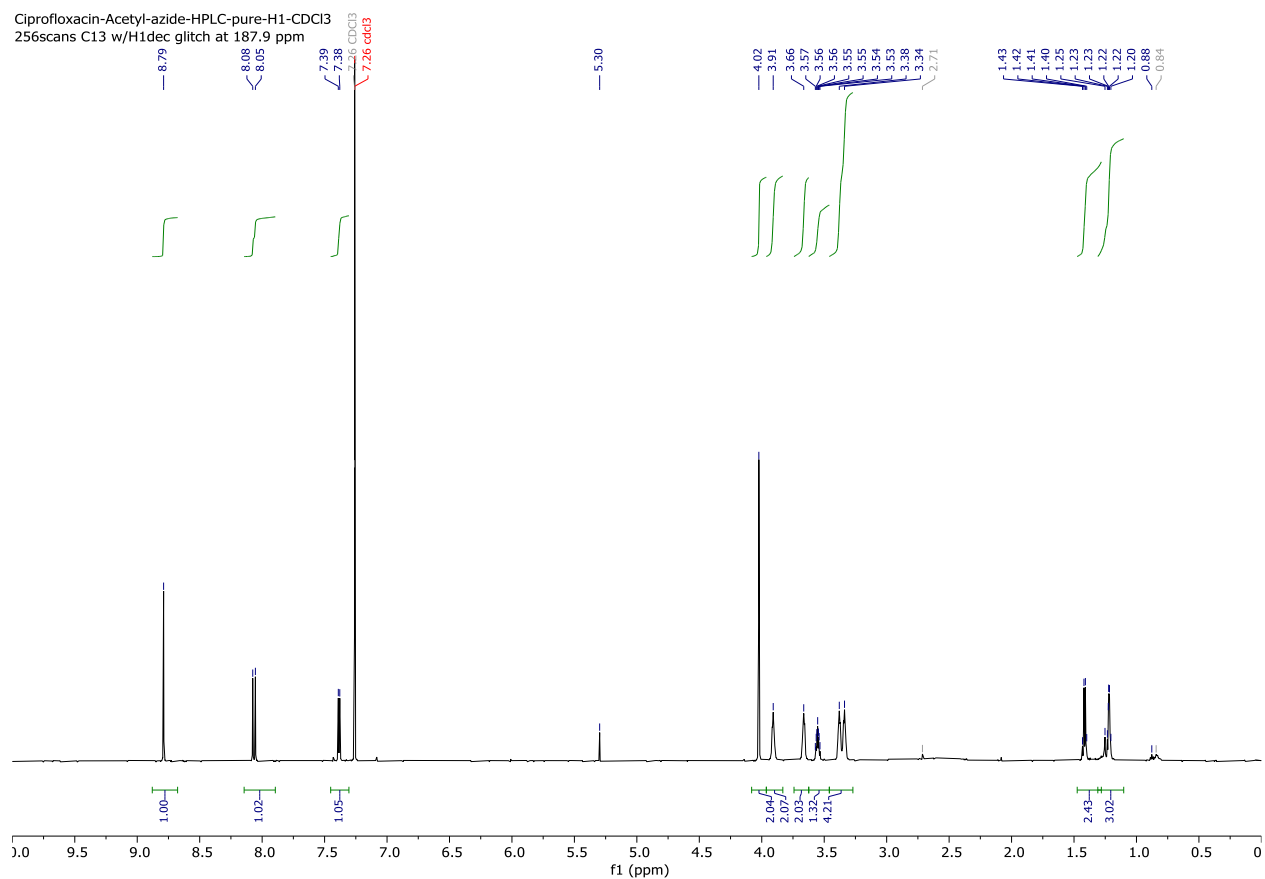
Calculated m/z, 414.4, found m/z, 415.2

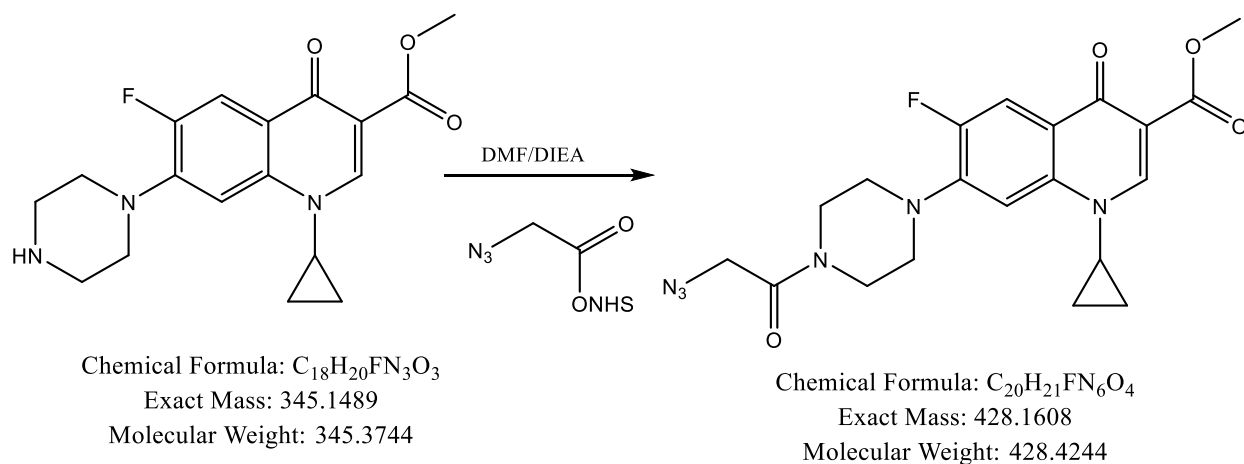
Spectrum RT 1.14 - 2.00 (72 scans) - Background Subtracted 0.04 - 1.04  
Cipro-N-Azidocarboxamide-MW414.datx 2022.09.28 20:30:29 Type in summary here;  
ESI + Settings for tune mix using source type ESI Positive. Max: 5E5



# <sup>1</sup>H-NMR

Ciprofloxacin-Acetyl-azide-HPLC-pure-H1-CDCl<sub>3</sub>  
 256scans C13 w/H1dec glitch at 187.9 ppm



**Scheme S5.** Synthesis of Ciprofloxacin-azidoacetyl methyl ester

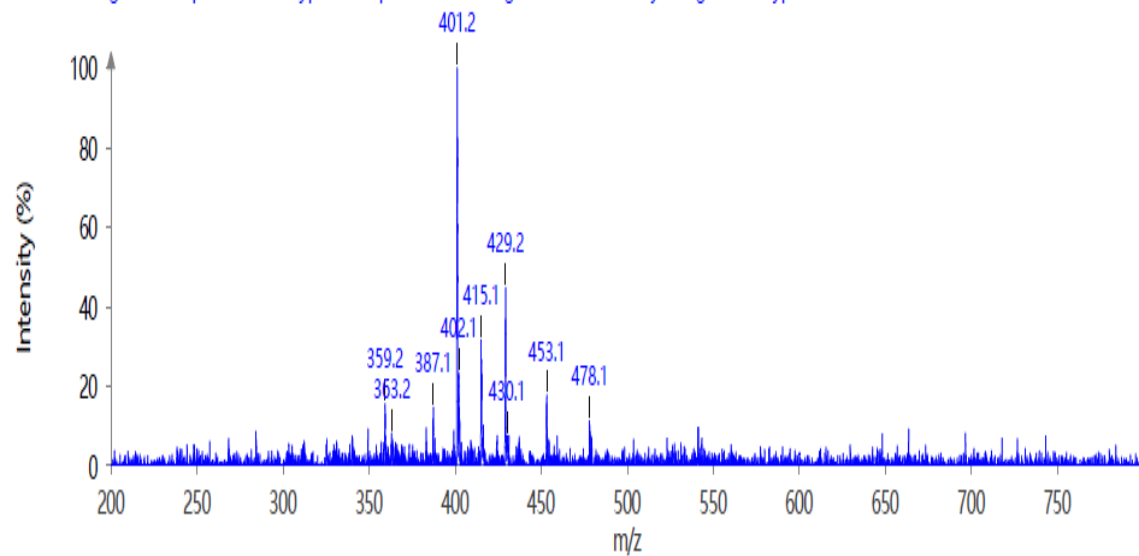
Ciprofloxacin-methyl ester as white solid was synthesized and characterized as per reported procedure using MeOH,  $SOCl_2$ . The ciprofloxacin-methyl ester (34.5 mg, 0.1mmol) was dissolved in anhydrous DMF (1.0 mL) and DIEA (50.0uL), followed by Azido-acetic acid NHS ester (25.3mg, 0.13 mmol) were added to it at room temperature and stirred for 4 hr. The TLC analysis indicated formation of new compound. The mixture was then diluted with chloroform (15.0mL), transferred to separatory funnel and washed thoroughly with water, and dil. HCl (0.1M). The organic layer was finally washed with brine, dried over  $Na_2SO_4$  and concentrated under reduced pressure to yield crude material, which was purified with silica gel column chromatography using chloroform:methanol gradient (98:2), Homogenous fractions as analyzed by TLC were combined and concentrated on rotary evaporator, to afford white solid (32.5mg, 76%). Molecular weight was confirmed using an Advion Expression® CMS mass spectrometer.

Calculated m/z, 428.4, found m/z, 429.2

Spectrum RT 8.94 - 9.06 (13 scans) - Background Subtracted 6.01 - 8.70

MDC-Ciprofloxacin-Acetylazide1 2021.10.27 18:25:31 Type in summary here;

ESI + Settings for compounds with typical temperature and fragmentation stability using source type ESI Positive. Max: 1.2E7



# <sup>1</sup>H-NMR

Ciprofloxacin-Acetyl-azide-pure-2nd-H1-DMSO  
 256scans C13 w/H1dec glitch at 187.9 ppm

